

I) Characterization of LytR-CpsA-Psr enzymes  
and their role in *Staphylococcus aureus* cell wall  
formation

II) Elucidating the mode of action of Cacaoidin,  
a novel class V lantibiotic

**Dissertation**

zur Erlangung des Doktorgrades (Dr. rer. nat.)  
der  
Mathematisch-Naturwissenschaftlichen Fakultät  
der  
Rheinischen Friedrich-Wilhelms-Universität Bonn

vorgelegt von

**Julia Patricia Deisinger**

aus

Moers

Bonn, 2021

Angefertigt mit Genehmigung der Mathematisch-Naturwissenschaftlichen Fakultät der  
Rheinischen Friedrich-Wilhelms-Universität Bonn

1. Gutachterin: Prof. Dr. Tanja Schneider
2. Gutachterin: Priv.-Doz. Dr. Christiane Dahl

Tag der Promotion: 31.01.2022  
Erscheinungsjahr: 2022

# Contents

<b>1</b>	<b>Summary</b>	<b>2</b>
<b>2</b>	<b>Introduction</b>	<b>4</b>
2.1	Cell envelope architecture of <i>Staphylococcus aureus</i> . . . . .	5
2.2	Function and relevance of capsule polysaccharides . . . . .	6
2.3	Organization of the capsule locus and capsule biosynthesis . . . . .	7
2.4	Regulation of capsule biosynthesis . . . . .	9
2.5	Anchoring of glycopolymers in the staphylococcal cell wall . . . . .	12
2.6	LytR-CpsA-Psr enzymes from a structural perspective . . . . .	18
2.7	The cell wall as an antibiotic target . . . . .	23
2.8	Natural product antibiotics . . . . .	27
2.9	Ribosomally synthesized and post-translationally modified peptides . . . . .	28
<b>3</b>	<b>Aim of the thesis</b>	<b>32</b>
<b>4</b>	<b>Publications included in this thesis</b>	<b>33</b>
4.1	Coordination of capsule assembly and cell wall biosynthesis in <i>Staphylococcus aureus</i> . . . . .	33
4.2	Cacaoidin, first member of the new lanthidin RiPP family . . . . .	69
4.3	Dual targeting of the lanthidin antibiotic Cacaoidin . . . . .	145
<b>5</b>	<b>Discussion</b>	<b>162</b>
<b>6</b>	<b>List of Publications</b>	<b>194</b>

# 1 Summary

Antibiotic resistance poses a serious threat to human health, demanding for the discovery and development of antibiotics with resistance-breaking properties. New antibiotics should be sought with the focus on novel chemistry and mechanisms of actions. Furthermore, a profound understanding of the antibiotic target, in the biological context as well as on a cellular level, the target-antibiotic interaction, and the cellular consequences of antibiotic treatment is necessary.

This work is divided in two major parts. The first part encloses the complete *in vitro* reconstitution of capsule assembly in *Staphylococcus aureus* as well as the identification and characterization of regulatory circuits which coordinate capsule assembly and peptidoglycan synthesis, elucidated by the combined efforts of three first authors. Furthermore, LcpC a member of the LytR-CpsA-Psr (LCP) protein family was demonstrated to catalyze the previously elusive attachment of capsular polysaccharides to the cell wall and the peptidoglycan precursor lipid II was identified as the acceptor substrate. The detailed characterization of the LcpC catalyzed reaction further provided the foundation to screen for inhibitors. The second part of this work describes the discovery and elucidation of the mechanism of action of the lantibiotic cacaoidin.

In the following the publications included in this thesis will be briefly summarized:

Subject of the first publication was the **Coordination of capsule assembly and cell wall biosynthesis in *Staphylococcus aureus* (Chapter 4.1)**. In Gram-positive bacteria the bacterial cell wall peptidoglycan is functionalized with glycopolymers, such as wall teichoic acid (WTA) and capsular polysaccharide (CP), and this highly complex assembly plays crucial roles in cell division, maintenance of cell shape and structural integrity, host-cell interaction and immune evasion, and antibiotic drug activity and resistance. Importantly, building up a vital cell wall requires a precise synchronization of various multi-enzyme machineries. This chapter describes the reconstitution of the entire capsule biosynthesis pathway and the elucidation of mechanisms that couple and control the major biosynthetic machineries, leading to a new model of cell wall assembly regulation. Importantly, *in vitro* reconstitution of capsule biosynthesis enabled the purification of lipid-linked synthesis intermediates allowing for the investigation of the previously elusive attachment reaction that transfer CP building blocks to a so far unidentified cell wall acceptor substrate. The work provided the first biochemical proof that the transfer of the capsular phospho-sugar moiety to the peptidoglycan network is catalyzed by LcpC, a member of the LytR-CpsA-Psr (LCP) protein family and show that the membrane-bound peptidoglycan precursor lipid II is the likely acceptor substrate. Strikingly, the work further revealed that CP transfer was significantly enhanced in the presence of CapA1, the membrane-anchored component of the CapAB kinase complex, indicating cooperative function of these enzymes. Further, the CapA1 activator was shown to exhibit a yet unknown and unexpected activity by which it catalyzes the cleavage of lipid-linked CP precursors. Thus, CapA1 has a novel dual function in signaling and processing of capsular polysaccharide precursor.

The second publication **Cacaoidin, first member of the new lanthidin RiPP family (Chapter 4.2)** describes the identification, isolation and structural elucidation of the natural product antibiotic cacaoidin (CAO), produced by a *Streptomyces cacaoi* CA-170360 strain. Cacaoidin was initially classified as a new family, designated lanthidins of ribosomally synthesized and post-translationally modified peptides (RiPPs) due to its unique structural features. The term lanthidin was defined as a hybrid of lanthipeptides (lanthionine rings) and linaridins (because of the presence in cacaoidin of a N,N-dimethyl amino terminals). Further outstanding structural features of cacaoidin comprise the high number of D-amino acids and an unusual glycosylated tyrosine-residue. The antimicrobial activity of cacaoidin is limited to gram positive bacteria, including methicillin-resistant *S. aureus* and *Clostridium difficile*. Cacaoidin was shown to interfere with cell wall biosynthesis and to interact with the peptidoglycan precursor lipid II.

In the third publication **Dual targeting of the lanthidin antibiotic Cacaoidin (Chapter 4.3)** a more comprehensive analysis of the mode of action of cacaoidin was conducted. The findings on the mode of action portrayed in Chapter 4.2 revealed that cacaoidin binds to the cell wall precursor lipid II, as demonstrated for numerous representatives of lanthipeptide family. In depth mechanism of action analysis revealed that cacaoidin exhibits a dual mode of action. Besides targeting lipid II, cacaoidin interfered with cell wall transglycosylases. The unique structural features of cacaoidin could guide the synthesis of hybrid antibiotics with improved and resistance-breaking properties as a result of multi-targeting.

## 2 Introduction

The clinical use of antibiotics represents a major breakthrough of the 20th century and increased the average human life expectancy by 23 years (Hutchings, Truman, & Wilkinson, 2019). In addition to treating infectious diseases, antibiotics revolutionized medical practices, such as chemotherapy, implantation of prosthetic devices, and organ transplantations. These achievements are severely threatened by the rapid rise of antibiotic resistance. According to a groundbreaking report released in December 2014, antibiotic resistance is considered to be a major threat to global health, as it has the potential to cause 10 million deaths per year by 2050 (O’neill, 2014). In 2017, the world health organization (WHO) published a list that highlights antibiotic-resistant priority pathogens (see Tab. 1) for which novel antibiotics are urgently needed, as therapeutic options became limited.

Table 1: WHO priority pathogens list for research and development of new antibiotics. Priority groups were divided based on the urgency of need for new antibacterials. Released in february 2017. ESBL, extended spectrum  $\beta$ -lactamase.

<b>Multidrug-resistant and extensively-resistant <i>Mycobacterium tuberculosis</i></b>
<b>Priority 1: CRITICAL</b> <i>Acinetobacter baumannii</i> , carbapenem-resistant <i>Pseudomonas aeruginosa</i> , carbapenem-resistant <i>Enterobacteriaceae</i> , carbapenem-resistant, ESBL-producing
<b>Priority 2: HIGH</b> <i>Enterococcus faecium</i> , vancomycin-resistant <i>Staphylococcus aureus</i> , methicillin-resistant, vancomycin-intermediate and resistant <i>Helicobacter pylori</i> , clarithromycin-resistant <i>Campylobacter</i> spp., fluoroquinolone-resistant <i>Salmonellae</i> , fluoroquinolone-resistant <i>Neisseria gonorrhoeae</i> , cephalosporin-resistant, fluoroquinolone-resistant
<b>Priority 3: MEDIUM</b> <i>Streptococcus pneumoniae</i> , penicillin-non-susceptible <i>Haemophilus influenzae</i> , ampicillin-resistant <i>Shigella</i> spp., fluoroquinolone-resistant

The opportunistic high priority pathogen *Staphylococcus aureus* is the major cause of wound infections and has the potential to cause invasive infections, e.g., pneumonia, endocarditis, and sepsis (Klevens et al., 2007). Soon after the clinically use of methicillin in 1961, methicillin resistant *S. aureus* (MRSA) strains were isolated (Jevons, 1961). Since then, methicillin resistance emerged rapidly and despite extensive measures (hand and environmental hygiene etc.), death rates are still high. An estimate of 10,600 deaths in the U.S. and 6,810 deaths in Europe were attributed to infections caused by MRSA in 2017 and 2015 respectively according to the Centers for Disease Control and Prevention (CDC) and the European Centre for Disease Prevention and Control (ECDC, Cassini et al. (2019)). MRSA has the outstanding ability to disseminate in different epidemiological settings including hospitals, community and animals (Rossolini, Arena, Pecile, & Pollini, 2014). Even though some drugs retain activity against MRSA (e.g., vancomycin, teicoplanin, linezolid) resistances to last resort antibiotics emerge (Mendes, Deshpande, & Jones, 2014) resulting in limited treatment options.

The antibiotic crisis the world faces today describes the race for the effective treatment of bacterial infections and the emergence of resistance. The underlying reasons for the crisis are diverse and include the overuse and misuse of antibiotics, as well as the lack of new drug development, since they

are generally regarded as non-lucrative investments for pharmaceutical companies (Ventola, 2015a, 2015b). Strategies to overcome the antibiotic resistance crisis comprise I) prevention of infections and transmission of resistant bacteria by e.g. hygiene, disinfection, and vaccine development, II) monitoring of resistant pathogens by e.g. healthcare surveillance networks, III) antibiotic stewardship programs aimed at the improvement of antibiotic use by e.g. optimized prescribing practices, IV) elimination of diagnostic uncertainty by the implementation of faster and more accurate diagnostic tools, and V) development of new antimicrobial agents. Some of these issues can only be addressed if a profound understanding of the pathogens is provided, foremost factors of pathogenicity, host interaction, and potential antibiotic target structures.

However, the highly dynamic bacterial evolution and transfer of resistance conferring genes can promote the rapid emergence of antimicrobial resistance even towards novel therapeutics, by e.g. adaptation of the antibiotic target structure. To prevent this, the identification of additional target structures which are i) essential for virulence e.g. capsular polysaccharides, ii) accessible by therapeutics, and at best iii) specific for virulent strains or species, is needed, since the synergistic targeting of multiple structures is regarded to reduce resistance development. The cell envelope synthesis machinery proved to be a particularly effective target structure for antibiotic therapy and a profound understanding of the underlying cellular mechanisms and potential antibiotic targets is of utmost importance.

## 2.1 Cell envelope architecture of *Staphylococcus aureus*

The bacterial cell wall is a highly conserved structure, which is essential for the survival and growth of most bacteria (Dörr, Moynihan, & Mayer, 2019). In *S. aureus* the cell wall primarily consists of a thick densely packed peptidoglycan mesh decorated with teichoic and teichuronic acid polymers, as well as surface proteins and encloses the cytoplasmic membrane (Figure 1; reviewed by Geoghegan and Foster (2015); Swoboda, Campbell, Meredith, and Walker (2009); Weidenmaier and Lee (2015)). Particularly in strains causing invasive diseases an additional polysaccharides capsule is present, which is anchored to the peptidoglycan mesh (Verdier et al., 2007) and represents the outermost layer of the staphylococcal cell envelope. The cell envelope separates the interior towards the surrounding milieu, while enabling the transport of substances as well as signal transduction from the exterior.

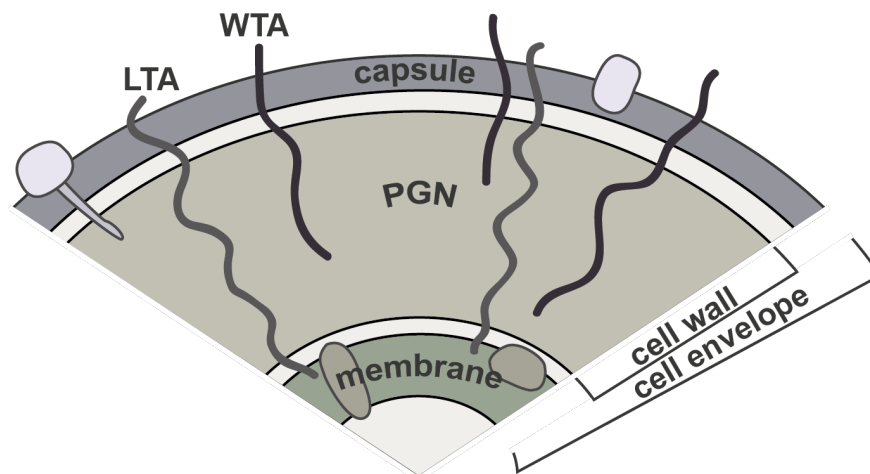


Figure 1: Schematic overview of the *S. aureus* cell envelope. The cytoplasmic membrane is surrounded by a thick layer of peptidoglycan. In some strains a polysaccharide capsule is covalently linked to peptidoglycan. Lipoteichoic acid (LTA) and wall teichoic acid (WTA) glycopolymers are attached to the membrane and peptidoglycan respectively and span through the PGN layer.

In addition to providing shape and stability, the cell wall represents a dynamic structure facilitating growth and proliferation. The major cell wall component, peptidoglycan, accounts for 90% of the cell dry weight in gram-positive bacteria (Malanovic & Lohner, 2016), and its main function is to preserve cell integrity and to withstand turgor pressure. It consists of alternating UDP-*N*-acetylglucosamine (UDP-GlcNAc) and UDP-*N*-acetylmuramic acid-pentapeptide (UDP-MurNAc-pp)-disaccharide units which are further crosslinked via peptide moieties to generate a rigid network (for review see Lovering, Safadi, and Strynadka (2012)). Surface proteins and wall teichoic acids (WTA) are covalently linked to peptidoglycan, while lipoteichoic acids are anchored within the membrane (Figure 1). In *S. aureus*, WTAs are the most abundant glycopolymers attached to PGN and are of great importance for cell physiology and pathogenicity (reviewed by Weidenmaier and Peschel (2008)). They are composed of 30-50 ribitol phosphate (Rbo-P) repeating units linked by a phosphodiester bond, which is tethered to PGN via a

D-ManNAc-D-GlcNAc-(glycerol phosphate [Gro-P])<sub>2-3</sub> murein linkage unit (Yokoyama, Miyashita, Araki, & Ito, 1986). Capsular polysaccharides of *S. aureus* appear to be covalently attached to the peptidoglycan, however the nature of the bond remains debated. The biosynthesis of peptidoglycan and WTA is well characterized, whereas the underlying biochemistry of capsule formation in *S. aureus* is not completely understood yet.

## 2.2 Function and relevance of capsule polysaccharides

The production of extracellular capsular polysaccharides is a common feature of pathogens which cause invasive diseases (O’Riordan & Lee, 2004; Robbins, Schneerson, Egan, Vann, & Liu, 1980). Bacterial capsules can provide protection against desiccation and can be important for adhesion, and biofilm formation. Importantly, the bacterial capsule contributes to virulence and plays a role for the survival within the host, e.g., protection from phagocytic clearance, complement-mediated lysis by shielding the bacterial surface and surface associated proteins from opsonization and prevents recognition by phagocytes (Kuipers et al., 2016; Thakker, Park, Carey, & Lee, 1998). Interestingly, capsule shedding has been observed for some *S. aureus* isolates and was accounted to interference with anti-capsular antibody binding elicited by the host to opsonize the pathogen (Liu, Park, Thompson, Li, & Lee, 2016).

Although older literature suggests as many as eleven staphylococcal capsule serotypes only four, namely serotypes 1, 2, 5, and 8, have been chemically defined, and evidence supporting the existence of others is tenuous at best<sup>1</sup> (Cocchiario et al., 2006). In fact, the majority of *S. aureus* clinical isolates are encapsulated (~87-92%) and serotypes 5 and 8 are predominant accounting for ~42-50% and ~42-45%, respectively (Roghmann et al., 2005; Verdier et al., 2007). Capsule serotyping is usually achieved using respective capsular polysaccharide type specific antibodies and strains not reacting to antibodies of serotypes 1, 2, 5 or 8 are referred to as nontypeable. Interestingly, many studies showed that the majority of nontypeable isolates, if not all, still possess genes to direct synthesis of capsule serotypes 5 or 8 (Cocchiario et al., 2006; Mohamed et al., 2019; Verdier et al., 2007) and produced a transcript of the respective capsule locus. The lack of capsule expression was attributed to mutations or deletions affecting essential capsule genes or genes and regions with regulatory function (Cocchiario et al., 2006; Lattar et al., 2009). Type 5 and 8 capsular polysaccharides (CP5 and CP8) share very similar structures (Figure 2). Both contain trisaccharide repeating units of *N*-acetyl-D-mannosaminuronic acid (D-ManNAcA), *N*-acetyl-L-fucosamin (L-FucNAc) and *N*-acetyl-D-fucosamin (D-FucNAc), that only differ in two of the three glycosidic-linkages between the sugar residues and sites of O-acetylation. Structures of the repeat units of the type 5 and 8 polysaccharides are (→4)-β-D-ManNAcA-(1→4)-α-L-FucNAc(3OAc)-(1→3)-β-D-FucNAc-(1→)<sub>n</sub> and (→3)-β-D-ManNAcA(4OAc)-(1→3)-α-L-FucNAc-(1→3)-α-D-FucNAc-(1→)<sub>n</sub>, respectively (Jones, 2005). Capsule production strongly responds to environmental conditions, e.g., CO<sub>2</sub>, iron-limitation,

<sup>1</sup>Neither the antisera nor the prototype strains, which were used to define the strains of serotype 6, 7, 9, 10 and 11 are available.



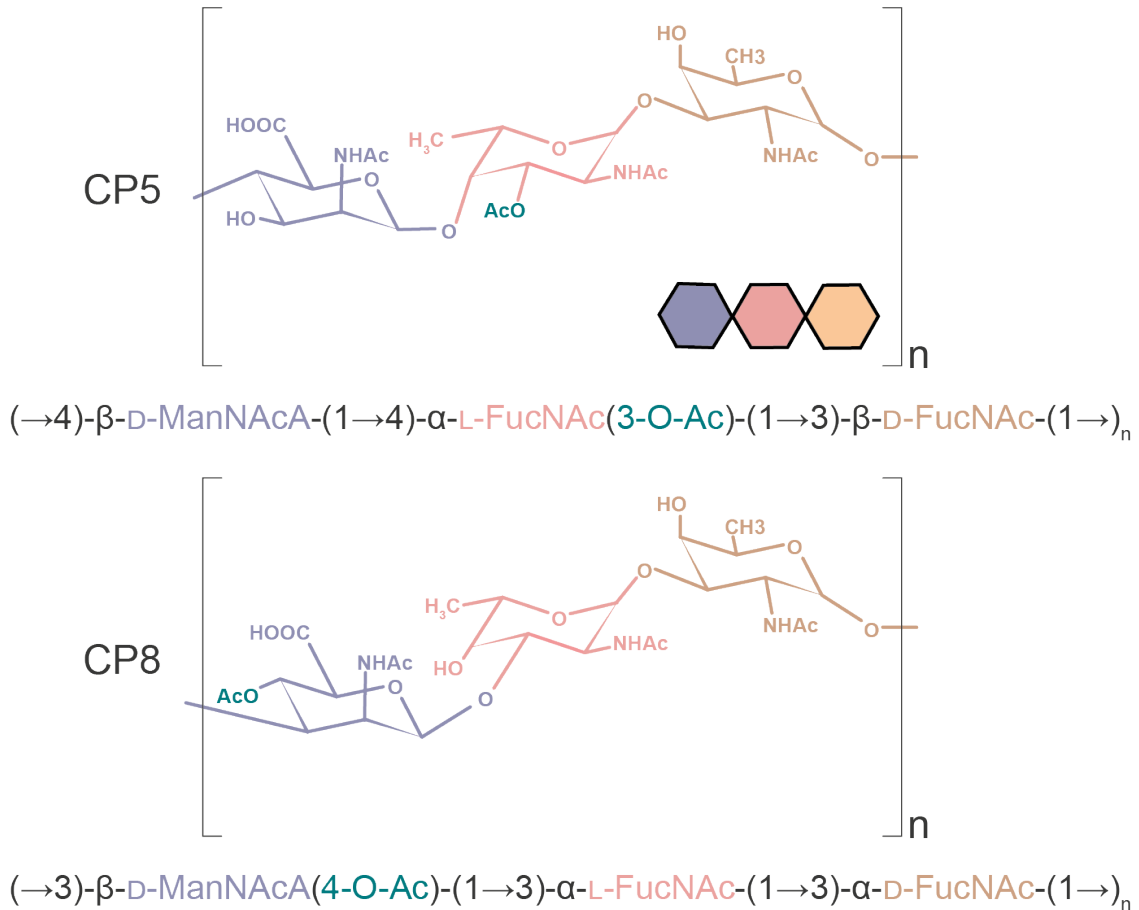


Figure 2: The prevalent *S. aureus* capsular serotypes CP5 and CP8 show a similar composition. Both polysaccharides are comprised of the trisaccharide subunits D-ManNAcA, L-FucNAc and D-FucNAc and only differ in their glycosidic linkages and the site of O-acetylation (highlighted green).

nutrients, pH, and anaerobiosis, reviewed by O’Riordan and Lee (2004). An intriguing example is that acapsular *S. aureus* adapted to infected bone regained the ability to produce a capsule when transferred to bloodstream (Suligoy et al., 2020). These observations are pointing out that capsule expression can be switched on or off according to the given niche in a host or other environments.

### 2.3 Organization of the capsule locus and capsule biosynthesis

Genes responsible for capsule production in *S. aureus* CP5 and CP8 are organized in one gene cluster localized on the chromosome and comprise 16 genes (ORFs), which are named *cap5(8)A* through *cap5(8)P* (Figure 3). The *cap5* and *cap8* loci are allelic and their type-specific genes are located at the central region of the loci, comprising *cap5(8)H*, *cap5(8)I*, *cap5(8)J* and *cap5(8)K* (Sau, Bhasin, et al., 1997; Wann, Dassy, Fournier, & Foster, 1999). The operon is mainly transcribed as a single 17 kb transcript under the control of promoter ( $P_{cap}$ ), located upstream of *cap5(8)A* (Herbert et al., 2001; Ouyang, Sau, & Lee, 1999). Data base homology searches allowed prediction of individual enzymatic functions (O’Riordan & Lee, 2004), of which some have already been verified.

The following remarks on capsule synthesis and involved *cap* gene products refer to *S. aureus* CP5. While gene products of *cap5A-C* are designated to have a regulatory function on capsule biosynthesis, *cap5D-P* gene products are attributed to enable synthesis, polymerization and translocation of capsule polysaccharides. The biosynthesis of all three soluble capsular precursors starts with the universal substrate uridine diphosphate *N*-acetyl-D-glucosamine (UDP-D-GlcNAc) in the cytoplasm and involves three reaction cascades generating the activated sugar building blocks UDP-D-FucNAc,

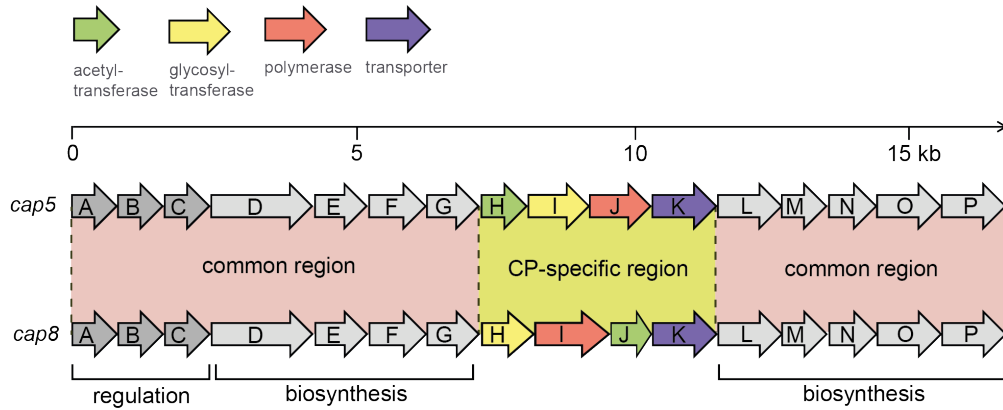


Figure 3: Comparison of *S. aureus* capsule biosynthesis gene clusters *cap5* and *cap8*. Gene designations and the orientation of transcription are indicated by arrows. The two clusters are allelic and capsule (CP) type-specific genes are flanked by genes conserved between both loci encoding for capsule biosynthesis directing enzymes.

UDP-L-FucNAc and UDP-D-ManNAcA (Figure 4). The membrane-bound Cap5D initiates synthesis of the first soluble capsule precursor by 4, 6-dehydration of UDP-D-GlcNAc generating UDP-2-acetamido-2,6-dideoxy- $\alpha$ -D-xylo-4-hexulose (UDP-xylo-sugar) (W. Li et al., 2014). Subsequent reduction of the intermediate by the membrane-associated Cap5N yields UDP-D-FucNAc (Ulm, 2016), which was shown to be a substrate of the initial glycosyltransferase Cap5M (Rausch, 2017). Membrane-anchored Cap5M catalyzes the transfer of D-FucNAc to the universal lipid carrier undecaprenyl-phosphate ( $C_{55}P$ ), generating lipid  $I_{cap}$ . Synthesis of the second soluble precursor UDP-L-FucNAc involves a three step reaction catalyzed by Cap5E, Cap5F and Cap5G. The 4, 6-dehydratase and 5-epimerase activity of Cap5E converts UDP-D-GlcNAc and leads to the formation of two products appearing sequentially. Dehydration of UDP-D-GlcNAc generates the intermediate UDP-xylo-sugar (aforementioned D-FucNAc precursor), this reaction is followed by C-5 inversion catalyzed by the 5-epimerase activity and generates UDP-2-acetamido-2,6-dideoxy- $\beta$ -L-arabino-4-hexulose (UDP-arabino-sugar, L-FucNAc precursor) (Kneidinger et al., 2002; W. Li et al., 2014; Miyafusa, Caaveiro, Tanaka, & Tsumoto, 2013). The UDP-xylo-sugar intermediate is regarded as a byproduct only detectable in absence of the downstream processing enzyme Cap5F. Cap5F reduces the UDP-arabino-sugar at C-4 generating UDP-2-acetamido-2,6-dideoxy-L-talose and a 2-epimerization step catalyzed by Cap5G yields UDP-L-FucNAc (Kneidinger et al., 2002). L-FucNAc is subsequently added to lipid  $I_{cap}$  by the glycosyltransferase Cap5L generating lipid  $II_{cap}$  (Rausch, 2017). The third and final soluble capsule intermediate UDP-D-ManNAcA is generated by the cooperative activity of Cap5P and Cap5O. Cap5P 2-epimerase activity catalyzes the conversion of UDP-D-GlcNAc to *N*-acetyl-D-mannosamine (UDP-D-ManNAc) (Kiser, Bhasin, Deng, & Lee, 1999) and the Cap5O dehydrogenase oxidizes the Cap5P-product to UDP-D-ManNAcA (Portolés, Kiser, Bhasin, Chan, & Lee, 2001). Subsequently, Cap5I is assumed to transfer the D-ManNAcA-moiety to lipid  $II_{cap}$ , generating the final lipid-bound capsule precursor lipid  $III_{cap}$ . Serotype-specific *O*-acetylation of CP5 is catalyzed by the *O*-acetyltransferase Cap5H at position C3 of L-FucNAc (Bhasin et al., 1998; Jones, 2005). After completion of the trisaccharide repeating unit (RU), the precursor is flipped across the membrane by the putative Wzx-like flippase Cap5K, where it is polymerized into the full-length capsule polymer by addition of new RUs to the reducing end of the glycopolymer in a reaction catalyzed by the putative Wzy-like polymerase Cap5J (Sau, Bhasin, et al., 1997). Final glycopolymer attachment to PGN is catalyzed by members of the LytR-CpsA-Psr enzyme family (Chan, Kim, Schneewind, & Missiakas, 2014; Rausch, 2017) summarized in chapters 2.5 and 2.6.

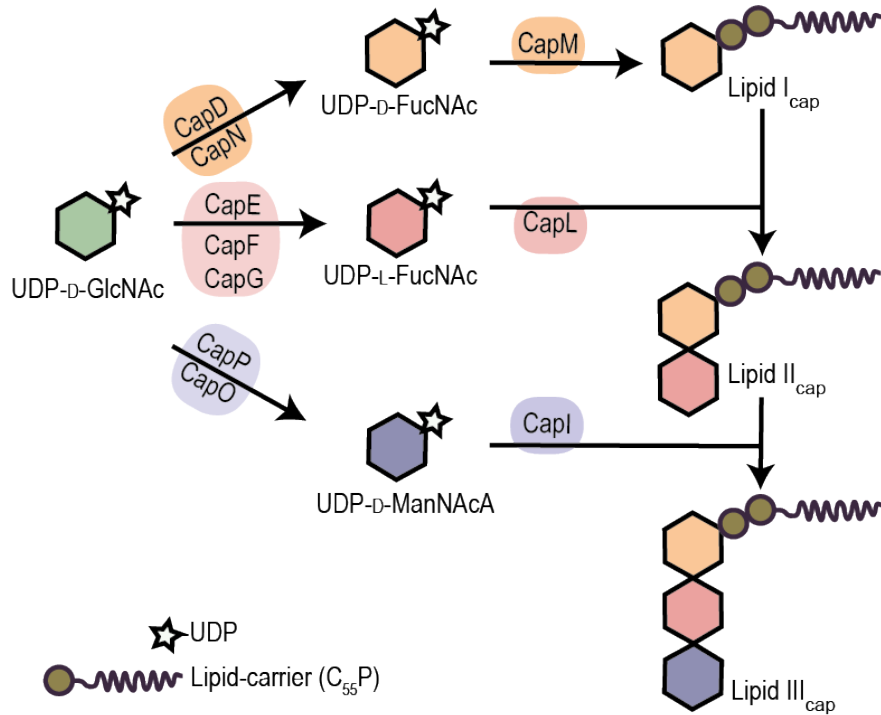


Figure 4: Schematic overview of the proposed pathway for *S. aureus* serotype 5 biosynthesis (adapted from O’Riordan and Lee (2004)). The universal soluble precursor uridine diphosphate *N*-acetyl-D-glucosamine (UDP-D-GlcNAc) is substrate for three distinct reaction cascades generating the nucleotide-coupled sugars *N*-acetyl-D-fucosamin (D-FucNAc), *N*-acetyl-L-fucosamin (L-FucNAc) and *N*-acetyl-D-mannosaminuronic acid (D-ManNAcA) in the cytoplasm. Saccharide-units are further assembled onto the membrane-anchored lipid-carrier undecaprenyl-phosphate, yielding the ultimate CP5 trisaccharide building block lipid III<sub>cap</sub>.

11 out of 16 genes have been shown to be essential for capsule production (Sau, Sun, & Lee, 1997). Genes *cap5A-C*, *cap5H*, and *cap5P* appear non-essential. The *cap5A-C* gene products are attributed to be post-transcriptional regulators of CP5 synthesis (Lee & Lee, 2014; Rausch, 2017), *cap5H* mutants produce O-deacetylated CP5 (Bhasin et al., 1998), and insertional inactivation of *cap5P* can be compensated by presence of a second UDP-GlcNAc-2-epimerase, which is usually attributed to WTA synthesis and encoded by *mnaA* (Kiser et al., 1999).

The fact that CapE, just like CapD is able to catalyze the formation of the UDP-*xylo*-sugar intermediate (UDP-D-FucNAc precursor) might represent a key determinant for the proposed ability of some USA300 strains to produce a capsule (Mohamed et al., 2019) under infectious conditions. Lack of capsule production in USA300 strains was, among other mutations, attributed to *cap5D* frameshift mutations resulting in non-functional Cap5D. Mohamed et al. (2019) proposed that USA300 strains in which the *cap5D* gene contains a premature stop codon, the UDP-D-FucNAc precursor UDP-2-acetoamino-2,6-dideoxy- $\alpha$ -D-xylo-4-hexulose is derived as byproduct of the reverse epimerase reaction catalyzed by CapE. In this scenario the membrane-spanning domains of the truncated Cap5D (devoid of enzyme activity) could still act as a docking station for the capsule synthesis machinery (Mohamed et al., 2019).

## 2.4 Regulation of capsule biosynthesis

Studies with encapsulated and non-encapsulated strains reveal that depending on the infection model used, capsule production can either enhance or attenuate virulence. Encapsulation is dominantly found in patients with acute systemic infections, whereas a heterogeneous proportion of *S. aureus*

not expressing a capsule are found in hosts with chronic infections. A putative advantage of non-encapsulated strains is the exposure of surface molecules, that confer adherence to host cells, which is essential to invade cells (avoiding immune clearance) and for colonization (reviewed by Tuchscher, Löffler, Buzzola, and Sordelli (2010)). Besides the high sensitivity to environmental changes, capsule production was also found to be strictly growth phase-dependent, with capsule expression only detected in post-exponential growing *S. aureus* cells. Furthermore, coexistence of capsule-positive and -negative bacteria was observed within the same population both in *in vitro* and *in vivo* (e.g., isolates from human nasal carriers), indicating that expression of capsular polysaccharides is heterogeneous and not necessarily dependent on the clonal complex or the capsule serotype (George et al., 2015). This raises the question which regulator is responsible for the particular earlyOff/lateHeterogen expression pattern.

Capsule heterogeneity could provide better adaptability of a population as a whole (Keinhörster et al., 2019). In order to achieve this degree of adaptability capsule expression must be tightly coordinated in time and space. Regulation of capsule expression was shown to be controlled at multiple levels. Experimental data suggests that regulation predominantly occurs at the transcriptional level, since  $P_{cap}$  controlled activities correlated with capsule synthesis (George et al., 2015). Keinhörster et al. (2019) demonstrated that capsule production is upregulated by alternative sigma factor B<sup>2</sup> ( $\sigma$ B), through direct promoter activation. The upstream region of  $P_{cap}$  was attributed to be of repressive function. Many regulators which bind to that region have been reported, including transcriptional factors and two component systems, which directly or indirectly repress expression of *cap*, by reducing  $\sigma$ B-dependent promoter activity. When transcription is rendered constitutive and the upstream region of  $P_{cap}$  is deleted, capsule production still remains growth-phase dependent. This observation was not reflected on the transcriptional level, since *capA* transcript levels<sup>3</sup> were very high throughout all growth phases (early exponential, exponential, and late exponential), while the majority of the bacterial population still remained capsule negative in the early exponential growth phase (Keinhörster et al., 2019). Therefore, capsule synthesis is not solely dependent on the regulation of *cap* expression but is also controlled by additional post-transcriptional regulatory circuits.

Several studies indeed demonstrated that capsule biosynthesis is also controlled on a post-translational level by reversible protein phosphorylation of CapM, CapE, and CapO (positively affecting protein activity) by the CapAB kinase complex (Gruszczuk et al., 2011; Rausch, 2017; Soulat, Grangeasse, Vaganay, Cozzone, & Duclos, 2007). The complex is composed of the transmembrane activator protein CapA, which induces autophosphorylation of the cytosolic bacterial (BY-) tyrosine kinase CapB. The kinase and its protein targets are in turn dephosphorylated by the histidinol phosphatase class phosphatase CapC (Rausch, 2017), which in the overall picture represents a regulative cycle for capsule polysaccharide biosynthesis (Figure 5). *S. aureus* harbors two paralogs of CapA, CapB and CapC and the encoding gene triplets are located at different positions on the bacterial chromosome. One is located at the 5'-end of the *cap* operon encoding *capA1*, *capB1*, and *capC1*, and the second highly similar triplet encoding *capA2*, *capB2*, and *capC2* is located elsewhere on the chromosome, adjacent to the *icaR* gene, a direct repressor of the intracellular adhesin (*ica*) operon (*icaADBC*). Enzymes encoded by the *ica* operon catalyze the synthesis of the adhesin poly-N-acetylglucosamine (PNAG) (Cerca, Brooks, & Jefferson, 2008; Sadykov et al., 2010; Schwartbeck et al., 2016)). Interestingly, the extracellular polysaccharides PNAG and CP5 were both shown to inhibit CapA2-mediated activation of CapB2, whereas CapA1-mediated activation

---

<sup>2</sup>In bacteria, alternative  $\sigma$  factors act as transcription factors involved in promoter recognition and RNA polymerase recruitment. The *S. aureus* alternative  $\sigma$ B is involved in the general stress response and has been shown to control the expression of multiple genes, including virulence determinants and global regulators playing an important role during infection (Schulthess et al., 2011; Supa-amornkul et al., 2019).

<sup>3</sup>Transcript levels of *capA* are indicative for *cap* expression since the *cap* operon is mainly transcribed as a single 17 kb transcript and *capA* is the first gene within the operon.

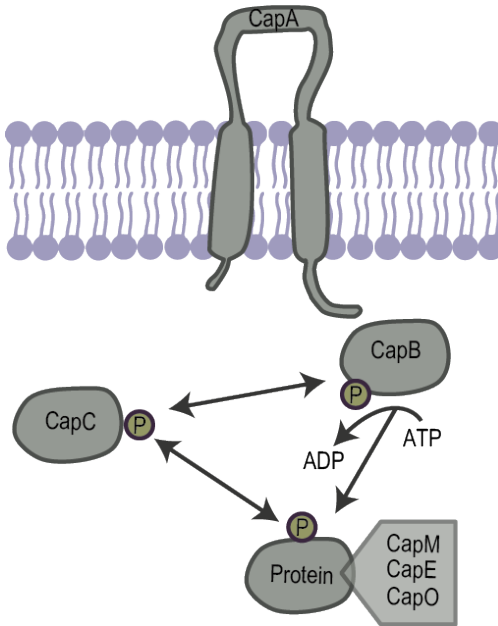


Figure 5: Schematic overview of the post-translational regulative circuit of capsule biosynthesis in *S. aureus*. The transmembrane activator CapA induces autophosphorylation of the cytosolic tyrosine kinase CapB, while CapB and its phosphorylation targets are in turn dephosphorylated by the histidinol phosphatase class phosphatase CapC.

of CapB2 remained unaffected (Rausch, 2017). These results suggest, that despite high sequence and structural similarity (Gruszczyk et al., 2013) the CapA1/B1 and CapA2/B2 complexes possess different physiological roles.

Another post-transcriptional regulator of capsule synthesis is the eukaryotic-like serine/threonine kinase (ESTK) PknB, also referred to as Stk. The general mechanism by which ESTKs and associated phosphatases mediate cell signaling is sensing and transduction of extracellular stimuli by the reversible phosphorylation of serine and threonine residues. PknB of *S. aureus* was found to reduce CapM and CapB activity by direct reversible phosphorylation and might therefore have a negative impact on capsule production (Rausch, 2017). Furthermore, PknB and its cognate phosphatase Stp play an important role for the coordination of cell wall synthesis, autolysis and cell division (Beltramini, Mukhopadhyay, & Pancholi, 2009; Donat et al., 2009; Hardt et al., 2017; Jarick et al., 2018; Tamber, Schwartzman, & Cheung, 2010). The finding that PknB specifically interacts with lipid II, via its extracellular PASTA (**p**enicillin-binding protein and **Ser/Thr** kinase **a**ssociated) domains, indicates that PknB likely senses and responds to lipid II pool levels, by the activation of its cytoplasmic N-terminal kinase domain and further triggers intracellular signaling cascades. Thus, PknB and its cognate phosphatase, might function as coordinators to regulate cell envelope biogenesis processes in response to the synthesis status of the essential cell wall precursor lipid II (Hardt et al., 2017).

Keinhörster et al. (2019) suggested that the transcriptional regulators are mainly responsible for heterogeneous capsule production pattern, while post-transcriptional regulation guarantees a link between capsule synthesis and the metabolic status of a cell. Since capsule, peptidoglycan and WTA synthesis pathways share a common pool of precursors (Figure 6), namely UDP-D-GlcNAc and the lipid carrier  $C_{55}P$ , which are only present in limited amounts in the cell, their consumption within the different biosynthetic pathways needs to be tightly controlled. In *S. aureus* PGN and WTA are predominantly synthesized during early and exponential growth phase, while capsule polysaccharides are mainly generated at the late exponential growth phase. Therefore, it is of utmost importance, that the consumption of shared precursors is prioritized in accordance to the metabolic state of the cell and the channeling of precursors into alternate metabolic pathways is tightly spatio-temporally

controlled. Especially the membrane-associated steps of the synthesis of capsule lipid intermediates are critical, since only the initial reaction catalyzed by CapM, where the undecaprenyl (C<sub>55</sub>P)-lipid carrier is coupled to the first sugar building block, is reversible. Uncontrolled consumption at that stage could cause adverse effects on cell viability. The fact that the activity of the priming capsule synthesis glycosyltransferase CapM is a (phosphorylation) target of PknB and the CapAB complex highlights the importance of CapM as an enzymatic checkpoint.

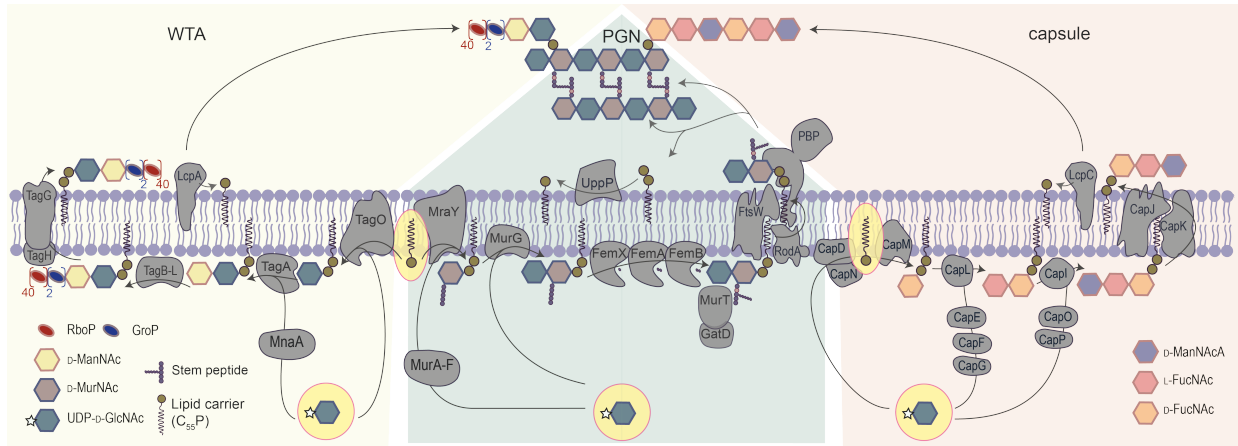


Figure 6: Overview of WTA (yellow background), PGN (green background) and capsule (orange background) biosyntheses in *S. aureus* which share a common precursor pool of UDP-D-GlcNAc and C<sub>55</sub>P (highlighted in yellow with pink outlines).

## 2.5 Anchoring of glycopolymers in the staphylococcal cell wall

Although there is substantial information on syntheses of cell wall glycopolymers (GPs) like wall teichoic acids and capsule polymers, the critical steps involved in their attachment to the cell surface remained elusive until recently. Mutational, structural, and biochemical investigations revealed that the LytR-CpsA-Psr (LCP) family of proteins commonly catalyze anchoring of different GPs to the PGN-backbone. Initially LCPs were suspected to be cell envelope-associated transcriptional attenuators. This assumption was also the origin of the "LCP" acronym, which derived from the first described representatives LytR (lytic repressor, now TagU) of *Bacillus subtilis* (Lazarevic, Margot, Soldo, & Karamata, 1992), CpsA (capsular polysaccharide expression regulator) of *Streptococcus agalactiae* (Cieslewicz, Kasper, Wang, & Wessels, 2000), and Psr (PBP5 synthesis repressor) of *Enterococcus hirae* (Ligozzi, Pittaluga, & Fontana, 1993). The characteristic feature of LCP family members is the unique LCP-domain. LCP homologous were discovered in eight bacterial phyla including *Actinobacteria*, *Bacteroidetes*, *Chloroflexi*, *Cyanobacteria*, *Deinococcus-Thermus*, *Firmicutes*, *Spirochaetes*, and *Thermotogae* (Hübscher, Lüthy, Berger-Bächli, & Meier, 2008). Although gram negative representatives are among these phyla, LCP enzymes are mostly absent in the majority of gram negative organisms. In contrast, they are present in all gram positive organisms, except for the cell wall-deficient *Mollicutes* and one strain of the *Clostridiales* (Hübscher et al., 2008). Until now, experimental evidence of LCP function was only provided for the phyla *Actinobacteria*, *Firmicutes*, and *Cyanobacteria* (Stefanović, Hager, & Schäffer, 2021). Deletion of *lcp* genes often correlates with pleiotropic phenotypes characterized by the release of cell wall GPs into the culture supernatant, aberrant septum formation, increased susceptibility to  $\beta$ -lactams and increased autolysis (Chan, Frankel, Dengler, Schneewind, & Missiakas, 2013; Chan et al., 2014; Hübscher et al., 2009; Johnsborg & Håvarstein, 2009; Over et al., 2011). The majority of reported phenotypes were attributed to be indirect consequences of severe cell wall alterations. In particular, the observed altered virulence and antibiotic susceptibility of human pathogens resulting from the absence of LCPs attracted a particular interest in this enzyme family as potential drug targets. The immense diversity of LCP-encoding

bacteria with regard to their morphology, ultrastructure, motility, metabolic characteristics, and habitat preferences is also reflected on the sequence level, except for the highly similar LCP domain (Hübscher et al., 2008).

Most organisms carry multiple versions of LCP encoding genes often located in close proximity to clusters encoding for genes involved in the biosynthesis of secondary polymer biosynthesis (Chan et al., 2014). *Bacillus subtilis* for example, harbors three LCP encoding genes *tagT*, *tagU* and *tagV* (*yvhJ*, *lytR*, *ywtF*, respectively) that are located within a 50 kb region on the chromosome, directly adjacent to genes coding for teichuronic acid and minor teichoic acid biosynthetic enzymes and within six open reading frames of the WTA biosynthesis gene cluster (Kawai et al., 2011). In case of *Streptococcus agalactiae* and *Streptococcus pneumoniae* enzymes for capsule biosynthesis are encoded in one operon starting with the conserved gene *cpsA* or *cps2A*, respectively, encoding a member of the LCP protein family. In *S. pneumoniae* additional *lcp* genes *psr* and *lytR* are located away from known cell wall biosynthesis related clusters. *S. aureus*, encodes for three LCP genes designated *lcpA* (*msrR*, SA1195), *lcpB* (SA0908) and *lcpC* (SA2103), of which none, is part of any biosynthetic cluster. Of interest, the *S. aureus* transcriptional activator LytR (SA0251; response regulator of TCS LytSR) shows no sequence similarity to LCP proteins and is therefore not part of the LCP family.

Deletion of individual *S. aureus lcp* genes had only minor effects on cell physiology and growth, while a variant lacking all three *lcp* genes ( $\Delta lcp$ ) is barely viable, indicating gene products have semi-redundant functions. However, enzymes cannot fully complement each other arguing against the complete redundancy of the gene products. In a  $\Delta lcp$  mutant WTA and capsule polysaccharides are no longer attached to the cell wall but released into the culture supernatant, indicating that WTA and capsule attachment requires at least one LCP enzyme. Investigations of single and double *lcp* knock-out mutants revealed a certain substrate preference and a certain physiological link to one and the other biosynthetic pathway, respectively. Mutants with a deletion of *lcpA* or *lcpB* for instance display significantly stronger reduction in WTA anchoring than a variant lacking *lcpC* (Chan et al., 2013). These results indicate that LcpA and LcpB are more relevant for WTA attachment than LcpC. On the other hand, a mutant lacking *lcpC* was reported to release capsular polysaccharides in the supernatant, while the deletion of *lcpA*, *lcpB* or a combination of both did not display impaired CP5 anchoring, suggesting LcpC predominantly catalyzes the attachment of capsular polysaccharides (Figure 7).

The viability of a complete *lcp* gene knockout mutant has only been reported for *S. aureus* so far and the lethal effect observed in other organisms might be attributed to the build up of toxic intermediates and/or the sequestration of the essential carrier lipid undecaprenyl phosphate (C<sub>55</sub>P highlighted in yellow), which is usually released during LCP action (Figure 7). The fact that the *S. aureus*  $\Delta lcp$  mutant is viable indicates the presence of an additional rescue mechanism which prevents either the accumulation of toxic intermediates and/or the sequestration of C<sub>55</sub>P. In case of *B. subtilis*, a triple knockout of all LCP genes (*tagTUV*) is lethal unless bacilli lack the *tagO* gene<sup>4</sup> encoding for the glycosyltransferase catalyzing the first membrane-committed step in WTA synthesis (Kawai et al., 2011). In a *tagO* deleted strain the WTA polymer synthesis is disrupted and the mutant strain is subsequently devoid of WTAs (D'Elia et al., 2006). The absence of an intact WTA synthesis machinery might circumvent accumulation of toxic WTA-intermediates in a *tagTUV* gene deletion background. To investigate the phenotype of a *tagTUV* deletion, a mutant with inducible depletion of *tagV* in a  $\Delta tagTU$  background was created. Interestingly, the  $\Delta tagTU(V)$  mutant neither released anionic polymers in the supernatant, nor did it attach WTA in

---

<sup>4</sup>In *B. subtilis* early steps of WTA synthesis, catalyzed by the *tagO* and *tagA* gene products, are dispensable for cell viability, while the late steps are essential. However, late WTA genes were found to be only conditionally essential, since respective gene knockouts are viable in either a *tagO* or *tagA* deletion background, indicating the importance of the reversibility of the TagO reaction. This is referred to as the essential gene paradox and also observed for the respective *S. aureus* gene homologous. Two hypotheses were given to explain this intriguing finding, I) the accumulation of toxic intermediates in late-stage WTA mutants and/or II) the sequestration of the lipid carrier C<sub>55</sub>P causing depletion of peptidoglycan synthesis (D'Elia, Millar, Beveridge, & Brown, 2006; D'Elia, Pereira, & Brown, 2009).

the cell wall (Kawai et al., 2011). The reason for the lethality of  $\Delta tagTUV$  might be the dead end accumulation of anionic polymers bound to undecaprenyl phosphate and subsequent depletion of the essential carrier lipid ( $C_{55}P$ ), essential for multiple cell wall envelope biosyntheses, as outlined for *S. aureus* (Chapter 2.4, Figure 7). For *S. aureus*  $\Delta lcp$  accumulation of undecaprenyl-linked intermediates was not observed (Chan et al., 2013), instead cell wall polymers are released into the culture supernatant. The release of glycopolymers might be facilitated by CapA1, which was shown to exhibit phosphodiesterase activity towards lipid-bound capsule (Figure 7) and WTA precursors and might represent the putative rescue mechanism (for a complete model see chapter 4.1; Rausch (2017)). *B. subtilis* lacks a corresponding protein homolog with this specific hydrolase activity (cleaving undecaprenyl( $C_{55}P$ )-coupled GP precursor), and therefore cannot recycle WTA synthesis intermediates to subsequently return  $C_{55}P$  to the membrane for continuous peptidoglycan synthesis.

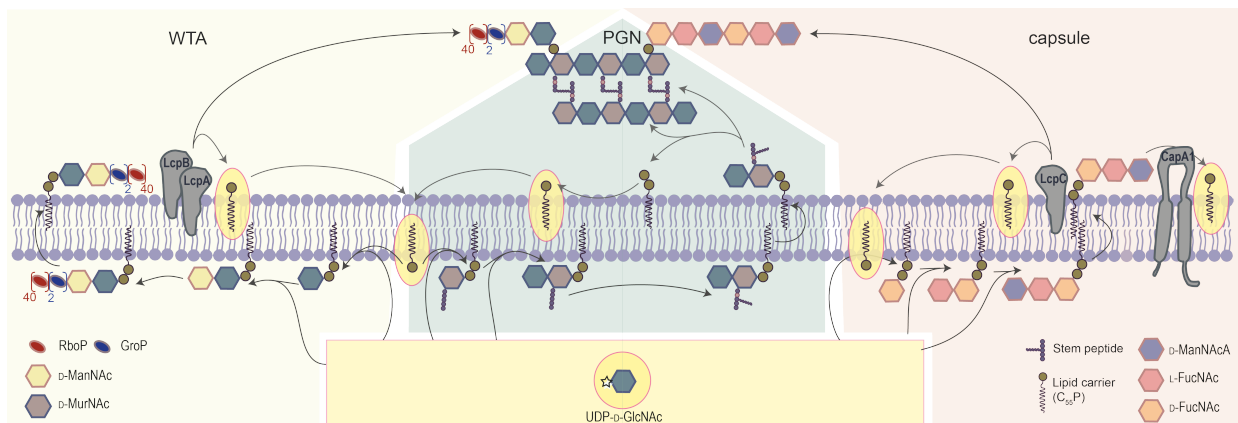


Figure 7: Proposed model for the glycopolymer attachment in *S. aureus*. WTA attachment is primarily catalyzed by LcpA and LcpB, while anchoring of capsular polysaccharides to PGN is majorly facilitated by LcpC. UDP-GlcNAc and  $C_{55}P$  (highlighted in yellow) represent essential precursors shared among PGN, WTA and capsule biosynthesis. The recycling and subsequent translocation of  $C_{55}P$  is necessary for continuous synthesis cycles. The phosphodiesterase activity of CapA1 (on the right) might represent a rescue mechanism against toxic dead end accumulation of  $C_{55}P$ -bound cell wall polymers on the periplasmic side of the bacterial membrane.

In *S. pneumoniae* mutational analysis suggested that Cps2A is responsible for the covalent attachment of capsular polysaccharides to the pneumococcal cell wall of capsular type 2 strain D39, and LytR (at least), and perhaps Psr are proposed to function in absence of Cps2A. However, biochemical proof is lacking so far. In contrast to *S. aureus*, individual deletion of *S. pneumoniae* LCP paralogs *cps2A* and *psr* did not trigger the release of capsular polysaccharides into the culture supernatant and mutants retained the capsule attached to the cell surface, whereby the overall capsule amount was reduced (the remaining capsule attached to the cell surface was significantly lower in the  $\Delta cps2A$  mutant, compared to the *psr* deleted strain). Based on the observations that lipid linked precursors did not accumulate in several *S. pneumoniae* *lcp* mutants and that the final polymer is only present in reduced amounts, it was suggested that cytoplasmic polymer synthesis, transport and attachment are coupled, and biosynthesis might be blocked by feedback regulation. Interestingly, a *S. pneumoniae* *lytR* deletion variant is only viable in an acapsular strain background and the deletion causes reduced growth and abnormal cell morphology. Presumably, the presence of a fully functional capsule assembly pathway induces growth problems and prevents isolation of viable mutants. On the other hand, in a *cps2AlytR* suppressor mutant substantial amounts of capsule material were released (Eberhardt et al., 2012). In this mutant the feedback regulation appears to be lost, since an excess of capsule material is produced, that cannot be retained in the cell wall and is subsequently released into the culture supernatant. It appears that the function and



regulation of LCPs within different biosynthetic pathways strongly diverges in various organisms. It should be further noted that, in contrast to *S. aureus*, capsule and peptidoglycan synthesis proceed side-by-side during early to mid-exponential growth phase (Carvalho et al., 2018; Hardy, Caimano, & Yother, 2000) in *S. pneumoniae* and regulatory circuits might therefore act on different levels. Besides WTAs and capsular polysaccharides, other types of glycopolymers are found to be attached to PGN, like arabinogalactan, pyruvylated, and rhamnose-containing GPs. These structures are highly diverse and often species- or even strain-specific. For most of these polymers transfer to the PGN backbone catalyzed by LCPs could already be demonstrated, while for some there is so far only strong indication for their involvement (reviewed by Stefanović et al. (2021)). Since deletion of *lep* alleles demonstrated biological importance, LCPs were investigated more closely for their biological activity and uncertainties regarding the nature of their substrates and products were addressed.

The LCP enzymes of *S. aureus* display overlapping functions in catalyzing the attachment of WTAs to the cell envelope. They form a phosphodiester bond between the C<sub>6</sub>-hydroxyl group of MurNAc in PGN and the ManNAc-(1→4)-GlcNAc disaccharide unit of the WTA polymer<sup>5</sup> (Figure 8; Chan et al. (2013); Schaefer, Matano, Qiao, Kahne, and Walker (2017)).

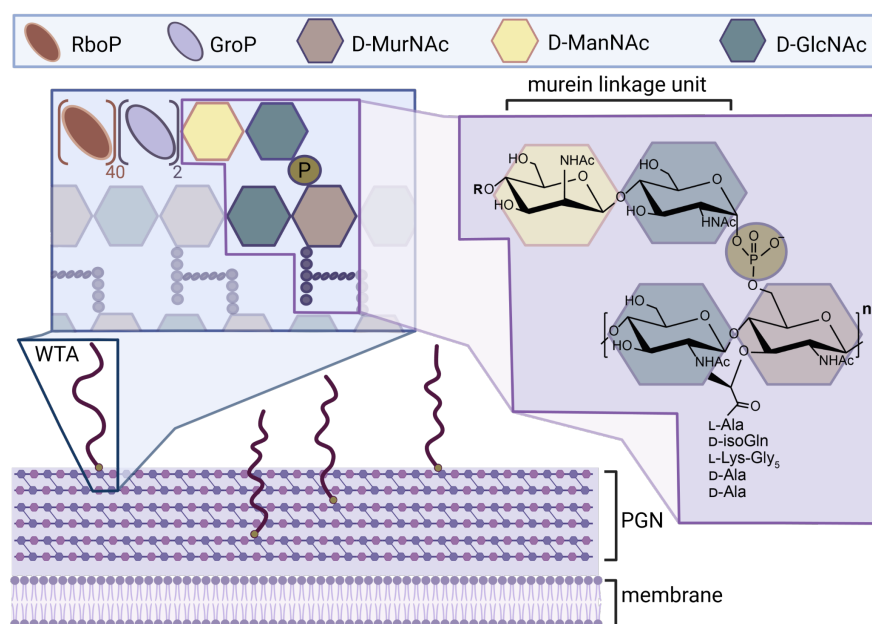


Figure 8: Close-up of WTA coupled to PGN via a phosphodiester bond to the C<sub>6</sub>-hydroxyl group of intermittent MurNAc units of the PGN backbone. The ManNAc-(1→4)-GlcNAc disaccharide moiety of WTAs represent the PGN linkage unit of the glycopolymer, also referred to as the murein linkage unit, and is located at the reducing end of the polymer. The non-reducing end of the murein linkage is tethered to two glycerol phosphate (GroP) units and up to 40 ribitol phosphate (RboP) units represented by an R in the chemical structure, while n indicates the number of PGN repeats. The figure was created with BioRender.com.

While mass spectrometry data verifies the presence of a phosphodiester bond between WTA and PGN, the final proof for the identity of the linkage between staphylococcal capsular polysaccharides and PGN has not yet been defined. In general, capsules of gram-positive bacteria were found to be either covalently linked to the cell wall or to the cytoplasmic membrane (Bender, Cartee, & Yother, 2003; Larson & Yother, 2017; Sørensen, Henrichsen, Chen, & Szu, 1990), but the exact nature of the cell wall linkage has only been characterized for a few organisms including *S. pneumoniae*

<sup>5</sup>The ManNAc-(1→4)-GlcNAc disaccharide unit is often referred to as the conventional murein linkage, because not only *S. aureus* WTA were found to be attached to PGN via this unit, but also various other cell wall GPs of different organisms, such as the pyruvylated GPs of *Bacillus anthracis*, the rhamnose-containing GPs of *Lactococcus lactis*, as well as WTAs of *B. subtilis*, and *Lactobacillus plantarum* (Stefanović et al., 2021).

capsular serotype 2 (CP2) (Larson & Yother, 2017) and partially for *S. agalactiae* type III capsular polysaccharides (Deng, Kasper, Krick, & Wessels, 2000). While *S. pneumoniae* CP2 is directly (no phosphodiester bond) glycosidically linked via its reducing end glucose to the GlcNAc (presumably GlcNAc-C<sub>6</sub>) residues of PGN, the linkage of *S. agalactiae* capsular polysaccharides is mediated by an oligosaccharide linker and a phosphodiester bond to GlcNAc of PGN (Figure 9). Out of 12 tested *S. pneumoniae* strains with different capsular polysaccharide serotypes, all but one *S. pneumoniae* serotype 3 strain produce a capsule, which is covalently attached to PGN (Sørensen et al., 1990). Interestingly, the serotype 3 strain also does not contain a *lcp* gene in their capsule gene cluster. However, in case of *S. aureus*, there is biochemical data strongly indicating the nature of the bond is phosphodiester linked to the C<sub>6</sub>-MurNAc residue of PGN (Figure 9).

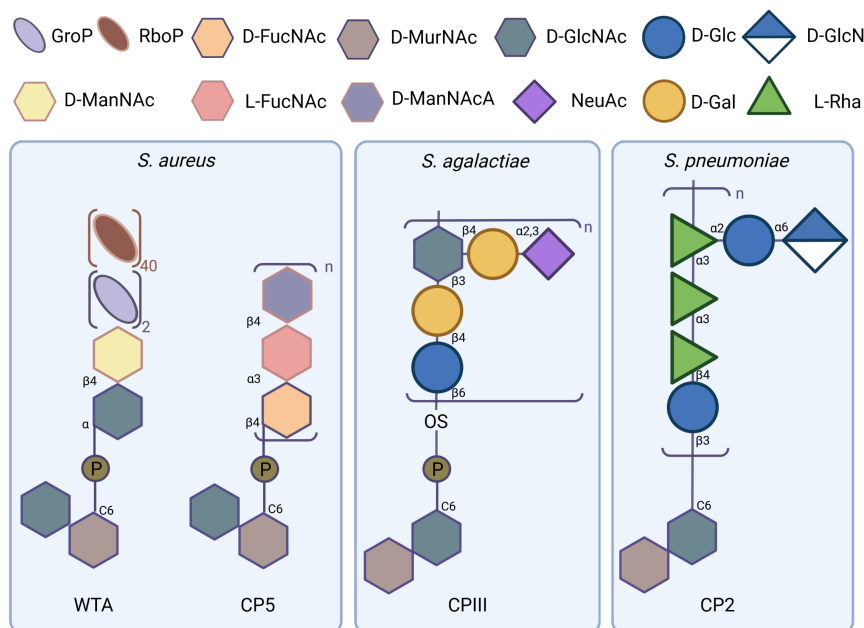


Figure 9: Overview of selected cell wall GPs and their (proposed) linkage to PGN. In contrast to the displayed *S. aureus* and *S. agalactiae* GPs which are linked via a phosphodiester bond, the CP2 of *S. pneumoniae* is directly glycosidically linked to PGN. Another notable difference is that the displayed GPs of *S. agalactiae* and *S. pneumoniae* are linked to the C<sub>6</sub>-hydroxyl group of GlcNAc of PGN, while the *S. aureus* WTA and CP5 polymers are bound to the C<sub>6</sub>-hydroxyl group of MurNAc of PGN. OS indicates the oligosaccharide linker in *S. agalactiae* of unknown structure. Glc, glucose; GlcN, glucosamine; NeuAc, *N*-acetylneuraminic acid; Gal, galactose; Rha, rhamnose. The figure was created with BioRender.com.

It was shown that capsular polysaccharides of *S. aureus* Newman are released from the cell wall by mild acid treatment. This kind of treatment is known to release phosphodiester and O-acetyl bonds, which are known to be acid labile (Bera, Herbert, Jakob, Vollmer, & Götz, 2004; de Jonge, Chang, Gage, & Tomasz, 1992; Kojima, Araki, & Ito, 1985). Furthermore, capsular polysaccharides are released when murein sacculi are incubated with an endopeptidase (cleave the pentaglycine cross-bridge) or amidase (cut the amide bond that links wall peptide to MurNAc) but not with an glucosaminidase (cleave GlcNAc-( $\beta$ 1-4)-MurNAc linkage). Since endopeptidases and amidases eliminate PGN crosslinking they would only cause release of capsular polysaccharides from murein sacculi if CP5 were attached to MurNAc- or GlcNAc-residues (Chan et al., 2014). The experimental data strongly indicate that the staphylococcal capsule is covalently attached to the glycan strands of PGN. In addition, a further experiment suggested that capsular polysaccharides occupy the same C<sub>6</sub>-hydroxyl group of MurNAc or proximal sites on PGN like the WTA polymer, since increased amounts of capsule were incorporated when WTA synthesis was inhibited (Chan et al., 2014).

It should be pointed out that capsular polysaccharides of *S. aureus* do not contain the murein linkage present in WTAs, that is comprised of a  $\beta$ -D-ManNAc-(1 $\rightarrow$ 4)- $\alpha$ -D-GlcNAc(1 $\rightarrow$ ) disaccharide (Figure 8), but are linked to PGN via  $\beta$ -D-FucNAc-(1 $\rightarrow$ ) (Figure 7).

There have been only a few attempts to characterize substrate selection and specificity of LCPs since putative substrates are not commercially available and their synthesis is tedious. In principal, the reaction requires a sugar(-phosphate) donor substrate, which is a lipid-phosphate-linked glycan precursor and PGN as an acceptor substrate, although the maturation status of PGN (lipid II, nascent PGN<sup>6</sup> or cross-linked PGN) is still a matter of debate. Partly contradictory *in vitro* evidence has been published on the nature of the acceptor substrate (Gale, Li, Sun, Strynadka, & Brown, 2017; Rausch, 2017; Schaefer et al., 2017; Schaefer, Owens, Kahne, & Walker, 2018). With regard to the donor substrate, *S. aureus* LcpA was shown to require WTA lipid substrates containing at least the disaccharide-murein linkage unit (lipid IV<sub>A</sub>/ LII<sub>A</sub><sup>WTA</sup>) to catalyze the transfer, while an additional glycerol phosphate (GroP) moiety at C<sub>4</sub> position of ManNAc (representing a more mature version of WTA; lipid IV<sub>B</sub>/ LII<sub>B</sub><sup>WTA</sup>) had no influence on enzyme activity (Schaefer et al., 2017). Ligation products were only observed for PGN tetrasaccharide, hexasaccharide and octasaccharide (lipid II-[MurNAc(-stem peptide)-GlcNAc]<sub>N</sub>; N= 1, 2, or 3, respectively) but not for lipid II. Of note, the lipid II substrate used during this study contained either a tetraprenyl (C20) or heptaprenyl (C35) lipid moiety instead of the native undecaprenyl (C55) chain. LcpB and LcpC were also shown to transfer phosphate-linked WTA disaccharides (ManNAc-GlcNAc-P) to nascent PGN oligosaccharides. Gale et al. (2017) proposed *B. subtilis* LCPs TagTUV catalyze the attachment of WTA to mature PGN (insoluble, crosslinked). Whether WTA attachment occurs before or after glycan strands are further processed by PBPs was addressed in a more recent study. Within this work it was possible to demonstrate that both of the tested LCPs, namely *S. aureus* LcpB and *B. subtilis* TagT were only able to process uncrosslinked PGN oligomers (lipid II-[MurNAc(-stem peptide)-GlcNAc]<sub>N</sub>; N= 1-5). The authors could further demonstrate that the stem peptide of the PGN acceptor substrate is not required for WTA ligation reactions, while the C<sub>2</sub>-N-acetyl groups (NHAc) play crucial roles in substrate recognition (Figure 8; Schaefer et al. (2018)). Since lipid II itself was proposed not to serve as a suitable acceptor substrate for transfer (Schaefer et al., 2017), the findings imply that nascent (uncrosslinked) PGN is first made and then modified with WTA before cross-linking. The authors further reasoned that neither lipid II nor nascent PGN tetrasaccharide (lipid II-[MurNAc(-stem peptide)-GlcNAc]<sub>2</sub>), pose physiologically relevant substrates, since the presence of large glycopolymers attached to the MurNAc C<sub>6</sub>-hydroxyl groups of the lipid II or nascent PGN tetrasaccharide, would prevent binding to the active site of PGN glycosyltransferases. Only if at least a PGN hexasaccharide (lipid II-[MurNAc(-stem peptide)-GlcNAc]<sub>6</sub>) is formed there will be a MurNAc C<sub>6</sub>-hydroxyl group exposed from the long active site cleft (Schaefer et al., 2017). Interestingly, while Walker and coworkers ruled out lipid II as a suitable substrate for LCP catalyzed reactions, it was demonstrated to serve as an acceptor substrate for LcpC in an *in vitro* attachment reaction where the capsule saccharide D-FucNAc(-phosphate) was transferred and the respective ligation product could be further processed by the PGN glycosyltransferase PBP2(see chapter 4.1 for a model and further elaboration of the attachment reaction; Rausch (2017); Rausch et al. (2019)).

In addition to or as part of their function as phosphotransferases, LCPs have also been described to have a hydrolase activity towards pyrophosphate lipids. Of the *S. aureus* LCPs, LcpA was demonstrated to possess the highest pyrophosphatase activity towards C<sub>10</sub>-PP, with ~14% cleavage, whereas LcpB and LcpC were found to only cleave 2-3% (F. K. K. Li et al., 2020). Surprisingly, no products of enzymatic hydrolysis (phosphate lipid) of the WTA disaccharide precursor were detected when LcpA was incubated in absence of the PGN acceptor (Schaefer et al., 2017). The catalytic release of P<sub>i</sub> from pyrophosphate lipids has also been reported for Cps2A and TagT, (Baumgart, Schubert, Bramkamp, & Frunzke, 2016; Eberhardt et al., 2012; Grzegorzewicz et al.,

---

<sup>6</sup>Lipid-coupled uncrosslinked PGN oligomers of defined length (lipid II-[MurNAc(-stem peptide)-GlcNAc]<sub>N</sub>; N= 1-7). The physiological relevance of nascent PGN is subject of debate.

2016; Kawai et al., 2011; Siegel et al., 2019). Both enzymes were also found co-crystallized with (pyro)phosphorylated polyprenyl lipids strongly bound to their LCP domain (Eberhardt et al., 2012; Kawai et al., 2011). The identity of the lipid-ligand was found to be dependent on the expression strain used for protein purification.

## 2.6 LytR-CpsA-Psr enzymes from a structural perspective

Structural *in silico* analyses were performed to shed light on the different functions of LCP enzymes. According to secondary structure predictions, all representatives of the LCP family contain an intracellular N-terminus, one consensus transmembrane region (except for CpsA which is predicted to have three), an optional accessory domain, the core catalytic extracellular LCP domain, and in some cases a C-terminal domain of unknown function (Figure 10; Hübscher et al. (2008); Stefanović et al. (2021)).

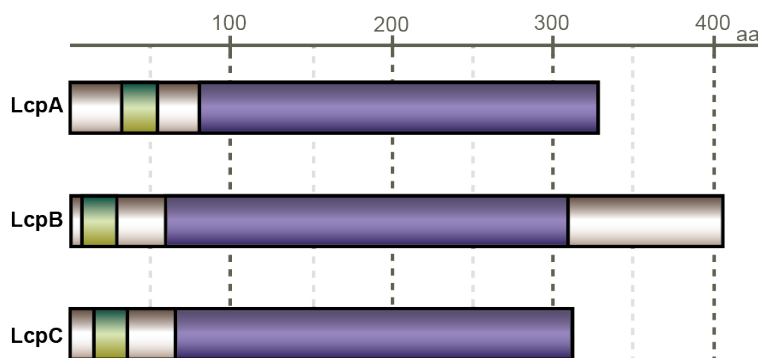


Figure 10: Overview on domain organization of *S. aureus* strain N315 LcpABC enzymes (adapted from F. K. K. Li et al. (2020)). The characteristic organization of the secondary structure of LCPs are displayed containing a single transmembrane domain (green) and extracellular catalytic LCP domain (purple).

Crystallographic analysis yielded a structure of *S. aureus* LcpA with endogenously captured  $C_{40}$ -PP-GlcNAc at the substrate binding site (Figure 11A1; F. K. K. Li et al. (2020)).  $C_{40}$ -PP-GlcNAc is a lipid substrate in the synthesis of O7-specific lipopolysaccharide of the *E. coli* strain used for overexpression of LcpA, but also highly resembles the staphylococcal lipid bound WTA-monosaccharide precursor (lipid III<sub>WTA</sub>,  $C_{55}$ P-GlcNAc). To enable crystallization of LcpA a truncated construct lacking the single N-terminal transmembrane anchor was used (residues 80-327,  $\Delta$ TM). The structure was solved by molecular replacement to 1.9 Å and encompasses the extracellular catalytic region corresponding to the LCP domain. The LCP domain comprises a six-stranded  $\beta$ -sheet in the center of multiple  $\alpha$ -helices and three double-stranded  $\beta$ -sheets (Figure 11A1). This or a very similar fold could commonly be observed in LCP enzymes crystallized so far, especially within the *Firmicutes* representatives *B. subtilis* and *S. pneumoniae* (Figure 11B-E). The central six-stranded  $\beta$ -sheet and helices 3-7 of LcpA form a large hydrophobic lipid-binding pocket with a narrow opening and a wide base. The lipid tail surrounding residues display low sequence conservation with other LCP family members but are largely hydrophobic. The electropositive entrance of the binding pocket (blue, Figure 11A2) is formed by invariant arginine residues (alignment displayed in Figure 12), which form the active site for binding of the pyrophosphate group of the lipid-bound donor substrate (Figure 11A3). The active site is surrounded by four regions (Figure 11A), which were designated as region A (blue, residues 92-100), region B (red, residues 188-201), region C (purple, residues 217-224), and region D (turquoise, residues 296-312). Structural comparison by molecular replacement of the conserved active site residues of LcpA revealed the highest similarity to *B. subtilis* TagT bound to a hexaprenyl-disaccharide WTA precursor ( $C_{30}$ PP-GlcNAc-ManNAc; Figure 11B; F. K. K. Li et al. (2020)). Comparison of regions A-D of *S. aureus* LcpA with *B. subtilis* LCPs show some

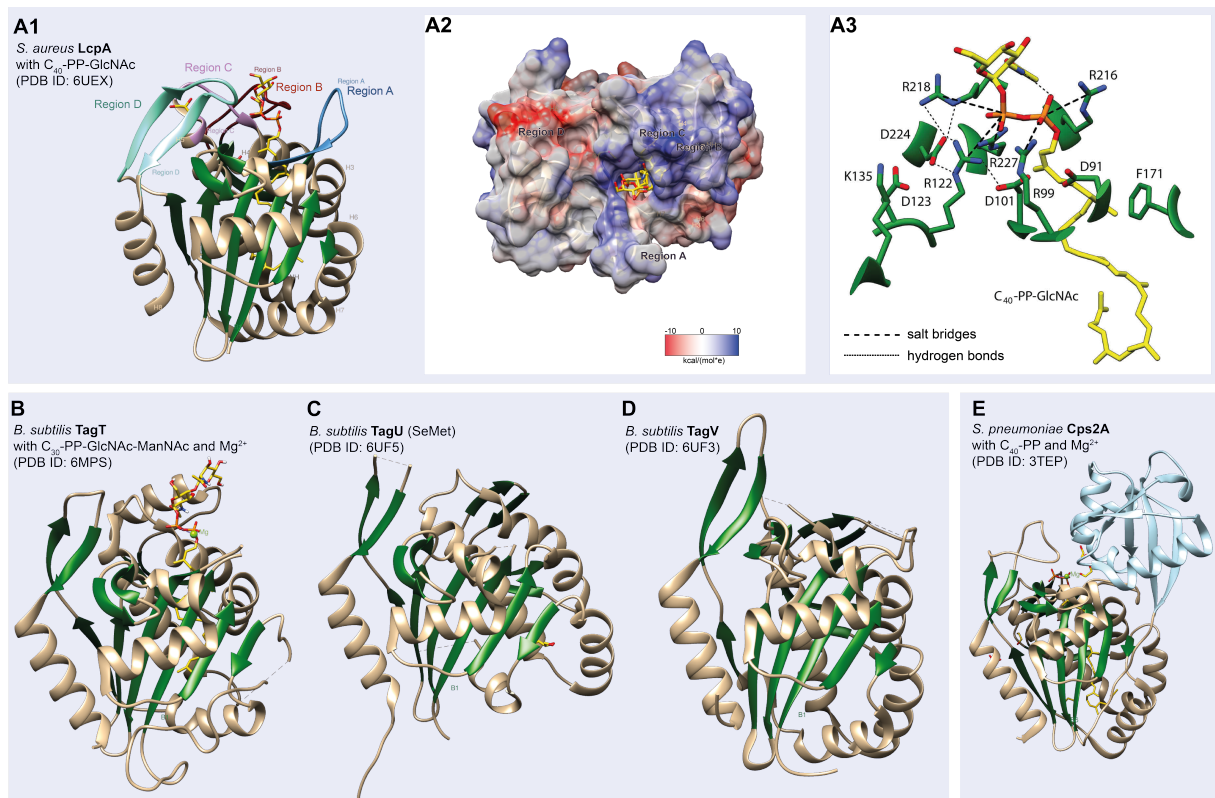


Figure 11: Comparison of different LCP protein crystals reveals a recurring fold of the LCP domain, composed of a six-stranded  $\beta$ -sheet sandwiched between multiple  $\alpha$ -helices and double-stranded  $\beta$ -sheets. Ribbon structures of *S. aureus* LcpA bound to  $C_{40}$ -PP-GlcNAc, the active site surrounding regions are designated A, B, C and D (A1), *B. subtilis* TagT bound to  $C_{30}$ -PP-GlcNAc-ManNAc and  $Mg^{2+}$  (B), *B. subtilis* TagU SeMet (selenomethionine-substituted; (C)), *B. subtilis* TagV (D), and *S. pneumoniae* Cps2A bound to  $C_{40}$ -PP and  $Mg^{2+}$ , in which the accessory domain is displayed in lightblue (E), are displayed.  $\beta$ -strands are illustrated in green, ligands are highlighted in yellow, heteroatoms are colored by type (oxygen, red; phosphorus, orange; nitrogen, blue) and structural features are labeled as follows, H, helix; B,  $\beta$ -strand; NH, nonconserved helix; Mg, magnesium. *S. aureus* LcpA is further displayed from top view of the active site of *S. aureus* LcpA in complex with  $C_{40}$ -PP-GlcNAc, where the protein surface is colored according to the electrostatic potential (A2; blue positive and red negative potential). A3 shows a close up of the interactions between the conserved LcpA residues and the pyrophosphate moiety of the bound  $C_{40}$ -PP-GlcNAc (A3; Figure modified after F. K. K. Li et al. (2020)).

structural variability, occurring especially in Region B. Where LcpA has a large loop, TagT has an  $\alpha$ -helix and TagU and TagV a double-stranded  $\beta$ -sheet. The structures are similar in regions A and C, which encompass flexible loops and in region D that adopts a two-stranded  $\beta$ -sheet. The latter is often enriched with aromatic residues (Figure 12), which are presumably relevant for PGN binding. In the majority of the LCP crystals the loop of region C is held away from the active site by a resident acidic acid residue that forms a salt bridge with a nearby basic residue<sup>7</sup>. Schaefer et al. (2018) proposed that the placement of region C is induced by the presence of a second sugar within the donor substrate binding site. However, this is contradictory to the finding that loop C of apo (ligand-free) TagT has higher similarity to TagT in complex with the WTA disaccharide substrate than the monosaccharide bound structure<sup>8</sup> (F. K. K. Li et al., 2020).

<sup>7</sup>reported for *S. aureus* LcpA, *B. subtilis* TagTUV, *A. oris* LcpA, and *S. pneumoniae* Cps2A

<sup>8</sup>RMSD of 0.4 Å instead of 2.7 Å for 7 C $\alpha$ -atoms

The binding site of the lipid-bound ligand, which represents the putative donor substrate binding site for LcpAs ligase activity is defined in the following. The guanidinyll groups of active site arginines form salt bridges with the pyrophosphate moiety of the polyprenyl. Whereas, residues R-99 and R-216 are in contact with the  $\alpha$ -phosphate group, while R-122, R-218, and R-227 interact with the  $\beta$ -phosphate group (Figure 11A3). Earlier mutagenesis studies confirmed the importance of these conserved arginines for growth and activity in various species (Baumgart et al., 2016; Kawai et al., 2011; Schaefer et al., 2018). Orientation of the saccharide headgroup was shown to rely on hydrophobic and van der Waals contacts rather than polar interactions with the enzyme. Thereby, the *N*-acetyl group of GlcNAc interacts with residues N-194, I-195, R-216, F-217, R-218, and H-219, which are part of the regions B or C (Figure 12). Comparison of TagT protein crystals complexed with either monosaccharide (C<sub>30</sub>PP-GlcNAc) or disaccharide (C<sub>30</sub>PP-GlcNAc-ManNAc) WTA precursor demonstrated significant structural differences concerning the orientation of saccharide moieties and pyrophosphate unit of the precursors (Schaefer et al., 2018). It was suggested the latter might influence coordination of a Mg<sup>2+</sup> cation, which was only present in the active site of the structure complexed with the disaccharide precursor. The second saccharide is presumed to position the pyrophosphate group of the substrate in a conformation that enables binding of a divalent cation (Schaefer et al., 2018). This hypothesis is based on the observation that TagT and other LCPs are metal-ion dependent transferases (Eberhardt et al., 2012; Kawai et al., 2011; Schaefer et al., 2018) and on the assumption that *S. aureus* LcpA requires donor substrates, which contain at least a disaccharide to catalyze transfer (Schaefer et al., 2017)). Interestingly, TagT and Cps2A were reported to possess divalent cation-dependent pyrophosphatase activity towards pyrophosphorylated polyprenyl lipids substrates devoid of any saccharide moieties and Mg<sup>2+</sup>-, as well as Mn<sup>2+</sup>-ions were found within the substrate binding sites of Cps2A protein crystals complexed with merely C<sub>40</sub>-PP (Eberhardt et al., 2012; Kawai et al., 2011). No metal ion has been observed within the LcpA structure but there is the possibility that it might have been displaced during crystallization. Coordination of Mg<sup>2+</sup> in LcpA is proposed to be facilitated by residues D91 and/or D101, since mutations of the corresponding residues D70A of LcpB, and D82A of TagT, or D87A of TagT respectively, resulted in no or significantly reduced ligase activity *in vitro*.

Since LCPs are commonly found complexed with pyrophosphorylated lipids the interactions between protein residues and the lipid, as well as the pyrophosphoryl part seem sufficient for binding. This observation might explain their (semi)redundant roles in attachment of different anionic polymer precursors.

The putative PGN binding groove of is outlined by regions A, C, and D (Eberhardt et al., 2012; Kawai et al., 2011; Schaefer et al., 2018). Region A of LcpA exhibits low sequence conservation except for the invariant arginine residue R-99 (Figure 12), which is expected to shift when a divalent cation is bound (Schaefer et al., 2018) and proposed to be involved in PGN binding. As mentioned above, region D commonly adopts a double-stranded  $\beta$ -sheet fold often enriched with aromatic residues, which could aid binding of PGN through carbohydrate-aromatic interactions. Additionally, conserved residues D-123, K-135 and N-137 of LcpA could play a potential role in PGN binding, since they are found within the putative binding groove and equivalent residues have been demonstrated to be essential for activity of TagT. Data-driven biomolecular docking studies led to the identification of three potential PGN saccharide binding subsites in proximity to the conserved residues R-99, K-135, N-137, and D-224. But the variability in interactions with the glycan among these three saccharide-bound structures prevented accurate assignment of PGN binding (F. K. K. Li et al., 2020). Comparison with LcpA of *A. oris* provides further clues concerning the putative PGN binding site, since this LCP was demonstrated to use proteins as acceptor substrates for glycosylation (Siegel et al., 2019) instead of PGN or the respective lipid II intermediate. Among differences in region B and C, the double-stranded  $\beta$ -sheet that forms region D in conventional LCPs is replaced by a loop that is shifted away from the active site, thereby closing off one end of the putative acceptor site while enlarging the opposite end, which is presumed to enable accommodation of the protein substrate. These variations highlight the importance of the anti-parallel  $\beta$ -strands of region D for

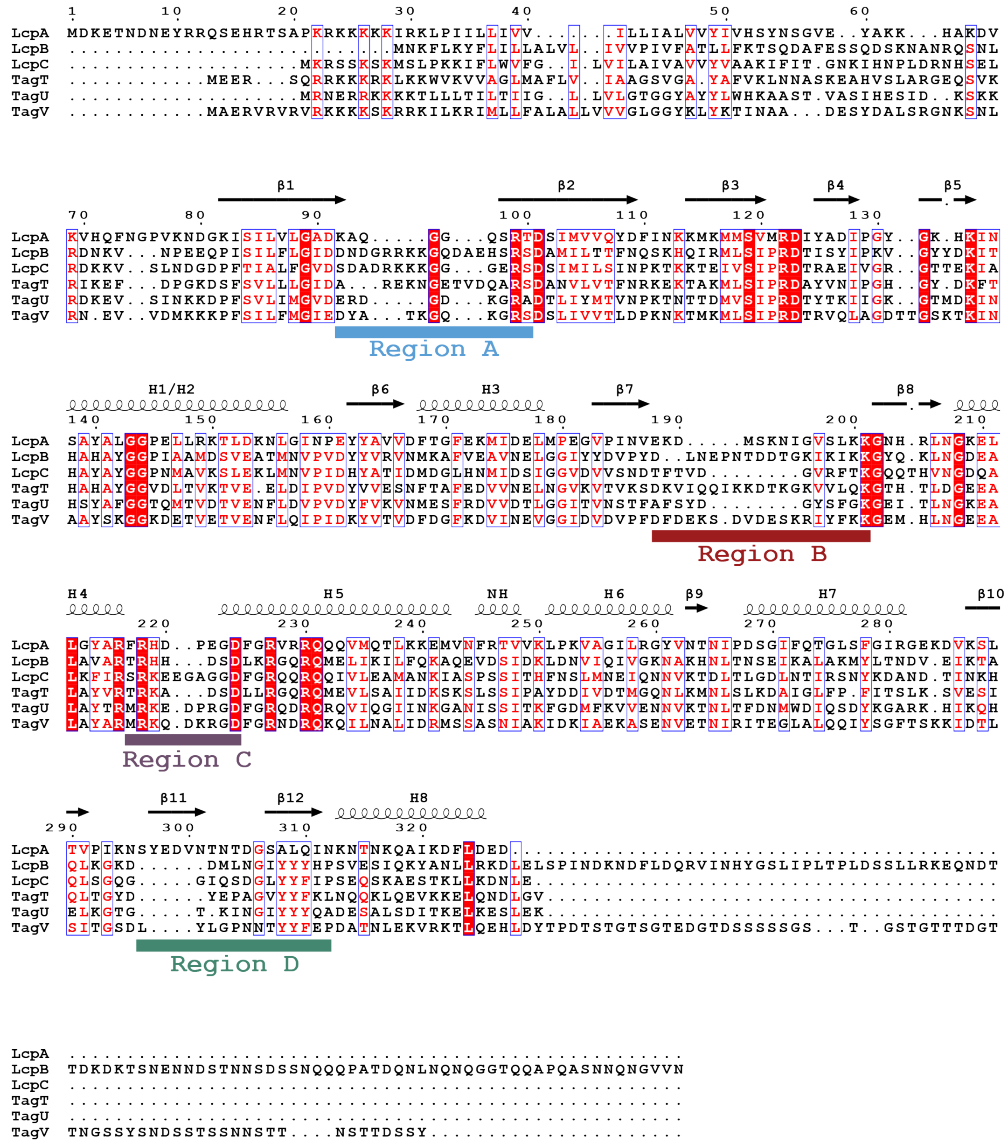


Figure 12: Sequence alignment of *S. aureus* (LcpA-C) and *B. subtilis* (TagT-V) LCP enzymes. Conserved residues are displayed in white on red background, and conservative substitutions are red on white background. The secondary structure of LcpA is depicted above the amino acid sequences. Structural features are labeled as follows,  $\beta$ ,  $\beta$ -strands; H,  $\alpha$ -helices; NH, nonconserved helix. Active site surrounding regions of LcpA are highlighted below the alignment A (blue), B (red), C (pink), and D (green).

PGN binding in conventional LCPs. Whether WTA attachment occurs before or after glycan strand polymerization was also addressed from a structural perspective. Protein crystals of TagT in complex with WTA precursor indicate that the PGN substrate binds in a long and narrow groove, which is adjacent to WTA binding pocket (Schaefer et al., 2018). The basis for acceptor substrate selectivity (nascent or mature PGN) appears to be steric exclusion of cross-linked PGN from the narrow binding groove.

Presumably, the reaction catalyzed by LCPs is similar to other biological phosphoryl-transfer reactions, where the nucleophile aligns with the electrophilic phosphorous ( $\beta$ -phosphorous of C<sub>55</sub>PP-WTA) and the leaving group ( $\alpha$ -phosphorous of C<sub>55</sub>PP-WTA) for an in line attack (Figure 13; Lassila, Zalatan, and Herschlag (2011); Schaefer et al. (2018)). The C<sub>6</sub>-hydroxyl group of MurNAc (PGN-intermediate) is assumed to act as the nucleophile and sits adjacent to the  $\beta$ -phosphorous

group of the donor lipid substrate in the PGN binding groove. The arginine residues R-122/R-218<sup>9</sup> of LcpA could function as a general base. Both candidates are adjacent to the aspartic acid carboxylate groups of D-123 and D-224, which might play a role in the activation of the general base<sup>10</sup>. R-216 was proposed to act as the general acid with proton exchange of its guanidinium side chain. Catalysis is initiated when transient deprotonated form of R-122 abstracts a proton from the C<sub>6</sub>-hydroxyl group of MurNAc (PGN intermediate). The magnesium ion and invariant arginine residues might be involved in stabilizing the transition state, besides coordination of the pyrophosphate moiety for catalysis. Upon collapse of the transition state a covalent bond between the PGN intermediate and saccharides of the WTA intermediate is formed, and the  $\alpha$ -phosphate leaving groups abstracts a proton from the guanidinium of R-216.

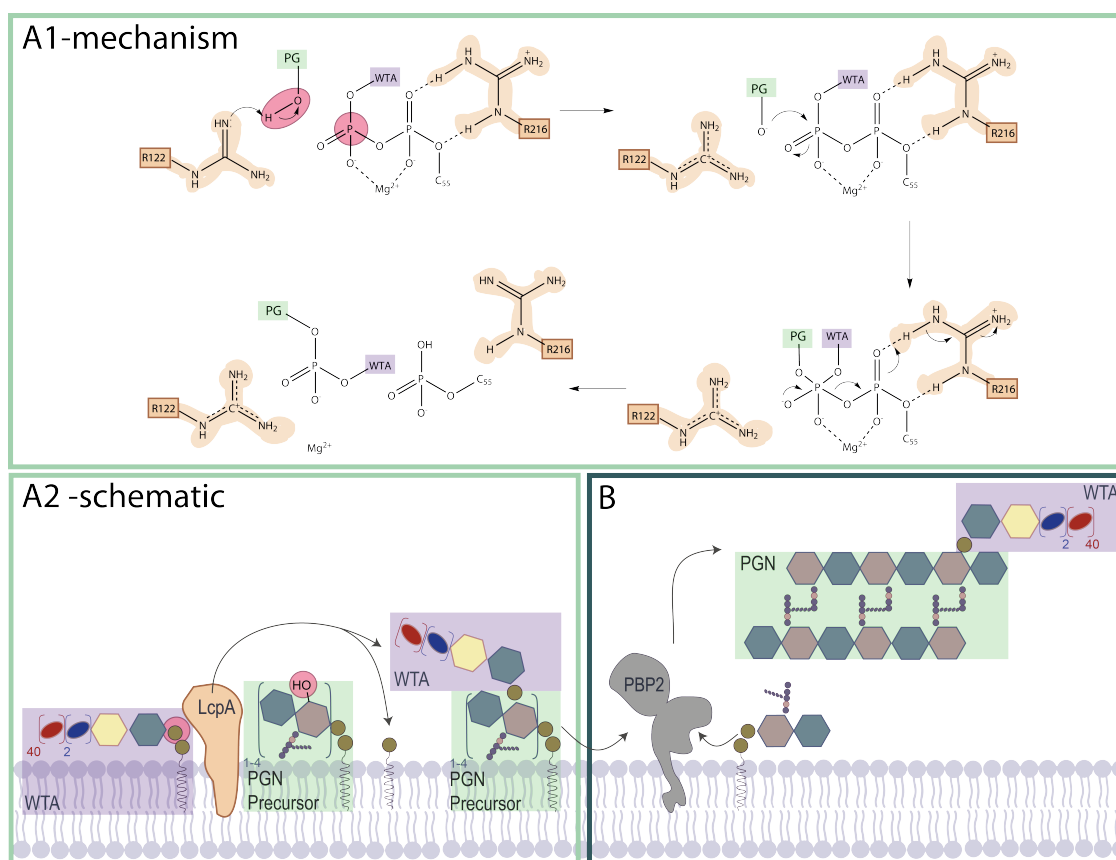


Figure 13: Proposed mechanism of WTA ligation to a peptidoglycan (PGN) intermediate catalyzed by *S. aureus* LcpA (A1; adapted to F. K. K. Li et al. (2020)) and schematic of the reaction at the membrane interface (A2), followed by PGN polymerization catalyzed by PBP2 (B). The active site residues R122 and R216 of LcpA are highlighted in orange. The WTA precursor (highlighted in purple) represents the glycopolymer donor substrate for the transfer reaction, while the displayed acceptor substrate is a lipid-bound PGN intermediate (highlighted in green; such as lipid II or nascent PGN). The  $\beta$ -phosphorous of the C<sub>55</sub>-PP-WTA donor substrate and the C<sub>6</sub>-hydroxyl group of the MurNAc unit of the PGN-intermediate acceptor substrate are highlighted in pink.

<sup>9</sup>Both of the equivalent TagT residues (R-118 and R-219) were essential for enzyme activity (Schaefer et al., 2018).

<sup>10</sup>Of the two LcpA general base and activating residue candidate pairs the arginine residue R-122 has a higher likelihood to act as the general base, since the adjacent carboxylate of D-123 is both conserved and essential, while R-218 can only interact with the carboxylate group of D-224, which is a nonessential for activity. Of note, enzyme activity was only assessed for the equivalent TagT D-123 and D-224 mutants (Schaefer et al., 2018). However, D-224 represents an invariant residue among LCPs which was attributed to play a role in PGN binding and although the mutation of D-224 did not abolish the TagT activity it was still strongly reduced.



A glycerol molecule (pink) and a cluster of water molecules were found within the structure of LcpA, highlighting the presence of an accessible hydrophilic pocket buried below the active site and close to the lipid-binding pocket (Figure 14). This hydrophilic pocket contains the highly conserved residues S-119, R-122, D-224, R-227, and Q-231 (Figure 12) and F. K. K. Li et al. (2020) suggested, this site represents an attractive target for the design of inhibitors.

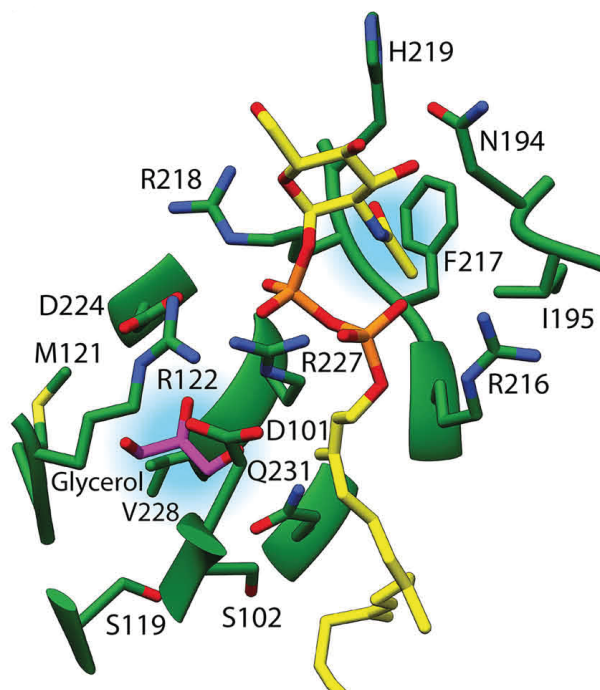


Figure 14: Putative target structure for the design of LCP inhibitors. The highly conserved residues S-119, R-122, D-224, R-227, and Q-231 surround a glycerol molecule (pink) outline a hydrophilic pocket located below the active site and next to the lipid binding pocket of LcpA. The figure was adapted to F. K. K. Li et al. (2020). A selection of LcpA residues are illustrated in green including their ribbon structures and respective atoms/bonds are depicted as sticks, the C<sub>40</sub>-PP-GlcNAc ligand is highlighted in yellow and depicted as sticks, heteroatoms are colored by type (oxygen, red; phosphorus, orange; nitrogen, blue; sulfur, yellow)

In order to complete cell wall assembly, pathways for PGN, WTA and capsule biosynthesis must converge and the generated GPs are subsequently attached to the cell wall by the ligase activity of LCP enzymes. Since an intact cell wall is a prerequisite for cell viability and virulence, LCP enzymes are attractive new drug and/or anti-virulence targets. Defects in capsule production were reported to make cells easier recognized by the immune system, and absence or reduced levels of WTA on the cell surface are associated with higher autolysis rates, reduced biofilm production and increased antibiotic susceptibility. Further, inhibitors may induce synergistic activities and restore antibiotic activities towards resistant strains. Another advantage of LCP enzymes, as a drug target, is that they are easily accessible on the outside of the cell, limiting challenges to pass the cytoplasmic membrane.

## 2.7 The cell wall as an antibiotic target

Inhibitors of cell wall biosynthesis proved to be among the most successful antibiotics in therapeutic use (e.g.  $\beta$ -lactams; reviewed by Müller, Klöckner, and Schneider (2017)). The biosynthetic machineries synthesizing cell wall components like peptidoglycan, wall teichoic acids, and capsular polysaccharides constitute attractive targets for new antibiotics, since these pathways are absent in

humans. Cell wall synthesis starts in the cytoplasm and extends over the cytoplasmic membrane to the extracytoplasmic space. Various inhibitors have been identified for all of these stages (Figure 15). While some of these antibiotics exert their activity by the formation of complexes with PGN intermediates

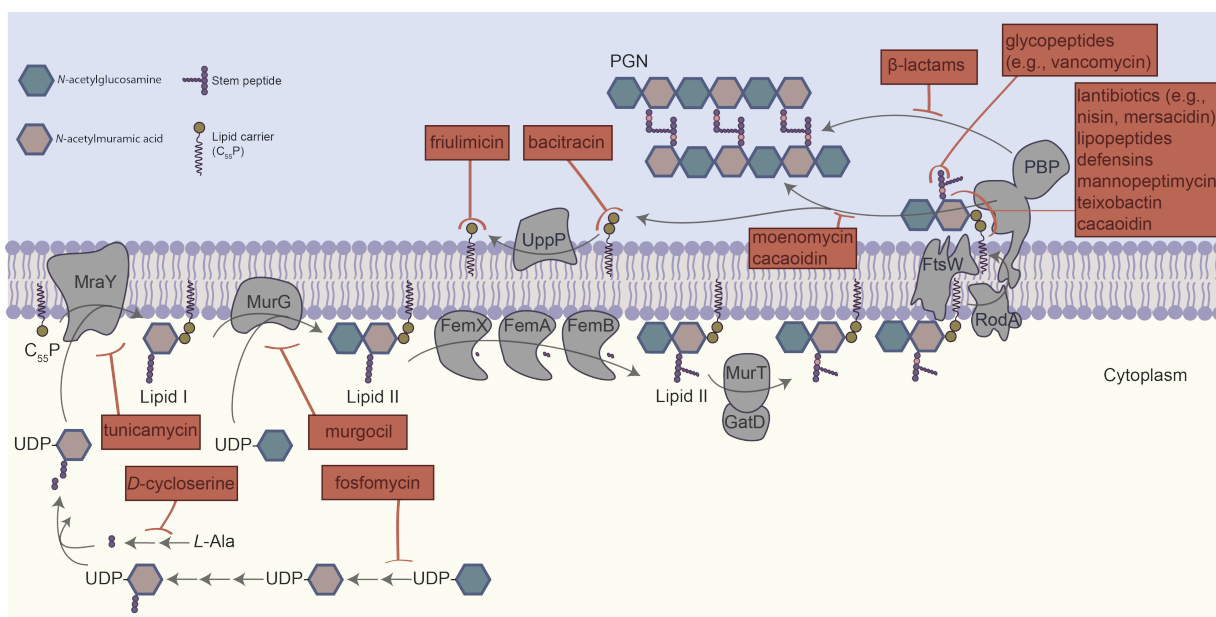


Figure 15: Overview of PGN synthesis in *S. aureus* including the target sites of various antibiotics (red boxes). Antibiotics block key enzymatic cell wall biosynthesis reactions by formation of a complexes with non-protein PGN intermediates or via direct enzyme inhibition.

intermediates (e.g., vancomycin and teixobactin), others explicitly target the enzymes (e.g.,  $\beta$ -lactams and moenomycin) that catalyze cell wall biosynthesis key reactions. Targeting of the final PGN precursor lipid II seems to be particularly effective and nature itself invented at least five different classes of antibiotics (e.g., (lipo)glycopeptides, lantibiotics, teixobactin, defensins, and lipo(depsi)peptides) to target this ultimate cell wall precursor. The benefits of lipid II targeting include that (i) it is structurally conserved in bacteria, (ii) it is essential, (iii) it is only present in limited amounts, and (iv) it is readily accessible on the outside of the cytoplasmic membrane. Importantly, modifications of non-protein targets, like lipid II, are not easily achieved by mutations and inhibitors thus generally appear less prone to resistance development. Nevertheless, several resistance mechanisms attributed to the modification of the lipid II molecule, such as glycopeptide antibiotic resistance, have been reported. These modifications are largely restricted to variations of the stem peptide (Figure 16), such as the incorporation of alternative amino acids i.e., by replacement of the terminal D-Ala residue by D-Lac or D-Ser; orange. The amino acid exchange, initially described for vancomycin resistant enterococci (VRE; Arthur, Reynolds, and Courvalin (1996)), represents the most prominent and clinically relevant lipid II modification conferring resistance towards several glycopeptide antibiotics. The resistance mechanism is based on the decreased binding affinity of glycopeptides to the modified lipid II target. Important reservoirs of genes conferring glycopeptide resistance include determinants that confer self-resistance in glycopeptide antibiotic producing organisms. These genes are believed to be horizontally transferred to clinical pathogenic bacteria, rather than being orchestrated *de novo* upon continued treatment (Unsleber, Wohlleben, & Stegmann, 2019; Yushchuk, Binda, & Marinelli, 2020). The high degree of vancomycin resistance observed in VRSA is conferred by the acquisition of the *vanA* operon often located in the plasmid-borne transposon Tn1546, which can transfer from VRE to *S. aureus*. Although the prevalence of VRSA might be underestimated (Moravvej et al., 2013), the limited amount of VRSA isolates suggests that the *vanA*-mediated vancomycin resistance has not evolved or quickly spread, presumably because of the high fitness cost of the altered PGN synthesis pathway (Foucault, Courvalin, & Grillot-Courvalin,

2009). The first VRSA cases were reported two decades after vancomycin was clinically used, while vancomycin-intermediate *S. aureus* (VISA) or its precursor heterogeneous VISA (hVISA)<sup>11</sup> emerged earlier and are more frequently isolated. The 'intermediate' resistance phenotype is conferred by reduced autolysis, a thickened cell wall with drastically reduced cross-linking and, in accordance, a high amount of free D-Ala-D-Ala residues, leading to an accumulation of vancomycin within the cell wall preventing the access to membrane-bound lipid II, referred to as "clogging". This phenotype is stabilized by a combination of multiple background mutations, the most prevalent occur in genes encoding for the TC regulatory systems VraRS and WalRK (Shoji et al., 2011). While, the *vraRS* mutations results in the activation and subsequent upregulation of cell wall synthesis (Katayama, Murakami-Kuroda, Cui, & Hiramatsu, 2009), mutations in *walRK* contribute to downregulation of the WalRK system, associated with reduced expression of PBP4 and autolysins thereby decreasing PGN crosslinking and autolysis respectively (Hu, Peng, & Rao, 2016; Shoji et al., 2011). In contrast to VRSA, where resistance is acquired by horizontal gene transfer, VISA are generated by stepwise adaptation to the antibiotic, through the accumulation of mutations and, although VISA share a major phenotype (thickened cell wall and altered autolysis), the genetic mechanisms underlying the phenotype are diverse.

Interestingly, resistance mechanisms attributed to modifications of the undecaprenyl-phosphate unit or the pyrophosphate-sugar linkage of lipid II have not been reported so far. Accordingly, it appears that the highly conserved core structure cannot be easily altered. Consequentially, the probability of resistance development appears to correlate with the interaction/binding sites on lipid II (pyrophosphate moiety versus stem peptide) and the physico-chemical properties of the antibiotic. The lipid II-binding antibiotics nisin and plectasin for instance are both positively charged peptide antibiotics interacting with the pyrophosphate-sugar unit of lipid II. While the stem peptide of lipid II is not required for high-affinity interaction (Müller et al., 2017) with nisin, the lipid II-plectasin interaction comprises the D-Glu residue at position two of the lipid II stem peptide (blue; Figure 16). The amidation of the  $\alpha$ -carboxyl group of D-Glu results in a less negatively charged PGN. In line with this, increased efficacy of plectasin was observed against cells depleted for the MurT/GatD enzyme complex, that catalyzes the formation of D-Gln in position two of the stem peptide (Münch et al., 2012). The overall reduction of the cell surface charge is a common resistance mechanism against defensins and other cationic antimicrobial peptides (CAMPs), such as nisin and vancomycin. Resistance to CAMPs not primarily depending on modification of the specific lipid II interaction site often develops gradually and involve the reversible reduction of the overall cell wall surface charge, such as the lysinylation of phosphatidylglycerol and the D-alanylation of teichoic acids, and lead to a reduced accumulation of the positively charged antibiotics in the cell wall mesh. These modifications commonly confer moderate levels of resistance and are relatively non-specific, because they generally repel CAMPs from reaching the membrane surface through electrostatic repulsion (Staubitz, Neumann, Schneider, Wiedemann, & Peschel, 2004). However, since the negative surface charge is vital, most of the charge modulation systems are only activated in presence of CAMPs to limit the degree of these substitutions (Münch & Sahl, 2015), while the amidation D-Glu of the lipid II stem peptide (blue; Figure 16), represents a more constitutive modification. Since antimicrobial peptides are central players in the innate immune defense against pathogenic bacteria, it is not surprising that pathogens developed several other strategies to overcome CAMP activity, such as alterations in the membrane composition, CAMP sequestration and inactivation, including proteolytic degradation of CAMPs and transporter-based detoxification (Assoni et al., 2020).

Antibiotics binding to or interfering with lipid II can trigger multifaceted secondary cellular consequences and often possess activities that go beyond passive blocking of one target (reviewed by Müller et al. (2017)). Lipid II is discussed to play a central scaffold in the coordination of

---

<sup>11</sup>Vancomycin-susceptible *S. aureus* with a subset of resistant colonies. VISA are generated by spontaneous mutations from hVISA, that increase vancomycin resistance to a MIC of 4 mgml<sup>-1</sup> or higher (Hiramatsu et al., 2014). Of note, a retrospective study demonstrated the occurrence of hVISA even before clinical introduction of vancomycin (Yamakawa et al., 2012).

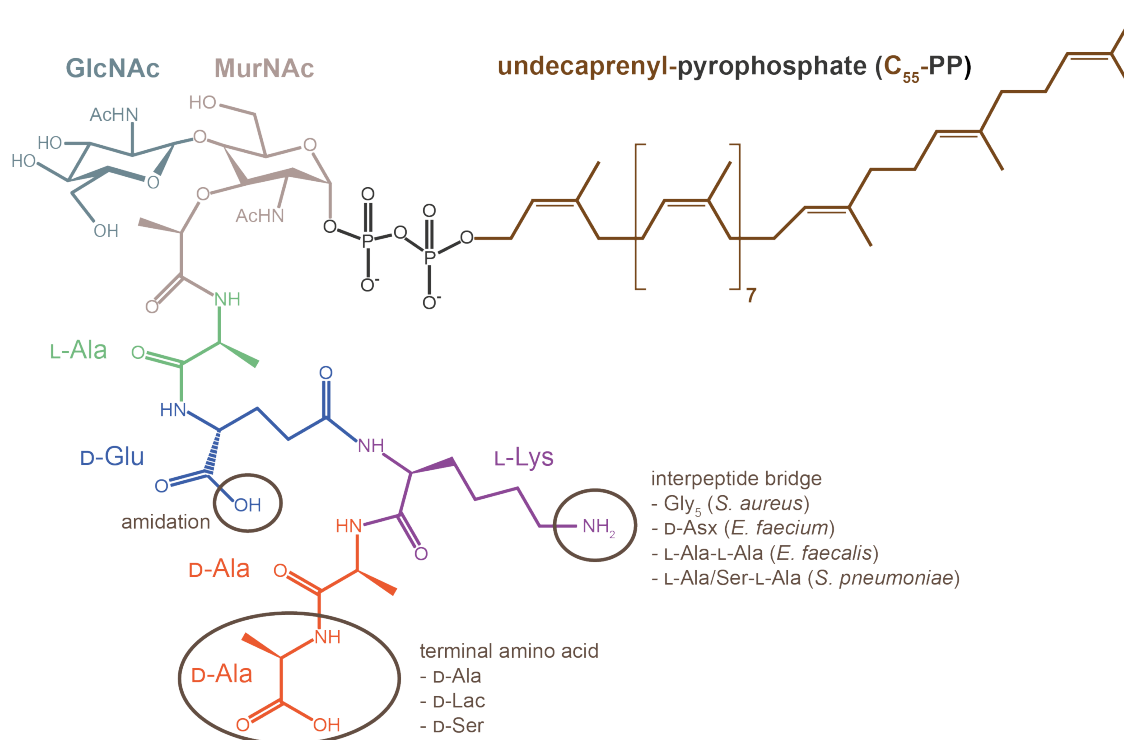


Figure 16: Schematic of the ultimate peptidoglycan precursor lipid II (undecaprenyl-pyrophosphate-GlcNAc-MurNAc-pentapeptide). The L-lysine (purple) at position three of the peptide stem is characteristic for most gram positive bacteria, while gram negatives often contain diaminopimelic acid instead. Species-specific modifications are highlighted with circles. GlcNAc, *N*-acetylmuramic acid; MurNAc, *N*-acetylmuramic acid; Ac, acetyl. Figure was modified according to Bouhss, Trunkfield, Bugg, and Mengin-Lecreulx (2008) and Müller et al. (2017).

the complex membrane-associated network of protein-protein interactions of the PGN biosynthesis machinery, by spatio-temporal orchestration of cell growth and division (Grein, Schneider, & Sahl, 2019). This hypothesis is supported by the fact that sequestration of lipid II can cause disintegration of membrane-bound multi-enzyme machineries, misplaced septum formation, and defects in cell division (Müller et al., 2017)). Furthermore, lipid II was demonstrated to act as a signal molecule for the kinase PknB, which is involved in coordination of PGN cross-wall formation, autolysis, and cell division pointing towards the involvement of lipid II or cellular levels of lipid II in bacterial signal transduction pathways (Hardt et al., 2017; Müller et al., 2017). Another example where the activity of a lipid II-targeting antibiotic goes beyond mere blocking of the incorporation of lipid II is the antibiotic teixobactin, which simultaneously binds to multiple undecaprenyl-coupled precursors that represent the building blocks for the syntheses of various surface polymers such as PGN, WTA, CPS, and arabinogalactan (Ling et al., 2015; Müller et al., 2017). The synergistic inhibition of PGN and WTA synthesis by teixobactin in *S. aureus* was demonstrated to result in cell wall damage, delocalization of autolysins and subsequent cell lysis (Homma et al., 2016). The multi-targeting of teixobactin might be causative for the apparent absence of resistance development. There are also several examples of compounds which combine sequestration of the building block with membrane damage. The well-characterized antibiotic nisin, for instance, uses lipid II as a docking molecule, producing a major impact on membrane integrity, ultimately resulting in pore formation and cell lysis (Grein et al., 2019; Oman et al., 2011; Wiedemann et al., 2006). In summary, the binding of or the interference with lipid II causes complex cellular downstream effects and triggers irreversible physical damage to cells, such as the delocalization of spatially-organized enzymes and other cell wall components and divisome machineries (Grein et al., 2019). These properties make lipid II an exceptional antibiotic target structure.

While the pace of antibiotic discovery has slowed down, the overall use of antibiotics and respective resistance mechanisms rises. It is estimated that the global death rate caused by antimicrobial resistance is 700 000 patients each year and predictions state an increase to 10 million every year by 2050, if no counter measurements are taken (O’neill, 2014). The discovery of novel antibiotics with unique chemistry and unprecedented mode of action and resistance-breaking properties is, therefore, of increasing interest and represents an inevitable measure to counteract the predicted scenario.

## 2.8 Natural product antibiotics

The mainstay of our current antibiotic arsenal is represented by (I) microbial natural products, (II) their derivatives, and (III) compounds of synthetic origin inspired by natural products (Wright, 2017). Although, natural products are produced in every domain of life, drugs originating from microbial species proved to be particularly potent in the anti-infective area, while we just begin to understand the function of plant and mammalian host derived antibiotics, such as phytoalexins and defensins respectively (González-Lamothe et al., 2009; D. Xu & Lu, 2020). Natural product antibiotics represent secondary metabolites of the producing organism and are generally regarded as non-essential but to possess extrinsic functions, such as increasing the competitiveness of organisms within its environment. The therapeutic success of microbial natural product antibiotics is attributed to the fact that they are often produced precisely for the purpose of interfering with the growth of others microorganisms, thereby providing an advantage for the producing organism. Evolution has shaped these molecules for optimized interaction with their cellular targets, providing the necessary structural and physicochemical properties for biological activity e.g. penetration of bacterial cells (Wright, 2017).

In comparison with conventional synthetic molecules, which follow the lipinski rule of five<sup>12</sup>, natural products are usually larger molecules, enriched with characteristic properties, which improve active target engagement, such as a high amount of chiral centers and sp<sup>3</sup>-carbon atoms<sup>13</sup>, fewer aromatic rings, larger macrocyclic aliphatic rings, a lower nitrogen and halogen, but an increased oxygen content (Atanasov, Zotchev, Dirsch, & Supuran, 2021; Wright, 2018). All of these features contribute to a more complex 3D structure and greater molecular rigidity. Consequentially, natural products can engage biological targets more productively than more planar and less stereochemically complex molecules dominant in the synthetic compound libraries (Atanasov et al., 2021; Rodrigues, Reker, Schneider, & Schneider, 2016; Wright, 2018). The high structural diversity goes along with a broad bioactivity spectrum, such as antiviral, antifungal, and antibacterial (Arnison et al., 2013; Essig et al., 2014; Férier et al., 2013; Ortega & van der Donk, 2016), which further favors sourcing of natural products with novel chemical matter as therapeutics or leads for drug design. Greatly enhanced knowledge and techniques concerning mining, extraction, production, characterization and manipulation of natural products could fill the antibiotic discovery gap of the 21<sup>st</sup> century, corresponding to a lull of 30 years and bring new drug candidates to the clinic (Wright, 2017). Lewis and Epstein’s laboratory have pioneered efforts, such as the iChip, to enable growth of previously unculturable bacteria to facilitate the isolation of antibiotic ‘dark matter’ (Nichols et al., 2010) and the discovery of teixobactin successfully demonstrated that such efforts can yield unique chemistry (Ling et al., 2015; Wright, 2017). This approach represents a kind of reboot of the bioactivity guided Waksman antibiotic discovery platform, which majorly contributed to the antibiotic scaffolds in clinical use today. The Waksman platform basically comprises of a screening platform where soil-derived streptomycetes are grown on various media followed by analysis of extracted metabolites for

---

<sup>12</sup>The rule of five is a set of in silico guidelines applied to drug discovery to prioritize compounds with increased pharmacokinetics for oral absorption. According to this rules 90% of oral compounds that have achieved phase II clinical status pass three of the four following parameters i)  $MW \leq 500$  Da, ii) calculated  $\text{LogP} \leq 5$  and  $\geq 0$ , iii) hydrogen bond acceptors  $\leq 10$ , and iv) hydrogen bond donors  $\leq 5$  (Doak, Over, Giordanetto, & Kihlberg, 2014; Lipinski, Lombardo, Dominy, & Feeney, 2001).

<sup>13</sup>The combination of one s and three p orbitals forms four identical hybrid sp<sup>3</sup> atomic orbitals, the resulting tetravalent carbon atom forms single covalent bonds

antibiotic activity against susceptible test microorganisms (Lewis, 2013; Schatz, Bugle, & Waksman, 1944). In the end this kind of approach was overmined, since only 1% of the isolated organisms can grow under laboratory conditions, subsequently leading to the frequent rediscovery of already known compounds and no discovery of novel chemistry. Therefore, the iChip enables the exploration of rare genera of soil-bourne organisms and surpasses the drawback of limitations in laboratory cultivation techniques, by enhancing the growth recovery to 50% (Ling et al., 2015).

Another approach to complement the activity- and chemistry-guided identification of new compounds is the mining of genomic data for the presence of biosynthetic pathways enabling organisms to produce secondary metabolites (Blin et al., 2019; Ziemert, Alanjary, & Weber, 2016). Two essential findings guiding the identification of biosynthetic genes in producing organisms are I) that the genes are clustered within the genomes of bacteria and filamentous fungi and II) that many natural products are based on polyketide or peptide cores and, although they display a huge diversity (structure- and activity-wise), their biosynthetic machineries involve enzymes encoded by large genes with highly conserved modules (Ziemert et al., 2016). Accordingly, genome-mining based drug discovery tools often rely on the conserved genetic markers located within the biosynthetic gene clusters (BGCs) which encode the respective core biosynthetic enzymes. Classes of natural products that use the aforementioned conserved machineries include polyketides (biosynthesized by a polyketide synthase; PKS), non-ribosomal peptides (NRPs), ribosomally synthesized and post-translationally modified peptides (RiPPs), aminoglycosides, and many more (Ziemert et al., 2016). Nearly all complex modified peptides identified so far belong to the RiPP and NRP class (Imani & Freeman, 2018), which are synthesized by two distinct biosynthetic routes. While the first class incorporates amino acids via the ribosome, with further modifications occurring after the initiation of translation, the latter requires large multimodular enzyme complexes for the incorporation of non-proteinogenic amino acids. Especially in direct comparison to the other natural product classes, the RiPP group is very heterogeneous and is further subdivided into over 40 families (likely expanding further), lacking overarching biosynthetic and structural commonalities between the groups (Arnison et al., 2013).

## 2.9 Ribosomally synthesized and post-translationally modified peptides

Historically, RiPPs were subdivided based on their biological activities (e.g. bacteriocins; Klaenhammer (1993)) or producers (e.g. microcins produced by gram negatives; Arnison et al. (2013); Duquesne, Destoumieux-Garzón, Peduzzi, and Rebuffat (2007)). In 2013, a comprehensive review by Arnison et al. (2013) presented the first uniform nomenclature for RiPPs taking common features of their biosynthetic pathways and specific modifications into consideration, and subdividing the class in over 20 distinct compound families, irrespective of their biological functions. Since then, new sequencing techniques and bioinformatic tools, developed specifically for this compound class, enabled the discovery of additional 17 entirely new RiPP members, recently summarized in a review by Montalbán-López et al. (2021). Of interest, the suggested nomenclature is not suited to describe all post-translationally modified natural metabolites, because final products can be devoid of peptide bonds, as in the case of pyrroloquinoline (PQQ), which is generated in a process overall similar to other RiPPs but with a final product that is no longer a peptide (Arnison et al., 2013).

Most of these compounds have in common that they are synthesized as a longer precursor peptide, containing an N-terminal leader peptide that usually guides the secretion and is excised from the C-terminal core peptide, which finally becomes the mature RiPP after undergoing extensive post-translationally modifications. A size limit of 10 kDa was defined to exclude post-translationally modified proteins (Arnison et al., 2013). Common RiPP modifications represent the presence of unusual non-proteinogenic amino acids, such as dehydroalanine (Dha) and dehydrobutyrine (Dhb), modifications of the N- and C-termini to reduce the susceptibility to degradation by exoproteases, as well as macrocyclization, which increases the metabolic stability and decreases the conformational

flexibility (Arnison et al., 2013). RiPPs usually contain several co- and post-translational modifications but are classified according to their primary post-translational modifications (PTMs), such as the eponymous (methyl)lanthionine residues of the lanthipeptide family.

Lanthipeptides represent the most prominent and extensively studied RiPP class. The most popular and best characterized representative of that family is nisin, which was already introduced in Chapter 2.7 as a PGN synthesis inhibiting antibiotic that combines binding of lipid II and pore formation. The growth inhibitory effect of nisin was already described in 1928 (Rogers, 1928) and it has been used as a food preservative since 1969 (Cotter, Hill, & Ross, 2005). **Lanthipeptides with antibiotic activity** are generally termed lantibiotics, their efficacy is often restricted to gram positives, and their mechanism of action is often attributed to their ability to interact with the ultimate PGN precursor lipid II. Interestingly, lantibiotics were the first lipid II-binding compounds ever studied in combination with purified full length lipid II, in the course of the mode of action studies on the lantibiotic mersacidin (Brötz, Bierbaum, Leopold, Reynolds, & Sahl, 1998; Grein et al., 2019). Lantibiotics are further grouped into two major categories according to their structural features (globular or flexible) and based on their mode of action as nisin-like (group A) or mersacidin-like (group B) lantibiotics. Nisin and related peptides display an elongated and flexible structure, are positively-charged, and act through the formation of membrane pores/membrane damage. On the other hand, the globular mersacidin (see Figure 17) and related lantibiotics are either negatively charged or carry no net charge they block PGN synthesis through interaction with lipid II and cause only marginal effects on membrane integrity (Müller et al., 2017). In the case of two-component lantibiotics, where two peptides assemble to a functional antibiotic, one is usually mersacidin-like, whereas the other one is often rather long and flexible (Müller et al., 2017).

The lanthipeptide class-defining  $\beta$ -thioether crosslinked bis amino acids lanthionine (Lan) and 3-methyl-lanthionine (MeLan) are introduced by initial dehydration of Ser and Thr residues to the corresponding dehydro amino acids Dha and Dhb. Subsequent addition of Cys thiols to these dehydrated amino acids result in Lan- and MeLan-based intramolecular thioether rings (Bierbaum & Sahl, 2009; Müller et al., 2017), which were reported to play a pivotal role in lipid II binding (e.g., for nisin and mersacidin). Interestingly, this particular PTM can be introduced by multiple types of enzymes and the lanthipeptides are grouped into class I-IV, according to the four different types of dehydratases (including their mechanism of catalysis and protein organization) responsible for lanthionine ring formation. The recently discovered lantibiotic cacaoidin (see Figure 17) represents the founding member of class V lanthipeptides and the characterization of its biological activity was subject of this work. The BGC cluster *cao* of cacaoidin (Chapter 4.2) showed no ORFs with homology to one of the proteins involved in the lanthionine ring synthesis of the four different lanthipeptide classes. Accordingly, the Lan bridge must be installed via an independent biosynthetic pathway, which is at present not yet well understood. Therefore, cacaoidin represents the first-in-class V lanthipeptide and shortly after its discovery the two additional family members pristin A3 (Kloosterman et al., 2020) and lexapeptide have been identified (see Figure 17; M. Xu et al. (2020)). M. Xu et al. (2020) proposed that the lexapeptide lanthionine moiety is formed by the three monofunctional proteins LxmK, LxmX, and LxmY constituting the class V-defining three-component lanthionine synthetase. Cao7-9-14 show a certain degree of homology to LxmK-X-Y and could function accordingly (Román-Hurtado, Sánchez-Hidalgo, Martín, Ortiz-López, & Genilloud, 2021).

The lanthionine residue of cacaoidin is dimethylated and positioned at the N-terminus generating an *N,N*-dimethyl lanthionine (NMe<sub>2</sub>Lan). While N-terminal methylation is commonly found among proteins, it is rarely found in RiPPs. There have been no reports of N-terminal bis-*N*-methylation for known lanthipeptides (class I-IV), but for the linaridin (see Figure 17) and linear azol(in)e-containing peptide (LAP) RiPP families, that both lack lanthionines. The other class V lanthipeptides lexapeptide and pristin A3 share the N-terminal *N,N*-dimethylation of cacaoidin. Another rare PTM, thus far only present in thioamitides, linaridins, class V lanthipeptides, and also in several other lanthipeptide classes is a 2-aminovinyl-(3-methyl)-cysteine (Avi(Me)Cys)-containing carboxyl-terminal ring. This structure is the result of oxidative decarboxylation of the C-terminal cysteine.

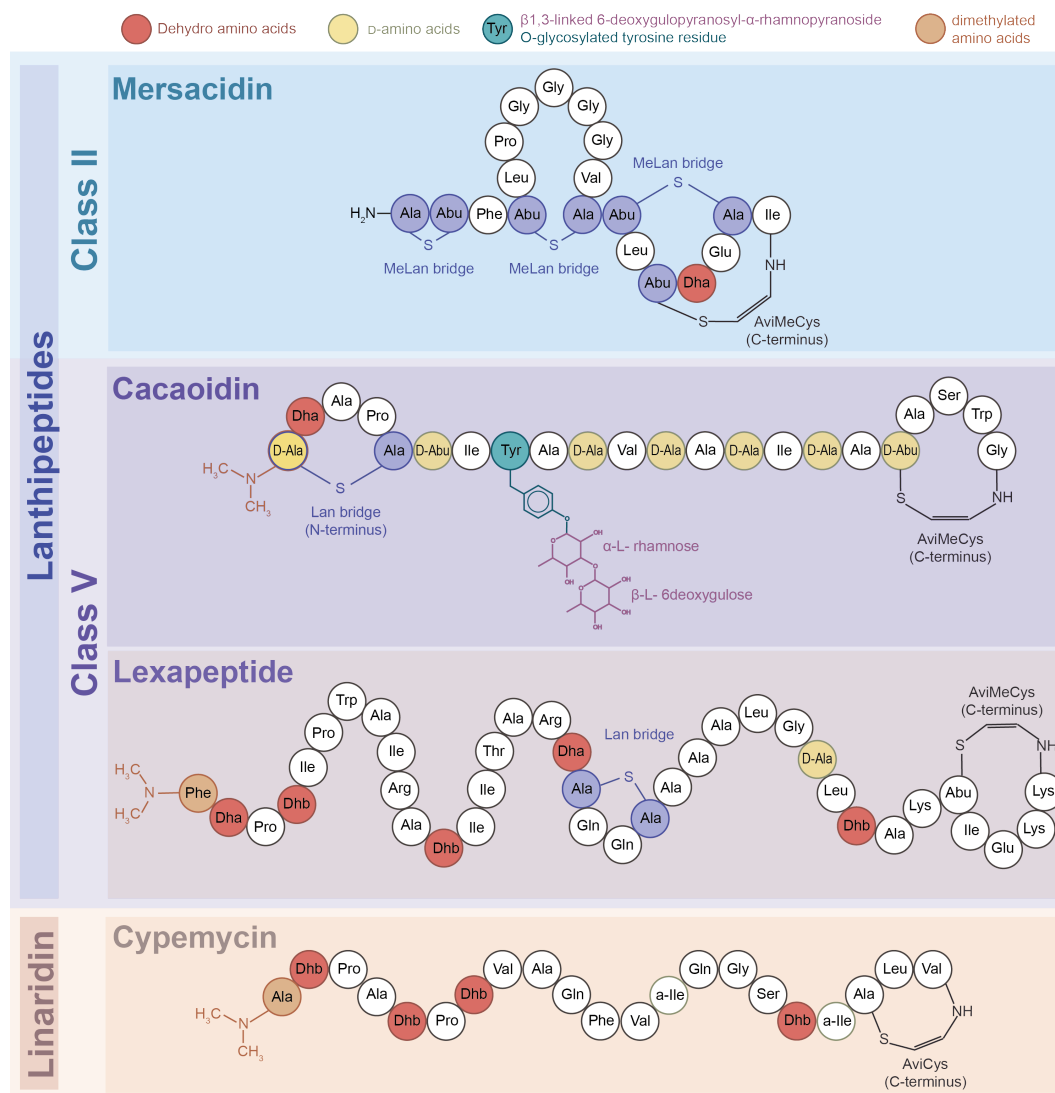


Figure 17: Structural comparison of selected lanthipeptide and linaridin RiPP family representatives. Dha, 2,3-dihydro-alanine; Dhb, 2,3-dihydrobutyrine; AviMeCys, 2-aminovinyl(-3-methyl)-cysteine; (Me)Lan bridge (purple),  $\beta$ -thioether crosslinked bis amino acid (3-methyl-)lanthionine (Abu-*S*-Ala and Ala-*S*-Ala, respectively)

Linaridins, as the name already indicates, are linear dehydrated (*arid* is greek and means dry) peptides and were initially classified as lanthipeptides due to the presence of Dhb and AviCys moieties. However, because they lack lanthionine residues and the respective synthetase-like enzyme encoding genes, and the alternative route predicted for installation of AviCys, a separate RiPP class was established. The linaridins constitute a moderately sized RiPP class with only four representatives, cypemycin (see Figure 17), grismycin, legonaridin, and salinipeptins (Ma & Zhang, 2020), and the only characteristic PTM common to all is the dehydration of Thr to Dhb. Cacaooidin combines structural elements of **lanthipeptides** and **linaridins**, but since the latter family is characterized by Dhb residues as their class-defining PTM, a feature absent in cacaooidin, it was initially classified as a new RiPP family referred as **lanthidins** (Montalbán-López et al., 2021). In contrast to cacaooidin, both lexapeptide and pristin A3 contain Dhb residues. Another rare PTM of cacaooidin is the presence of D-amino acids (D-alanine and D-aminobutyric acid; Figure 17, highlighted in light yellow), thus far only reported for a limited number of RiPPs. D-amino acids are introduced by hydrogenation of Dha and Dhb, resulting in D-Ala and D-amino butyric acid residues, respectively. Most D-amino acid containing RiPPs are members of the lanthipeptide family, comprising lactocin S



(Skaugen et al., 1994), lacticin 3147 (Ryan et al., 1999), carnolysin (Lohans, Li, & Vederas, 2014), and bicereucin (Huo & van der Donk, 2016), whereas the salinipeptins are the only members of the linaridin subfamily reported to contain D-amino acids (Shang, Winter, Kauffman, Yang, & Fenical, 2019). Compared to the lanthipeptide representatives, CAO contains a relatively high number of D-amino acids (a total of seven, compared to one-four in the representatives), displaying a greater similarity with salinipeptins, that contain nine D-amino acids. Lexapeptide contains one (Figure 17, highlighted in light yellow), whereas pristin A3 has no D-amino acids (Kloosterman et al., 2020; M. Xu et al., 2020).

### 3 Aim of the thesis

Cell wall biosynthesis represents a very efficient target pathway for antibiotic intervention. Enzymes as well as intermediates of peptidoglycan synthesis are effective and validated antibiotic targets. Particularly binding bactoprenyl-coupled cell envelope precursors, such as the ultimate peptidoglycan building block lipid II has proven an attractive antibiotic strategy against Gram-positive pathogens. Besides the individual reactions, building up a vital bacterial cell envelope requires the precise synchronization of various multi-enzyme machineries of diverse cell envelope polymers, i.e. peptidoglycan, teichoic acids and capsules, as well as the cell division apparatus, which need to be intimately controlled in time and space. Understanding the dense cell wall biosynthesis interaction network and the molecular roles of individual reactions within, will unravel novel points for antiinfective attack.

The aims of this thesis were:

- Reconstitution of staphylococcal capsule biosynthesis reactions
- Characterization of LCP enzymes and their role in cell wall assembly
- Detailed analysis of the mode of action of cacaoidin, the founding member of a new RiPP subfamily

## 4 Publications included in this thesis

### 4.1 Coordination of capsule assembly and cell wall biosynthesis in *Staphylococcus aureus*

Capsular polysaccharides are commonly found attached to the peptidoglycan of most clinical *S. aureus* isolates and contribute substantially to pathogenicity. Despite its relevance for disease the biochemistry of capsule biosynthesis have yet not been characterized in detail, while the cytoplasmic steps have been investigated, particularly the membrane associated steps as well as the critical step of anchoring capsular polysaccharides to the cell envelope were unexplored and reconstituted in this chapter. Although the structures of different *S. aureus* capsule serotypes have been determined over three decades ago (Fournier, Vann, & Karakawa, 1984; Moreau et al., 1990), there has been no biochemical evidence for the corresponding membrane-dedicated synthetic steps until now. Evidence for the function of individual capsule gene products whose activities are located in the bacterial cytoplasm, e.g. *capE*, *capF*, *capG*, *capH*, *capO*, and *capP*, was demonstrated long ago (Bhasin et al., 1998; Jones, 2005; Kiser et al., 1999; Kneidinger et al., 2002). New insights in the remaining pathways were only given recently as a result of the cooperative work of various researchers and published in two articles (W. Li et al., 2014), one of them presented in the following.






Accordingly, the first chapter of this thesis, describes the reconstitution of the entire capsule biosynthesis pathway in *S. aureus*, regulatory circuits and the attachment, of capsule polysaccharides to PGN. The study was published in Nature Communications in 2019 and comprises the work of three first authors, Dr. M. Rausch, Dr. H. Ulm and myself, that equally contributed to the work. This work was included partially in the the doctoral theses of Dr. M. Rausch (Rausch, 2017). Already published content will be marked as such with asterisk-symbols (\*), whereby two asterisks indicate identical content and one asterisk indicates contents which only partially overlap. In the following the work to which I have contributed significantly will be outlined: I) Optimization of capsular lipid I and lipid II synthesis, with regard to the product yield and to overcome limitations for the detection via mass analysis; II) reconstitution of capsular lipid III synthesis reaction, including the expression and purification of CapI, CapO, and CapP; III) processing of all three capsular lipid precursors by LcpC; IV) the *in vivo* role of CapA1 in a LCP-deficient *S. aureus* strain ( $\Delta$ *lcp* mutant).

ARTICLE

<https://doi.org/10.1038/s41467-019-09356-x>

OPEN

# Coordination of capsule assembly and cell wall biosynthesis in *Staphylococcus aureus*

Marvin Rausch <sup>1,2</sup>, Julia P. Deisinger<sup>1,2</sup>, Hannah Ulm<sup>1</sup>, Anna Müller <sup>1</sup>, Wenjin Li<sup>3</sup>, Patrick Hardt<sup>1</sup>, Xiaogang Wang<sup>4</sup>, Xue Li<sup>4</sup>, Marc Sylvester <sup>5</sup>, Marianne Engeser <sup>6</sup>, Waldemar Vollmer<sup>7</sup>, Christa E. Müller <sup>3</sup>, Hans Georg Sahl<sup>8</sup>, Jean Claire Lee<sup>4</sup> & Tanja Schneider<sup>1,2</sup>

The Gram-positive cell wall consists of peptidoglycan functionalized with anionic glycopolymers, such as wall teichoic acid and capsular polysaccharide (CP). How the different cell wall polymers are assembled in a coordinated fashion is not fully understood. Here, we reconstitute *Staphylococcus aureus* CP biosynthesis and elucidate its interplay with the cell wall biosynthetic machinery. We show that the CapAB tyrosine kinase complex controls multiple enzymatic checkpoints through reversible phosphorylation to modulate the consumption of essential precursors that are also used in peptidoglycan biosynthesis. In addition, the CapA1 activator protein interacts with and cleaves lipid-linked CP precursors, releasing the essential lipid carrier undecaprenyl-phosphate. We further provide biochemical evidence that the subsequent attachment of CP is achieved by LcpC, a member of the LytR-CpsA-Psr protein family, using the peptidoglycan precursor native lipid II as acceptor substrate. The Ser/Thr kinase PknB, which can sense cellular lipid II levels, negatively controls CP synthesis. Our work sheds light on the integration of CP biosynthesis into the multi-component Gram-positive cell wall.

<sup>1</sup>Pharmaceutical Microbiology, University of Bonn, Bonn 53115, Germany. <sup>2</sup>German Center for Infection Research (DZIF), partner site Bonn-Cologne, Bonn 53115, Germany. <sup>3</sup>Pharma Center Bonn, Pharmaceutical Institute, Pharmaceutical Chemistry I, University of Bonn, Bonn 53121, Germany. <sup>4</sup>Division of Infectious Diseases, Department of Medicine, Brigham and Women's Hospital, Harvard Medical School, Boston 02115 MA, USA. <sup>5</sup>Institute of Biochemistry and Molecular Biology, University of Bonn, Bonn 53115, Germany. <sup>6</sup>Kekulé Institute for Organic Chemistry and Biochemistry, University of Bonn, 53121 Bonn, Germany. <sup>7</sup>Center for Bacterial Cell Biology, Medical School, Newcastle University, Newcastle upon Tyne NE2 4AX, UK. <sup>8</sup>Institute of Medical Microbiology, Immunology and Parasitology, University of Bonn, Bonn 53127, Germany. These authors contributed equally: Marvin Rausch, Julia P. Deisinger, Hannah Ulm. Correspondence and requests for materials should be addressed to T.S. (email: [tschneider@uni-bonn.de](mailto:tschneider@uni-bonn.de))

The bacterial cell envelope is a complex multilayered structure consisting of peptidoglycan (PG), which in Gram-positive bacteria is densely decorated with glyco-polymers such as wall teichoic acid (WTA) and capsular polysaccharide (CP). The coordinated synthesis and assembly of these polymers is pivotal for maintenance of cell wall architecture and function<sup>1</sup>. In contrast to the biosyntheses of PG and WTA, for which the individual enzymatic reactions have already been characterized *in vitro*<sup>2,3</sup>, the biochemistry underlying capsule formation in Gram-positive bacteria is not well understood. Even more so, it is largely unknown how the different cell wall synthesis pathways, which share building blocks and membrane carriers, function in a coordinated and integrated fashion.

In the case of *Staphylococcus aureus*, an important opportunistic pathogen<sup>4</sup>, the expression of a polysaccharide capsule contributes substantially to the ability to cause invasive disease<sup>5–7</sup>. Serotype 5 and 8 capsular polysaccharide (CP5 and CP8) types are dominant among clinical isolates<sup>6</sup>. *S. aureus* USA300, which is prevalent in the United States, lacks a capsule due to several conserved mutations within the *cap5* locus<sup>8</sup>. However, the majority of USA300-associated infections involved superficial wounds or abscesses<sup>9</sup>, and USA300 isolates are not common outside of North America<sup>10</sup>. Among predominant methicillin-resistant *S. aureus* clones worldwide are the CP8 + lineages ST1, ST30, ST59, ST80, and ST239 and the CP5 + lineages ST5 and ST22.

CP5 and CP8 share similar trisaccharide repeating units, which are identical in monosaccharide composition and sequence, only differing in the glycosidic linkages between the sugars and the sites of *O*-acetylation<sup>11</sup>.

The CP5 biosynthetic gene cluster comprises 16 genes (*cap5A–cap5P*; Fig. 1a)<sup>12</sup> encoding for proteins involved in polymer biosynthesis<sup>7,13,14</sup>, acetylation<sup>15</sup>, transport, and the regulation of CP production<sup>16,17</sup>. Database homology searches with amino acid sequences of *cap5* operon gene products allowed for the prediction of individual enzymatic functions and the proposal of a pathway for capsule (CP) biosynthesis in *S. aureus*<sup>18</sup>.

Within this pathway (Fig. 1b), synthesis of the soluble building blocks occurs in the cytoplasm via three distinct reaction cascades, through which the universal cell envelope substrate UDP-D-*N*-acetylglucosamine (UDP-D-GlcNAc), is converted into the three different nucleotide-coupled sugars UDP-*N*-acetyl-D-fucosamine (UDP-D-FucNAc), UDP-*N*-acetyl-L-fucosamine (UDP-L-FucNAc) and UDP-*N*-acetyl-D-mannosaminuronic acid (UDP-D-ManNAcA). The synthesis of the first soluble precursor UDP-D-FucNAc is allegedly catalyzed in a two-step process by the enzymes CapD and CapN. Only recently, the integral membrane protein CapD was shown to function as a 4,6-dehydratase, which generates the intermediate UDP-2-acetamido-2,6-dideoxy-D-xylo-4-hexulose<sup>19</sup>, proposed to be further converted to UDP-D-FucNAc by the action of the membrane-associated reductase CapN, though experimental evidence is lacking so far. Subsequently, CapM is supposed to transfer the phosphosugar moiety

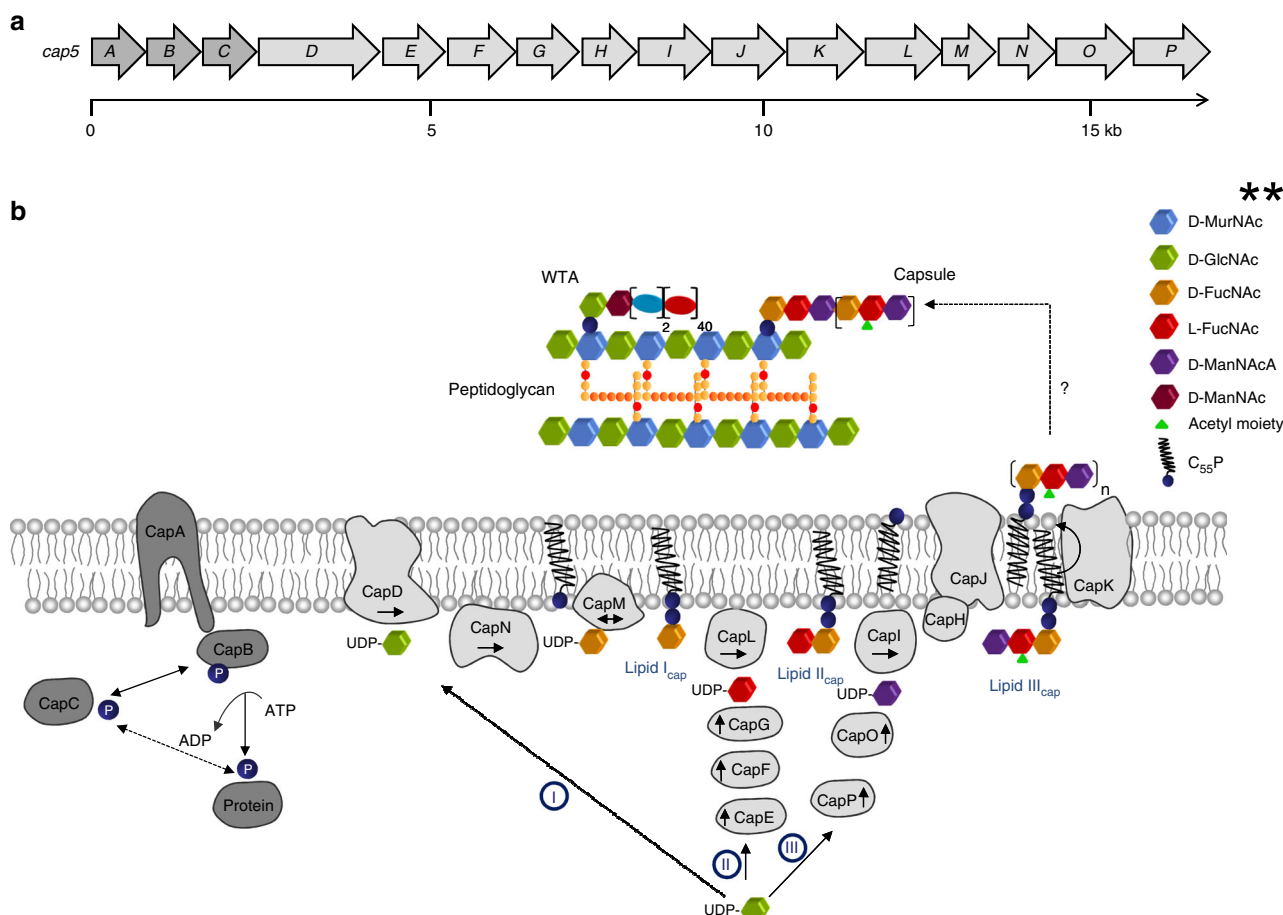


**Fig. 1** *S. aureus* capsule biosynthesis. **a** *S. aureus* capsule (CP5) biosynthesis gene cluster (NWMN\_0095-0110). **b** Model for the capsule (CP) biosynthesis pathway in *S. aureus* and its regulation by the tyrosine kinase complex CapA1B1. C<sub>55</sub>P, undecaprenyl-phosphate; GlcNAc, *N*-acetyl-glucosamine; FucNAc, *N*-acetyl-fucosamine; ManNAc, *N*-acetyl-mannosamine; ManNAcA, *N*-acetyl-mannosaminuronic acid. Arrows indicate synthesis direction. Double arrow indicates reaction reversibility

of UDP-D-FucNAc to the membrane-anchored lipid carrier undecaprenyl-phosphate ( $C_{55}P$ ), yielding lipid  $I_{cap}$ .

The second cytoplasmic reaction cascade generating the soluble precursor UDP-L-FucNAc involves the enzymes CapE, CapF and CapG, the enzymatic functions of which have already been elucidated biochemically<sup>13</sup>. The transferase CapL is assumed to further attach L-FucNAc to lipid  $I_{cap}$  leading to the formation of the second CP lipid intermediate, lipid  $II_{cap}$ .

The third nucleotide-activated monosaccharide required for CP5 production, UDP-D-ManNAcA, is generated by the epimerase CapP and the dehydrogenase CapO<sup>7,14</sup>. The transmembrane protein CapI has been proposed to transfer the ManNAcA moiety to lipid  $II_{cap}$ , thereby generating the final capsule precursor lipid  $III_{cap}$ . The  $C_{55}P$ -coupled trisaccharide is most likely further modified by the putative acetyltransferase CapH<sup>15</sup>, which catalyzes the *O*-acetylation of L-FucNAc residues in position C3 in CP5 strains<sup>11</sup>. The complete, modified precursor is then translocated to the outer surface of the cell membrane, where polymerization is assumed to take place. These processes are proposed to be facilitated by the putative flippase CapK and the polymerase CapJ, respectively<sup>12,18</sup>. The attachment of CP precursors to the MurNAc (*N*-acetylmuramic acid) moiety of peptidoglycan is achieved by a yet unknown mechanism possibly involving a member of the LCP (LytR-CpsA-Psr) family of proteins<sup>20,21</sup>. This process likely releases the lipid carrier  $C_{55}P$ , which enters new synthesis cycles.

The fact that the undecaprenyl-phosphate carrier is found in limited amounts within the cell<sup>22</sup> and required for the biosyntheses of diverse cell envelope components, like CP, WTA and PG<sup>2,3,18</sup>, makes a well-orchestrated spatial and temporal regulation of these processes crucial for the viability of the cell. The consequences arising from perturbation of this balanced biosynthetic network have been well exemplified for WTA biosynthesis. Interference with late WTA biosynthesis steps has been shown to be lethal, although the polymer per se is not crucial for viability<sup>23</sup>. Similarly, late stage genes are conditionally essential since they are dispensable for viability in an early gene (*tarO* or *tarA*) deletion background, a phenomenon referred to as the “essential gene paradox”<sup>24</sup>. Inhibition of late WTA biosynthesis steps causes the accumulation of dead-end lipid-linked intermediates and thus depletes the cellular pool of  $C_{55}P$  to critical levels impeding peptidoglycan biosynthesis, resulting in cell death<sup>25</sup>.

In *S. aureus*, the regulation of CP biosynthesis is not only achieved by differential gene expression<sup>26–28</sup>, but has additionally been linked to tyrosine phosphorylation<sup>16,17</sup>. Bacterial tyrosine kinases (BY-kinases) are widespread in bacteria and have multifaceted roles in bacterial exopolysaccharide production<sup>29</sup>. BY-kinases belong to the family of P-loop containing kinases<sup>30</sup>, whereby “P-loop” designates a characteristic amino acid sequence resembling the Walker A nucleotide binding motif. BY-kinases of Firmicutes are composed of two interacting polypeptides, a transmembrane activator protein and a cytoplasmic BY-kinase<sup>31</sup>. The cytoplasmic kinase carries a C-terminal tyrosine cluster that undergoes autophosphorylation in the presence of ATP. Based on studies in *S. aureus* and *Streptococcus pneumoniae*, the cytoplasmic kinase protein alone is not sufficient for phosphotransfer, but has to interact with the C-terminus of the transmembrane adaptor to undergo autophosphorylation<sup>16,32,33</sup>. Concomitantly, phosphate groups can be transferred to tyrosine residues of target proteins, thus modulating their activity. Two triplets of adjacent BY genes encoding for a transmembrane adaptor, a cytoplasmic BY-kinase, and a cognate phosphotyrosine phosphatase were identified in the genome of *S. aureus* serotype 5: The *capA1/capB1/capC1* triplet (also referred to *cap5A/cap5B/cap5C*) is located at the 5'-end of the *cap5* operon (Fig. 1a), whereas the highly similar *capA2/capB2/capC2* triplet

is found elsewhere on the bacterial chromosome<sup>12,16</sup>. So far, the cellular roles of the distinct CapAB complexes are not fully understood. Particularly, the nature of the stimulus that triggers CapAB signaling and the exact mode of signal transduction are still elusive.

In this study, we functionally reconstitute the entire CP biosynthetic reaction cascade generating the three membrane-anchored CP precursors lipid  $I_{cap}$ , lipid  $II_{cap}$  and lipid  $III_{cap}$ , allowing us to identify crucial enzymatic check points, which are regulated by the tyrosine kinase CapA1B1 complex to control the consumption of essential precursors. Reconstitution of the membrane anchored CapA1 adaptor protein further reveals a yet elusive function. We show that CapA1 is a dual-function kinase activator/phosphodiesterase protein crucial for signaling and processing of the CP polymer. CapA1 interacts with lipid-bound CP precursors to catalyze the cleavage of the pyrophosphate linkage, releasing the essential lipid carrier  $C_{55}P$ . Moreover, we elucidate the principles of CP attachment to murein precursors in Gram-positive bacteria. We show that the transfer of the capsular phosphosugar moiety is conducted by a member of the LCP protein family and identify the acceptor substrate. We provide biochemical evidence that the attachment of the anionic precursor likely occurs on the level of the lipid-linked peptidoglycan precursor lipid II, and is facilitated in the presence of CapA1, indicating its cooperative functioning with LCP proteins.

## Results

**In vitro reconstitution of capsule biosynthesis.** Homology searches with CapD and CapN suggested that both proteins are involved in the synthesis of the first soluble capsule precursor UDP-D-FucNAc<sup>18</sup>. More recently, CapD was characterized at the molecular level, and the enzymatic product was shown to be UDP-2-acetamido-2,6-dideoxy-D-xylo-4-hexulose<sup>19</sup>. CapN is proposed to further convert the CapD reaction product to UDP-D-FucNAc by stereospecific reduction of the C-4 keto group<sup>18</sup>.

As confirmed by capillary electrophoresis (CE) and mass spectrometry (MS), purified CapN (Supplementary Figure 1) catalyzed the NADPH-dependent conversion of the intermediate UDP-2-acetamido-2,6-dideoxy-D-xylo-4-hexulose to a sugar nucleotide species having a molecular mass of  $m/z$  590.4 for the negatively charged molecule, consistent with the formation of UDP-D-FucNAc (Supplementary Figure 2). The subsequent transfer of the phosphosugar moiety of UDP-D-FucNAc to the lipid anchor  $C_{55}P$  is thought to be catalyzed by the polyprenyl-phosphoglycosyltransferase CapM, to initiate the assembly of the lipid-anchored trisaccharide repeating units<sup>18</sup>. Incubation of purified CapM protein with  $C_{55}P$  and UDP-D-[<sup>14</sup>C]FucNAc revealed the formation of a new radiolabeled lipid species, not present in the negative control (Fig. 2a). In comparison to  $C_{55}P$  (Fig. 2a, lane 1;  $R_f = 0.95$ ), migration of the lipid product was retarded (lane 3;  $R_f = 0.87$ ), consistent with the addition of a sugar moiety. The product displayed the same  $R_f$  value as determined for the WTA lipid intermediate undecaprenyl-pyrophosphoryl-D-GlcNAc (lipid III), which is structurally very similar to the proposed first CP lipid intermediate<sup>34</sup>. The newly formed purified lipid intermediate had a mass of  $m/z$  1112.7058 for the negatively charged molecule (Fig. 2b), which is consistent with the calculated neutral mass for undecaprenyl-pyrophosphoryl-D-FucNAc (lipid  $I_{cap}$ ) of 1113.7162. Moreover, the GT-B type<sup>35</sup> glycosyltransferase CapL was able to use lipid  $I_{cap}$  as acceptor substrate and to catalyze the addition of the second <sup>14</sup>C-labeled sugar moiety L-FucNAc, yielding lipid  $II_{cap}$  (Fig. 2a, lane 4;  $R_f = 0.83$ ). Mass spectrometry analysis of lipid  $II_{cap}$  revealed a mass of  $m/z$  1299.7896  $[M-H]^-$  matching the

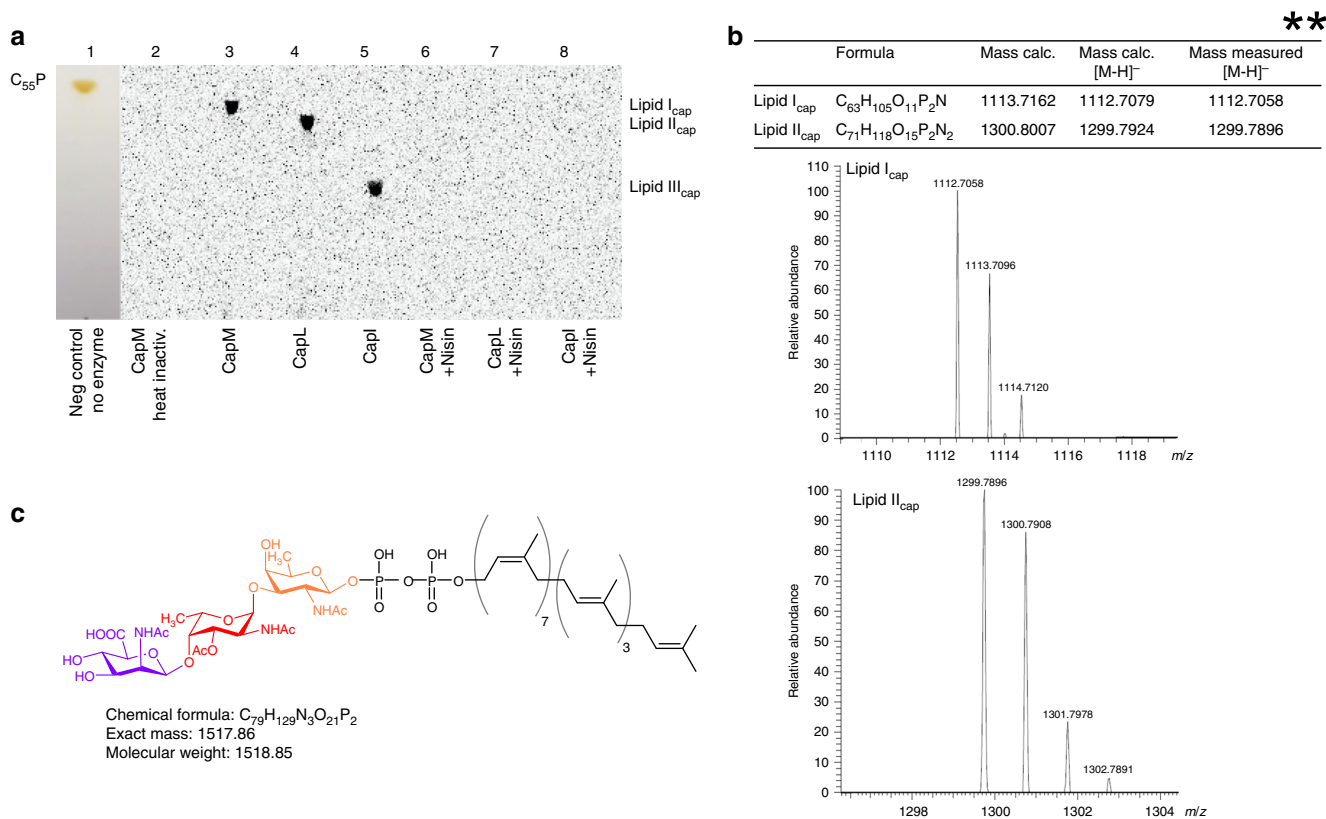


**Fig. 2** Synthesis of CP lipid intermediates. Glycosyltransferases (GT) CapM, CapL and CapI catalyze the *in vitro* synthesis of CP lipid intermediate lipid I<sub>cap</sub> (C<sub>55</sub>PP-D-FucNAc), lipid II<sub>cap</sub> (C<sub>55</sub>PP-D-FucNAc-L-FucNAc) and lipid III<sub>cap</sub> (C<sub>55</sub>PP-D-FucNAc-L-FucNAc-D-ManNAc), respectively. **a** Purified GTs were incubated with the respective purified acceptor lipid substrate in the presence of radiolabeled UDP-activated sugars. After extraction with BuOH/PyrAc, synthesis products were analyzed by TLC and phosphorimaging. Counterstain with iodide (lane 1) was used to visualize the migration behavior relative to C<sub>55</sub>P. Nisin, known to bind to the pyrophosphate-sugar moiety of cell wall lipid intermediates was added posterior and formed complexes with all lipid<sub>cap</sub> intermediates that are not extracted from the reaction mixture. Heat-inactivated CapM was used as a negative control. **b** ESI-MS analysis of lipid I<sub>cap</sub> and lipid II<sub>cap</sub>. The peaks at *m/z* 1112.70 and 1299.78 correspond to the negatively charged lipid I<sub>cap</sub> and lipid II<sub>cap</sub> molecules, respectively. **c** Structure of the ultimate CP lipid intermediate lipid III<sub>cap</sub>. Sugar residues are colored: D-FucNAc (orange), L-FucNAc (red), D-ManNAc (purple)

calculated neutral mass of *m/z* 1300.801 for undecaprenyl-pyrophosphoryl-D-FucNAc-L-FucNAc.

Conversion to the ultimate lipid-linked CP precursor lipid III<sub>cap</sub> was achieved by the attachment of a <sup>14</sup>C-D-ManNAc residue to lipid II<sub>cap</sub>, catalyzed by the glycosyltransferase CapI (Fig. 2a, lane 5; R<sub>f</sub> = 0.53). Mass spectrometric analysis of lipid III<sub>cap</sub> did not yield any signal, presumably due to reduced ionization with addition of further sugar moieties. However, in line with the altered migration behavior of the different CP intermediates on TLC (Fig. 2a, lanes 3–5) resulting from the consecutive sugar residue addition, the lantibiotic nisin formed extraction-stable complexes with all C<sub>55</sub>P-containing CP precursors further validating their identity (Fig. 2a, lanes 6–8). Taken together, these findings confirm the proposed functions of the different glycosyltransferases (GT) and demonstrate that CapM functions as priming GT, initiating the synthesis of membrane-bound CP precursors by coupling the first sugar moiety to the lipid carrier C<sub>55</sub>P.

CapM is homologous to a wide range of GTs from various pathogens (Supplementary Figure 3a), which catalyze the transfer of UDP-activated sugars to C<sub>55</sub>P<sup>36,37</sup>. Prediction of transmembrane topology (<http://www.cbs.dtu.dk/services/TMHMM/>) and comparison with hydrophobicity plots (ProtScale<sup>38</sup>) of homologous GTs predicts that CapM is anchored to the cytoplasmic membrane by a 28-amino acid long α-helical transmembrane domain that is linked to a large C-terminal catalytic domain located in the cytoplasm (Supplementary Figure 3b). In contrast

to the *in silico* predicted single-pass transmembrane (TM) helix geometry, structural analysis of the homologous PglC of *Campylobacter concisus* suggests that the TM segment adopts an unusual architecture<sup>37</sup>. Structural modelling of CapM revealed a similar architecture (Supplementary Figure 3c), in which the TM segment is broken into two helices (A and B) with an interhelix angle of 118° by a Ser-Pro motif (Supplementary Figure 3c), suggesting a similar membrane embedment as PglC. Shared structural features further include a conserved Arg residue (Arg3) positioned at the membrane interface as well as a catalytic Asp-Glu dyad and a strictly conserved PRP motif (residues 110–112 in CapM) in the cytoplasmic GT domain, involved in Mg<sup>2+</sup> and substrate binding, respectively<sup>37</sup> (Supplementary Figure 3). CapM activity *in vitro* depends on the presence of MgCl<sub>2</sub>, and was completely lost in the presence of EDTA (Supplementary Figure 4a), as reported for homologous glycosyltransferases<sup>36,37,39</sup>.

Interestingly, CapM was inhibited in the presence of tunicamycin (Supplementary Figure 4a), a nucleoside antibiotic shown to inhibit members of the UDP-HexNAc-1-phosphate transferase family (i.e., WecA, MraY or TarO) through competitive binding to the DDxxD Mg<sup>2+</sup>-binding site<sup>39</sup>. Tunicamycin had an IC<sub>50</sub> of 129 μM for CapM, which is in the range determined for PglC of *C. jejuni* (IC<sub>50</sub> = of 100 μM)<sup>40</sup>. The lower potency of tunicamycin for these monotopic GTs compared to the polytopic WecA (IC<sub>50</sub> of 11 nM), MraY (IC<sub>50</sub> of ~22.5 μM) or TarO (IC<sub>50</sub> of ~59 nM) may likely result from the distinct

architectures and catalytic sites. Since we observed a major impact of anionic phospholipids (dioleoylphosphatidylglycerol and cardiolipin) on the enzymatic activity of CapM, we further investigated the effect of different detergents. However, CapM showed lower activity in the presence of detergents or DMSO indicating that the enzyme preferred the native phospholipid environment (Supplementary Figure 4b).

**\*\* CapAB phosphorylation positively modulates CapM and CapE activity.** Full-length integral membrane proteins CapA1 and CapA2 and cytoplasmic kinases CapB1 and CapB2 were over-expressed as His<sub>6</sub>-tag fusion proteins, purified by Ni-NTA chromatography (Supplementary Figure 1), and utilized to reconstitute CapAB tyrosine kinase activity in vitro in the

presence of  $\gamma$ -labeled [<sup>33</sup>P]ATP. CapB2 autophosphorylation was effectively activated by full-length CapA1 or CapA2 (Fig. 3a) producing a single radiolabeled band with an apparent molecular mass of 25.3 kDa, corresponding to phosphorylated CapB2 (lanes 3 & 4). In contrast, the negative control in which a CapA activator was absent (Fig. 3a, lane 1 and 2, Supplementary Figure 5a) showed no autophosphorylation. In line with previous findings<sup>16</sup>, phosphorylation of the individual kinase protein CapB1 was neither observed with CapA1 nor with CapA2 (Fig. 3a, lanes 5 & 6, Supplementary Figure 5a, lanes 6 & 7). However, when CapB1 was fused to its cognate activator CapA1, the recombinant chimera CapAB full-length fusion protein (50.2 kDa) efficiently autophosphorylated in the presence of  $\gamma$ -labeled [<sup>33</sup>P]ATP, demonstrating functionality of CapB1

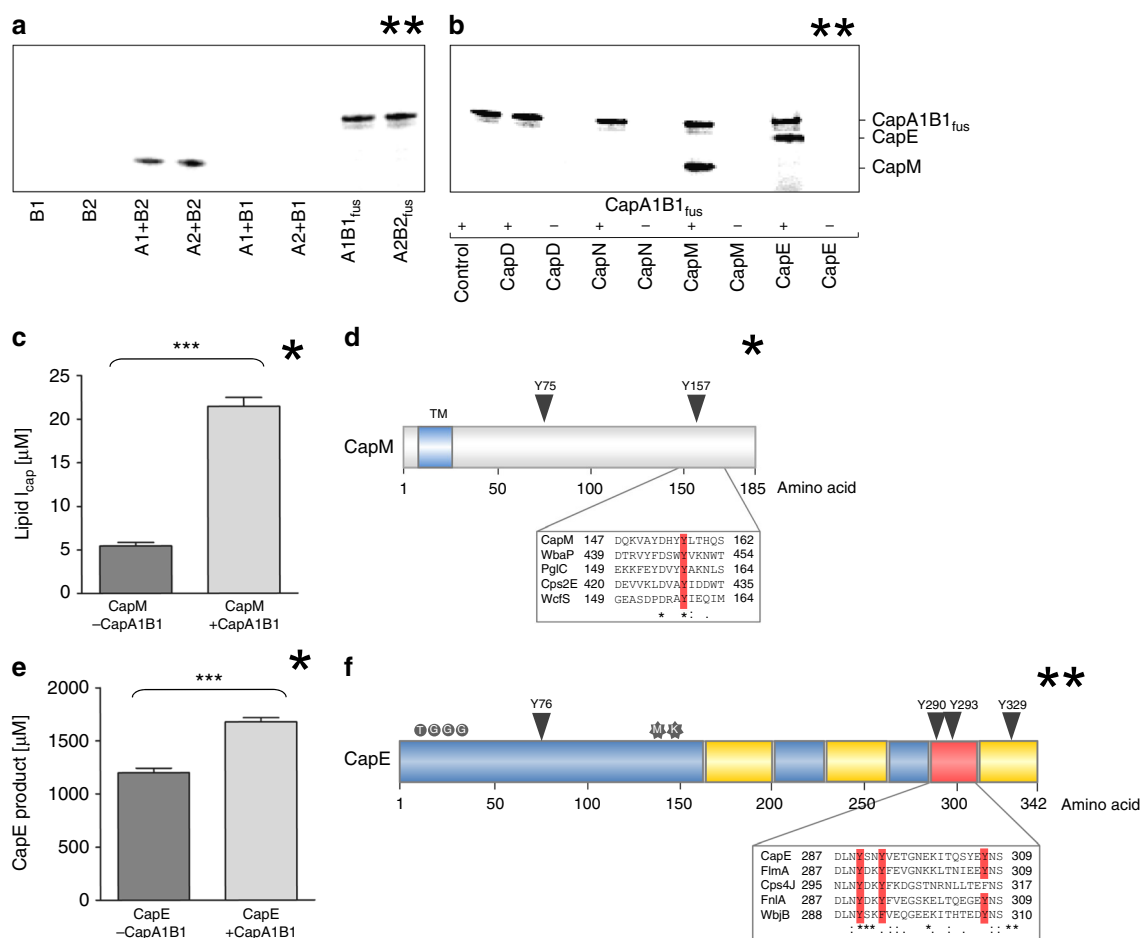


**Fig. 3** Tyrosine phosphorylation positively controls CapM and CapE activity. **a** CapAB autokinase activity was assayed in the presence of [<sup>33</sup>P]ATP using either native proteins or kinase activator CapA1 and tyrosine kinase CapB1 fused into a single polypeptide (CapA1B1<sub>fus</sub>). Phosphotransfer was analyzed by SDS-PAGE and phosphoimaging. **b** CapM and CapE are phosphorylated by the CapA1B1<sub>fus</sub> tyrosine kinase complex. Putative target proteins (3 μg) were assayed for phosphotransfer in the presence and absence of CapA1B1<sub>fus</sub>, CapA1B1<sub>fus</sub>, 50.2 kDa; CapB2, 25.3 kDa; CapE, 38.6 kDa; CapD, 69.1 kDa; CapM, 21 kDa; CapN, 33.7 kDa. **c** Impact of CapA1B1 kinase activity on CapM glycosyltransferase activity. CapM was incubated in presence of either active CapA1B1 (light grey) or heat-inactivated CapA1B1 (dark grey) with UDP-D-[<sup>14</sup>C]FucNAc and C<sub>55</sub>P. After extraction with BuOH/PyrAc, reactions were analyzed by TLC and phosphoimaging. **d** Topology and CapAB phosphorylation site (arrow) of CapM. The protein is anchored in the membrane by one reentrant transmembrane domain. The catalytic domain is located in the cytoplasm. Sequence alignment of homologous proteins containing the conserved Tyr phosphorylation site (red) is boxed. (from top to bottom: *S. aureus*, *Salmonella enterica*, *Campylobacter concisus*, *Streptococcus pneumoniae* and *Bacteroides fragilis*). **e** Impact of CapA1B1 kinase activity on CapE-mediated substrate conversion. CapE was incubated in presence of either active CapA1B1 (light grey) or heat-inactivated CapA1B1 (dark grey) with UDP-D-GlcNAc. Reactions were analyzed by CE. **f** Mapping of CapE phosphorylation sites. Tyr phosphorylation sites are marked by arrows. Cofactor binding site, substrate-binding site and the mobile loop are marked blue, yellow and red, respectively. The active site motif MxxxK (stars) and the cofactor binding motif TGxxGxxG (circles) are highlighted. A sequence alignment of the mobile latch (red) of selected homologous proteins from different species is boxed (from top to bottom: *S. aureus*, *Bacillus cereus*, *Streptococcus pneumoniae*, *Enterococcus faecium*, *Pseudomonas aeruginosa*). Experiments were performed in triplicate. The error bars represent the  $\pm$  standard deviation (SD) from three biological replicates. Statistical significance was analyzed by an unpaired *t* test (\*\*\*) *p* < 0.005



(Fig. 3a, lane 7). A full-length CapA2B2 fusion protein, which was constructed for reasons of comparison, showed comparable autokinase activity (lane 8). This finding contradicts recent suggestions that CapB1 might be a pseudokinase devoid of catalytic activity<sup>41</sup>.

CapA1B1-mediated phosphotransfer on putative target proteins involved in CP biosynthesis revealed tyrosine phosphorylation of the glycosyltransferase CapM (21 kDa) and the dehydratase CapE (38.6 kDa) (Fig. 3b, Supplementary Figure 5b). In contrast, recombinant CapD, CapN, CapF, CapG or CapL were not phosphorylated (Fig. 3b, Supplementary Figure 5c). The opposing PHP class phosphatases CapC1 and CapC2 were able to antagonistically dephosphorylate CapB kinase and target proteins (Supplementary Figure 5d).

Phosphorylation of CapM by the CapA1B1 fusion increased lipid  $I_{cap}$  synthesis 4-fold (Fig. 3c), showing that CapAB-mediated signaling stimulates the priming step of CP biosynthesis in *S. aureus* by enhancing the rate of CapM-catalyzed glycosyl transfer and thus likely controlling the consumption of the shared carrier  $C_{55}P$ .

In silico phosphorylation site prediction (NetPhos 3.1)<sup>42</sup> identified tyrosines 75 and 157 as putative phosphosites in CapM (Fig. 3d). The highly conserved Tyr157 appears to be the primary phosphorylation site in CapM, since tyrosine phosphorylation and the concomitant stimulatory effect on the catalytic activity was completely abolished in the CapM\_Y157F mutant (Supplementary Figure 6a,b). In contrast, changing Tyr75 to Phe had only a minor effect on the protein's ability to be catalytically activated by CapA1B1-mediated phosphotransfer. Both mutant proteins retained catalytic activity comparable to wild-type CapM in the absence of CapA1B1 (Supplementary Figure 6b) showing that Tyr157 represents the crucial regulatory CapAB phosphorylation site on CapM.

The CapA1B1-mediated stimulation of CapM activity is also reflected by enzyme kinetics, revealing a  $K_m$  value of  $2,309 \pm 311.8 \mu M$  for UDP-D-FucNAc and a  $V_{max}$  value of  $0.5559 \pm 0.02645 \text{ pmol min}^{-1} \mu g^{-1}$  in the absence of CapA1B1 and a lowered  $K_m$  value of  $996.2 \pm 136.2 \mu M$  and an increased  $V_{max}$  of  $1.0688 \pm 0.0358 \text{ pmol min}^{-1} \mu g^{-1}$  in the presence of CapA1B1 (Supplementary Figure 6c). Moreover, a CapM phosphomimetic in which Tyr157 was exchanged to Glu displayed a  $K_m$  value of  $1383 \pm 267.3 \mu M$  and a  $V_{max}$  value of  $0.8625 \pm 0.04708 \text{ pmol min}^{-1} \mu g^{-1}$  in the absence of CapA1B1, substantiating the stimulatory impact of CapM phosphorylation on Tyr157 (Supplementary Figure 6c).

In vitro kinase assays further identified CapE as a CapA1B1 target (Fig. 3e). Tryptic fragments of in vitro phosphorylated CapE were analyzed by nanoscale liquid chromatography coupled to tandem mass spectrometry (nanoLC-MS/MS), and Tyr76 of the CapE protein was found to be phosphorylated (Supplementary Figure 7a). This residue is located in proximity to the conserved TGxxGxxG motif required for cofactor binding and to the MxxxK catalytic site<sup>43</sup> (Fig. 3f). Three other phosphotyrosine residues (Tyr290, Tyr293 and Tyr329), were mapped to a C-terminal loop of CapE (Fig. 3f; Supplementary Figure 7a). In CapE in vitro assays with active CapAB, the conversion of UDP-D-GlcNAc was increased by 40%, demonstrating that the CapE catalyzed reaction is positively modulated through phosphorylation (Fig. 3e).

The role of the potential regulatory CapAB phosphorylation sites was probed in a site-directed mutagenesis study. As determined by CE quantification, replacing either Tyr76 of CapE or the three C-terminal tyrosine residues Tyr290, Tyr293, and Tyr329 with Phe diminished the activating effect of CapA1B1 on CapE. The stimulatory effect of CapA1B1 on the conversion of UDP-GlcNAc was completely abolished when all four tyrosine

residues were mutated to Phe, confirming their role as regulatory phosphorylation sites on CapE (Supplementary Figure 7b).

### CapA1 is a dual-function phosphodiesterase/kinase activator protein.

When purified lipid  $I_{cap}$  was incubated in the presence of CapA1, an additional lipid band was detected by TLC analysis (Fig. 4a), which was not visible in the negative control with heat-inactivated CapA1, indicating enzymatic conversion of the first CP lipid precursor. Intriguingly, the reaction product displayed an identical  $R_f$  value as the lipid carrier  $C_{55}P$ . MALDI-TOF MS analysis determined a mass of  $m/z$  845.610 (negative mode;  $[M-H]^-$ ) for the purified lipid product, confirming that CapA1 is able to catalyze the cleavage of the pyrophosphate linkage within the lipid  $I_{cap}$  intermediate to release  $C_{55}P$  (Fig. 4b). Of note, CapA1 was unable to cleave the peptidoglycan precursor lipid  $II_{PG}$ , but was able to hydrolyze the WTA precursor lipid III (Supplementary Figure 8). The facts that CapA1 interacts with lipid-linked CP precursors, and exhibits phosphodiesterase activity towards lipid  $I_{cap}$ , implies additional functions for this protein in CP biosynthesis, polymerization and attachment processes that go beyond being a mere “transmembrane activator”. Importantly, no cleavage of lipid  $I_{cap}$  or lipid  $III_{WTA}$  was observed with the CapA1 paralogue CapA2 (Fig. 4a), revealing functional differences between the two proteins.

CapA1 is anchored to the cytoplasmic membrane via two transmembrane domains flanking an outside loop comprising 130 amino acids (Fig. 4c), which likely represents a dual function sensory/catalytic domain involved in recognition and processing of membrane-bound CP precursors.

As evidenced in previous research, CapA1 is crucial for efficient capsule formation in *S. aureus*<sup>44</sup>. Corroborating these studies, complementation with pCapA1 *in trans* enhanced CP production in the serotype 8 strain MW2 (Fig. 4d). Strain MW2 carries a frameshift mutation in *capA1* (*cap5A*) that results in expression of a truncated version (171 aa) of the full-length gene product (222 aa)<sup>45</sup>. In contrast, deletion of *capA2* in *S. aureus* Newman did not affect in vivo CP production (Fig. 4d). Similarly, the deletion of cognate CapB kinases revealed, that *capB1* but not *capB2* is required for CP production (Supplementary Figure 7c). In spite of the functional redundancy and overlapping protein target specificities of CapA1B1 and CapA2B2 observed in our in vitro phosphorylation assays, the two kinase complexes clearly have distinct roles in cell physiology.

In contrast to CapA1, CapA2 is not encoded within the *cap5* operon, and does not exhibit phosphodiesterase activity towards lipid  $I_{cap}$ , which led us to conclude that CapA2 has a distinct function in the biosynthesis of the bacterial cell envelope. More recently, the *S. aureus* exopolysaccharide poly-N-acetyl- $\beta$ -(1,6)-glucosamine (PNAG; also referred to as polysaccharide intercellular adhesin) has been reported to bind to the CapA2 receptor loop<sup>46</sup>, suggesting that PNAG might represent a molecular signal detected by CapA2. We therefore investigated the influence of purified PNAG and CP5 on the autophosphorylation rate of the CapAB complexes. As revealed by in vitro kinase assays, CapA2-induced autophosphorylation of CapB2 was inhibited in the presence of PNAG, as well as in the presence of CP5, in a concentration-dependent manner (Supplementary Figure 9). In contrast, CapA1-induced phosphorylation of CapB2 was not diminished, indicating that the observed modulatory effect of exopolysaccharide molecules is mediated via an interaction with the transmembrane activator protein CapA2, and not via a direct inhibitory interaction with the protein kinase CapB2. This finding further substantiates differential roles for CapA1 and CapA2 in cell envelope biosynthesis.

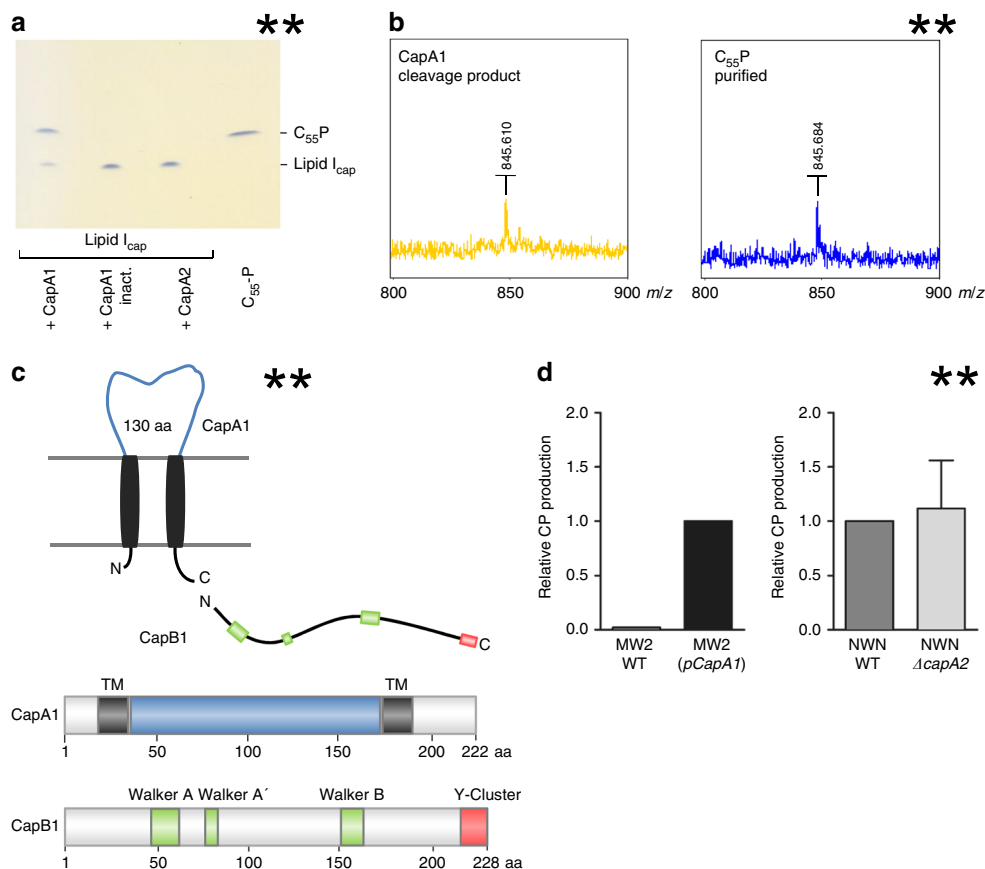


**Fig. 4** Cap1 exhibits phosphodiesterase activity towards lipid-linked capsule precursors. **a** Purified lipid  $I_{cap}$  (2 nmol) was incubated in the presence of either CapA1 or CapA2 (4  $\mu$ g each). After extraction with BuOH/PyAc, reactions were analyzed by TLC and PMA staining. **b** MS analysis of the CapA1 cleavage product isolated via preparative TLC. MALDI-TOF MS spectra were obtained with a Biflex III instrument running in negative mode. The  $m/z$  of 845.61 corresponds to the singly charged  $C_{55}P$  molecule, which has a measured mass of 845.68 and a calculated neutral mass of 846.67. **c** CapA1 is anchored to the cytoplasmic membrane via two transmembrane helices flanking an extracytoplasmic loop of 130 amino acids. The catalytic domains of CapB1 contains the Walker A, A' and B motifs (green); a tyrosine-rich region containing the phosphorylation sites is present at the C-terminus (red). **d** ELISA-based quantification of CP production in *S. aureus* MW2 complemented *in trans* with pCapA1 (left) and *S. aureus* Newman wild type and a  $\Delta capA2$  deletion mutant (right). Experiments were performed in triplicate. The error bars represent the mean  $\pm$  SEM from three biological replicates

**LcpC catalyzes the ligation of CP to lipid II.** Structural analysis and phenotypic studies suggest that members of the LCP protein family catalyze the transfer of undecaprenyl-linked intermediates onto the C6-hydroxyl function of *N*-acetylmuramic acid in PG, thereby promoting attachment of WTA and CP in Gram-positive bacteria<sup>20,47</sup>. *S. aureus* encodes three LCP enzymes with semi-redundant functions<sup>21</sup>. As deduced from knockout mutant studies, CP attachment is preferentially catalyzed by LcpC, though LcpA and LcpB may partially compensate for the loss of LcpC<sup>21</sup>.

To investigate the proposed role of LcpC *in vitro* purified [<sup>14</sup>C] lipid  $I_{cap}$  was incubated with purified LcpC protein and lipid  $II_{PG}$  as a potential acceptor substrate. In this setup, LcpC was able to catalyze cleavage of the donor substrate lipid  $I_{cap}$  and catalyze attachment of the phosphoryl-sugar moiety to the ultimate PG precursor lipid II (Fig. 5a), resulting in a reaction product ( $II_{PG}$ -<sup>14</sup>C-CP) that migrates slower on TLC. Identical results were obtained when [<sup>14</sup>C]-labeled lipid  $II_{PG}$  and non-labeled lipid  $I_{cap}$  were used as the reaction substrates (Fig. 5b), further verifying the identity of the ligation product. Quantitative analysis revealed that ~50% of the CP lipid precursor was attached to lipid II (Fig. 5c). Strikingly, the LcpC-mediated transferase reaction was significantly enhanced when CapA1 was included in the reaction mixture, indicating cooperative action of the transmembrane activator/phosphodiesterase protein and LcpC (Fig. 5c).

CapA1 alone was unable to catalyze the attachment of the CP precursor (Supplementary Figure 10a). Of note, LcpC was able to catalyze hydrolytic cleavage of lipid  $I_{cap}$ , but not of lipid  $II_{PG}$ , a reaction that would likely be deleterious *in vivo* (Supplementary Figure 10b, c).

Interestingly, PBP2 added posterior to the LcpC reaction efficiently catalyzed the transglycosylation of lipid  $II_{PG}$ -CP (Fig. 5a, b). The resulting polymerized PBP reaction product is not extracted from the reaction mixture, thus lipid bands vanish from the TLC. The antibiotic moenomycin, known to inhibit the PBP2 catalyzed transglycosylation, fully blocked the polymerization reaction (Fig. 5b). Importantly, LcpC was further able to efficiently transfer the disaccharide of lipid  $II_{cap}$  and the trisaccharide of the ultimate CP lipid intermediate lipid  $III_{cap}$  to lipid  $II_{PG}$ , as evidenced by the altered migration of the respective ligation products ( $R_f = 0.26$  and  $R_f = 0.22$ , respectively). Efficient processing of ligation products by PBP2 shows that CP attachment could occur in parallel to PG assembly (Fig. 5d).

Interestingly, antisense-RNA mediated depletion of CapA1 in a triple  $\Delta lcp$  mutant was lethal, indicating that CapA1 hydrolysis of  $C_{55}P$ -coupled CP and WTA precursors contributes to rescue *S. aureus* from the accumulation of toxic intermediates (Supplementary Figure 10d) and further supports a functional link between CapA1 and LcpC.

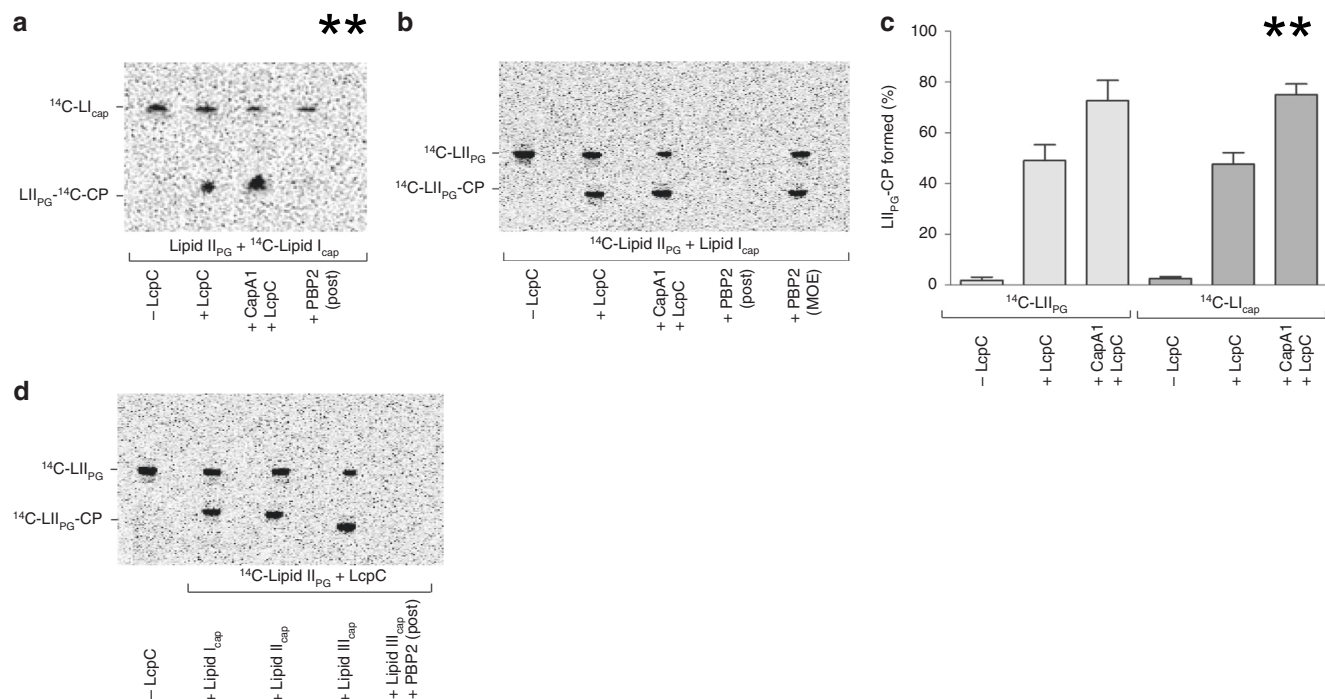


**Fig. 5** Attachment of CP to the ultimate PG building block lipid II<sub>PG</sub> is mediated by LcpC. **a** [<sup>14</sup>C]lipid I<sub>cap</sub> and lipid II<sub>PG</sub> or **b** lipid I<sub>cap</sub> and [<sup>14</sup>C]lipid II<sub>PG</sub> were incubated with LcpC in the absence or presence of CapA1. The resulting reaction product (LII<sub>PG</sub>-CP; bold) exhibits an altered migration behavior on the TLC compared to the individual substrates, lipid II<sub>PG</sub> and lipid I<sub>cap</sub>. PBP2 catalyzes the transglycosylation of the LcpC reaction product LII<sub>PG</sub>-CP (lane 4) resulting in the polymerization of radiolabeled lipid II<sub>PG</sub>-CP into hydrophilic glycan strands that retain in the water phase and are not extracted after BuOH/PyAc treatment resulting in disappearance of the corresponding band on the chromatogram. The PBP2 catalyzed conversion is inhibited in the presence of the antibiotic moenomycin (MOE; 10 μM) (B, lane 5). **c** Quantification of lipid I<sub>cap</sub> attachment to lipid II<sub>PG</sub>. Radiolabeled bands were quantified by phosphoimaging. Experiments were performed in triplicate. The error bars represent the ± SD from three biological replicates. **d** LcpC catalyzes the attachment of lipid II<sub>cap</sub> (lane 3) and the ultimate CP lipid intermediate lipid III<sub>cap</sub> (lane 4) and the final reaction product is processed by PBP2 added posterior to the LcpC reaction (lane 5). Representative TLC of 2 independent experiments

**Capsule biosynthesis is negatively controlled by PknB.** As evidenced in previous research, the eukaryotic serine/threonine kinase (ESTK) PknB of *S. aureus* is involved in the regulation of cell envelope biogenesis processes<sup>48–50</sup> and was more recently shown to sense lipid II<sub>PG</sub><sup>51</sup>. Testing CapM in an in vitro kinase assay showed PknB-mediated phosphorylation of the priming GT (Fig. 6a). Moreover, quantitative analysis of the in vitro CapM-catalyzed reaction revealed an up to 30% decrease in lipid I<sub>cap</sub> synthesis when purified PknB kinase and ATP were included in the reaction mixture, compared to a control reaction containing heat-inactivated PknB, suggesting that ESTK signaling negatively controls the activity of CapM (Fig. 6b). LC/MS-analysis revealed PknB-mediated phosphotransfer onto Thr67, Thr128 and Thr134 of CapM (Supplementary Figure 11). Thr134 is highly conserved among homologous bacterial glycosyltransferases, located in proximity of the membrane interface and the amphipathic helices D and I (Supplementary Figure 3c) and may thus be the most promising candidate for a regulatory PknB-phosphorylation site on CapM.

Intriguingly, the kinase protein CapB1 was also identified as potential phosphorylation target of PknB (Fig. 6c), indicating the possibility of kinase cross-talk. To further explore this finding, the autophosphorylation activity of the CapA1B1 complex was assessed in the presence of PknB. The overall phosphorylation intensity of CapA1B1 was decreased by 34% in the presence of active PknB (Fig. 6d), compared to the heat-inactivated negative control, showing that PknB-mediated serine/threonine phosphorylation inhibits CapB1 autophosphorylation on tyrosine. Thr8 was identified as the specific phosphorylation site on CapB1 by

LC/MS analysis (Supplementary Figure 12a) and a CapA1B1<sub>fus</sub> phosphomimetic in which this Thr was exchanged to Glu resulted in a significantly reduced CapB1 autophosphorylation (Supplementary Figure 12b, c), suggesting that PknB-mediated phosphorylation interferes with the CapB1 activation by CapA1<sup>41,52</sup>. In contrast, an exchange of Thr8 to Ala did not affect CapA1B1<sub>fus</sub> autophosphorylation (Supplementary Figure 12b,c).

To determine whether the observed inhibitory effect of PknB in vitro would translate into an in vivo effect, we compared CP5 production in *S. aureus* Newman and in an isogenic *pknB* deletion mutant. Consistent with the proposed role of PknB as negative regulator of CP biosynthesis, the amount of cell-associated CP5 was 5-fold higher in the *pknB* mutant compared to the parental strain and complementation of the  $\Delta pknB$  mutant *in trans* restored CP production to wild-type level (Fig. 6e).

The in vitro and in vivo data reveal that PknB signaling serves to reduce CapM GT activity, as well as CapA1B1 autokinase activity, allowing for a shutdown of CP production likely ensuring a sufficient supply of precursors for PG formation, and thus maintenance of cell wall architecture and function.

## Discussion

Biosynthesis of the *S. aureus* CP shows similarity to the syntheses of PG and WTA, in that all pathways share a pool of essential precursors, i.e. the lipid carrier undecaprenyl-phosphate and UDP-D-GlcNAc<sup>1,53</sup>. Since the availability of C<sub>55</sub>P within the bacterial cell is limited<sup>22</sup>, distribution and prioritization for the alternate metabolic pathways need to be tightly controlled in time and space to ensure bacterial viability.

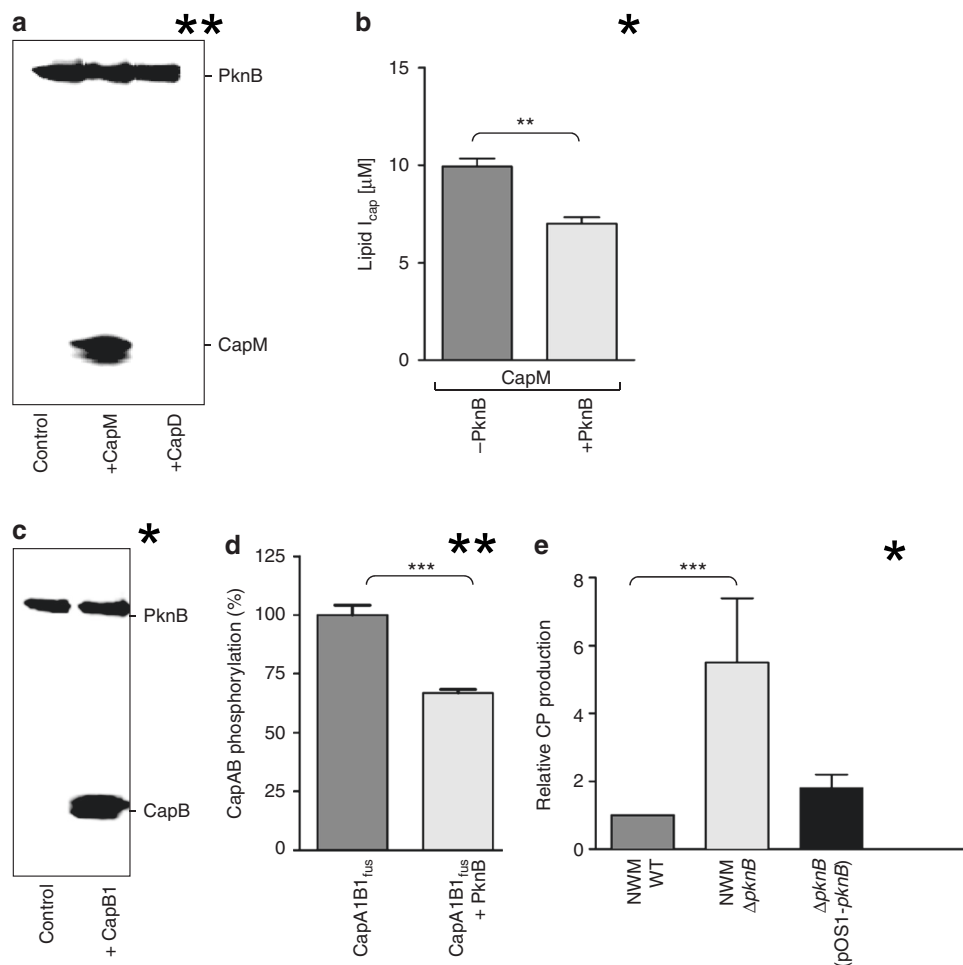


**Fig. 6** CapM and CapB1 are protein targets of the ESTK PknB. **a** CapM is phosphorylated by PknB. Putative target proteins (3 μg) were incubated with PknB in the presence of [<sup>33</sup>P]ATP and reactions were analyzed by SDS-PAGE and phosphoimaging. **b** Impact of PknB kinase activity on CapM GT activity. CapM was incubated in presence of either active PknB (light grey) or heat-inactivated PknB (dark grey) with UDP-D-[<sup>14</sup>C]FucNAc and C<sub>55</sub>P. After extraction with BuOH/PyrAc, reactions were analyzed by TLC and phosphoimaging. Experiments were performed in triplicate. The error bars represent the ± SD from three biological replicates. Statistical significance was analyzed by an unpaired *t*-test (\*\**p* < 0.05). **c** CapB1 is phosphorylated by PknB. Putative target proteins (3 μg) were incubated with PknB in the presence of [<sup>33</sup>P]ATP, and reactions were analyzed by SDS-PAGE and phosphoimaging. **d** Quantification of CapB autophosphorylation in the absence and presence of PknB. Experiments were performed in triplicate. The error bars represent the ± SD from three biological replicates. Statistical significance was analyzed by an unpaired *t*-test (\*\*\*) *p* < 0.005). **e** ELISA-based quantification of CP production in a Δ*pknB* deletion strain, the corresponding parental strain *S. aureus* Newman (WT) and complementation of the Δ*pknB* mutant *in trans*. Experiments were performed in triplicate. The error bars represent the ± standard error of the mean (SEM) from three biological replicates. Statistical significance was analyzed by an unpaired *t*-test (\*\*\*) *p* < 0.005)

Reversible protein phosphorylation appears an elegant mechanism to ensure a coordinated and temporally controlled flux of intimately shared cell envelope metabolites. Several biosynthetic enzymes involved in polysaccharide production have been identified as endogenous substrates of bacterial tyrosine kinases, for instance the UDP-glucose 6-dehydrogenases TaaA and YwqF of *Bacillus subtilis*<sup>54</sup>, the homologous *E. coli* UDP-glucose dehydrogenase Ugd<sup>55</sup> and the UDP-ManNAc dehydrogenase CapO<sup>17</sup> involved in *S. aureus* CP biosynthesis.

The fact that CapO, involved in the third CP reaction cascade (Fig. 1), is a regulatory target of the CapAB kinase complex<sup>17</sup>, led us to assume that additional checkpoints within the biosynthetic pathway are also controlled by CapAB, which turned out to be the case for CapE and CapM. Four tyrosine residues in the dehydrogenase CapE were identified as the specific phosphorylation sites, with Tyr76, Tyr290 and Tyr293 being widely conserved among homologous proteins from different pathogens. Interestingly, these residues are located in strategic functional

regions of CapE: next to the cofactor binding site, in close proximity to the active site, and within a recently described mobile loop (Fig. 3f). Crystal structure analysis identified this mobile latch to connect two CapE protomers within the hexameric complex (trimer of dimers) and showed that the latch of one dimerization partner is associated with the substrate-binding domain of the contiguous CapE monomer, and *vice versa*, suggesting that this mobile loop is involved in regulating the access of the UDP-D-GlcNAc substrate to the active site<sup>56</sup>. Since contacts to Tyr290 and Tyr293 appear to be involved in the interaction, phosphorylation might induce conformational changes that facilitate access of UDP-D-GlcNAc to the active site, thereby increasing CapE enzymatic activity.

For the monotopic GT CapM, we identified the conserved tyrosine residue at position 157 as the CapA1B1 regulatory phosphorylation site which is in good agreement with the work of Minic et al. (2007) and supports the hypothesis that phosphorylation of the equivalent site in the *S. thermophilus*

\*\*

\*\*

phosphogalactosyl-transferase EpsE results in activation *in vivo*<sup>57</sup>. A recent structural analysis showed, that the equivalent tyrosine residue in PglC is involved in a hydrogen-bonding network that establishes intramolecular interactions between helices A, F and G<sup>37</sup> (Supplementary Figure 3c), suggesting that the phosphorylated amino acid side chain may affect relative strengths of hydrogen bonds and critical interactions in CapM.

**\*\*** Current hypotheses suggest a multifaceted role for BY-kinases in bacterial exopolysaccharide production. BY-kinase signalling may not only regulate the catalytic activity of polysaccharide biosynthetic enzymes, but also ensure the correct cellular localization of protein targets<sup>58</sup>. Moreover, it has been suggested that BY-kinases may interact with the export and polymerization machinery to control the level of CP production and/or CP chain length<sup>52,59</sup>. However, the exact mechanism through which this control is exerted, as well as the molecular signal sensed, remains enigmatic so far.

The phosphodiesterase activity of CapA1 described here is in good agreement with previous studies demonstrating the release of CP and WTA into the culture supernatant in LCP deletion mutants of different species<sup>60–63</sup>. An *lcpC* deletion mutant of *S. aureus* accumulated CP in the culture supernatant, indicating that LcpC is the key LCP enzyme for attachment of CP to the peptidoglycan in *S. aureus*<sup>21</sup>.

This study provides biochemical proof that LcpC catalyzes the attachment of CP to PG. Importantly, CP lipid precursor cleavage and transfer of the phosphosugar moiety were found to be enhanced in the presence of CapA1, suggesting that the transmembrane activator cooperates with LcpC by forming an interaction complex, thereby modulating the attachment of CP to the cell wall precursor. In line with this interpretation, Toniolo et al. (2015) reported that the extracellular domain of the CapA1 homolog CpsC of *Streptococcus agalactiae* may modulate LCP-mediated CP attachment in response to the phosphorylation state of the BY kinase CpsD<sup>64</sup>.

The natural PG acceptor substrate of LcpC is elusive; possible acceptor structures include the ultimate PG precursor lipid II, as well as “nascent” and crosslinked PG. More recently, LcpA and LcpB were shown to attach a shortened, soluble (C<sub>20</sub>P) WTA precursor to a preformed “nascent PG” oligomer<sup>65</sup>, but not to a lipid II<sub>PG</sub> mimetic lacking the natural undecaprenyl tail. In contrast, the biochemical analyses presented here clearly demonstrate that CP is efficiently attached to lipid II<sub>PG</sub> by the LcpC enzyme, and that PBPs are able to polymerize the resulting reaction product. With regard to the membrane localization of both, substrates and enzymes, and the interdependence and intimate connection of the enzymatic machineries, lipid II<sub>PG</sub> seems the most plausible acceptor.

**\*\*** CP lipid intermediates were further hydrolyzed by LcpC in the absence of the acceptor substrate as predicted by structural analysis of Cps2A of *S. pneumoniae*<sup>20</sup>, which was not observed for LcpA and LcpB proteins<sup>65</sup>. *In vitro*, all three CP lipid intermediates were efficiently processed by LcpC, although the proximal full-length undecaprenyl-pyrophosphoryl-linked sugar moiety appears sufficient for CP precursor recognition. Likewise, the first C<sub>55</sub>P-linked sugar unit of the O-antigen repeat unit contains the recognition information necessary for catalysis by the O-antigen ligase Waal<sup>66</sup>.

The biosyntheses of the cell envelope components PG, WTA and CP have to be coordinated in time and space, since the enzymatic machineries and their individual components are functionally related to each other or intimately connected<sup>1,53</sup>. The complex interplay between different cell envelope pathways becomes evident upon inhibition of individual biosynthetic steps. In analogy to the WTA biosynthesis in *S. aureus*, where late stage biosynthetic genes have been shown to be conditionally essential

(“essential gene paradox”;<sup>67</sup>), Yother and co-workers reported that deletion of the late stage CP biosynthesis genes, responsible for side chain assembly, polymerization or transport (*cps2K*, *cps2J*, and *cps2H*) in *Streptococcus pneumoniae*, is lethal<sup>68</sup>. Since the capsule is not required for cell viability *per se*, the damage to the cell envelope is most likely due to an inhibitory effect on PG biosynthesis, resulting from sequestration of CP lipid intermediates probably reducing the undecaprenyl-phosphate level to a critical point where PG synthesis is affected. Since we found CapA1 to hydrolyze CP lipid intermediates even in the absence of LCP proteins and that depletion of CapA1 in a *S. aureus*  $\Delta$ *lcp* triple mutant was lethal, we conclude that CapA1-mediated cleavage of dead-end lipid-linked products might serve as a rescue mechanism counteracting depletion of C<sub>55</sub>P to critical levels.

The ESTK PknB is another important player in the orchestration of cell wall polymer biosynthesis and has been implicated in coordinating PG cross-wall formation, autolysis and cell division in *S. aureus*<sup>48–50</sup>. Our findings that PknB downregulates CapM and with the BY-kinase CapA1B1 operating in an antagonistic manner underpins the importance of CapM as crucial enzymatic checkpoint. Moreover, *in vitro* kinase assays indicate that PknB-mediated phosphotransfer onto CapB1 modulates the activity of the CapA1B1 BY-kinase complex itself, thus identifying another activity by which PknB may exert control on CP biosynthesis. Cross-phosphorylation of ESTKs and BY-kinases has also been reported in *B. subtilis*<sup>69</sup>. The CapB homolog PtkA was identified as *in vitro* phosphorylation target of the ESTK PrkC<sup>69</sup>. Moreover, PtkA autophosphorylation *in vivo* was strongly enhanced in a  $\Delta$ *prkC* strain, suggesting that PtkA BY-kinase activity is negatively regulated by PrkC-mediated phosphotransfer<sup>70</sup>.

Corroborating the *in vitro* results, CP production was substantially elevated in a *pknB* deletion mutant of *S. aureus*. Besides decreasing the activity of CP biosynthesis proteins by direct phosphorylation, PknB kinase activity may serve to increase the cellular concentration of UDP-MurNAc-pentapeptide and lipid II<sub>PG</sub><sup>71</sup>, cell wall metabolites that were identified as inhibitors of CapD enzymatic activity<sup>19</sup>. Moreover, PknB signaling was reported to influence the transcription of the *cap5* gene cluster<sup>72</sup>, suggesting that this sensor kinase is part of a multilayered signal-transduction network that coordinates CP formation in space and time.

The finding that CP and PG production are inversely controlled by PknB further substantiates a key role for PknB in the coordinate regulation of Gram-positive cell surface glycopolymers. In exponentially growing cells, PknB-mediated Ser/Thr phosphorylation positively controls PG biosynthesis, while exerting negative control on CP production (Fig. 7).

With respect to biosynthesis of the *S. aureus* CP, the CapA1B1 complex may be particularly important for short-term regulation. More recently, Elsholz and co-workers showed that exopolysaccharide (EPS) production in *Bacillus subtilis* is subject to a positive feedback loop that ties the synthesis of the polymer to its own concentration<sup>46</sup>. Regulation of EPS synthesis is mediated by the EpsAB tyrosine kinase complex, whereby direct recognition of EPS by the extracellular domain of the membrane component EpsA seems to result in stimulation of kinase activity<sup>46</sup>.

The activator/phosphodiesterase CapA1 directly and specifically interacts with lipid-bound CP precursors, and CapA1B1 signaling stimulates the activity of CP biosynthetic enzymes, triggering enhanced CP production in late-exponential and stationary phase (Fig. 7).

*S. aureus* PknB specifically interacts with lipid II<sub>PG</sub>, likely responding to cellular pool levels of the ultimate peptidoglycan precursor<sup>51</sup>. It is thus conceivable that in order to balance the pool levels of the lipid II<sub>PG</sub> acceptor and the CP donor substrate,

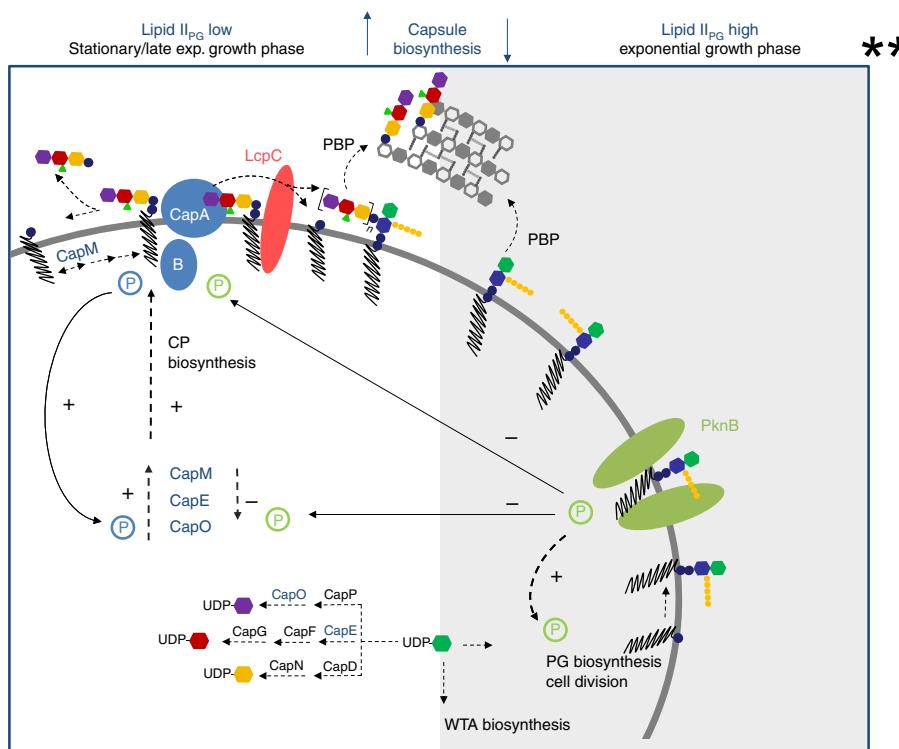


**Fig. 7** Model for the regulation of CP biosynthesis and the attachment to PG in *S. aureus*. The CapA1B1 tyrosine complex (blue) positively controls multiple enzymatic checkpoints to orchestrate CP biosynthesis and precursor consumption during late exponential growth phase (white box). By catalyzing tyrosine phosphorylation (blue 'P') of biosynthetic enzymes CapE, CapO and CapM, CapA1B1 positively controls the synthesis of both soluble and lipid-linked CP precursors. The membrane-anchored component CapA1 possesses a dual function; CapA1 recognizes lipid-bound CP building blocks and catalyzes the cleavage of the pyrophosphate linkage, releasing the essential isoprenoid lipid carrier C<sub>55</sub>P. CP transfer is catalyzed by LcpC (red), which uses the ultimate peptidoglycan (PG) precursor lipid II<sub>PG</sub> as an acceptor substrate. During exponential growth phase (grey shading), the insertion of new PG material (LII<sub>PG</sub>) into the cell wall network is increased; UDP-GlcNAc and C<sub>55</sub>P are preferably channeled into PG and WTA biosynthesis, while CP production is low. The Ser/Thr kinase PknB (green) contributes to the control of cell wall biosynthesis and cell division. Control of CP formation during ongoing PG synthesis is achieved by PknB via Ser/Thr phosphorylation (green 'P'). PknB negatively controls the activity of the priming glycosyltransferase CapM to regulate the initial C<sub>55</sub>P-consuming reaction within the CP biosynthetic pathway. Furthermore, PknB cross-talks with the CapAB complex, thus allowing control of the CP biosynthetic machinery on multiple levels, in response to the status of PG biosynthesis. The model highlights central biosynthetic precursors as important signal molecules situated at the interface of different pathways, integrated in feedback loops to control biosyntheses and the flux of shared precursors

which are both built on the lipid carrier C<sub>55</sub>P, PknB and CapA1B1 antagonistically control biosyntheses to ensure vital cycling of the essential C<sub>55</sub>P lipid carrier. In addition, CapA1 might contribute to the correct localization of the CP assembly machinery, as proposed for *S. agalactiae*<sup>64</sup>, which has to integrate precursor transport and CP polymerization. This interaction protein network thus appears to contribute to the spatiotemporal coordination of CP biosynthesis with PG synthesis (Fig. 7), rendering proteins such as CapA1 and LcpC, exposed at the cell surface and devoid of eukaryotic homologs, potentially attractive antibacterial or antivirulence targets.

**Methods**

**Strains.** *S. aureus* Newman NCTC8178 was maintained on blood or lysogeny broth (LB; Oxoid) agar. *Escherichia coli* strains BL21 and C43 used for over-expression of recombinant His<sub>6</sub>-tag fusion proteins were maintained on LB-agar plates containing 50 µg ml<sup>-1</sup> ampicillin or 25 µg ml<sup>-1</sup> kanamycin. CP5 production was quantified from *S. aureus* cultivated on Columbia medium supplemented with 2% NaCl and 1.5% agar. The Newman  $\Delta$ *pknB* mutant was kindly provided by Dr. Knut Olsen (Wuerzburg, Germany), and RN4220 carrying pCapA1 was provided by Dr. Gabriele Bierbaum (Bonn, Germany)<sup>44</sup>. *S. aureus* strain MW2 (NRS123) and strains from the Nebraska transposon mutant library<sup>73</sup> were obtained from the Network on Antimicrobial Resistance in *Staphylococcus aureus* program, which was supported by the National Institute of Allergy and Infectious Diseases of the National Institutes of Health (contract HHSN272200700055C). The Nebraska library is comprised of derivatives of the serotype 5 strain USA300 LAC (cured of

three plasmids) in which individual nonessential genes were disrupted by the insertion of the mariner transposon (Tn) *bursa aurealis* and includes mutants in *capA2* (NE1286), *capB2* (NE75), *capA1* (NE302a), and *capB1* (NE135). Construction of *cap* deletion mutants is described in the Supplementary Methods. The *pknB* and Tn mutants were maintained on tryptic soy agar (TSA) plates with 5 µg ml<sup>-1</sup> erythromycin, and pCapA1 was maintained in *S. aureus* cultivated on TSA with 10 µg ml<sup>-1</sup> chloramphenicol. *S. aureus* Newman  $\Delta$ *lcpABC* mutants were kindly provided by Dr. Olaf Schneewind (Chicago, USA)<sup>21</sup> maintained on LB-agar plates. *S. aureus* strains carrying the plasmid pEPSA5 or the antisense plasmid pEPSA5-*capA1As* were maintained on TSA-agar plates supplemented with 34 µg ml<sup>-1</sup> chloramphenicol.

**Plasmid construction and site-directed mutagenesis.** Oligonucleotide primers were purchased from Eurofins MWG Operon (Germany). Primer pairs used for amplification of genomic sequences encoding *capA1*, *capA2*, *capB1*, *capB2*, *capA1B1fus*, *capA2B2fus*, *capA1As*, *capC1*, *capC2*, *capI*, *capL*, *capN*, *capM* and *lcpC* are listed in Supplementary Table 1. PCR reactions were carried out using Phusion DNA polymerase (NEB) and genomic DNA of the serotype 5 strain *S. aureus* Newman as template. PCR products were digested with type II restriction endonucleases (NEB; Supplementary Table 1) and ligated (T4 DNA ligase, Roche) with appropriately restricted expression vectors (Novagen). The PCR amplicon of the gene *capN* was inserted into pET24a. The vector pET21b was utilized for cloning of the *capI* and *capL* genes. The antisense fragment of *capA1* was inserted into pEPSA5. All other amplicons were introduced into pET28a. The resulting plasmids (Supplementary Table 2) were confirmed by DNA sequencing (Sequiseive, Germany). Plasmids pET24a-*capD*, pKBK50d, pET5F1.1, pKBK6a, pET28a-*pglF* and pET52b-*pknB* used for overexpression of CapD-His<sub>6</sub>, CapE-His<sub>6</sub>, CapF-His<sub>6</sub>, CapG-His<sub>6</sub>, PglF-His<sub>6</sub> and PknB-His<sub>6</sub> have been described previously<sup>13,19</sup>. To

enable expression of N-terminally His<sub>6</sub>-tagged CapA1B1 and CapA2B2 fusion proteins, the constructs *capA1B1fus* and *capA2B2fus* were amplified using the primer pairs *capA1\_F* and *capB1\_R*, and *capA2\_F* and *capB2\_R*, respectively. The QuikChange Lightning Mutagenesis Kit (Stratagene) was used according to the manufacturer's instructions to remove the stop codon of *capA* by site-directed mutagenesis (TTA > GCA); the respective mutagenesis primers (*capA1B1fus\_mut\_F*, *capA1B1fus\_mut\_R* and *capA2B2fus\_mut\_F* and *capA2B2fus\_mut\_R* (TAA > TAT) are given in Supplementary Table 1. Site-directed mutagenesis of plasmid pET28a-*capM* was performed to introduce amino acid exchanges Tyr75 (TAT) > Phe (TTT) (primers: *capM\_mutY75\_F*, *capM\_mutY75\_R*) and Tyr157 (TAC) > Phe (TTC) (*capM\_mutY157\_F*, *capM\_mutY157\_R*) in CapM. Likewise, plasmid pKBK50 was mutated to introduce amino acid exchanges Tyr76 (TAC) > Phe (TTC) (*capE\_mutY76\_F*, *capE\_mutY76\_R*), Tyr290/293 (TAT) > Phe (TTT) (*capE\_mutY290/293\_F*, *capE\_mutY290/293\_R*), and Tyr329 (TAT) > Phe (TTT) (*capE\_mutY329\_F*, *capE\_mutY329\_R*) into CapE. Site-directed mutagenesis of plasmid pET28a-*capA1B1* was performed to introduce amino acid exchanges Thr8 (ACA) > Glu (GAA) (primers: *capA1B1fus\_mutT8E\_F*, *capA1B1fus\_mutT8E\_R*) and Thr8 (ACA) > Ala (GCA) (primers: *capA1B1fus\_mutT8A\_F* and *capA1B1fus\_mutT8A\_R*) into CapA1B1<sub>fus</sub>. In order to produce a CapB2\_T8E mutant, site-directed mutagenesis of plasmid pET28a-*capB2* was performed using the primer pair *capB2\_mutT8E\_F* and *capB2\_mutT8E\_R* to introduce an amino acid exchange Thr8 (ACA) > Glu (GAA). PCR-mediated base pair exchange was confirmed by sequencing. The resulting plasmids, which were utilized for expression and purification of CapM and CapE mutant proteins containing single or multiple Tyr to Phe exchanges, are listed in Supplementary Table 2. pCapA1 was transduced from *S. aureus* RN4220 to strain MW2 with phage 11, with selection on medium containing 10 µg ml<sup>-1</sup> chloramphenicol. *S. aureus* Newman  $\Delta$ lcpABC was transformed by electroporation<sup>74</sup> with pEPSA5-*capAIAS* purified from *E. coli* DC10B, with selection on TSA containing 2.5% glucose and 34 µg ml<sup>-1</sup> chloramphenicol. Expression of the appropriate antisense fragment was induced on TSA-agar plates containing 500 mM xylose.

**Overexpression and purification of recombinant proteins.** *E. coli* strain BL21 (DE3) (Promega) was used as host for the recombinant expression of cytoplasmic enzymes (CapB1-His<sub>6</sub>, CapB2-His<sub>6</sub>, CapC1-His<sub>6</sub>, CapC2-His<sub>6</sub>, CapE-His<sub>6</sub>, CapF-His<sub>6</sub>, CapG-His<sub>6</sub>, CapO-His<sub>6</sub>, CapP-His<sub>6</sub> and PglF-His<sub>6</sub>) and *E. coli* strain C43 (DE3) (Promega) was used for the recombinant expression of integral membrane or membrane associated proteins (CapA1-His<sub>6</sub>, CapA2-His<sub>6</sub>, CapAB-His<sub>6</sub> fusion constructs, CapI-His<sub>6</sub>, CapL-His<sub>6</sub>, CapM-His<sub>6</sub>, CapD-His<sub>6</sub>, LcpC-His<sub>6</sub> and Strep-tagged PknB). *E. coli* strain BL21 (DE3) cells were grown at 37 °C in lysogeny broth (LB; Oxoid) and *E. coli* C43 (DE3) cells were grown at 30 °C in double-strength yeast extract-tryptone broth (2YT, Difco) containing the appropriate selective antibiotic (50 µg ml<sup>-1</sup> ampicillin or 25 µg ml<sup>-1</sup> kanamycin). At an OD<sub>600</sub> of 0.6, IPTG was added at a final concentration of 0.5 mM to induce expression of the recombinant protein. Expression times and temperatures were optimized for the individual constructs to ensure high yields of the different fusion proteins. The cultures for overexpression of CapA1, CapA2, CapAB fusion constructs, CapD, CapI, CapL, CapN, LcpC and PknB were induced at 20 °C for 16 h. All other *E. coli* BL21 (DE3) cultures and the *E. coli* C43 (DE3) cultures for the expression of CapM were induced at 30 °C for 4 h. After induction, cells were harvested (15 min, 4 °C, 7000 × g) and resuspended in lysis buffer (50 mM Tris-HCl, 300 mM NaCl, pH 7.5), which was supplemented with 1% (v/v) Triton X-100 (Sigma-Aldrich) for purification of CapA1, CapA2, CapAB fusion constructs and CapN or with 29 mM *n*-dodecyl-β-D-maltoside (DDM, Glycon Biochemicals) for purification of CapD, CapI, CapL, CapM and LcpC. Lysozyme (250 µg ml<sup>-1</sup>), DNase (50 µg ml<sup>-1</sup>) and RNase (10 µg ml<sup>-1</sup>) (Sigma-Aldrich) were added to the suspension; cells were incubated on ice for 30 min and sonicated. Cell debris was removed by centrifugation (20 min, 4 °C, 21,000 × g).

The supernatant was incubated with Ni-NTA-agarose slurry (Qiagen, Germany) for 2 h at 4 °C under gentle stirring. The mixture was then loaded onto a column support. After washing with lysis buffer, weakly bound material was removed with 10 and 20 mM imidazole. Recombinant proteins were eluted with buffer containing 300 mM imidazole. Five 500-µl fractions were collected each and stored in 30% (v/v) glycerol at -20 °C; preparations of CapE were dialyzed against 10 mM potassium phosphate buffer (KPi), pH 7.5 before storage. For PknB purification the pellet was resuspended in lysis buffer containing 1% (v/v) Triton X-100 and the suspension was incubated on ice for 1 h. Cell debris was spun down (20 min, 4 °C, 34,000 × g) and the clear supernatant was loaded onto a Strep-tactin agarose column (IBA, Germany). The column was washed twice with lysis buffer and PknB was eluted with Strep-tactin elution buffer (IBA, Germany). Purity of elution fractions was assessed by SDS-Page (NuPAGE; Invitrogen); protein concentrations were measured using Bradford reagent (Bio-Rad, Germany). Expression and purification of CapA1B1<sub>fus</sub>, CapE and CapM protein variants were carried out as described for the wild-type proteins.

**In vitro syntheses of soluble CP precursors.** UDP-D-GlcNAc and cofactors for enzyme assays were obtained from Sigma-Aldrich. Synthesis of the precursor UDP-2-acetamido-2,6-dideoxy-D-xylo-4-hexulose for mass spectrometric analysis was performed with a recombinant truncated version of the enzyme PglF from *C. jejuni*, as previously described<sup>19</sup>. The PglF reaction product was used as

substrate for reconstitution of CapN catalytic activity. For this purpose, PglF reactions were carried out overnight and quenched by heating (5 min, 95 °C). CapN catalyzed synthesis of UDP-D-FucNAc was carried out in a total volume of 40 µl. CapN (12 µg) was incubated in the presence of ~3 mM UDP-2-acetamido-2,6-dideoxy-D-xylo-4-hexulose, 1.875 mM NADPH, 8% (v/v) Triton X-100 and 10 mM KPi, pH 7.5, for 2 h at 30 °C. Synthesis of larger quantities of soluble capsule precursors for MALDI-TOF MS analysis was achieved by a 10-fold upscale of the synthesis reaction.

Alternatively, synthesis of UDP-D-FucNAc was performed in an one-pot assay containing 4 µg CapD, 4 µg CapN, 2 mM UDP-D-GlcNAc, 2 mM NADPH and 0.5 mM NADP in 50 mM Tris-HCl, 10 mM MgCl<sub>2</sub>, pH 7.5, in a total volume of 30 µl. UDP-L-FucNAc was synthesized by incubating CapE, CapF and CapG in presence of 2 mM UDP-D-GlcNAc, 2 mM NADPH and 0.5 mM NADP in 50 mM Tris-HCl, 10 mM MgCl<sub>2</sub>, pH 7.5.

The third soluble precursor UDP-D-ManNAcA was synthesized by incubating 2 mM UDP-D-GlcNAc with CapO and CapP (4 µg each), 6 mM NAD<sup>+</sup> and 0.5 mM dithiothreitol (DTT; Sigma-Aldrich) in 50 mM Tris-HCl, 10 mM MgCl<sub>2</sub>, pH 7.5. All enzymatic synthesis reactions were quenched by heating 5 min, 90 °C.

**In vitro modulation of CapE catalytic activity by CapAB.** The influence of CapAB-mediated tyrosine phosphorylation on CapE catalytic activity was examined in vitro using purified recombinant proteins. Assays were performed in a total volume of 100 µl containing 17 µg of CapE (or of a CapE protein variants) and 8.5 µg of purified CapAB kinase complex. The enzymes were incubated in the presence of 3 mM UDP-D-GlcNAc and 1 mM ATP, in 10 mM KPi, 10 mM MgCl<sub>2</sub>, pH 7.5 supplemented with 1 mM DTT, for 30 min at 30 °C. Reactions were quenched by heating (5 min, 90 °C), then subjected to capillary electrophoresis (CE) analysis<sup>19</sup>. Control reactions were performed with heat-inactivated (10 min, 100 °C) CapAB protein.

**MALDI-TOF mass spectrometric analysis.** Soluble capsule precursors were purified by RP18-HPLC<sup>19</sup>, and cleaved C<sub>55</sub>P intermediates were purified by preparative TLC. Lipid spots were visualized using iodine vapour and extracted off the silica plates with methanol. Samples were spotted onto a ground steel MALDI-TOF target plate and allowed to dry at room temperature. Subsequently, each sample was overlaid with 1 µl of matrix (saturated solution of 6-Aza-2-thiothymine in 50% (v/v) ethanol, 10 mM diammonium hydrogen citrate) and air dried at room temperature again. Spectra were recorded either in the reflector negative mode within a mass range from 300 to 3000 Da (soluble capsule precursors) or in the linear negative mode within a mass range from 400 to 3000 Da (lipid intermediates), at a laser frequency of 9 Hz on a Biflex III mass spectrometer (Bruker Daltonics). Data analysis was performed using flexAnalysis software (Bruker Daltonics).

**In vitro kinase assays.** In vitro BY-kinase assays were carried out in a total volume of 10 µl containing either 0.5 µg of CapA and CapB, or 2 µg of a CapAB protein fusion construct. For identification of protein substrates, 2 µg of a recombinant target protein were added. The proteins were incubated in the presence of 10 µCi γ-labeled [<sup>33</sup>P]ATP (~300 nM; Hartmann Analytic) in 50 mM Tris-HCl, 10 mM MgCl<sub>2</sub>, pH 7.5 supplemented with 0.5 mM DTT, 0.5 mM EDTA and 10 µM ATP. Assays with CapAB protein variants were carried out as described for the wild-type proteins.

For identification of PknB protein substrates, purified PknB (0.5 µg) was incubated in presence of 3 mM MnCl<sub>2</sub> in the reaction mixture described above. Cross-phosphorylation of CapAB by PknB was assessed analogously.

After 30 min of incubation at 30 °C, reactions were stopped by addition of 4x LDS sample buffer (Invitrogen), and analyzed by SDS-PAGE (NuPAGE, Invitrogen). Radioactive protein bands were visualized using a storage phosphor screen in a Storm imaging system (GE Healthcare). A detailed description of the identification of phosphorylation sites by nanoLC-MS/MS is given in the Supplementary Methods.

**In vitro phosphatase assays.** CapC phosphatase activity was examined in vitro by the addition of CapC1 or CapC2 (2 µg each) with 2 mM MnCl<sub>2</sub> to the CapAB in vitro kinase assays (see above) and subsequent heat-inactivation. After incubation for 1 h at 30 °C, phosphatase reaction was stopped by the addition of 4x LDS sample buffer (Invitrogen), and analyzed by SDS-PAGE (NuPAGE, Invitrogen). Radioactive protein bands were visualized using a storage phosphor screen in a Storm imaging system (GE Healthcare).

**In vitro syntheses of lipid I<sub>cap</sub>, lipid II<sub>cap</sub>, and lipid III<sub>cap</sub>.** Lipid I<sub>cap</sub> synthesis was carried out in a total volume of 50 µl containing 5 nmol C<sub>55</sub>P (Larodan, Sweden), 2 mM UDP-D-GlcNAc, 10 mM NADPH, 0.5 mM NADP and 0.6% (v/v) DMSO in 50 mM Tris-HCl, 10 mM MgCl<sub>2</sub>, pH 7.5. The reaction was initiated by the addition of 4 µg of biosynthetic enzymes CapD, CapN and CapM, and incubated for 16 h at 30 °C.

To assess the influence of different detergents and phospholipids on CapM activity, newly synthesized UDP-D-FucNAc (described above) was incubated with 4 µg CapM, 5 nmol C<sub>55</sub>P in a reaction mixture containing 50 mM Tris-HCl, 10 mM

MgCl<sub>2</sub>, pH 7.5 supplemented with an appropriate amount of triton X-100, *n*-dodecyl-β-D-maltoside (DDM), *n*-lauroyl sarcosine (LS), dimethylsulfoxide (DMSO), dioleoylphosphatidylglycerol (DOPG) or cardiolipin (CL). To investigate the modulatory effect of CapAB on CapM activity 4 μg CapAB and 10 mM ATP were added to the CapM reaction mixture. To assess the influence of PknB on CapM activity in vitro, 1 μg PknB was added to the CapM reaction mixture supplemented with 2 mM MnCl<sub>2</sub> and 10 mM ATP.

The second precursor lipid II<sub>cap</sub> was synthesized in a total volume of 50 μl by incubating the capsule biosynthesis proteins CapE, CapF, CapG and CapL (4 μg each) in the presence of 2 nmol purified lipid I<sub>cap</sub> and 2 mM UDP-D-GlcNAc, 2 mM NADPH, 0.5 mM NADP and 0.6% (v/v) DMSO in 50 mM Tris-HCl, 10 mM MgCl<sub>2</sub>, pH 7.5.

Lipid III<sub>cap</sub> was synthesized by incubating 2 nmol purified lipid II<sub>cap</sub> with CapO, CapP and CapI (4 μg each) and 2 mM UDP-D-GlcNAc, 6 mM NAD<sup>+</sup>, 0.5 mM dithiothreitol (DTT; Sigma-Aldrich) in 50 mM Tris-HCl, 10 mM MgCl<sub>2</sub>, pH 7.5. Synthesized CP precursors were extracted from the reaction mixture with an equal volume of *n*-butanol/pyridine acetate, pH 4.2 (2:1, v/v) and analyzed by TLC on silica plates (Merck) according to Rick (chloroform, methanol, water, ammonium hydroxide, 88:48:10:1)<sup>75</sup>. Nisin was added at a molar ratio of 2:1 with respect to the lipid precursor prior to the extraction procedure. Reaction mixtures were extracted and unbound lipids were analyzed by TLC. For mass spectrometric analysis of lipid intermediates see Supplementary Methods.

For synthesis of [<sup>14</sup>C]-labeled lipid-bound precursors, the assays were further supplemented with 0.333 nmol UDP-D-[<sup>14</sup>C]GlcNAc (Hartmann Analytic, Germany). Radiolabeled spots were visualized using a storage phosphor screen in a Storm imaging system (GE Healthcare). Non-radiolabeled lipid intermediates were analyzed using PMA staining reagent (2.5% (w/v) phosphomolybdate, 1% (w/v) ceric sulfate, 6% (v/v) sulfuric acid). Isolation of small quantities of CP precursors was achieved by synthesis and subsequent purification via preparative TLC. To this end, lipid spots were visualized using iodine vapour and material was scratched off the silica plates. Lipids were extracted by incubation in 100 μl of methanol for 60 min. Larger quantities of CP precursor were purified using high-performance liquid chromatography (HPLC) over a DEAE-FF (5 ml; GE Healthcare) and eluted in a linear gradient from chloroform/ methanol/ water (2:3:1) to chloroform, methanol, 300 mM ammonium bicarbonate (2:3:1).

**CapA1 catalyzed cleavage of lipid-bound CP precursor.** For reconstitution of the CapA1 mediated cleavage of the pyrophosphate-linkage of lipid-linked cell wall intermediates, purified CapA1 (8 μg) was incubated with 2 nmol lipid I<sub>cap</sub>, lipid III<sub>WTA</sub>, lipid II<sub>PG</sub> in 10 mM MgCl<sub>2</sub> and 50 mM Tris-HCl, pH 7.5. After incubation for 16 h at 30 °C, cleavage products were extracted from the reaction mixture with an equal volume of *n*-butanol/pyridine acetate, pH 4.2 (2:1, v/v) and analyzed by TLC on silica plates (Merck) according to Rick (chloroform, methanol, water, ammonium hydroxide, 88:48:10:1) and visualized by PMA staining<sup>75</sup>.

**In vitro LCP assays.** For reconstitution of the CP ligation reaction purified lipid I<sub>cap</sub> or [<sup>14</sup>C]lipid I<sub>cap</sub> was incubated in the presence of LcpC (4 μg), using 2 nmol of purified lipid II<sub>PG</sub> or [<sup>14</sup>C]lipid II<sub>PG</sub> as acceptor substrate in a 50 μl reaction mixture with 0.6% DMSO, 18 μg DOPG, 10 mM MgCl<sub>2</sub> in 50 mM MES buffer, pH 5.5. Synthesis and purification of the acceptor substrate lipid II is described in the supplementary methods. If indicated, assays additionally contained 4 μg of CapA1. After incubation for 16 h at 30 °C, samples were analyzed by TLC, followed by phosphoimaging. Polymerization of LcpC reaction products were catalyzed by the subsequent addition of PBP2 with 2 mM CaCl<sub>2</sub> to the LCP reaction mixture, followed by incubation at 30 °C for 1 h. Moenomycin (MOE) was used to block the PBP2 catalyzed reaction and added at a final concentration of 10 μM. For evaluation of LcpC mediated hydrolysis of CP precursor in the absence of the acceptor substrate, 2 nmol of the individual lipid-linked precursor was incubated with 4 μg LcpC, 18 μg DOPG, 10 mM MgCl<sub>2</sub> and 0.6% DMSO in 50 mM MES buffer, pH 5.5. After incubation for 16 h at 30 °C, samples were analyzed by TLC and visualized by PMA staining.

**Reporting summary.** Further information on experimental design is available in the Nature Research Reporting Summary linked to this article.

## Data availability

The authors declare that all data supporting the findings of this study are available within the Article and its Supplementary Information.

Received: 21 March 2016 Accepted: 28 February 2019

Published online: 29 March 2019

## References

1. Hanson, B. R. & Neely, M. N. Coordinate regulation of Gram-positive cell surface components. *Curr. Opin. Microbiol.* **15**, 204–210 (2012).

- Bouhss, A., Trunkfield, A. E., Bugg, T. D. H. & Mengin-Lecreux, D. The biosynthesis of peptidoglycan lipid-linked intermediates. *FEMS Microbiol. Rev.* **32**, 208–233 (2008).
- Xia, G., Kohler, T. & Peschel, A. The wall teichoic acid and lipoteichoic acid polymers of *Staphylococcus aureus*. *Int. J. Med. Microbiol.* **300**, 148–154 (2010).
- David, M. Z. & Daum, R. S. Community-Associated Methicillin-Resistant *Staphylococcus aureus*: Epidemiology and Clinical Consequences of an Emerging Epidemic. *Clin. Microbiol. Rev.* **23**, 616–687 (2010).
- Thakker, M., Park, J.-S., Carey, V. & Lee, J. C. *Staphylococcus aureus* serotype 5 capsular polysaccharide is antiphagocytic and enhances bacterial virulence in a murine bacteremia model. *Infect. Immun.* **66**, 5183–5189 (1998).
- Nilsson, I. M., Lee, J. C., Bremell, T., Rydén, C. & Tarkowski, A. The role of staphylococcal polysaccharide microcapsule expression in septicemia and septic arthritis. *Infect. Immun.* **65**, 4216–4221 (1997).
- Portolés, M., Kiser, K. B., Bhasin, N., Chan, K. H. N. & Lee, J. C. *Staphylococcus aureus* cap50 has udp-mannac dehydrogenase activity and is essential for capsule expression. *Infect. Immun.* **69**, 917–923 (2001).
- Boyle-Vavra, S. et al. USA300 and USA500 clonal lineages of *Staphylococcus aureus* do not produce a capsular polysaccharide due to conserved mutations in the cap5 locus. *mBio* **6**, e0258–14 (2015).
- Diekema, D. J. et al. Continued emergence of USA300 methicillin-resistant *Staphylococcus aureus* in the united states: results from a nationwide surveillance study. *Infect. Control. Hosp. Epidemiol.* **35**, 285–292 (2014).
- van der Mee-Marquet, N. et al. The incidence of *Staphylococcus aureus* ST8-USA300 among French pediatric inpatients is rising. *Eur. J. Clin. Microbiol. Infect. Dis.* **34**, 935–942 (2015).
- Jones, C. Revised structures for the capsular polysaccharides from *Staphylococcus aureus* Types 5 and 8, components of novel glycoconjugate vaccines. *Carbohydr. Res.* **340**, 1097–1106 (2005).
- Sau, S. et al. The *Staphylococcus aureus* allelic genetic loci for serotype 5 and 8 capsule expression contain the type-specific genes flanked by common genes. *Microbiology* **143**, 2395–2405 (1997).
- Kneidinger, B. et al. Three highly conserved proteins catalyze the conversion of UDP-*n*-acetyl-d-glucosamine to precursors for the biosynthesis of O antigen in *Pseudomonas aeruginosa* O11 and capsule in *Staphylococcus aureus* type 5 implications for the udp-*n*-acetyl-l-fucosamine biosynthetic pathway. *J. Biol. Chem.* **278**, 3615–3627 (2003).
- Kiser, K. B., Bhasin, N., Deng, L. & Lee, J. C. *Staphylococcus aureus* cap5P encodes a UDP-*N*-acetylglucosamine 2-epimerase with functional redundancy. *J. Bacteriol.* **181**, 4818–4824 (1999).
- Bhasin, N. et al. Identification of a gene essential for O-acetylation of the *Staphylococcus aureus* type 5 capsular polysaccharide. *Mol. Microbiol.* **27**, 9–21 (1998).
- Soulat, D. et al. *Staphylococcus aureus* operates protein-tyrosine phosphorylation through a specific mechanism. *J. Biol. Chem.* **281**, 14048–14056 (2006).
- Soulat, D., Grangeasse, C., Vaganay, E., Cozzone, A. J. & Duclos, B. UDP-acetyl-mannosamine dehydrogenase is an endogenous protein substrate of *Staphylococcus aureus* protein-tyrosine kinase activity. *J. Mol. Microbiol. Biotechnol.* **13**, 45–54 (2007).
- O’Riordan, K. & Lee, J. C. *Staphylococcus aureus* capsular polysaccharides. *Clin. Microbiol. Rev.* **17**, 218–234 (2004).
- Li, W. et al. Analysis of the *Staphylococcus aureus* capsule biosynthesis pathway in vitro: Characterization of the UDP-GlcNAc C6 dehydratases CapD and CapE and identification of enzyme inhibitors. *Int. J. Med. Microbiol. IJMM* **304**, 958–969 (2014).
- Kawai, Y. et al. A widespread family of bacterial cell wall assembly proteins. *EMBO J.* **30**, 4931–4941 (2011).
- Chan, Y. G.-Y., Kim, H. K., Schneewind, O. & Missiakas, D. The capsular polysaccharide of *Staphylococcus aureus* is attached to peptidoglycan by the LytR-CpsA-Psr (LCP) family of enzymes. *J. Biol. Chem.* **289**, 15680–15690 (2014).
- Barreteau, H. et al. Quantitative high-performance liquid chromatography analysis of the pool levels of undecaprenyl phosphate and its derivatives in bacterial membranes. *J. Chromatogr. B* **877**, 213–220 (2009).
- Swoboda, J. G. et al. Discovery of a small molecule that blocks wall teichoic acid biosynthesis in *Staphylococcus aureus*. *ACS Chem. Biol.* **4**, 875–883 (2009).
- D’Elia, M. A., Millar, K. E., Beveridge, T. J. & Brown, E. D. Wall teichoic acid polymers are dispensable for cell viability in *Bacillus subtilis*. *J. Bacteriol.* **188**, 8313–8316 (2006).
- Sewell, E. W. & Brown, E. D. Taking aim at wall teichoic acid synthesis: new biology and new leads for antibiotics. *J. Antibiot. (Tokyo)* **67**, 43–51 (2014).
- Pohlmann-Dietze, P. et al. Adherence of *Staphylococcus aureus* to endothelial cells: influence of capsular polysaccharide, global regulator agr, and bacterial growth Phase. *Infect. Immun.* **68**, 4865–4871 (2000).



27. Wamel, Wvan et al. Regulation of *Staphylococcus aureus* type 5 capsular polysaccharides by *agr* and *sarA* in vitro and in an experimental endocarditis model. *Microb. Pathog.* **33**, 73–79 (2002).
28. Luong, T. T. & Lee, C. Y. The *arl* locus positively regulates *Staphylococcus aureus* type 5 capsule via an *mgrA*-dependent pathway. *Microbiology* **152**, 3123–3131 (2006).
29. Grangeasse, C., Nessler, S. & Mijakovic, I. Bacterial tyrosine kinases: evolution, biological function and structural insights. *Philos. Trans. R. Soc. B* **367**, 2640–2655 (2012).
30. Lee, D. C. & Jia, Z. Emerging structural insights into bacterial tyrosine kinases. *Trends Biochem. Sci.* **34**, 351–357 (2009).
31. Grangeasse, C., Cozzone, A. J., Deutscher, J. & Mijakovic, I. Tyrosine phosphorylation: an emerging regulatory device of bacterial physiology. *Trends Biochem. Sci.* **32**, 86–94 (2007).
32. Bender, M. H., Cartee, R. T. & Yother, J. Positive Correlation between tyrosine phosphorylation of CpsD and capsular polysaccharide production in *Streptococcus pneumoniae*. *J. Bacteriol.* **185**, 6057–6066 (2003).
33. Morona, J. K., Paton, J. C., Miller, D. C. & Morona, R. Tyrosine phosphorylation of CpsD negatively regulates capsular polysaccharide biosynthesis in *Streptococcus pneumoniae*. *Mol. Microbiol.* **35**, 1431–1442 (2000).
34. Müller, A., Ulm, H., Reder-Christ, K., Sahl, H.-G. & Schneider, T. Interaction of type A lantibiotics with undecaprenol-bound cell envelope precursors. *Microb. Drug. Resist.* **18**, 261–270 (2012).
35. Breton, C., Snajdrová, L., Jeanneau, C., Koca, J. & Imberty, A. Structures and mechanisms of glycosyltransferases. *Glycobiology* **16**, 29R–37R (2006).
36. Patel, K. B., Ciepichal, E., Swiezewska, E. & Valvano, M. A. The C-terminal domain of the *Salmonella enterica* WbaP (UDP-galactose: Und-P galactose-1-phosphate transferase) is sufficient for catalytic activity and specificity for undecaprenyl monophosphate. *Glycobiology* **22**, 116–122 (2012).
37. Ray, L. C. et al. Membrane association of monotopic phosphoglycosyl transferase underpins function. *Nat. Chem. Biol.* **14**, 538–541 (2018).
38. Gasteiger, E. et al. in *The Proteomics Protocols Handbook* (ed. Walker, J.) 571–607 (Humana Press, Totowa, NJ, 2005).
39. Price, N. P. & Momany, F. A. Modeling bacterial UDP-HexNAc: polyprenol-P HexNAc-1-P transferases. *Glycobiology* **15**, 29R–42R (2005).
40. Walvoort, M. T. C., Lukose, V. & Imperiali, B. A modular approach to phosphoglycosyltransferase inhibitors inspired by nucleoside antibiotics. *Chem. - Eur. J.* **22**, 3856–3864 (2016).
41. Gruszczak, J. et al. Comparative analysis of the Tyr-kinases CapB1 and CapB2 fused to their cognate modulators CapA1 and CapA2 from *Staphylococcus aureus*. *PLOS ONE* **8**, e75958 (2013).
42. Blom, N., Sicheritz-Pontén, T., Gupta, R., Gammeltoft, S. & Brunak, S. Prediction of post-translational glycosylation and phosphorylation of proteins from the amino acid sequence. *Proteomics* **4**, 1633–1649 (2004).
43. Kavanagh, K. L., Jörnvall, H., Persson, B. & Oppermann, U. Medium- and short-chain dehydrogenase/reductase gene and protein families. *Cell. Mol. Life Sci.* **65**, 3895–3906 (2008).
44. Jansen, A. et al. Production of capsular polysaccharide does not influence *Staphylococcus aureus* vancomycin susceptibility. *Bmc. Microbiol.* **13**, 65 (2013).
45. Montgomery, C. P. et al. Comparison of virulence in community-associated methicillin-resistant *Staphylococcus aureus* pulsotypes USA300 and USA400 in a rat model of pneumonia. *J. Infect. Dis.* **198**, 561–570 (2008).
46. Elsholz, A. K., Wacker, S. A. & Losick, R. Self-regulation of exopolysaccharide production in *Bacillus subtilis* by a tyrosine kinase. *Genes Dev.* **28**, 1710–1720 (2014).
47. Eberhardt, A. et al. Attachment of capsular polysaccharide to the cell wall in *Streptococcus pneumoniae*. *Microb. Drug. Resist.* **18**, 240–255 (2012).
48. Donat, S. et al. Transcriptome and functional analysis of the eukaryotic-type serine/threonine kinase PknB in *Staphylococcus aureus*. *J. Bacteriol.* **191**, 4056–4069 (2009).
49. Beltrami, A. M., Mukhopadhyay, C. D. & Pancholi, V. Modulation of cell wall structure and antimicrobial susceptibility by a *Staphylococcus aureus* eukaryote-like serine/threonine kinase and phosphatase. *Infect. Immun.* **77**, 1406–1416 (2009).
50. Tamber, S., Schwartzman, J. & Cheung, A. L. Role of PknB kinase in antibiotic resistance and virulence in community-acquired methicillin-resistant *Staphylococcus aureus* Strain USA300. *Infect. Immun.* **78**, 3637–3646 (2010).
51. Hardt, P. et al. The cell wall precursor lipid II acts as a molecular signal for the Ser/Thr kinase PknB of *Staphylococcus aureus*. *Int. J. Med. Microbiol.* **307**, 1–10 (2017).
52. Olivares-Illana, V. et al. Structural basis for the regulation mechanism of the tyrosine kinase CapB from *Staphylococcus aureus*. *PLoS Biol.* **6**, e143 (2008).
53. Yother, J. Capsules of *Streptococcus pneumoniae* and other bacteria: paradigms for polysaccharide biosynthesis and regulation. *Annu. Rev. Microbiol.* **65**, 563–581 (2011).
54. Mijakovic, I. et al. Transmembrane modulator-dependent bacterial tyrosine kinase activates UDP-glucose dehydrogenases. *EMBO J.* **22**, 4709–4718 (2003).
55. Grangeasse, C. et al. Autophosphorylation of the *Escherichia coli* protein kinase Wzc regulates tyrosine phosphorylation of Ugd, a UDP-glucose dehydrogenase. *J. Biol. Chem.* **278**, 39323–39329 (2003).
56. Miyafusa, T., Caaveiro, J. M. M., Tanaka, Y., Tanner, M. E. & Tsumoto, K. Crystal structure of the capsular polysaccharide synthesizing protein CapE of *Staphylococcus aureus*. *Biosci. Rep.* **33**, 463–474 (2013).
57. Mimic, Z. et al. Control of EpsE, the phosphoglycosyltransferase initiating exopolysaccharide synthesis in *Streptococcus thermophilus*, by EpsD tyrosine kinase. *J. Bacteriol.* **189**, 1351–1357 (2007).
58. Jers, C. et al. *Bacillus subtilis* BY-kinase PtkA controls enzyme activity and localization of its protein substrates. *Mol. Microbiol.* **77**, 287–299 (2010).
59. Whitfield, C. & Larue, K. Stop and go: regulation of chain length in the biosynthesis of bacterial polysaccharides. *Nat. Struct. Mol. Biol.* **15**, 121–123 (2008).
60. Massidda, O., Kariyama, R., Daneo-Moore, L. & Shockman, G. D. Evidence that the PBP 5 synthesis repressor (*psr*) of *Enterococcus hirae* is also involved in the regulation of cell wall composition and other cell wall-related properties. *J. Bacteriol.* **178**, 5272–5278 (1996).
61. Cieslewicz, M. J., Kasper, D. L., Wang, Y. & Wessels, M. R. Functional analysis in type Ia group B streptococcus of a cluster of genes involved in extracellular polysaccharide production by diverse species of streptococci. *J. Biol. Chem.* **276**, 139–146 (2001).
62. Morona, J. K., Morona, R. & Paton, J. C. Attachment of capsular polysaccharide to the cell wall of *Streptococcus pneumoniae* type 2 is required for invasive disease. *Proc. Natl. Acad. Sci.* **103**, 8505–8510 (2006).
63. Hübscher, J. et al. MsrR contributes to cell surface characteristics and virulence in *Staphylococcus aureus*. *FEMS Microbiol. Lett.* **295**, 251–260 (2009).
64. Toniolo, C. et al. *Streptococcus agalactiae* capsule polymer length and attachment is determined by the proteins CpsABCD. *J. Biol. Chem.* **290**, 9521–9532 (2015).
65. Schaefer, K., Matano, L. M., Qiao, Y., Kahne, D. & Walker, S. In vitro reconstitution demonstrates the cell wall ligase activity of LCP proteins. *Nat. Chem. Biol.* **13**, 396–401 (2017).
66. Horzempa, J., Dean, C. R., Goldberg, J. B. & Castric, P. *Pseudomonas aeruginosa* 1244 pilin glycosylation: glycan substrate recognition. *J. Bacteriol.* **188**, 4244–4252 (2006).
67. D'Elia, M. A. et al. Lesions in teichoic acid biosynthesis in *Staphylococcus aureus* lead to a lethal gain of function in the otherwise dispensable pathway. *J. Bacteriol.* **188**, 4183–4189 (2006).
68. Xayarath, B. & Yother, J. Mutations blocking side chain assembly, polymerization, or transport of a Wzy-dependent *Streptococcus pneumoniae* capsule are lethal in the absence of suppressor mutations and can affect polymer transfer to the cell wall. *J. Bacteriol.* **189**, 3369–3381 (2007).
69. Shi, L. et al. Cross-phosphorylation of bacterial serine/threonine and tyrosine protein kinases on key regulatory residues. *Front. Microbiol.* **5**, 495 (2014).
70. Ravikumar, V. et al. Quantitative phosphoproteome analysis of *Bacillus subtilis* reveals novel substrates of the kinase PrkC and phosphatase PrpC. *Mol. Cell. Proteom. MCP* **13**, 1965–1978 (2014).
71. Liebeke, M., Meyer, H., Donat, S., Ohlsen, K. & Lalk, M. A Metabolomic view of *Staphylococcus aureus* and its Ser/Thr kinase and phosphatase deletion mutants: involvement in cell wall biosynthesis. *Chem. Biol.* **17**, 820–830 (2010).
72. Burnside, K. et al. Regulation of hemolysin expression and virulence of *Staphylococcus aureus* by a serine/threonine kinase and phosphatase. *PLoS ONE* **5**, e11071 (2010).
73. Fey, P. D. et al. A genetic resource for rapid and comprehensive phenotype screening of nonessential *Staphylococcus aureus* genes. *mBio* **4**, e00537–00512 (2013).
74. Monk, I. R., Shah, I. M., Xu, M., Tan, M.-W. & Foster, T. J. Transforming the untransformable: application of direct transformation to manipulate genetically *Staphylococcus aureus* and *Staphylococcus epidermidis*. *mBio* **3**, e00277 (2012).
75. Rick, P. D. et al. Characterization of the lipid-carrier involved in the synthesis of enterobacterial common antigen (ECA) and identification of a novel phosphoglyceride in a mutant of *Salmonella typhimurium* defective in ECA synthesis. *Glycobiology* **8**, 557–567 (1998).

## Acknowledgements

We would like to thank Michael Josten for mass spectrometry, and Katie O'Riordan for providing plasmids pKBK4, pKBK6a, pKBK10, pKBK50d, pET24-*capD*, pET24-*capN*,

and pET5F1.1. We thank Jerry Pier for providing purified PNAG, Knut Ohlsen for providing strain *S. aureus* Newman  $\Delta pknB$ , Gabriele Bierbaum for providing plasmid pCapA1, Andreas Peschel for providing *E. coli* DC10 $\beta$  and Olaf Schneewind for kindly providing the  $\Delta lcpABC$  mutant. Marvin Rausch is grateful for support by the Juergen Manchot Foundation. This work was supported by the German Research Foundation (DFG; SCHN 1284/1–2) and the BONFOR program of the Medical Faculty of the University of Bonn.

### Author contributions

M.R., J.P.D., H.U., A.M., W.L., P.H., M.S., M.E., X.W., X.L. performed experiments. C.E. M., W.V., H.G.S., J.C.L., T.S. contributed to the study design, planning of the experiments and interpretation of data. H.U. and T.S. wrote the manuscript. M.R., A.M., C.E. M., W.V., J.C.L., H.G.S., T.S. contributed to revision of the manuscript.

### Additional information

**Supplementary Information** accompanies this paper at <https://doi.org/10.1038/s41467-019-09356-x>.

**Competing interests:** The authors declare no competing interests.

**Reprints and permission** information is available online at <http://npg.nature.com/reprintsandpermissions/>

**Journal peer review information:** *Nature Communications* thanks Eric Brown and the other anonymous reviewer(s) for their contribution to the peer review of this work. Peer reviewer reports are available.

**Publisher's note:** Springer Nature remains neutral with regard to jurisdictional claims in published maps and institutional affiliations.



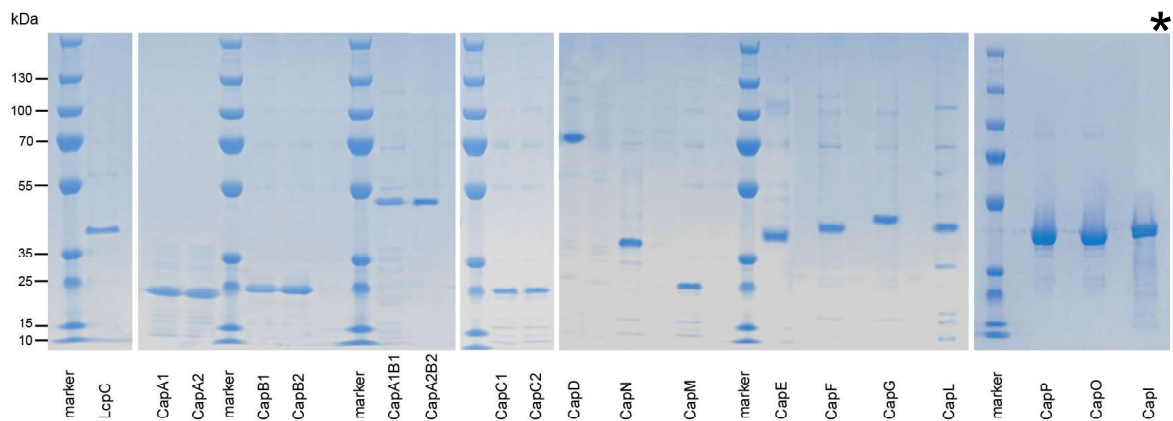
**Open Access** This article is licensed under a Creative Commons Attribution 4.0 International License, which permits use, sharing, adaptation, distribution and reproduction in any medium or format, as long as you give appropriate credit to the original author(s) and the source, provide a link to the Creative Commons license, and indicate if changes were made. The images or other third party material in this article are included in the article's Creative Commons license, unless indicated otherwise in a credit line to the material. If material is not included in the article's Creative Commons license and your intended use is not permitted by statutory regulation or exceeds the permitted use, you will need to obtain permission directly from the copyright holder. To view a copy of this license, visit <http://creativecommons.org/licenses/by/4.0/>.

© The Author(s) 2019

**Supplementary Information**

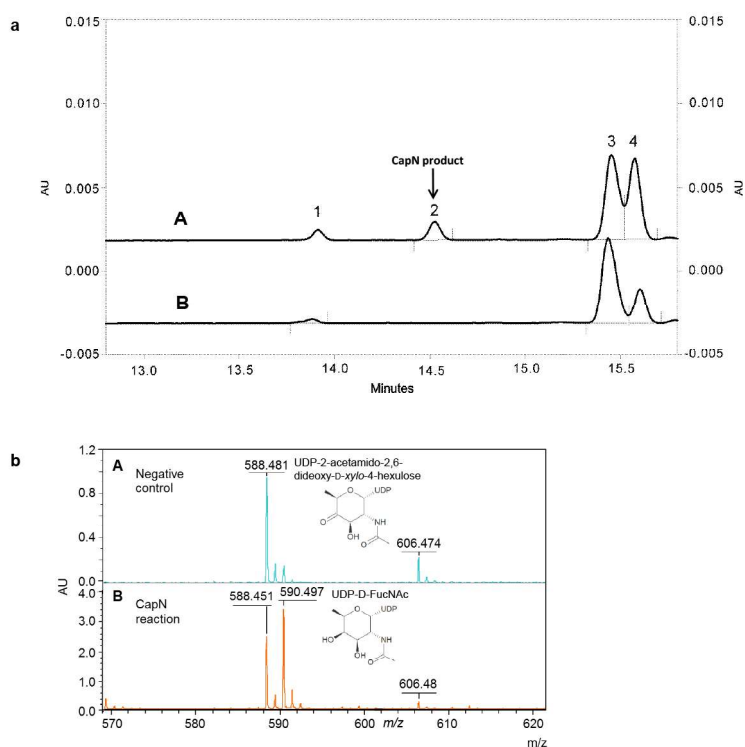
**Coordination of capsule assembly and cell wall biosynthesis in  
*Staphylococcus aureus***

**Rausch *et al.***



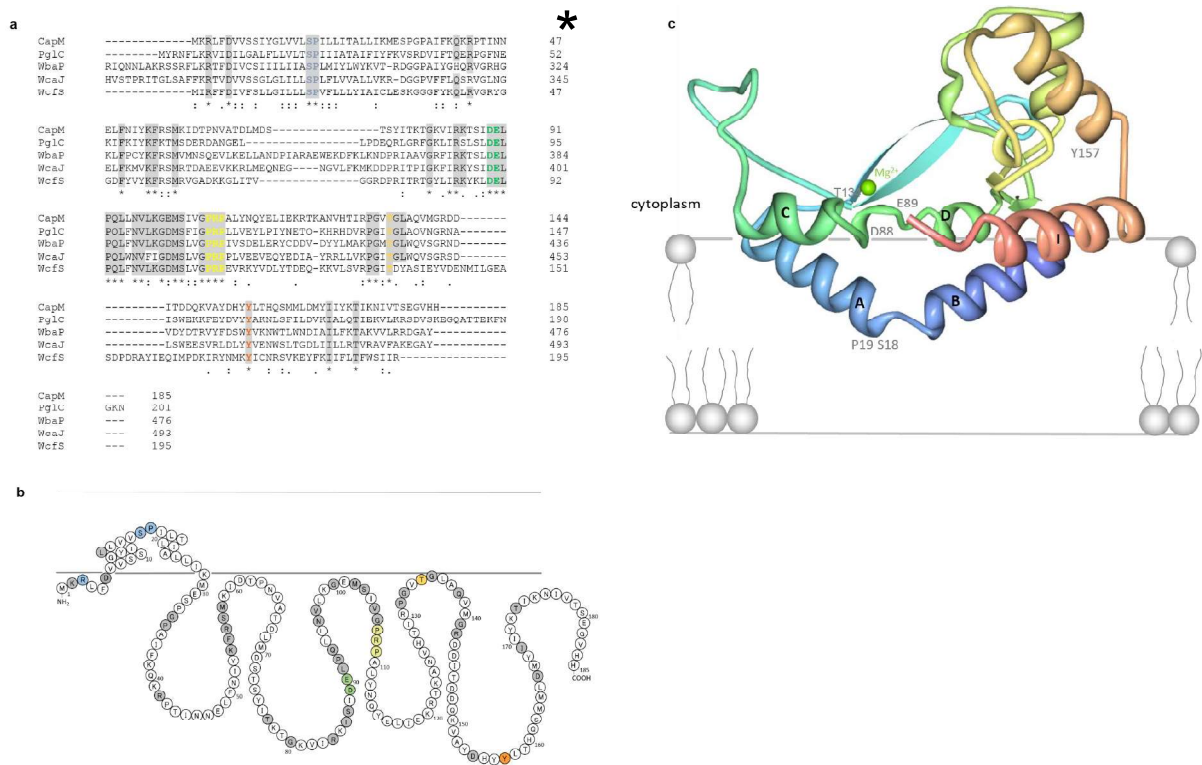
### Supplementary Figure 1

**SDS-PAGE analysis of purified recombinant His<sub>6</sub>-tagged proteins.** Protein marker: PageRuler Plus Pre-Stained Protein Ladder (10–250 kDa); Fermentas. Calculated molecular weights: LcpC, 34.7 kDa; CapA1, 24.8 kDa; CapA2, 24.3 kDa; CapB1, 25.3 kDa; CapB2, 25.3 kDa; CapA1B1<sub>fus</sub>, 50.2 kDa; CapA2B2<sub>fus</sub>, 49.7 kDa; CapC1, 28.9 kDa; CapC2, 28.9 kDa; CapD, 69.1 kDa; CapN, 33.7 kDa; CapM, 21.0 kDa; CapE, 38.6 kDa; CapF, 42.2 kDa; CapG, 42.9 kDa; CapL, 46.6 kDa; CapP, 44.3 kDa; CapO, 46.8 kDa; CapI, 42.6 kDa.



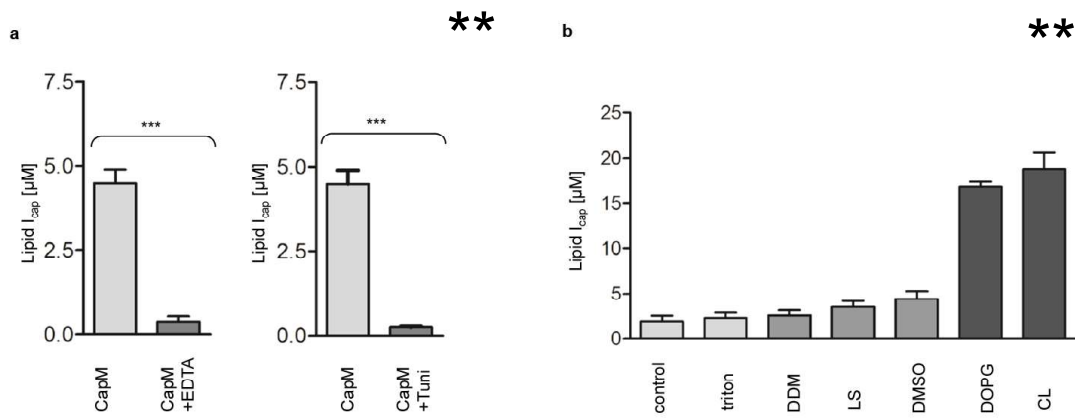
## Supplementary Figure 2

**CapN enzymatic activity.** (a) Capillary electrophoresis (CE) analysis of CapN *in vitro* activity. Purified CapN and PglF were incubated simultaneously in a combined assay in the presence of UDP-GlcNAc and NADPH. (A) PglF/CapN reaction. (B) control reaction containing heat-inactivated CapN. 1, UDP-GlcNAc; 2, UDP-D-FucNAc (CapN product); 3, UDP-2-acetamido-2,6-dideoxy-D-xylo-4-hexulose (PglF product); 4, NADP. (b) Mass spectrometric analysis of CapN *in vitro* activity. HPLC-purified sugar nucleotides were analyzed by negative-mode MALDI-TOF mass spectrometry. (A) Mass spectrum of a control reaction containing heat-inactivated CapN. (B) UDP-GlcNAc converted with PglF and CapN. Peaks at  $m/z$  588.4 ( $[M-H]^-$ ) correspond to the deprotonated molecular ion of UDP-2-acetamido-2,6-dideoxy-D-xylo-4-hexulose (neutral mass 589.3). The peak at  $m/z$  590.4 ( $[M-H]^-$ ) corresponds to UDP-D-FucNAc (neutral mass 591.4) and peaks at  $m/z$  606.5 ( $[M-H]^-$ ) arise either from UDP-GlcNAc (neutral mass 607.4) or from the hydrated (diol) form of UDP-2-acetamido-2,6-dideoxy-D-xylo-4-hexulose. AU, arbitrary units.



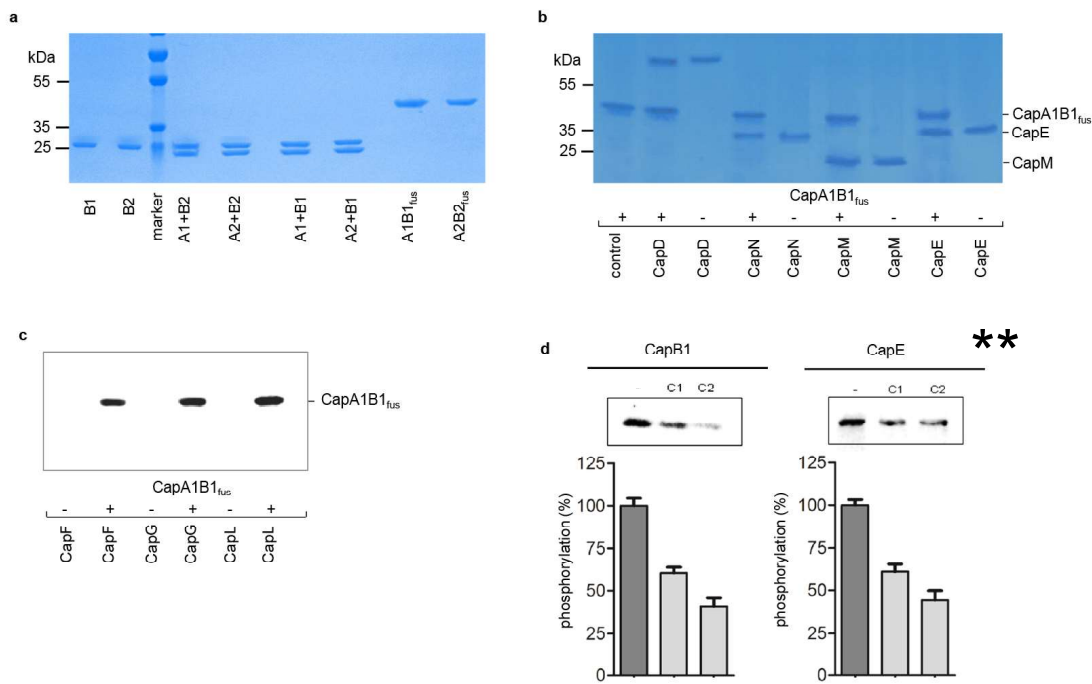
### Supplementary Figure 3

**Membrane topology and predicted architecture of *S. aureus* CapM.** (a) Sequence alignment of CapM (*S. aureus*) with glycosyltransferases WbaP (*Salmonella enterica*), PglC (*Campylobacter concisus*), WcaJ (*Mycobacterium tuberculosis*) and WcfS (*Bacteroides fragilis*). Conserved amino acids are highlighted grey. The highly conserved Tyr157 residue is highlighted orange and Thr134 is highlighted yellow. The catalytic DE dyad is marked green and a strictly conserved PRP motif (107-109) yellow<sup>1</sup>. (b) CapM is anchored in the membrane by a reentrant membrane helix. (c) Structural model obtained by SWISS-MODEL (based on PglC structure of *C. concisus*<sup>1</sup>). The reentrant membrane helix is formed by a helix-break-helix motif of helices A and B (blue) with an interhelix angle of 118° by a Ser-Pro motif (residues 18 and 19). The catalytic DE dyad (residues 88 and 89) is located in the cytoplasm. Mg<sup>2+</sup> cofactor is highlighted in green.



#### Supplementary Figure 4

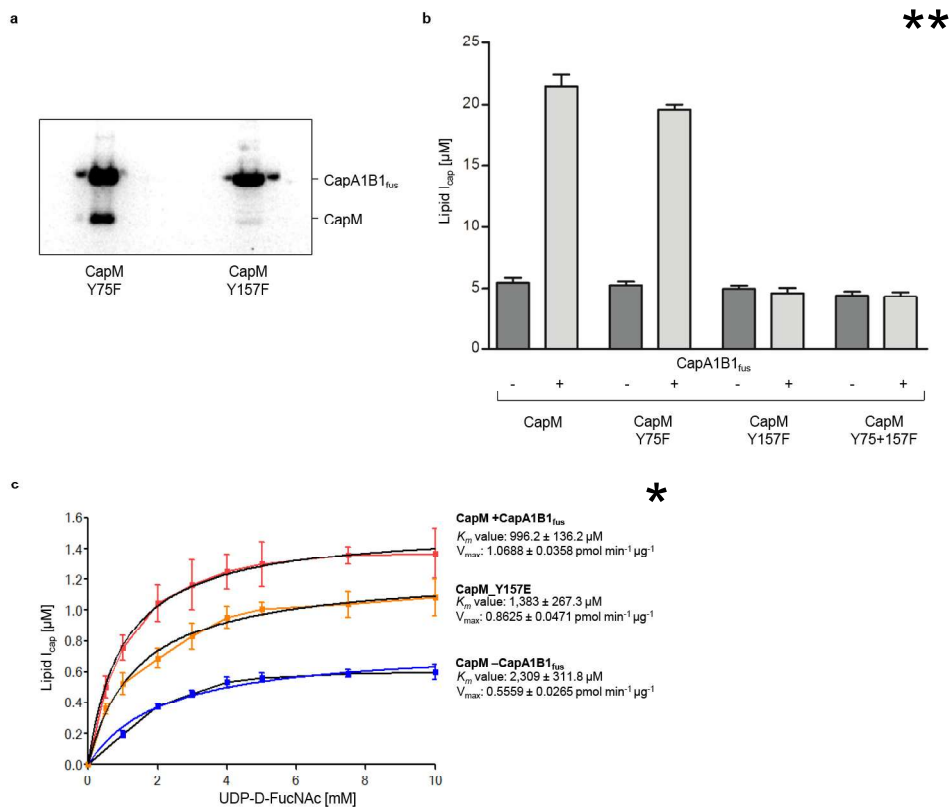
**CapM enzymatic activity.** (a) The impact of MgCl<sub>2</sub> (50 mM EDTA) and tunicamycin (Tuni; 200 μM) on CapM *in vitro* activity was tested in the presence of DMSO. (b) Impact of detergents and anionic lipids on CapM *in vitro* enzyme activity. Triton, triton X-100; DDM, *n*-dodecyl-β-D-maltoside; LS, *n*-lauroyl sarcosine; DMSO, dimethylsulfoxide; DOPG, dioleoylphosphatidylglycerol (9 nmol); CL, cardiolipin (20 nmol). Experiments were performed in triplicate. The error bars represent the ± SD from three biological replicates. Statistical significance was analyzed by an unpaired *t*-test (\*\*\*)  $p < 0.005$ .



### Supplementary Figure 5

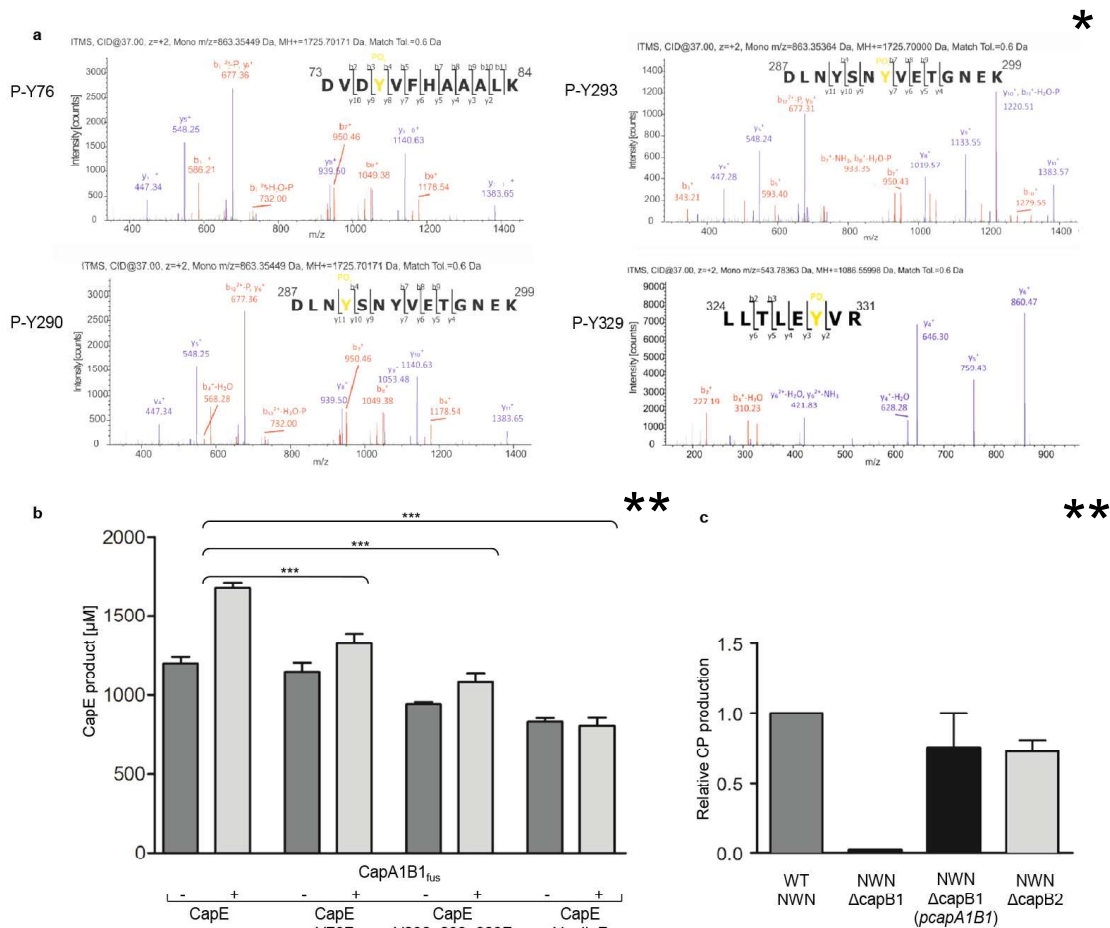
**CapA1B1 phosphorylation and CapC mediated dephosphorylation.** (a) Representative SDS page of CapAB phosphorylation analysis. (b) Representative SDS page of phosphorylation target protein analysis. (c) Analysis of CapA1B1 mediated phosphotransfer to CapF, CapG and CapL by SDS-PAGE and phosphoimaging. (d) The phosphatases CapC1 and CapC2 catalyze the dephosphorylation of target proteins CapB1 and CapE. Experiments were performed in triplicate. The error bars represent the  $\pm$  SD from three biological replicates.





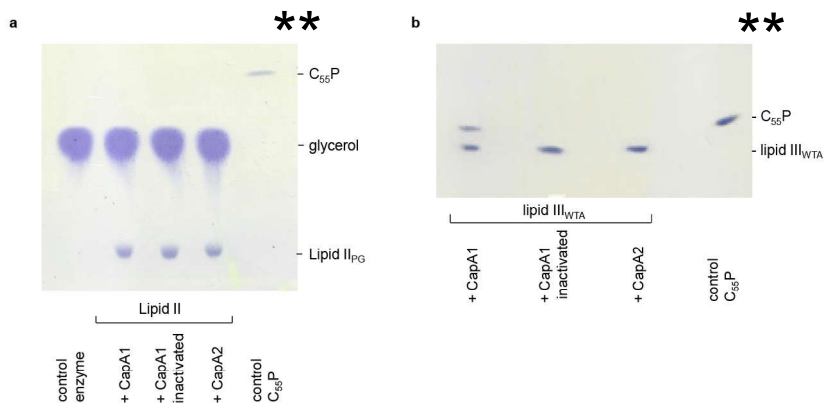
## Supplementary Figure 6

**Identifying Tyr157 as regulatory phosphorylation site on CapM.** (a) CapM mutant proteins carrying Tyr to Phe exchanges in position 75 and/or 157 were assayed for GT activity in the presence of either active CapA1B1 (light grey) or heat-inactivated CapAB (dark grey) in DMSO. Experiments were performed in triplicate. The error bars represent the  $\pm$  SD from three biological replicates. (b) Determination of  $K_m$  and  $V_{max}$  values of CapM in the presence (red), absence (blue) of CapA1B1 and of a CapM phosphomimetic variant (Tyr157Glu, orange). (c) CapA1B1 *in vitro* kinase assay with CapM Y75F and CapM Y157F. Phosphotransfer was analyzed by SDS-PAGE and phosphoimaging.



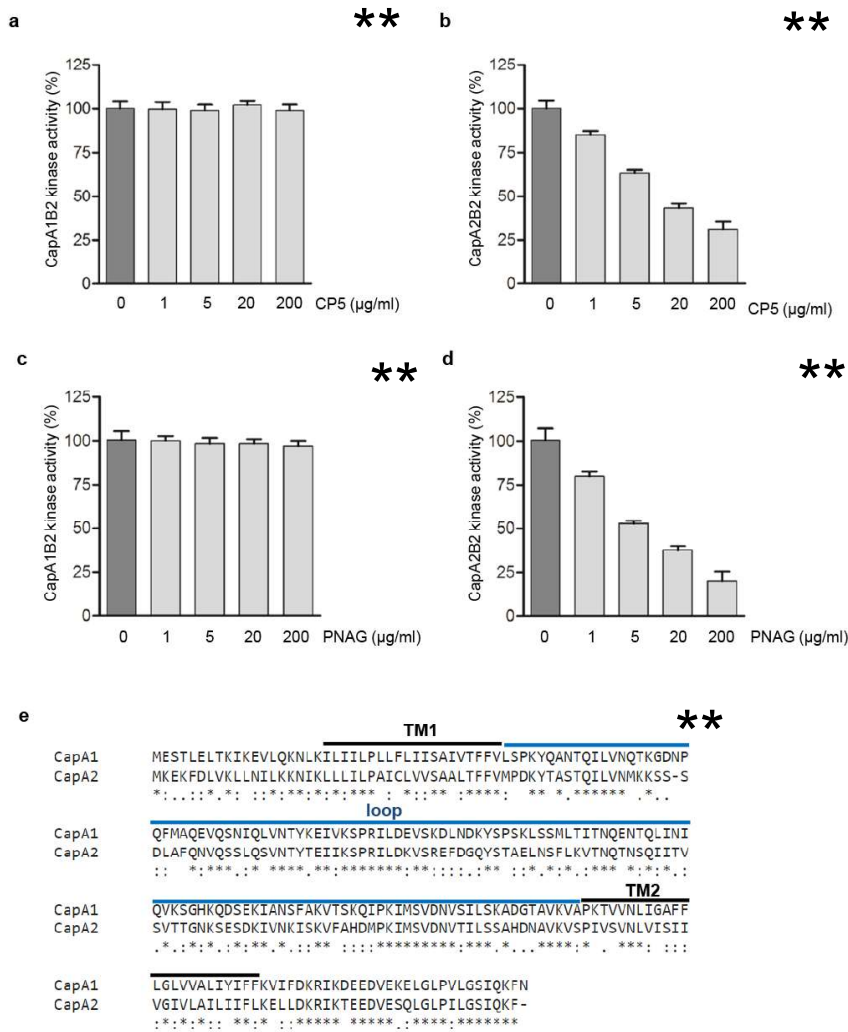
## Supplementary Figure 7

**CapAB positively controls CapE enzymatic activity.** (a) Representative LC/MS spectrum for identification of CapAB phosphorylation sites on CapE. (b) Site-directed mutagenesis of CapE tyrosine phosphorylation sites. CapE mutant proteins carrying Tyr to Phe exchanges were assayed for dehydratase activity in the presence of either active CapA1B1<sub>fus</sub> (light grey) or heat-inactivated CapA1B1<sub>fus</sub> (dark grey) using CE detection. Experiments were performed in triplicate, with duplicate measurements. The error bars represent the  $\pm$  SD from three biological replicates. Statistical significance was analyzed by an unpaired *t*-test (\*\* $p < 0.005$ ). (c) ELISA-based quantification of CP production by *S. aureus* Newman (NWN) wildtype compared to  $\Delta capB1$ ,  $\Delta capB2$  deletion mutants and  $\Delta capB1$  mutant complemented *in trans*. Experiments were performed in triplicate. The error bars represent the  $\pm$  SEM from three biological replicates.



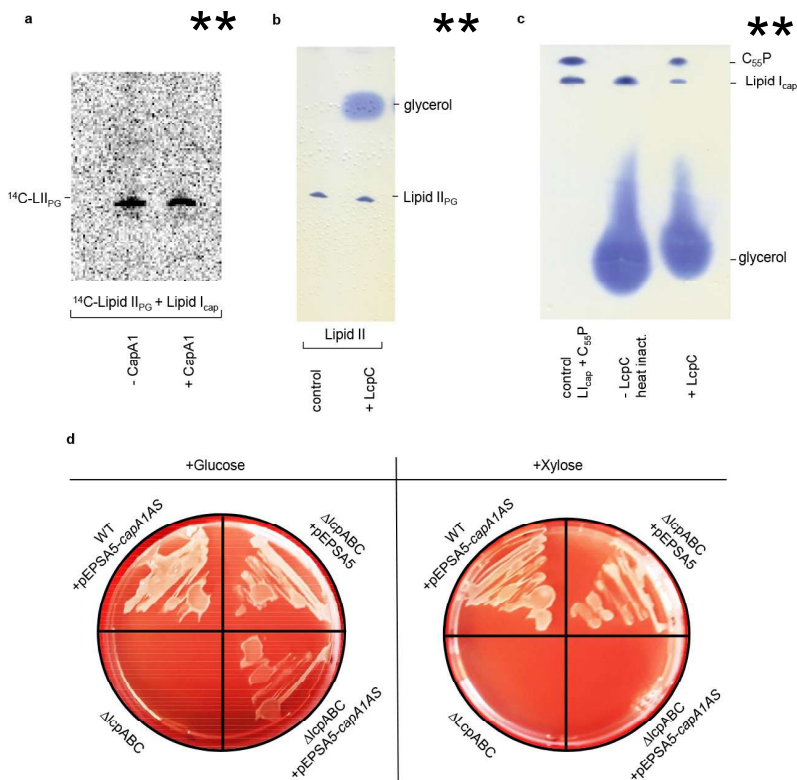
### Supplementary Figure 8

**The ultimate PG precursor lipid II is no phosphodiesterase substrate for CapA1.** (a) Purified lipid II (2 nmol) was incubated with CapA1, CapA2 and heat-inactivated CapA1 (4  $\mu$ g each). Reaction mixtures were extracted with BuOH/PyAc and analyzed by TLC and PMA staining. Purified C<sub>55</sub>P was used as a migration control. (b) The WTA precursor lipid III (C<sub>55</sub>PP-GlcNAc) (2 nmol) is a CapA1 substrate.



### Supplementary Figure 9

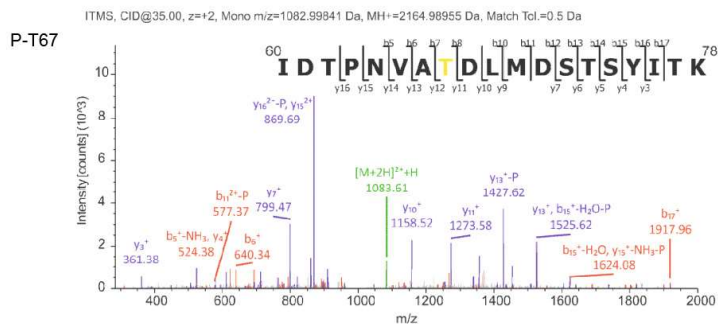
**CapA2 senses extracellular polysaccharides.** CapA2-mediated activation of CapB2 is inhibited by purified polysaccharides CP5 (b) and PNAG (d) in a concentration-dependent manner. In contrast, CapA1-mediated activation of CapB2 is neither affected in the presence of CP5 (a), nor in the presence of PNAG (c). Experiments were performed in triplicate. The error bars represent the  $\pm$  SD from three biological replicates. (e) Sequence alignment of CapA1 and CapA2 of *S. aureus* Newman. The extracellular loop is highlighted blue.



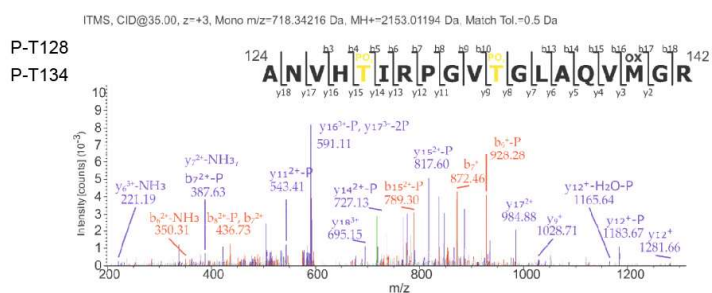
### Supplementary Figure 10

#### The ultimate PG precursor lipid II is no phosphodiesterase substrate for LcpC.

(a) CapA1 alone does not catalyze CP-to-PG attachment. Lipid I<sub>cap</sub> and [ $^{14}\text{C}$ ]lipid II<sub>PG</sub> were incubated in the absence or presence of CapA1 and reactions were analyzed by TLC and phosphoimaging. (b) Purified lipid II<sub>PG</sub> (2 nmol) was incubated with LcpC (4  $\mu\text{g}$ ). Purified lipid II<sub>PG</sub> was used as control. (c) Lipid I<sub>cap</sub> is a phosphodiesterase substrate for LcpC. LcpC alone is able to catalyze cleavage of lipid I<sub>cap</sub> releasing C<sub>55</sub>P (lane 3) compared to the heat-inactivated control (lane 2). Reaction mixtures were extracted with BuOH/PyrAc and analyzed by TLC and PMA staining. Purified lipid I<sub>cap</sub> and C<sub>55</sub>P were used as migration controls. (d) Antisense-RNA mediated depletion of CapA1 in a *S. aureus* Newman  $\Delta\text{lcpABC}$  mutant is lethal. (right) Expression of a pEPSA5-*capA1AS* encoded *capA1* antisense fragment in a *S. aureus* Newman  $\Delta\text{lcpABC}$  mutant induced with 500 mM xylose lead to growth inhibition whereas a wildtype (WT) strain was able to grow. Of note, a  $\Delta\text{lcpABC}$  mutant harbouring the empty vector (pEPSA5) as a control grew under similar conditions. (left) *S. aureus* Newman  $\Delta\text{lcpABC}$  harbouring pEPSA5 or pEPSA5-*capA1AS* grew under non-inducing conditions (2.5% glucose). All strains were grown on TSA-agar plates containing 34  $\mu\text{g ml}^{-1}$  chloramphenicol supplemented with either 2.5% glucose or 500 mM xylose. Strains lacking the pEPSA5 mediated chloramphenicol resistance were not able to grow. Pictures were taken against a red background.

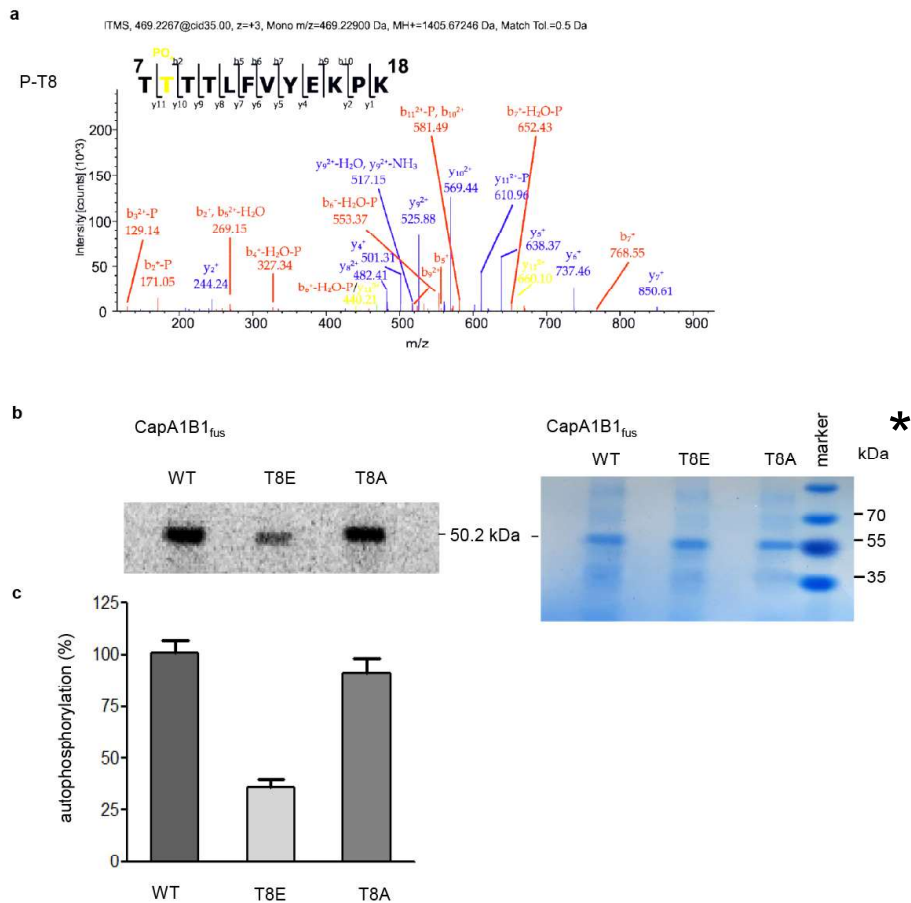


\*



## Supplementary Figure 11

Representative LC/MS spectrum for identification of PknB phosphorylation sites on CapM.



## Supplementary Figure 12

**PknB negatively controls CapB1 kinase activity.** (a) Representative LC/MS spectrum for identification of PknB phosphorylation sites on CapB1. (b) Analysis with loading controls (right) and (c) quantification of the autophosphorylation of a CapA1B1<sub>fus</sub>\_T8E-phosphomimetic and a CapA1B1<sub>fus</sub>\_T8A-phosphoablative variant compared to the wild-type protein. Experiments were performed in triplicate. The error bars represent the  $\pm$  SD from three biological replicates.

**Supplementary Table 1. Primers used in this study**

Primer	Sequence (5'→3')*
<i>capA1_F</i>	GCGCGGCTAGCATGGAAAGTACATTAGAATTAAC
<i>capA1_R</i>	GCGCGCTCGAGTTAATTAATTTTTGAATTGAACCC
<i>capA2_F</i>	GCGCGGCTAGCATGAAAGAAAAGTTTGATTTAGTAA
<i>capA2_R</i>	GCGCGCTCGAGTTAAAATTTTTGTATTGAACCTAAAA
<i>capB1_F</i>	GCGCGGCTAGCATGCTACTTATGTCAAAAAAGGA
<i>capB1_R</i>	GCGCGCTCGAGTTATTCATCTCCATAATAGTGAT
<i>capB2_F</i>	GCGCGGCTAGCATGACGAATACACGAAGAAGTA
<i>capB2_R</i>	GCGCGCTCGAGTCATTCATCAGTCCCATAATATG
<i>capC1_F</i>	GCGCGGCTAGCATGAATAAGTATGATTGATATTCAT
<i>capC2_R</i>	GCGCGCTCGAGTTATAACCCAAACCATCTTTTCT
<i>capA1B1fus_mut_F</i>	GATTGCCTGTATTGGGTTCAATTCAAAAATTTAATGCAG GATGGTTGCTACTTAT
<i>capA1B1fus_mut_R</i>	ATAAGTAGCAACCATCCTGCAATTAATTTTTGAATTGAA CCCAATACAGGCAATC
<i>capA2B2fus_mut_F</i>	AGGATTACCTATTTTAGGTTCAATACAAAAATTTTATTTA CGAGGAATTACCATG
<i>capA2B2fus_mut_R</i>	CATGGTAATTCCTCGTAAATAAAAATTTTTGTATTGAACCT AAAATAGGTAATCCT
<i>capA1B1fus_mutT8E_F</i>	GGAAAATACGGAAACAACACTATTTG
<i>capA1B1fus_mutT8E_R</i>	TTTTTTGACATAAGTAGCAAC
<i>capA1B1fus_mutT8A_F</i>	GTTTTTCATATACAAATAGTGTTGTTGCCGTATTTTCCTTT TTTGACATAAGTAG
<i>capA1B1fus_mutT8A_R</i>	CTACTTATGTCAAAAAAGGAAAATACGGCAACAACACTA TTTGTATATGAAAAAC
<i>capA1As_F</i>	GCGCGCGAGCTCTATATAAGCGCGACAACACTAATC
<i>capA1As_R</i>	GCGCGCGTTCGACAAACTGTAGTGAATCTAATCGG
<i>capE_mutY76_F</i>	GCGAGATGTTGATTTTCGTATTCCATGCAGCAGC
<i>capE_mutY76_R</i>	GCTGCTGCATGGAATACGAAATCAACATCTCGC
<i>capE_mutY290/293_F</i>	TACCGGTTTCAACAAAATTACTAAAATTTAAATCTCTGG AGTCTGCCGGCA



*capE\_mutY290/293\_R* TGCCGGCAGACTCCAGAGATTTAAATTTTAGTAATTTTG  
 TTGAAACCGGTA  
*capE\_mutY329\_F* TTATAATCATTCAATTCGTTTCTAACAAATTCTAGTGTTA  
 AAAGTTTTTCTTTTATCTCTTC  
*capE\_mutY329\_R* GAAGAGATAAAAGAAAACTTTTAACACTAGAATTTGTT  
 AGAAACGAATTGAATGATTATAA  
*capI\_F* AAAAGGATACTTAATCATATGAG  
*capI\_R* TAGTCTACCTCCTCGAGAAATT  
*capL\_F* AAGGACGTCGCTAGCATGAGTG  
*capL\_R* ATCGTCGACCTTCAACAGATTGTAATAC  
*capM\_F* GCGCGGCTAGCATGAAGCGATTATTCGATGTAG  
*capM\_R* GCGCGCTCGAGTTAGTGATGCACACCTTCTGA  
*capM\_mutY75\_F* ATTTAATGGATTCAACATCGTATTTAACAAAGACAGGGA  
 AGGTCAT  
*capM\_mutY75\_R* ATGACCTTCCCTGTCTTTGTTAAATACGATGTTGAATCCA  
 TTAAAT  
*capM\_mutY157\_F* GTAGCGTATGATCATTATTTCTTAACACATCAATCTATGA  
 GGG  
*capM\_mutY157\_R* CCCTCATAGATTGATGTGTTAAGAAATAATGATCATACG  
 CTAC  
*capN\_F* GTGCAGCTAGCATGAGAAAAAATATT  
*capN\_R* AATAGATCTCGAGTGCCTTATCTTTG  
*lcpC\_F* GCGCGGCTAGCATGAAACGTTTCGTCTAAAAGTAAA  
*lcpC\_R* GCGCGCTCGAGCTACTCTAGATTATCTTTTAATAAC

---

\*Restriction sites are underlined, nucleotide exchanges are indicated in bold.

### Supplementary Table 2. Plasmids used in this study

Plasmid	Description*	Source/Reference
pET21b	<i>E. coli</i> expression vector, C-terminal His <sub>6</sub> -tag, Amp <sup>R</sup>	Novagen
pET21b- <i>capI</i>	pET21b containing <i>capI</i> via <i>NheI/XhoI</i>	This work
pET21b- <i>capL</i>	pET21b containing <i>capL</i> via <i>NheI/SalI</i>	This work
pET24a	<i>E. coli</i> expression vector, C-terminal His <sub>6</sub> -tag, Amp <sup>R</sup>	Novagen

pET24a- <i>capD</i>	pET24a containing <i>capD</i> via <i>NheI/XhoI</i>	2
pET24a- <i>capN</i>	pET24a containing <i>capN</i> via <i>NheI/XhoI</i>	This work
pET28a	<i>E. coli</i> expression vector, N-terminal His <sub>6</sub> -tag, Kan <sup>R</sup>	Novagen
pET28a- <i>capA1</i>	pET28a containing <i>capA1</i> via <i>NheI/XhoI</i>	This work
pET28a- <i>capA2</i>	pET28a containing <i>capA2</i> via <i>NheI/XhoI</i>	This work
pET28a- <i>capB1</i>	pET28a containing <i>capB1</i> via <i>NheI/XhoI</i>	This work
pET28a- <i>capB2</i>	pET28a containing <i>capB2</i> via <i>NheI/XhoI</i>	This work
pET28a- <i>capA1B1fus</i>	pET28a derivative for expression of a N-terminally His <sub>6</sub> -tagged CapA1B1 fusion protein	This work
pET28a- <i>capA2B2fus</i>	pET28a derivative for expression of a N-terminally His <sub>6</sub> -tagged CapA2B2 fusion protein	This work
pET28a- <i>capA1B1fus_T8A</i>	pET28a- <i>capA1B1fus</i> derivative for expression of CapA1B1 <sub>fus</sub> _T8A	This work
pET28a- <i>capA1B1fus_T8E</i>	pET28a- <i>capA1B1fus</i> derivative for expression of CapA1B1 <sub>fus</sub> _T8E	This work
pET28a- <i>capM</i>	pET28a containing <i>capM</i> via <i>NheI/XhoI</i>	This work
pET28a- <i>capM_mut1</i>	pET28a- <i>capM</i> derivative for expression of CapM_Y75F	This work
pET28a- <i>capM_mut2</i>	pET28a- <i>capM</i> derivative for expression of CapM_Y157F	This work
pET28a- <i>capM_mut3</i>	pET28a- <i>capM</i> derivative for expression of CapM_Y[75,157]F	This work
pET28a- <i>lcpC</i>	pET28a containing <i>lcpC</i> (SA2103) via <i>NheI/XhoI</i>	This work
pET28a- <i>pglF</i>	pET28a containing truncated <i>C. jejuni pglF</i> via <i>NdeI/XhoI</i>	2
pET5F1.1	pET24a containing <i>capF</i> via <i>XhoI/NheI</i>	3
pET52b	<i>E. coli</i> expression vector, N-terminal Strep-tag, Amp <sup>R</sup>	Novagen
pET52b- <i>pknB</i>	pET52b containing <i>pknB</i> via <i>BamHI/SacI</i>	4
pKBK4	pET24a containing <i>capO</i> via <i>XbaI/EcoRI</i>	5
pKBK10	pET24a containing <i>capP</i> via <i>HindIII/EcoRI</i>	5
pKBK6a	pET24a containing <i>capG</i> via <i>XbaI/EcoRI</i>	3
pKBK50d	pET24a containing <i>capE</i> via <i>XhoI/NheI</i>	3
pKBK50d_mut1	pKBK50d derivative for expression of CapE_Y76F	This work

pKKBK50d_mut2	pKKBK50d derivative for expression of CapE_Y[290,293,329]F	This work
pKKBK50d_mut3	pKKBK50d derivative for expression of CapE_Y[76,290,293,329]F	This work
pCU1	<i>E. coli</i> - <i>S. aureus</i> shuttle plasmid, Amp <sup>R</sup> , Cm <sup>R</sup>	6
pCapA1	pCU1 harbouring <i>capA1</i>	7
pEPSA5	<i>E. coli</i> - <i>S. aureus</i> shuttle plasmid, Amp <sup>R</sup> , Cm <sup>R</sup>	8
pEPSA5- <i>capA1AS</i>	pEPSA5 containing <i>capA1</i> antisense fragment via <i>SacI/SalI</i>	This work
pCapA1B1	pOS1-Plgt harbouring <i>capA1B1</i> fusion fragment via <i>NdeI/XhoI</i>	This work

\*Resistance marker: Amp<sup>R</sup>, ampicillin; Cm<sup>R</sup>, chloramphenicol; Kan<sup>R</sup>, kanamycin.

## Supplementary Methods

\*\*

***ESI-TOF mass spectrometric analysis of lipid intermediates.*** Electrospray. MS spectra were recorded on a micrOTOF-Q quadrupole time of flight instrument (Bruker Daltonics) working in negative mode. Samples were infused at 0.05 ml h<sup>-1</sup>, (in methanol-chloroform, 1:1). Signals from the [M-H]<sup>-</sup> ions were accompanied in all cases by those from the monosodium adduct and those from the monopotassium adduct.

***Identification of phosphorylation sites by nanoLC-MS/MS.*** *In vitro* phosphorylation of recombinant His<sub>6</sub>-tagged proteins, followed by SDS-PAGE separation with omission of radiolabeled ATP from the reaction mixture. For peptide preparation, protein bands were excised from the Coomassie-stained polyacrylamide gels and subjected to tryptic in-gel digestion<sup>9,10</sup>. In brief, proteins were reduced with 20 mM DTT, slices were washed with 50 mM ammonium bicarbonate, and proteins were alkylated with 40 mM iodoacetamide. The slices were washed again and dehydrated with acetonitrile. Slices were dried in a vacuum concentrator and incubated with 400 ng sequencing grade trypsin at 37 °C overnight. The peptide extract was dried in a vacuum concentrator and stored at -20 °C. Dried peptides were dissolved in 10 µl 0.1% formic acid (solvent A), and aliquots (1 µl) were injected onto a C18 trap column (20 mm x 100 µm, NanoSeparations). Bound peptides were eluted onto a C18 analytical column (200 mm x 75 µm, NanoSeparations). Peptides were separated during a

linear gradient from 0% to 55% solvent B (80% acetonitrile, 0.1% formic acid) within 40 min at a flow rate of 400 nl min<sup>-1</sup>. The nanoHPLC was coupled online to an LTQ Orbitrap Velos mass spectrometer (Thermo Fisher Scientific). Peptide ions between 395 and 1800 *m/z* were scanned in the orbitrap detector with a resolution of 30,000 (maximum fill time 400 ms, AGC target 10<sup>6</sup>). The 25 most intense precursor ions (threshold intensity 5000) were subjected to collision induced dissociation and fragments were analyzed in the linear ion trap. Fragmented peptide ions were excluded from repeat analysis for 15 s.

Raw data processing and analysis of database searches were performed with Proteome Discoverer software version 1.40.288 (Thermo Fisher Scientific). Peptide identification was done with an in house Mascot server version 2.3 (Matrix Science Ltd, UK). MS2 data was searched against *S. aureus* N315 NCBI nr (release 20130323) and *E. coli* sequences from SwissProt (release 2013\_03). Precursor ion *m/z* tolerance was 8 ppm, fragment ion tolerance 0.6 Da, b- and y-ion series were included. Semitryptic peptides with up to one missed cleavage were searched. The following dynamic modifications were set: Alkylation of Cys by iodoacetamide or acrylamide, phosphorylation (Ser, Thr, Tyr), and oxidation (Met). The PhosphoRS3.0 node was used for scoring of the phosphosite assignment<sup>11</sup>. Mascot results from searches against SwissProt were sent to the percolator algorithm<sup>12</sup> version 2.04 as implemented in Proteome Discoverer 1.4.

***In vitro* lipid II synthesis.** Synthesis and purification of lipid II was performed using membranes of *Micrococcus luteus* as described<sup>13-15</sup>. In short, membrane preparations (200 µg protein) were incubated in the presence of purified substrates, 5 nmol undecaprenylphosphate (C<sub>55</sub>P), 50 nmol UDP-MurNAc-pp and 50 nmol [<sup>14</sup>C]-UDP-GlcNAc in 60 mM Tris-HCl, 5 mM MgCl<sub>2</sub>, pH 7.5, and 0.5% (w/v) Triton X-100 in a total volume of 50 µl for 1 h at 30 °C. Bactoprenol containing products were extracted with the same volume of butanol/pyridine acetate (2:1; vol:vol; pH 4.2) and analyzed by TLC using phosphomolybdic acid (PMA) staining. For synthesis of higher quantities of lipid II the assay was scaled up and purification was performed as described<sup>16</sup>. Reaction mixtures were incubated for 4 h at 30 °C, and lipids were extracted with the same volume of BuOH/PyrAc. Purification of lipid II was performed on a DEAE-cellulose column (0.9 × 25 cm, DEAE SS-Typ; Serva) and eluted in a linear gradient from chloroform-methanol-water (2:3:1) to chloroform-methanol-30 mM ammonium bicarbonate (2:3:1).

**Construction of cap deletion mutants.** Tn mutations in the *cap* genes (*capA2*, *capB2*, *capA1* and *capB1*) were transduced from USA300 mutants into Streptomycin-resistant strain Newman with phage 80 as described by Foster<sup>17</sup> with selection on erythromycin (5 µg ml<sup>-1</sup>) plates. The mutations were confirmed by PCR, antibiotic resistance, and hemolytic phenotype, and CP5 production was assessed by colony immunoblot<sup>18</sup> and ELISA inhibition assays<sup>19</sup> CP5 was purified from *S. aureus* as described previously<sup>20</sup>.

### Supplementary References

1. Ray, L. C. *et al.* Membrane association of monotopic phosphoglycosyl transferase underpins function. *Nat. Chem. Biol.* **14**, 538–541 (2018).
2. Li, W. *et al.* Analysis of the Staphylococcus aureus capsule biosynthesis pathway in vitro: Characterization of the UDP-GlcNAc C6 dehydratases CapD and CapE and identification of enzyme inhibitors. *Int. J. Med. Microbiol. IJMM* **304**, 958–969 (2014).
3. Kneidinger, B. *et al.* Three Highly Conserved Proteins Catalyze the Conversion of UDP-N-acetyl-d-glucosamine to Precursors for the Biosynthesis of O Antigen in Pseudomonas aeruginosa O11 and Capsule in Staphylococcus aureus Type 5 IMPLICATIONS FOR THE UDP-N-ACETYL-1-FUCOSAMINE BIOSYNTHETIC PATHWAY. *J. Biol. Chem.* **278**, 3615–3627 (2003).
4. Hardt, P. *et al.* The cell wall precursor lipid II acts as a molecular signal for the Ser/Thr kinase PknB of Staphylococcus aureus. *Int. J. Med. Microbiol.* **307**, 1–10 (2017).
5. Kiser, K. B. & Lee, J. C. Staphylococcus aureus cap5O and cap5P genes functionally complement mutations affecting enterobacterial common-antigen biosynthesis in Escherichia coli. *J. Bacteriol.* **180**, 403–406 (1998).
6. Augustin, J. & Götz, F. Transformation of Staphylococcus epidermidis and other staphylococcal species with plasmid DNA by electroporation. *FEMS Microbiol. Lett.* **66**, 203–207 (1990).
7. Jansen, A. *et al.* Production of capsular polysaccharide does not influence Staphylococcus aureus vancomycin susceptibility. *BMC Microbiol.* **13**, 65 (2013).
8. Forsyth, R. A. *et al.* A genome-wide strategy for the identification of essential genes in Staphylococcus aureus. *Mol. Microbiol.* **43**, 1387–1400 (2002).
9. Rosenfeld, J., Capdevielle, J., Guillemot, J. C. & Ferrara, P. In-gel digestion of proteins for internal sequence analysis after one- or two-dimensional gel electrophoresis. *Anal. Biochem.* **203**, 173–179 (1992).

10. Jenö, P., Mini, T., Moes, S., Hintermann, E. & Horst, M. Internal sequences from proteins digested in polyacrylamide gels. *Anal. Biochem.* **224**, 75–82 (1995).
11. Taus, T. *et al.* Universal and confident phosphorylation site localization using phosphoRS. *J. Proteome Res.* **10**, 5354–5362 (2011).
12. Käll, L., Storey, J. D., MacCoss, M. J. & Noble, W. S. Assigning significance to peptides identified by tandem mass spectrometry using decoy databases. *J. Proteome Res.* **7**, 29–34 (2007).
13. Umbreit, J. N. & Strominger, J. L. Isolation of the lipid intermediate in peptidoglycan biosynthesis from *Escherichia coli*. *J. Bacteriol.* **112**, 1306–1309 (1972).
14. Brötz, H. *et al.* Role of lipid-bound peptidoglycan precursors in the formation of pores by nisin, epidermin and other lantibiotics. *Mol. Microbiol.* **30**, 317–327 (1998).
15. Wiedemann, I. *et al.* Specific binding of nisin to the peptidoglycan precursor lipid II combines pore formation and inhibition of cell wall biosynthesis for potent antibiotic activity. *J. Biol. Chem.* **276**, 1772–1779 (2001).
16. Schneider, T. *et al.* In vitro assembly of a complete, pentaglycine interpeptide bridge containing cell wall precursor (lipid II-Gly5) of *Staphylococcus aureus*. *Mol. Microbiol.* **53**, 675–685 (2004).
17. Foster, T. J. 7.9 Molecular Genetic Analysis of Staphylococcal Virulence. *Methods Microbiol. JK Peter Williams George Acad. Press* **27**, 433–454 (1998).
18. Lee, J. C., Liu, M. J., Parsonnet, J. & Arbeit, R. D. Expression of type 8 capsular polysaccharide and production of toxic shock syndrome toxin 1 are associated among vaginal isolates of *Staphylococcus aureus*. *J. Clin. Microbiol.* **28**, 2612–2615 (1990).
19. Lee, J. C., Takeda, S., Livolsi, P. J. & Paoletti, L. C. Effects of in vitro and in vivo growth conditions on expression of type 8 capsular polysaccharide by *Staphylococcus aureus*. *Infect. Immun.* **61**, 1853–1858 (1993).
20. Tzianabos, A. O., Wang, J. Y. & Lee, J. C. Structural rationale for the modulation of abscess formation by *Staphylococcus aureus* capsular polysaccharides. *Proc. Natl. Acad. Sci.* **98**, 9365–9370 (2001).

## 4.2 Cacaoidin, first member of the new lanthidin RiPP family

Natural products represent a rich source of compounds with highly diverse structures and wide-ranging bioactivities, especially if compared to conventional synthetic small molecule libraries. They play pivotal roles in drug discovery and were found to be particularly effective as treatment options for cancerous and infectious diseases (Rodrigues et al., 2016). A decline in natural product antibiotic discovery by the pharmaceutical industry from the 1990s onwards was due to different obstacles, such as technical difficulties in screening, isolation, and characterization. Today, improved analytical tools, genome mining and engineering strategies, and microbial culturing advances bring natural products back into the spotlight as interesting drug leads, particularly to combat antimicrobial resistance.

The Fundación MEDINA, Spain runs a natural product drug discovery platform aimed at the I) production of new microbial natural products, II) the development of chemical and molecular tools to support natural products discovery, and III) the identification of new potential therapeutic applications. As part of the screening program focused on finding novel substance classes with antimicrobial activity, cacaoidin (CAO), produced by a *Streptomyces cacaoi* CA-170360 strain, was isolated. With the discovery of CAO, a new subfamily of ribosomally synthesized and post-translationally modified peptides (RiPPs) was introduced. This peptide family has been designated **lanthidins**, due to the co-occurrence of a lanthionine ring and a dimethylated N-terminus, which are characteristic features of the **lanthipeptide** and **linaridin** RiPP families. The initial classification at the time of publication was based on the observation that the *cao* biosynthetic gene cluster shows low homology with those associated with linaridin and lanthipeptide biosynthesis, suggesting an alternative pathway for lanthionine ring synthesis distinct from class I-IV lanthipeptides. Further investigations and latest findings on the structurally similar lanthionine-containing lexapeptide and the associated three-component lanthionine synthetase, proposed to catalyze lanthionine ring formation, redefined the categorization of cacaoidin and lexapeptide as class V lanthipeptides. The initial classification of cacaoidin as a new lanthidin RiPP family might therefore not be entirely correct and it is important to highlight this dual classification in future communications.

Isolation and structural elucidation (via NMR spectroscopy, mass spectrometry and chemical derivatization) as well as preliminary assessment of cacaoidin's antimicrobial activity were conducted at MEDINA by the work group of Olga Genilloud. Further investigations of the antibiotic activity spectrum as well as whole cell reporter assays aimed at elucidating the mode of action and potential molecular targets of cacaoidin were performed as part of this work.

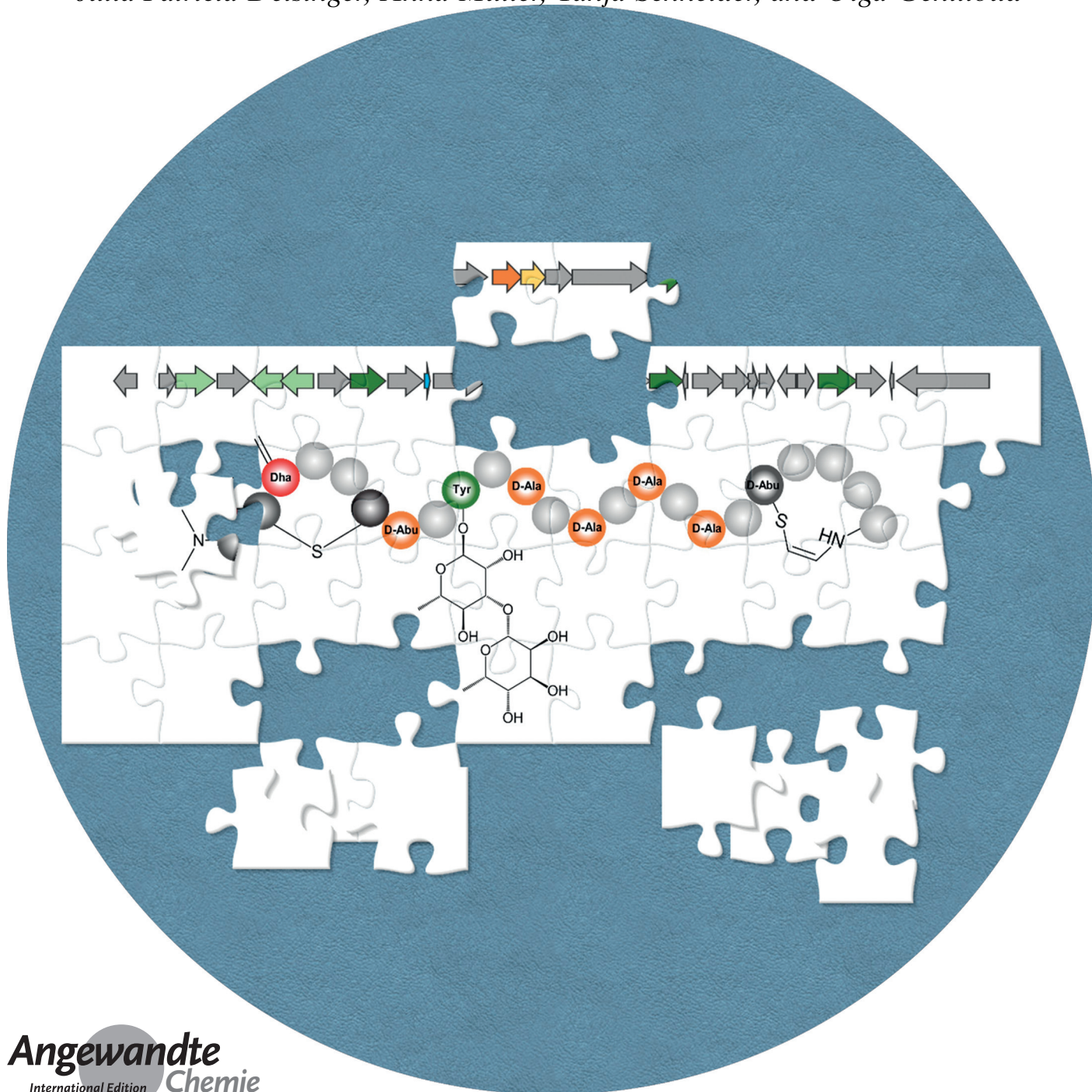
Natural Products **Hot Paper**How to cite: *Angew. Chem. Int. Ed.* **2020**, 59, 12654–12658

International Edition: doi.org/10.1002/anie.202005187

German Edition: doi.org/10.1002/ange.202005187

# Cacaoidin, First Member of the New Lanthidin RiPP Family

Francisco Javier Ortiz-López,\* Daniel Carretero-Molina, Marina Sánchez-Hidalgo, Jesús Martín, Ignacio González, Fernando Román-Hurtado, Mercedes de la Cruz, Sergio García-Fernández, Fernando Reyes, Julia Patricia Deisinger, Anna Müller, Tanja Schneider, and Olga Genilloud





**Abstract:** Lantibiotics are ribosomally synthesized and post-translationally modified peptides (RiPPs) characterized by the presence of lanthionine or methyllanthionine rings and their antimicrobial activity. Cacaoidin, a novel glycosylated lantibiotic, was isolated from a *Streptomyces cacaoi* strain and fully characterized by NMR, mass spectrometry, chemical derivatization approaches and genome analysis. The new molecule combines outstanding structural features, such as a high number of D-amino acids, an uncommon glycosylated tyrosine residue and an unprecedented N,N-dimethyl lanthionine. This latter feature places cacaoidin within a new RiPP family located between lanthipeptides and linaridins, here termed lanthidins. Cacaoidin displayed potent antibacterial activity against Gram-positive pathogens including *Clostridium difficile*. The biosynthetic gene cluster showed low homology with those of other known lanthipeptides or linaridins, suggesting a new RiPP biosynthetic pathway.

**R**ibosomally synthesized and post-translationally modified peptides (RiPPs) represent a major class of natural products which comprise numerous families covering a wide structural diversity.<sup>[1]</sup> One of the most thoroughly studied RiPP classes are the lanthipeptides,<sup>[2]</sup> which are characterized by the presence of the thioether-bridged amino acids lanthionine (Lan) and methyllanthionine (MeLan). Many lanthipeptides are also named lantibiotics due to their potent antimicrobial activities.<sup>[3,4]</sup> Lantibiotics may exert their effects by different mechanisms of action,<sup>[5]</sup> one of the most prominent being the interaction with Lipid II, an essential component of the peptidoglycan (PGN) barrier considered as the “Achilles’ heel” of cell wall biosynthesis in bacteria.<sup>[6]</sup>

The global threat posed by the current antibiotic resistance crisis makes the discovery of novel antibacterial agents an urgent need. During a screening program aimed at finding bacterial cell wall inhibitors, culture extracts of the strain *Streptomyces cacaoi* CA-170360 showed potent activity against methicillin-resistant *Staphylococcus aureus* (MRSA) and triggered the induction of the LiaRS (Lipid II cycle

interfering antibiotic response regulator and sensor) bioreporter,<sup>[7,8]</sup> which indicated interference with the Lipid II biosynthesis cycle (Supporting Information, Figure S1). Bioassay-guided fractionation of the culture extracts and subsequent HPLC-HRESIMS analysis of the active fractions led to the identification of the bioactive compound, cacaoidin (**1**), as a peak with a  $[M+H]^+$  ion at  $m/z$  2360.1332, indicative of the molecular formula  $C_{107}H_{162}N_{24}O_{32}S_2$  ( $\Delta + 1.27$  ppm). This was further supported by the presence of  $[M+2NH_4]^{2+}$  and  $[M+2H+NH_4]^{3+}$  ions at  $m/z$  1197.5932 and 793.0555 respectively. Additionally, the presence of two in-source fragment ions at  $m/z$  2068.0164 and 2214.0745 indicated the sequential loss of two deoxyhexose units, thus revealing the partial glycosidic nature of the compound. (Supporting Information, Figures S2–S6). Searches in different natural products databases failed to identify any known metabolite with the observed exact mass, suggesting that **1** was a new natural product. The producing strain CA-170360 was then cultivated in large scale and the novel compound, cacaoidin (**1**), was isolated as described in the Supporting Information (SI, section 2.2), yielding approximately 6 mg of compound from a 3 L culture. The structure of cacaoidin (**1**, Figure 1) was fully characterized by combining NMR spectroscopy, HRMS/MS and chemical derivatization approaches. The core peptide sequence derived from the biosynthetic gene cluster (BGC) was lastly used as a reference to corroborate the sequence of the mature peptide and the stereochemistry of the constituent amino acids. Further inspection of the glycosyltransferases found in the BGC (see description below) served us to propose the absolute configuration for the monosaccharide units present in the molecule.

NMR spectroscopy was extensively applied to partially elucidate the structure of **1** (see SI, section 2.3 for details). Along with different proteinogenic amino acids, modified residues such as aminobutyric acid (Abu), dehydroalanine (Dha) and aminovinyl-methyl-cysteine (AviMeCys) were found in **1**. The glycosylating unit was identified as the disaccharide  $\beta$ -6-deoxygulopyranosyl-(1 $\rightarrow$ 3)- $\alpha$ -rhamnopyranoside, which as far as we know, has not been previously reported in any other natural product. This unit was found to be attached to the phenolic oxygen of a tyrosine residue in **1** on the basis of the corresponding HMBC correlations (SI, sections 2.3 and 2.11; Figure S28). Tyr-*O*-glycosylation within a peptide is uncommon in natural products, being mannopeptimycins<sup>[9]</sup> the only compounds isolated from bacteria with this feature. Overall, this makes cacaoidin only the second example of a glycosylated lantibiotic after NAI-112.<sup>[10]</sup>

Furthermore, an unprecedented N,N-dimethyl lanthionine system (NMe<sub>2</sub>Lan) was found to be present in **1**, based on the characteristic chemical shifts in the HSQC and the key cross-peaks in the HMBC spectrum (SI, sections 2.3 and 2.11; Figure S28). Thus far, the N-terminus dimethylation has been reported only for the rare linaridin family,<sup>[11–14]</sup> whose members lack lanthionine rings. The involvement of a dimethylated N-terminus in a Lan ring (NMe<sub>2</sub>Ala-S-Ala) is reported here for the first time within RiPPs and further highlights the structural novelty of cacaoidin.


Collectively, the NMR data allowed us to unambiguously connect the major fragments of the peptide sequence in

[\*] Dr. F. J. Ortiz-López, M. Sc. D. Carretero-Molina, Dr. M. Sánchez-Hidalgo, M. Sc. J. Martín, Dr. I. González, M. Sc. F. Román-Hurtado, Dr. M. de la Cruz, Dr. F. Reyes, Dr. O. Genilloud  
Fundación MEDINA, Centro de Excelencia en Investigación de Medicamentos Innovadores en Andalucía, Avenida del Conocimiento, 34. Parque Tecnológico de Ciencias de la Salud, 18016 Armilla, Granada (Spain)  
E-mail: javier.ortiz@medinaandalucia.es

Dr. S. García-Fernández  
Hospital Universitario, Ramón y Cajal. Ctra. de Colmenar Viejo, km. 9,100, 28034 Madrid (Spain)

M. Sc. J. P. Deisinger, Dr. A. Müller, Dr. T. Schneider  
Institute for Pharmaceutical Microbiology, University Clinic Bonn, University of Bonn, Meckenheimer Allee 168, 53115 Bonn (Germany)

M. Sc. J. P. Deisinger, Dr. T. Schneider  
DZIF, German Center for Infection Research, partner site Bonn-Cologne, Bonn (Germany)

 Supporting information and the ORCID identification number(s) for the author(s) of this article can be found under <https://doi.org/10.1002/anie.202005187>.

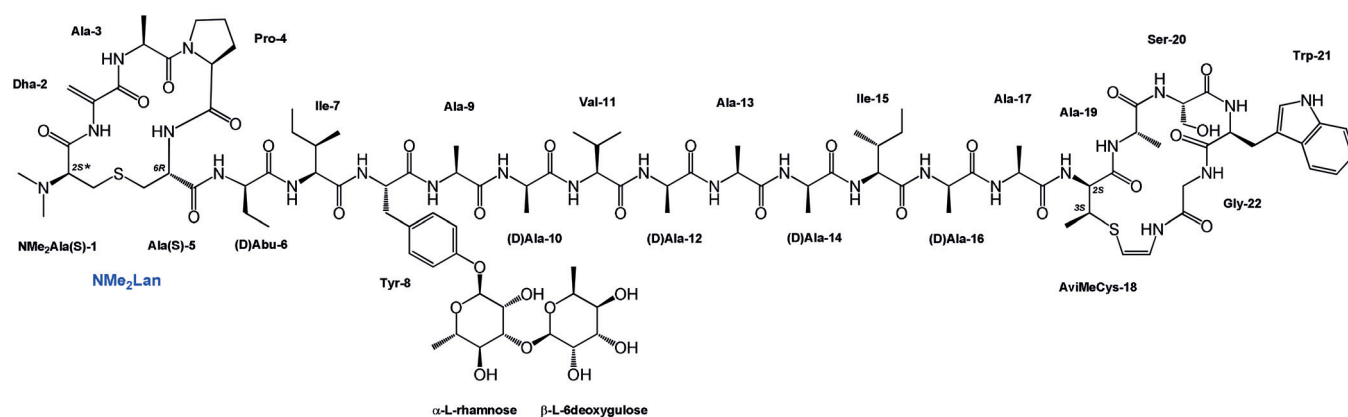


**Figure 1.** Structure of cacaoidin (**1**). Stereochemistry of NMe<sub>2</sub>Lan is proposed as DL (2S\*, 6R). (\* indicates tentative stereochemistry).

cacaoidin, including the NMe<sub>2</sub>Lan-Dha fragment at the N-terminus and the AviMeCys-containing ring at the C-terminus of **1** (SI, Figure S14). We then took advantage of whole genome sequencing of the producing strain. Genome mining using the C-terminus sequence as a probe led to the identification of a 162 bp open reading frame (ORF) encoding the precursor peptide (*caoA*) and within it, a core sequence comprising a 23-mer peptide (Figures 2 and S15). The cleavage site for the proteolytic removal of the leader peptide<sup>[15]</sup> was identified as the only region in the precursor peptide in which two adjacent serine residues were found, since only such sequence could finally render the NMe<sub>2</sub>Ala-Dha substructure at the N-terminus of **1**. The mass difference of 152 Da between the predicted peptide (2219 Da) (SI, Figure S15), and the aglycon of the mature peptide (2067 Da) was partially explained by the post-translational modifications (PTMs) occurred on **1**, that is, dimethylation of the N-terminus, three dehydrations (ultimately resulting in Dha, NMe<sub>2</sub>Lan and AviMeCys), and one oxidative decarboxylation at the C-terminal Cys residue (AviMeCys). The remaining difference of 80 Da could be attributed to dehydrations and subsequent hydrogenations for five amino acids in the core peptide, thus advancing the presence of five D-amino acids in the final structure (see discussion below).

To corroborate the relationship between the genomic and NMR-based sequences, tandem-mass spectrometry was applied so that pseudo molecular ions  $[M+H]^+$  and  $[M+2NH_4]^{2+}$  were alternatively subjected to MS/MS fragmentation. The in-source fragment ion at  $m/z$  523.2328 ( $b_6$  ion) was also fragmented in a pseudo-MS<sup>3</sup> approach (Figures 2 and S20) and the annotation of the resulting product ions allowed us to fill the gaps from NMR data and validated the amino acid sequence of **1** (SI, Figures S16–S21). Additionally, the topology of the N-terminus ring in cacaoidin was definitively confirmed by reduction-desulfurization<sup>[16]</sup> and subsequent HRMS/MS analysis (SI, section 2.5). Jointly, these MS results allowed us to establish the full connectivity of **1** and integrate all its NMR data (SI, Figure S28 and Table S1).

The planar structure of **1** confirmed the dehydration of genetically encoded Ser-1, Ser-2 and Thr-18 and the subsequent addition of Cys-5 and (decarboxylated) Cys-23 to the

transients Dha-1 and Dhb-18 respectively (to ultimately originate the N-terminus Lan and the C-terminus AviMeCys rings) (SI, Figure S48). The biosynthetic origin of AviMeCys in **1** is therefore the same as that described for lanthipeptides and lipolanthines,<sup>[17]</sup> and different to that reported for linaridins, in which the AviCys is formed between two cysteine residues.<sup>[11–14]</sup>

At the same time, it was shown that four of the serine amino acids in the genomic sequence (Ser-10, Ser-12, Ser-14 and Ser-16) were present in the final structure as Ala residues and remarkably, Thr-6 had been modified to finally appear as an aminobutyric acid residue (Abu) in **1**. The conversion of L-Ser or L-Thr to D-Ala or D-Abu, respectively has been reported for a few RiPPs such as lacticin 3147,<sup>[18]</sup> carnolysin,<sup>[19]</sup> and bicereucin<sup>[20]</sup> and proved to occur through dehydration and subsequent reduction (hydrogenation) of the genetically encoded amino acid. To confirm those conversions and determine the absolute configurations for all the amino acids in **1**, we proceeded in different stages. First, advanced Marfey's analysis<sup>[21]</sup> of **1** led us to determine that Pro-4, Ile-7 and Ile-15, Tyr-8, Val-11, Ser-20 and Trp-21 were all L-amino acids (SI, Figures S32–S38). It also revealed the presence of both L- and D-Ala, the relative peak area suggesting a ratio of 5 L-Ala to 4 D-Ala (SI, Figures S40 and S41). This was consistent with the formation of the D-Ala stereoisomer in **1** exclusively from the four genetically encoded serine residues (SI, Figure S48). Furthermore, the presence of D-Abu was confirmed (SI, Figure S39), which makes cacaoidin the third example of RiPP with this structural feature, after carnolysin<sup>[19]</sup> and bicereucin.<sup>[20]</sup>

Regarding the AviMeCys ring, a Z-geometry for the double bond was determined based on the corresponding  $^3J_{H,H}$  value (7.5 Hz). (SI, Table S1). By combining desulfurization approaches and Marfey's analysis (SI, section 2.8), the (2S, 3S) configuration was established for the Abu-S unit within the C-terminus ring of **1**, which matches with the stereochemistry reported thus far for AviMeCys in all lanthipeptides.

To determine the absolute configuration of NMe<sub>2</sub>Lan by Marfey's analysis, a comparison with pure DL or LL (the two different stereochemistries reported for Lan or MeLan) standard samples was unfortunately not possible since they

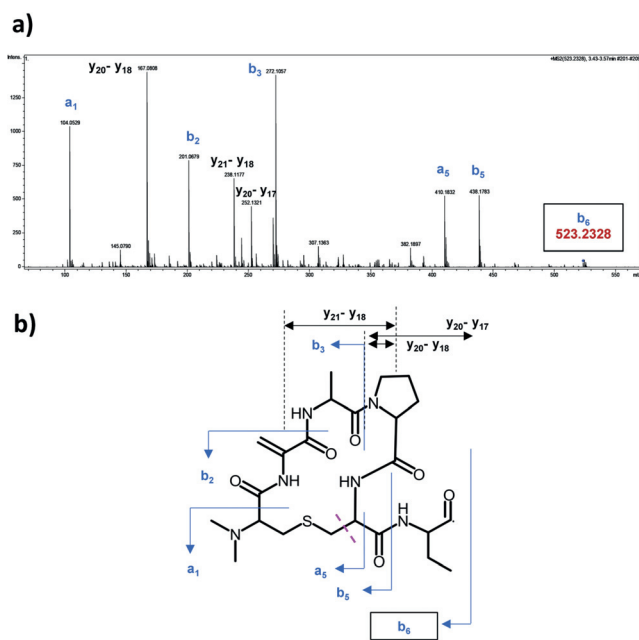


**Figure 2.** a) Key MS/MS fragmentation of in source fragment  $b_6$  ion ( $m/z$  523.2328). b) Key fragments within the N-terminal ring of **1**, comprising NMe<sub>2</sub>Lan.

are not commercially available. Nevertheless, the elution order “D before L” observed for the FDVA derivatives of NMe<sub>2</sub>Lan in **1** resembled the behavior of the Marfey-derivatives (both mono- and di-) of DL-MeLan in nisin A and pinensin B,<sup>[22]</sup> so a DL (2*S*, 6*R*) absolute configuration for NMe<sub>2</sub>Lan was tentatively assigned (SI, Figures S42–S44). Although DL is the configuration mostly found for (Me)Lan in lanthipeptides,<sup>[23]</sup> the alternative LL-(Me)Lan stereochemistry has been recently reported for cytolysins S and L (CylL<sub>S</sub>, CylL<sub>L</sub>)<sup>[24]</sup> and haloduracin  $\beta$  (Hal $\beta$ ),<sup>[25]</sup> all of them bearing a common Dh<sub>x</sub>-Dh<sub>x</sub>-X<sub>xx</sub>-X<sub>xx</sub>-Cys (Dh<sub>x</sub> = Dha or Dhb) sequence motif in their dehydrated precursors. The Dha-Dha-Ala-Pro-Cys sequence in the cacaoidin precursor (SI, Figure S48) thus suggests it might also cyclize with LL-stereochemistry. Based on the experimental result from Marfey’s analysis we propose here a DL stereochemistry for NMe<sub>2</sub>Lan, although additional evidences are needed to confirm it.

The analysis of the ORFs contiguous to *caoA* led to the identification of a putative 30 Kb BGC containing 27 ORFs (GenBank MT210103). Genes involved in some of the post-translational modifications of cacaoidin were assigned (Figure 3, Table S2). A homologous protein to cypemycin decarboxylase CypD<sup>[11]</sup> (CaoD) would account for the generation of the C-terminal AviMeCys ring, while a protein with homology to flavin-dependent oxidoreductases (Cao12) might be involved in the hydrogenation of both Dha and Dhb to D-Ala and D-Abu, respectively, as previously described for LanJ<sub>B</sub> enzymes such as CrnJ<sup>[19]</sup> and BsjJ<sub>B</sub>.<sup>[20]</sup> Conversely, the *cao* cluster does not encode any protein homologous to dehydratases described in class I lanthipeptide (i.e., LanB) or linaridin (e.g., CypH) BGCs. Moreover, the cluster lacks classical type I–IV lanthipeptide biosynthetic

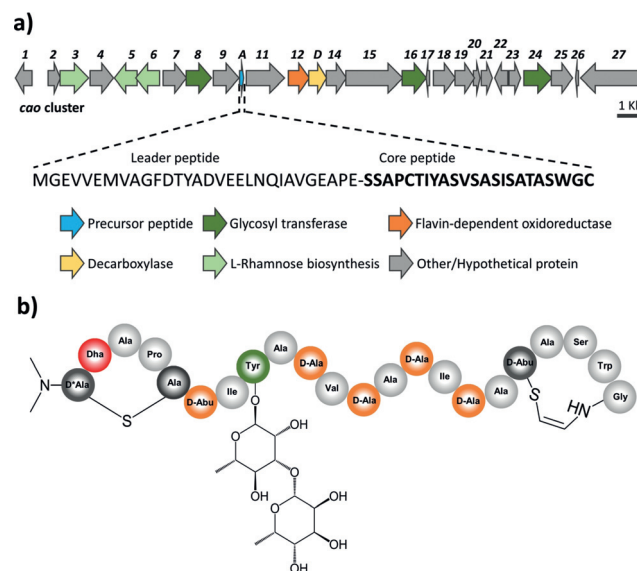


**Figure 3.** a) The cacaoidin (*cao*) BGC. Genes with predicted functions are color-coded as shown. The sequences of the putative leader peptide and the core peptide of cacaoidin are indicated. b) Depiction of cacaoidin showing amino acids as coloured balls according to different PTMs. (\* indicates tentative stereochemistry).

enzymes involved in the formation of lanthionine rings (i.e., LanC, LanM, LanKC and LanL), suggesting a modified or non-enzymatic cyclization mechanism. On the other hand, homologous proteins to CypM, reported to be responsible for the N-terminal Ala dimethylation in cypemycin,<sup>[11]</sup> are not found in the cluster. Although Cao4 shows homology to a methyltransferase, the analysis of its conserved domains suggests a role as *O*-methyltransferase (SI, Table S2).

Regarding the glycosylation of **1**, three glycosyl-transferases (GTs) are encoded in the BGC (Cao8, Cao16 and Cao24; see Figure 3 and Table S2). Additionally, genes involved in the biosynthesis of L-rhamnose<sup>[26]</sup> are also found in the cluster, strongly supporting the L configuration for the rhamnose unit in **1**. On the basis of these findings and the inverting or retaining nature of these GTs,<sup>[27]</sup> the absolute configuration for 6-deoxygulose sugar moiety was tentatively assigned as follows: Cao8 and Cao16 are similar proteins belonging to the inverting GT-2 family (SI, Figure S49), so we propose that one of them, or perhaps both in a cooperative fashion, are responsible for the introduction of the  $\alpha$ -L-rhamnose unit. Cao24, belonging to the retaining GT-4 family (SI, Figure S49), can then be involved in the attachment of the  $\beta$ -6-deoxygulose unit, so a L configuration is also proposed for this sugar. This analysis ultimately completed the proposal for the full stereochemistry of cacaoidin (**1**, Figure 1).

Finally, the antibacterial activity of **1** was evaluated against different Gram-positive pathogens (Table 1). Cacaoidin showed potent activity against MRSA (MIC 0.5  $\mu\text{g mL}^{-1}$ ) and moderate activity against a set of *Clostridium difficile* strains. Induction of LiaRS bioreporter in a dose-dependent manner was confirmed for **1** (SI, Figure S50) and  $\beta$ -galactosidase gene expression bioreporters for major biosynthetic pathways clearly suggested the cell wall synthesis as the specific target pathway (SI, Figure S51). Further antagoniza-

**Table 1:** Minimum inhibitory concentration (MIC) of **1** against selected strains.

Strain <sup>[a]</sup>	MIC [ $\mu\text{g mL}^{-1}$ ]	MIC [ $\mu\text{M}$ ]
<i>Staphylococcus simulans</i> 22	0.25	0.11
MRSA MB5393 <sup>[a]</sup>	0.5	0.22
<i>S. aureus</i> SG511	2	0.85
<i>S. aureus</i> SG511 DapR	32	13.60
<i>Mycobacterium tuberculosis</i> H37Ra	32	13.60
<i>Bacillus subtilis</i> 168	8	3.40
<i>Clostridium difficile</i> RyC 11872343 (toxigenic) <sup>[a]</sup>	8	3.40
<i>C. difficile</i> RyC 11945271 (toxigenic) <sup>[a]</sup>	4	1.70

[a] Clinical isolate.

tion of the LiaRS stress response by purified cell wall precursor strongly supported Lipid II binding as the most plausible mechanism of action (SI, Figure S52).

In summary, cacaoidin (**1**) is a novel glycosylated lantibiotic which combines remarkable structural features, such as an uncommon Tyr-*O*-glycosylation with a 6-deoxygulopyranosyl-(rhamnopyranose) disaccharide and a high number of D-amino acids including D-Abu. Unique among RiPPs, cacaoidin exhibits an unprecedented *N,N*-dimethyl lanthionine system (NMe<sub>2</sub>Lan). While (Me)Lan rings are a specific feature of lanthipeptides, the terminal *N*-methylation is restricted to linaridins, which in turn lack lanthionine rings. The co-occurrence in **1** of structural elements exclusive to different families appoints cacaoidin the first member of a new RiPP (sub-)family located between lanthipeptides and linaridins, which we suggest naming lanthidins. Consistently, the gene cluster shows low homology with those of other lanthipeptides or linaridins, thus advancing an alternative RiPP biosynthetic pathway whose details are currently being explored.

## Acknowledgements

We thank Dr. Ignacio Pérez-Victoria for assistance in the acquisition of special NMR experiments and helpful discussions. Funding was provided by Fundación MEDINA and the German Center for Infection Research (DZIF).

## Conflict of interest

The authors declare no conflict of interest.

**Keywords:** lanthidin · lantibiotic · natural products · RiPP family · tyrosine-*O*-glycosylation

- [1] P. G. Arnison, M. J. Bibb, G. Bierbaum, A. A. Bowers, T. S. Bugni, G. Bulaj, J. A. Camarero, D. J. Campopiano, G. L. Challis, J. Clardy, et al., *Nat. Prod. Rep.* **2013**, *30*, 108–160.

- [2] L. M. Repka, J. R. Chekan, S. K. Nair, W. A. van der Donk, *Chem. Rev.* **2017**, *117*, 5457–5520.
- [3] J. M. Willey, W. A. van der Donk, *Annu. Rev. Microbiol.* **2007**, *61*, 477–501.
- [4] M. Montalbán-López, L. Zhou, A. Buivydas, A. J. Van Heel, O. P. Kuipers, *Expert Opin. Drug Discovery* **2012**, *7*, 695–709.
- [5] L. E. Cooper, B. Li, W. A. van der Donk, *Comprehensive Natural Products II Chemistry and Biology*, Vol. 5, Elsevier, Amsterdam, **2010**, pp. 217–256.
- [6] A. Müller, A. Klöckner, T. Schneider, *Nat. Prod. Rep.* **2017**, *34*, 909–932.
- [7] T. Mascher, S. L. Zimmer, T.-A. Smith, J. D. Helmman, *Antimicrob. Agents Chemother.* **2004**, *48*, 2888–2896.
- [8] M. de la Cruz, I. González, C. A. Parish, R. Onishi, J. R. Tormo, J. Martín, F. Peláez, D. Zink, N. El Aouad, F. Reyes, et al., *Front. Microbiol.* **2017**, *8*, 343.
- [9] H. He, R. T. Williamson, B. Shen, E. I. Graziani, H. Y. Yang, S. M. Sakya, P. J. Petersen, G. T. Carter, *J. Am. Chem. Soc.* **2002**, *124*, 9729–9736.
- [10] M. Iorio, O. Sasso, S. I. Maffioli, R. Bertorelli, P. Monciardini, M. Sosio, F. Bonezzi, M. Summa, C. Brunati, R. Bordoni, et al., *ACS Chem. Biol.* **2014**, *9*, 398–404.
- [11] J. Claesen, M. Bibb, *Proc. Natl. Acad. Sci. USA* **2010**, *107*, 16297–16302.
- [12] M. E. Rateb, Y. Zhai, E. Ehrner, C. M. Rath, X. Wang, J. Tabudravu, R. Ebel, M. Bibb, K. Kyeremeh, P. C. Dorrestein, et al., *Org. Biomol. Chem.* **2015**, *13*, 9585–9592.
- [13] T. Mo, W. Q. Liu, W. Ji, J. Zhao, T. Chen, W. Ding, S. Yu, Q. Zhang, *ACS Chem. Biol.* **2017**, *12*, 1484–1488.
- [14] Z. Shang, J. M. Winter, C. A. Kauffman, I. Yang, W. Fenical, *ACS Chem. Biol.* **2019**, *14*, 415–425.
- [15] T. J. Oman, W. A. van der Donk, *Nat. Chem. Biol.* **2010**, *6*, 9–18.
- [16] C. T. Lohans, J. C. Vederas, *J. Antibiot.* **2014**, *67*, 23–30.
- [17] V. Wiebach, A. Mainz, M. A. J. Siebert, N. A. Jungmann, G. Lesquame, S. Tirat, A. Dreux-Zigha, J. Aszodi, D. Le Beller, R. D. Süssmuth, *Nat. Chem. Biol.* **2018**, *14*, 652–654.
- [18] N. I. Martin, T. Sprules, M. R. Carpenter, P. D. Cotter, C. Hill, R. P. Ross, J. C. Vederas, *Biochemistry* **2004**, *43*, 3049–3056.
- [19] C. T. Lohans, J. L. Li, J. C. Vederas, *J. Am. Chem. Soc.* **2014**, *136*, 13150–13153.
- [20] L. Huo, W. A. Van Der Donk, *J. Am. Chem. Soc.* **2016**, *138*, 5254–5257.
- [21] K. Fujii, K. I. Harada, *Anal. Chem.* **1997**, *69*, 5146–5151.
- [22] K. I. Mohr, C. Volz, R. Jansen, V. Wray, J. Hoffmann, S. Bernecker, J. Wink, K. Gerth, M. Stadler, R. Müller, *Angew. Chem. Int. Ed.* **2015**, *54*, 11254–11258; *Angew. Chem.* **2015**, *127*, 11406–11410.
- [23] P. J. Knerr, W. A. van der Donk, *Annu. Rev. Biochem.* **2012**, *81*, 479–505.
- [24] W. Tang, W. A. Van Der Donk, *Nat. Chem. Biol.* **2013**, *9*, 157–159.
- [25] W. Tang, G. Jiménez-Osés, K. N. Houk, W. A. Van Der Donk, *Nat. Chem.* **2015**, *7*, 57–64.
- [26] M. F. Giraud, J. H. Naismith, *Curr. Opin. Struct. Biol.* **2000**, *10*, 687–696.
- [27] D. M. Liang, J. H. Liu, H. Wu, B. Bin Wang, H. J. Zhu, J. J. Qiao, *Chem. Soc. Rev.* **2015**, *44*, 8350–8374.

Manuscript received: April 9, 2020

Accepted manuscript online: May 14, 2020

Version of record online: June 15, 2020

## Supporting Information

### **Cacaoidin, First Member of the New Lanthidin RiPP Family**

*Francisco Javier Ortiz-López,\* Daniel Carretero-Molina, Marina Sánchez-Hidalgo, Jesús Martín, Ignacio González, Fernando Román-Hurtado, Mercedes de la Cruz, Sergio García-Fernández, Fernando Reyes, Julia Patricia Deisinger, Anna Müller, Tanja Schneider, and Olga Genilloud*

anie\_202005187\_sm\_miscellaneous\_information.pdf

## Author Contributions

F.O. Conceptualization: Lead; Formal analysis: Lead; Investigation: Lead; Methodology: Equal; Supervision: Lead; Writing—Original Draft: Lead; Writing—Review & Editing: Lead; Structural elucidation: Lead

D.C. Investigation: Supporting; Methodology: Supporting; Experimental: Isolation and purification: Lead

M.S. Formal analysis: Equal; Writing—Original Draft: Supporting; Writing—Review & Editing: Supporting; Gene cluster analysis: Lead

J.M. Investigation: Supporting; Methodology: Equal; Writing—Review & Editing: Supporting; HRMS/MS analysis: Equal

I.G. Investigation: Supporting; Writing—Review & Editing: Supporting; Fermentations, taxonomic identification: Lead

F.R. Formal analysis: Supporting; Gene cluster analysis: Supporting

M.d. Investigation: Supporting; Writing—Review & Editing: Supporting; Antibacterial tests: Lead

S.G. Investigation: Supporting; Antibacterial tests: Lead

F.R. Resources: Lead; Writing—Review & Editing: Equal

J.D. Formal analysis: Supporting; Investigation: Supporting; Methodology: Supporting; Antibacterial tests. mode of action studies: Equal

A.M. Formal analysis: Supporting; Investigation: Supporting; Writing—Review & Editing: Supporting; Antibacterial tests. mode of action studies: Equal

T.S. Formal analysis: Lead; Funding acquisition: Lead; Methodology: Lead; Supervision: Equal; Writing—Review & Editing: Supporting; Antibacterial tests. mode of action studies: Lead

O.G. Funding acquisition: Lead; Project administration: Lead; Resources: Lead; Writing—Review & Editing: Supporting.

## Table of Contents

<b>1. Experimental procedures.....</b>	<b>2</b>
1.1 General experimental procedures .....	2
1.2 NMR spectroscopy.....	3
1.3 Bacterial strain .....	3
1.4 DNA extraction and genome sequencing .....	3
<b>2. Results and discussion.....</b>	<b>4</b>
2.1 Culture conditions for screening campaign. Bioassay-guided isolation of cacaoidin (1) .....	4
2.2 Large-scale fermentation and isolation of cacaoidin (1) .....	8
2.3 Structural elucidation: NMR spectroscopy.....	9
2.4 Structural elucidation: Tandem Mass spectrometry (HRMS / MS).....	16
2.5 Structural elucidation: Reduction and desulfurization of cacaoidin (1). HRMS / MS.....	20
2.6 Structural characterization data of cacaoidin (1) .....	26
2.7 Advanced Marfey's analysis of cacaoidin (1) .....	31
2.8 Advanced Marfey's analysis after reduction-desulfurization.....	39
2.9 Biosynthetic gene cluster of cacaoidin (1).....	42
2.10 Biological assays .....	44
2.11 NMR spectra of cacaoidin (1).....	47
<b>3. References .....</b>	<b>69</b>

## 1. Experimental Procedures

### 1.1 General Experimental Procedures

Solvents employed were all HPLC grade. Chemical reagents and standards were purchased from Sigma-Aldrich unless indicated otherwise. Optical rotations were measured on a Jasco P-2000 polarimeter (JASCO Corporation, Tokyo, Japan). IR spectra were recorded with a JASCO FT/IR-4100 spectrometer (JASCO Corporation) equipped with a PIKE MIRacle™ single reflection ATR accessory. LC-UV-LRMS analyses were performed on an Agilent 1100 (Agilent Technologies, Santa Clara, CA, USA) single quadrupole LC-MS system as previously described.<sup>[1]</sup> HRESIMS and MS/MS spectra were acquired using a Bruker maXis QTOF mass spectrometer (Bruker Daltonik GmbH, Bremen, Germany) coupled to an Agilent Rapid Resolution HPLC. The mass spectrometer was operated in positive ESI mode. The instrumental parameters were 4 kV capillary voltage, drying gas flow of 11 L min<sup>-1</sup> at 200 °C, and nebulizer pressure of 2.8 bar. TFA-Na cluster ions were used for mass calibration of the instrument prior to sample injection. Pre-run calibration was done by infusion with the same TFA-Na calibrant. Medium pressure liquid chromatography (MPLC) was performed on a CombiFlash Teledyne ISCO Rf400x apparatus with a preloaded C<sub>18</sub> column (Phenomenex, 5 μm). Preparative or semi-preparative HPLC purifications were performed on a Gilson GX-281 322H2 HPLC (Gilson Technologies, USA) using reversed-phase preparative (Agilent Zorbax SB-C<sub>18</sub>, 21.2 × 250 mm, 7 μm) or semi-preparative (Agilent Zorbax SB-C<sub>18</sub>, 9.4 × 250 mm, 5 μm) columns. Molecular models were generated using Chem3D Pro 12.0 (CambridgeSoft, PerkinElmer Informatics, Waltham, MA, USA). The structures were energy-minimized by molecular mechanics with the MM2 force field using as gradient convergence criteria an RMS value of 0.001. Molecular modeling figures were generated with PyMol (W. L. DeLano, The PyMOL Molecular Graphics System, DeLano Scientific LLC, Palo Alto, CA, USA, 2002).

### 1.2 NMR spectroscopy

1D and 2D NMR spectra were recorded at 297K on a Bruker Avance III spectrometer (500, 125 and 50 MHz for  $^1\text{H}$ ,  $^{13}\text{C}$  and  $^{15}\text{N}$  NMR, respectively) equipped with a 1.7 mm TCI MicroCryoProbe™ (Bruker Biospin, Fällanden, Switzerland). Unless other thing is indicated, NMR experiments were performed with an appropriate water suppression scheme. All 2D NMR experiments were recorded with 512 increments in F1. HSQC and HMBC experiments were recorded at  $J$  values of 145 and 8 Hz respectively. Band-Selective constant time HMBC spectrum was performed with a spectral width of 16 ppm, centered at 174 ppm to better resolve the peptide carbonyl region. Mixing times were 90 ms for TOCSY and 400 ms for NOESY.  $^1\text{H}$  and  $^{13}\text{C}$  chemical shifts were reported in ppm using the signals of the residual solvents as internal reference ( $\delta_{\text{H}}$  1.94 and  $\delta_{\text{C}}$  1.32 ppm for  $\text{CD}_3\text{CN}$ ;  $\delta_{\text{H}}$  4.75 ppm for  $\text{D}_2\text{O}$ ).  $^{15}\text{N}$  chemical shifts were reported in ppm and referred to liquid ammonia (spectrometer default reference).

### 1.3 Bacterial strain.

The producing strain CA-170360, belonging to Fundación MEDINA's microbial collection, was isolated from the rhizosphere collected from a specimen of *Brownanthus corallinus* in the region of Namaqualand (South Africa). On the basis of its nearly complete 16S rDNA sequence (1410bp) the strain was identified as a closest neighbor of the species *Streptomyces cacaoi* subsp. *cacaoi* NBRC 12748<sup>T</sup>, (similarity of 99.93%), according to the EzTaxon server analysis. <sup>[2]</sup> (<http://www.ezbiocloud.net/eztaxon>)

### 1.4 DNA extraction and genome sequencing

Genomic DNA of the strain *Streptomyces cacaoi* CA-170360 was extracted and purified as previously described <sup>[3]</sup> from cultures in ATCC-2 liquid medium (soluble starch 20 g/L, glucose 10 g/L, NZ Amine Type E 5 g/L, meat extract 3 g/L, peptone 5 g/L, yeast extract 5 g/L, calcium carbonate 1 g/L, pH 7) grown during two days on an orbital shaker at 28 °C, 220 rpm and 70% relative humidity. The genome of CA-170360 was fully sequenced *de novo*, assembled and annotated by Macrogen (Seoul, Korea; <http://www.macrogen.com/>), using a combined strategy of Illumina HiSeq 2500 and PacBio RSII platforms. The predicted protein functions were assigned using antiSMASH and BLAST. The Conserved Domain Database (CDD) from NCBI was used to search for protein conserved domains.<sup>[3-6]</sup>



## 2. Results and Discussion

### 2.1 Culture conditions for screening campaign. Bioassay-guided isolation of cacaoidin (1)

The strain CA-170360 was cultivated in 10 mL of MPG medium (see description below) and shaken at 220 rpm at 28 °C for 13 days. The whole broth was extracted with an equal volume of acetone under shaking for 1h. After evaporation of the organic solvent, the mycelial debris was discarded by centrifugation and filtration. The aqueous broth was then extracted with MEK (2 × 5 mL). The organic extract was evaporated to dryness and a portion of the residue was redissolved in 20% DMSO: H<sub>2</sub>O (2 × WBE, Whole Broth Equivalent units). This sample showed potent activity against MRSA and triggered the expression of the LiaRS bioreporter (section 2.10, Figure S1). Subsequent bioassay-guided purification by semipreparative RP-HPLC led to the identification of the bioactive compound (1) as the peak indicated in the chromatogram below (Figure S2). The purity of the bioactive compound was assessed by LC-UV-HRMS analysis (Figure S3). HRESIMS analyses of 1 were performed using two different ISCID values (0 eV; 75 eV). A molecular formula of C<sub>107</sub>H<sub>162</sub>N<sub>24</sub>O<sub>32</sub>S<sub>2</sub> ( $\Delta$  +1.27 ppm) was assigned to 1 based on the mono- (ISCID 75 eV) or doubly and triply charged adducts (ISCID 0 eV) (Figures S4 and S5 respectively). Ions accounting for the sequential loss of two 6-deoxyhexose units were also detected (ISCID 75 eV; Figure S6).

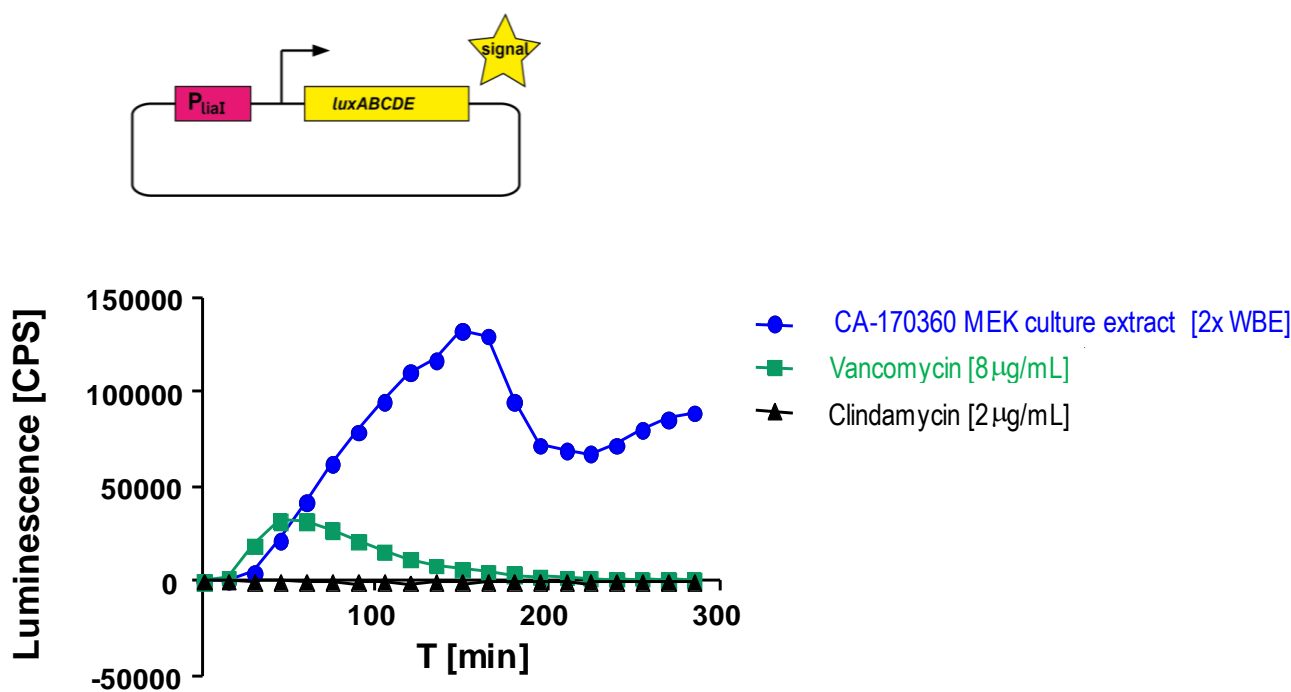


**Figure S1.** Induction of the LiaRS bioreporter by a MEK culture extract (2 × WBE) of strain CA-170360 (MPG medium), compared to vancomycin (positive control) and clindamycin (negative control)

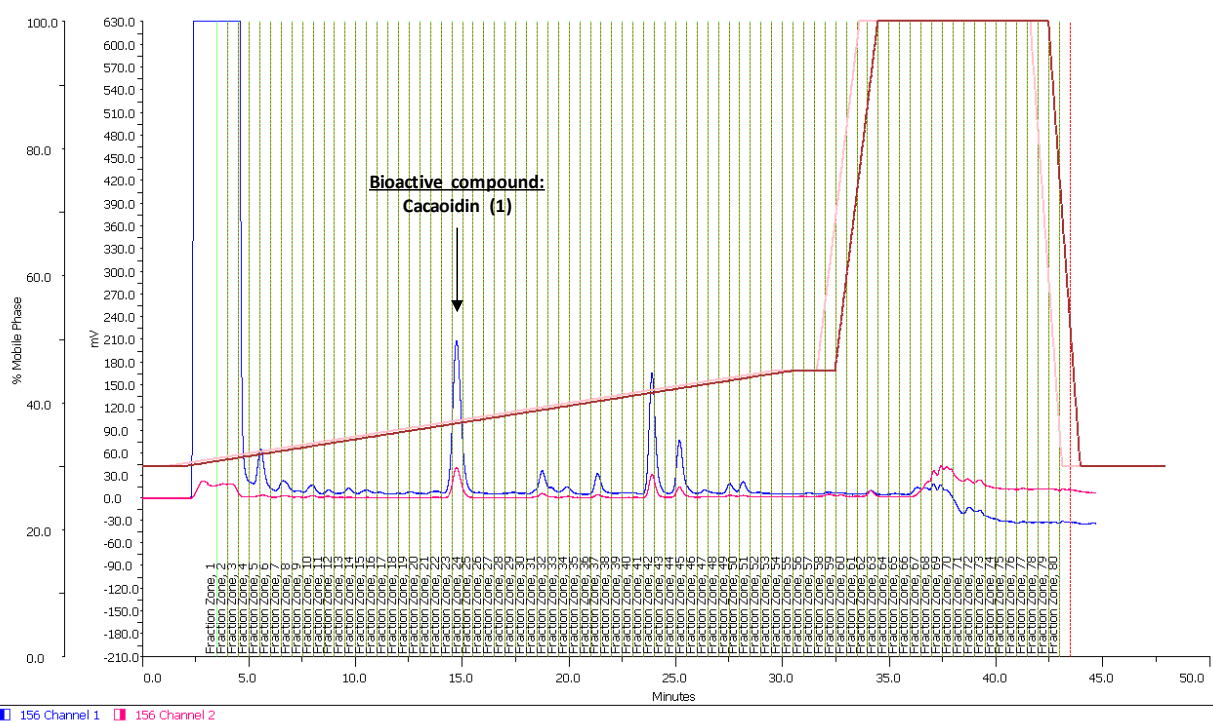
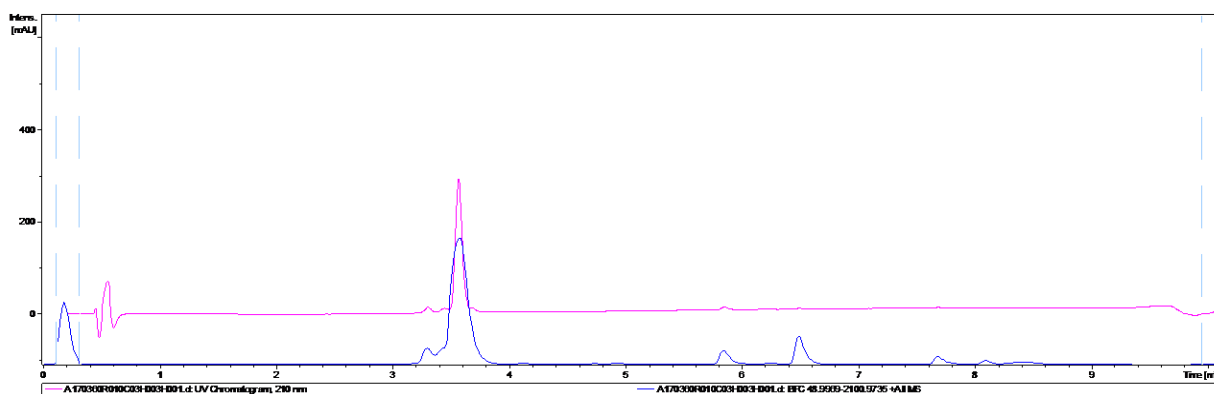


**Figure S2.** Bioassay-guided isolation of cacaoidin (1). LC-UV semipreparative chromatogram recorded at both 210 (blue trace) and 280 nm (pink trace)

a)



b)

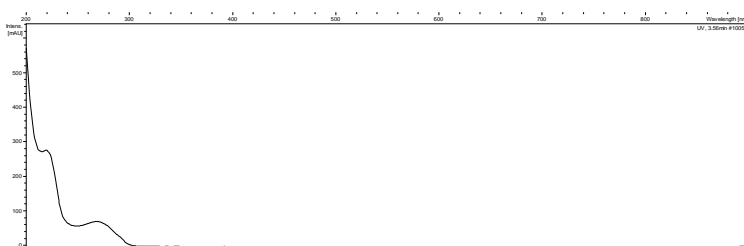


**Figure S3.** a) LC-UV-HRMS chromatogram (UV 210 nm: pink trace; MS+: blue trace). b) UV spectrum (bottom) of the bioactive compound, cacaoidin (1)

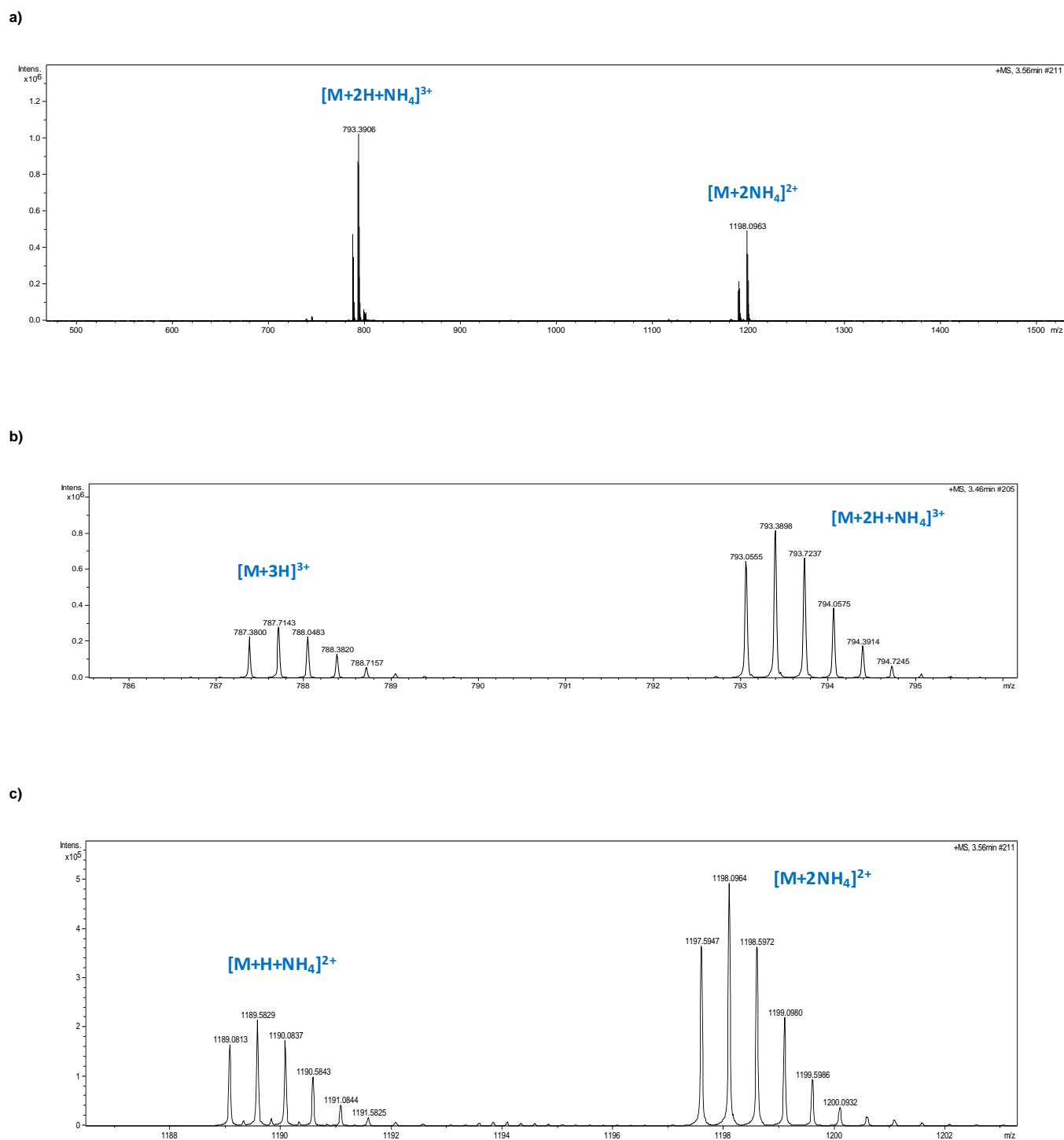
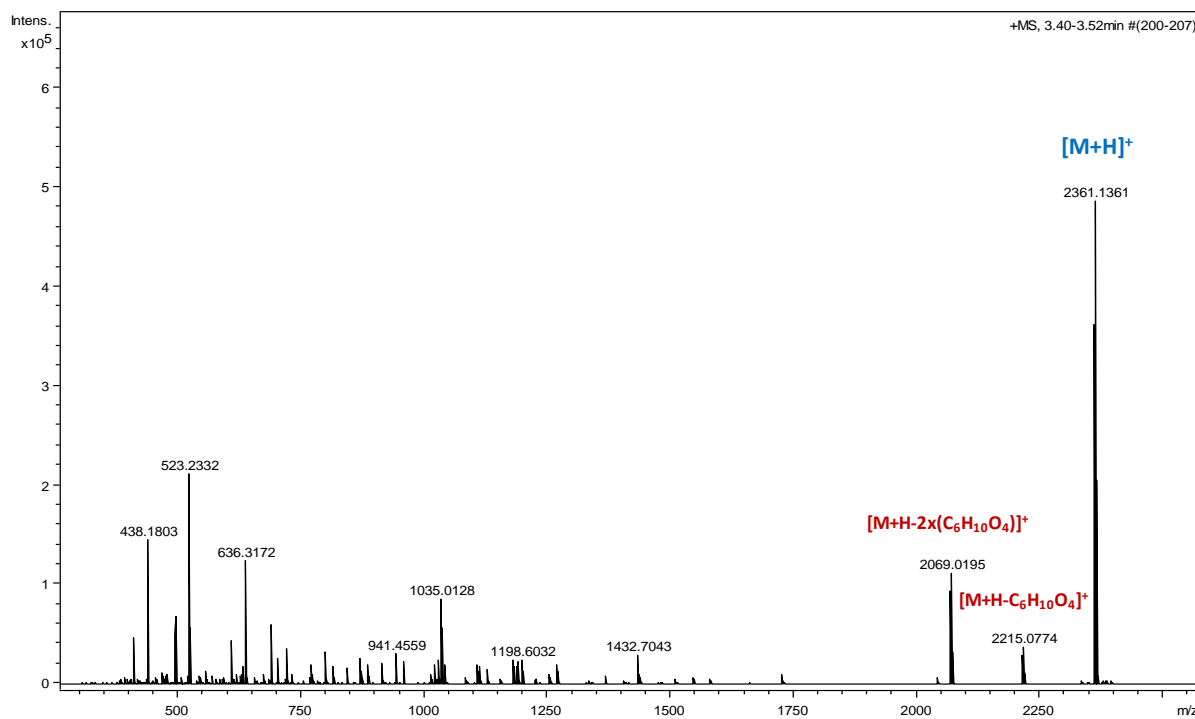


**Figure S4.** HRESIMS(+)-TOF spectra (ISCID 0 eV) of the bioactive compound, cacaoidin (**1**). a) Overview; b) Triply-charged adducts (zoom in region); c) Doubly-charged adducts (zoom in region).

a)



b)

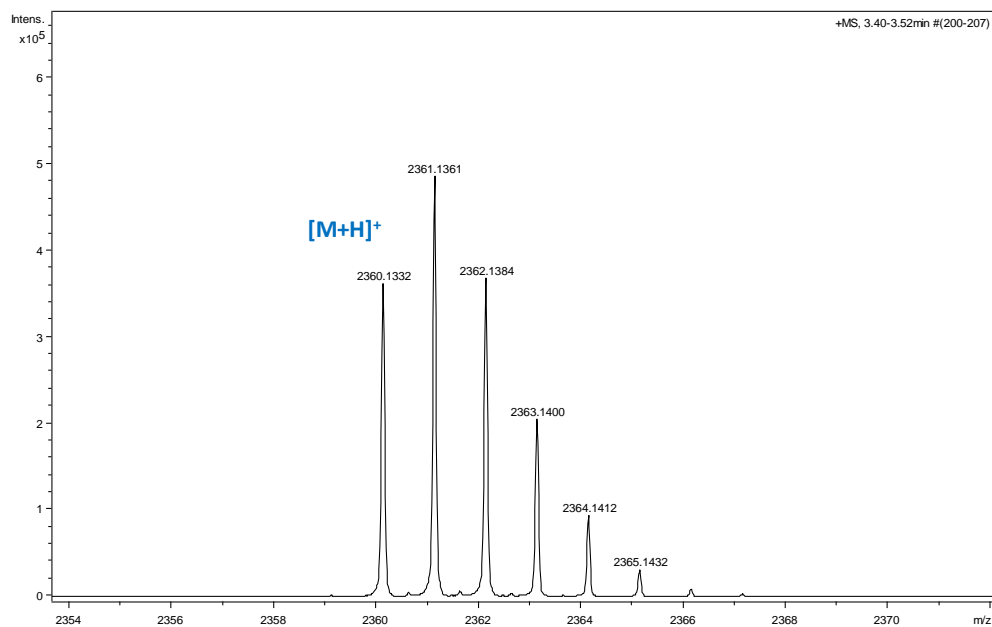


**Figure S5.** a) HRESIMS(+)-TOF spectra (ISCID 75 eV) of the bioactive compound, cacaoidin (**1**), showing the mono-charged proton adduct (in blue) and in-source fragment ions. Those corresponding to the sequential loss of two deoxyhexose units are marked in red. b) Mono-charged proton adduct (zoom in region)

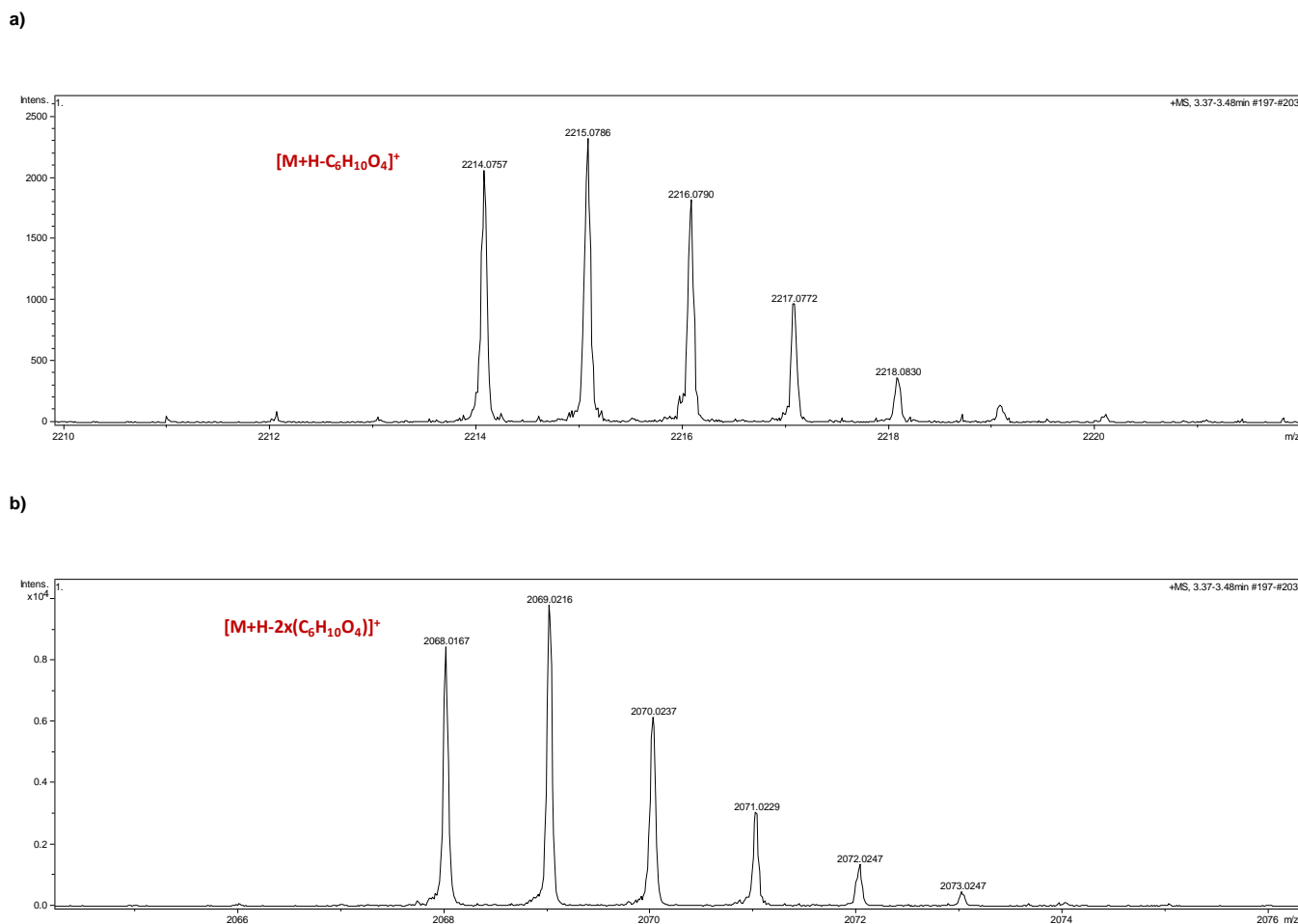


**Figure S6.** (a, b): HRESIMS(+)-TOF spectra (ISCID 75 eV) of the bioactive compound, cacaoidin (**1**). In-source fragment ions revealing the sequential loss of two deoxyhexose units are marked in red.

## 2.2 Large-scale fermentation and isolation of cacaoidin (**1**)

The producing strain CA-170360 was cultured in a 3L-scale as follows: A first seed culture of the producing organism was prepared by inoculating 10 mL of seed medium ATCC-2 which consists of [soluble starch (20 g/L), dextrose (10 g/L), NZ amine EKC (Sigma) (5 g/L), Difco beef extract (3 g/L), Bacto peptone (5 g/L), yeast extract (5 g/L), and  $CaCO_3$  (1 g/L), adjusted to pH 7.0 with NaOH before addition of  $CaCO_3$ ], in a 40 mL tube with 0.5 mL of a frozen inoculum stock of the producing strain and incubating the tube at 28 °C with shaking at 220 rpm for about 48 h. A second seed culture was prepared by inoculating 50 mL of seed medium in two 250 mL flasks with 2.5 mL of the first seed. A 5% aliquot of the second seed culture was transferred to each of the 20 × 500 mL Erlenmeyer flasks containing 150 mL of the production medium MPG consisting of glucose (10 g/L), millet meal (20 g/L), cottonseed flour (20 g/L), MOPS (20 g/L), pH 7.0. The flasks were incubated at 28 °C for 13 days in a rotary shaker at 220 rpm and 70% humidity before harvesting.

The 3 L whole broth was then extracted with an equal volume of acetone under continuous shaking for 1h. After evaporating most of the organic solvent (concentration to initial volume) under a  $N_2$  stream, the mycelial debris was discarded by centrifugation and vacuum filtration. The resulting aqueous broth was adjusted to pH 10.0 (previous optimization, data not shown), extracted with MEK (3 × 800 mL), and the extract was rotary evaporated to dryness (160 mg). Attempts of pre-purification by MPLC resulted in loss of the target compound (data not shown), so successive portions of the residue were directly purified by preparative RP-HPLC (Agilent Zorbax SB-C<sub>18</sub>, 21.2 × 250 mm, 7 μm) applying a linear  $H_2O-CH_3CN$  gradient (15 mL/min; 30-45%B in 30 min, then 100% B; UV detection at 210 nm), both solvents containing 0.1% trifluoroacetic acid (TFA). Selected fractions (eluting at 14-15 min) were pooled, the organic solvent was evaporated under a  $N_2$  stream and the resulting aqueous sample was freeze-dried. Cacaoidin (**1**) was thus obtained as an amorphous white powder (6 mg).

### 2.3 Structural elucidation: NMR spectroscopy

NMR spectroscopy was extensively applied to partially determine the structure of **1**.

i) The overall peptide nature of the compound was deduced from NMR spectroscopic data. The  $^1\text{H}$  spectrum of **1** (Figure S53 and S54) exhibited characteristic signals for multiple exchangeable protons ( $\delta_{\text{H}}$  7.0-10.0 ppm), numerous  $\alpha$ -protons of amino acids ( $\delta_{\text{H}}$  3.8-4.6 ppm), and different alkyl ( $\delta_{\text{H}}$  0.6-3.8 ppm) or aromatic ( $\delta_{\text{H}}$  6.9-7.6 ppm) side chain protons. Additionally, a minimum of three olefinic protons ( $\delta_{\text{H}}$  5.46, 5.94, 6.01 ppm), two diagnostic anomeric signals ( $\delta_{\text{H}}$  5.40, 4.80 ppm) and another two chemically equivalent proton signals ( $\delta_{\text{H}}$  2.87 ppm) assigned to a *N,N*-dimethyl group were found in the spectrum.

Analysis of COSY, TOCSY and HSQC-TOCSY spectra (Figures S56, S57 and S66 respectively) allowed the identification of spin systems consistent with different proteinogenic amino acids such as Trp ( $\times 1$ ), Tyr ( $\times 1$ ), Gly ( $\times 1$ ), Ile / *allo*-Ile ( $\times 2$ ), Val ( $\times 1$ ), Ser ( $\times 1$ ), *trans* Pro<sup>[7]</sup> ( $\times 1$ ) and a set of nearly overlapping alanine (Ala) residues. It also accounted for the presence of one aminobutyric residue (Abu), one dehydroalanine (Dha), one aminovinyl-methyl-cysteine (AviMeCys) and two 6-deoxyhexose units in the molecule (as advanced by the HRMS data, see section 2.1).

The presence of two Ile (but not *allo*-Ile) residues in the structure was confirmed by comparison of the HSQC NMR spectra of a hydrolysate of **1** (HCl 6N, 110 C, 16 h) with those of Ile and *allo*-Ile standard amino acids.<sup>[8]</sup> (Supporting Information, Figures S7, S8).

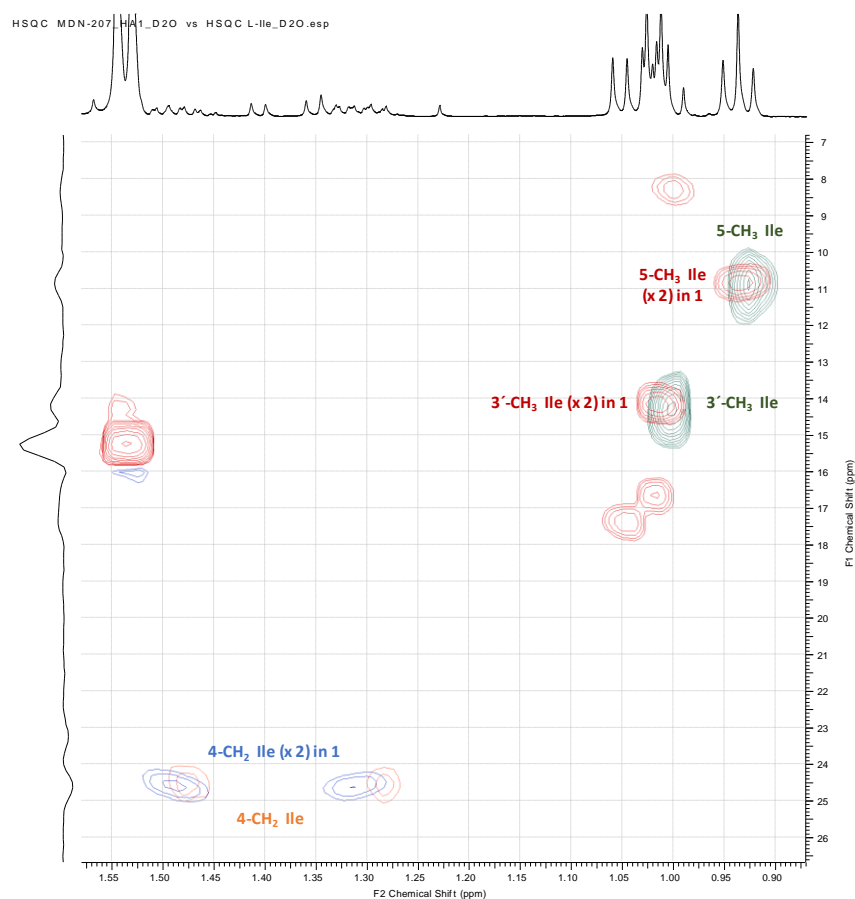


**Figure S7.** Overlay of HSQC NMR spectra (D<sub>2</sub>O, 500 MHz, 24C) of hydrolysate of **1** (red and blue NMR signals; F1 resolution: 256 increments) and Ile standard amino acid (green and orange NMR signals; F1 resolution: 128 increments).

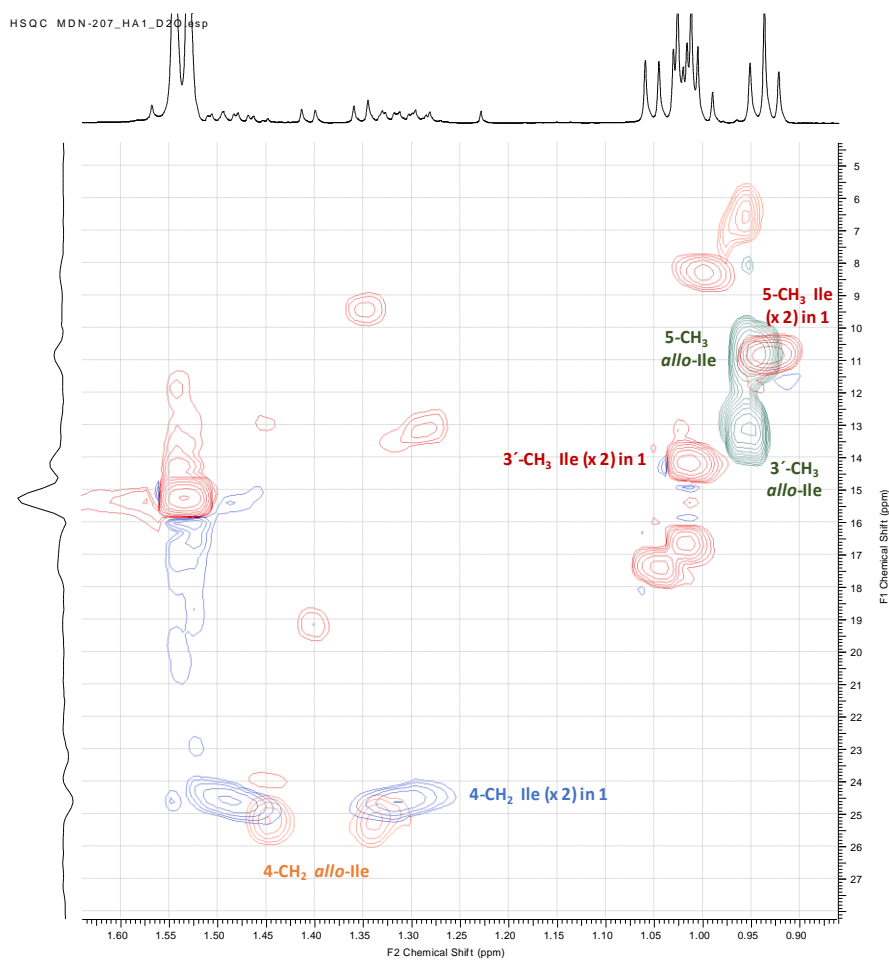
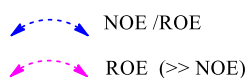
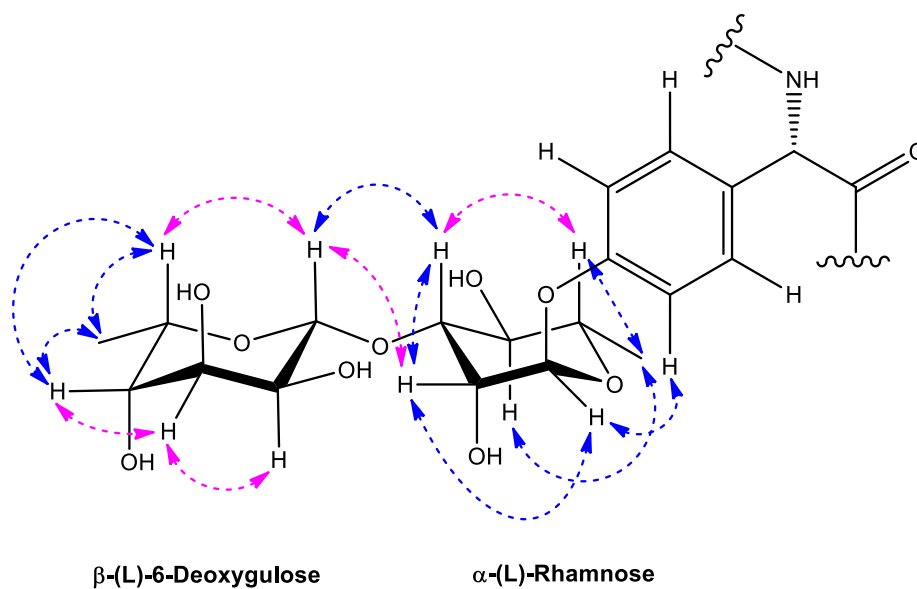


**Figure S8.** Overlay of HSQC NMR spectra (D<sub>2</sub>O, 500 MHz, 24C) of hydrolysate of **1** (red and blue NMR signals; F1 resolution: 256 increments) and *allo*-Ile standard amino acid (green and orange NMR signals; F1 resolution: 128 increments).

ii) Inspection of the HMBC (Figures S67 and S68) spectra allowed us to establish that both sugar units were interconnected through a (1→3) linkage and the resulting disaccharide was in turn O-linked to the aromatic ring of the tyrosine residue. Based on  $^3J_{H,H}$  values from the  $^1\text{H}$  or *J*-resolved (JRES) spectra and *nOe* cross-peaks from NOESY NMR spectrum (Figures S58 and S70 respectively), the disaccharide was identified as  $\beta$ -6-deoxygulopyranosyl-(1→3)- $\alpha$ -rhamnopyranoside (Figure S9).

a)



b)

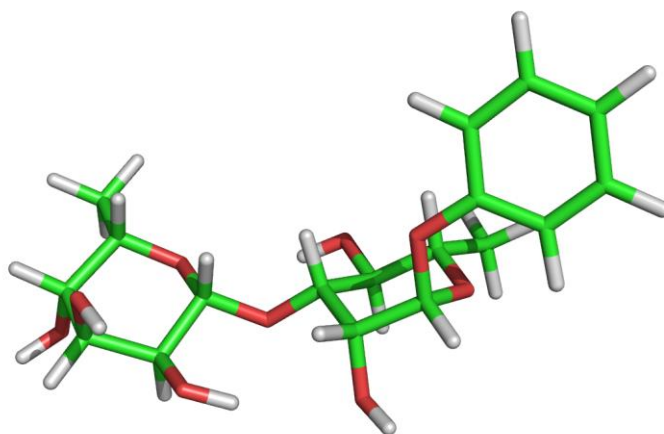
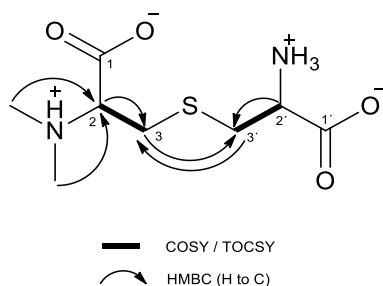


**Figure S9.** a) Key NOE and ROE correlations showing the relative stereochemistry of monosaccharide units in **1**. Both sugar units are shown in their L forms, as supported in section 2.9. b) Energy-minimized 3D molecular model of the Tyr-O glycosylating disaccharide  $\beta$ -(L)-6-deoxygulopyranosyl-(1→3)- $\alpha$ -(L)-rhamnopyranoside.



iii) An unprecedented *N,N*-dimethyl lanthionine system ( $\text{NMe}_2\text{Ala-S-Ala}$ ) was found to be present in cacaoidin based on the characteristic chemical shifts in the HSQC (Figures S59-S65) and the cross-peaks in the HMBC spectra of **1** (Figures S67 and S68; see also Figure S28 for depicted HMBC correlations). The identity of this subunit in **1** was furtherly confirmed in a hydrolysate sample of **1**, by analysis of the corresponding 2D NMR data ( $\text{D}_2\text{O}$ , 500 MHz, 24 C) (Figures S10-S13; see below).

a)



b)

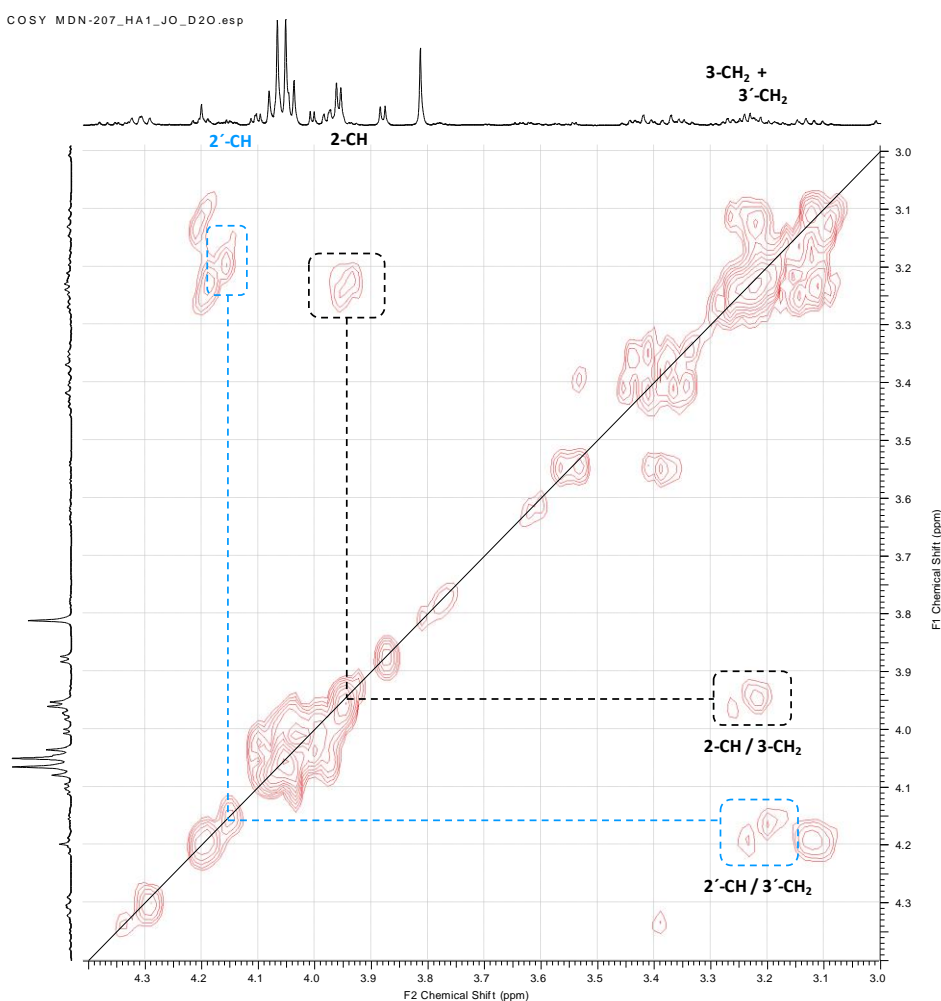


**Figure S10.** a) Key COSY/TOCSY and HMBC correlations within the *N,N*-dimethyl lanthionine ( $\text{NMe}_2\text{Ala-S-Ala}$ ) subunit in the sample hydrolysate of **1**. The substructure is shown in the most probable protonation state in neutral water ( $\text{D}_2\text{O}$ ). b) Key cross-peaks within the  $\text{NMe}_2\text{Ala-S-Ala}$  system in the COSY spectrum of the hydrolysate sample of **1**

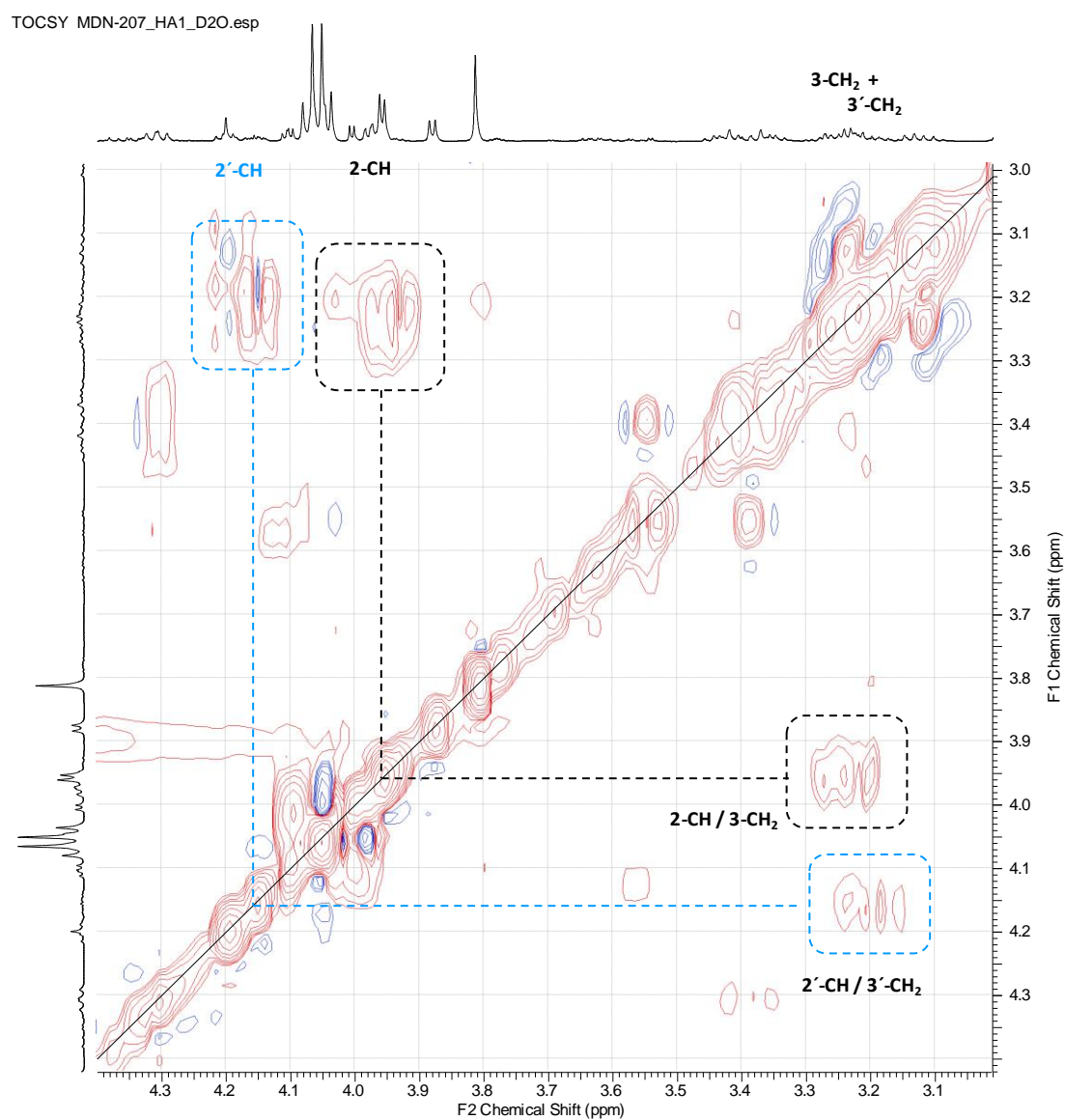


**Figure S11.** Key cross-peaks within the NMe<sub>2</sub>Ala-S-Ala subunit in the TOCSY spectrum of the hydrolysate sample of **1**

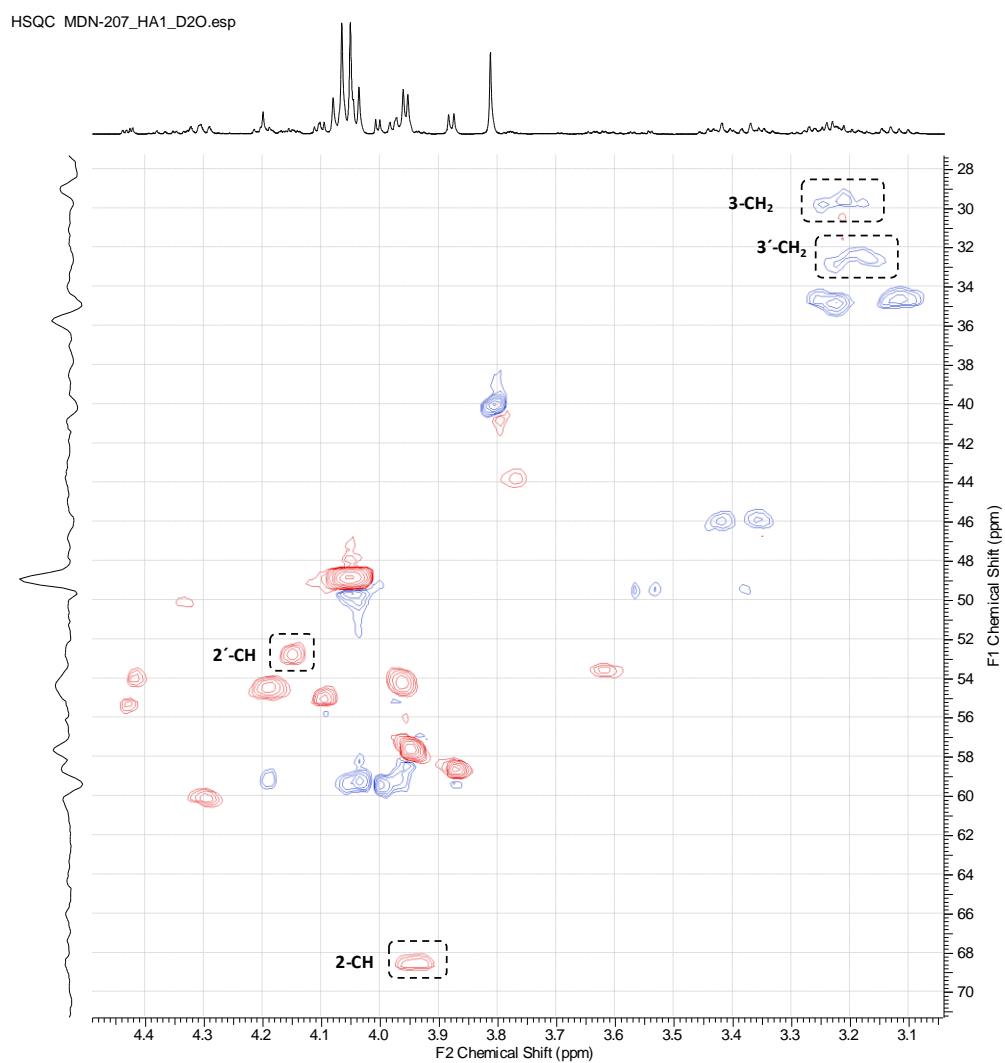


**Figure S12.** Key cross-peaks within the NMe<sub>2</sub>Ala-S-Ala system in the HSQC spectrum of the hydrolysate sample of **1**

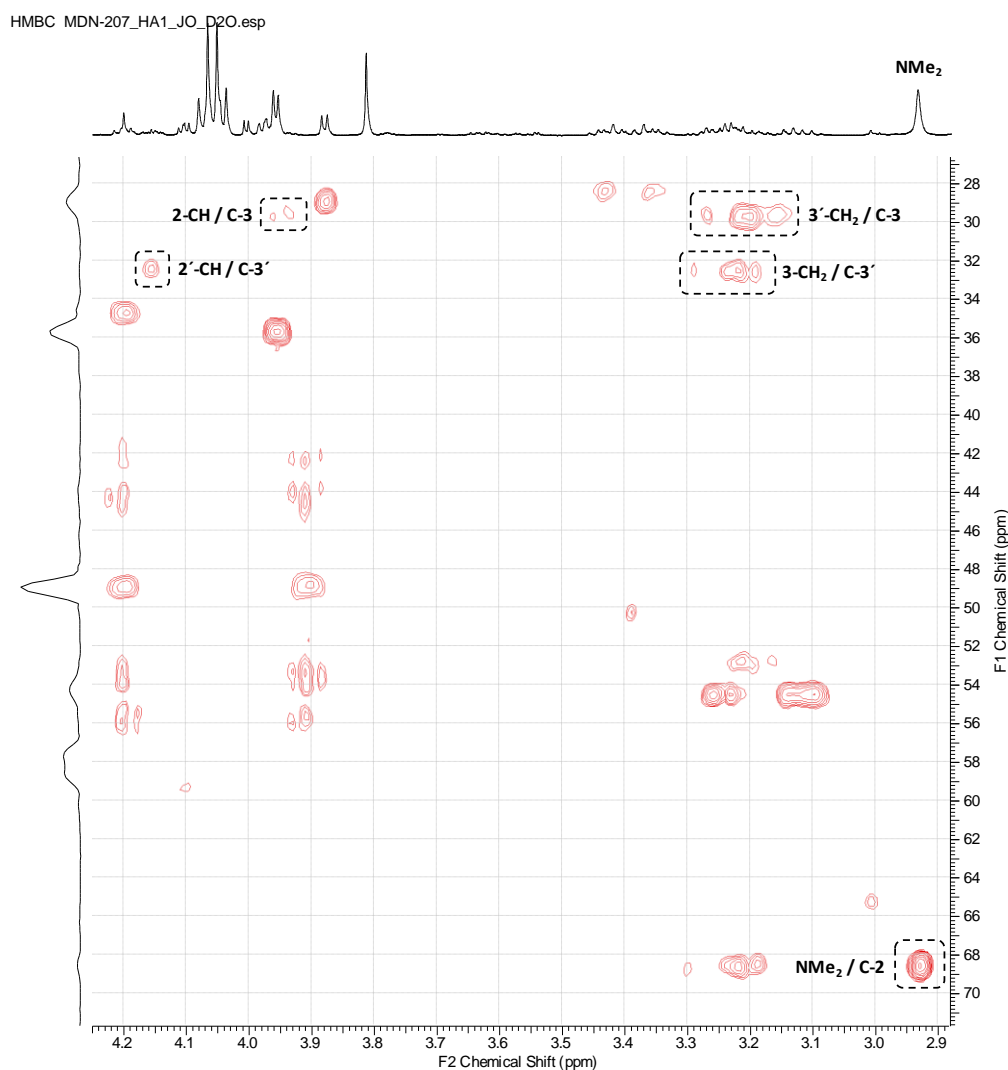


**Figure S13.** Key HMBC cross-peaks within the  $\text{NMe}_2\text{Ala-S-Ala}$  system in a hydrolysate sample of **1**

**iv)** Detailed analysis of  $\text{H}_\alpha\text{-NH}$  ( $i, i+1$ ) NOESY correlations and  $\text{NH-}$  to  $\text{-CO}$  HMBC cross-peaks within each amide bond allowed to partially determine the sequence of the peptide. Due to overlapping of different  $\text{NH}$  and  $\text{CO}$  signals, the fragments connected unambiguously by NMR were limited to  $[\text{NMe}_2\text{Ala-(S-Ala-Abu)-Dha-Ala}]$ ,  $\text{Ile-Tyr-Ala-Ala-Val}$ ,  $\text{Ile-Ala-Ala}$  and the C-termini ring ( $\text{AviMeCys-Ala-Ser-Trp-Gly}$  cyclic substructure)

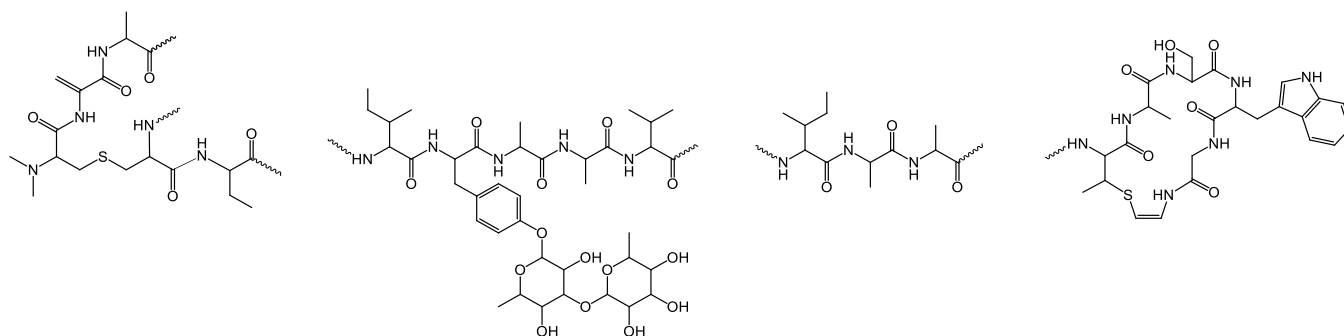


**Figure S14.** Structural fragments in **1** unambiguously connected by NMR through  $\text{H}_\alpha\text{-NH}$  ( $i, i+1$ ) NOESY and  $\text{NH-}$  to  $\text{-CO}$  HMBC correlations.

## 2.4 Structural elucidation: Tandem Mass spectrometry (HRMS / MS)

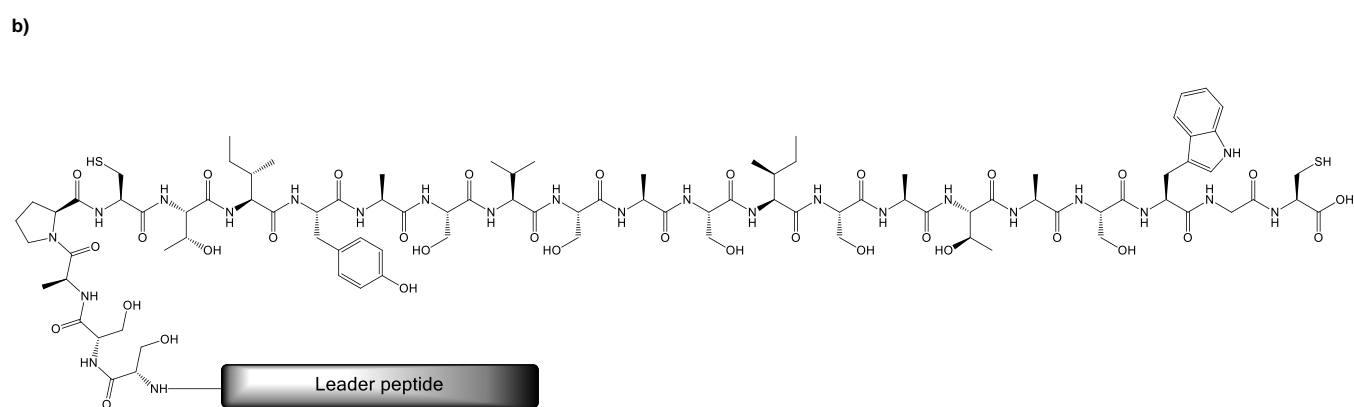


**Figure S15.** a) Protein sequence of the cacaoidin precursor peptide (CaoA), showing the cleavage site and the predicted mass for the unmodified peptide. b) Structure of unmodified core peptide (attached to leader peptide)

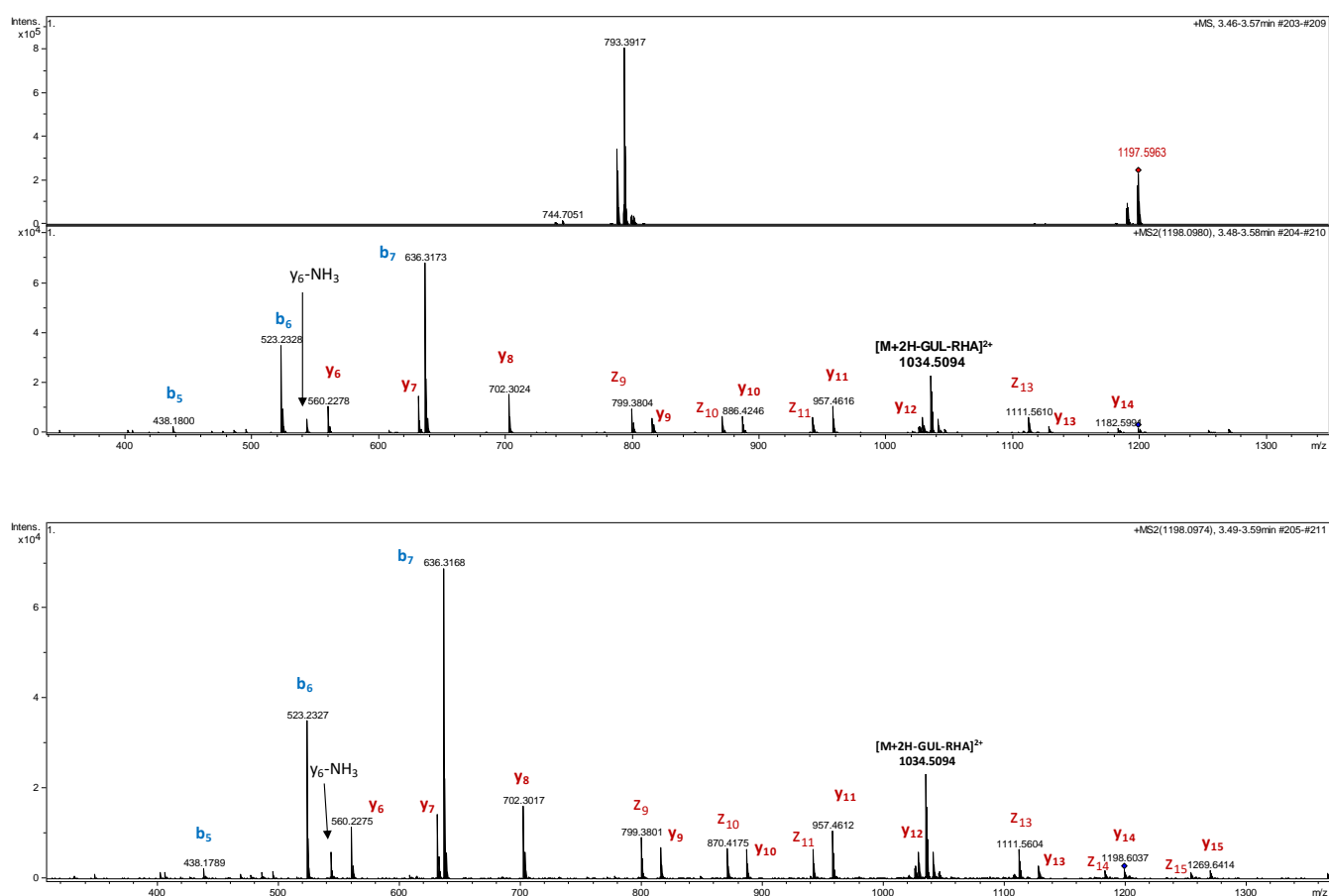


**Figure S16.** Experimental MS/MS fragmentation of the  $[M+2NH_4]^{2+}$  adduct (bottom: zoom). Annotation of b, y and z ions

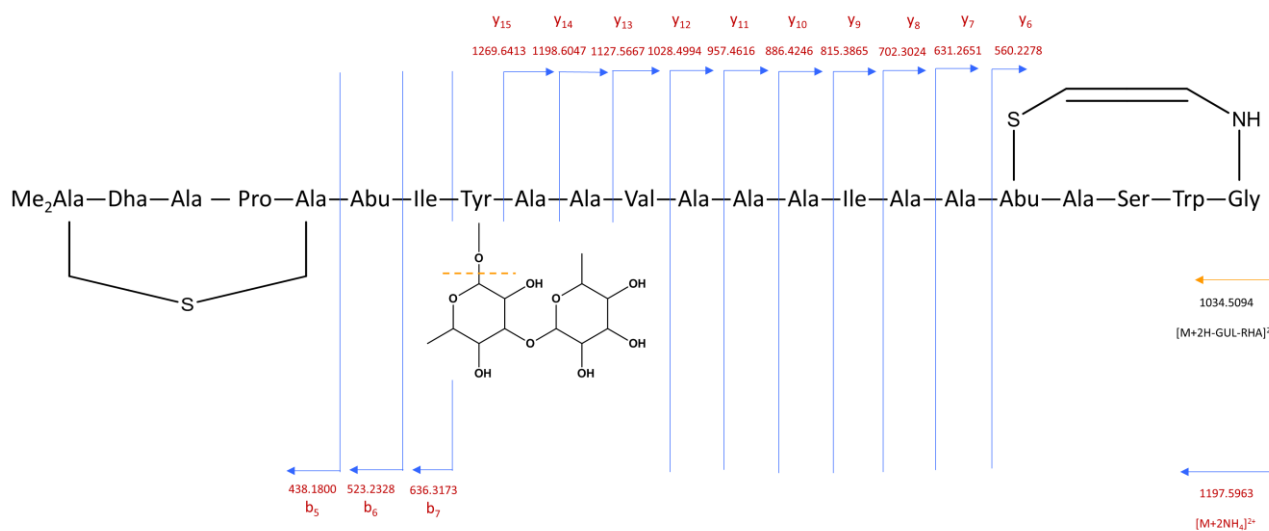


**Figure S17.** Key MS/MS fragmentation of the  $[M+2NH_4]^{2+}$  adduct

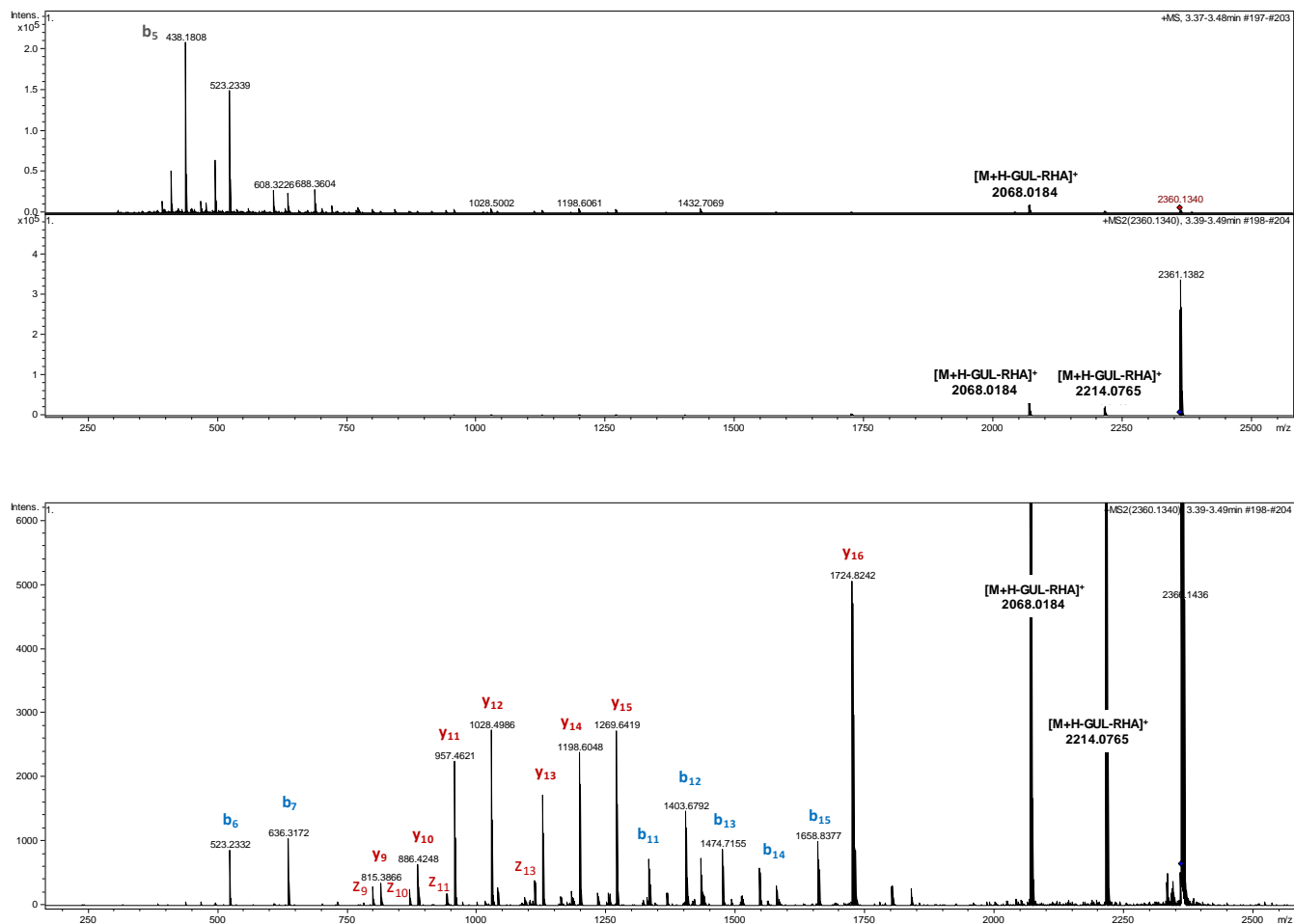


Figure S18. Experimental MS/MS fragmentation of the  $[M+H]^+$  adduct (bottom: zoom). Annotation of b, y and z ions

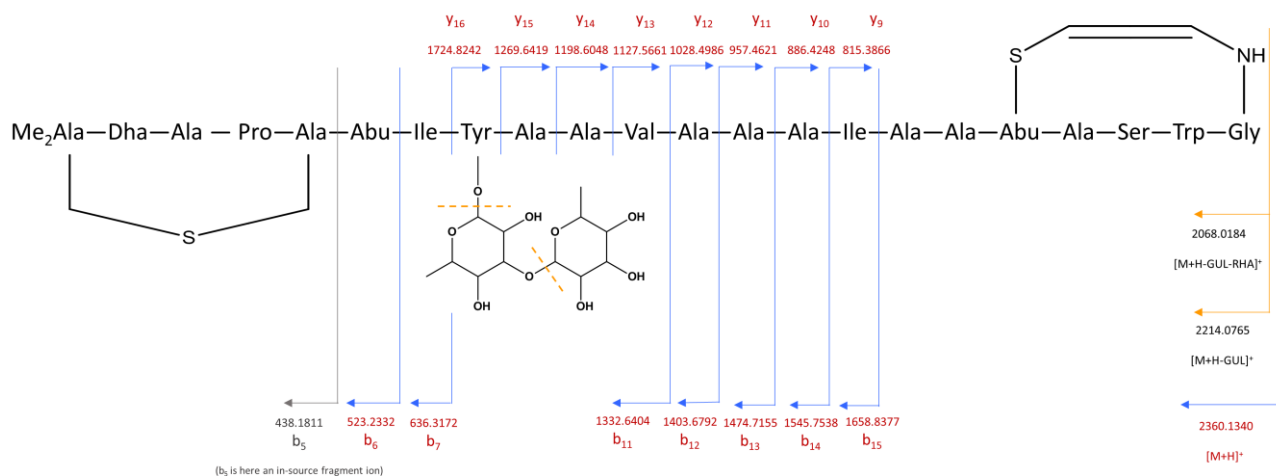


Figure S19. Key MS/MS fragmentation of the  $[M+H]^+$  adduct

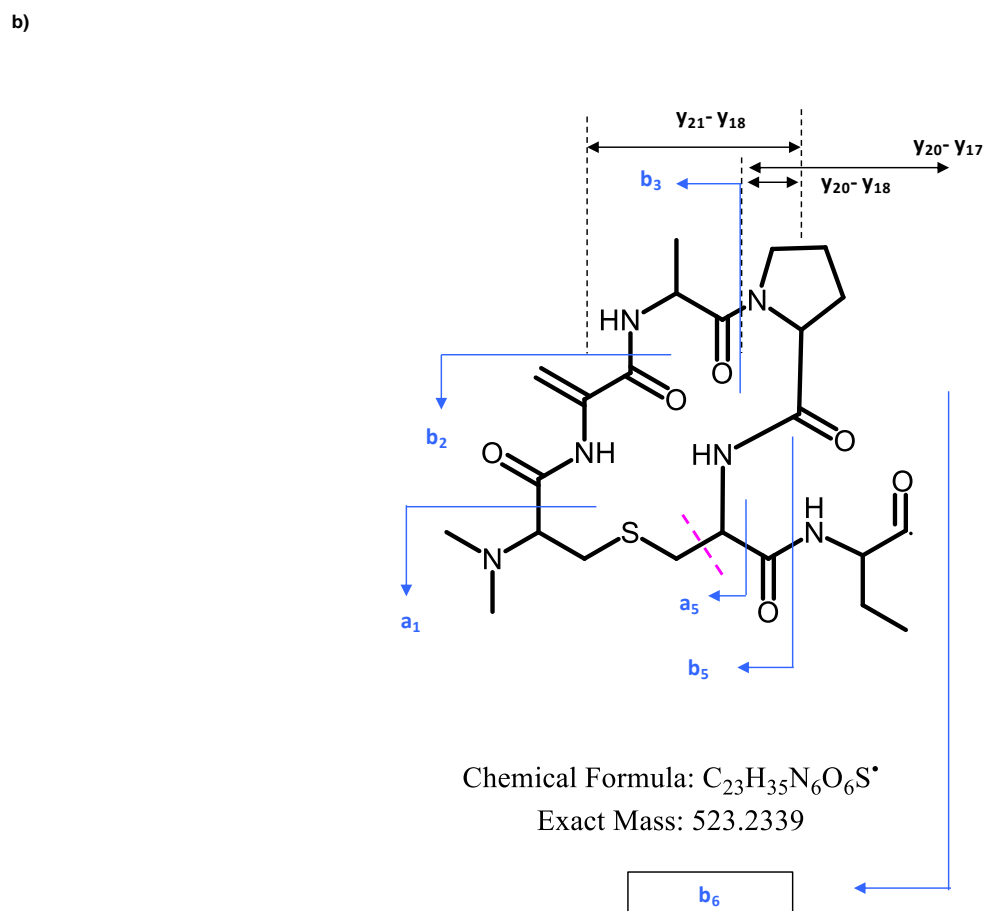
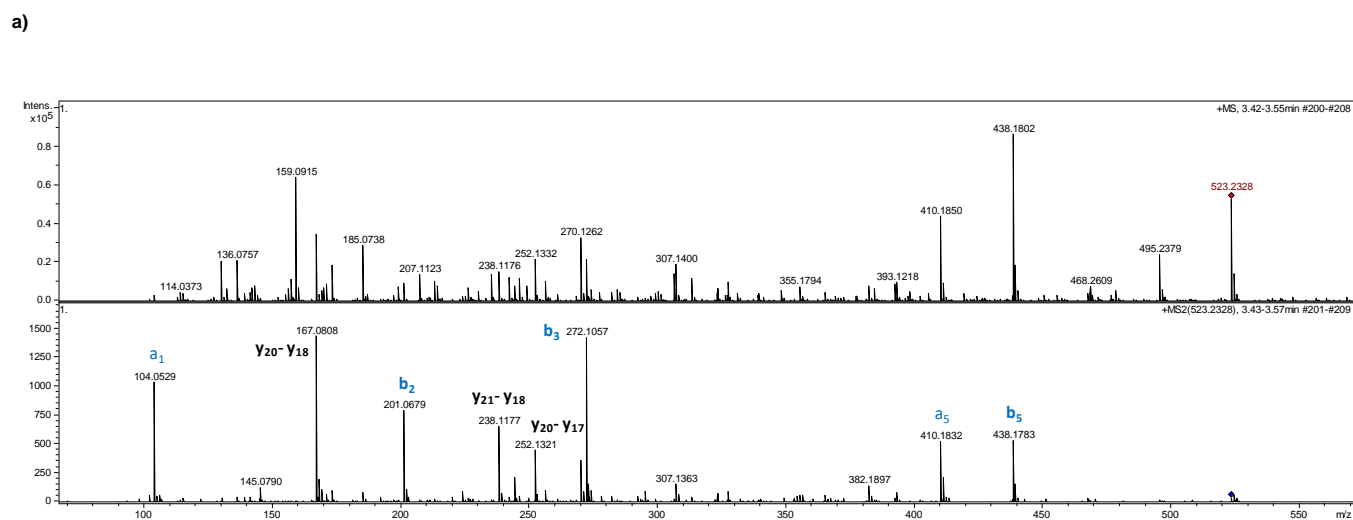
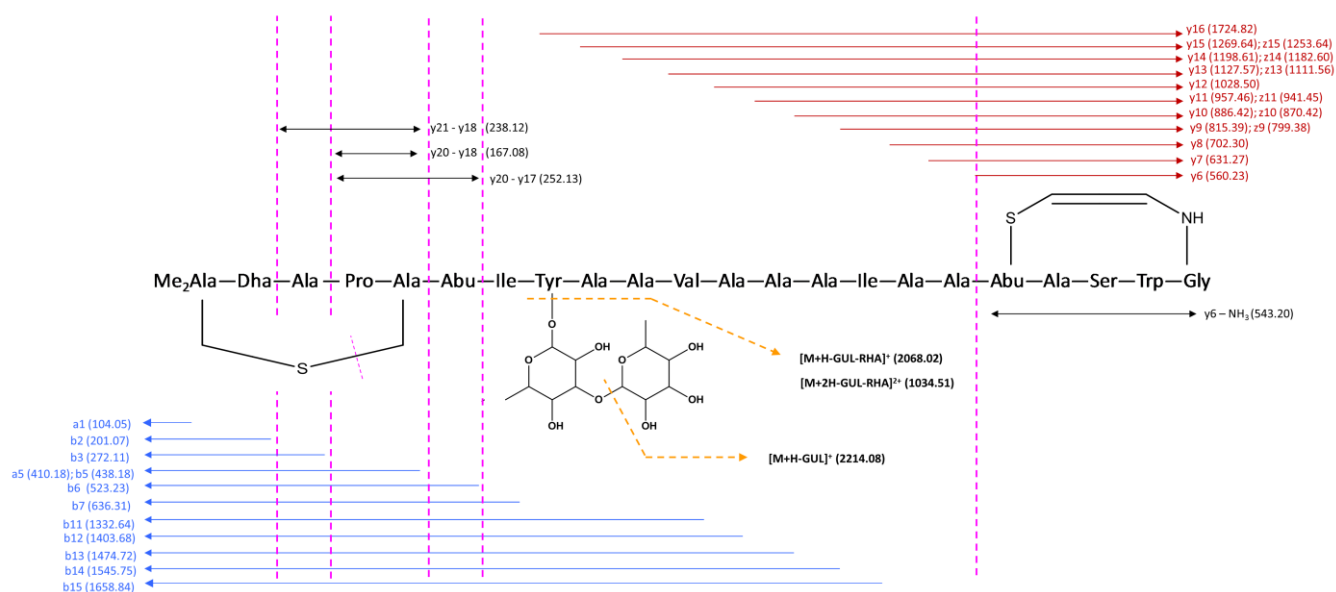


Figure S20. a) Key MS/MS fragmentation of in source fragment b6 ion ( $m/z$  523.2328). b) Key product ions within the N-terminus of **1**





**Figure S21.** Global MS<sup>n</sup> fragmentation of cacaoidin (**1**) Annotation of product ions

## 2.5 Structural elucidation: Reduction and desulfurization of cacaoidin (**1**). HRMS / MS

To definitely establish the ring topology in cacaoidin, a sample of **1** was reduced and desulfurized with nickel boride under standard (sample **a**) and deuterated conditions<sup>[9]</sup> (sample **b**). The reaction mixtures were separately analyzed by HPLC-HRMS and the major species in both cases were found to be peaks with [M+H]<sup>+</sup> ions at *m/z* 2334.2094 (standard conditions, sample **a**) or 2340.2487 (deuterated conditions, sample **b**) (Figures S22 and S24 respectively). These results were consistent with the reduction of two double bonds (Dha, AviMeCys) and the desulfurization of only one of the two thioether bridges present in the molecule (NMe<sub>2</sub>Lan, AviMeCys rings).

Attempts to fragment these protonated adducts for reduced and desulfurized peptides were unsuccessful (Figures S23a, S25a). The presence in the sample **a** of a set of “in-source” fragment *b* ions differing 2 Da (*b<sub>n</sub>+2*) with respect to the homologous ions detected in **1** (*b<sub>7</sub>+2*: *m/z* 638; *b<sub>6</sub>+2*: *m/z* 525; *b<sub>5</sub>+2*: *m/z* 440) (Figure S22a) and the analogous set of *b<sub>n</sub>+4* ions in sample **b** (*b<sub>7</sub>+4*: *m/z* 640; *b<sub>6</sub>+4*: *m/z* 527; *b<sub>5</sub>+4*: *m/z* 442) (Figure S24a), both indicated that only the reduction of the Dha-2 residue had occurred at the *N*-terminus of **1**. This was further confirmed by MS-MS fragmentation of *b<sub>6</sub>+2* (*m/z* 525) (Figures S23b and S26a) and *b<sub>6</sub>+4* (527 *m/z*) (Figures S25b and S26a) ions in samples **a** and **b** respectively. Thus, it became clear that the C-terminus AviMeCys had been fully reduced and desulfurized while the NMe<sub>2</sub>Lan ring remained intact (Figure S26b).

### Experimental procedure<sup>[9]</sup>

Cacaoidin (**1**; 0.1 mg each sample) and NiCl<sub>2</sub> (0.3 mg) were suspended in 0.4 mL of a mixture CH<sub>3</sub>OH: H<sub>2</sub>O (1:1) for the standard (non-deuterated) conditions or CD<sub>3</sub>OD: D<sub>2</sub>O (1:1) for the experiment under deuterated conditions. The mixtures were transferred into screw-cap vials containing 0.3 mg of NaBH<sub>4</sub> or NaBD<sub>4</sub> and the tubes were rapidly sealed. A black precipitate appeared immediately with gas evolution (H<sub>2</sub> or D<sub>2</sub> gas). The reaction mixture was shaken at 50 °C for 2 h, after which the mixtures were significantly decolored. After centrifugation (12K rpm, 5 min, rt) and retention of the supernatant, fresh solvent (CH<sub>3</sub>OH: H<sub>2</sub>O (1:1) or CD<sub>3</sub>OD: D<sub>2</sub>O (1:1)) was added, and the mixture sonicated and re-centrifuged to recovery any residual peptide. Combined supernatants in each case were dried under vacuum and stored at -20 °C. Before the MS/MS analysis, the crude mixture from deuterated conditions was incubated in MeOH for NH/OH protons exchange.

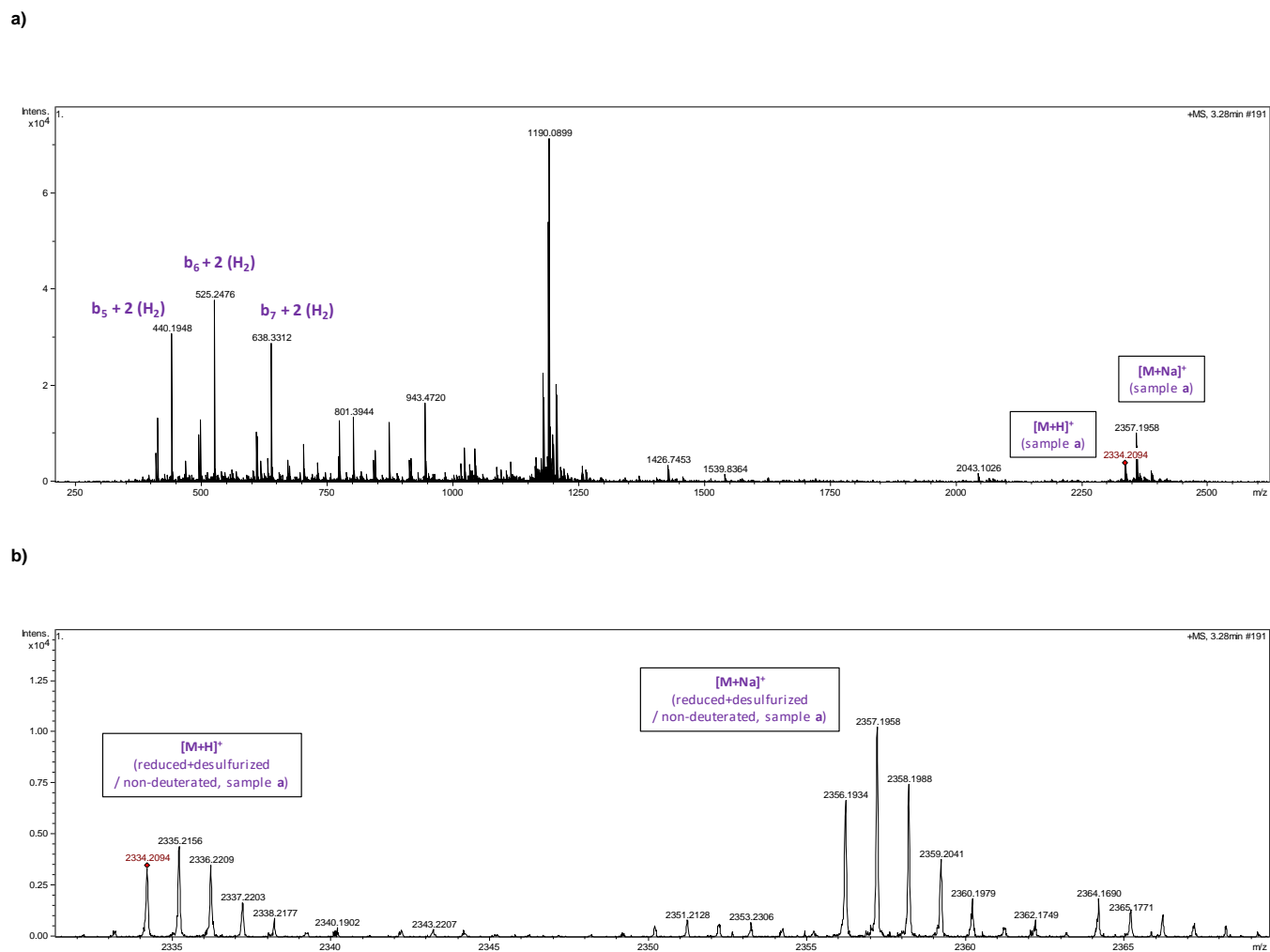
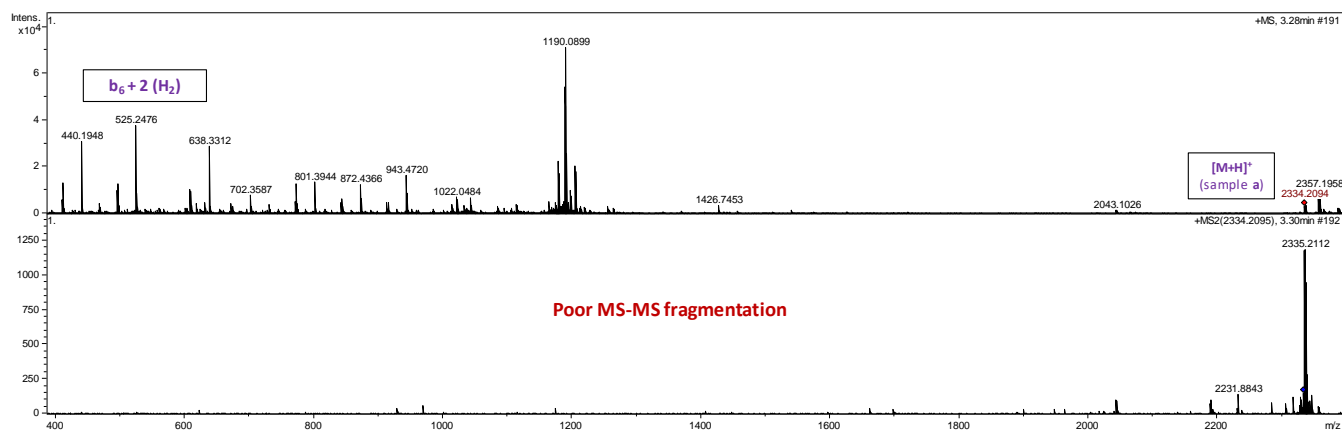


Figure S22. a) HRESIMS(+)-TOF spectrum of the crude reaction (sample a); overview. b) HRESIMS(+)-TOF spectrum sample a (zoom in region)

a)



b)

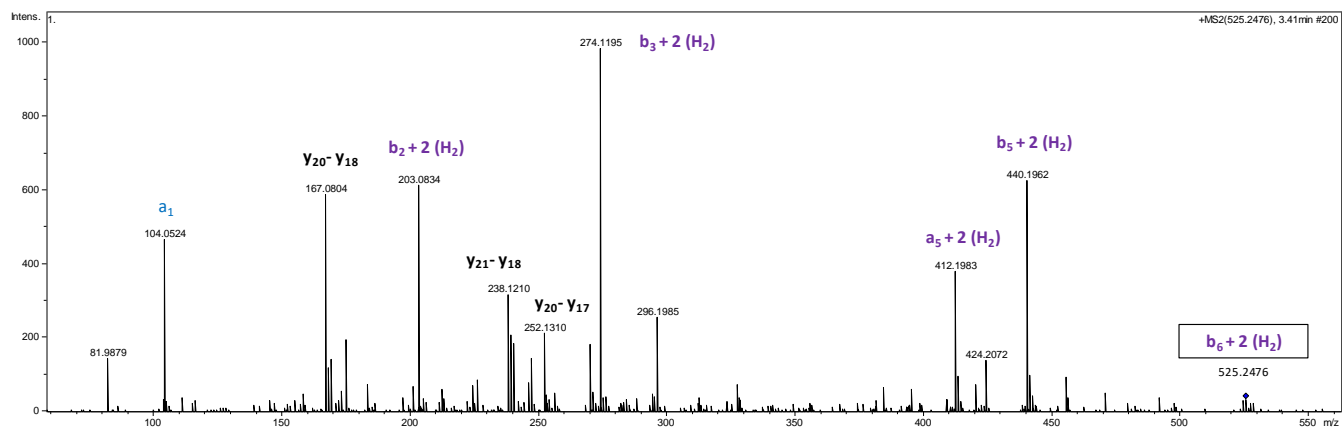


Figure S23. a) MS/MS fragmentation of ion  $m/z$  2334 resulted in very poor ion production. b) MS/MS fragmentation of “in-source” fragment ion at  $m/z$  525 ( $b_6+2$ )

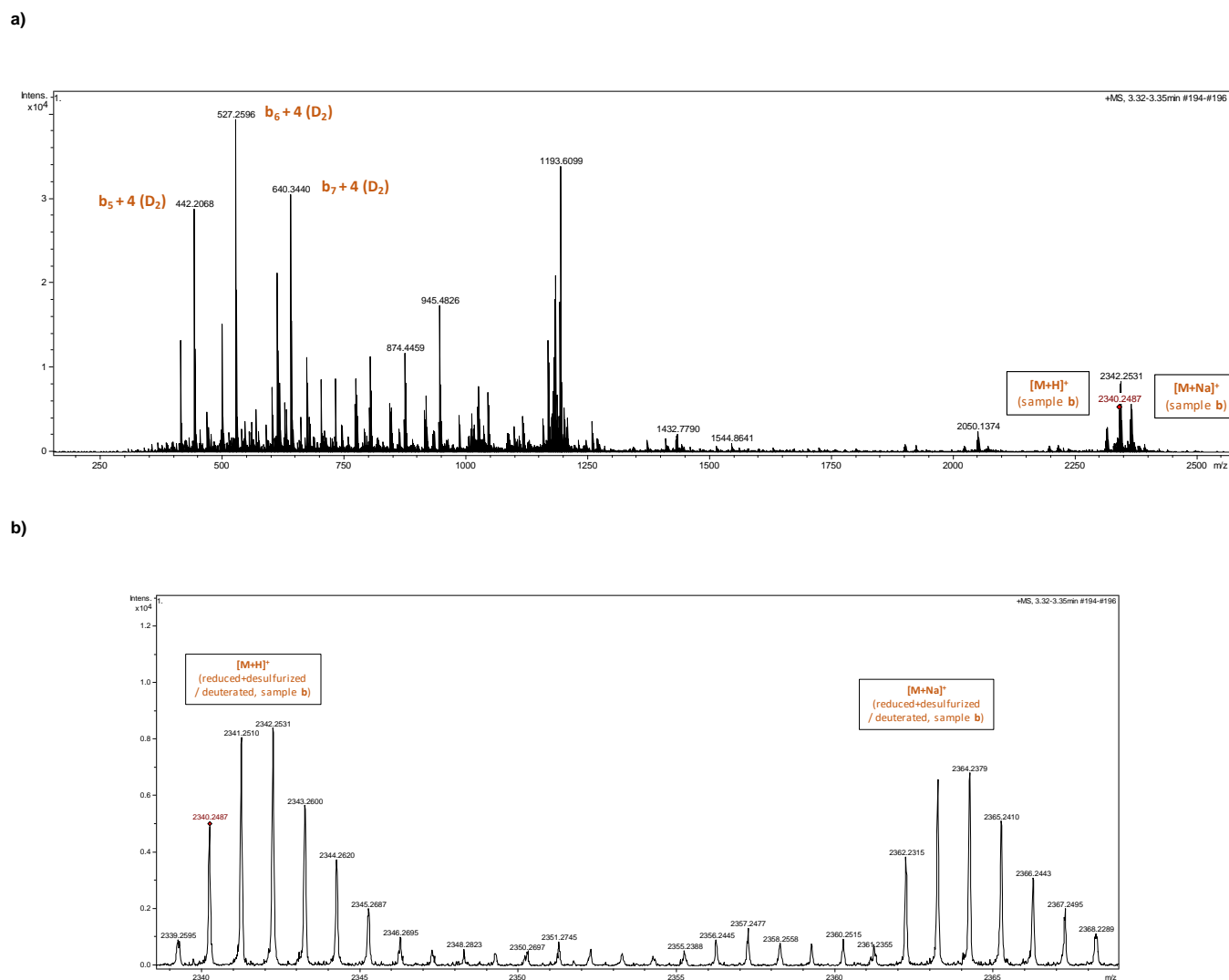


Figure S24. a) HRESIMS(+)-TOF spectrum of the crude reaction (sample b); overview. b) HRESIMS(+)-TOF spectrum sample b (zoom in region)

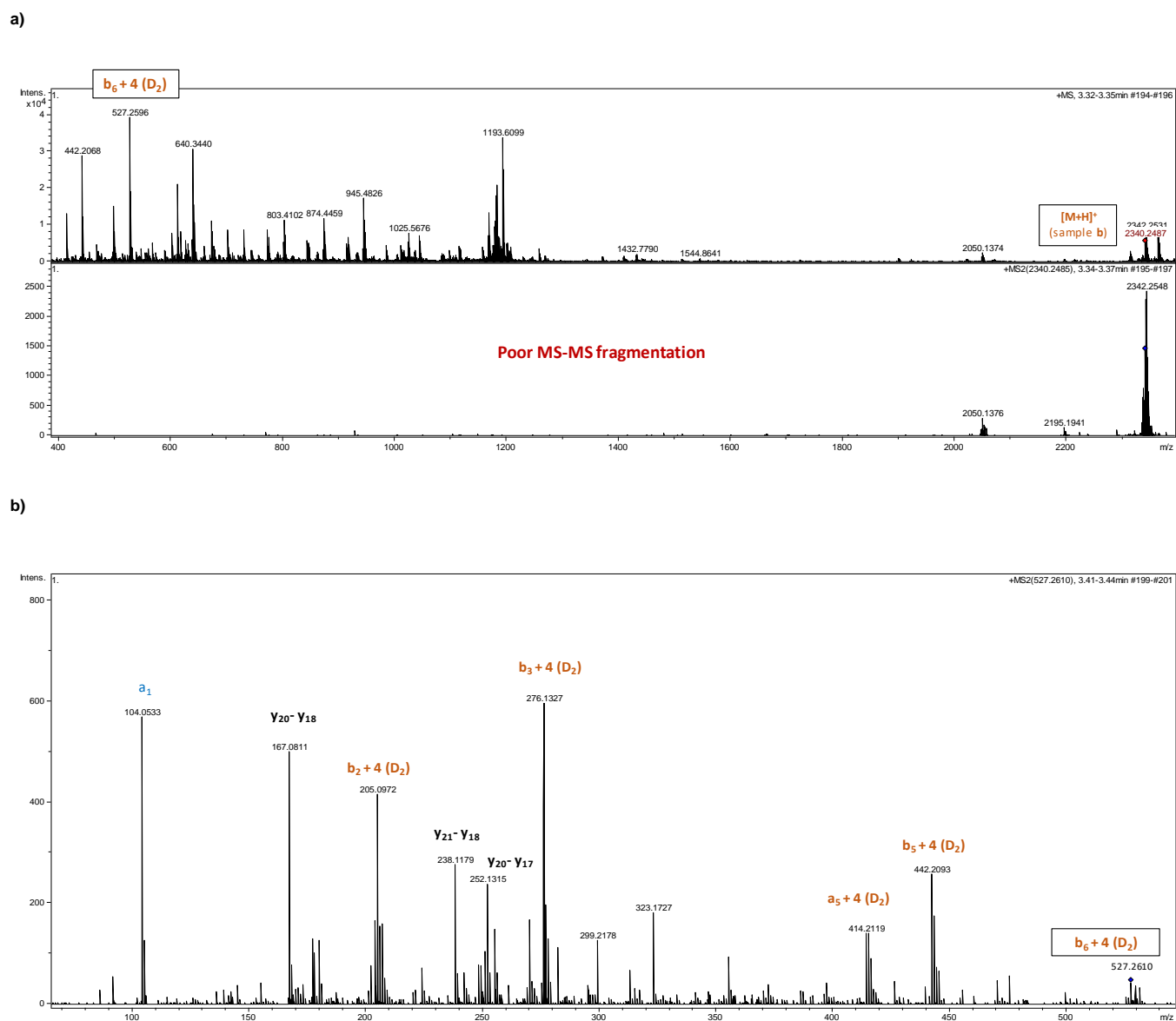
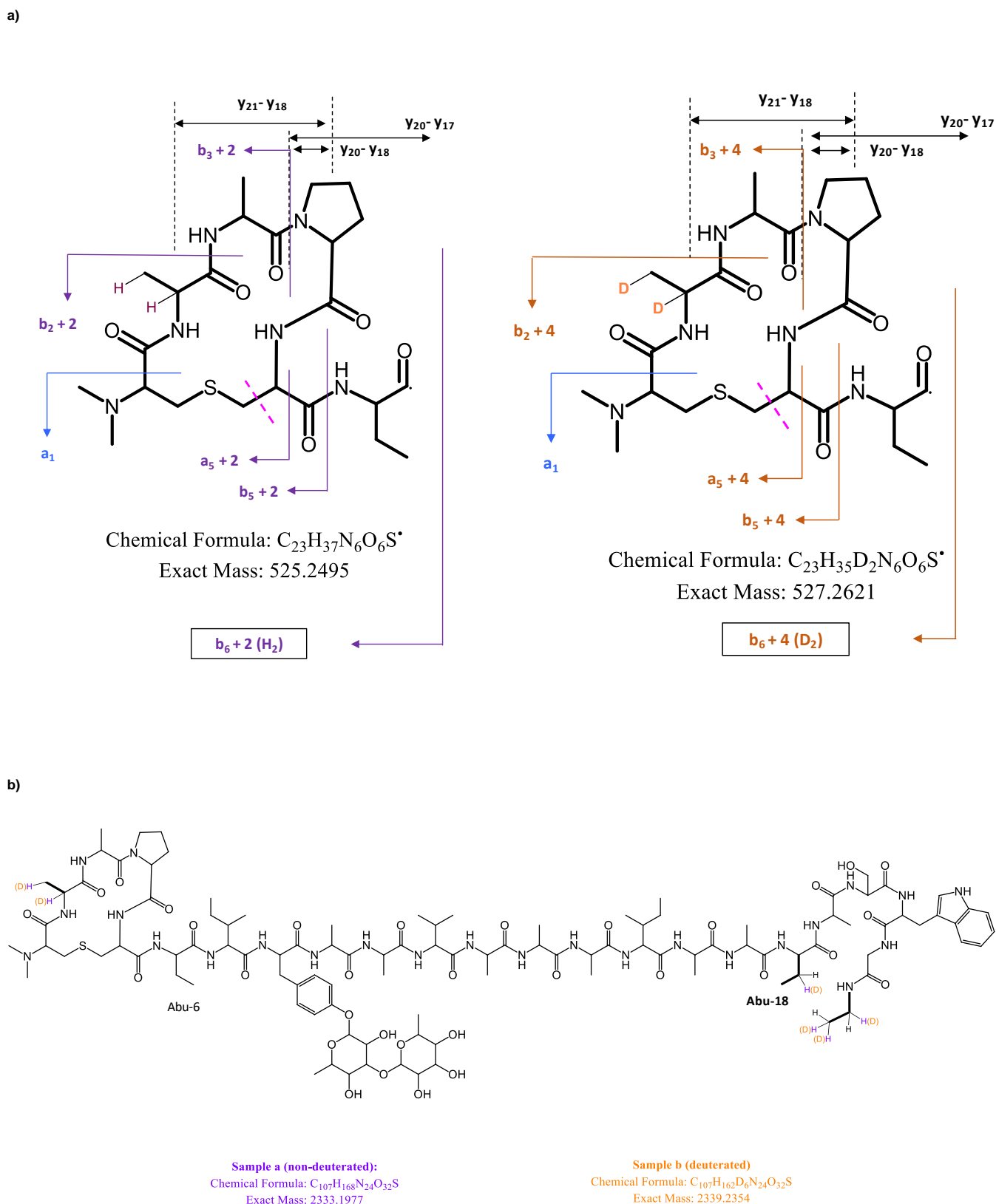
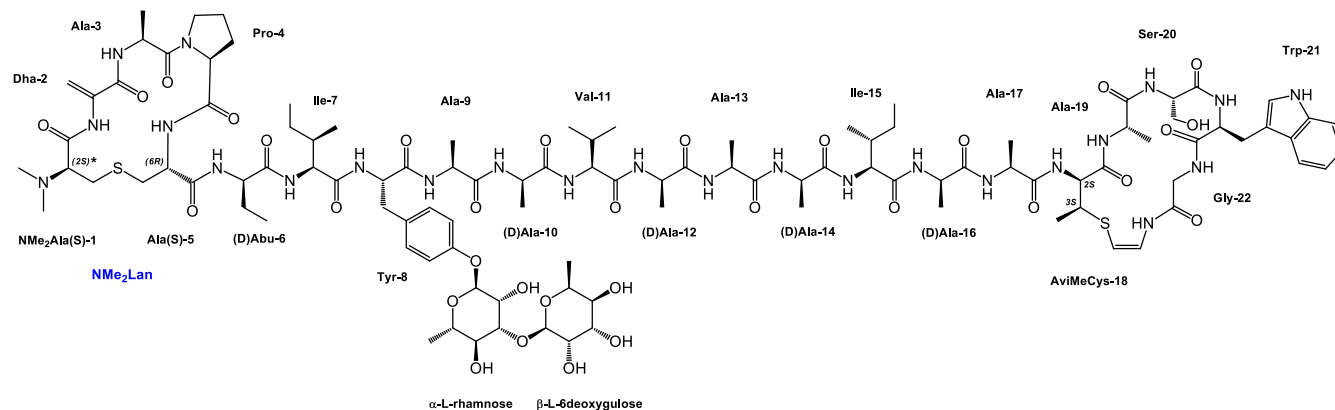


Figure S25. a) MS/MS fragmentation of ion  $m/z$  2340 resulted in very poor ion production. b) MS/MS fragmentation of “in-source” fragment ion at  $m/z$  527 ( $b_6+4$ )



**Figure S26.** a) Key MS/MS fragmentation of  $b_6+2$  (sample a; left) and  $b_6+4$  (sample b, right). b) Structure of reaction (reduction and partial desulfurization) products under standard (sample a; in purple) and deuterated (sample b, in orange) conditions

## 2.6 Structural characterization data of cacaoidin (1)



**Figure S27.** Structure of cacaoidin (1). Stereochemistry of NMe<sub>2</sub>Lan is proposed as DL (2*S*<sup>\*</sup>, 6*R*) (see section 2.7, below)

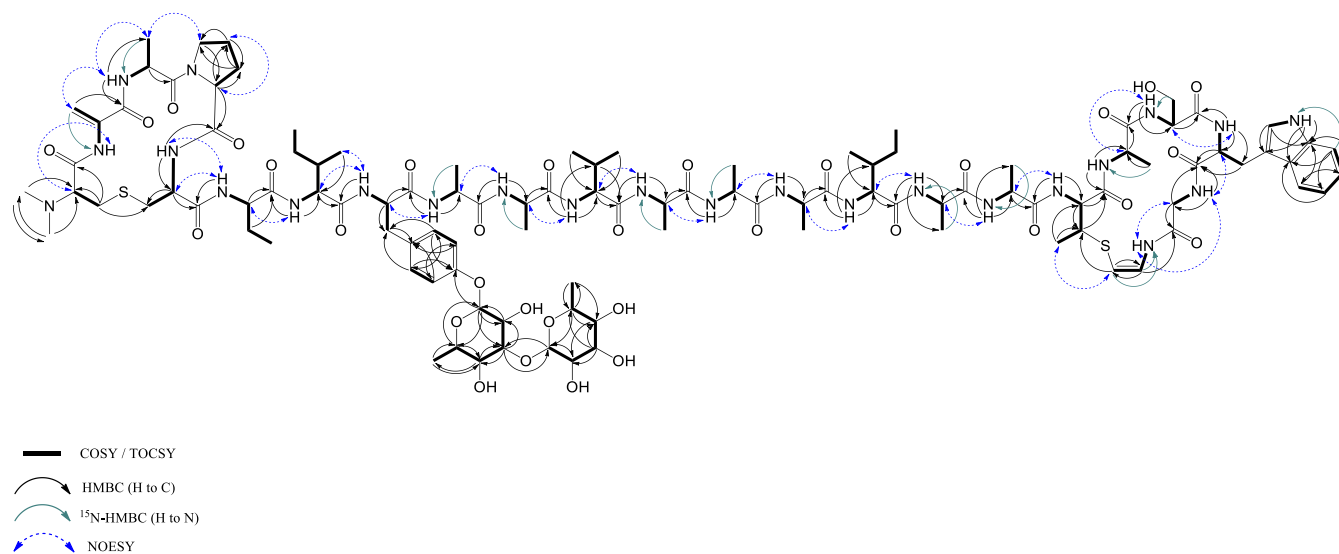


**Figure S28.** COSY / TOCSY, HMBC (H to C), <sup>15</sup>N-HMBC (H to N) and NOESY correlations observed for cacaoidin (1). (NOESY / ROESY correlations for the Tyr-O-disaccharide subunit previously shown in Figure S9).

## Cacaoidin (1)

**C<sub>107</sub>H<sub>162</sub>N<sub>24</sub>O<sub>32</sub>S<sub>2</sub>.**

White amorphous powder,  $[\alpha]_{\text{D}}^{25} = -7.1^\circ$  (c 0.20, MeOH); <sup>1</sup>H NMR (500 MHz, CD<sub>3</sub>CN:H<sub>2</sub>O, 9:1): see Table S1; <sup>13</sup>C NMR (125 MHz, CD<sub>3</sub>CN:H<sub>2</sub>O, 9:1): see Table S1; IR (ATR)  $\nu$  (cm<sup>-1</sup>): 3285, 2969, 2937, 1650, 1537, 1453, 1382, 1201, 1182, 1137, 1024; UV/Vis (DAD):  $\lambda_{\text{max}}$  219, 268 nm. HRMS (ESI+, 0 eV):  $m/z$  793.0555 [M+2H+NH<sub>4</sub>]<sup>3+</sup> (calcd. for C<sub>107</sub>H<sub>168</sub>N<sub>25</sub>O<sub>32</sub>S<sub>2</sub>: 793.0571),  $m/z$  1197.5932 [M+2NH<sub>4</sub>]<sup>2+</sup> (calcd. for C<sub>107</sub>H<sub>170</sub>N<sub>26</sub>O<sub>32</sub>S<sub>2</sub>: 1197.5953); HRMS (ESI+, 75 eV):  $m/z$  2360.1332 [M+H]<sup>+</sup> (calcd. for C<sub>107</sub>H<sub>163</sub>N<sub>24</sub>O<sub>32</sub>S<sub>2</sub>: 2360.1301); HRMS/MS: see section 2.4 in Supporting information.

**Table S1.** <sup>1</sup>H and <sup>13</sup>C NMR (500 MHz; CD<sub>3</sub>CN: H<sub>2</sub>O, 9:1; 24 C) data for **cacaoidin (1)**

Residue	Position	$\delta_C / \delta_N$ [a, b]	$\delta_H$ , mult* (J in Hz) [c, d, e, f]	Residue	Position	$\delta_C / \delta_N$ [a, b]	$\delta_H$ , mult* (J in Hz) [c, d, e, f]	
<b>NMe<sub>2</sub>-Ala(S)-1</b>	1	167.6, C		<b>Tyr-8</b>	1	173.1, C		
	2	68.6, CH	3.91, d (11.5) <sup>e</sup>		2	55.8, CH	4.46	
	3	29.6, CH <sub>2</sub>	3.53, d (14.2) <sup>e</sup> / 2.74, dd (14.2, 11.5)		3	36.2, CH <sub>2</sub>	3.30 <sup>c, d</sup> / 2.81	
	N(CH <sub>3</sub> ) <sub>2</sub>	42.8, 2 x CH <sub>3</sub>	2.87, s		4	132.6, C		
<b>Dha-2</b>	1	167.0, C		5/9	131.2 <sup>a</sup> , 2 x CH	7.19, d (8.8)		
	2	134.8, C		6/8	117.7 <sup>a</sup> , 2 x CH	6.98, d (8.8)		
	3	119.7, CH <sub>2</sub>	6.02, brs / 5.94, brs	7	156.1, C			
	NH	133.5	9.90 <sup>c</sup> , br s	NH	117.1 <sup>a</sup>	7.66, d (8.1)		
<b>Ala-3</b>	1	173.8 <sup>a</sup> , C		<b>Ala-9</b>	1	175.2 <sup>a</sup> , C		
	2	55.9, CH	4.24		2	51.4, CH	4.03	
	3	14.5, CH <sub>3</sub>	1.48, d (7.4)		3	17.8, CH <sub>3</sub>	1.26, d (6.9)	
	NH	123.7 <sup>a</sup>	8.82, d (2.6)		NH	122.1 <sup>a</sup>	7.54, d (4.8)	
<b>Pro-4</b>	1	173.7, C		<b>Ala-10</b>	1	175.2 <sup>a</sup> , C		
	2	63.7, CH	4.34, dd (8.6, 8.6)		2	50.4 <sup>a</sup> , CH	4.26	
	3	29.7, CH <sub>2</sub>	a: 2.31 / b: 1.65		3	18.0, CH <sub>3</sub>	1.28, d (7.1)	
	4	26.6, CH <sub>2</sub>	1.93 / 1.87		NH	121.4	7.95, d (6.9)	
	5	49.1, CH <sub>2</sub>	3.69 / 3.30 <sup>c, d</sup>		<b>Val-11</b>	1	173.9, C	
<b>Ala(S)-5</b>	1	172.8, C		2		61.0 <sup>a</sup> , CH	4.00	
	2	54.2, CH	4.22	3		30.7, CH	2.13	
	3	35.3, CH <sub>2</sub>	3.15 <sup>c, d</sup>	4		19.6, CH <sub>3</sub>	0.91, d (6.8)	
	NH	110.7	8.15, d (7.5) <sup>f</sup>	4'		19.4, CH <sub>3</sub>	0.91, d (6.8)	
<b>Abu-6</b>	1	176.3, C		NH	116.7	7.76, d (7.0)		
	2	57.8, CH	3.97	<b>Ala-12</b>	1	174.8 <sup>a</sup> , C		
	3	24.6, CH <sub>2</sub>	1.77		2	50.8, CH	4.21	
	4	10.7, CH <sub>3</sub>	0.90, t (7.4)		3	17.6, CH <sub>3</sub>	1.33, d (6.9)	
	NH	120.2 <sup>a</sup>	7.69, d (4.3)		NH	125.7	8.16, d (5.5) <sup>f</sup>	
<b>Ile-7</b>	1	173.4, C			<b>Ala-13</b>	1	174.8 <sup>a</sup> , C	
	2	61.0 <sup>a</sup> , CH	3.95	2		50.4 <sup>a</sup> , CH	4.25	
	3	36.3, CH	1.72	3		17.5, CH <sub>3</sub>	1.29, d (6.9)	
	3'	15.9, CH <sub>3</sub>	0.67, d (7.0)	NH		120.2 <sup>a</sup>	7.80 <sup>a</sup>	
	4	25.1, CH <sub>2</sub>	0.98 / 0.84 <sup>*</sup>	<b>Ala-14</b>		1	175.6 <sup>a</sup> , C	
	5	12.1, CH <sub>3</sub>	0.66, t (7.4)			2	51.0, CH	4.19
	NH	120.2 <sup>a</sup>	7.80 <sup>a</sup>			3	17.7, CH <sub>3</sub>	1.32, d (6.9)
						NH	120.2 <sup>a</sup>	7.80 <sup>a</sup>



<b>Ile-15</b>	1	173.8 <sup>a</sup> , C		<b>Trp-21</b>	1	174.3, C	
	2	60.3, CH	3.99, dd (7.3, 7.3)		2	55.7, CH	4.52
	3	37.0, CH	1.85		3	27.8, CH <sub>2</sub>	3.27 <sup>c,d</sup> / 3.04 <sup>c,d</sup> , d (14.9, 9.5)
	3'	15.7, CH <sub>3</sub>	0.87, d (6.8)		4	111.0, C	
	4	26.0, CH <sub>2</sub>	1.48 / 1.14		5	128.3, C	
	5	11.3, CH <sub>3</sub>	0.83, t (7.4)		6	119.3, CH	7.52, d (8.2)
	NH	117.1 <sup>a</sup>	7.72, d (7.3)		7	119.8, CH	7.01, dd (8.2, 7.2)
<b>Ala-16</b>	1	175.3, C		8	122.4, CH	7.08, dd (8.1, 7.2)	
	2	50.4 <sup>a</sup> , CH	4.17	9	112.5, CH	7.35, d (8.1)	
	3	17.0, CH <sub>3</sub>	1.30	10	137.4, C		
	NH	123.7 <sup>a</sup>	8.10, d (6.8)	11	125.0, CH	7.14, d (2.4)	
<b>Ala-17</b>	1	175.6 <sup>a</sup> , C		NH (indol)	127.2	9.69, br s	
	2	52.2, CH	4.02	NH	117.1 <sup>a</sup>	7.87, d (6.8)	
	3	17.2, CH <sub>3</sub>	1.23, d (6.9)	<b>Gly-22</b>	1	169.8, C	
NH	121.8	7.96, d (5.6)	2		45.2, CH <sub>2</sub>	3.89, dd (16.1, 6.1) / 3.73, dd (16.1, 6.1)	
<b>AviMeCys-18</b>	1	172.6, C		NH	106.6	7.75, dd (6.1, 6.1)	
	2	58.1, CH	3.90	<b>α-Rhamnose</b>	1	99.2, CH	5.40, br s
	3	44.8, CH	3.32 <sup>c,d</sup> , m		2	71.2, CH	4.18
	3'	20.5, CH <sub>3</sub>	1.31, d (7.0)		3	82.4, CH	3.86, dd (9.4, 3.1)
	4	102.0 <sup>b</sup> , CH	5.46, d (7.5)		4	72.1, CH	3.54, dd (9.4, 9.4)
	5	130.8 <sup>b</sup> , CH	7.03, dd (10.4, 7.5)	5	70.0 <sup>a</sup> , CH	3.67, dq (9.4, 6.2)	
	5-NH	131.5	9.40, d (10.4)	6	18.3, CH <sub>3</sub>	1.15, d (6.2)	
NH	115.9	8.17, d (6.7) <sup>f</sup>	<b>β-6-Deoxy-gulose</b>	1	103.5, CH	4.80, d (8.1)	
<b>Ala-19</b>	1	175.2 <sup>a</sup> , C			2	69.6, CH	3.62, dd (8.1, 3.4)
	2	52.4, CH		4.18	3	72.6, CH	3.96
	3	17.3, CH <sub>3</sub>		1.34, d (7.4)	4	72.7, CH	3.47, br d (2.7)
	NH	123.7 <sup>a</sup>		8.19, d (6.0)	5	70.0 <sup>a</sup> , CH	4.01
<b>Ser-20</b>	1	172.4, C			6	16.4, CH <sub>3</sub>	1.14, d (6.9)
	2	58.4, CH	4.25				
	3	62.6, CH <sub>2</sub>	3.71 / 3.55				
	NH	110.4	7.73, d (6.7)				

[a] Overlapping with other isochronous <sup>13</sup>C-NMR / <sup>15</sup>N-NMR / <sup>1</sup>H-NMR signals. [b] Weak <sup>13</sup>C-NMR / <sup>15</sup>N-NMR signal

[c] <sup>1</sup>H-NMR signal intensity decreased in water suppression experiments. [d] Water masked <sup>1</sup>H-NMR signal in non-presaturated experiments. [e] *J*s determined from HSQC traces. [f] *J*s determined from <sup>15</sup>N-HSQC traces.

\* No multiplicity is given for <sup>1</sup>H-NMR signals for which coupling constants (*J*s) could not be measured directly in <sup>1</sup>H or JRES spectra nor determined from HSQC / <sup>15</sup>N-HSQC traces. The assignments were supported by HSQC (<sup>15</sup>N-HSQC if applicable), HMBC (<sup>15</sup>N-HMBC if applicable), TOCSY and HSQC-TOCSY.

As observed in many small cyclic peptides, the 2D NMR data revealed the N-terminus ring of cacaoidin (**1**) to appear in two distinct conformations (in a 5:1 ratio) interconverting on the NOESY NMR time scale (Figures S29-S31). (**Note:** NMR data reported in Table S1 corresponds exclusively to the major conformer). The signals within the N-terminus of the minor conformer were partially assigned by TOCSY, HSQC and HMBC interpretation (for NMR assignments of minor conformer in HSQC, see Figures S61, S63 and S65). The characteristic chemical shift difference between C $\beta$  and C $\gamma$  for the proline residue in the minor conformer (see HSQC spectrum, Figure S63) strongly suggest a cis configuration<sup>[7]</sup> for the Ala-Pro amide bond within the N-terminus. This cis / trans isomerization at Pro residues with the trans isomer predominating (as occurs in **1**) has been previously reported for synthetic analogues of Lan rings found in other lantibiotics.<sup>[10,11]</sup>

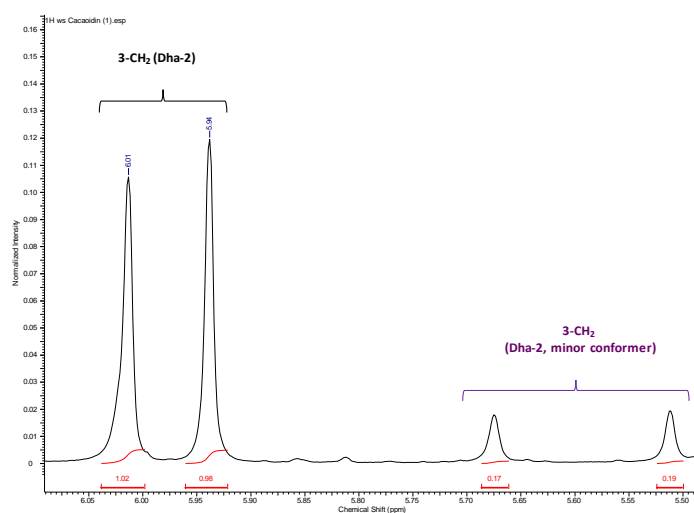


**Figure S29.** Olefinic proton signals for Dha-2 residue in both major (black) and minor (purple) conformers showing a 5:1 ratio between them.

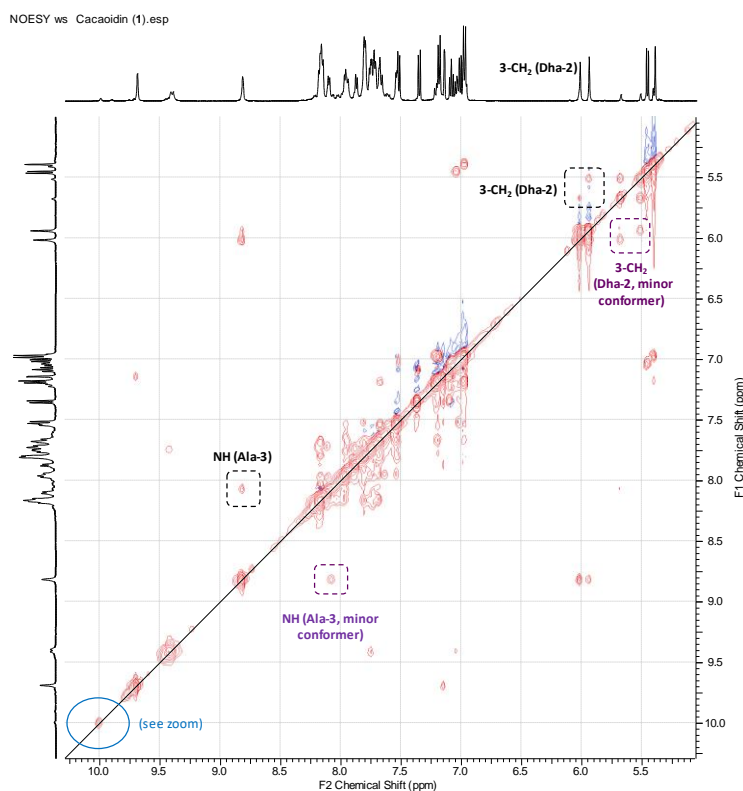


**Figure S30.** Conformational exchange in the N-terminus of cacaoidin (**1**). Section of the NOESY spectrum showing key chemical exchange (EXSY) cross-peaks. Water suppression was applied for the acquisition.

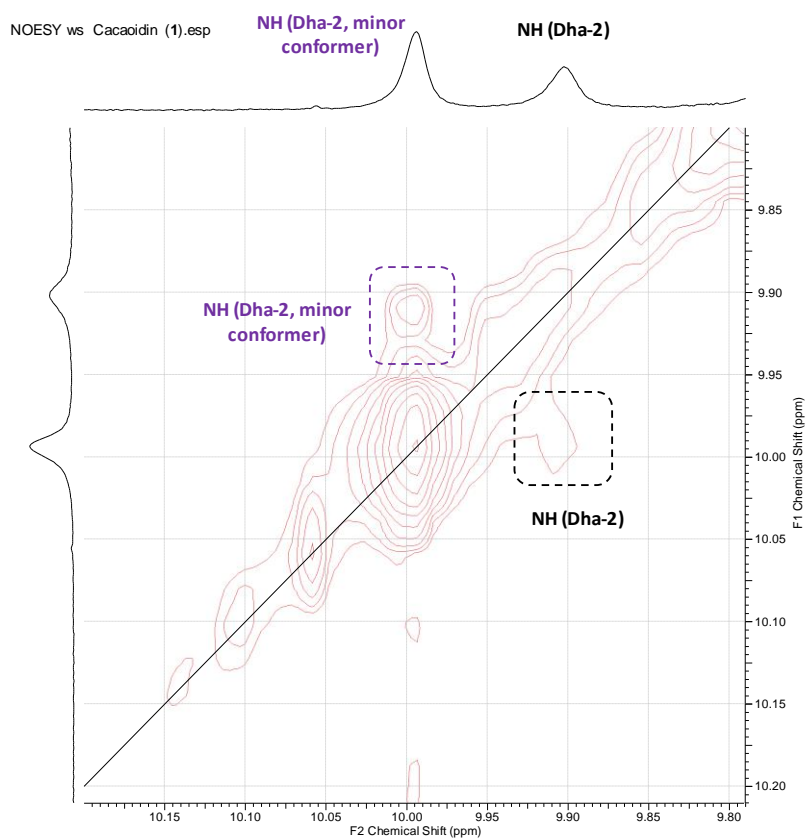


**Figure S31.** Expansion of the NOESY spectrum showing key chemical exchange (EXSY) cross-peaks (zoom in region). Water suppression was applied for the acquisition.

## 2.7 Advanced Marfey's analysis of cacaoidin (1)

The absolute configuration for virtually all constituent amino acids in cacaoidin (**1**) was determined by advanced Marfey's analysis.<sup>[12]</sup> First, a sample of **1** (**sample M1**) was subjected to hydrolysis (HCl 6N, 110 °C, 16 h) and subsequent derivatization with L- and D-FDVA reagents. Comparison of the retention times of Marfey-derivatized hydrolysate of **1** with those of standard amino acids (Figure S32) showed that Pro-4, Ile-7 and Ile-15, Tyr-8, Val-11 and Ser-20 were all L-amino acids (Figures S33-S37). Trp-(21)-derivative, however, was not found due to degradation during hydrolysis, so a second sample of cacaoidin (**sample M2**) was hydrolyzed in presence of 5% thioglycolic acid to prevent degradation issues. After derivatization, L-Trp was confirmed in **1** (Figure S38).

For the first sample (**sample M1**), aminobutyric acid was determined to be present in its D- form (D-Abu; Figure S39). It was also revealed the presence of both L- and D-Ala in **1**. The relative peak areas showed a ratio of 5 L-Ala to 4 D-Ala (Figures S40-S41). This result strongly supports that D-Ala residues in **1** arise from amino acids genetically encoded as serine (Ser-10, Ser-12, Ser-14 and Ser-16) and perfectly agrees with the 9 Ala residues present in cacaoidin (**1**).

To determine the absolute configuration of NMe<sub>2</sub>Lan subunit (NMe<sub>2</sub>-Ala(S)-Ala) by advanced Marfey's analysis, DL and LL (the two different stereochemistries reported for Lan or Melan) standard samples of this diamino acid should be used but unfortunately, they are not commercially available. The double derivatization (with both L- and D-FDVA) of the hydrolysate of **1** revealed and elution order "D before L" for the corresponding derivatives (Figures S42-S43). This behavior is the same as that reported for Marfey-derivatives (both mono- and di-) of DL-MeLan in nisin A and pinensin B, so a DL (2*S*, 6*R*) absolute configuration was tentatively assigned for NMe<sub>2</sub>Lan in cacaoidin (**1**).

### Experimental details<sup>[13]</sup>

A sample of **1** (0.3 mg; **samples M1 or M2**) was dissolved in 0.6 mL of 6 N HCl (additionally containing 5% (v/v) of thioglycolic acid for **sample M2**) and heated at 110 °C for 16 h. Each crude hydrolysate was evaporated to dryness under a N<sub>2</sub> stream, the residues were separately dissolved in 100 µL of water and aliquoted into two portions of 50 µL each one. After addition of 20 µL of 1 M NaHCO<sub>3</sub> solution, a 1% (w/v) solution (100 µL) of L-FDVA (Marfey's reagent, N-(2,4-dinitro-5-fluorophenyl)-L-valinamide) in acetone was added to an aliquot (50 µL) of a 50 mM solution of each standard amino acid in its hydrochloride form (D, L, or DL mixture). Analogously, NaHCO<sub>3</sub> aq. 1 M (30 µL) was added to each peptide hydrolysate (M1 or M2) and they were separately treated with a 1% (w/v) solution (200 µL) of L-FDVA or D-FDVA. All the reaction mixtures were heated at 40 °C for 1 h, then quenched by addition of 20 µL of 1 N HCl. For the HPLC analysis, the crude mixtures were diluted 4-fold with acetonitrile and analyzed by LC/MS on an Agilent 1100 single quadrupole. Separations were carried out on a Waters XBridge C<sub>18</sub> column (4.6 x 150 mm, 5 µm) maintained at 40 °C. A mixture of two solvents, A (10% acetonitrile, 90% water) and B (90% acetonitrile, 10% water), both containing 1.3 mM trifluoroacetic acid and 1.3 mM ammonium formate, was used as the mobile phase under a linear gradient elution mode (25–65% B in 28 min, 65–100% B in 0.1 min, then isocratic 100% B for 4 min) at a flow rate of 1.0 mL/min.

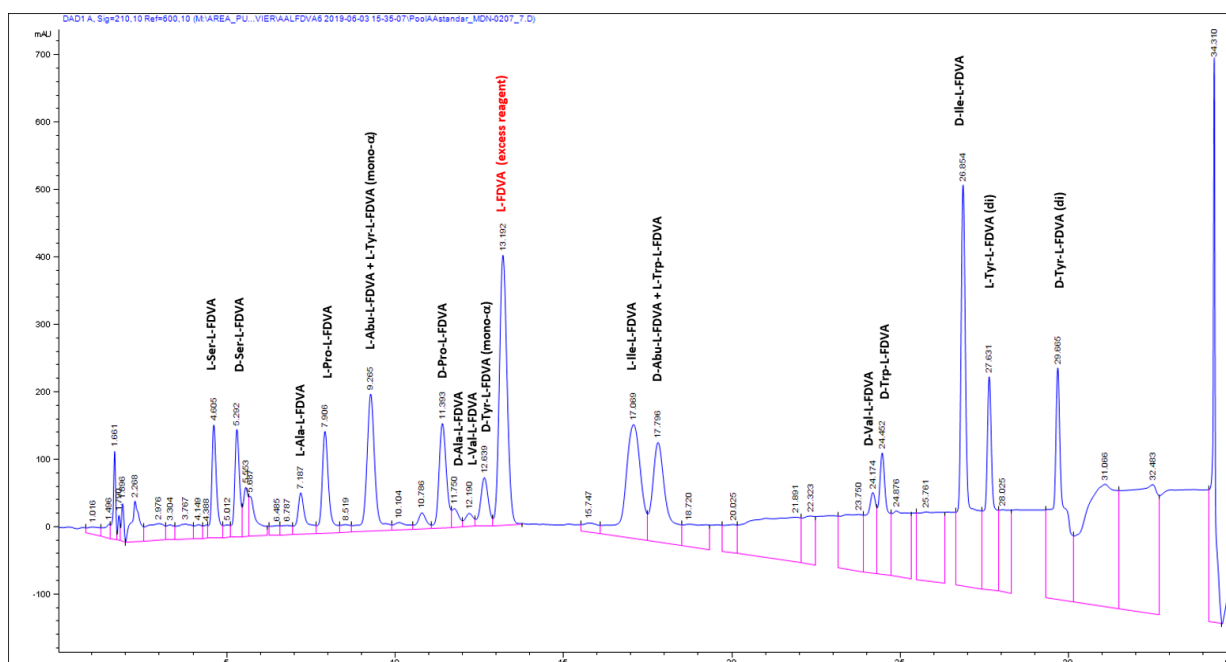


**Figure S32.** LC-UV chromatogram of the pool of L-FDVA derivatized standard amino acids (both L- and D- forms) present in **1**

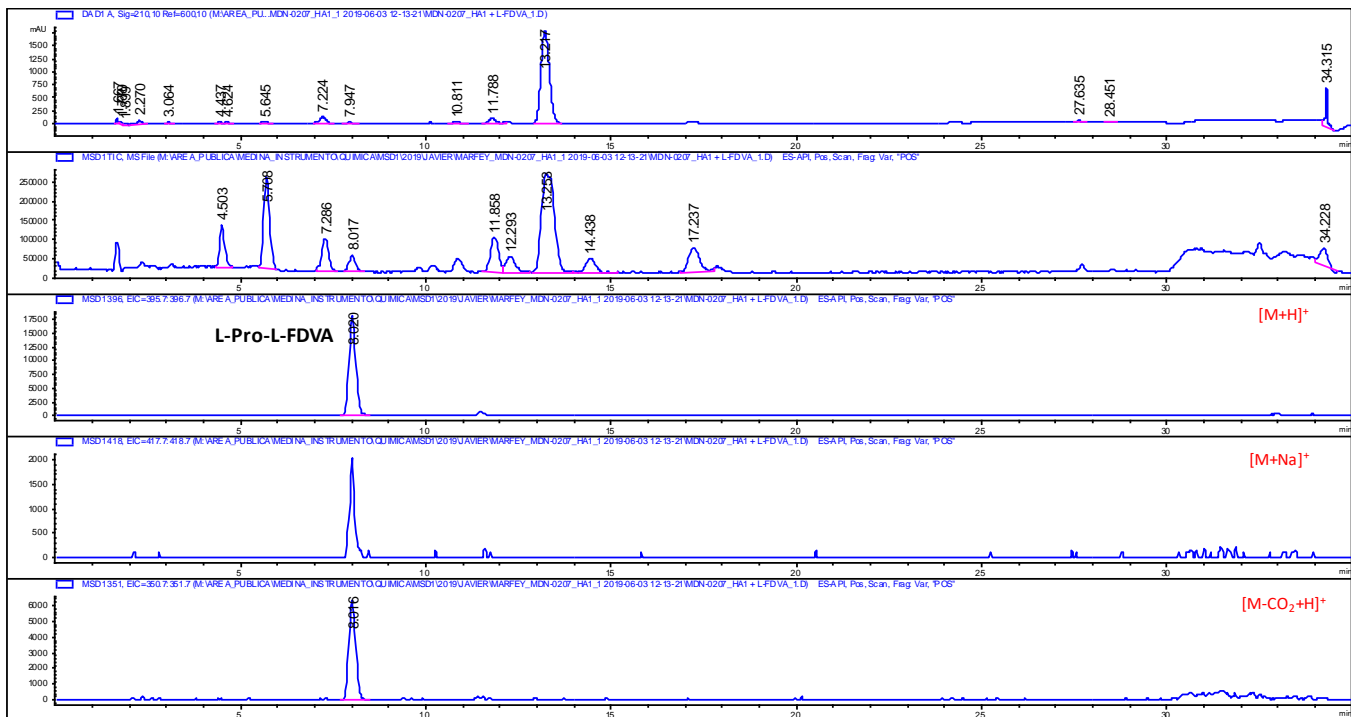


**Figure S33.** LC-UV and extracted-ion chromatograms (EIC) of Pro-L-FDVA derivative (**sample M1**). L-Pro was found in 1

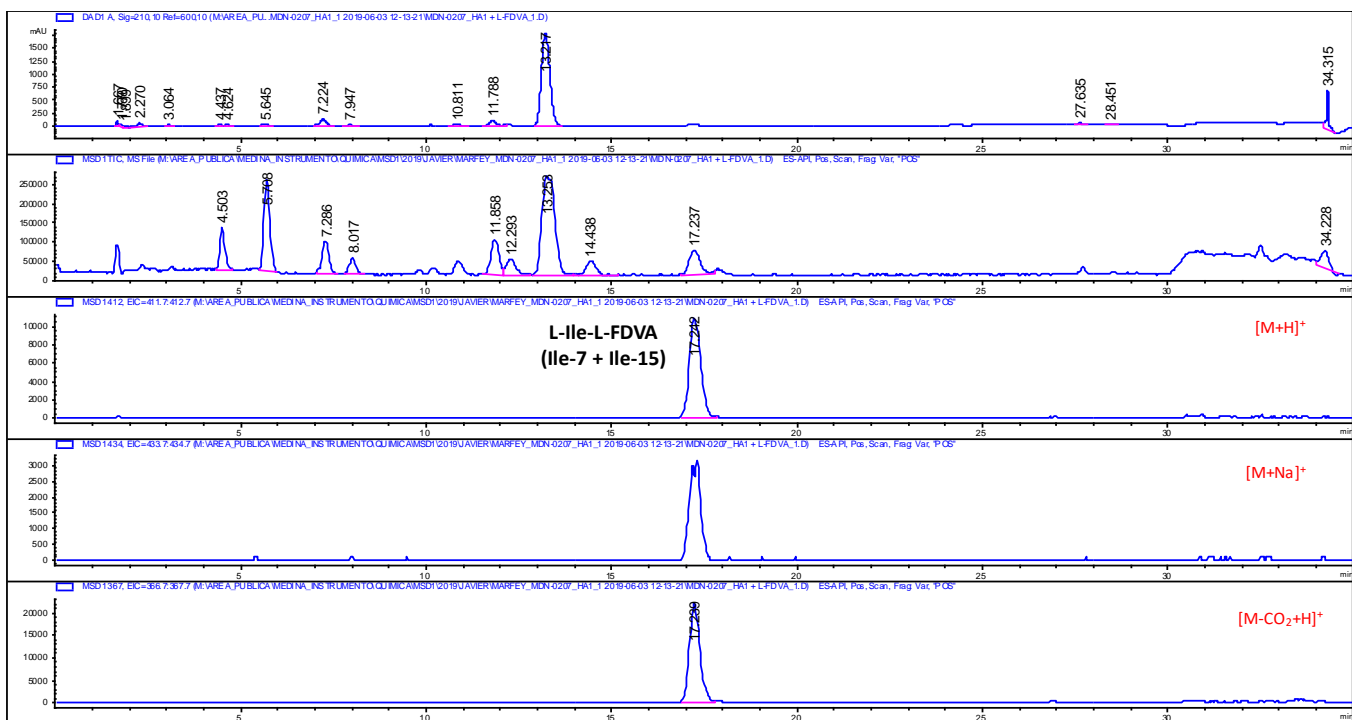


**Figure S34.** LC-UV chromatogram and EIC of Ile-L-FDVA derivative (**sample M1**). A unique peak corresponding to L-Ile-L-FDVA was found in the hydrolysate M1, so both Ile-7 and Ile-15 were determined as L-amino acids.

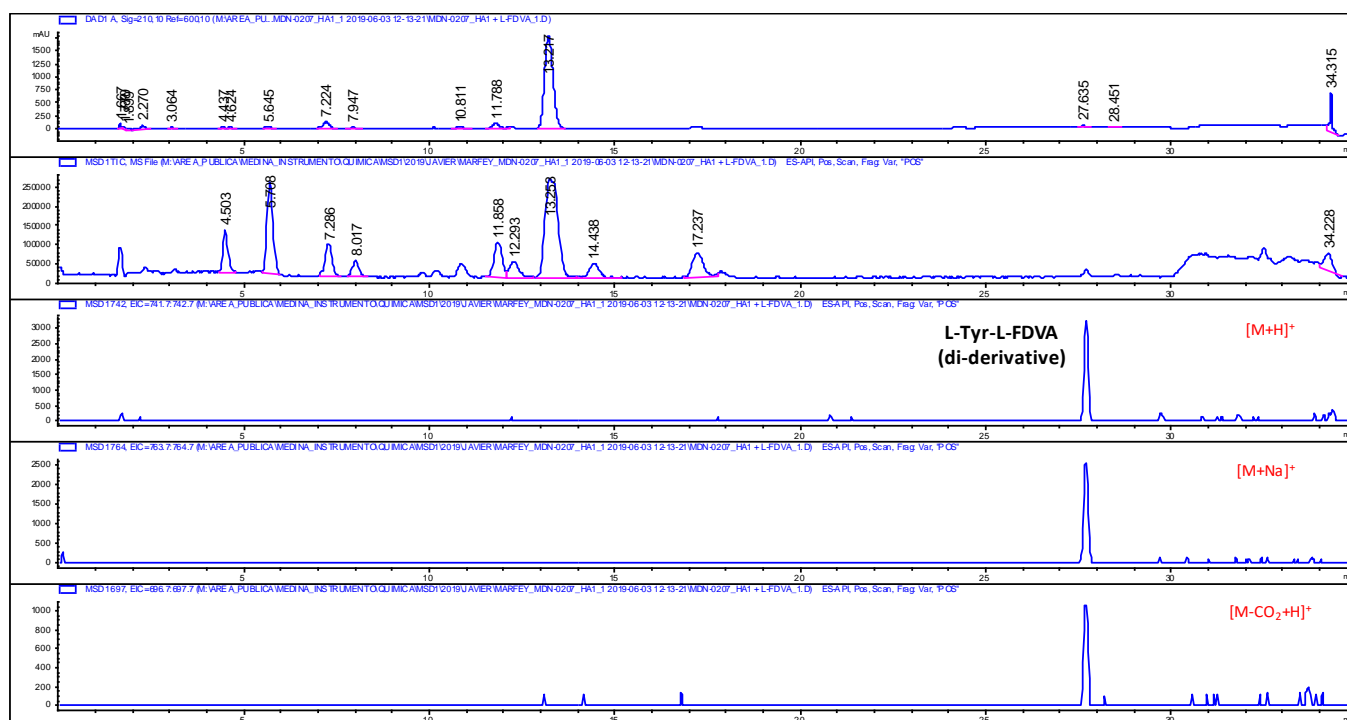


Figure S35. LC-UV chromatogram and EIC of Tyr-L-FDVA di-derivative (sample M1). L-Tyr was found in 1 (mono-derivatives were not detected in sample M1)

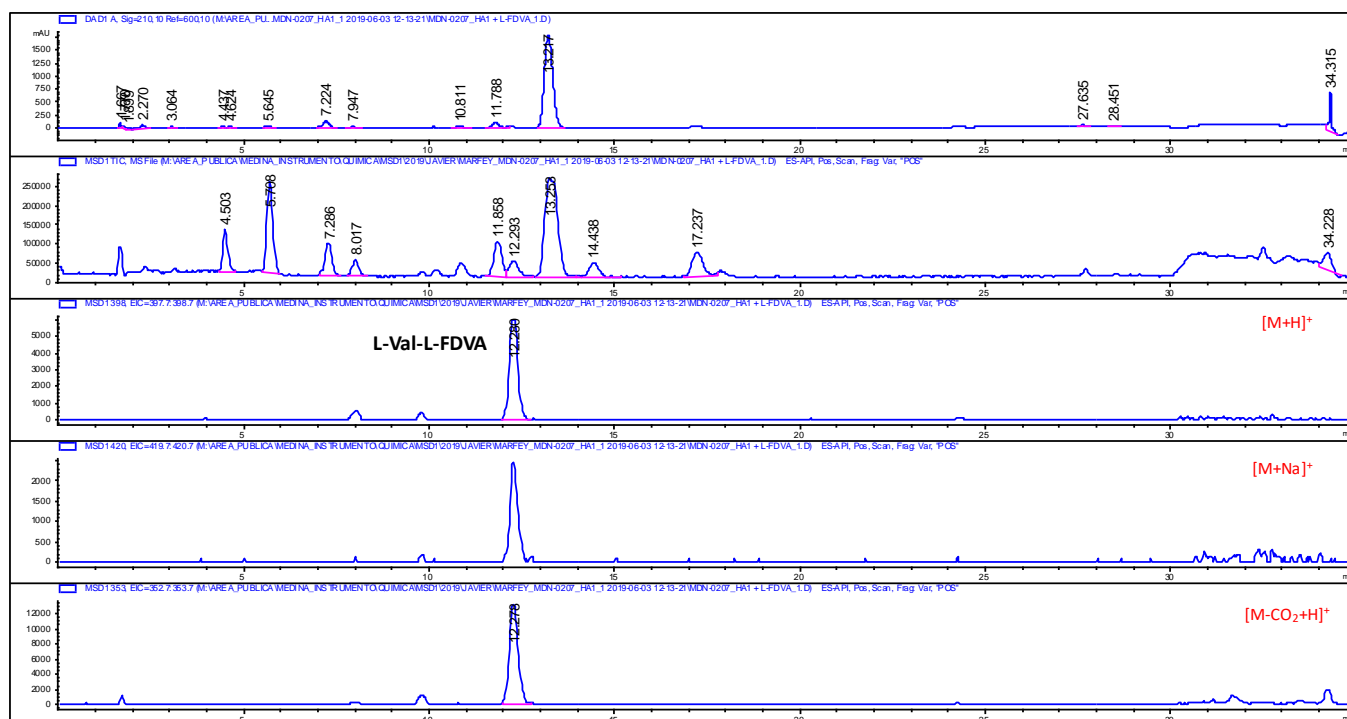


Figure S36. LC-UV chromatogram and EIC of Val-L-FDVA di-derivative (sample M1). L-Val was found in 1

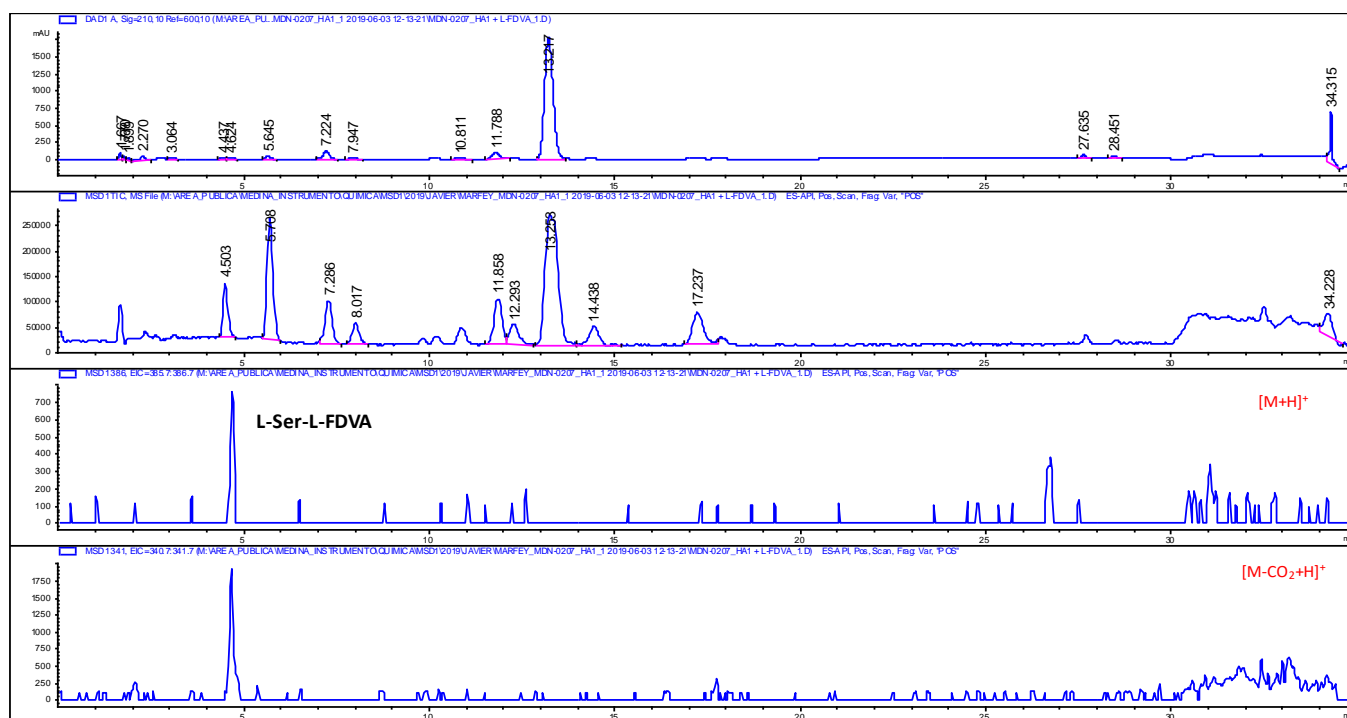


Figure S37. LC-UV chromatogram and EIC of Ser-L-FDVA derivative (sample M1). L-Ser was found in 1

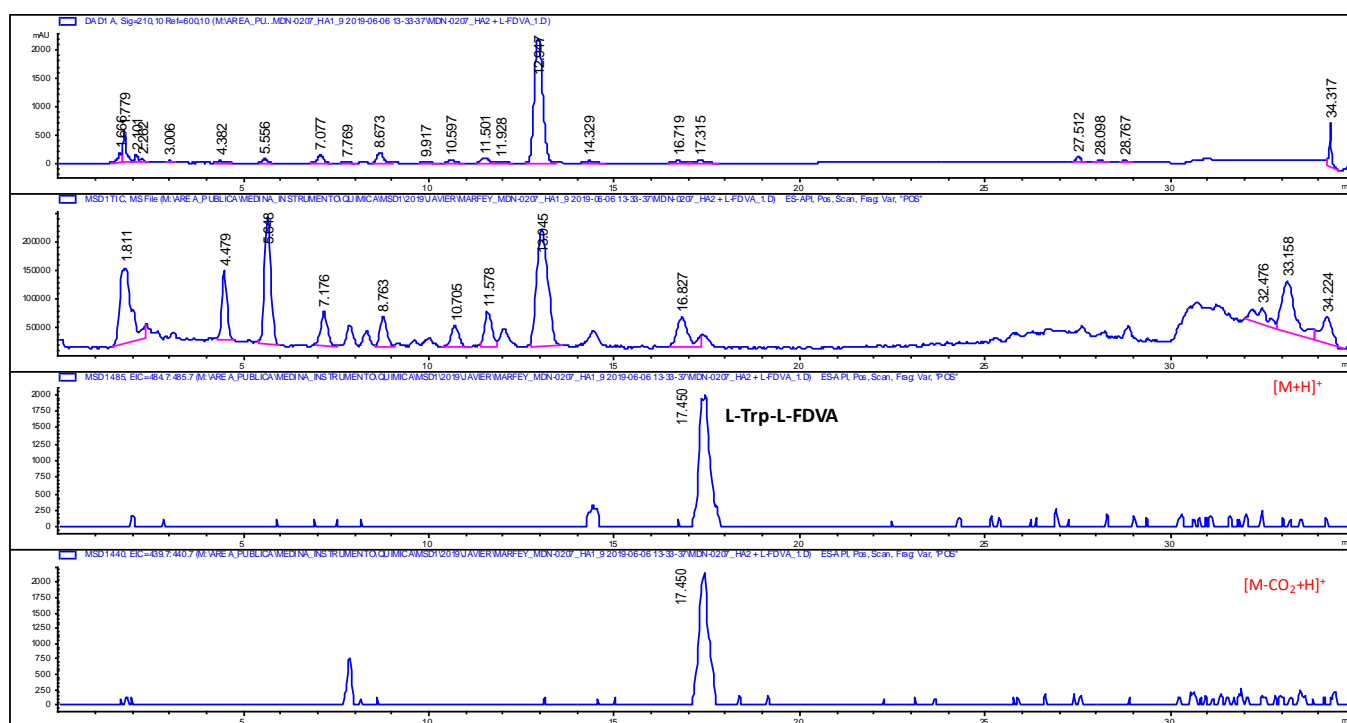


Figure S38. LC-UV chromatogram and EIC of Trp-L-FDVA derivative (sample M2: 5% thioglycolic acid was added during the hydrolysis to prevent Trp-degradation). L-Trp was found in 1

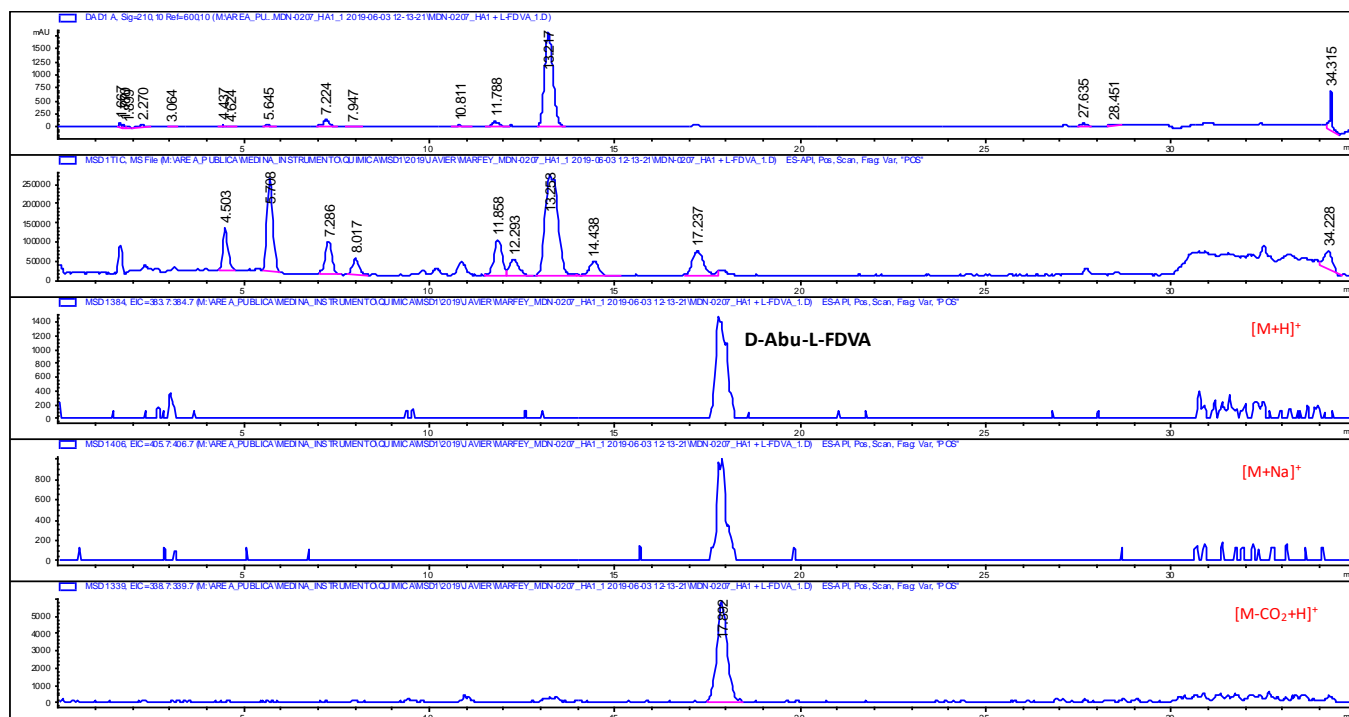


Figure S39. LC-UV chromatogram and EIC of Abu-L-FDVA derivative (sample M1). D-Abu was found in 1

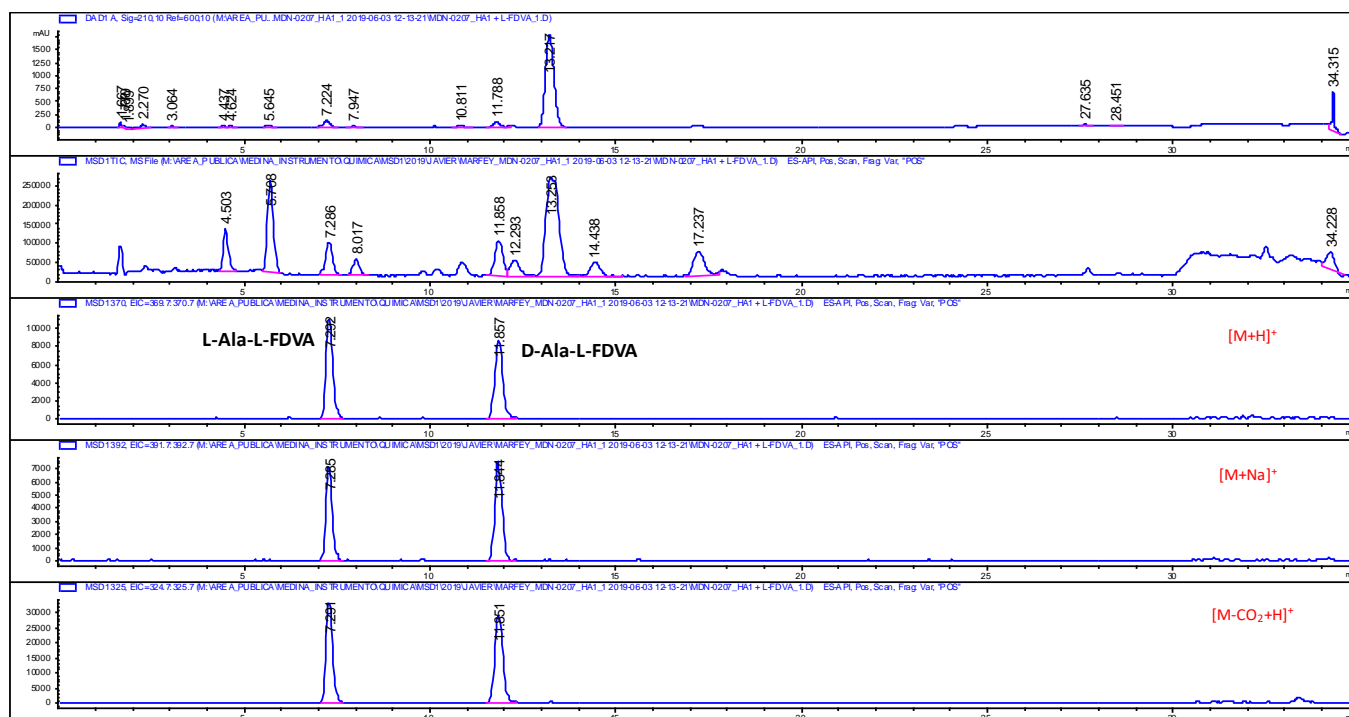


Figure S40. LC-UV chromatogram and EIC of Ala-L-FDVA derivatives (sample M1). Both L- and D-Ala-L-FDVA derivatives were found.



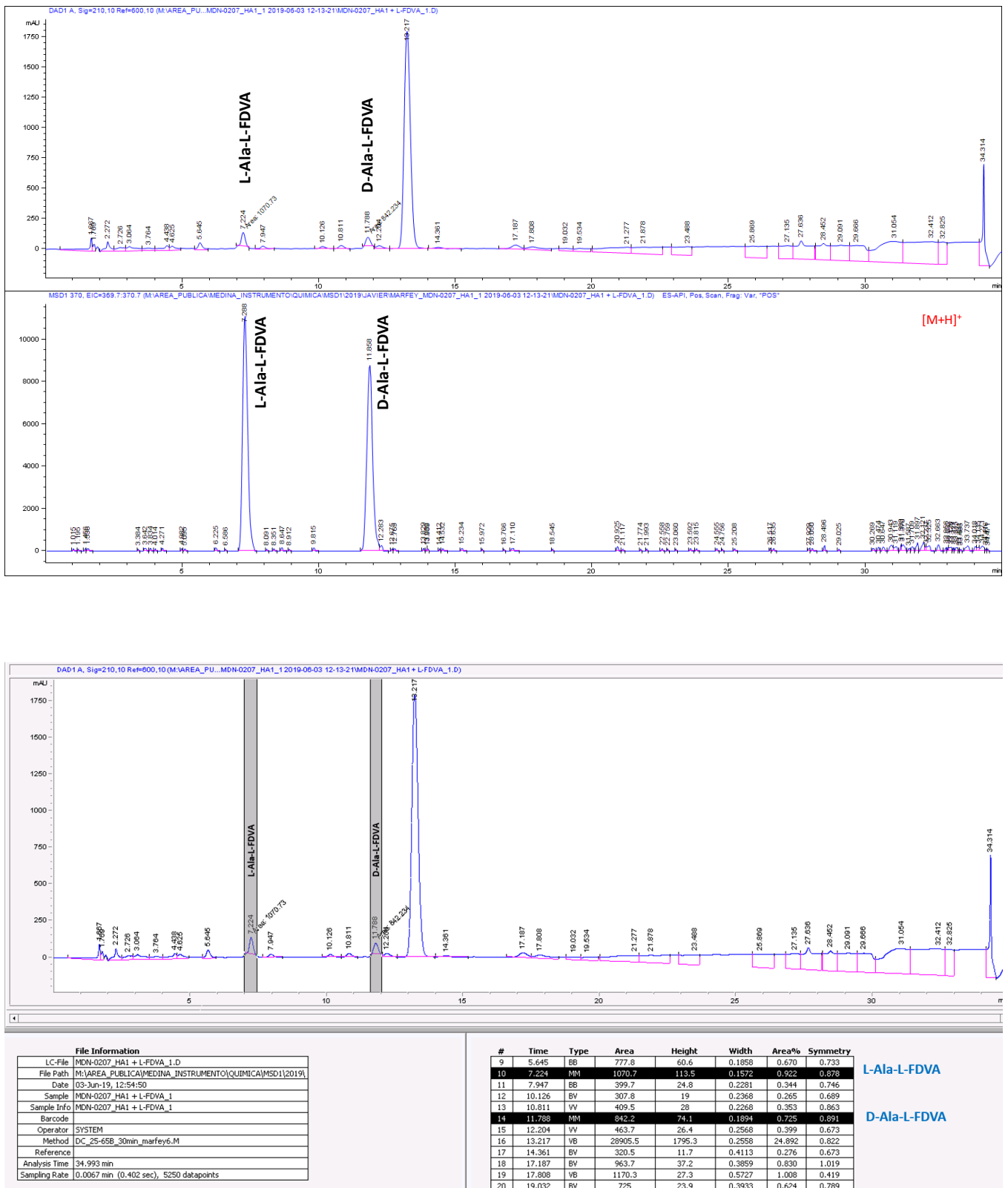
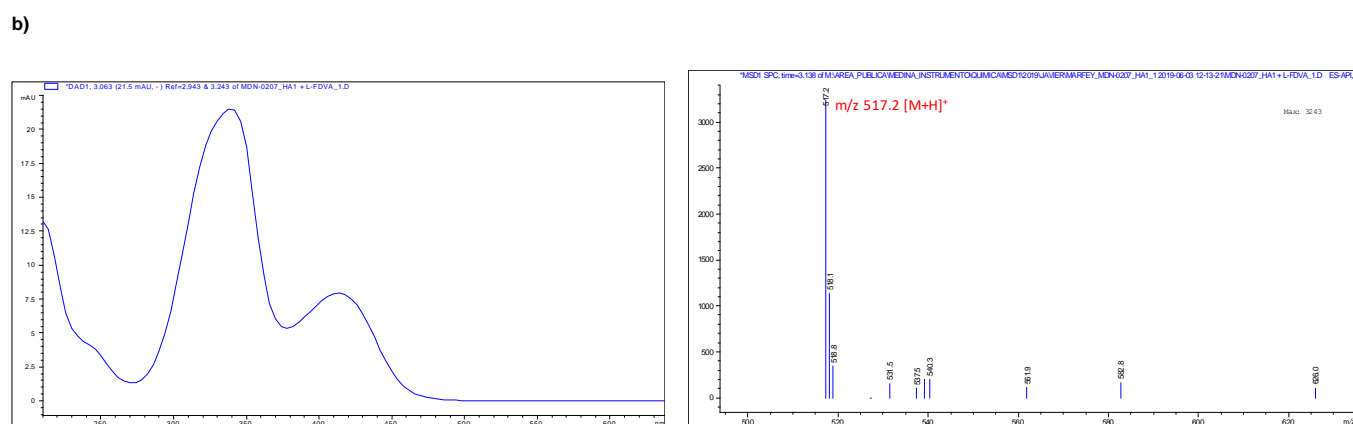
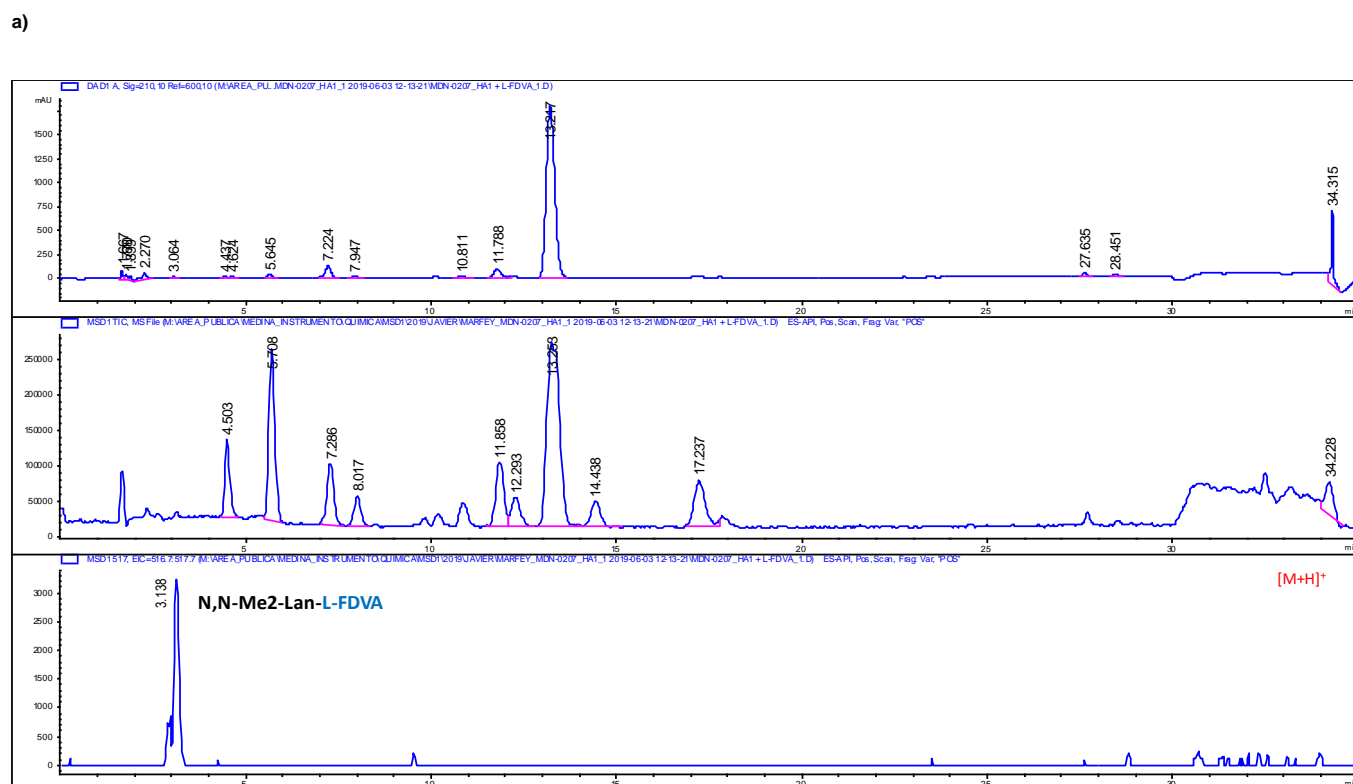
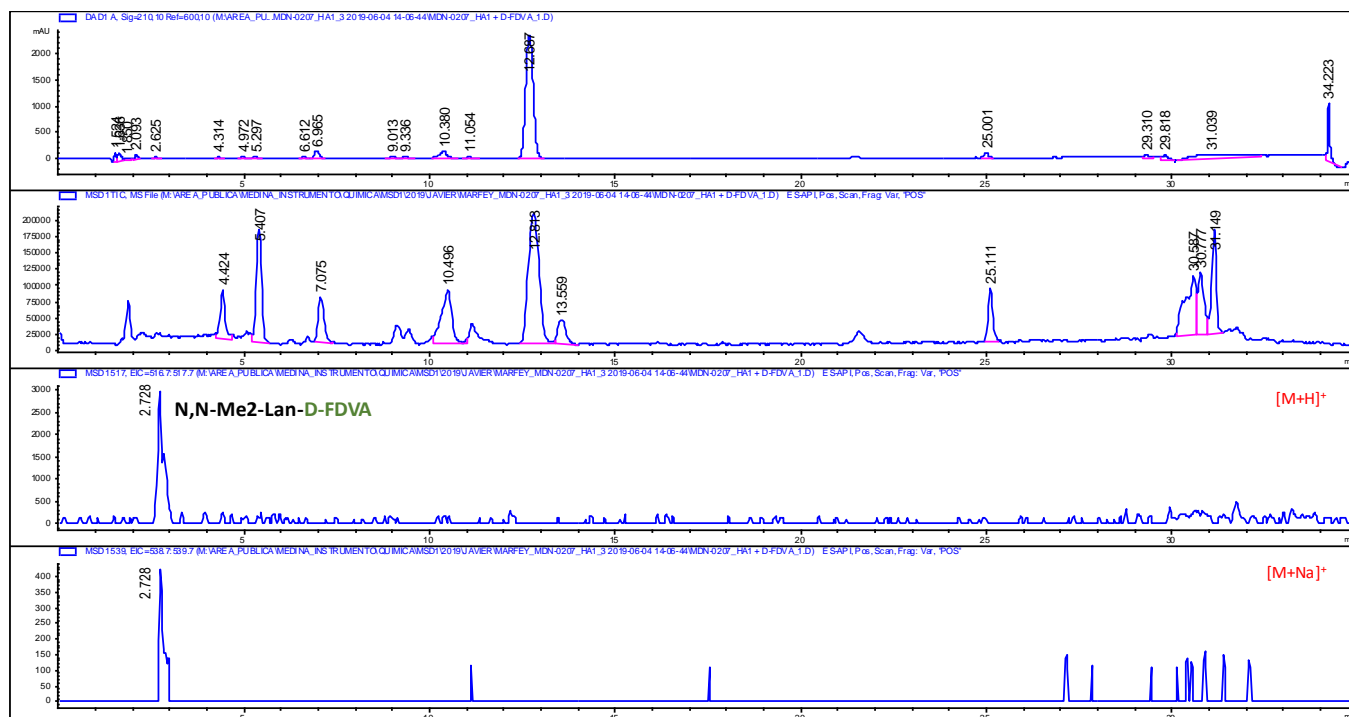


Figure S41. LC-UV chromatogram and EIC of Ala-L-FDVA derivatives (sample M1). L- and D-Ala-L-FDVA derivatives were present in a 5:4 ratio.



**Figure S42.** a) LC-UV chromatogram and EIC of NMe<sub>2</sub>Lan-L-FDVA derivative (**sample M1**). b) UV (left) and MS (right) spectra of NMe<sub>2</sub>Lan-L-FDVA.

a)



b)

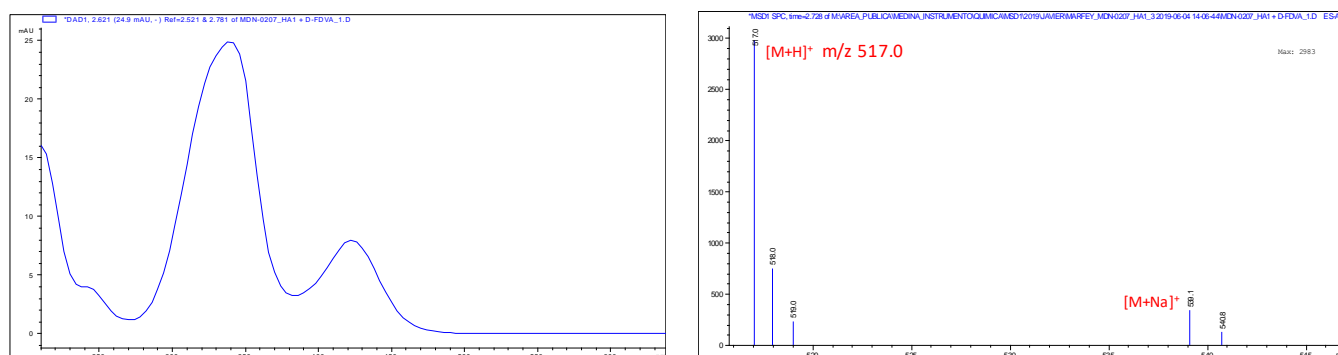
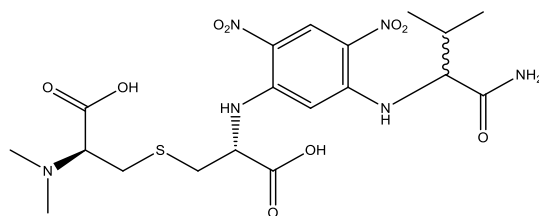


**Figure S43.** a) LC-UV chromatogram and EIC of NMe<sub>2</sub>Lan-D-FDVA derivative (**sample M1**). b) UV (left) and MS (right) spectra of NMe<sub>2</sub>Lan-D-FDVA.



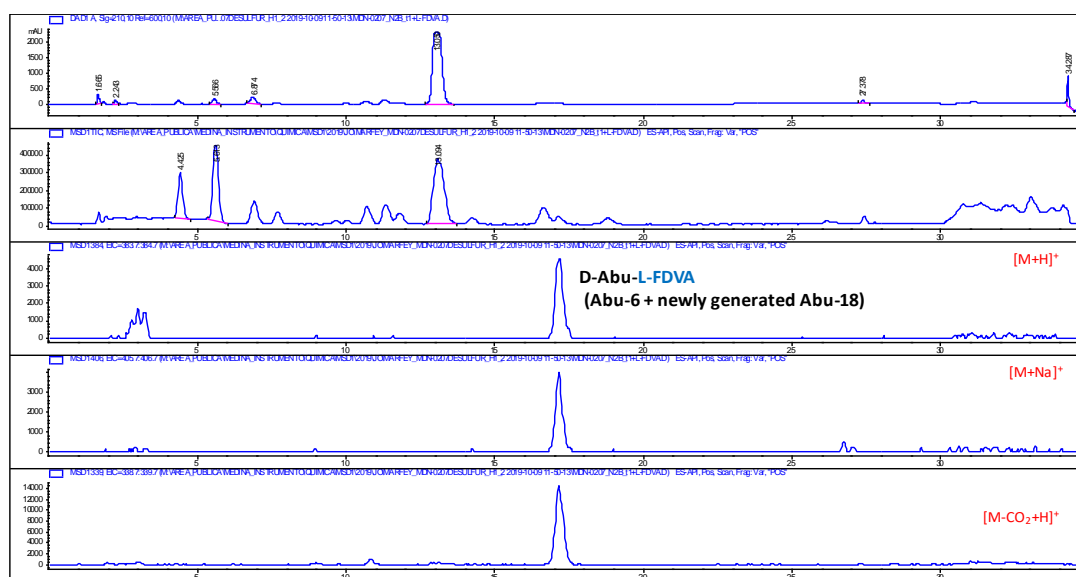
Chemical Formula: C<sub>19</sub>H<sub>28</sub>N<sub>6</sub>O<sub>9</sub>S  
Exact Mass: 516.1638

**Figure S44.** Structure of FDVA-derivatized NMe<sub>2</sub>Lan (DL-NMe<sub>2</sub>Lan stereochemistry is shown in the figure)

## 2.8 Advanced Marfey's analysis after reduction-desulfurization.

The stereochemistry of the AviMeCys unit in cacaoidin (**1**) was established by advanced Marfey's analysis on a sample of previously reduced and desulfurized compound ("sample **a**", see section 2.5 of Supporting Information). As previously shown, the AviMeCys unit had been reduced and desulfurized to originate a second Abu residue (Abu-18) in the structure (Figure S26b). This sample **a** was hydrolyzed (HCl 6N, 110 C, 16 h) and then doubly derivatized with both L- and D-FDVA reagents (**sample M3**). The presence of a unique peak in both cases corresponding to D-Abu-FDVA derivatives revealed that both Abu residues (Abu-6 and Abu-18) had the same absolute configuration (D-Abu) (Figure S45). The increased ratios D-Abu to L-Val or D-Abu to L-Ile (considering the relative peak areas for the L-FDVA derivatives) in sample M3 respect to those found in sample M1 also support this result (Figures S46 and S47). Lastly, the overall anti-stereochemistry of the Michael-type addition<sup>[14–16]</sup>, in this case of decarboxylated Cys-23 onto Dhb-18 in the dehydrated precursor (Figure S48), imposes a (3*S*) absolute configuration and consequently support the canonical *S*-[(*Z*)-aminovinyl-(3*S*)-3-methyl]-*D*-cysteine configuration for AviMeCys in **1**.

a)



b)

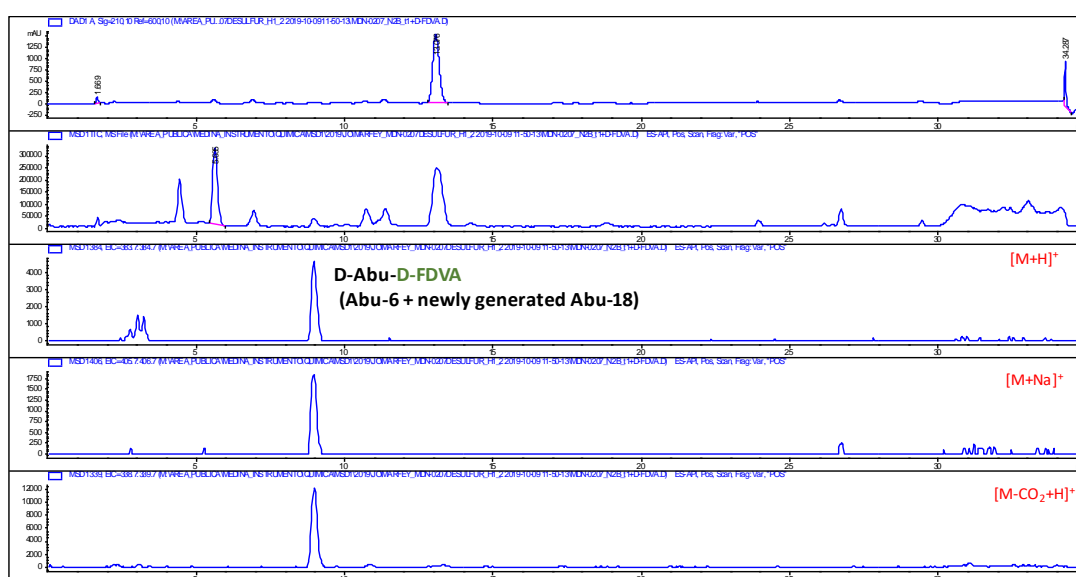


Figure S45. a) LC-UV chromatogram and EIC of Abu-L-FDVA derivative (**sample M3**). b) LC-UV chromatogram and EIC of Abu-D-FDVA derivative (**sample M3**).

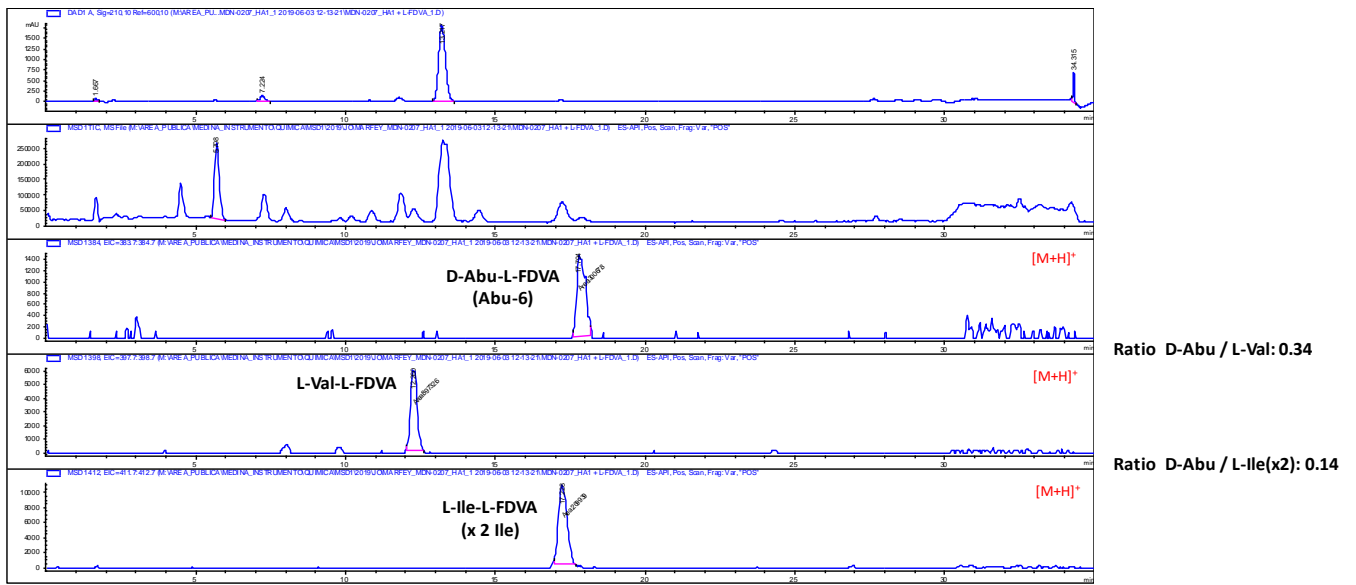


Figure S46. LC-UV chromatogram and EIC of Abu-, Val- and Ile-L-FDVA derivatives (sample M1) showing the ratios D-Abu to L-Val and D-Abu to L-Ile (x2)

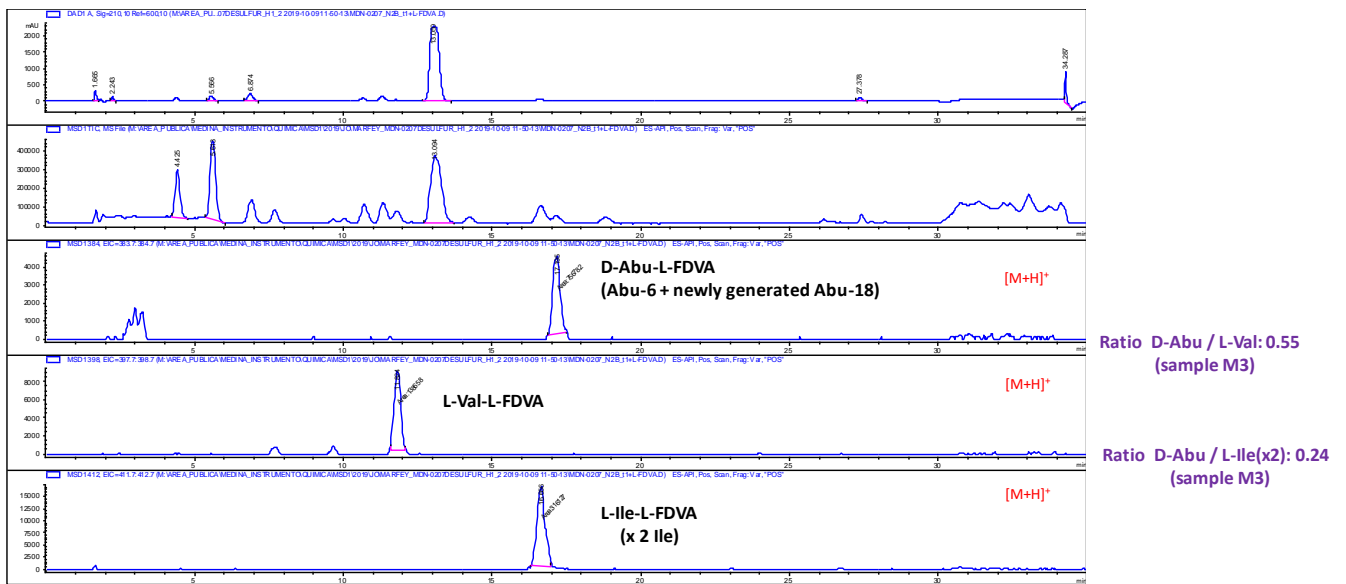
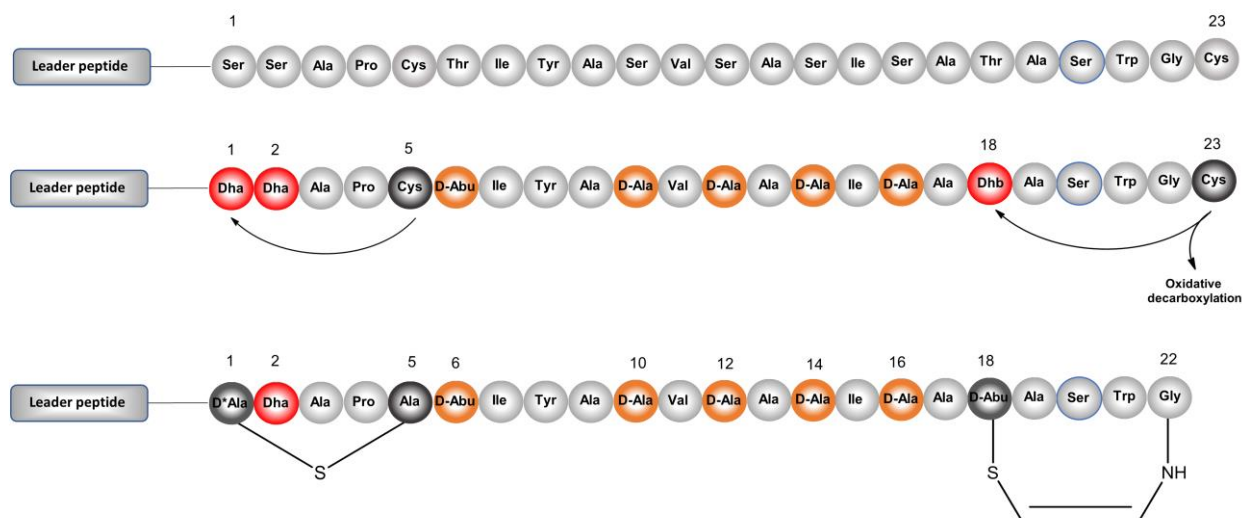


Figure S47. a) LC-UV chromatogram and EIC of Abu-, Val- and Ile-L-FDVA derivatives (sample M3) showing increased ratios D-Abu to L-Val and D-Abu to L-Ile (x2) respect to the Marfey's analysis of the intact peptide (sample M1).



**Figure S48.** Top: Ribosomally-encoded sequence of the cacaoidin precursor peptide (CaoA). Middle: Dehydrated precursor showing the Michael-type additions of Cys-5 onto Dha-1 and (decarboxylated) Cys-23 addition onto Dhb-18 (conversion of L- to D-aa through dehydration and hydrogenation are already indicated as orange balls, although the relative timing of all these modifications may not be as shown). Bottom: Lanthionine (N-terminus) and AviMeCys rings (C-terminus) in core peptide of cacaoidin precursor. Absolute configuration for NMe<sub>2</sub>Ala(S) is tentatively proposed as D (2*R*).

## 2.9 Biosynthetic gene cluster of cacaoidin (cao)

Putative functions for proteins found in the biosynthetic gene cluster were predicted based on BLAST analysis.

Protein	Length (AA)	Closest BLAST homolog (GenBank accession number)	Putative function
Cao1	241	GEB47959.1	Regulator
Cao2	192	WP_159401550.1	Regulator
Cao3	411	GEB47961.1	L-rhamnose biosynthesis
Cao4	349	WP_149563574.1	O-Methyltransferase
Cao5	326	WP_030874945.1	L-rhamnose biosynthesis
Cao6	355	WP_030874943.1	L-rhamnose biosynthesis
Cao7	344	WP_149563571.1	Hypothetical protein
Cao8	383	WP_051846339.1	Glycosyl transferase family 2
Cao9	380	WP_051855537.1	Hypothetical protein
CaoA	53	GEB47968.1	Cacaoidin precursor peptide
Cao11	583	WP_030890022.1	ABC transporter
Cao12	316	WP_030890020.1	Flavin-dependent oxidoreductase
CaoD	267	GEB47971.1	Decarboxylase
Cao14	301	WP_030890015.1	Hypothetical protein
Cao15	865	WP_159787532.1	Hypothetical protein
Cao16	359	WP_086816368.1	Glycosyl transferase family 2
Cao17	48	WP_158102314.1	Hypothetical protein
Cao18	325	WP_030890006.1	ABC transporter
Cao19	286	WP_030874928.1	ABC transporter
Cao20	111	GEB47977.1	Hypothetical protein
Cao21	182	WP_158933426.1	Hypothetical protein
Cao22	205	WP_037865472.1	Hypothetical protein
Cao23	164	GEB47980.1	Hypothetical protein
Cao24	417	WP_030874924.1	Glycosyl transferase family 4
Cao25	320	WP_086816358.1	Hypothetical protein
Cao26	33	WP_030741653.1	Hypothetical protein
Cao27	1016	WP_030874922.1	Hypothetical protein

**Table S2.** Predicted functions of proteins from *cao* cluster based on BLAST analysis.

The amino acid sequences of the conserved domains for the three glycosyltransferases present in the *cao* cluster were analyzed with BLAST and CDD. Cao8 and Cao16 showed homology with family 2 glycosyltransferases (Table S2, figure S49a) and shared a 45.6% identity and 55.9% similarity between them. Cao24 was shown to belong to family 4 glycosyltransferases (Table S2, figure S49b).

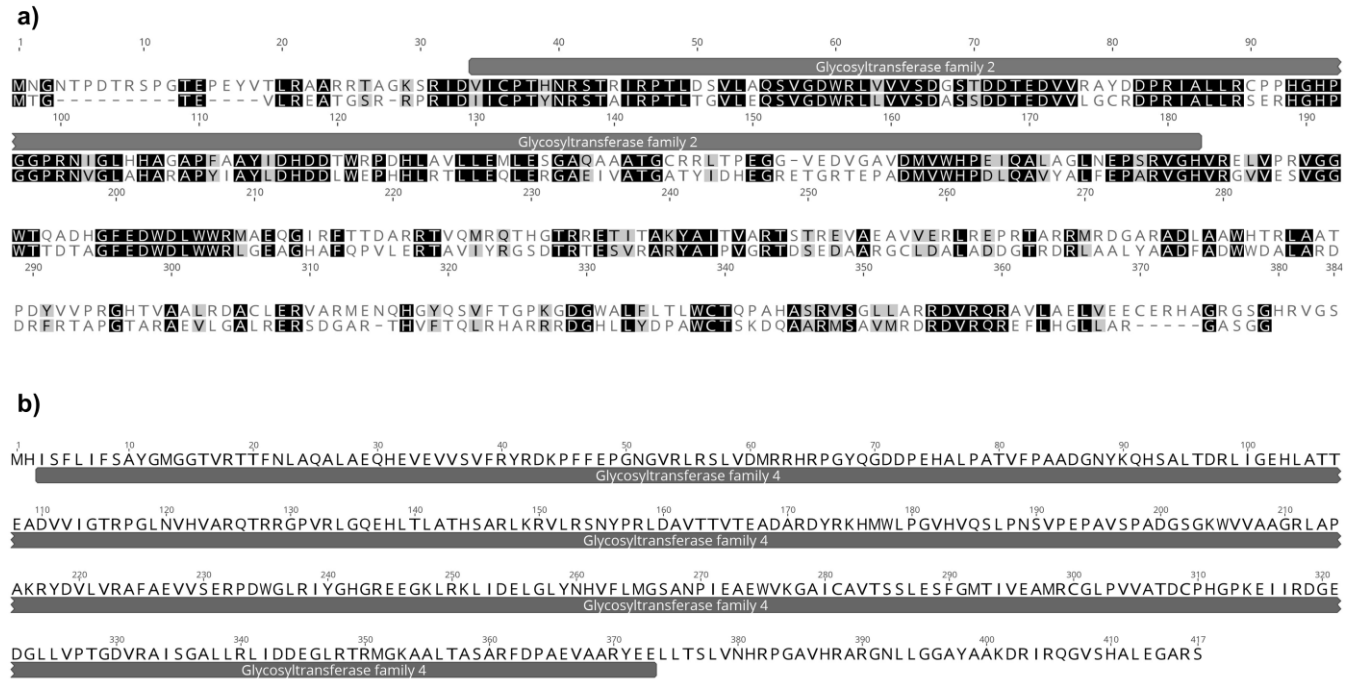


**Figure S49.** Analysis of the glycosyltransferases present in the *cao* BGC. a) Alignment of Cao8 (top) and Cao16 (bottom). Identical residues are shown in black and similar residues in grey. The conserved glycosyltransferase family 2 domain is highlighted. b) Sequence of Cao24, indicating the conserved glycosyltransferase family 4 domain.



## 2.10 Biological assays

Cacaoidin (**1**) was tested for its antibacterial activity against a set of Gram-positive strains (Table 2 in article). Briefly, **1** was serially diluted in DMSO with a dilution factor of 2 to provide 10 concentrations starting at 64 µg/mL for all the antimicrobial assays. The MIC was defined as the lowest concentration of compound that inhibited 90% of the growth of a microorganism after overnight incubation. Genedata Screener software (Genedata, Inc., Basel, Switzerland) was used to process and analyze the data and to calculate the RZ' factor, which predicts the robustness of an assay.<sup>[17]</sup> In all experiments performed in this work the RZ' factor obtained was between 0.87 and 0.98.

### Antibacterial assay against methicillin-resistant *Staphylococcus aureus* (MRSA)

Antibacterial activity against MRSA was tested as described previously.<sup>[18,19]</sup> Thawed stock inoculum suspension from a cryovial of MRSA was streaked onto Brain Heart Infusion (BHI) agar plate and incubated at 37 °C overnight to obtain isolated colonies. Single colonies of this microorganism were inoculated into 10 mL of BHI broth medium in 250 mL Erlenmeyer flask and incubated overnight at 37 °C with shaking at 220 rpm and then diluted in order to obtain an assay inoculum of  $1.1 \times 10^6$  CFU mL<sup>-1</sup>. For the assay, 90 µL/well of the diluted inoculum were mixed with 1.6 µL/well of compound dissolved in DMSO and 8.4 µL/well of BHI medium. Vancomycin was included as internal plate control. Absorbance at OD 612 nm was measured with an EnVision Microplate Reader (PerkinElmer) at T<sub>0</sub> (zero time) and immediately after that, plates were statically incubated at 37 °C for 20 h. After this period, the assay plates were shaken using the DPC Micromix-5 and once more the absorbance at OD 612 nm was measured at T<sub>f</sub> (final time). Percentage of growth inhibition was calculated using the following normalization:

$$\% \text{ Inhibition} = 100 \times \{1 - [(T_f \text{ Sample} - T_0 \text{ Sample}) - (T_f \text{ Blank} - T_0 \text{ Blank})] / [(T_f \text{ Growth} - T_0 \text{ Growth}) - (T_f \text{ Blank} - T_0 \text{ Blank})]\}$$

### Antibacterial assay against *Staphylococcus simulans*, *S. aureus* and *Bacillus subtilis* strains

MIC values against *Staphylococcus simulans* 22, *Bacillus subtilis* 168, *S. aureus* SG511 and *S. aureus* SG511 DapR (Daptomycin-resistant) were determined by the broth microdilution method, using BSA-coated plates as previously described.<sup>[20]</sup>

### Anti-mycobacterium assay

Bioactivity of **1** against *Mycobacterium tuberculosis* was determined using the resazurin microtiter assay (REMA) method<sup>[21]</sup> and following previously described methodologies.<sup>[22]</sup> *M. tuberculosis* H37Ra ATCC 25177 was grown for 15 days in Middlebrook 7H9 broth (Becton Dickinson ref 271310) supplemented with 10 % ADC enrichment (Becton Dickinson ref. 211887) containing albumin, dextrose, and catalase; 0.5% glycerol as a carbon source; and 0.25% Tween 20 to prevent clumping. Suspensions were prepared, and the turbidity was adjusted to 0.5 OD at 600nm. Then, further dilutions were made to reach the final bacterial suspension concentration of  $5 \times 10^5$  CFU mL<sup>-1</sup> for the assay. A volume of 90 µL of the inoculum was added to each well of a 96-well microtiter plate containing 1.6 µL of compound (100% DMSO). Growth controls containing no antibiotic and sterility controls without inoculation were also included, as well as streptomycin that was used as positive control. Plates were incubated for 7 days at 37°C, 5% CO<sub>2</sub> and 95% humidity. After this incubation, 30 µL of 0.02% resazurin and 15 µL of Tween 20 were added to each well, and the plates were incubated four 24 hours and assessed for color development. A change from blue to pink indicated reduction of resazurin and therefore, bacterial growth. The wells were read for color change and the data were quantified by measuring fluorescence (excitation 570 nm, emission 615 nm) using a EnVision Microplate Reader (PerkinElmer). The MIC (minimum inhibitory concentration) was defined as the lowest concentration resulting in a 90% growth inhibition of microorganism. The percentage of resazurin reduction and growth inhibition was calculated using the following normalization:

$$\% \text{ reduction} = 100 \times (\text{fluorescent intensity of test agent} - \text{fluorescent intensity of untreated control}) / (\text{fluorescent intensity of reduced resazurin} - \text{fluorescent intensity of untreated control})$$

$$\% \text{ inhibition} = 100 - \% \text{ reduction.}$$

### Antibacterial assay against *Clostridium difficile*

MIC values against *C. difficile* clinical isolates and control strains (*C. difficile* RyC 11945271 (toxigenic); *C. difficile* RyC 11872343 (toxigenic) and *C. difficile* ATCC 750057) were determined by the broth microdilution method using Wilkins Chalgren Anaerobe Broth (Oxoid), as previously reported<sup>[23]</sup>. Final inocula in the 96-well microtiter plates were ca. 10<sup>6</sup> CFU mL<sup>-1</sup>.

### *Bacillus subtilis* β-galactosidase bioreporter assay

*B. subtilis* bioreporter strains with selected promoter-*lacZ* gene fusions were used to identify interference with major biosynthesis pathways (DNA (*pyorB*), RNA (*pyvgS*), protein (*pyhel*), cell wall (*pypuA*)).<sup>[24,25]</sup> Induction of a specific stress response results in expression of β-galactosidase, cleaving the chromogenic substrate 5-bromo-4-chloro-3-indolyl-β-D-galactopyranoside (X-Gal) indicated by a blue halo around the inhibition zone. The reporter strains were grown in Mueller-Hinton (MH) broth supplemented with chloramphenicol (5 µg mL<sup>-1</sup>). After reaching OD<sub>600</sub> = 0.5 the cells were mixed with liquid MH agar containing chloramphenicol (5 µg mL<sup>-1</sup>) and X-Gal (75-250 µg mL<sup>-1</sup>) yielding a final cell inoculum of 1x10<sup>7</sup> CFU mL<sup>-1</sup> and poured into an OmniTray™ plate. Six µl of test compounds (8 µg cacaoidin, 6 µg vancomycin, 0.3 µg ciprofloxacin, 3 µg clindamycin or 6 µg rifampicin) were spotted on the solidified agar plates, incubated for 16 h at 30 °C and visually evaluated for appearance of a blue stain (Figure S51).

**Induction of *liaI-lux* cell wall stress response.**

*B. subtilis liaI-lux*<sup>[26]</sup> was grown in Mueller–Hinton broth with chloramphenicol ( $5 \mu\text{g mL}^{-1}$ ) to  $\text{OD}_{600} = 0.5$ . The antibiotics cacaoidin ( $8 \mu\text{g mL}^{-1}$ ), vancomycin ( $8 \mu\text{g mL}^{-1}$ ) and clindamycin ( $2 \mu\text{g mL}^{-1}$ ) were diluted in a Greiner LUMITRAC™ 96-well-microtiter plate prior to addition of the reporter strain. Induction of cell wall stress indicated by an increase in luminescence was measured using the Tecan Spark 10 M microplate reader for 400 min at  $30^\circ\text{C}$  (Figures S1 and S50)

**Antagonization of *liaI-lux* cell wall stress response.**

Antagonization of the *liaI-lux* luminescence response was used as a method to investigate the direct interaction of an inducing antibiotic with putative antagonists as previously reported.<sup>[27]</sup> The central peptidoglycan precursor lipid II was added in a molar ratio of 5:1 with respect to cacaoidin ( $4 \mu\text{g mL}^{-1}$ ) or vancomycin ( $4 \mu\text{g mL}^{-1}$ ) and luminescence was measured as described above (Figure S52).

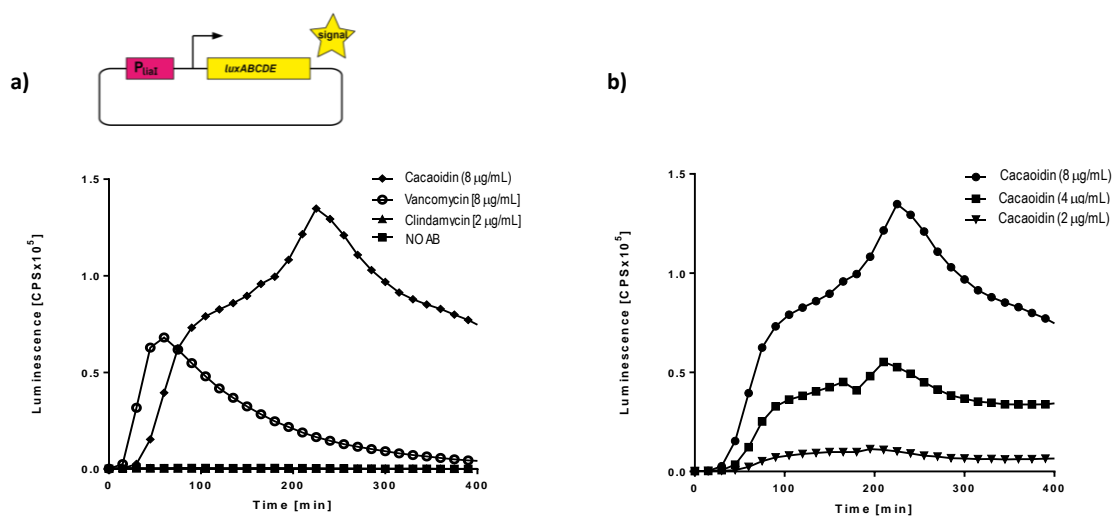


**Figure S50.** a) Induction of the LiaRS bioreporter by pure cacaoidin compared to vancomycin, clindamycin and a negative control (no antibiotic added). b) Dose-dependency of the LiaRS response for pure cacaoidin.

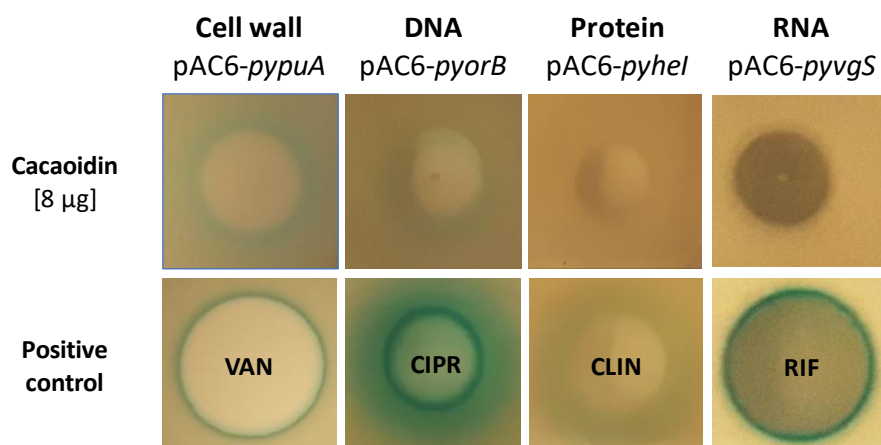


**Figure S51.** Tests of cacaoidin (**1**) against a set of *Bacillus subtilis*  $\beta$ -galactosidase bioreporters compared to positive controls (vancomycin, ciprofloxacin, clindamycin and rifampicin). Results identify cell wall biosynthesis as the specific target pathway.

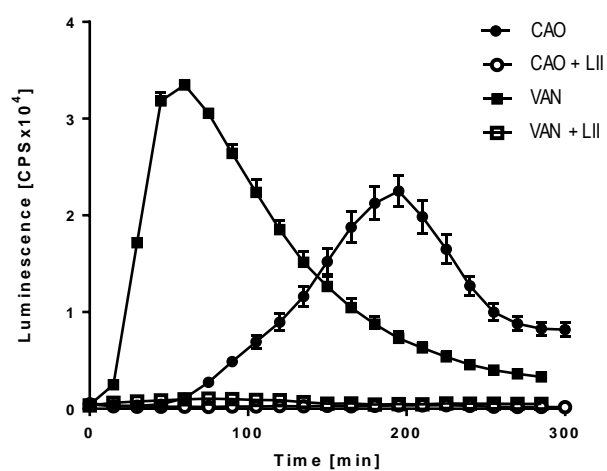


**Figure S52.** Antagonization of the LiaRS stress response by addition of purified Lipid II (LII) to cacaoidin (CAO) or vancomycin (VAN)

## 2.11 NMR spectra of cacaoidin (1)

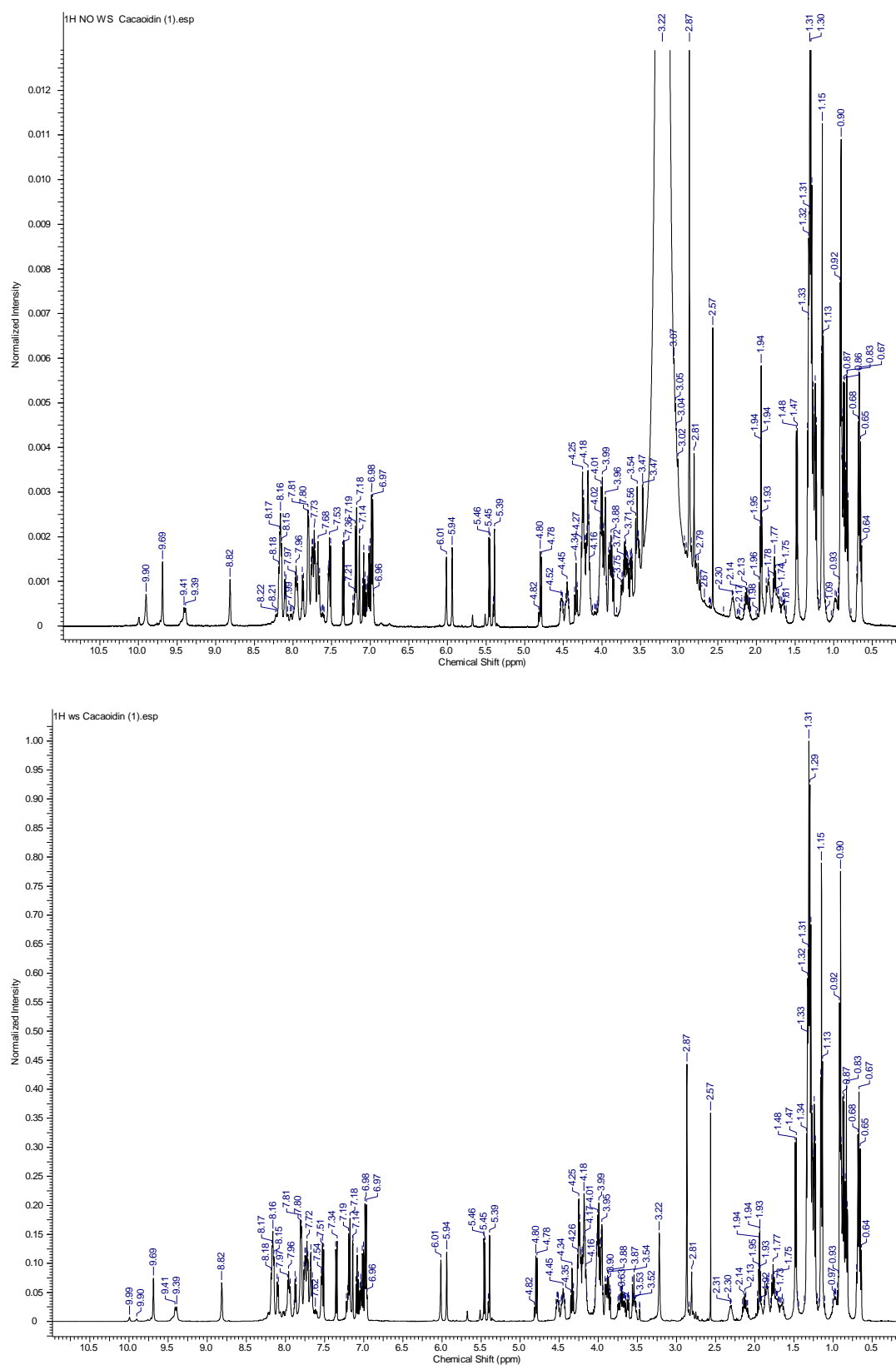


Figure S53. <sup>1</sup>H-NMR spectrum (CD<sub>3</sub>CN: H<sub>2</sub>O; 9:1) of cacaoidin (1) with (bottom) or without (top) water suppression.

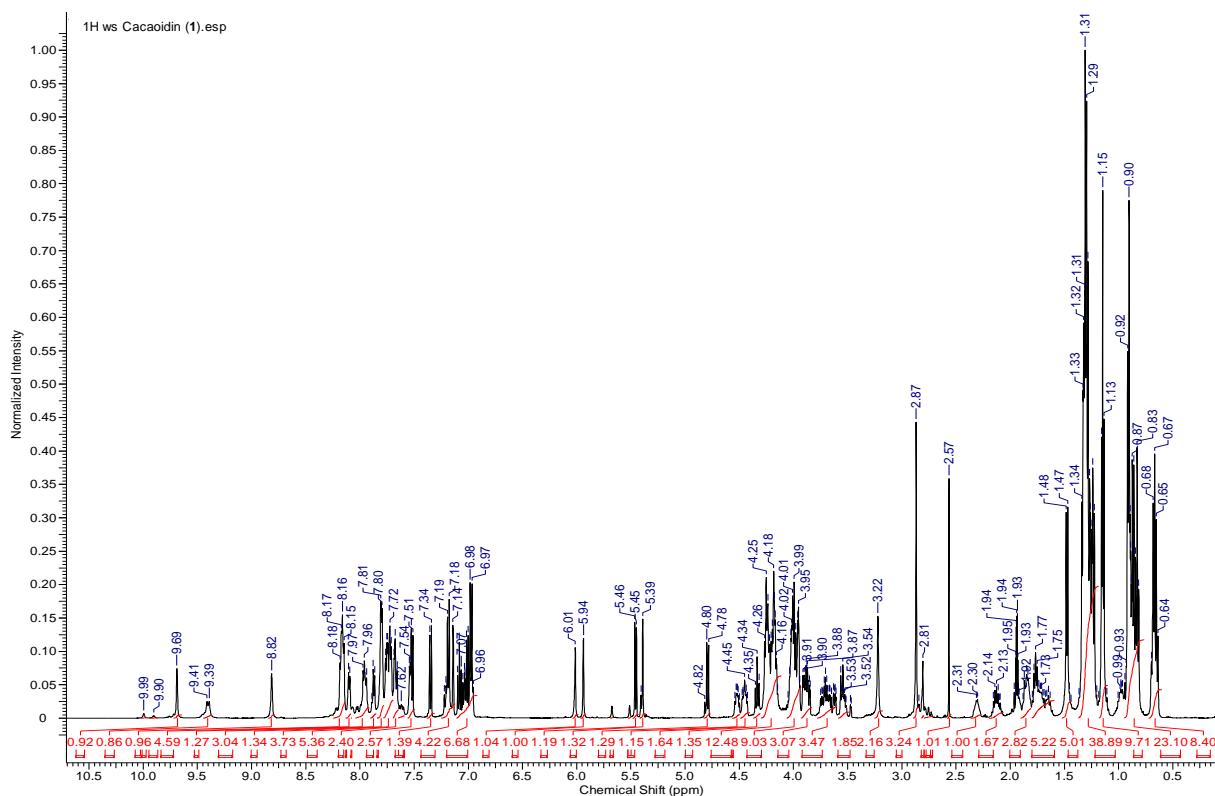


Figure S54.  $^1\text{H}$ -NMR spectrum ( $\text{CD}_3\text{CN}:\text{H}_2\text{O}:\text{9:1}$ ) of cacaoidin (**1**) with water suppression, showing integral values.

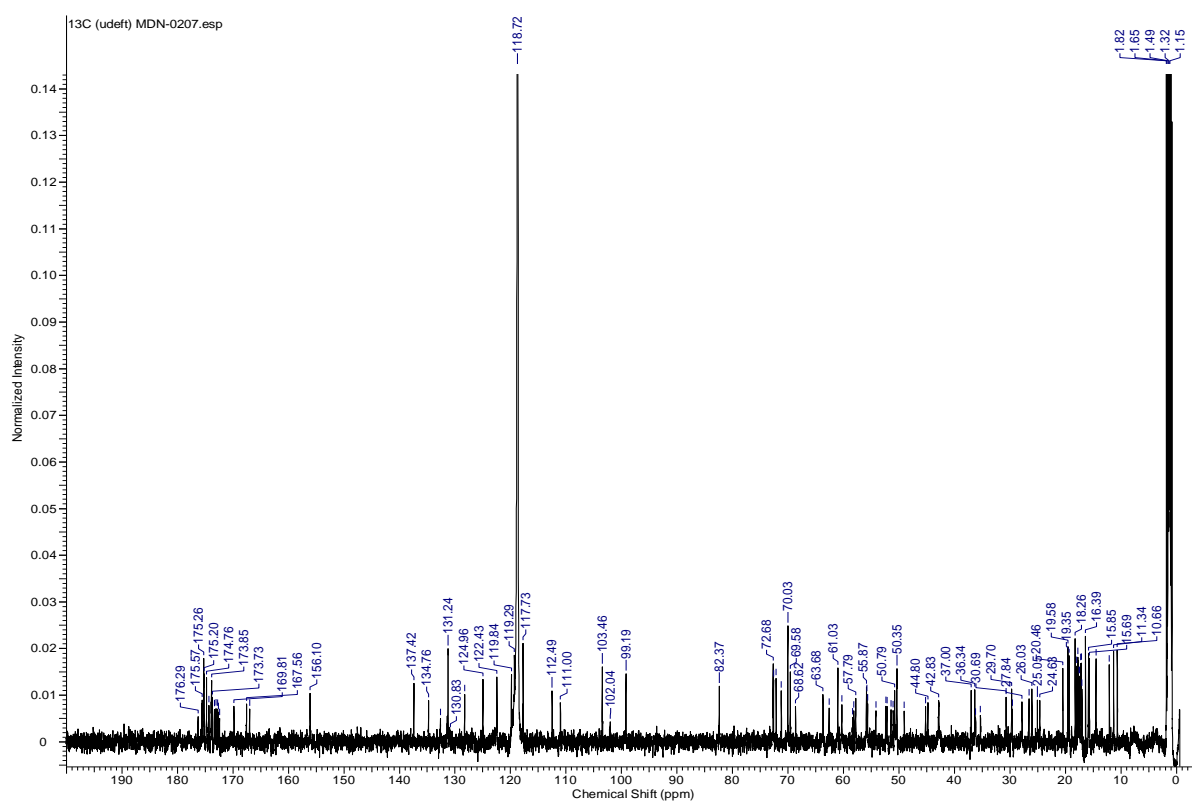


Figure S55.  $^{13}\text{C}$ -NMR spectrum ( $\text{CD}_3\text{CN}:\text{H}_2\text{O}:\text{9:1}$ ) of cacaoidin (**1**).

COSY ws Cacaoidin (1).esp

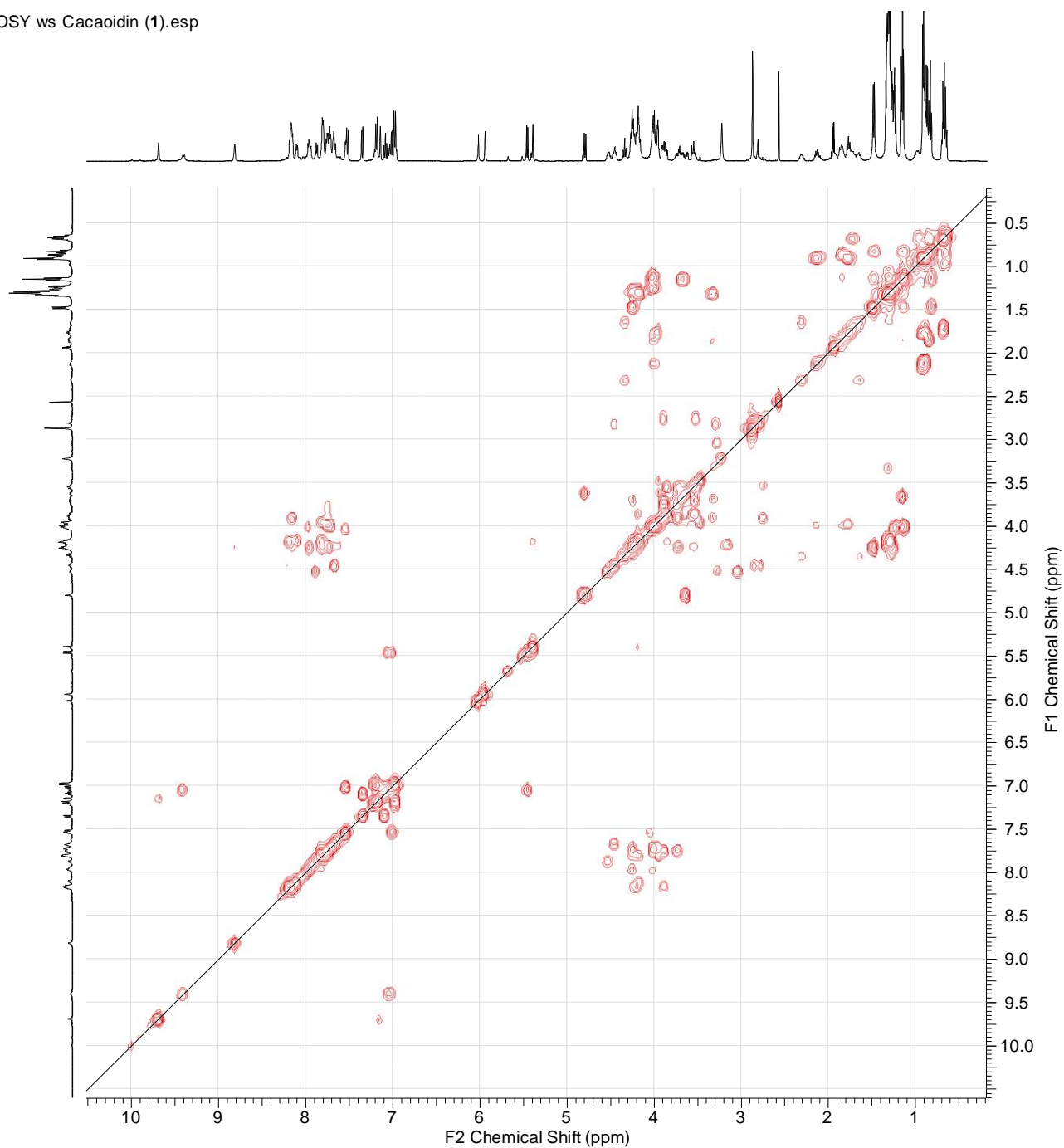
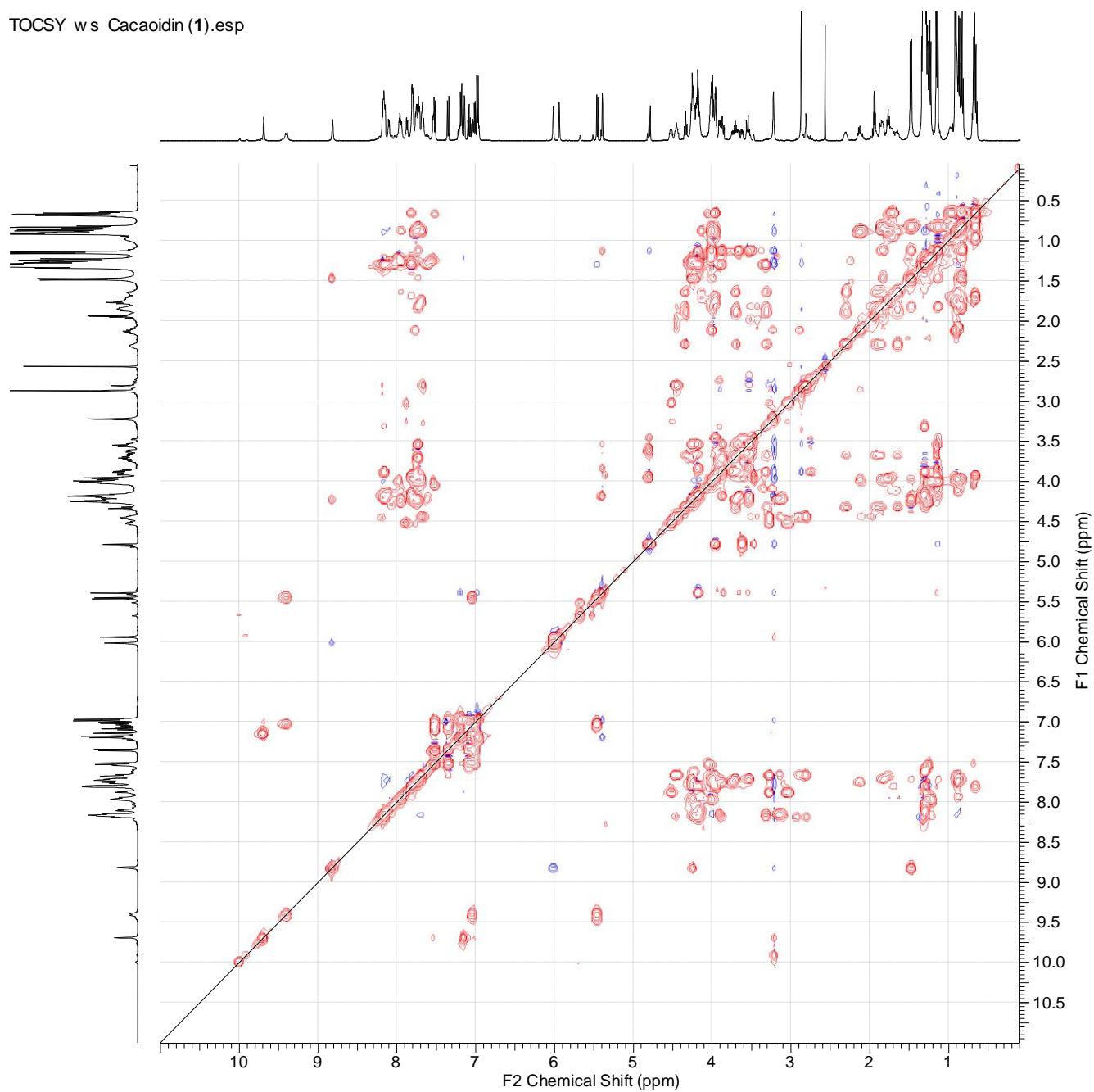


Figure S56. COSY spectrum ( $\text{CD}_3\text{CN}:\text{H}_2\text{O}; 9:1$ ) of cacaoidin (1).

TOCSY w s Cacaoidin (1).esp



**Figure S57.** TOCSY spectrum (CD<sub>3</sub>CN: H<sub>2</sub>O; 9:1) of cacaoidin (1).

JRES w s Cacaoidin (1).esp

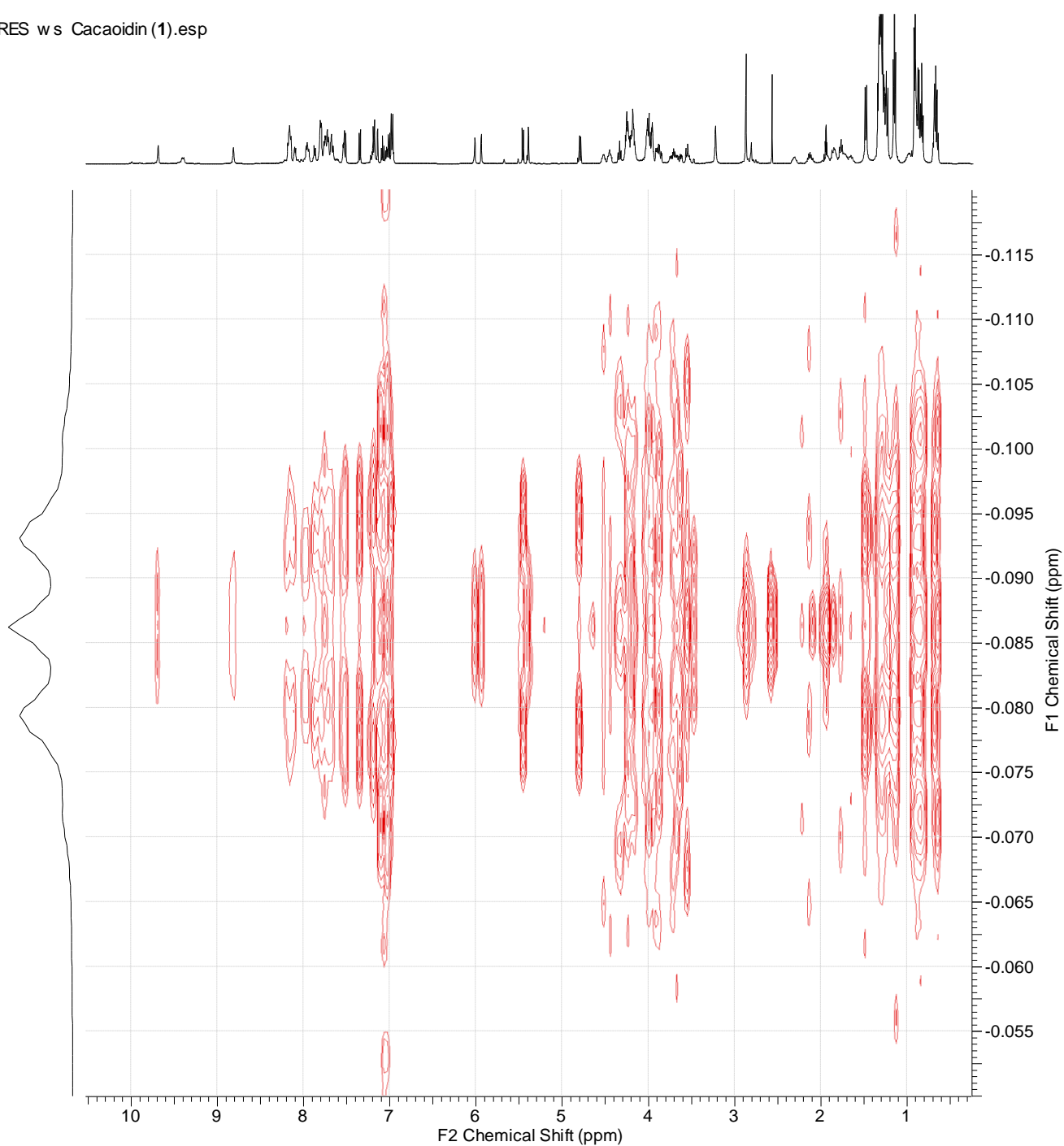


**Figure S58.** J-resolved (JRES) spectrum ( $\text{CD}_3\text{CN}:\text{H}_2\text{O}; 9:1$ ) of cacaoidin (1).



HSQC Cacaoidin (1).esp

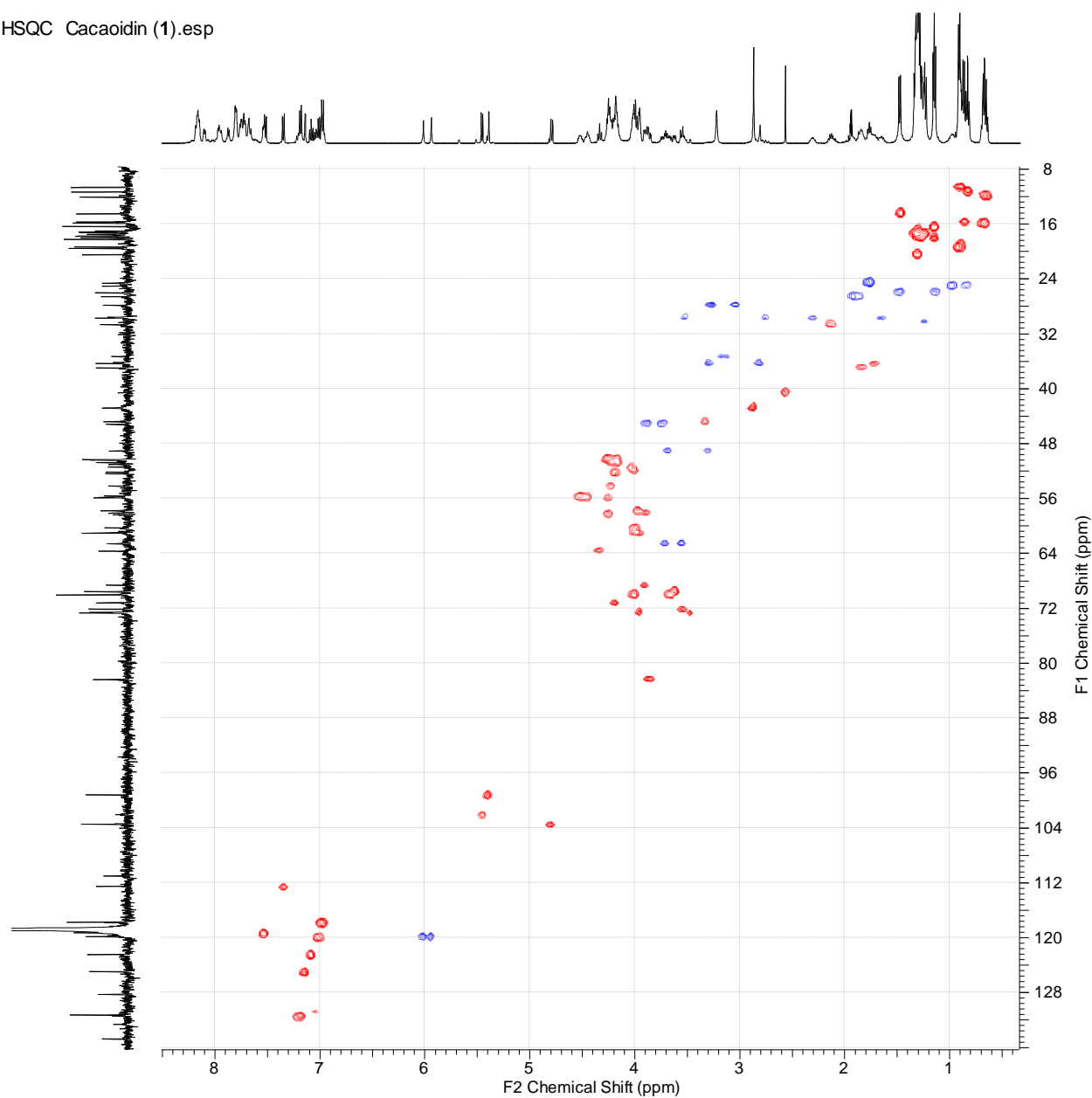


Figure S59. HSQC spectrum ( $\text{CD}_3\text{CN}:\text{H}_2\text{O}; 9:1$ ) of cacaoidin (1).

HSQC Cacaoidin (1).esp

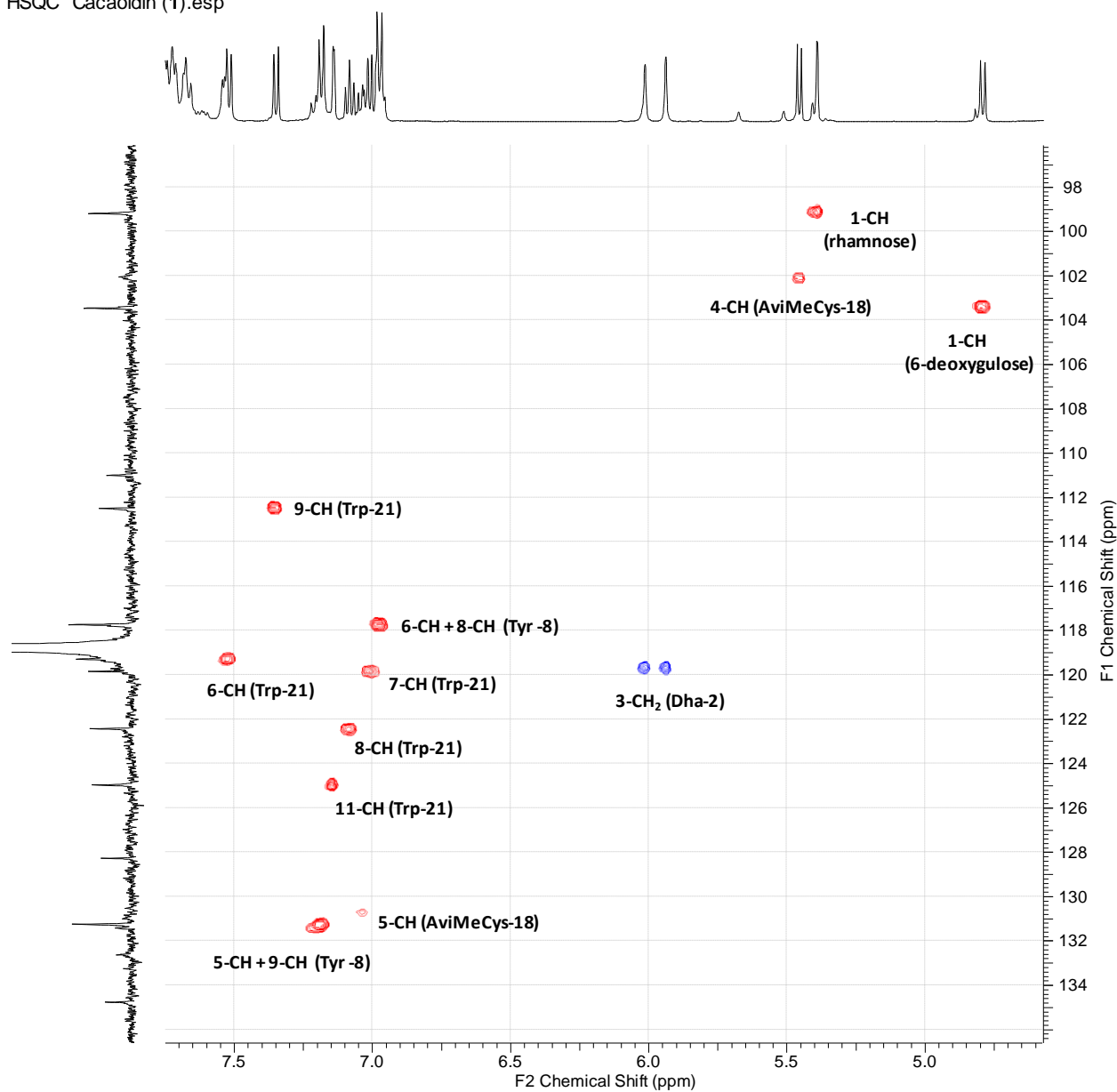
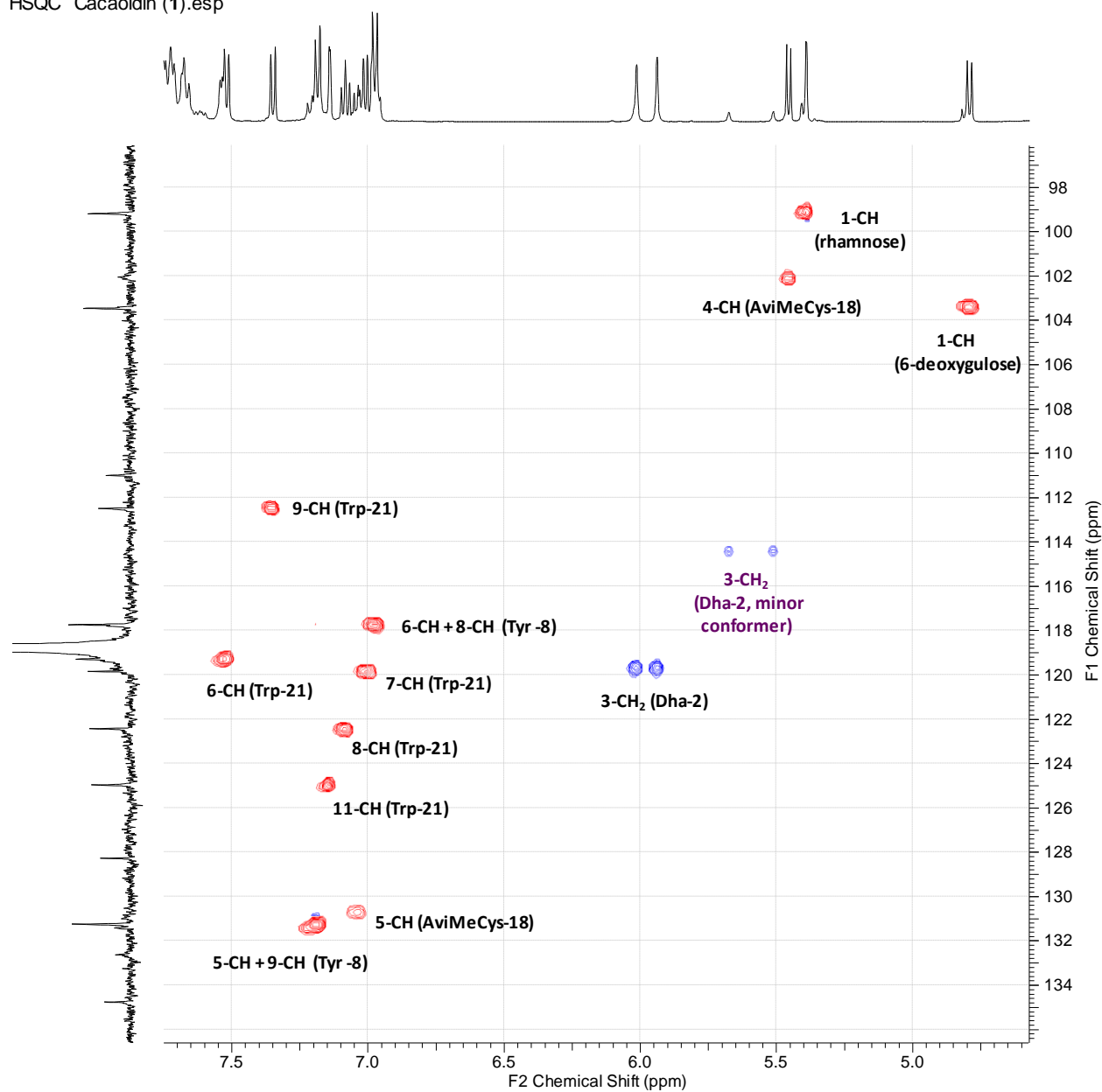


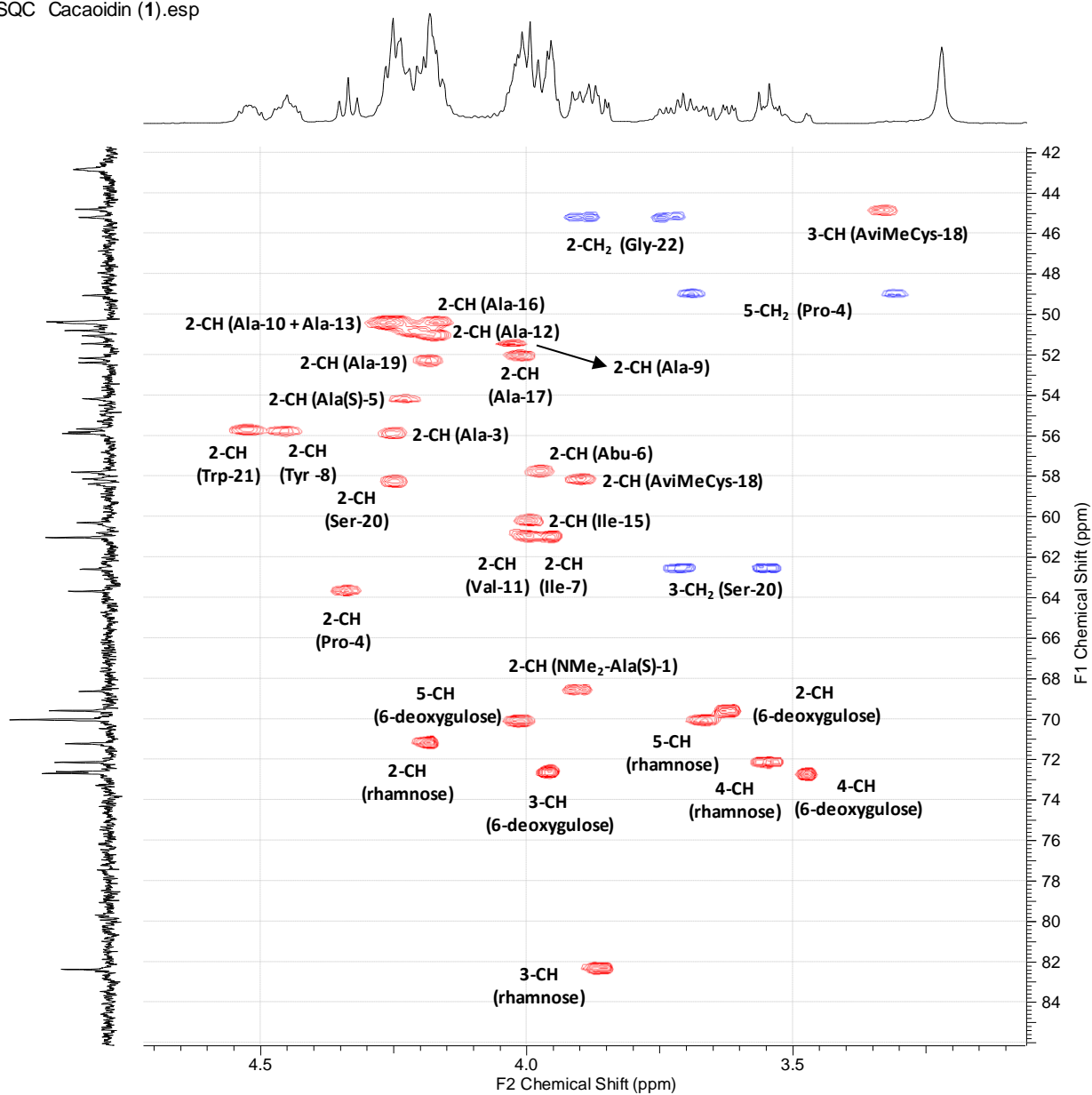
Figure S60. Expansion 1 of the HSQC spectrum ( $\text{CD}_3\text{CN}:\text{H}_2\text{O}; 9:1$ ) of cacaoidin (1).

HSQC Cacaoidin (1).esp



**Figure S61.** Expansion 1 of the HSQC spectrum (CD<sub>3</sub>CN: H<sub>2</sub>O; 9:1) of cacaoidin (1). Signals corresponding to the minor conformer are indicated in purple

HSQC Cacaoidin (1).esp

**Figure S62.** Expansion2 of the HSQC spectrum ( $\text{CD}_3\text{CN}:\text{H}_2\text{O}; 9:1$ ) of cacaoidin (1).

HSQC Cacaoidin (1).esp

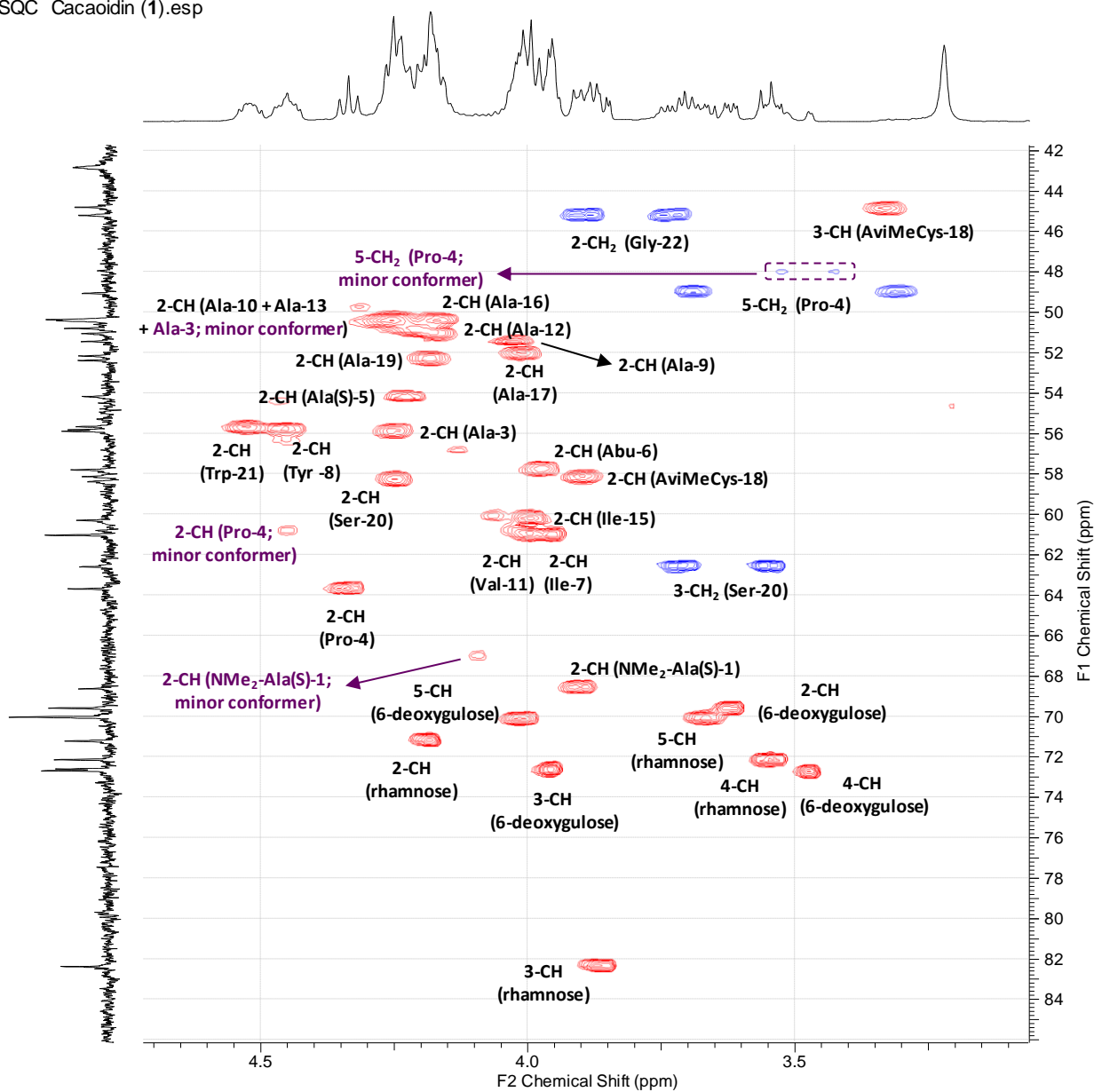


**Figure S63.** Expansion 2 of the HSQC spectrum ( $\text{CD}_3\text{CN}:\text{H}_2\text{O}; 9:1$ ) of cacaoidin (1). Signals corresponding to the minor conformer are indicated or framed in purple

HSQC Cacaoidin (1).esp

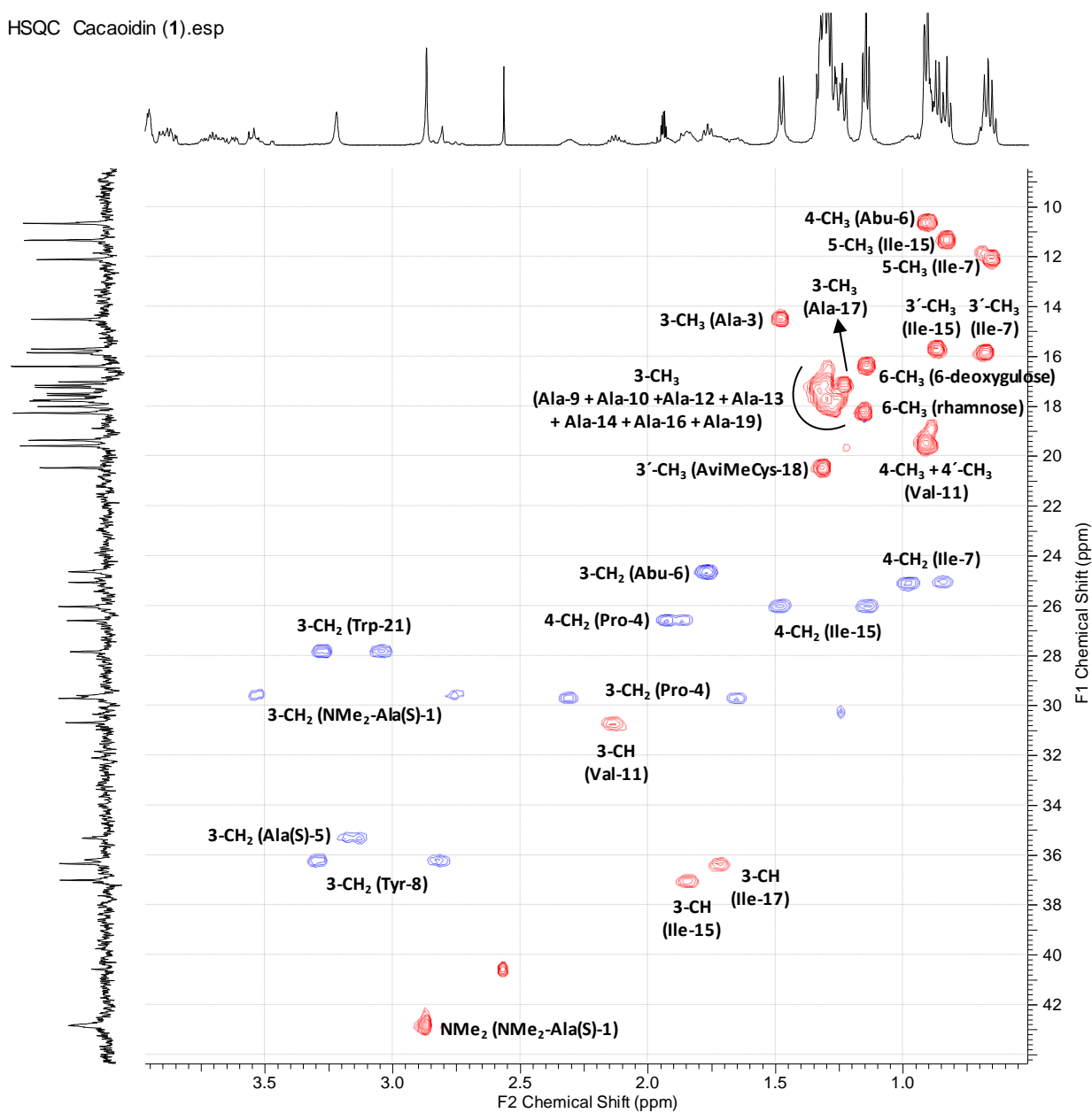
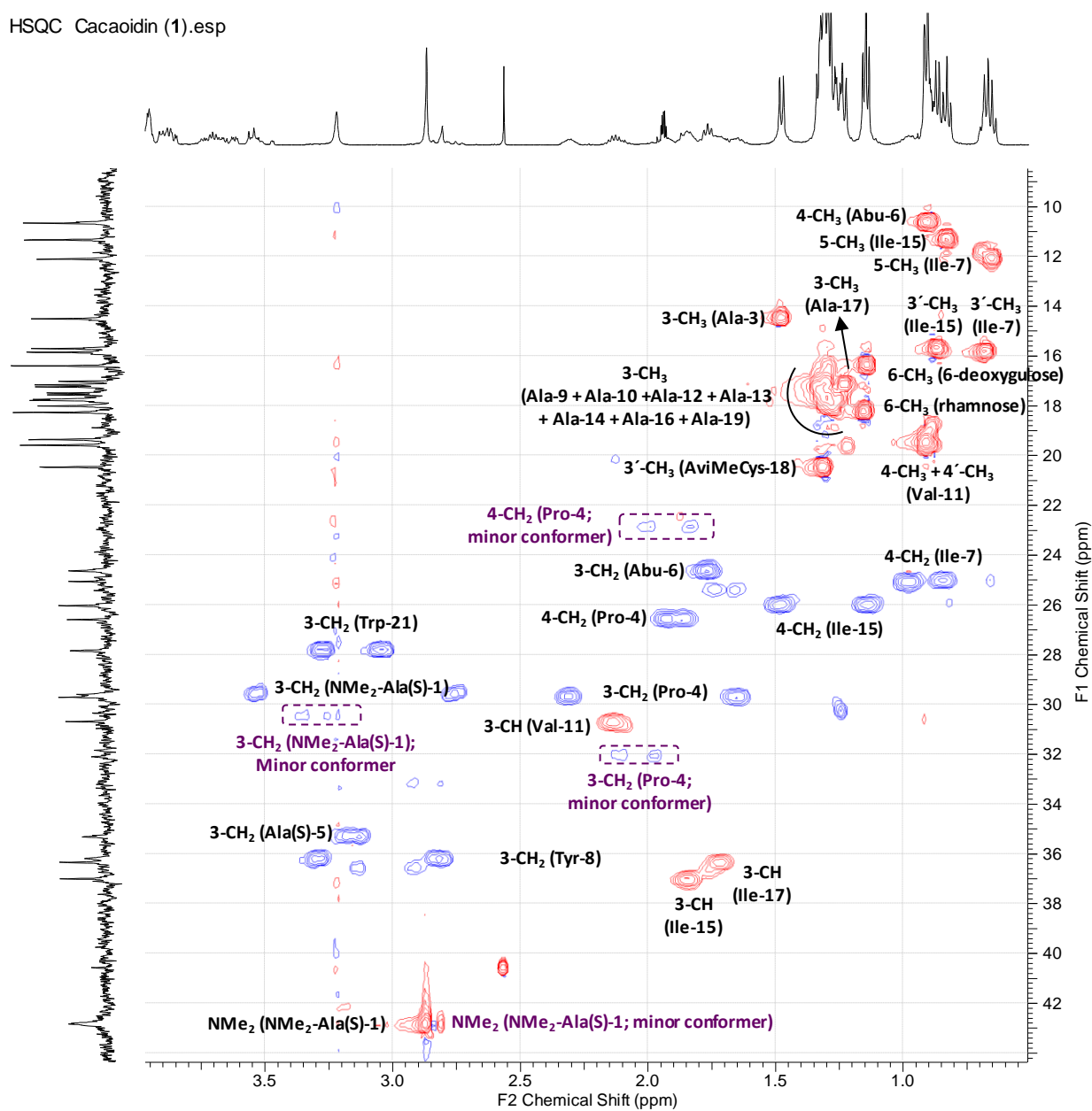


Figure S64. Expansion 3 of the HSQC spectrum (CD<sub>3</sub>CN: H<sub>2</sub>O; 9:1) of cacaoidin (1).

HSQC Cacaoidin (1).esp



**Figure S65.** Expansion 3 of the HSQC spectrum ( $\text{CD}_3\text{CN}$ :  $\text{H}_2\text{O}$ ; 9:1) of cacaoidin (1). Signals corresponding to the minor conformer are indicated or framed in purple

HSQC-TOCSY Cacaoidin (1).esp

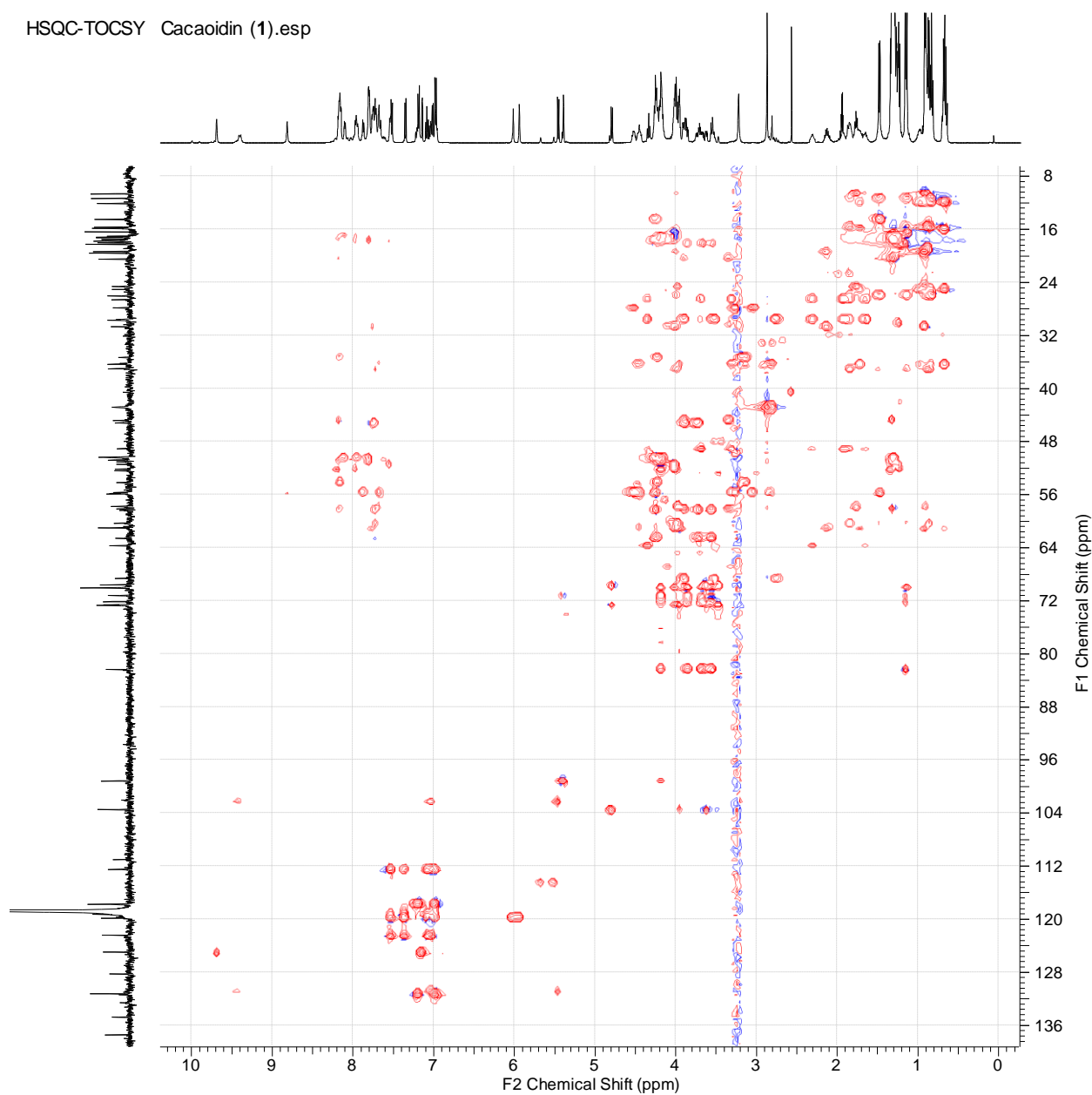


Figure S66. HSQC-TOCSY spectrum ( $\text{CD}_3\text{CN}:\text{H}_2\text{O}$ ; 9:1) of cacaoidin (1).



HMBC ws Cacaoidin (1).esp

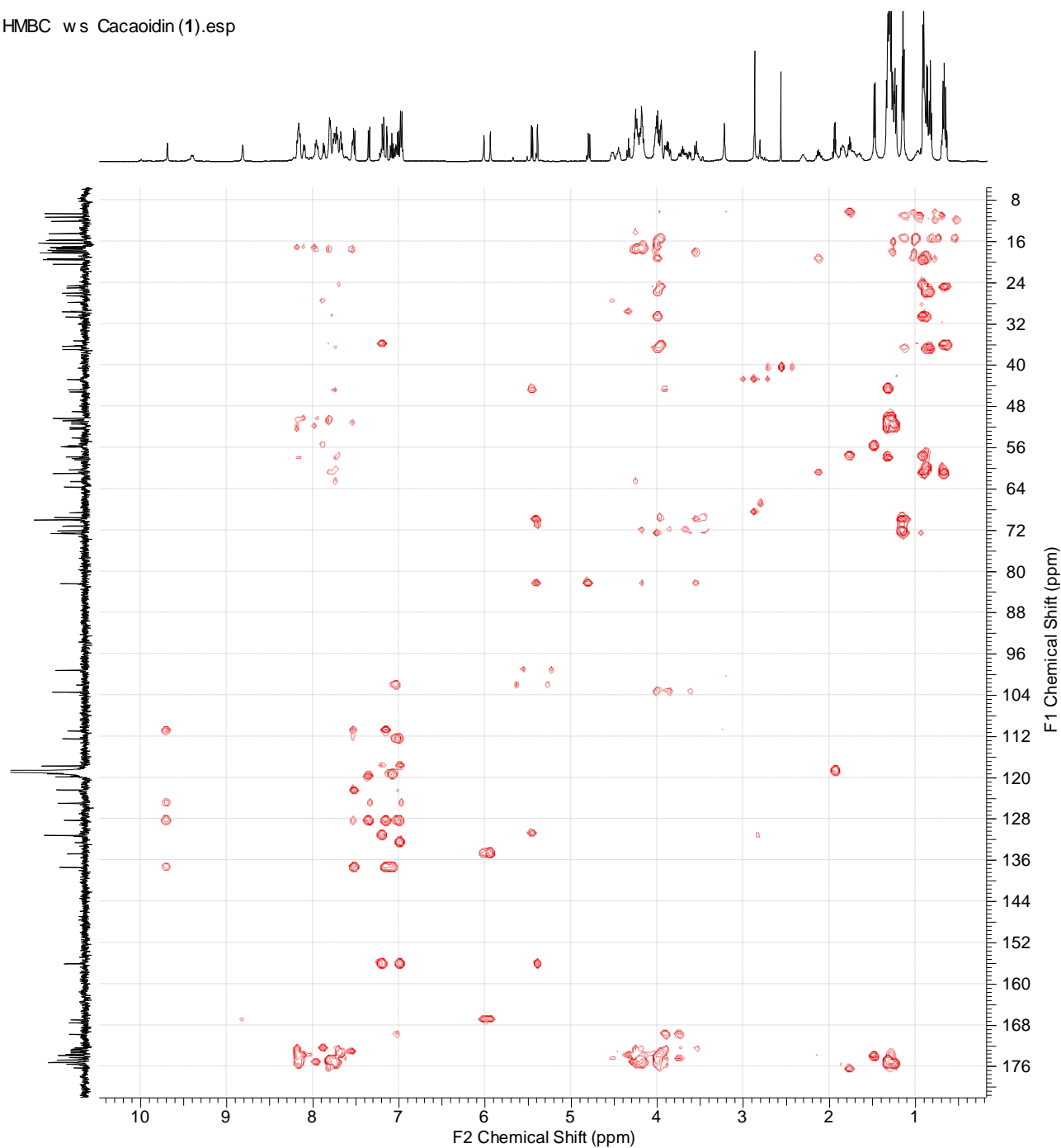


Figure S67. HMBC spectrum (CD<sub>3</sub>CN: H<sub>2</sub>O; 9:1) of cacaoidin (1).

HMBC Cacaoidin .esp

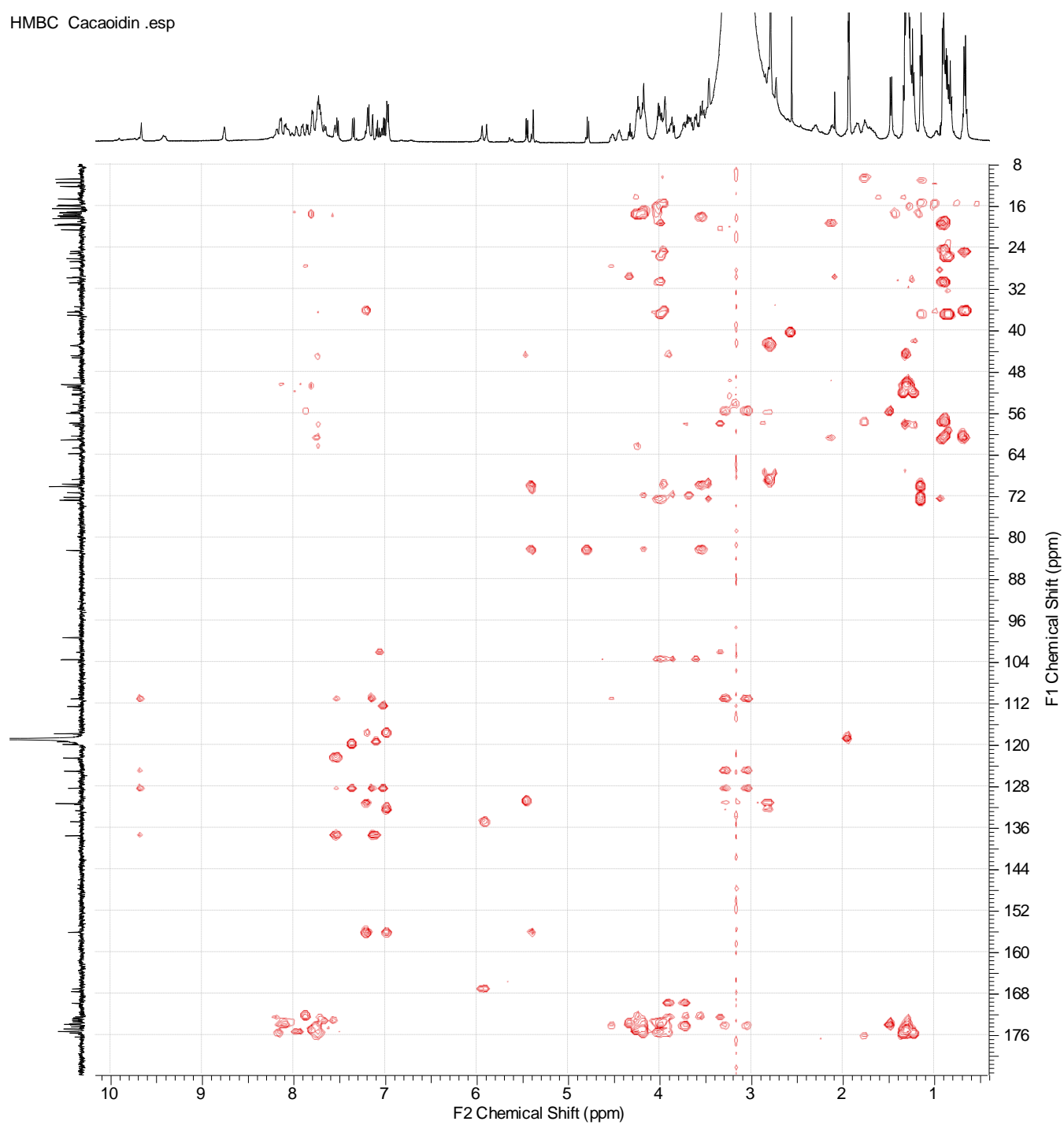
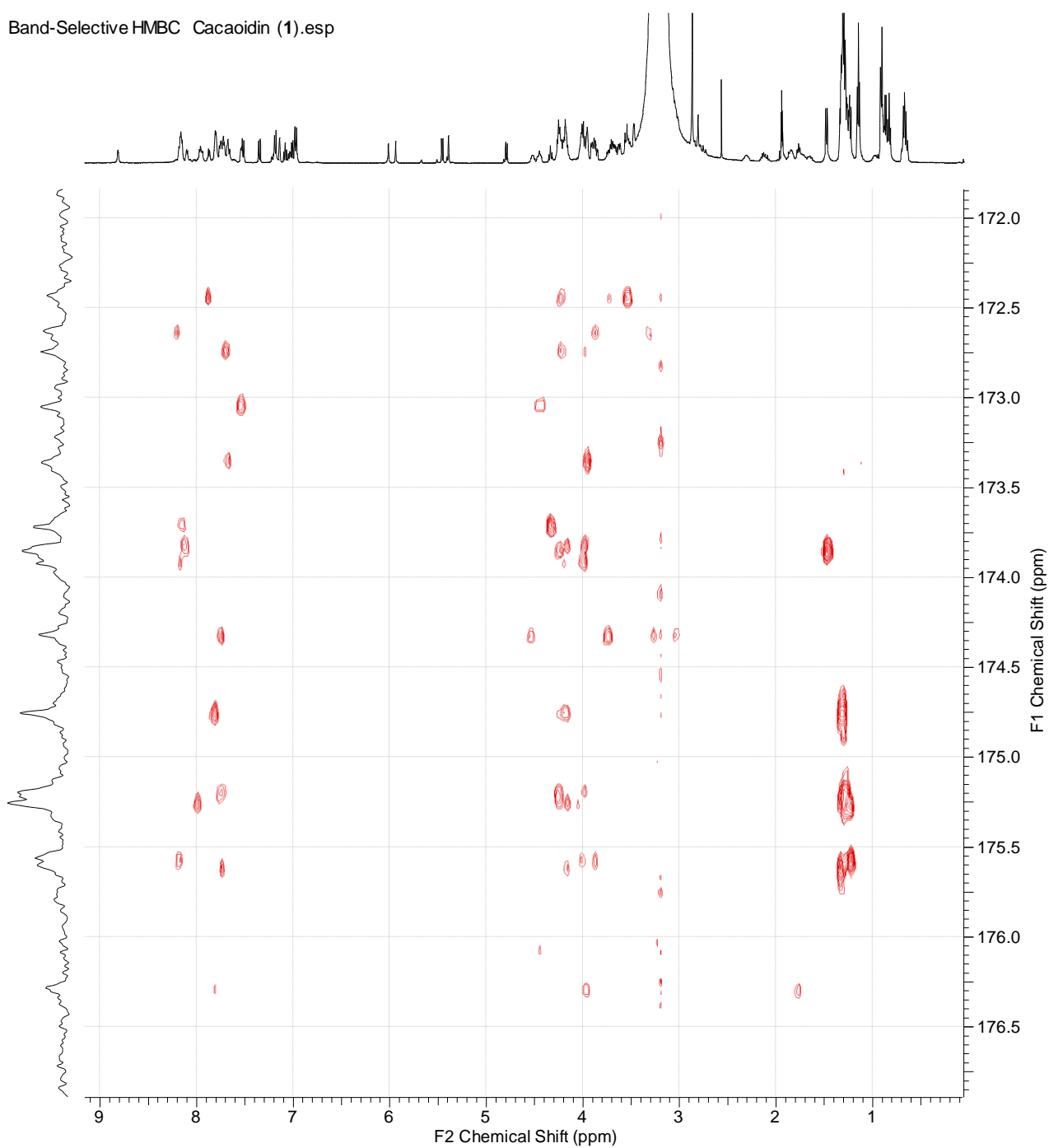


Figure S68. HMBC (no water suppression) spectrum ( $\text{CD}_3\text{CN}:\text{H}_2\text{O}; 9:1$ ) of cacaoidin (1).

Band-Selective HMBC Cacaoidin (1).esp



**Figure S69.** Band-Selective HMBC (no water suppression) spectrum ( $\text{CD}_3\text{CN}:\text{H}_2\text{O}; 9:1$ ) of cacaoidin (1).

NOESY ws Cacaoidin (1).esp

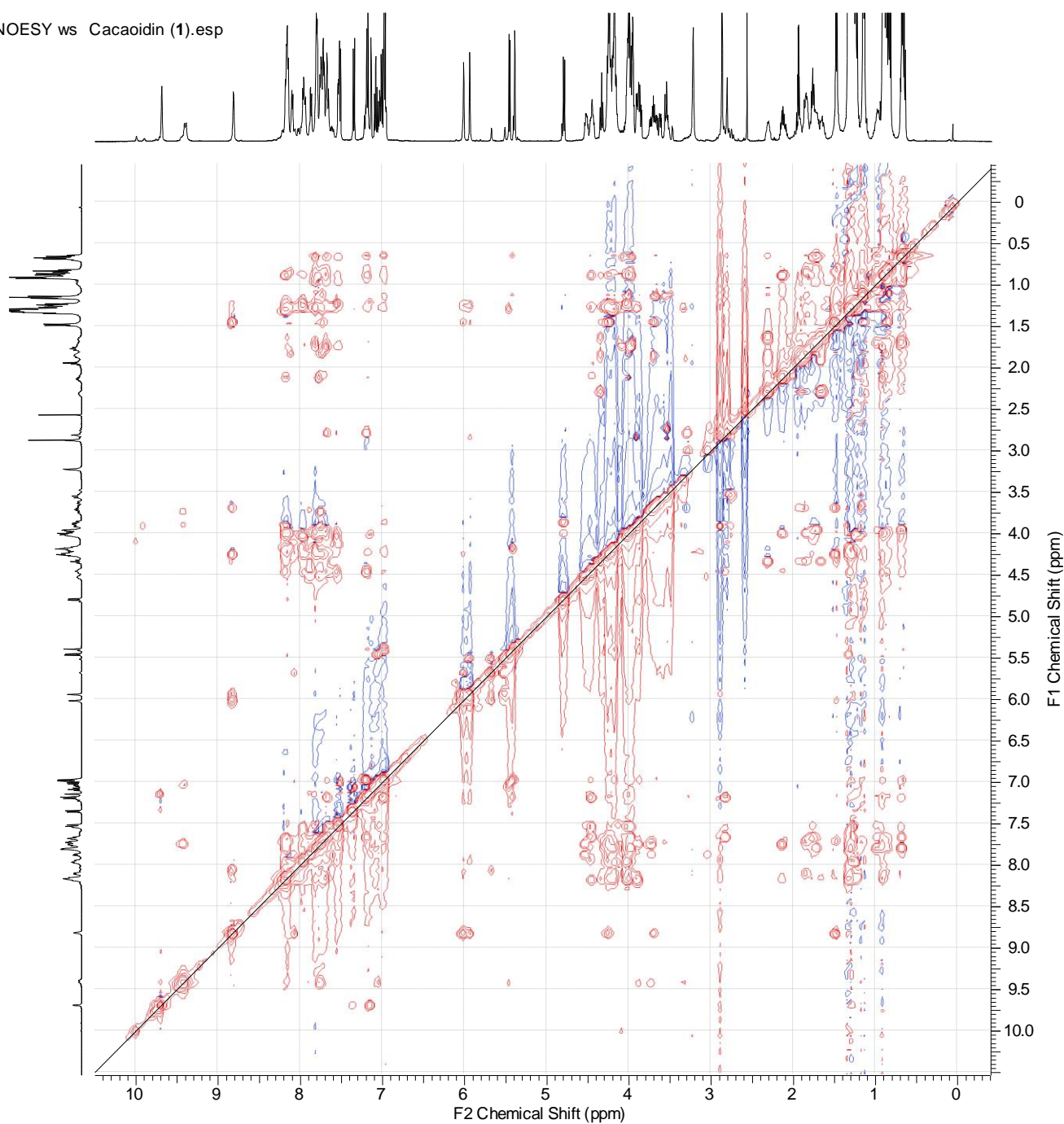


**Figure S70.** NOESY spectrum (CD<sub>3</sub>CN: H<sub>2</sub>O; 9:1) of cacaoidin (1).

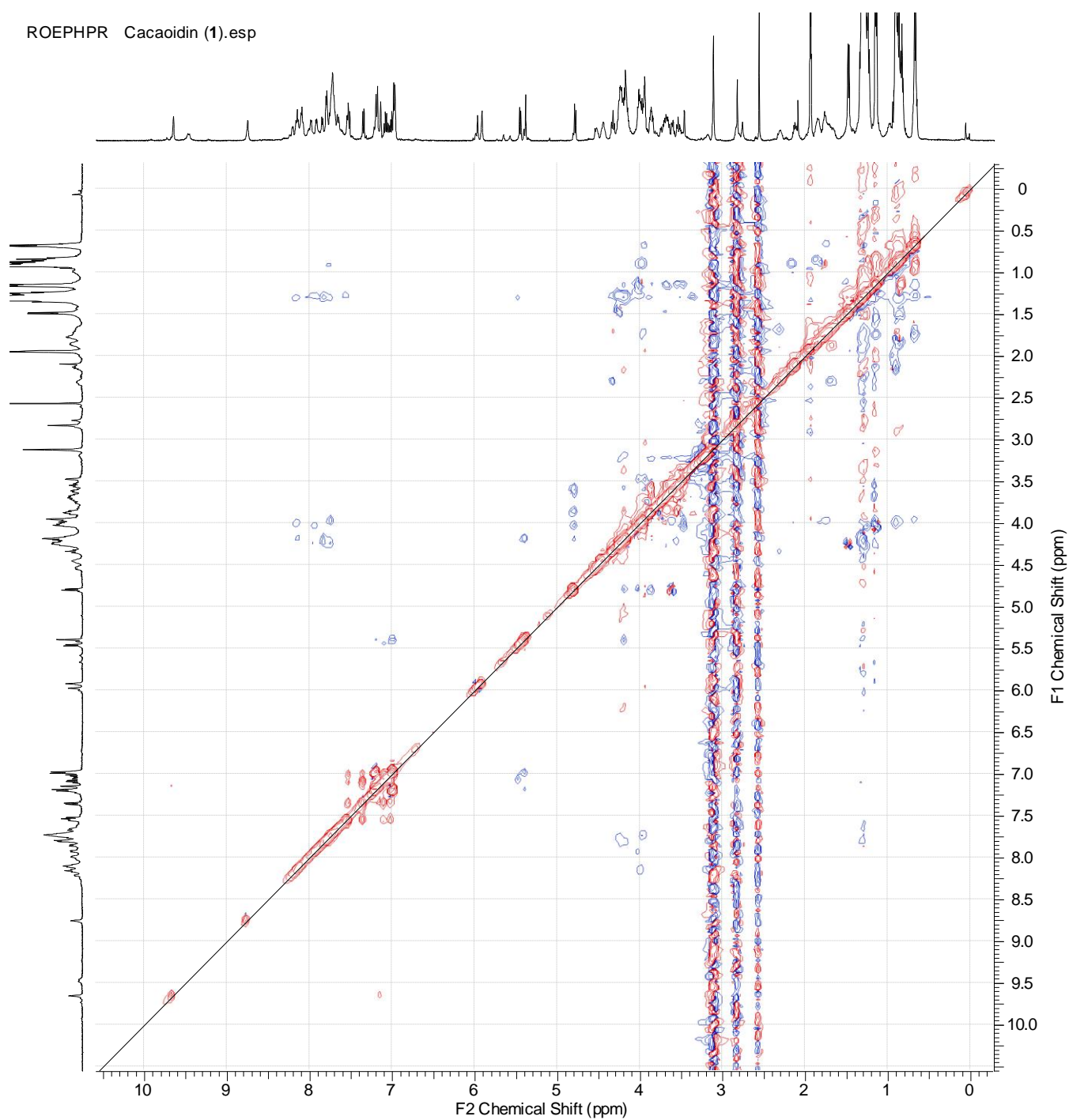
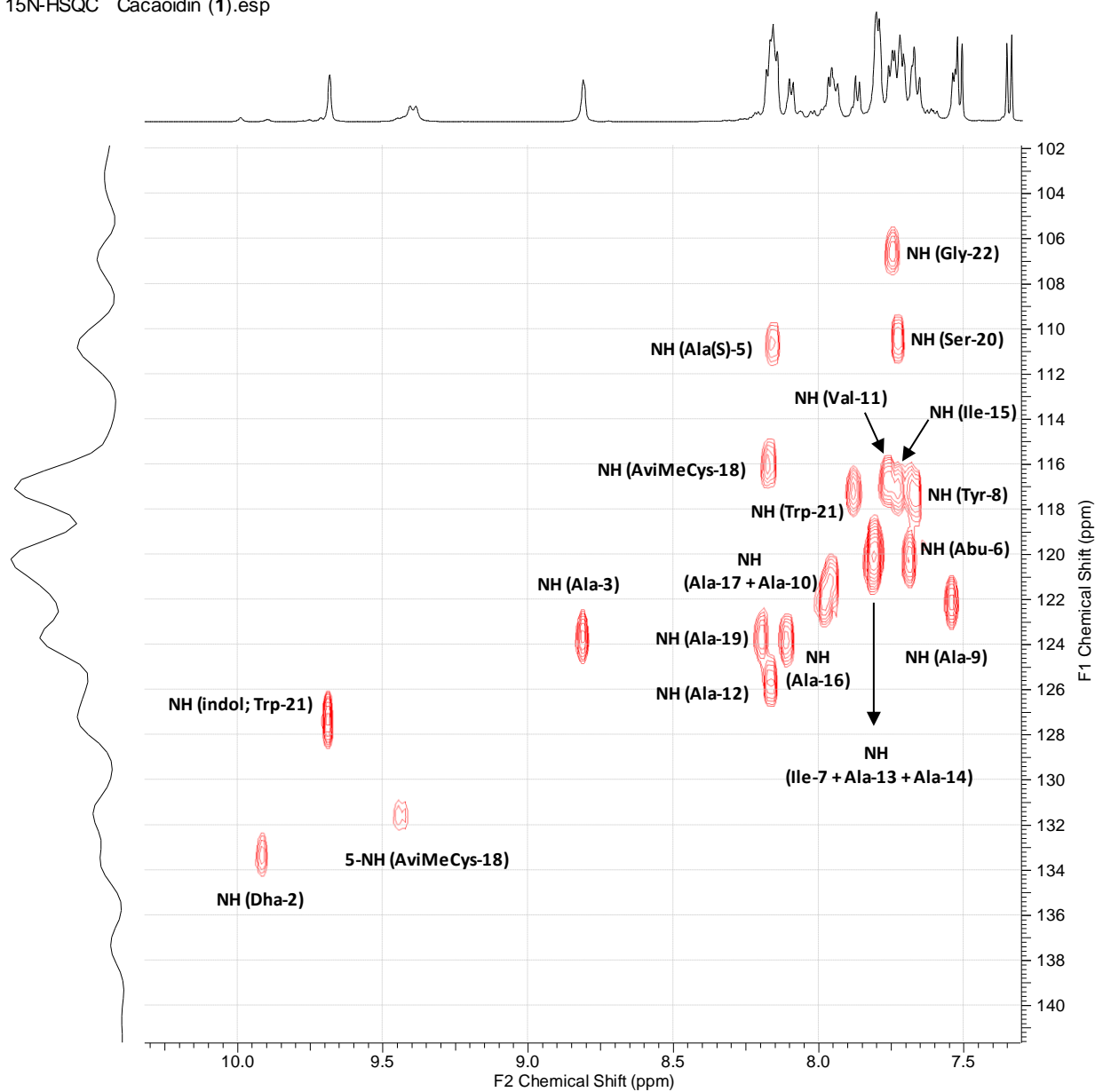


Figure S71. ROESY spectrum ( $\text{CD}_3\text{CN}:\text{H}_2\text{O}; 9:1$ ) of cacaoidin (1).

15N-HSQC Cacaoidin (1).esp



**Figure S72.** Expansion of the <sup>15</sup>N-HSQC spectrum (CD<sub>3</sub>CN: H<sub>2</sub>O; 9:1) of cacaoidin (1)

15N-HSQC Cacaoidin (1).esp

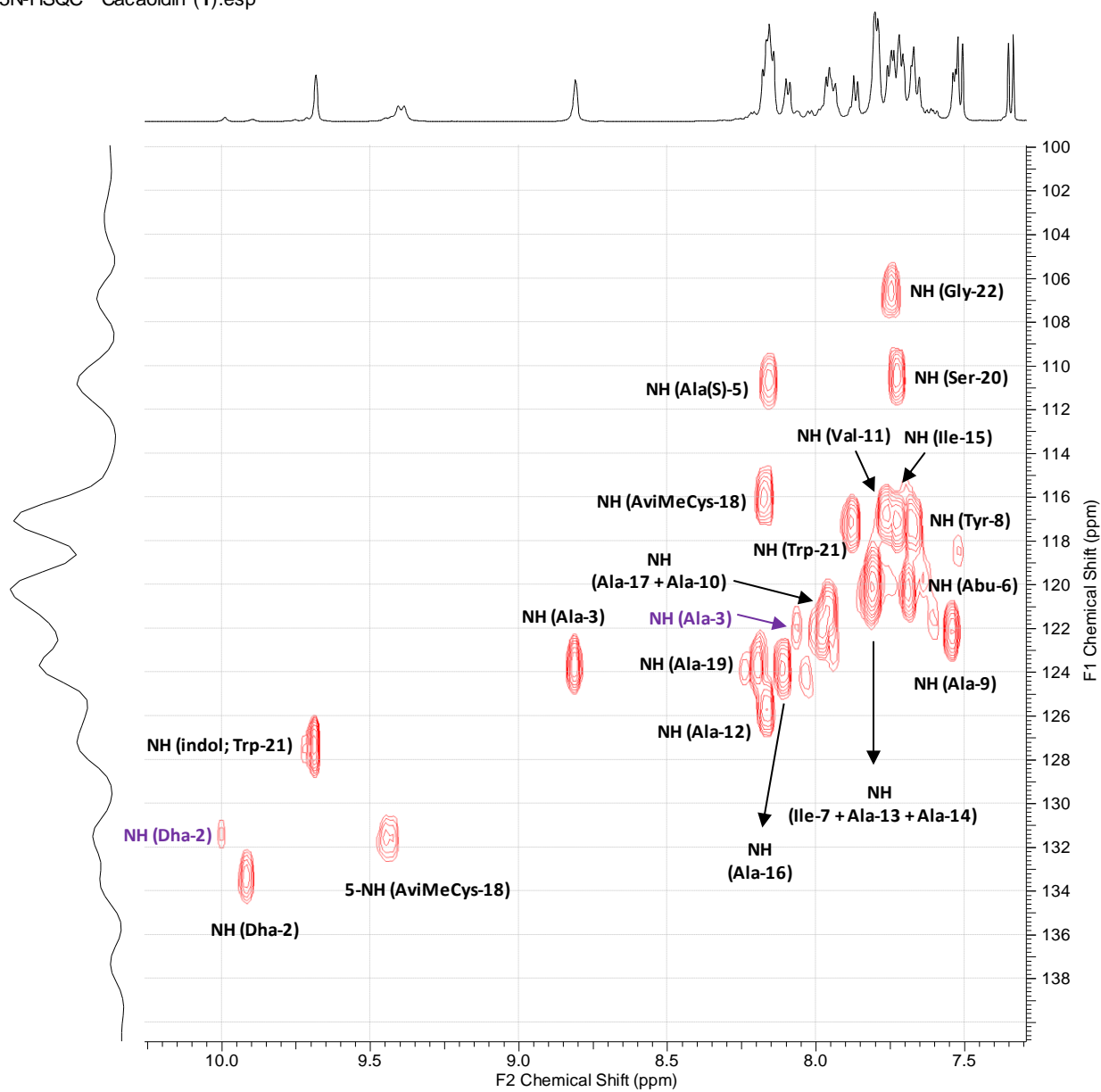


**Figure S73.** Expansion of the  $^{15}\text{N}$ -HSQC spectrum ( $\text{CD}_3\text{CN}:\text{H}_2\text{O}$ ; 9:1) of cacaoidin (1). Signals corresponding to the minor conformer are indicated or framed in purple.

15N-HMBC ws Cacaoidin (1).esp

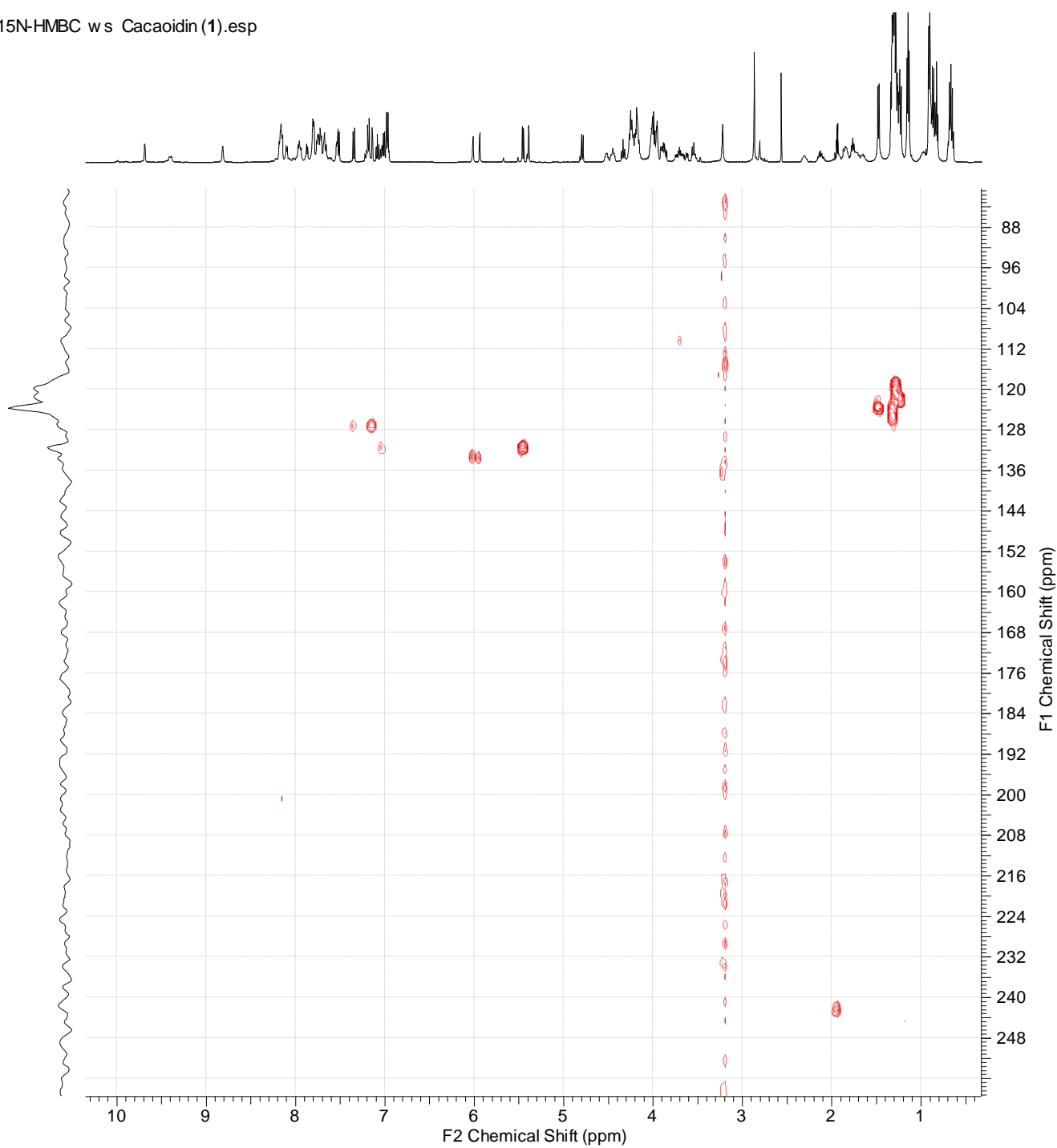
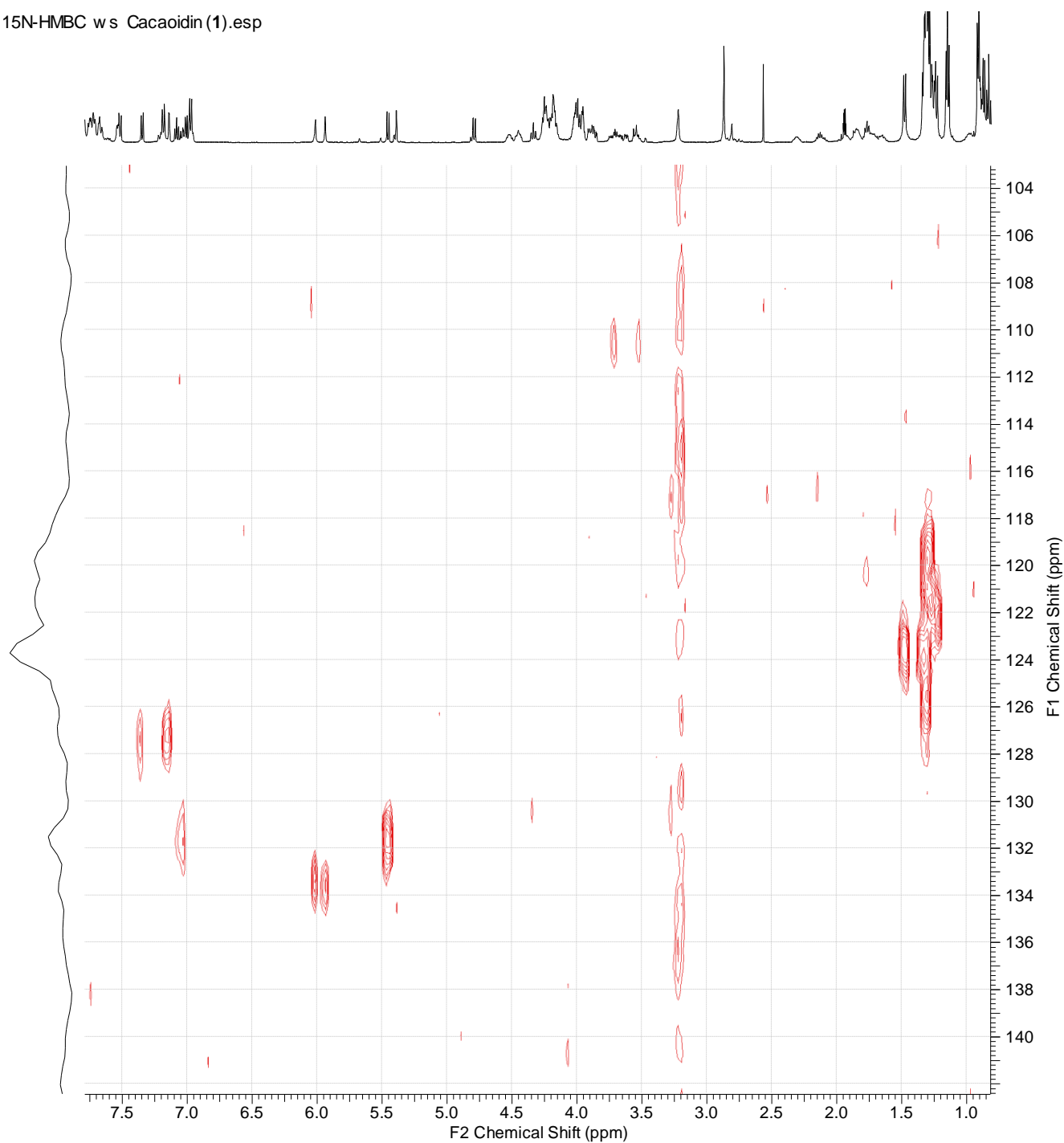


Figure S74. <sup>15</sup>N-HMBC spectrum (CD<sub>3</sub>CN: H<sub>2</sub>O; 9:1) of cacaoidin (1).



15N-HMBC ws Cacaoidin (1).esp



**Figure S75.** Expansion of the <sup>15</sup>N-HMBC spectrum (CD<sub>3</sub>CN: H<sub>2</sub>O; 9:1) of cacaoidin (1)

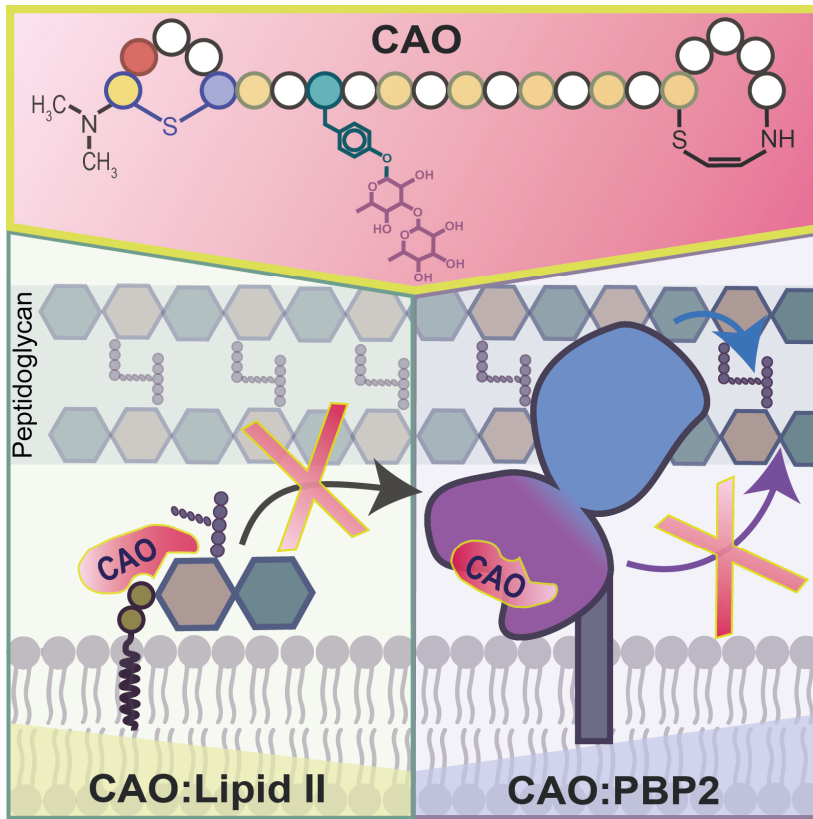
### 3. References

- [1] J. Martín, G. Crespo, V. González-Menéndez, G. Pérez-Moreno, P. Sánchez-Carrasco, I. Pérez-Victoria, L. M. Ruiz-Pérez, D. González-Pacanowska, F. Vicente, O. Genilloud, et al., *J. Nat. Prod.* **2014**, *77*, 2118–2123.
- [2] O. S. Kim, Y. J. Cho, K. Lee, S. H. Yoon, M. Kim, H. Na, S. C. Park, Y. S. Jeon, J. H. Lee, H. Yi, et al., *Int. J. Syst. Evol. Microbiol.* **2012**, *62*, 716–721.
- [3] T. Kieser, M. J. Bibb, M. J. Buttner, K. F. Chater, D. A. Hopwood, *Practical Streptomyces Genetics. A Laboratory Manual.*, John Innes Foundation, **2000**.
- [4] K. Blin, S. Shaw, K. Steinke, R. Villebro, N. Ziemert, S. Y. Lee, M. H. Medema, T. Weber, *Nucleic Acids Res.* **2019**, *47*, W81–W87.
- [5] M. Johnson, I. Zaretskaya, Y. Raytselis, Y. Merezuk, S. McGinnis, T. L. Madden, *Nucleic Acids Res.* **2008**, *36*, W5–9.
- [6] S. Lu, J. Wang, F. Chitsaz, M. K. Derbyshire, R. C. Geer, N. R. Gonzales, M. Gwadz, D. I. Hurwitz, G. H. Marchler, J. S. Song, et al., *Nucleic Acids Res.* **2020**, *48*, D265–D268.
- [7] H. Kessler, *Angew. Chemie Int. Ed. English* **1982**, *21*, 512–523.
- [8] T. Hamada, S. Matsunaga, G. Yano, N. Fusetani, *J. Am. Chem. Soc.* **2005**, *127*, 110–118.
- [9] C. T. Lohans, J. C. Vederas, *J. Antibiot. (Tokyo)*. **2014**, *67*, 23–30.
- [10] D. E. Palmer, D. F. Mierke, C. Pattaroni, M. Goodman, T. Wakamiya, K. Fukase, M. Kitazawa, H. Fujita, T. Shiba, *Biopolymers* **1989**, *28*, 397–408.
- [11] P. L. Toogood, *Tetrahedron Lett.* **1993**, *34*, 7833–7836.
- [12] K. Fujii, K. I. Harada, *Anal. Chem.* **1997**, *69*, 5146–5151.
- [13] F. J. Ortiz-López, M. C. Monteiro, V. González-Menéndez, J. R. Tormo, O. Genilloud, G. F. Bills, F. Vicente, C. Zhang, T. Roemer, S. B. Singh, et al., *J. Nat. Prod.* **2015**, *78*, 468–475.
- [14] H. Zhou, W. A. Van Der Donk, *Org. Lett.* **2002**, *4*, 1335–1338.
- [15] X. Yang, W. A. Van Der Donk, *ACS Chem. Biol.* **2015**, *10*, 1234–1238.
- [16] W. Tang, G. Jiménez-Osés, K. N. Houk, W. A. Van Der Donk, *Nat. Chem.* **2015**, *7*, 57–64.
- [17] J.-H. Zhang, T. D. Y. Chung, K. R. Oldenburg, *J. Biomol. Screen.* **1999**, *4*, 67–73.
- [18] J. Martín, T. S. Da Sousa, G. Crespo, S. Palomo, I. González, J. R. Tormo, M. De La Cruz, M. Anderson, R. T. Hill, F. Vicente, et al., *Mar. Drugs* **2013**, *11*, 387–398.
- [19] D. Carretero-Molina, F. J. Ortiz-López, J. Martín, D. Oves-Costales, C. Díaz, M. De La Cruz, B. Cautain, F. Vicente, O. Genilloud, F. Reyes, *Mar. Drugs* **2020**, *18*, DOI 10.3390/md18010022.
- [20] A. Hoffmann, T. Schneider, U. Pag, H. G. Sahl, *Appl. Environ. Microbiol.* **2004**, *70*, 3263–3271.
- [21] C. A. G. Haasnoot, F. A. A. M. de Leeuw, C. Altona, *Tetrahedron* **1980**, *36*, 2783–2792.
- [22] C. Lauritano, J. Martín, M. De La Cruz, F. Reyes, G. Romano, A. Ianora, *Sci. Rep.* **2018**, *8*, 1–10.
- [23] J. Freeman, S. Pilling, J. Vernon, M. H. Wilcox, *Antimicrob. Agents Chemother.* **2017**, *61*, 1–5.
- [24] A. Urban, S. Eckermann, B. Fast, S. Metzger, M. Gehling, K. Ziegelbauer, H. Rübsamen-Waigmann, C. Freiberg, *Appl. Environ. Microbiol.* **2007**, *73*, 6436–6443.
- [25] H. Harms, A. Klöckner, J. Schrör, M. Josten, S. Kehraus, M. Crüsemann, W. Hanke, T. Schneider, T. F. Schäberle, G. M. König, *Planta Med.* **2018**, *84*, 1363–1371.
- [26] J. Radeck, S. Gebhard, P. S. Orchard, M. Kirchner, S. Bauer, T. Mascher, G. Fritz, *Mol. Microbiol.* **2016**, *100*, 607–620.
- [27] S. Tan, K. C. Ludwig, A. Müller, T. Schneider, J. R. Nodwell, *ACS Chem. Biol.* **2019**, *14*, 966–974.

### 4.3 Dual targeting of the lanthidin antibiotic Cacaoidin

Antibiotic resistance is reaching alarming levels, demanding for the discovery and development of antibiotics with novel chemistry and mechanism of action. The recently discovered antibiotic cacaoidin (CAO) combines structural features of the lanthipeptide and the linaridin families of ribosomally synthesized and post-translationally modified peptides (RiPP), introduced by alternative RiPP biosynthetic pathways. Therefore CAO represents the founding member of a new RiPP subfamily referred to as lanthidins or class V lanthipeptides. CAO displays several rare or unprecedented post-translational modifications, including a dimethylated N-terminal lanthionine (NMe<sub>2</sub>Lan), a C-terminal 2-aminovinyl-methyl-cysteine (AviMeCys), one dehydro alanine residue, a high amount of D-amino acids, and a unique disaccharide substitution attached to the tyrosine residue.

Investigating if the novel chemistry also goes along with an unprecedented mode of action was subject of this work. In the previous publication (Chapter 4.2), interference with cell wall biosynthesis, or more precisely, binding of the ultimate peptidoglycan precursor lipid II was suggested to be the mode of action of CAO. Lipid II represents a validated target structure of many successful antibiotics (a general overview has been given in Chapter 2.7), including lanthipeptide antibiotics. The lipid II interaction is among other potential cellular consequences (e.g. pore formation) causative for interference with peptidoglycan synthesis. In contrast to known lipid II-binding antibiotics, treatment with CAO triggers deviating cellular effects which further initiated in-depth mode of action studies. Using a combination of biochemical and molecular interaction studies, we provide evidence that CAO combines binding to the ultimate cell wall precursor lipid II and direct inhibition of murein transglycosylases, both validated target structures of most successful antibiotics. In accordance with the unique hybrid structural features of lanthipeptide and the linaridin families and the unique disaccharide substitution attached to the tyrosine residue of CAO, we demonstrate that CAO exhibits an unprecedented dual mechanism of action. To the best of our knowledge, CAO thus represents the first natural product combining these mechanisms.



Graphical Abstract

# Dual targeting of the lanthidin antibiotic Cacaoidin

Julia P. Deisinger<sup>†,§</sup>, Anna Müller<sup>†</sup>, Francisco Javier Ortiz-López<sup>‡</sup>, Olga Genilloud<sup>‡</sup>, Tanja Schneider<sup>\*,†,§</sup>

<sup>†</sup>Institute for Pharmaceutical Microbiology, University of Bonn, Meckenheimer Allee 168, 53115 Bonn, Germany

<sup>§</sup>DZIF, German Center for Infectious Research, partner site Bonn-Cologne, Bonn, Germany

<sup>‡</sup>Fundación MEDINA, Centro de Excelencia en Investigación de Medicamentos Innovadores en Andalucía, Avenida del Conocimiento, 34. Parque Tecnológico de Ciencias de la Salud, 18016 Armilla, Granada, Spain.

**KEYWORDS** *lantibiotic, lanthipeptide, peptidoglycan, antibiotic, glycosyltransferase inhibitor, PBP*

**Cacaoidin combines the characteristic lanthionine residue of lanthipeptides and the linaridin-specific N-terminal dimethylation, therefore designated as the first class-V lanthipeptide (lanthidin). Notable features further include the high D-amino acid content and a unique disaccharide substitution attached to the tyrosine residue. Cacaoidin shows antimicrobial activity against gram-positive pathogens and was shown to interfere with peptidoglycan biosynthesis. Initial investigations indicated an interaction with the peptidoglycan precursor LII<sub>PGN</sub> as described for several lanthipeptides. We here provide evidence that cacaoidin is a first-in-class lantibiotic that exhibits a dual mode of action combining binding to LII<sub>PGN</sub> and direct inhibition of cell wall transglycosylases.**

## INTRODUCTION

Ribosomally synthesized and post-translationally modified peptides (RiPPs) represent a family of structurally diverse peptide natural products with a variety of activities including antifungal, antibacterial or antiviral.<sup>1-4</sup> Lanthipeptides with antibiotic activity, so-called lantibiotics,<sup>5</sup> are among the best characterized classes of RiPPs. Structurally distinct features of this family include the presence of the thioester amino acids lanthionine (Lan) and/or methyllanthionine (MeLan), as well as dehydroamino acids which result from extensive post-translational modifications.<sup>6,7</sup>

Recently discovered cacaoidin (CAO) is the first member of a new family of RiPPs termed lanthidins,<sup>8</sup> sharing characteristic features of the lanthipeptide and the linaridin family, i.e. a thioether-based lanthionine residue and a linaridin-specific dimethylated N-terminus, respectively. Further analysis of its biosynthetic gene cluster has designated it as the first class-V lanthipeptide.<sup>8,9</sup>

CAO is a 23 amino acid peptide produced by *Streptomyces cacaoides* characterized by the presence of a C-terminal S-[(Z)-2-aminovinyl-3-methyl]-D-cysteine (AviMeCys), found in both lanthipeptides and linaridins,<sup>10,11</sup> and a glycosylated tyrosine residue, rarely found in natural products with mannopeptimycins being the only representatives reported so far.<sup>12</sup> In contrast to most representatives of the lanthipeptide family, CAO contains only a single Lan residue with a unique *N,N*-dimethyl modification, located at the N-terminus (Figure 1). The latter is a characteristic feature of the linaridins, which in turn lack Lan/MeLan residues. The linaridins represent a small family of linear, dehydrated (*arid*) peptides presently comprising four members, cypemycin, grismycin, legonaridin, and salinipeptins.<sup>11</sup>

Another feature of CAO is the presence of D-amino acids D-alanine and D-aminobutyric acid (Figure 1), only reported for a limited number of RiPPs.<sup>13-17</sup>

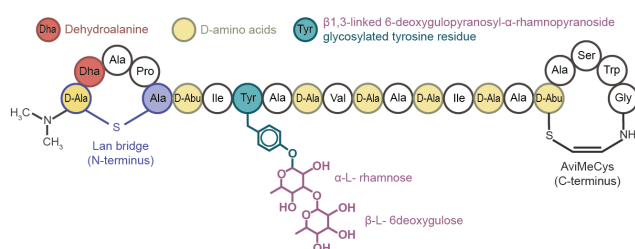


Figure 1. Structure of cacaoidin. D-aminobutyric acid (D-Abu).

## RESULTS AND DISCUSSION

CAO shows potent activity against methicillin resistant *Staphylococcus aureus* (MRSA; 0.25  $\mu\text{g ml}^{-1}$ ) and good to moderate activity against vancomycin resistant enterococci and *Clostridium difficile* (Table S1)<sup>8</sup> but lacks activity against gram-negative organisms. The antimicrobial activity of lantibiotics (e.g. globular mersacidin) is often conferred by interaction with the ultimate peptidoglycan (PGN) precursor LII<sub>PGN</sub> (undecaprenyl-pyrophosphate-MurNAC-pentapeptide-GlcNAc), thereby blocking cell wall biosynthesis. Flexible lantibiotics, such as nisin, combine LII<sub>PGN</sub>-binding and pore formation.<sup>18</sup> LII<sub>PGN</sub> represents the essential PGN building block that is readily accessible on the outside of gram-positive bacteria, where the lipid intermediate is incorporated into the growing PGN network by glycosyl transferases (GTs) and subsequently crosslinked by the activity of transpeptidases (TPs).<sup>19</sup> Cell wall biosynthesis was identified as the target pathway for CAO, as indicated by pathway specific bioreporters, and the

induction of a *liaI-lux* reporter fusion pointed to interference with the LII<sub>PGN</sub> biosynthesis cycle.<sup>8</sup>

**Targeting of cell wall building blocks.** In accordance, CAO and the LII<sub>PGN</sub>-binding lantibiotic mersacidin (MRS) both induced the expression of *liaI-lux* as indicated by an increase in the luminescence signal (Figure 2). Pre-incubation with purified LII<sub>PGN</sub> in a two-fold molar excess resulted in the antagonization of *liaI* induction indicating a direct interaction with the PGN precursor.<sup>8</sup>

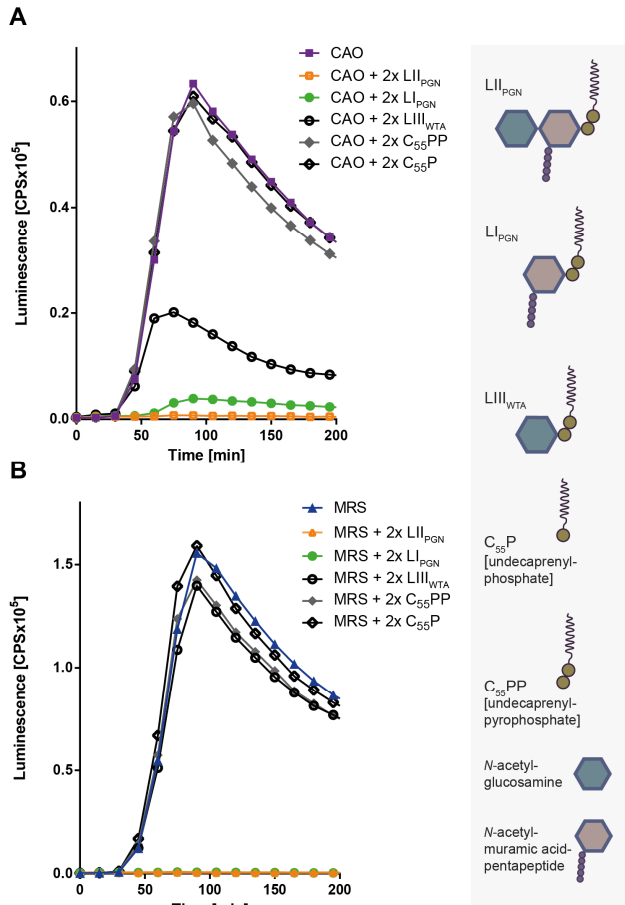


Figure 2. Cacaoidin (CAO; A) and mersacidin (MRS; B)-induced *liaI-lux* expression is antagonized by purified LI<sub>PGN</sub> or LII<sub>PGN</sub> at a two-fold molar excess with respect to CAO and MRS, while C<sub>55</sub>P and C<sub>55</sub>PP did not antagonize antibiotic activity. LIII<sub>WTA</sub> had no influence on MRS-induced *liaI-lux* expression but reduced the CAO-induced signal three-fold.

To identify the minimal binding motif of CAO, different undecaprenyl-containing cell wall precursors were tested for their ability to antagonize the CAO-induced response. As observed for LII<sub>PGN</sub>, pre-incubation of antibiotics with purified LI<sub>PGN</sub> (undecaprenyl-pyrophosphate-MurNac-pentapeptide) in a two-fold molar excess almost completely antagonized *liaI* induction (Figure 2), while equivalent amounts of C<sub>55</sub>PP or C<sub>55</sub>P had virtually no effect (Figure 2). Even a 20-fold molar excess of C<sub>55</sub>PP reduced the luminescence signal only by ~30% (Figure S1A&B), indicative for unspecific hydrophobic interactions. The results demonstrate that in contrast to nisin and flexible

lantibiotics, interaction with the pyrophosphate moiety is not sufficient and that binding of CAO and MRS involves interactions with the first sugar of lipid intermediates. To evaluate the relevance of the nature of the sugar, purified wall teichoic precursor LIII<sub>WTA</sub> (undecaprenyl-pyrophosphate-GlcNAc) was tested. Interestingly, CAO-induced *liaI-lux* expression was suppressed three-fold when preincubated with LIII<sub>WTA</sub> (Figure 2A), while MRS-induced *liaI-lux* expression remained unaffected (Figure 2B), indicating that, in contrast to CAO, the interaction with the MurNac-pentapeptide sugar of LII<sub>PGN</sub> is crucial for MRS-binding, likely involving interactions with the pentapeptide moiety. Indeed, MRS, but not CAO, was able to inhibit amidation of D-glutamate in position 2 of the LII<sub>PGN</sub>-stem peptide *in vitro* (Figure S2). Together these results support differential binding modes, involving binding to the pyrophosphate-sugar-peptide portion of LII<sub>PGN</sub> for MRS, while the interaction of CAO primarily involves binding to the phosphate sugar moiety, with the nature of the first sugar being less relevant. Moreover, interactions with the second sugar in LII<sub>PGN</sub> are not mandatory for high affinity binding for both antibiotics, as efficient antagonization was observed with LI<sub>PGN</sub> lacking the GlcNAc residue (Figure 2).

In contrast to other LII<sub>PGN</sub>-binding antibiotics, including vancomycin and MRS, treatment with CAO did not result in accumulation of the soluble PGN precursor (Figure S3A&B), suggesting that CAO activity triggers additional cellular effects. Absence of UDP-MurNac-pentapeptide accumulation was also observed for the lantibiotic nisin (Figure S3B). In contrast to MRS, nisin exhibits a dual mode of action. It forms a complex with LII<sub>PGN</sub> leading to inhibition of late-stage PGN biosynthesis reactions and in addition uses LII<sub>PGN</sub> as a docking molecule for the formation of a defined membrane pore<sup>20</sup>, ultimately leading to leakage of cytoplasmic content, thus interfering with UDP-MurNac-pentapeptide accumulation. However, in contrast to nisin, neither pore formation nor rapid membrane disrupting effects were observed for CAO. While nisin treatment triggers the release of intracellular potassium ions from *Staphylococcus simulans* cells, CAO did not lead to potassium ion leakage (Figures S4). Furthermore, the cellular localization of GFP-MinD in *Bacillus subtilis* was almost unaffected by CAO treatment (Figure S5). MinD accumulates at the cell poles in growing cells to facilitate selection of the mid-cell division site, specific FtsZ placement and formation of the division septum.<sup>21</sup> MinD localization is sensitive to alterations of the membrane potential that stimulates membrane binding.<sup>21</sup> Treatment with compounds that dissipate the membrane potential, such as the ionophore carbonyl cyanide m-chlorophenylhydrazone (CCCP) or the pore forming nisin, results in rapid MinD delocalization.<sup>21</sup> Such effects were not observed for CAO (Figure S5) and the MinD localization pattern at concentrations up to 10xMIC remained unchanged.

**Direct inhibition of cell wall transglycosylases.** The distinct cellular effects observed for CAO prompted a more detailed analysis of CAO's effect on LII<sub>PGN</sub>-consuming reactions, catalyzed by penicillin binding proteins (PBPs) and monofunctional transglycosylases. To this end the

impact of CAO on transglycosylase activity was investigated *in vitro* (Figure 3).

Bifunctional PBP2 catalyzes the formation of polymeric PGN from monomeric LII<sub>PGN</sub> *in vitro*. To enable individual analysis of the transglycosylase activity a PBP2 variant harboring a loss of function mutation in the transpeptidase domain was used in all experiments (PBP2<sub>mutTP</sub>, Figure 3).

Reactions were initiated by the addition of increasing enzyme concentrations. At lower enzyme concentration (0.75  $\mu\text{M}$ ) about 50% of the LII<sub>PGN</sub> substrate was converted and full inhibition was observed in presence of CAO, MRS, and the transglycosylase inhibitor moenomycin (MOE) (Figure 3). For MRS and other LII<sub>PGN</sub>-binding antibiotics, it is known that binding of LII<sub>PGN</sub> leads to steric hindrance, ultimately resulting in interference with PBP2 action.<sup>20,22</sup> In line with the formation of an antibiotic-LII<sub>PGN</sub> complex, increasing concentrations of PBP2 were unable to outcompete the inhibitory effect of MRS. In contrast, incrementing enzyme concentrations gradually restored LII<sub>PGN</sub> transglycosylation in the presence of the phosphoglycolipid antibiotic MOE, that acts by direct enzyme inhibition.<sup>23</sup> Interestingly, increasing PBP2 concentrations successively restored transglycosylase activity in presence of CAO, pointing to direct inhibition of the PBP2 enzyme as observed with MOE (Figure 3).

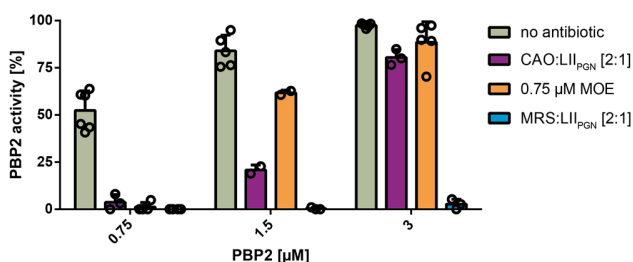


Figure 3. PBP2 mediated transglycosylation of LII<sub>PGN</sub> is inhibited by CAO and transglycosylase inhibitor moenomycin (MOE) and restored by increasing PBP2 concentrations. Incrementing PBP2 concentrations did not affect the inhibitory effect of LII<sub>PGN</sub>-binding mersacidin (MRS). The extent of inhibition relates to enzyme activity in absence of antibiotics at respective enzyme concentrations.

To further characterize transglycosylase inhibition, the impact of CAO on the monofunctional transglycosylase SgtB was analyzed. In absence of antibiotics and at low SgtB concentration (0.2  $\mu\text{M}$ ) approximately 50% of monomeric LII<sub>PGN</sub> was transglycosylated, while full conversion was achieved at 0.8  $\mu\text{M}$  of SgtB (Figure 4). At the lowest enzyme concentrations tested SgtB, was almost completely inhibited by CAO (Figure 4). With increasing SgtB concentration enzyme activity was gradually restored to the level of the respective control without antibiotic. As observed for the PBP-catalyzed reaction, MOE strongly inhibited SgtB activity at low enzyme concentrations and full recovery of activity was achieved at 1.6  $\mu\text{M}$  (Figure 4). Once more, the inhibitory effect of MRS remained unaffected with elevating enzyme amounts (Figure 4), in

agreement with the LII<sub>PGN</sub>-binding mechanism of this compound.

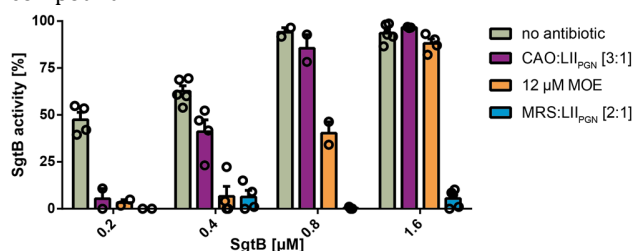


Figure 4. Inhibitory effect of CAO and MOE on SgtB activity is restored by increasing enzyme concentrations, whereas inhibition of MRS remains unaltered. The extent of inhibition relates to enzyme activity in absence of antibiotics at respective enzyme concentrations.

**Binding to *S. aureus* PBP2.** The *in vitro* data obtained analyzing CAO's inhibitory effect on GTs, compared to the substrate binding antibiotic MRS and the enzyme inhibitor MOE, strongly pointed to a direct GT inhibition by CAO. To validate a direct CAO-GT interaction, surface plasmon resonance (SPR) analysis was performed. Since the transmembrane domain of PBPs is critical for binding of MOE,<sup>24</sup> experiments were conducted with full-length PBP2<sub>mutTP</sub> (Figure S6A). A dose-dependent binding response of MOE to PBP2 was observed (Figure 5A) confirming the interaction. Kinetic analysis was performed by fitting of the curves to a 1:1 interaction model (Figure S7A) resulting in a  $K_D$  of 0.728  $\mu\text{M}$  (Table S2), comparable to steady state kinetics previously determined (0.393  $\mu\text{M}$ ).<sup>24</sup> Furthermore, the  $K_D$  was in the range of  $10^{-7}$  M, correlating with the reported inhibitory concentration of MOE for the transglycosylation reaction.<sup>24,25</sup> To investigate the interaction of CAO with PBP2, a series of CAO concentrations were analyzed, resulting in a dose-dependent binding response (Figure 5B). Kinetic analysis was fitted to a 1:1 interaction model (Figure S7B), that proved to be the most suitable to describe the observed interaction (Table S2) and resulted in a  $K_D$  of 16.1  $\mu\text{M}$ . Compared to MOE, full dissociation of CAO was not achieved at higher concentrations ( $\geq 16$   $\mu\text{M}$ ). Furthermore, the association curve at higher concentrations ( $\geq 16$   $\mu\text{M}$ ) differs compared to lower concentrations. This observation may indicate a more complex interaction pronounced at higher concentrations.

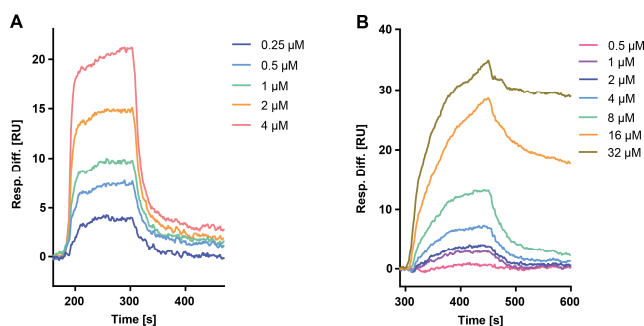


Figure 5. Dose-dependent SPR binding response of MOE (A) and CAO (B) to immobilized full-length *S. aureus* PBP2<sub>mutTP</sub> indicates a direct interaction.

Analysis of the CAO and MOE binding curves, revealed clear differences in association and dissociation rates, with slower association and dissociation for CAO. Indeed, the half-life of the CAO-PBP2 complex is approximately 10-fold higher (12 min) than for the MOE-PBP2 complex (1.1 min; Table S2). Nevertheless, the determined  $K_D$  of CAO at equilibrium is about 22-fold higher. The binding strength of MOE to PBPs from *S. aureus*, *E. faecalis* and *E. coli*, was shown to correlate with antibiotic activity.<sup>24,25</sup> For CAO a correlation of  $K_D$  (16.1  $\mu\text{M}$ ) and MIC value (0.106-0.847  $\mu\text{M}$ ) was not observed. This discrepancy can be explained by CAOs dual mechanism of action, that combines binding to LII<sub>PGN</sub> and direct transglycosylase inhibition (Figure 6). It is tempting to speculate that the latter mechanism relies on the unique disaccharide unit of CAO mimicking and thus competing with the natural transglycosylase substrate, i.e. the  $\beta$ 1,4-linked MurNAc-GlcNAc-chain. MOE represents the only natural product acting specifically as an inhibitor of the GT active site. Crystal structure analysis revealed that the antibiotic binds to the glycosyl donor site of GTs, involving interactions with the disaccharide and the phosphoglycerate portion of the MOE pharmacophore.<sup>23,26-28</sup> Semisynthetic GT inhibitors harboring  $\beta$ 1,2-,  $\beta$ 1,3- or  $\beta$ 1,4-linked disaccharides moieties were shown to facilitate inhibition of PGN synthesis *in vitro*<sup>29,30</sup> and to exhibit antimicrobial activity.<sup>31-34</sup> Interestingly, neither the positioning of the glycosidic bond nor the identity of the disaccharide hexoses were determinants for the overall activity of the inhibitors, supporting the involvement of the  $\beta$ 1,3-linked 6-deoxygulopyranosyl- $\alpha$ -rhamnopyranoside disaccharide of CAO in GT binding in a similar fashion.

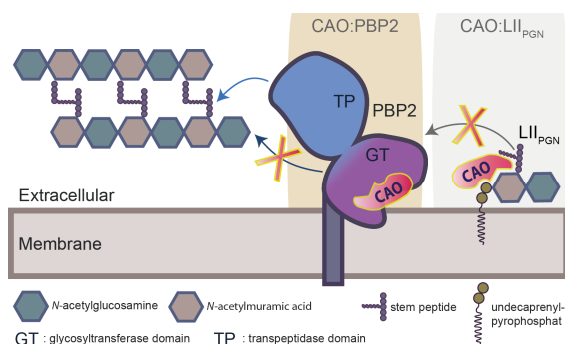


Figure 6. Proposed model for the dual mode of action of cacaoidin (CAO).

To identify the motifs crucial for binding to GTs and LII<sub>PGN</sub> and for rational SAR analysis, determination of the crystal structures of the individual complexes would be of importance. Furthermore, deglycosylated CAO variants could provide valuable information on the role of the disaccharide unit for GT interaction. Thus far, chemical attempts to generate such variants were unsuccessful and proved incompatible with the stability of the thioether-bridged rings and particularly the AviMeCys rings (data not shown). Attempts to generate a deglycosylated variant through knockout of the respective glycosyltransferase genes in the producing strain were also unsuccessful so far.

## CONCLUSIONS

CAO represents the first natural product with a dual mode of action comprising binding of the LII<sub>PGN</sub> PGN synthesis intermediate and simultaneous direct inhibition of murein transglycosylases (Figure 6), both representing validated target structures of successful antibiotics. The unique structural features of CAO could guide the synthesis of hybrid antibiotics with resistance breaking properties due to multitargeting.

## MATERIALS AND METHODS

**Antibacterial assay.** MIC values were determined by broth microdilution using BSA-coated plates as previously described.<sup>35</sup>

**Induction and antagonization of *lial-lux* cell wall stress response.** *B. subtilis lial-lux*<sup>36</sup> was grown in Mueller–Hinton broth supplemented with chloramphenicol (5  $\mu\text{g mL}^{-1}$ ) to OD<sub>600</sub> = 0.5. The antibiotics CAO and MRS were added in a BSA-coated Greiner LUMITRACTM 96-well-microtiter plate at a final concentration of 8  $\mu\text{g mL}^{-1}$  and 4  $\mu\text{g mL}^{-1}$  respectively prior to addition of the reporter strain. Induction of cell wall stress indicated by an increase in luminescence was measured using the Tecan Spark 10 M microplate reader for 400 min at 30 °C.

Antagonization of the CAO and MRS induced *lial-lux* luminescence response was used as a method to investigate the direct interaction of the antibiotics with putative antagonists as previously reported.<sup>8,37</sup> To this end, purified PGN (LI<sub>PGN</sub>, LII<sub>PGN</sub>) and WTA precursors (LIII<sub>WTA</sub>) were first preincubated with CAO and MRS at a two-fold molar excess with respect to the antibiotics. The central lipid carrier undecaprenyl-phosphate (C<sub>55</sub>P) and undecaprenyl-pyrophosphate (C<sub>55</sub>PP) were tested in equivalent amounts, but additionally in a 20-fold molar excess with respect to the antibiotics. After preincubation, the experiment was performed, and luminescence was measured as described above. At least three independent biological replicate experiments were conducted.

**Overexpression and affinity purification of recombinant proteins.** Purification of the GatD-His<sub>6</sub>/MurT complex was performed as previously described<sup>38</sup>. *E. coli* strain BL21 (DE3) was used as a host for the recombinant expression of *S. aureus* proteins PBP2<sub>mutTP</sub>-His<sub>6</sub> (pET21b-*pbp2*<sub>mutTP</sub>), SgtB-His<sub>6</sub> (pET28a-*sgtB*), and PBP4-His<sub>6</sub> (pET21b-*pbp4*). Cells were grown at 37 °C in lysogeny broth (LB; Oxoid) supplemented with the appropriate antibiotic (100  $\mu\text{g mL}^{-1}$  ampicillin or 50  $\mu\text{g mL}^{-1}$  kanamycin). Proteins were expressed in mid-log phase cultures (OD<sub>600</sub> 0.6) after induction with 1 mM IPTG for 4 h at 37 °C. Cells were harvested by centrifugation (12 min, 7000 xg, 4 °C), washed once with buffer (50 mM Tris-HCl, 500 mM NaCl, pH 7.5), and resuspended in buffer supplemented with 1% (v/v) Triton X-100, lysozyme (250  $\mu\text{g mL}^{-1}$ ), DNase (50  $\mu\text{g mL}^{-1}$ ), RNase (10  $\mu\text{g mL}^{-1}$ ) and 0.5% N-Laurylsarcosine. After incubation on ice for 60 min, cells were sonicated and centrifuged (20 min, 15000 xg, 4 °C), the cleared lysate was subjected to Ni<sup>2+</sup>-affinity chromatography. In case of the purification of SgtB-His<sub>6</sub> the cleared lysate was incubated for 1 h with NiNTA-agarose



(1 ml NiNTA-agarose per 10 ml supernatant) under gentle stirring and transferred onto a column support. After washing of the NiNTA-agarose matrix with buffer W (50 mM Tris-HCl, 500 mM NaCl, 1% (v/v) Triton X-100, pH 7.5), subsequent rinsing with buffer W supplemented with 10 mM and 20 mM imidazole removed weakly bound proteins. SgtB-His<sub>6</sub> was eluted with buffer containing 300 mM imidazole. Elution fractions were collected and stored in 30% (v/v) glycerol at -20 °C.

Since PBP2\_mutTP and PBP4 were utilized for SPR measurements, these proteins had to be of particularly high purity. The required purity was ensured by two successive purification cycles via a fast protein liquid chromatography (FPLC) system (BioRad) with a 1 ml Bio-Scale™ Mini Nuvia™ IMAC Ni-charged resin. After the cleared lysate was loaded to the column, the resin was rinsed with buffer (50 mM Tris-HCl, 500 mM NaCl, 0.06% (v/v) Triton X-100, pH 7.5). Subsequently, an imidazole gradient (up to 50-100 mM) was applied in order to remove weakly bound proteins. The protein of interest (PBP2\_muTP or PBP4) was eluted with 500 mM imidazole containing buffer. Purity of elution fractions was assessed by SDS-PAGE (NuPAGE; Invitrogen) analysis and relevant fractions were pooled. Those fractions were dialyzed against buffer without imidazole (50 mM Tris-HCl, 500 mM NaCl, 0.06% (v/v) Triton X-100, pH 7.5) and concentrated using a spin column with molecular weight cut off (MWCO) of at least half the proteins size before the second run. After the second FPLC run (performed in the same way described above), elution fractions were assessed for purity, pooled and concentrated as mentioned above. Finally, proteins used for SPR coupling were dialyzed against coupling buffer (10 mM sodium maleate, pH 5.6). Protein concentrations were measured using Bradford reagent (BioRad).

***In vitro* reactions of PGN biosynthesis in presence of CAO.** In all *in vitro* assays, the PGN intermediate LII<sub>PGN</sub> was used as a substrate and CAO was added in molar ratios with regard to LII<sub>PGN</sub>. MRS and MOE were used as control antibiotics. LII<sub>PGN</sub> was purified as described previously.<sup>39</sup> The polyprenyl containing products and non-processed substrate were extracted from the reaction mixture with an equal volume of n-butanol/pyridine acetate, pH 4.2 (2:1; v/v), and analyzed by thin-layer chromatography (TLC) using chloroform/methanol/water/concentrated ammonium hydroxide (88:48:10:1, v/v/v/v) as solvent<sup>40</sup> and phosphomolybdic acid staining.<sup>39</sup> Quantification was carried out using ImageJ 1.52a software.

*In vitro* amidation was assayed by incubating 2 nmol of LII<sub>PGN</sub> in 160 mM Tris-HCl, 40 mM MgCl<sub>2</sub>, 50 mM KCl, pH 7.5, 0.26% Triton X-100, 6 mM ATP, and 6.6 mM glutamine in a total volume of 30 µl. The reaction was initiated by the addition of 3.8 µg of the purified GatD-His<sub>6</sub>/MurT complex and incubated for 2 h at 30 °C. In case of reactions containing antibiotics, CAO and MRS were added in a two-fold molar excess with regard to LII<sub>PGN</sub>, and preincubated for 20 min prior to the addition of enzyme. The MRS containing reaction further included 1.25 mM CaCl<sub>2</sub>. The experiment was performed in at least two biological replicates.

To investigate the impact of CAO on *in vitro* transglycosylase activity generating polymeric PGN by the

consumption of monomeric LII<sub>PGN</sub>, the activity of the bifunctional PBP2 and monofunctional SgtB of *S. aureus* were analyzed. In the case of the bifunctional PBP2, the PBP2\_mutTP (S398G) variant<sup>41,42</sup> was used in all experiments to ensure analysis of transglycosylase activity exclusively. Enzymatic activity of PBP2\_mutTP-His<sub>6</sub> was determined in 20 mM 2-(N-morpholino)-ethane sulfonic acid (MES) buffer, 2 mM MgCl<sub>2</sub>, 2 mM CaCl<sub>2</sub> and 0.06% TritonX-100, pH 5.5. CAO or MRS were added at a two-fold molar excess (120 µM) with respect to the substrate LII<sub>PGN</sub> (2 nmol; 60 µM). MOE containing reactions were supplemented with 0.75 µM MOE corresponding to the lowest PBP2\_mutTP concentration tested. After preincubation of the antibiotics with LII<sub>PGN</sub> for 20 min, the transglycosylation reaction was initiated by addition of the enzyme added at incrementing concentrations of 0.75, 1.5, and 3 µM, respectively. For each enzyme concentration tested, a control reaction without antibiotic was prepared. After incubation for 2 h at 30 °C, the reactions were stopped and analyzed as described above and the amount of remaining LII<sub>PGN</sub> was quantified to indirectly determine enzyme activity. Control reactions were supplemented with respective amounts of antibiotics after the reactions were stopped to match the extraction properties. The total signal of 2 nmol unprocessed LII<sub>PGN</sub> substrate served as a reference for calculation of enzyme activity, calculated as  $100 - 100 / [\text{total LII}_{\text{PGN}} \text{ signal}] * [\text{LII}_{\text{PGN}} \text{ signal of respective reaction}]$ .

The enzymatic activity of SgtB-His<sub>6</sub> was analyzed in 20 mM MES and 10 mM CaCl<sub>2</sub>, pH 5.5. The reactions contained 2 nmol (60 µM) LII<sub>PGN</sub> substrate. CAO was added in a three-fold molar excess (180 µM), MRS in a two-fold molar excess (120 µM) towards LII<sub>PGN</sub> and MOE was added at a final concentration of 12 µM. The antibiotics were preincubated for 20 min with LII<sub>PGN</sub> prior to addition of SgtB. The amount of SgtB was titrated from 0.2 to 1.6 µM, while the concentration of respective antibiotics remained unchanged. All reactions were stopped after 2 h incubation at 30 °C, analyzed and quantified as described above.

**Intracellular accumulation of UDP-MurNAc-pp.** Analysis of the cytoplasmic UDP-MurNAc-pp precursor pool was performed as described before<sup>43</sup> with some modifications: cell extracts were acidified, sterile filtered and directly analyzed using high-performance liquid chromatography (HPLC). The concentrations of antibiotics used were chosen to inhibit growth without significant lysis of the cells.

**Membrane disruption-potassium release from whole cells.** Potassium release from *S. simulans* whole cells was performed as previously described<sup>43</sup> in presence and absence of 10 mM glucose. Compound-induced potassium leakage was plotted relative to the total amount of potassium release after the addition of 1 µM (5xMIC) nisin (NIS, 100%, positive control); non-treated cells were used as the negative control. CAO was added at 0.2 µM and 1 µM (1x and 5xMIC, respectively). Both compounds were added after 20 s and potassium release was monitored.

**Fluorescence microscopy.** Fluorescence microscopy to analyze the cellular localization of the GFP-MinD fusion protein was performed as previously described.<sup>21</sup> *B. subtilis*

HS17 cells were treated with increasing concentrations of CAO (1xMIC to 10xMIC, corresponding to 2  $\mu\text{g ml}^{-1}$  to 20  $\mu\text{g ml}^{-1}$ ) or 100  $\mu\text{M}$  CCCP (positive control) before mounting on microscope slides covered with a thin film of 1% agarose. Imaging was carried out within 2 min after addition of CAO or CCCP. Fluorescence microscopy was performed on a Zeiss Axio Observer Z1 microscope equipped with HXP 120 V light source and an Axio Cam MR3 camera. Images were acquired using a 100x objective with ZEN2 software (Zeiss) and processed with Adobe Illustrator CS5.

**SPR measurements of PBP2 interaction.** All SPR measurements were performed on a Biacore 3000 apparatus (BIACORE) with research grade sensor chips (HC1500M, XanTec) and evaluated using the BIACORE Control Software 3.1.1.

Both, PBP4-His<sub>6</sub> and PBP2\_mutTP-His<sub>6</sub>, were immobilized on the respective flow cell via amine coupling<sup>44</sup> according to the manufacturer's instructions (XanTec): PBP2\_mutTP-His<sub>6</sub> was immobilized on the active flow cell, *S. aureus* PBP4-His<sub>6</sub> on the reference cell, since *in vitro* carboxypeptidase activity of PBP4 was unaltered in presence of CAO (data not shown). Briefly, the chip surface was conditioned with elution buffer (1 M sodium chloride, 0.1 M sodium borate pH 9.0; 3 min, 40  $\mu\text{l min}^{-1}$ ) and washed with deionized water until a stable baseline was reached. The surface of the reference cell was activated with freshly prepared activation mix (100 mM N-hydroxysuccinimide in 50 mM MES buffer at pH 5.0, supplemented with 26 mM N-ethyl-N'-(dimethylaminopropyl)-carbodiimide hydrochloride; 7.5 min, 40  $\mu\text{l min}^{-1}$ ). After a brief wash with deionized water (5 min, 40  $\mu\text{l min}^{-1}$ ), the PBP4 protein was injected (22  $\mu\text{g ml}^{-1}$ ; 7.5 min, 40  $\mu\text{l min}^{-1}$ ). To complete the coupling reaction, the surface was rinsed with deionized water for 40 min. The remaining active NHS esters were quenched with quenching buffer (1 M ethanolamine hydrochloride, pH 8.5; 15 min, 40  $\mu\text{l min}^{-1}$ ). The matrix of the analytic flow cell was activated as described above and PBP2\_mutTP-His<sub>6</sub> protein solution (10  $\mu\text{g ml}^{-1}$ ) was injected (7.5 min, 40  $\mu\text{l min}^{-1}$ ). After rinsing the surface with deionized water for 40 min, the residual active ester groups were deactivated as described above.

Following the immobilization, the whole system was rinsed thoroughly with freshly filtered running buffer (50 mM Tris-HCl, 150 mM NaCl, 0.005% Tween20, pH 7.5) at high flow rates. The known and characterized peptidoglycan glycosyltransferase inhibitor moenomycin<sup>24</sup> was used as positive control to analyze the interaction with PBP2. MOE complex, which is a mixture of moenomycins A, A12, C1, C3 and C4 (Cayman chemicals), was freshly dissolved in 100% dimethyl sulfoxide (DMSO) to a concentration of 10 mg mL<sup>-1</sup> (6.31 mM). CAO was freshly dissolved in deionized water to a concentration of 10 mg mL<sup>-1</sup> (4.24 mM). For the SPR measurements, the compounds were diluted in running buffer at the respective concentrations of 0.25  $\mu\text{M}$ -4  $\mu\text{M}$  for MOE and 0.5  $\mu\text{M}$ -32  $\mu\text{M}$  for COA. The interactions were investigated under constant conditions (40  $\mu\text{l min}^{-1}$  flow rate). Immobilization and data collection was performed at 25 °C. The direct binding assays were performed as a muticycle. Each cycle consisted of

10 min stabilization time, a 2.5 min injection and a dissociation phase of 30 min. Binding response (RU) was recorded continuously and presented as a sensorgram. Running buffer injections were used at the beginning of a run and in between cycles where higher concentrations of compounds were injected ( $\geq 4 \mu\text{M}$ ). CAO in a concentration of 8  $\mu\text{M}$  was injected in duplicate to monitor the reproducibility of the binding response. Different kinetic models were applied to the crude data and examined for consistency between crude data and the fit, but kinetic evaluation by fitting the data to a 1:1 Langmuir binding model with drifting baseline created the lowest deviation of data and fit (data not shown).

## ASSOCIATED CONTENT

### Supporting Information.

Supplemental figures and tables, experimental procedures, and protein purification protocols (PDF)

## AUTHOR INFORMATION

### Corresponding Author

\*tschneider@uni-bonn.de

### Author Contributions

All authors have given approval to the final version of the manuscript.

### Notes

The authors declare no competing financial interest.

## ACKNOWLEDGMENT

We thank M. Arts for her help with the antagonization assay, J. Siegl for assistance in the acquisition of SPR data, and Dr. V. Uzunova for helpful discussions. Funding was provided by the German Center for Infection Research (DZIF) and Fundación MEDINA.

## ABBREVIATIONS

CAO, cacaoidin; RiPPs, ribosomally synthesized and post-translationally modified peptides; Lan, lanthionine; MeLan, methylanthionine; D-Abu, D-aminobutyric acid, Dha, dehydroalanine; AviMeCys, S-[(Z)-2-aminovinyl-3-methyl]-D-cysteine; MRSA, methicillin resistant *Staphylococcus aureus*; PGN, peptidoglycan; LII<sub>PGN</sub>, undecaprenyl-pyrophosphate-MurNAc-pentapeptide-GlcNAc; C<sub>55</sub>P, undecaprenyl-phosphate; GTs, glycosyl transferases; TP, transpeptidase; MRS, mersacidin; LI<sub>PGN</sub>, undecaprenyl-pyrophosphate-MurNAc-pentapeptide; C<sub>55</sub>PP, undecaprenyl-pyrophosphate; LIII<sub>WTA</sub>, undecaprenyl-pyrophosphate-GlcNAc; CCCP, carbonyl cyanide m-chlorophenylhydrazide; PBP, penicillin binding protein; PBP2\_mutTP, PBP2 variant with a loss of function mutation in the transpeptidase domain; AB, antibiotic; SPR, surface plasmon resonance; HPLC, high-performance liquid chromatography.

## REFERENCES

(1) Essig, A.; Hofmann, D.; Münch, D.; Gayathri, S.; Künzler, M.; Kallio, P. T.; Sahl, H.-G.; Wider, G.; Schneider, T.; Aebi, M. Copsin, a Novel Peptide-based Fungal Antibiotic Interfering with the

Peptidoglycan Synthesis. *Journal of Biological Chemistry* **2014**, *289* (50), 34953–34964. DOI: 10.1074/jbc.m114.599878.

(2) Férir, G.; Petrova, M. I.; Andrei, G.; Huskens, D.; Hoorelbeke, B.; Snoeck, R.; Vanderleyden, J.; Balzarini, J.; Bartschek, S.; Brönstrup, M.; Süßmuth, R. D.; Schols, D.; Favoreel, H. The Lantibiotic Peptide Labyrinthopeptin A1 Demonstrates Broad Anti-HIV and Anti-HSV Activity with Potential for Microbicidal Applications. *PLoS ONE* **2013**, *8* (5), e64010. DOI: 10.1371/journal.pone.0064010.

(3) Arnison, P. G.; Bibb, M. J.; Bierbaum, G.; Bowers, A. A.; Bugni, T. S.; Bulaj, G.; Camarero, J. A.; Campopiano, D. J.; Challis, G. L.; Clardy, J.; Cotter, P. D.; Craik, D. J.; Dawson, M.; Dittmann, E.; Donadio, S.; Dorrestein, P. C.; Entian, K.-D.; Fischbach, M. A.; Garavelli, J. S.; Göransson, U.; Gruber, C. W.; Haft, D. H.; Hemscheidt, T. K.; Hertweck, C.; Hill, C.; Horswill, A. R.; Jaspars, M.; Kelly, W. L.; Klinman, J. P.; Kuipers, O. P.; Link, A. J.; Liu, W.; Marahiel, M. A.; Mitchell, D. A.; Moll, G. N.; Moore, B. S.; Müller, R.; Nair, S. K.; Nes, I. F.; Norris, G. E.; Olivera, B. M.; Onaka, H.; Patchett, M. L.; Piel, J.; Reaney, M. J. T.; Rebuffat, S.; Ross, R. P.; Sahl, H.-G.; Schmidt, E. W.; Selsted, M. E.; Severinov, K.; Shen, B.; Sivonen, K.; Smith, L.; Stein, T.; Süßmuth, R. D.; Tagg, J. R.; Tang, G.-L.; Truman, A. W.; Vederas, J. C.; Walsh, C. T.; Walton, J. D.; Wenzel, S. C.; Willey, J. M.; Wilfred A. van der Donk. Ribosomally synthesized and post-translationally modified peptide natural products: overview and recommendations for a universal nomenclature. *Nat. Prod. Rep.* **2013**, *30* (1), 108–160. DOI: 10.1039/c2np20085f.

(4) Ortega, M. A.; Wilfred A. van der Donk. New Insights into the Biosynthetic Logic of Ribosomally Synthesized and Post-translationally Modified Peptide Natural Products. *Cell Chemical Biology* **2016**, *23* (1), 31–44. DOI: 10.1016/j.chembiol.2015.11.012.

(5) Schnell, N.; Entian, K.-D.; Schneider, U.; Götz, F.; Zähler, H.; Kellner, R.; Jung, G. Prepeptide sequence of epidermin, a ribosomally synthesized antibiotic with four sulphide-rings. *Nature* **1988**, *333* (6170), 276–278.

(6) Dischinger, J.; Chipalu, S. B.; Bierbaum, G. Lantibiotics: Promising candidates for future applications in health care. *International Journal of Medical Microbiology* **2014**, *304* (1), 51–62. DOI: 10.1016/j.ijmm.2013.09.003.

(7) Montalbán-López, M.; Scott, T. A.; Ramesh, S.; Rahman, I. R.; van Heel, A. J.; Viel, J. H.; Bandarian, V.; Dittmann, E.; Genilloud, O.; Goto, Y.; Burgos, M. G.; Hill, C.; Kim, S.; Koehnke, J.; Latham, J. A.; Link, A. J.; Martínez, B.; Nair, S. K.; Nicolet, Y.; Rebuffat, S.; Sahl, H.-G.; Sareen, D.; Schmidt, E. W.; Schmitt, L.; Severinov, K.; Süßmuth, R. D.; Truman, A. W.; Wang, H.; Weng, J.-K.; van Wezel, G. P.; Zhang, Q.; Zhong, J.; Piel, J.; Mitchell, D. A.; Kuipers, O. P.; Wilfred A. van der Donk. New developments in RiPP discovery, enzymology and engineering. *Natural Product Reports* **2021**, *38* (1), 130–239. DOI: 10.1039/d0np00027b.

(8) Ortiz-López, F. J.; Carretero-Molina, D.; Sánchez-Hidalgo, M.; Martín, J.; González, I.; Román-Hurtado, F.; Cruz, M.; García-Fernández, S.; Reyes, F.; Deisinger, J. P.; Müller, A.; Schneider, T.; Genilloud, O. Cacaoidin, First Member of the New Lanthidin RiPP Family. *Angewandte Chemie International Edition* **2020**, *59* (31), 12654–12658. DOI: 10.1002/anie.202005187.

(9) Román-Hurtado, F.; Sánchez-Hidalgo, M.; Martópez, J.; Genilloud, O. Biosynthesis and Heterologous Expression of Cacaoidin, the First Member of the Lanthidin Family of RiPPs. *Antibiotics* **2021**, *10* (4), 403. DOI: 10.3390/antibiotics10040403.

(10) Sit, C. S.; Yoganathan, S.; Vederas, J. C. Biosynthesis of Aminovinyl-Cysteine-Containing Peptides and Its Application in the Production of Potential Drug Candidates. *Accounts of Chemical Research* **2011**, *44* (4), 261–268. DOI: 10.1021/ar1001395.

(11) Ma, S.; Zhang, Q. Linaridin natural products. *Natural Product Reports* **2020**, *37* (9), 1152–1163. DOI: 10.1039/c9np00074g.

(12) He, H.; Williamson, R. T.; Shen, B.; Graziani, E. I.; Yang, H. Y.; Sakya, S. M.; Petersen, P. J.; Carter, G. T. Mannopeptimycins, Novel

Antibacterial Glycopeptides from *Streptomyces hygrosopicus*, LL-AC98. *Journal of the American Chemical Society* **2002**, *124* (33), 9729–9736. DOI: 10.1021/ja020257s.

(13) Skaugen, M.; Nissen-Meyer, J.; Jung, G.; Stevanovic, S.; Sletten, K.; Inger, C.; Abildgaard, M.; Nes, I. F. In vivo conversion of L-serine to D-alanine in a ribosomally synthesized polypeptide. *The Journal of biological chemistry* **1994**, *269* (44), 27183–27185.

(14) Ryan, M. P.; Jack, R. W.; Josten, M.; Sahl, H. G.; Jung, G.; Ross, R. P.; Hill, C. Extensive post-translational modification, including serine to D-alanine conversion, in the two-component lantibiotic, lactacin 3147. *The Journal of biological chemistry* **1999**, *274* (53), 37544–37550. DOI: 10.1074/jbc.274.53.37544.

(15) Lohans, C. T.; Li, J. L.; Vederas, J. C. Structure and Biosynthesis of Carnolysin, a Homologue of Enterococcal Cytolysin with D-Amino Acids. *Journal of the American Chemical Society* **2014**, *136* (38), 13150–13153. DOI: 10.1021/ja5070813.

(16) Huo, L.; van der Donk, Wilfred A. Discovery and Characterization of Bicereucin, an Unusual D-Amino Acid-Containing Mixed Two-Component Lantibiotic. *Journal of the American Chemical Society* **2016**, *138* (16), 5254–5257. DOI: 10.1021/jacs.6b02513.

(17) Shang, Z.; Winter, J. M.; Kauffman, C. A.; Yang, I.; Fenical, W. Salinipeptins: Integrated Genomic and Chemical Approaches Reveal Unusual D-Amino Acid-Containing Ribosomally Synthesized and Post-Translationally Modified Peptides (RiPPs) from a Great Salt Lake *Streptomyces* sp. *ACS Chemical Biology* **2019**, *14* (3), 415–425. DOI: 10.1021/acscchembio.8b01058.

(18) Grein, F.; Schneider, T.; Sahl, H.-G. Docking on Lipid II\textemdashA Widespread Mechanism for Potent Bactericidal Activities of Antibiotic Peptides. *Journal of Molecular Biology* **2019**, *431* (18), 3520–3530. DOI: 10.1016/j.jmb.2019.05.014.

(19) Lovering, A. L.; Safadi, S. S.; Strynadka, N. C. J. Structural Perspective of Peptidoglycan Biosynthesis and Assembly. *Annual Review of Biochemistry* **2012**, *81* (1), 451–478. DOI: 10.1146/annurev-biochem-061809-112742.

(20) Müller, A.; Klöckner, A.; Schneider, T. Targeting a cell wall biosynthesis hot spot. *Natural Product Reports* **2017**, *34* (7), 909–932. DOI: 10.1039/c7np00012j.

(21) Strahl, H.; Hamoen, L. W. Membrane potential is important for bacterial cell division. *Proceedings of the National Academy of Sciences* **2010**, *107* (27), 12281–12286. DOI: 10.1073/pnas.1005485107.

(22) Brötz, H.; Bierbaum, G.; Reynolds, P. E.; Sahl, H.-G. The Lantibiotic Mersacidin Inhibits Peptidoglycan Biosynthesis at the Level of Transglycosylation. *European Journal of Biochemistry* **1997**, *246* (1), 193–199. DOI: 10.1111/j.1432-1033.1997.t01-1-00193.x.

(23) Derouaux, A.; Sauvage, E.; Terrak, M. Peptidoglycan Glycosyltransferase Substrate Mimics as Templates for the Design of New Antibacterial Drugs. *Frontiers in Immunology* **2013**, *4*. DOI: 10.3389/fimmu.2013.00078.

(24) Cheng, T.-J. R.; Sung, M.-T.; Liao, H.-Y.; Chang, Y.-F.; Chen, C.-W.; Huang, C.-Y.; Chou, L.-Y.; Wu, Y.-D.; Chen, Y.-H.; Cheng, Y.-S. E.; Wong, C.-H.; Ma, C.; Cheng, W.-C. Domain requirement of moenomycin binding to bifunctional transglycosylases and development of high-throughput discovery of antibiotics. *Proceedings of the National Academy of Sciences* **2008**, *105* (2), 431–436. DOI: 10.1073/pnas.0710868105.

(25) Stempera, K.; Vogel, S.; Buchynskyy, A.; Ayala, J. A.; Welzel, P. A surface plasmon resonance analysis of the interaction between the antibiotic moenomycin A and penicillin-binding protein 1b. *ChemBiochem: a European journal of chemical biology* **2002**, *3* (6), 559–565. DOI: 10.1002/1439-7633(20020603)3:6<559:AID-CBIC559>3.0.CO;2-#.

(26) Heaslet, H.; Shaw, B.; Mistry, A.; Miller, A. A. Characterization of the active site of *S. aureus* monofunctional glycosyltransferase (Mtg) by site-directed mutation and structural analysis of the protein complexed with moenomycin. *Journal of*

- Structural Biology* **2009**, *167* (2), 129–135. DOI: 10.1016/j.jsb.2009.04.010.
- (27) Lovering, A. L.; Castro, L. H. d.; Lim, D.; Strynadka, N. C. J. Structural Insight into the Transglycosylation Step of Bacterial Cell-Wall Biosynthesis. *Science* **2007**, *315* (5817), 1402–1405. DOI: 10.1126/science.1136611.
- (28) Gampe, C. M.; Tsukamoto, H.; Doud, E. H.; Walker, S.; Kahne, D. Tuning the Moenomycin Pharmacophore To Enable Discovery of Bacterial Cell Wall Synthesis Inhibitors. *Journal of the American Chemical Society* **2013**, *135* (10), 3776–3779. DOI: 10.1021/ja4000933.
- (29) Dumbre, S.; Derouaux, A.; Lescrinier, E.; Piette, A.; Joris, B.; Terrak, M.; Herdewijn, P. Synthesis of Modified Peptidoglycan Precursor Analogues for the Inhibition of Glycosyltransferase. *Journal of the American Chemical Society* **2012**, *134* (22), 9343–9351. DOI: 10.1021/ja302099u.
- (30) Baizman, E. R.; Branstrom, A. A.; Longley, C. B.; Allanson, N.; Sofia, M. J.; Gange, D.; Goldman, R. C. Antibacterial activity of synthetic analogues based on the disaccharide structure of moenomycin, an inhibitor of bacterial transglycosylase. *Microbiology (Reading, England)* **2000**, *146 Pt 12*, 3129–3140. DOI: 10.1099/00221287-146-12-3129.
- (31) Goldman, R. C.; Baizman, E. R.; Branstrom, A. A.; Longley, C. B. Differential antibacterial activity of moenomycin analogues on gram-positive bacteria. *Bioorganic & Medicinal Chemistry Letters* **2000**, *10* (20), 2251–2254. DOI: 10.1016/S0960-894X(00)00443-1.
- (32) Leimkuhler, C.; Chen, L.; Barrett, D.; Panzone, G.; Sun, B.; Falcone, B.; Oberthür, M.; Donadio, S.; Walker, S.; Kahne, D. Differential Inhibition of *Staphylococcus aureus* PBP2 by Glycopeptide Antibiotics. *Journal of the American Chemical Society* **2005**, *127* (10), 3250–3251. DOI: 10.1021/ja043849e.
- (33) Chen, L.; Walker, D.; Sun, B.; Hu, Y.; Walker, S.; Kahne, D. Vancomycin analogues active against vanA-resistant strains inhibit bacterial transglycosylase without binding substrate. *Proceedings of the National Academy of Sciences* **2003**, *100* (10), 5658–5663. DOI: 10.1073/pnas.0931492100.
- (34) Mesleh, M. F.; Rajaratnam, P.; Conrad, M.; Chandrasekaran, V.; Liu, C. M.; Pandya, B. A.; Hwang, Y. S.; Rye, P. T.; Muldoon, C.; Becker, B.; Zuegg, J.; Meutermaans, W.; Moy, T. I. Targeting Bacterial Cell Wall Peptidoglycan Synthesis by Inhibition of Glycosyltransferase Activity. *Chemical Biology & Drug Design* **2015**, *87* (2), 190–199. DOI: 10.1111/cbdd.12662.
- (35) Hoffmann, A.; Schneider, T.; Pag, U.; Sahl, H.-G. Localization and Functional Analysis of PepI, the Immunity Peptide of Pep5-Producing *Staphylococcus epidermidis* Strain 5. *Applied and Environmental Microbiology* **2004**, *70* (6), 3263–3271. DOI: 10.1128/aem.70.6.3263-3271.2004.
- (36) Radeck, J.; Gebhard, S.; Orchard, P. S.; Kirchner, M.; Bauer, S.; Mascher, T.; Fritz, G. Anatomy of the bacitracin resistance network in *Bacillus subtilis*. *Molecular Microbiology* **2016**, *100* (4), 607–620. DOI: 10.1111/mmi.13336.
- (37) Tan, S.; Ludwig, K. C.; Müller, A.; Schneider, T.; Nodwell, J. R. The Lasso Peptide Siamycin-I Targets Lipid II at the Gram-Positive Cell Surface. *ACS Chemical Biology* **2019**, *14* (5), 966–974. DOI: 10.1021/acscchembio.9b00157.
- (38) Münch, D.; Roemer, T.; Lee, S. H.; Engeser, M.; Sahl, H. G.; Schneider, T.; Peschel, A. Identification and in vitro Analysis of the GatD/MurT Enzyme-Complex Catalyzing Lipid II Amidation in *Staphylococcus aureus*. *PLoS Pathogens* **2012**, *8* (1), e1002509. DOI: 10.1371/journal.ppat.1002509.
- (39) Schneider, T.; Senn, M. M.; Berger-Bächli, B.; Tossi, A.; Sahl, H.-G.; Wiedemann, I. In vitro assembly of a complete, pentaglycine interpeptide bridge containing cell wall precursor (lipid II-Gly5) of *Staphylococcus aureus*. *Molecular Microbiology* **2004**, *53* (2), 675–685. DOI: 10.1111/j.1365-2958.2004.04149.x.
- (40) Rick, P. D.; Hubbard, G. L.; Kitaoka, M.; Nagaki, H.; Kinoshita, T.; Dowd, S.; Simplaceanu, V.; Ho, C. Characterization of the lipid-carrier involved in the synthesis of enterobacterial common antigen (ECA) and identification of a novel phosphoglyceride in a mutant of *Salmonella typhimurium* defective in ECA synthesis. *Glycobiology* **1998**, *8* (6), 557–567. DOI: 10.1093/glycob/8.6.557.
- (41) Murakami, K.; Fujimura, T.; Doi, M. Nucleotide sequence of the structural gene for the penicillin-binding protein 2 of *Staphylococcus aureus* and the presence of a homologous gene in other staphylococci. *FEMS Microbiology Letters* **1994**, *117* (2), 131–136. DOI: 10.1111/j.1574-6968.1994.tb06754.x.
- (42) Yao, X.; Lu, C.-D. A PBP 2 Mutant Devoid of the Transpeptidase Domain Abolishes Spermine *Staphylococcus aureus* Mu50. *Antimicrobial Agents and Chemotherapy* **2011**, *56* (1), 83–91. DOI: 10.1128/aac.05415-11.
- (43) Schneider, T.; Gries, K.; Josten, M.; Wiedemann, I.; Pelzer, S.; Labischinski, H.; Sahl, H.-G. The Lipopeptide Antibiotic Friulimicin B Inhibits Cell Wall Biosynthesis through Complex Formation with Bactoprenol Phosphate. *Antimicrobial Agents and Chemotherapy* **2009**, *53* (4), 1610–1618. DOI: 10.1128/aac.01040-08.
- (44) Johnsson, B.; Löfås, S.; Lindquist, G. Immobilization of Proteins to a Carboxymethyl-dextran-Modified Gold Surface for Biospecific Interaction Analysis in Surface Plasmon Resonance Sensors. *Analytical Biochemistry* **1991**, *198* (2), 268–277. DOI: 10.1016/0003-2697(91)90424-r.

## Supporting Information

### Dual targeting of the lanthidin antibiotic Cacaoidin

Julia P. Deisinger, Anna Müller, Francisco Javier Ortiz-López, Olga Genilloud, Tanja Schneider\*

\*To whom correspondence should be addressed: E-mail: [tschneider@uni-bonn.de](mailto:tschneider@uni-bonn.de)

Table S1. Antimicrobial activity of cacaoidin (CAO) assessed by determining the minimal inhibitory concentration (MIC) of CAO against selected strains. CAO activity remained unaltered in presence of 1.25 mM Ca<sup>2+</sup>.

Strain	MIC ( $\mu\text{g ml}^{-1}$ )
<i>S. simulans</i>	0.25
<i>S. aureus</i> SG511	2
<i>S. aureus</i> MRSA (MB5393)	0.25 <sup>1</sup>
<i>S. aureus</i> VISA (Mu50)	32
<i>Bacillus subtilis</i> 168	8
<i>Bacillus subtilis</i> HS17 MinD-GFP	2
<i>E. faecalis</i>	16
<i>E. faecalis</i> VRE (BM4223 pIP819)	8
<i>E. coli</i> MB5746	128

<sup>1</sup> Ortiz-López *et al.*, 2020 (DOI:10.1002/anie.202005187)



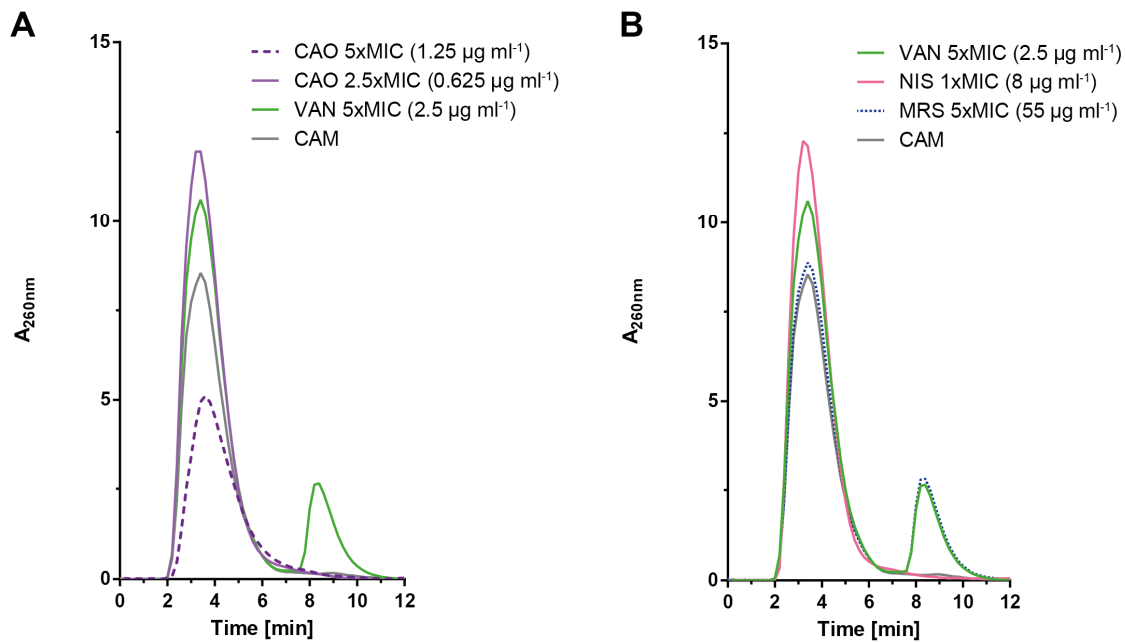


Figure S3. The accumulation of the soluble PGN precursor UDP-MurNac-pentapeptide (UDP-MurNac-pp) in the bacterial cytoplasm is frequently observed for antibiotics that block late steps of PGN biosynthesis e.g., vancomycin (VAN). *S. simulans* cells were treated with CAO and control antibiotics (respectively) and analyzed via HPLC. The accumulation of UDP-MurNac-pp is represented by the peak with a retention time of 8.5 min in the chromatograms (A, B). Treatment with CAO or with the translation inhibitor chloramphenicol (CAM, negative control, used to prevent the cellular stress response) did not result in accumulation of UDP-MurNac-pp (A), whereas treatment with VAN (A, positive control) and MRS, known to inhibit late stage PGN synthesis reactions, resulted in accumulation of UDP-MurNac-pp (B). Although nisin (NIS) binds to  $\text{LII}_{\text{PGN}}$  and thereby interrupts PGN production, no accumulation of UDP-MurNac-pp is observed. Nisin forms target-mediated pores in cellular membranes which is most likely causative for this finding.

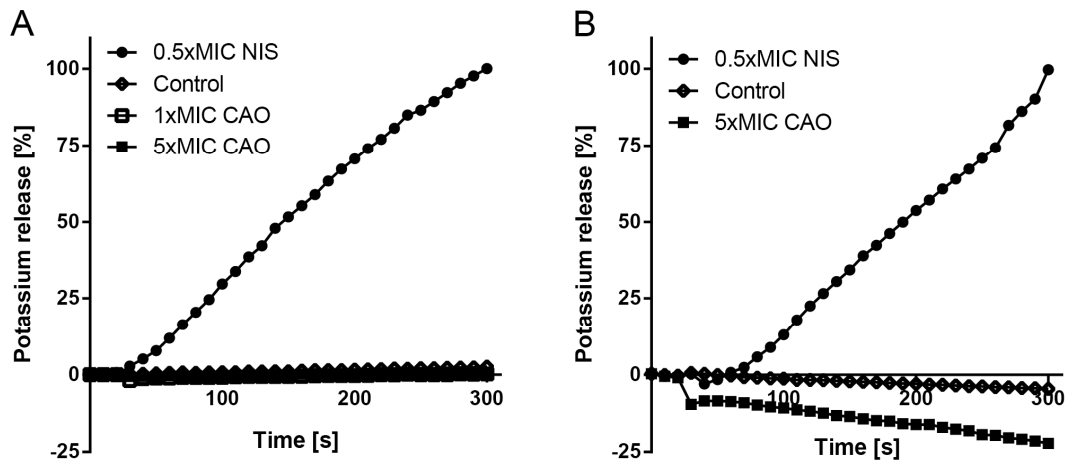


Figure S4. Potassium release from *S. simulans* cells is induced by NIS treatment, but not observed after addition of CAO, neither in absence (A) nor in presence of 10 mM glucose (B). 0.5xMIC NIS corresponds to a concentration of 1  $\mu\text{M}$ . 1xMIC and 5xMIC CAO correspond to concentrations of 0.2  $\mu\text{M}$  and 1  $\mu\text{M}$  respectively.



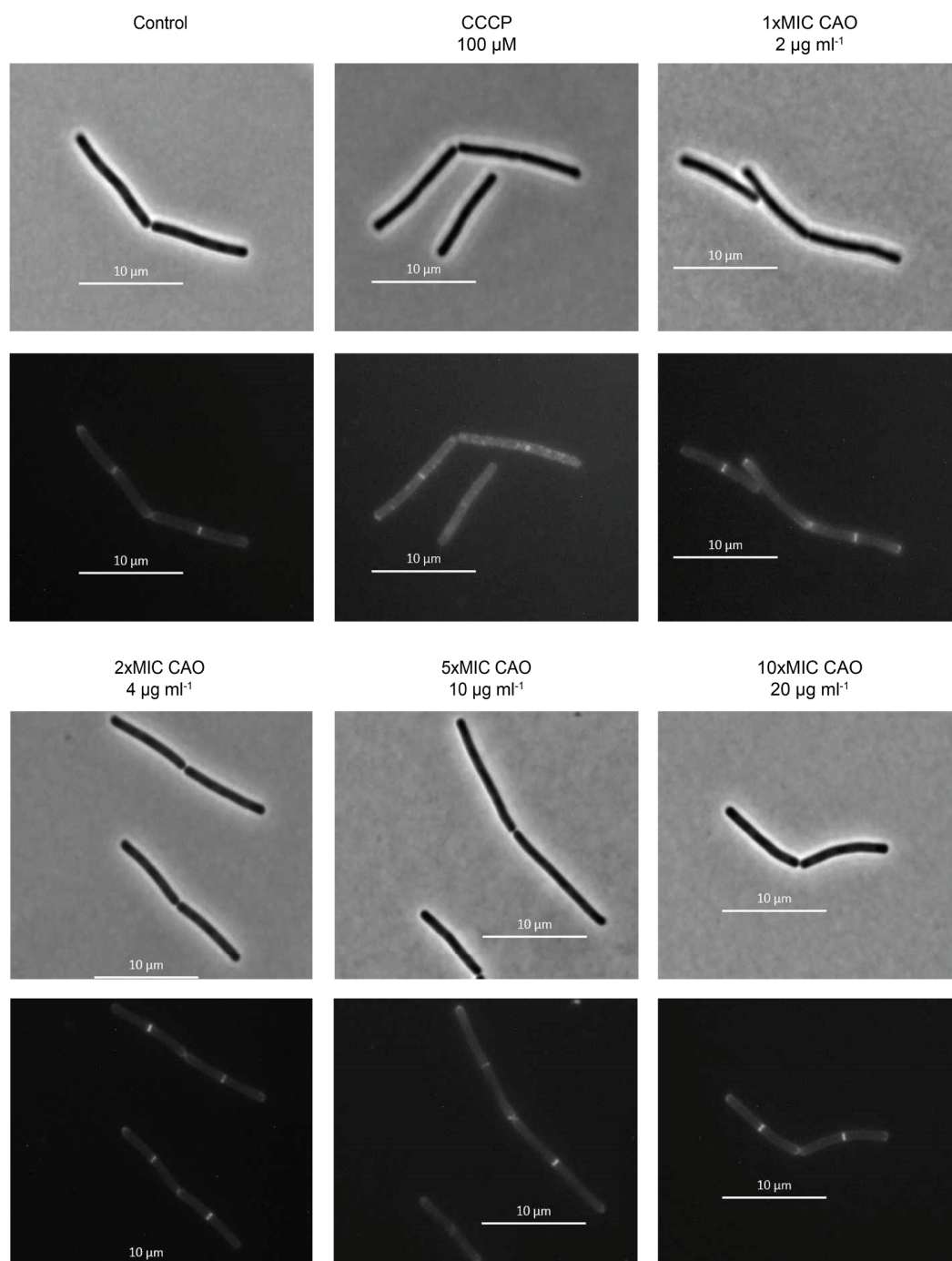


Figure S5. Localization pattern of MinD-GFP indicative for alterations of the membrane potential in response to treatment with CAO or the ionophore carbonyl cyanide m-chlorophenylhydrazone (CCCP). CCCP dissipates the transmembrane electric potential resulting in dispersed localization of MinD, whereas MinD clusters are localized at newly formed cell poles to prevent formation of new division sites in control cells. Images of cells in early exponential growth phase were taken after 2 min incubation with CCCP or CAO. Fluorescence microscopy was performed on a Zeiss Axio Observer Z1 microscope with a 100x objective. The images were acquired with ZEN software (Zen2) and processed with Adobe Illustrator CS5.

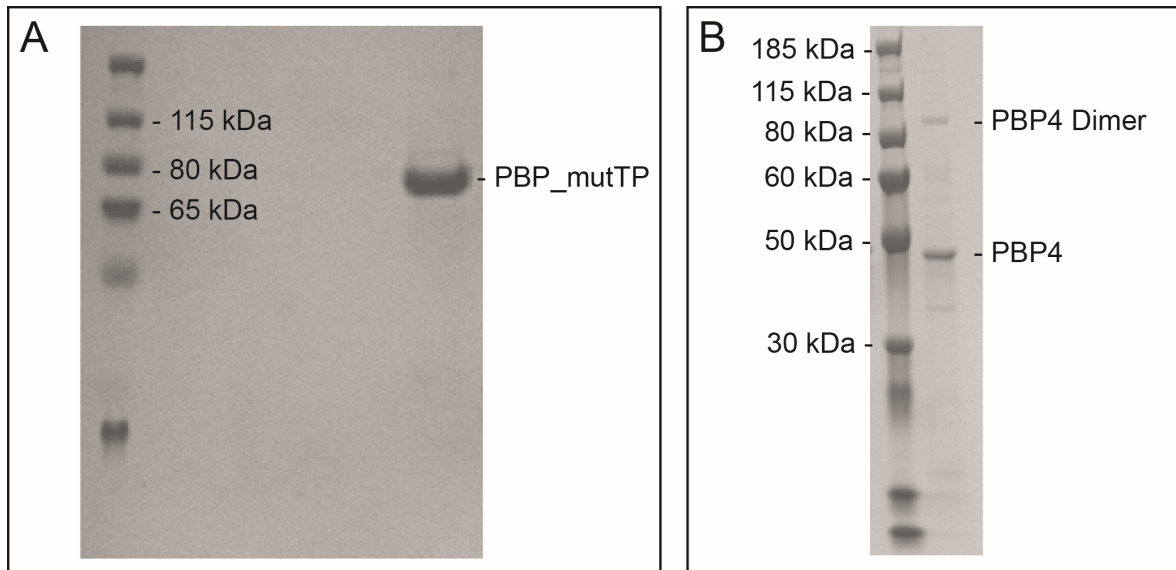


Figure S6. SDS-PAGE analysis of purified *S. aureus* penicillin binding proteins 2 with an amino acid mutation (S398G) in the active site of the transpeptidase domain (PBP2\_mutTP; A) and 4 (PBP4) (B). The expected molecular weights of the recombinant proteins including their affinity tags are 81159 Da for PBP2\_mutTP and 49040 Da for PBP4.

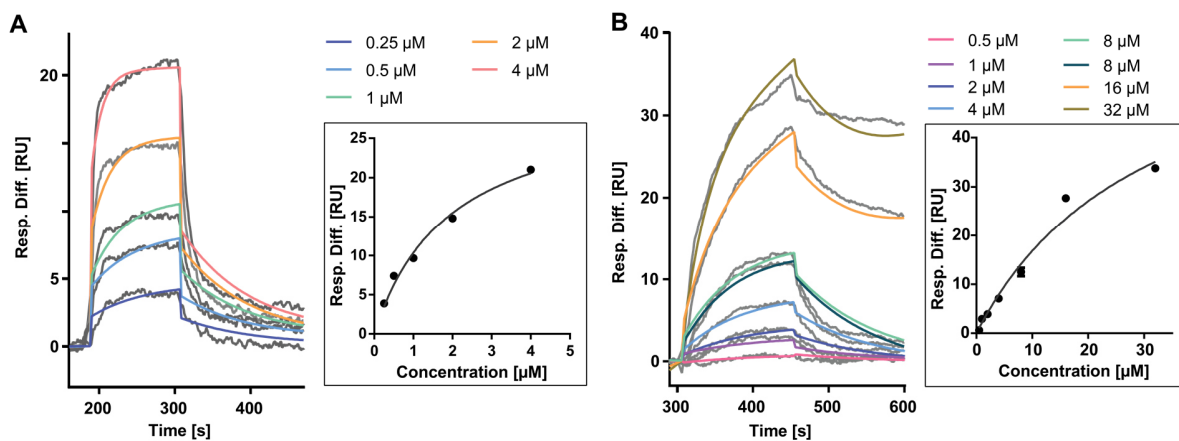


Figure S7. SPR analysis of moenomycin (MOE) (A) and CAO (B) binding to immobilized full-length *S. aureus* PBP2\_mutTP. Kinetic rate constants were determined by fitting the best equations (colored curves) describing a 1:1 interaction model with drifting baseline to the experimental data (grey curves). Insets show the binding levels plotted against analyte concentration and the course of the graphs visualize that a plateau was not reached.

Table S2. Overview of the kinetic and affinity data obtained by analysis of the binding of CAO and MOE to full length *S. aureus* PBP2\_mutTP. Different kinetic models were used to fit the crude data and examined for consistency between the crude data and the fit. Association rate constant ( $k_a$ ), dissociation rate constant ( $k_d$ ), equilibrium constant ( $K_D$ ), half-life of ligand-analyte complex ( $t_{1/2}$ ).

Analyte	CAO		MOE	
1:1 binding with drifting baseline	$k_a$ ( $M^{-1} s^{-1}$ ) = 595 $k_d$ ( $s^{-1}$ ) = 9.55e-3	$K_D$ = 16.1 $\mu M$ $t_{1/2}$ = 12 min	$k_a$ ( $M^{-1} s^{-1}$ ) = 1.44e4 $k_d$ ( $s^{-1}$ ) = 0.0105	$K_D$ = 0.728 $\mu M$ $t_{1/2}$ = 1.1 min
Bivalent analyte	$k_{a1}$ ( $M^{-1} s^{-1}$ ) = 306 $k_{d1}$ ( $s^{-1}$ ) = 0.031 $k_{a2}$ ( $M^{-1} s^{-1}$ ) = 1.84e-5 $k_{d2}$ ( $s^{-1}$ ) = 3.46e-4	$t_{1/2}$ = 0.4 min $t_{1/2}$ = 33.4 min	* $k_{a1}$ ( $M^{-1} s^{-1}$ ) = 4.64e3 $k_{d1}$ ( $s^{-1}$ ) = 0.0135 $k_{a2}$ ( $M^{-1} s^{-1}$ ) = 2.3e-4 $k_{d2}$ ( $s^{-1}$ ) = 1.14e-5	$t_{1/2}$ = 0.9 min $t_{1/2}$ = 16.9 h
Heterogeneous ligand- Parallel reactions	$k_{a1}$ ( $M^{-1} s^{-1}$ ) = 1.07e3 $k_{d1}$ ( $s^{-1}$ ) = 6.83e-4 $k_{a2}$ ( $M^{-1} s^{-1}$ ) = 146 $k_{d2}$ ( $s^{-1}$ ) = 0.0342	$t_{1/2}$ = 16.9 min $t_{1/2}$ = 0.3 min	* $k_{a1}$ ( $M^{-1} s^{-1}$ ) = 1.77e4 $k_{d1}$ ( $s^{-1}$ ) = 8.07e-5 $k_{a2}$ ( $M^{-1} s^{-1}$ ) = 1.06e4 $k_{d2}$ ( $s^{-1}$ ) = 7.2e-4	$t_{1/2}$ = 2.4 h $t_{1/2}$ = 16 min
Two state reaction	$k_{a1}$ ( $M^{-1} s^{-1}$ ) = 581 $k_{d1}$ ( $s^{-1}$ ) = 0.0316 $k_{a2}$ ( $M^{-1} s^{-1}$ ) = 1.45e-3 $k_{d2}$ ( $s^{-1}$ ) = 6.48e-4	$K_D$ = 16.75 $\mu M$ $t_{1/2}$ = 0.4 min $t_{1/2}$ = 17.8 min	* $k_{a1}$ ( $M^{-1} s^{-1}$ ) = 1.07e4 $k_{d1}$ ( $s^{-1}$ ) = 9.59e-6 $k_{a2}$ ( $M^{-1} s^{-1}$ ) = 7.82e-4 $k_{d2}$ ( $s^{-1}$ ) = 1e-5	$K_D$ = 0.01 nM $t_{1/2}$ = 20 h $t_{1/2}$ = 19.3 h
Steady state affinity		$K_D$ = 31.2 $\mu M$		$K_D$ = 1.95 $\mu M$

kinetic and affinity analysis was performed including all tested analyte concentrations

\* kinetic analysis was performed for the concentration range 0.5-8  $\mu M$

## REFERENCES

(1) Ortiz-López, F. J.; Carretero-Molina, D.; Sánchez-Hidalgo, M.; Martín, J.; González, I.; Román-Hurtado, F.; Cruz, M.; García-Fernández, S.; Reyes, F.; Deisinger, J. P.; Müller, A.; Schneider, T.; Genilloud, O. Cacaoidin, First Member of the New Lanthidin RiPP Family. *Angewandte Chemie International Edition* **2020**, *59* (31), 12654–12658. DOI: 10.1002/anie.202005187.

## 5 Discussion

"Understanding is a prerequisite for action."

Antimicrobial resistance represents a substantial threat to global health. It is an endemic condition that increases slowly and constantly causing a high and chronic burden of disease worldwide. Most of the estimated burden of infections with antibiotic-resistant bacteria was attributed to hospitals and other health care settings (Cassini et al., 2019). Even though resistance is a naturally occurring phenomenon, the widespread inappropriate use of antibiotics in humans and animals accelerates the process of both the emergence and the spread of resistance. As a result, a growing number of infections become harder or even impossible to treat. Among these, infections caused by MRSA, VISA, and VRSA (**v**ancomycin-**i**ntermediate and **r**esistant *S. aureus*) strains, causing thousands of deaths worldwide. Thus, *S. aureus* was ranked as a high priority pathogen by the WHO. Antibiotic stewardship interventions, which are aimed at optimizing prescribing practices and infection prevention are necessary to reduce the burden of these infections (Cassini et al., 2019). Furthermore, alternative treatment options for patients infected with resistant pathogens, especially the ones which have comorbidities or are otherwise vulnerable (infants and elderly population) are required. First and foremost, in order to overcome antibiotic resistance we need to promote the discovery of new antibiotics with unprecedented mode of action and resistance-breaking properties. Additionally, novel drug targets need to be identified combined with better understanding of their biological context and cellular function.

**The attachment of glycopolymers to the cell wall during staphylococcal cell envelope biogenesis as a putative drug target.** The staphylococcal cell wall is functionalized with glycopolymers, such as WTA and capsular polysaccharide. These structures play important roles in cell division, maintenance of the cell shape and structural integrity and were shown to significantly contribute to pathogenicity e.g., invasion of host immunity, adherence, cellular uptake, and biofilm formation. Accordingly, antibiotic interference with WTA and capsule synthesis reactions, is accompanied by alterations of the cell surface, such as the modulation of the cell surface charge caused by the absence of anionic WTA polymers. These changes can have a dramatic impact on the organism, such as cell division defects, increased autolysis, and increased antibiotic susceptibility. Furthermore, WTA- and/or capsule-deficient (or depleted) strains display altered interactions with the host immune system e.g., capsule-deficient strains display increased opsonization. The understanding of the underlying molecular processes is a prerequisite for rational antiinfective development and could further provide the essential foundation for deciphering the cellular consequences that arise from the interference with respective synthesis pathways. Accordingly, an assessment of these possible consequences could help to evaluate the potency of inhibitors or to take appropriate precautions to improve their efficacy. The essential role of bacterial cell walls makes the cell wall biosynthesis an attractive drug target pathway.

The cell wall of *S. aureus* contains a variety of glycopolymers, among which WTA and the capsular polysaccharides are covalently linked to PGN. The underlying biosynthesis reactions generating WTA and PGN have been extensively studied by now, but so far, investigations of capsule biosynthesis have been limited to the reconstitution of individual steps. Therefore it is not surprising, that many inhibitors of PGN synthesis (Chapter 2.7) and several late-stage WTA synthesis and WTA export inhibitors have already been identified (reviewed by Sewell and Brown (2013)), while there is only little information on potential capsule biosynthesis inhibitors. The final ligation step of cell wall glycopolymers to the PGN backbone is catalyzed by representatives of the conserved LCP family, which represent promising new targets for antibiotics. Biochemical analyses as well as the identification of donor and acceptor substrates allows for the development of screening approaches in search for inhibitors.

LCP proteins typically hydrolyze the pyrophosphate linkage between the lipid-carrier and the reducing-end sugar of the cell wall glycopolymer (GP) donor substrate, and subsequently attach the phosphoryl-sugar unit to either MurNAc (e.g. in *S. aureus*; Figure 18, relevant residues highlighted in pink) or GlcNAc (e.g. in *S. agalactiae*, Figure 9) residues of the PGN backbone. The nature of the linkage (if known) is in most organisms a phosphodiester bond. As part of this work *S. aureus* LcpC was demonstrated to process all three capsular lipid precursors, and catalyze the attachment of the respective (phosphoryl-)mono-, di-, and trisaccharide capsular glycopolymer to the PGN precursor lipid II. Furthermore, the ligation product was shown to be a sufficient substrate for PGN polymerization catalyzed by PBP2.

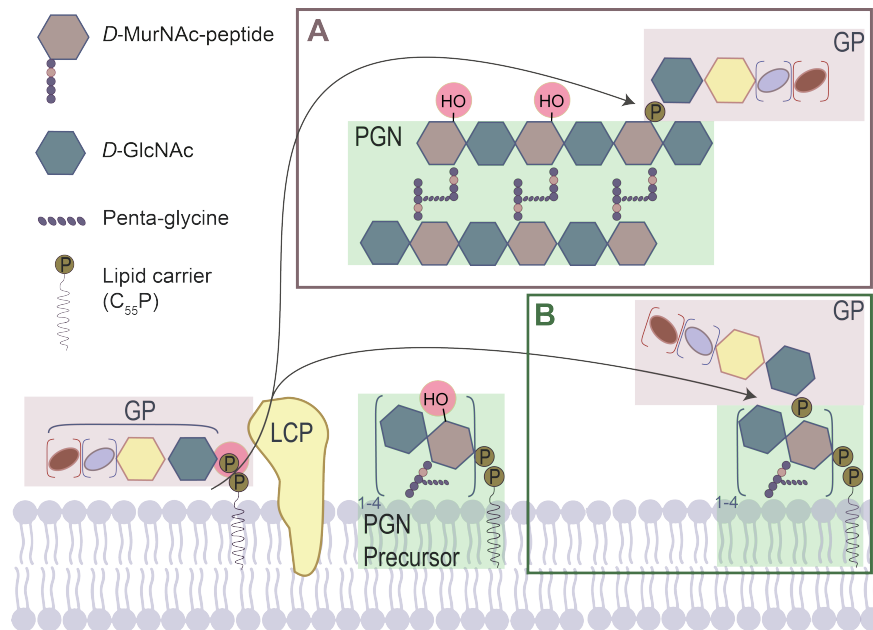


Figure 18: Model for the attachment of cell wall glycopolymers (GPs) to mature PGN (A) or to a lipid-bound PGN precursor (lipid II or nascent PGN; B) catalyzed by LCP enzymes in *S. aureus*. The displayed reaction is shown with a schematic GP structure, comprising either the WTA D-ManNAc-D-GlcNAc or a capsular polysaccharides (e.g., D-FucNAc) linkage unit. The ligation reaction involves the  $\beta$ -phosphorous of the GP donor substrate and the C<sub>6</sub>-hydroxyl group of the PGN MurNAc unit (highlighted in pink).

From a catalytic perspective open questions arise regarding:

- (i) The nature of the acceptor substrate
- (ii) The enzyme stringency versus promiscuity for the glycopolymer's PGN linkage unit (WTA D-ManNAc-D-GlcNAc versus CP5 capsular polysaccharides D-FucNAc linker)

These question will be discussed in the following.

#### (i) The nature of the acceptor substrate

Given the periplasmic location of the LCP catalytic domains, the most plausible physiological PGN acceptor substrates include mature PGN (cross-linked), nascent PGN (uncrosslinked), and/or lipid II. Since the extension of the catalytic LCP domain is relatively short, the enzymes may utilize only nascent PGN, lipid II, or if at all, the first few layers of the mature PGN sacculus. **The role of the PGN maturation stage for its function as an acceptor substrate.** In the present work, lipid II was shown to be a sufficient acceptor substrate for the attachment of the

(phosphoryl-)mono-, di-, and trisaccharide CP5 capsular glycopolymer catalyzed by *S. aureus* LcpC. However, contradictory *in vitro* evidences were published each postulating another 'maturation stage' of the natural PGN acceptor substrate of the LCP reaction. Gale et al. (2017) demonstrated that the transfer of WTA glycopolymers to insoluble (crosslinked) PGN was catalyzed by all of the three *B. subtilis* LCP enzymes (TagT, TagU, and TagV), while ligase activity of *S. aureus* LCPs could not be reconstituted in this *in vitro* setup or with this substrates. It should be noted that the authors were not able to ascertain LCP activity due to their inability to determine the amount of attached polymers in relation to the number of free C(6) MurNAc hydroxyl groups across the PGN substrate. Therefore, respective results should be regarded critically. On the other hand, Schaefer et al. (2018) established a method to generate crosslinked *S. aureus* PGN of defined composition and excluded crosslinked PGN as the physiological acceptor substrate (demonstrated for *S. aureus* LcpB and *B. subtilis* TagT). All attempts of other groups to reconstitute the transfer of WTA glycopolymers to lipid II by LCPs (*S. aureus* LcpA or *B. subtilis*) failed until now (Gale et al., 2017; Schaefer et al., 2017). Contrary to these findings, work enclosed in this thesis revealed that *S. aureus* LcpC efficiently catalyzes the attachment to lipid II. Potential explanations could be that they used truncated enzyme constructs lacking the predicted transmembrane helix and did not reconstitute a membrane interface during activity analysis, which might be required for the function and correct positioning of these proteins. Indeed, protein-lipid interactions are known to play crucial roles for structural and functional integrity of membrane proteins. **Relevance of the polyisoprenoid portion of the cell wall glycopolymer precursor.** All substrates used in this work comprised the natural undecaprenyl (C<sub>55</sub>P)-lipid portion which might be required to completely assess LCP activity. Schaefer et al. (2017) used shortened synthetic lipid II variants (heptaprenyl (C<sub>35</sub>)-, or tetraprenyl (C<sub>20</sub>)-lipid) as acceptor molecules and hexaprenyl (C<sub>35</sub>)-bound WTA intermediates as donor substrates. Although some of the results of Gale and coworkers should be evaluated critically, they demonstrated that the substitution of the undecaprenyl-lipid moiety of the WTA intermediate with tridecane abolished LCP activity, indicating that the polyisoprenoid moiety of the donor molecule is required for catalysis. The geometric configuration and number of isoprene units of the synthetic hexaprenyl-coupled WTA intermediates used by Schaefer et al. (2017, 2018) differ from the physiological undecaprenyl-coupled substrate, but they are identical if one focuses on the first three isoprene units. Since LCPs were shown to process hexaprenyl-coupled WTA intermediates, it was proposed that the key interaction between LCP enzymes and the donor substrate occur in the region of the polyisoprenoid lipid proximal to the pyrophosphate moiety.

**The sequence of events of the final steps in *S. aureus* cell wall assembly.** Final events of the *S. aureus* cell wall assembly were proposed to take place as follows, uncross-linked PGN is first made, than modified with WTA, and subsequently cross-linked (Schaefer et al., 2018). Furthermore, Schaefer et al. (2017) pointed out that neither lipid II nor the nascent PGN tetrasaccharide (lipid II-[MurNAc(-stem peptide)-GlcNAc]<sub>2</sub>), even though the latter was demonstrated to serve as a sufficient substrate for WTA transfer *in vitro*, pose physiologically relevant substrates for LCPs, since the respective ligation products could not be processed by PGN glycosyltransferases. The authors reasoned that the C<sub>6</sub>-hydroxyl group of the MurNAc unit of Lipid II (site for GP attachment) points directly into the active site of the monofunctional *S. aureus* glycosyltransferase SgtB, and that the presence of a large glycopolymer at this position would prevent substrate binding and thus block PGN polymerization. Since the active site cleft of SgtB and other PGN glycosyltransferases are quite long, MurNAc C<sub>6</sub>-hydroxyl groups would not be exposed until at least a PGN hexasaccharide (lipid II-[MurNAc(-stem peptide)-GlcNAc]<sub>6</sub>) has formed. Interestingly, while Walker and coworkers ruled out lipid II ligation products as suitable substrates for PGN glycosyltransferases, work enclosed in this thesis demonstrated that lipid II ligation products were efficiently processed by the *S. aureus* glycosyltransferase PBP2. An observation that could revise the sequence of final cell wall assembly events in *S. aureus* as follows, the PGN precursor lipid II is modified with glycopolymers, and subsequently polymerized and cross-linked.

## (ii) Enzyme stringency versus promiscuity for the glycopolymer's PGN linkage unit

The question arises why lipid II is a suitable acceptor substrate for the transfer of capsule saccharides catalyzed by LcpC *in vitro* (this work), while it was not for the transfer of WTA saccharides catalyzed by LcpA (Schaefer et al., 2017). Potential reasons for this observation are I) lipid II can only serve as an acceptor substrate for WTA ligation if appropriate reaction conditions are provided, including a full length protein, native substrates, and mimicry of a membrane interface, or II) the structural differences between the acceptor binding sites of LcpA and LcpC are decisive for substrate specificity.

**Identification of potential structural features causal for differential substrate specificity of LcpA and LcpC.** Until now attempts to crystallize *S. aureus* LcpC failed, but comparative analysis of known LCP 3D structures could help to identify key residues essential for substrate binding, substrate specificity as well as catalysis, and further provide the basis for mutational analysis. Phyre2 models were generated based on LcpCs amino acid sequence and the crystal structures of LcpA in complex with octaprenyl-pyrophosphate-GlcNAc and the apo (ligand-free) TagU (Figure 19). Both of the created LcpC models matched the respective protein template with a confidence of 100%. A confidence of >90% suggests that LcpC actually adopts the overall fold of the template structure and that the protein core is modeled at high accuracy (2-4 Å root-mean-square deviation (RMSD) from the native, true structure). The likely accuracy of a model is defined by the percentage identity (% i.d.) between a sequence and the template. In case of extremely high accuracy models this number is above 30-40%, which is the case for LcpC modeled to TagU with a % i.d. of 43%. However, even at lower sequence identities, models can still be very useful if the confidence is really high, which applies for LcpC modeled to LcpA with a % i.d. of 25%. Considering the high similarity between LcpA and TagT (3.22 Å over 216 residues), the former shows a relatively low overall structural similarity to TagU with a RMSD of 5.6 Å for 222 C $\alpha$  atom<sup>14</sup> pairs, indicating regions of significant difference. Comparison of just the highly conserved active-site residues shows a closer matched RMSD of 2.02 Å for 10 C $\alpha$  atom pairs<sup>15</sup>.

Complementary to this, the overall comparison of C $\alpha$  pairs of active site residues of LcpA and other LCPs revealed the highest similarity to TagT complexed with C<sub>30</sub>-PP-GlcNAc-ManNAc with a RMSD of 0.85 Å (F. K. K. Li et al., 2020). The comparison of the LcpA and TagU structures can provide information about which domains of LcpC have been modeled with a higher degree of certainty and which should be considered with caution. When comparing the active site surrounding regions of LcpA and TagU, the most prominent differences occur in region B (red), where LcpA displays a large loop and TagU contains a double-stranded  $\beta$ -sheet (see Figure 20A). Unfortunately, the resolution of region D (green) and especially region A (blue) is poor for the TagU protein crystal. Presumably, the electropositive entrance of the binding pocket becomes harder to observe when the guanidiny groups of the conserved active site arginines are not localized by a pyrophosphate group (F. K. K. Li et al., 2020). This is the case for apo TagU, whereas the regions were resolved for LcpA in complex with C<sub>40</sub>-PP-GlcNAc. For further evaluations, the structures of LcpC modeled to either TagU (LcpC<sub>U</sub>) or LcpA (LcpC<sub>A</sub>) via Phyre2 were superimposed (Figure 19B). The most prominent differences occur again in region B (red), with the presence versus the absence of a double-stranded  $\beta$ -sheet, but also in region A (blue), with a short  $\alpha$ -helix versus a flexible loop, for LcpC<sub>U</sub> and LcpC<sub>A</sub>, respectively. The active site residues of LcpA (R99, blue; R216; R122; R227; R218 and D224, pink; D101) surrounding the pyrophosphate moiety of the C<sub>40</sub>-PP-GlcNAc are conserved in LcpC (Figure 20A). As one can see the orientation of the modeled LcpC residues is similar to the ones of LcpA, except for residues R208 (pink) and D92 in the LcpC<sub>A</sub> structure which face into the complete opposite direction. A shallow pocket was described for LcpA to accommodate the *N*-acetyl group of the donor substrate's saccharide moiety. The residues which outline this pocket show only a low conservation in the LcpC structure (Figure 20B) and the putative binding pockets of the LcpC models

<sup>14</sup>First carbon atom attached to a functional group, in case of amino acids the central carbon atom represents the C $\alpha$  atom. Protein backbones are structurally compared by their C $\alpha$  atom coordinates.

<sup>15</sup>The 10 highly conserved active-site residues of LcpA are D77, R90, D92, R113, D114, K127, R206, R208, R216, R219

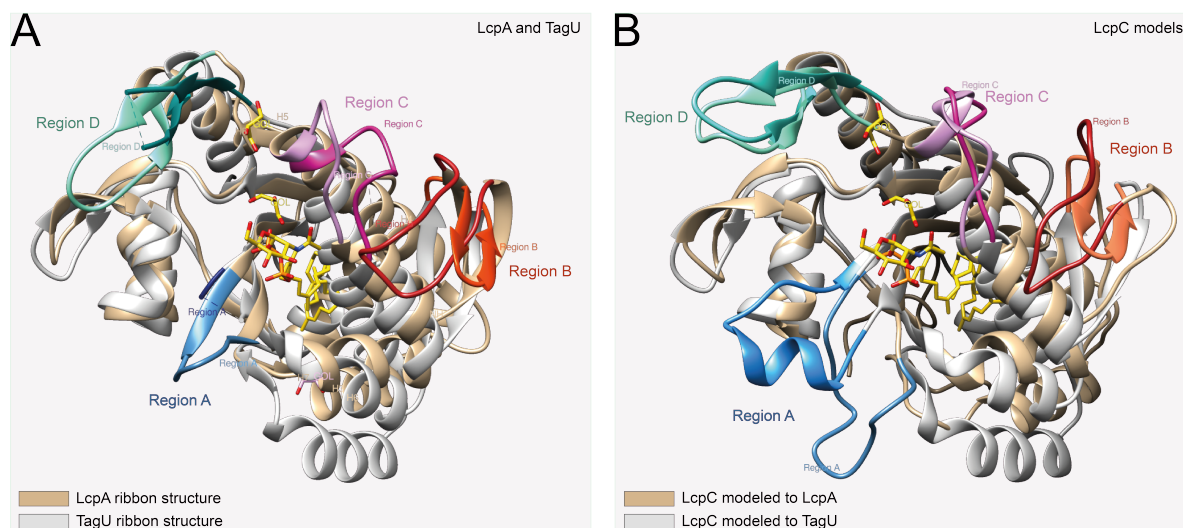


Figure 19: Structural comparison of *S. aureus* LcpA, *B. subtilis* TagU protein crystals, and respective models of *S. aureus* LcpC. Superimposed ribbon structures of *S. aureus* LcpA in complex with C<sub>40</sub>-PP-GlcNAc (yellow) and *B. subtilis* apo TagU (A). The active site of LcpA is surrounded by four regions, designated A (blue), B (red), C (pink), and D (green) and respective regions were highlighted in the other structures accordingly. Based on the protein crystals of *S. aureus* LcpA and *B. subtilis* TagU, high confidence structure models were generated for *S. aureus* LcpC via the Phyre<sup>2</sup> software and superimposed (B). Heteroatoms of the ligand are colored by type oxygen, red; phosphorus, orange; nitrogen, blue.

generally appear longer. The physiological substrates (WTAs and capsular polysaccharides) of LCPs would contain further saccharide moieties extending from the *N*-acetyl group. Low conservation of this region in addition to the observation that the position of the saccharide moiety is mainly stabilized by hydrophobic and van der Waals interactions (F. K. K. Li et al., 2020) could indicate a certain flexibility of that region towards different lipid-linked pyrophosphate saccharide substrates. Since LCPs are commonly found complexed with pyrophosphorylated lipids the interactions between protein residues and the lipid as well as the pyrophosphoryl part, might be sufficient for binding. This observation might also explain their (semi)redundant roles in attachment of different anionic polymer precursors *in vitro* and *in vivo* (single *lcp* gene knock outs can be compensated by other LCP enzymes). The PGN binding groove of LCPs is proposed to be outlined by regions A (blue), C (pink), and D (green, Figure 19 and 20C, F. K. K. Li et al. (2020)). The conserved arginine residue R99 of LcpA (corresponding to R90 in LcpC) is proposed to be involved in PGN binding and expected to shift in the event of binding a divalent cation (Schaefer et al., 2018). The orientation of this arginine is similar in LcpA and LcpC<sub>A</sub> (Figure 20C), while in case of LcpC<sub>U</sub> the orientation of the arginine residue is different. However, this part of the predicted structure could be inaccurate since this region was not resolved for the TagU template. The region D (green) is often found enriched with aromatic residues and its importance for PGN binding was already highlighted in chapter 2.6. Interactions between the protein residues and the PGN saccharides are presumably aided through carbohydrate-aromatic interactions. While region D of LcpA contains only one aromatic residue (Y297, green), LcpC contains three (Y294, Y295, and F296; turquoise; Figure 20C)). The higher amount of aromatic residues in the putative PGN binding site (highlighted with a pink circle) might facilitate a stronger interaction and, therefore, enable the binding of the lipid II disaccharide by LcpC. Interestingly, the other residues proposed to facilitate binding of PGN in LcpA are D123, K135, and N137, are, except for the latter, conserved in LcpC (D114 and K127, respectively), and could also enable binding of PGN from the predicted spatial orientation of the residues. Overall the LcpC<sub>A</sub> model might allow more reliable predictions than the LcpC<sub>U</sub> model, due to the superior resolution



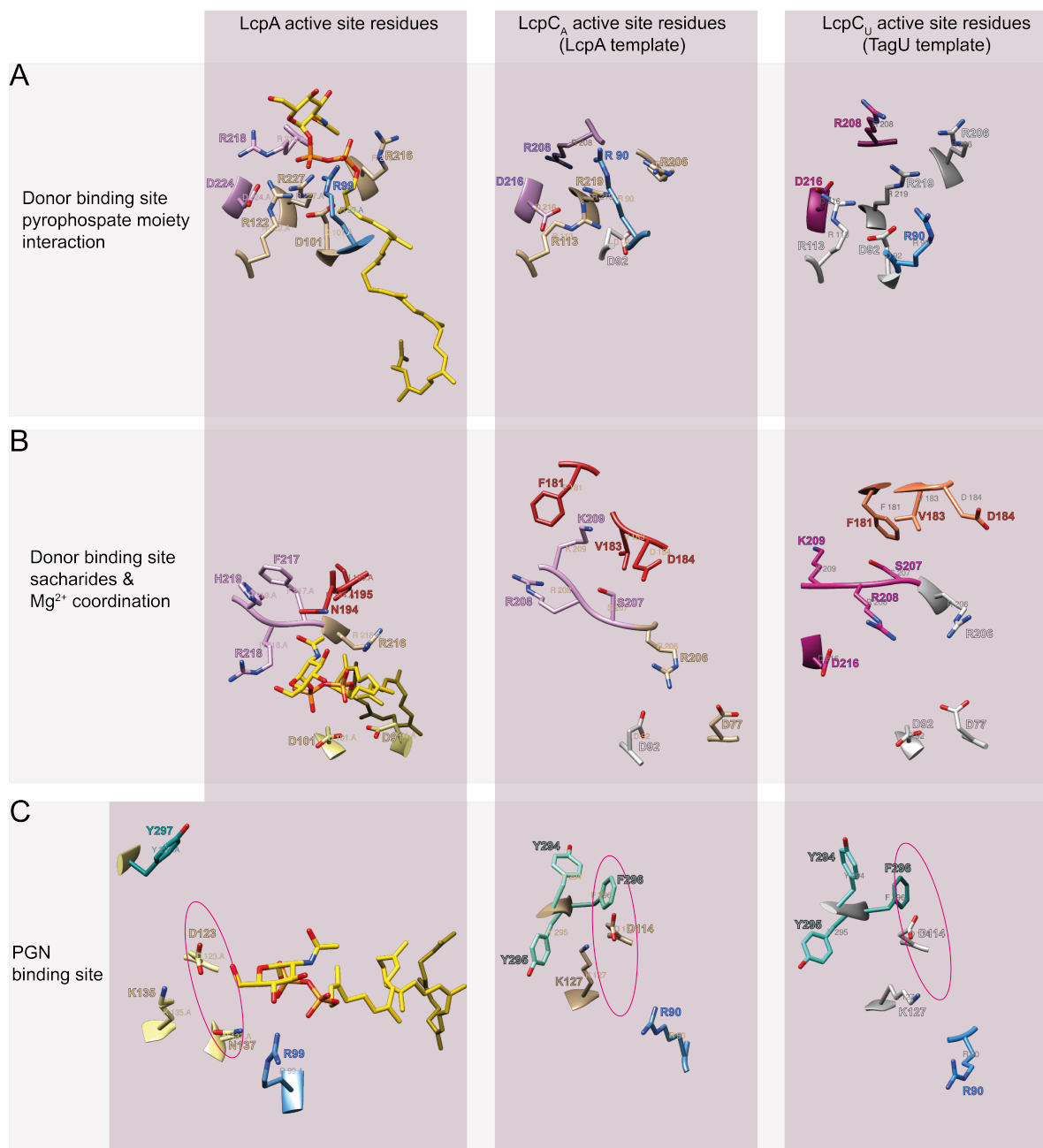


Figure 20: Evaluation of the putative structure and active site of *S. aureus* LcpC. High confidence models were generated using the amino acid sequence of LcpC and the protein crystals of *S. aureus* LcpA in complex with C<sub>40</sub>-PP-GlcNAc and *B. subtilis* apo TagU via the Phyre2 software. Selected active site residues of LcpA, LcpC modeled to either LcpA (LcpC<sub>A</sub>) or TagU (LcpC<sub>U</sub>) are displayed in the columns from left to right. The 'putative' active site residues involved in binding of the pyrophosphate moiety of the donor substrate (A), the saccharide moiety of the donor substrate (B), and the PGN acceptor substrate (C) are depicted as sticks. Pink circles indicate the putative location of the saccharide moiety of the PGN substrate.

of the active site of the LcpA template structure, the observation that structure rearrangements within the TagU protein crystal resulted in the collapse of the lipid-binding site, and the fact that there is more mechanistic data available for LcpA.

**The substrate preference of LcpC might be facilitated by membrane activator, phosphodiesterase and putative polysaccharide co-polymerase CapA1.** Ligand-bound LCP crystals have not yet been able to clearly show how the PGN precursor lipid II is discriminated from the WTA intermediate within the substrate binding site. One hypothesis is that the presence of the stem peptide sterically prevents binding of lipid II to the LCP donor substrate binding site. The substrate preference might also be facilitated by another enzyme that delivers the lipid-bound cell wall glycopolymer intermediate and returns C<sub>55</sub>-P to the membrane for further synthesis cycles. CapA1 represents a potential candidate for this role in *S. aureus*, since it was demonstrated to enhance LcpC's activity, indicating cooperative function of these enzymes. Of note, LCPs also cleave lipid-bound glycopolymers by themselves. The current hypotheses suggest a multifaceted role for CapA1, not only as part of the CapAB BY-kinase complex in the regulation of enzymes involved in polysaccharide synthesis by reversible protein phosphorylation, but also by cooperative interaction with LcpC to modulate the attachment of capsular glycopolymers. Further, CapA1 belongs to the polysaccharide co-polymerase (PCP) family, suggested to interact with cell wall machineries dedicated to the export, polymerization, and modal length determination of extracellular polysaccharides. Sequence comparison and 3D predictions via Phyre2 revealed a high structural similarity of CapA1 to the *E. coli* co-polymerase WzzB, with 87% of the CapA1 sequence being modeled with 100% confidence to WzzB (193 of CapA1 residues corresponding to 87% coverage), despite an overall low sequence identity of 14%. WzzB is one out of three components of the Wzy-dependent polysaccharide biosynthesis pathway, in which O-antigen or enterobacterial common antigen polymers of gram negative bacteria are synthesized at the inner membrane. The other two integral membrane proteins comprise the flippase Wzx (the *S. aureus* Wzx-like flippase is Cap5K), that flips the lipid-bound oligosaccharides from the inner to the outer leaflet, and the polymerase Wzy (the *S. aureus* homolog is Cap5J), that polymerizes the oligosaccharides into longer polysaccharide chains (Stähle & Widmalm, 2019; Wiseman, Nitharwal, Widmalm, & Högbom, 2021). WzzB was demonstrated to modulate the length of the growing polysaccharide chain (Kalynych, Ruan, Valvano, & Cygler, 2011; Kalynych, Yao, Magee, & Cygler, 2012) and crystal structure analysis shows it (homo)oligomerizes into a unique bell-shaped structure (Figure 21A) composed of eight identical protomers (Figure 21D) that form a circular octameric supercomplex (Figure 21E). The periplasmic base and linker region, the transmembrane (TM) domain, and  $\alpha$ -helix  $\alpha 0$  of WzzB (Figure 21B) were suggested to mainly play a structural role in the correct protein folding, in the interaction with Wzy, and the C<sub>55</sub>-PP-linked O-antigen, and in stabilizing of the Wzy-dependent supercomplex and are conserved in the CapA1 model (Figure 21B and C). CapA1 also contains many of the conserved residues of the PCP family of proteins, proposed to fulfill important roles for correct positioning, stabilization, and activity of the super complex, such as K31 (K16 or K19 in CapA1), P293 (P169 in CapA1), K294 (K170 in CapA1), and the GXXXG motif (GAFFLG in CapA1). On the other hand, the long periplasmic upper part of WzzB (light-green) containing  $\alpha$ -helices  $\alpha 6$ -8, as well as the L4 loop (yellow, Figure 21B and D) is missing in CapA1. The hollow L4 loop, located on the inside of the cavity (Figure 21E), is conserved in most PCPs and is required for chain length determination of the growing polysaccharide and synthesis of long polysaccharide chains (Kalynych et al., 2011, 2012; Wiseman et al., 2021). According to docking studies, the eight central L4 loops might create a pore that could accommodate a single polysaccharide and Wiseman et al. (2021) suggested that once the growing polysaccharide reaches the top of the periplasmic domain, it is captured by the L4 loops, which somehow stabilize the association with Wzz and allows continues elongation of the polymer. The WzzB structure supports the hypothesis that the Wzy polymerase and Wzz co-polymerase must work in close contact in order to modulate growing polysaccharide chain length.

It is very likely that also CapA1 monomers form an octameric structure, since many of the structure determining residues of the PCP protein family are conserved in CapA1, suggesting that it could adopt a similar overall fold as WzzB, except for the upper part of the periplasmic domain. Furthermore, the crystal structure of a CapAB chimera, comprised of the cytoplasmic tyrosine kinase CapB2 and the C-terminal activator domain of its cognate transmembrane modulator CapA1

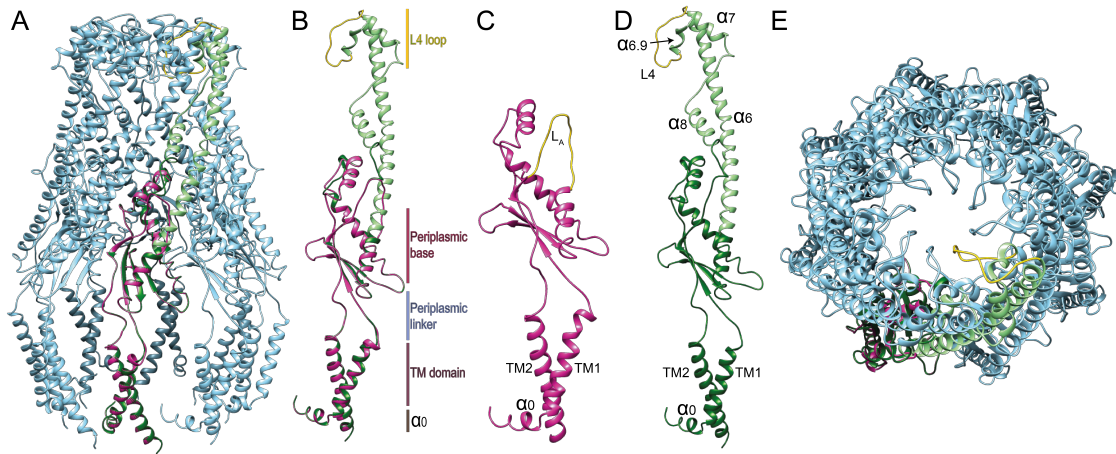


Figure 21: Structural comparison of a high confidence *S. aureus* CapA1 model with the template crystal structure of the circular octameric co-polymerase WzzB complex, which is a component of the Wzy-dependent lipopolysaccharide biosynthesis pathway in *E. coli*. A, Side view of the full-length octameric WzzB complex (light blue) with the periplasmic side at the top and the cytoplasmic side at the bottom. Alignment of the CapA1 model (highlighted in pink) and a single WzzB protomer (template structure, displayed in green). B, Isolated and superimposed structures of the single WzzB protomer (green) and the CapA1 model (pink). Prominent structures are highlighted and labeled. Comparison of the CapA1 model (C) and WzzB protomer (D), shows that the  $\alpha_0$ , the transmembrane (TM) domains and the periplasmic linker display high structural similarity, whereas the long periplasmic upper part of WzzB (light-green) containing  $\alpha$ -helices  $\alpha_6$ -8, as well as the conserved L4 loop (yellow) of the polysaccharide co-polymerase family is missing in CapA1. In contrast, CapA1 displays a loop ( $L_A$ , yellow) at that position. E, Top view of the circular octameric WzzB complex looking down from the periplasmic domain. The highly flexible L4 loops located at center of the complex are suggested to create a pore at the top of the periplasmic domain, which could accommodate and stabilize single polysaccharides and enable continued elongation.

(residues 197-222 of Cap5A1 linked to residues 1 to 215 of CapB2), reveals a ring-shaped octameric conformation. This arrangement was demonstrated to allow intramolecular autophosphorylation of the subunits before dissociation of the cytoplasmic kinase domains (Olivares-Illana et al., 2008). F. K. K. Li et al. (2020) observed the formation of decameric LcpC, although truncated protein variants which lacked the transmembrane domain were used. The direct interaction of LcpC and CapA1 oligomers might facilitate the transport of lipid-linked WTA/CP from the membrane to the hydrophobic pocket of LCP enzymes. In addition to the putative structural features of CapA1, that suggest a cooperative interaction with LcpC, CapA1 was further demonstrated to have a novel and unexpected hydrolase function. This hydrolase function is most likely situated within the periplasmic part of the protein. In direct comparison to WzzB the upper periplasmic part of the CapA1 model is replaced by another structure, referred to as  $L_A$  loop (yellow, Figure 21C and, for a close up, 22B), and it is tempting to narrow the location of additional hydrolase function down to this region. CapA1 catalyzes the cleavage of the pyrophosphate linkage of the WTA and CP5 C<sub>55</sub>-PP-coupled glycopolymer precursors, preferentially over lipid II, and might govern the correct localization of the capsule synthesis machinery, thereby integrating the precursor transport and capsule polymerization. This ability of CapA1 was suggested to provide a rescue mechanism against toxic dead end accumulation of lipid bound cell wall intermediates in a triple  $\Delta lcp$  knockout strain. Interestingly, although CapA1 was shown to cleave lipid-linked WTA precursors *in vitro*, its activity appears to be insufficient to compensate the lethal effects of late stage WTA inhibition *in vivo* (S. Brown, Maria, & Walker, 2013). Presumably, the catalytic site of CapA1 phosphodiesterase activity is extracellular, so CapA1 has no access to the cytoplasmic intermediates of the WTA

pathway and, therefore, cannot relieve growth-inhibitory attributes of inhibitors or lethal gene deletion in the WTA synthesis cluster. Despite a high sequence and structural similarity of CapA1 (encoded within the *cap5* operon) to the CapA2 paralog (encoded outside the *cap* operon, in close proximity to the *ica* operon; Figure 22), the latter was unable to hydrolyze pyrophosphate linkages. The most prominent differences in the modeled CapA1 and CapA2 structures occur in the positioning of the  $L_A$  loop, which is enlarged and appears to be more flexible in the case of CapA1, suggesting the loop is relevant for the hydrolase function. In addition to the findings that CapA2 is able to sense the extracellular polysaccharides PNAG and CP5, which results in decreased activation of the CapB2 kinase, while CapA1 is not, it is tempting to assume they sense different signals and pose different physiological significance.

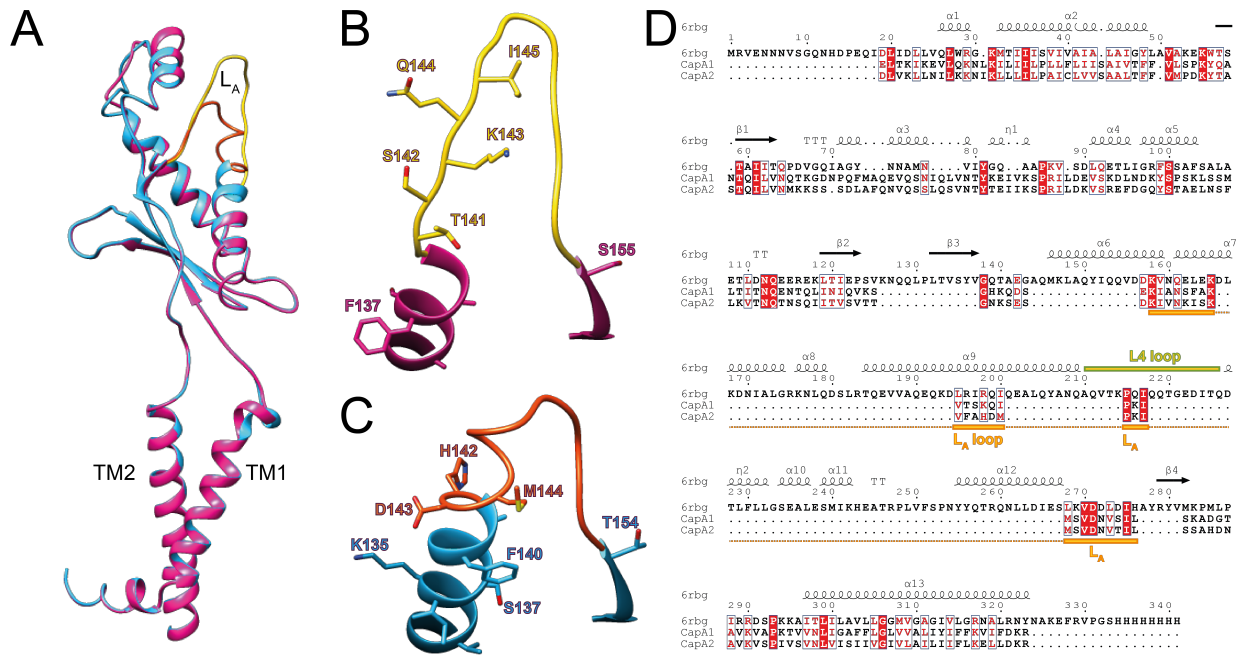


Figure 22: Sequence and structure comparison of *S. aureus* CapA1 and CapA2 modeled to a single *E. coli* WzzB protomer. A, The superimposed CapA1 (pink) and CapA2 (blue) models display a high similarity, except for the  $L_A$  loop region (yellow and orange, respectively). Close up of the  $L_A$  loop structures of CapA1 (B) and CapA2 (C), where non-conserved residues are depicted as sticks. D, Sequence alignment of WzzB (6rbg, PDB accession number), CapA1 and CapA2. Sequence similarities are highlighted and secondary structure elements of the WzzB template are displayed.

### Novel versus validated drug targets

In a recent study by F. Li et al. (2020), the role of LcpC, which was found to be overexpressed in a *S. aureus* COL adapted to high levels of oxacillin, was observed and LcpC was demonstrated to contribute to antimicrobial resistance and pathogenicity. The deletion of *lcpC* showed increased sensitivity to  $\beta$ -lactams in VISA, MRSA and MSSA strain backgrounds, and consequently, displayed decreased pathogenicity in the host (F. Li et al., 2020). The LcpC protein functions at the interface of two highly interlinked cellular processes, i.e. PGN and capsular polysaccharide synthesis (and to some extent also WTA). Although *S. aureus* LCPs were attributed to possess functional redundancy, the absence of LcpC was shown to cause severe morphological changes, characterized by deviant cell shapes and hollowed cell envelopes. The morphological defects, probably caused by impairing cell envelope biosynthesis, were especially pronounced in the  $\Delta lcpC$  *S. aureus* Mu50 VISA strain. Furthermore, LcpC deficiency caused attenuation in pathogenicity in a mouse septic shock model with oxacillin treatments. Therefore, LcpC appears particularly suitable as an effective target for drug

development, since it has a confirmed role in the pathophysiology of *S. aureus* infections. However, the understanding of the underlying molecular mechanism of the LCP reaction and its *in vitro* reconstitution provides the foundation for future screening approaches, as well as crystallographic analysis, computational modeling, and binding kinetics, and future analysis of potential interaction partners.

History showed that the selection of putative new targets alone is not the most expedient approach for drug discovery. Although, the exploitation of new drug targets poses several advantages, such as limited cross-resistance with existing therapeutics, a target's presence alone is not always sufficient to ensure the desired spectrum of a drug. The efficacy of a drug can be hampered by e.g. permeability issues and efflux systems, especially in gram negatives, not to mention pharmacokinetics or aspects of human physiology. In fact, the amount of appropriate molecular structures that are targeted by commonly used antibiotic therapeutics is limited and, with regard to this, an era of genomic approaches to search for novel unexploited targets began in the 1990s. It turned out that such target-based approaches were unproductive. The rising difficulties were subject to many reviews and reports (Chopra, 2012; Gwynn, Portnoy, Rittenhouse, & Payne, 2010; Payne, Gwynn, Holmes, & Pompliano, 2006; Silver, 2011; Tommasi, Brown, Walkup, Manchester, & Miller, 2015), but the major obstacles were the rapid development of resistance towards single enzyme targeting drugs and the insufficient target accessibility for the inhibitor (D. G. Brown, May-Dracka, Gagnon, & Tommasi, 2014; Silver, 2011; Tommasi et al., 2015). A thorough understanding of the cellular routes and functions is a prerequisite for the identification of suitable antibacterial targets and of vital importance for the development of novel antibiotics. According to the multitarget hypothesis, the essence of most successful systemic monotherapeutic agents is the interference in multiple gene and pathway products and causal for a low level of endogenous single-step resistance (Brötz-Oesterhelt & Brunner, 2008; Silver, 2007, 2016; Silver & Bostian, 1993). Monotherapeutic treatment of antibacterials targeting only single essential enzymes frequently results in the development of single-step resistance *in vitro* and in the clinic environment, with few exceptions (i.e., fosfomycin), while the major type of clinical resistance towards multiple target agents is caused by horizontal gene transfer. Most multi-targeting antibiotics have nonprotein targets like the ribosomal RNA, cell wall synthesis intermediates or membranes. The few classes of antibiotics with proteinous targets, where similar observations could be made, are the  $\beta$ -lactams and the fluoroquinolones, which are known to target multiple enzymes. The observations made with the focus on the discovery of novel target structures have demonstrated the indispensability and value of the classical and validated target structures, such as lipid II and PBPs, which are essential for PGN synthesis and cell viability. Therefore, new therapeutics that attack the classical validated targets should also be sought using novel chemical structures (Lange, Locher, Wyss, & Then, 2007; Payne et al., 2006; Silver, 2016). To increase the success of novel-target based drug discovery, the propensity of single enzyme inhibitors to rapidly select for resistance is a potential problem that must be considered. LCPs represent enzymatic targets and *S. aureus* contains three LCP homologs that show some degree of functional redundancy. In accordance with the multi-target hypothesis, resistance development towards LCP-targeting drugs could be hampered by the fact that all three enzyme targets would need to be mutated. If LCP inhibitors alone might not have the desired long-lasting antimicrobial effect, it might be effective in synergy with other antimicrobial agents, such as  $\beta$ -lactams. The advantage of a combinatory treatment would be that this form of therapy could re-sensitize resistant strains, as in the case of a LcpC deficient MRSA strain, which showed increased sensitivity towards  $\beta$ -lactams (F. Li et al., 2020). Inhibition of LCPs would interfere with capsule formation and anchoring of wall teichoic acid glycopolymers, unmask the bacterial surface, and could facilitate recognition by the innate immune system as well as antibody binding (Rasko & Sperandio, 2010).

There are numerous target identification strategies, but all are based on two principles either the targeted discovery or target deconvolution. In the first case potential targets are identified (such as LCP enzymes), compounds are subsequently screened for binding to these targets, and further analyzed if they elicit the desired effect. In the case of target deconvolution an efficacious drug with

desired activity is already in hand and target identification takes place retrospectively. There is no requirement to know the molecular target of a drug for its approval, because major concerns primarily apply to the safety and efficacy of a drug. Accordingly, there are a number of approved drugs for which the mechanism of action is (or was by the time of approval) unknown, such as the last resort antibiotic daptomycin. However, knowing the molecular targets of an antibiotic has several advantages, that greatly facilitates the drug development process, because it enables e.g. the rational design of derivatives and new molecules to improve potency and safety profiles.

### Cacaoidin, first-in-class lantibiotic interfering with validated drug target structures

CAO was discovered from, culture extracts of *S. cacaoi* screened for antimicrobial activity. The extracts showed potent activity against *S. aureus* MRSA strains and other gram positive pathogens and CAO was identified to be the bioactive compound. Therefore, target deconvolution was initiated for CAO, which was particularly interesting due to the unique structural features of the compound. This work demonstrated that CAO binds to the PGN building block lipid II, a feature commonly reported for other representatives of the lanthipeptide family and additionally interacts directly with the *S. aureus* PGN transglycosylases PBP2 and SgtB, a property that has been primarily attributed the natural product family of moenomycins so far. The interference with PGN synthesis by direct interaction with lipid II and binding of the catalyzing transglycosylase both represent validated target structures of successful antibiotics. It would further be interesting to decipher how the unique structural features of CAO contribute to its dual mode of action and antibiotic activity and if the two functions can be structurally dissected. CAO is an amphiphilic glycolanthipeptide containing mainly hydrophobic amino acids and a unique disaccharide moiety. Two sulfured bridges (NMe<sub>2</sub>Lan and AviMeCys) are located one at each extreme of the molecule. Besides one tertiary amine, which is a functional group of the NMe<sub>2</sub>Lan residue, no other ionizable groups are present in the molecule. At pH 7.5 or lower, the major CAO species (probably >98%) will be the +1 charged ones, due to the presence of the tertiary amine (pK<sub>a</sub> is around 9.5-10.5). All of these features facilitate the solubility of CAO in organic solvents as well as in water.

**CAO-lipid II binding depends on interactions with the phosphate-sugar moiety of the PGN precursor.** The high content of hydrophobic amino acids in CAO suggests that an interaction between lipid II and CAO is mainly hydrophobically driven, and could possibly also aid to the anchoring of CAO to the membrane. On the other hand, the weakly charged dimethylated N-terminus of CAO (+1, at physiological pH or lower) could interact with the pyrophosphate linkage of lipid II. Structural information on lipid II-binding lantibiotics revealed that the pyrophosphate moiety in lipid II and the conserved ring motifs in nisin-type and mersacidin-type lanthipeptides are the primary interaction sites (Hsu et al., 2003, 2004; Medeiros-Silva et al., 2018). In the case of nisin, the amino protons of the N-terminal rings A and B directly bind lipid II at the pyrophosphate group via hydrogen bonds. The mersacidin-lipid II binding motif comprises an essential Glu residue within an Abu-X-Glu-Ala amino acid conformation (Figure 17), where Ca<sup>2+</sup> ions are thought to bridge the Glu side chain to the negatively charged pyrophosphate moiety of lipid II (Böttiger, Schneider, Martínez, Sahl, & Wiedemann, 2009; Hsu et al., 2003). Accordingly, the activities of mersacidin and related lantibiotics, which are either negatively charged or carry no net charge, are often enhanced by the presence of divalent cations (Böttiger et al., 2009). Furthermore, achieving an overall positive net charge could also facilitate the interaction with bacterial membranes. The conserved ring motifs of nisin- and mersacidin-type lantibiotics (Böttiger et al., 2009) are absent in CAO and CAO activity was found to be completely independent of the presence of divalent cations. Antagonization experiments, in which different undecaprenyl-containing cell wall intermediates were tested for their ability to antagonize CAOs antimicrobial activity, showed that the undecaprenyl-phosphate moiety of lipid II alone is not sufficient for CAO binding and further involves the first sugar residue of cell wall lipid intermediates. The disaccharide moiety as well as the two aromatic amino acids (Tyr and Trp)

of CAO might also be involved in the interaction with lipid II, i.e. via carbohydrate-carbohydrate and carbohydrate-aromatic interactions, reported for the recognition of saccharides by proteins (Asensio, Ardá, Cañada, & Jiménez-Barbero, 2012; Hudson et al., 2015).

**Structural aspects of moenomycin GT inhibitors might provide insight on the CAO-GT interaction.** Besides binding to lipid II, CAO was shown to interact with the *S. aureus* PGN glycosyltransferases (GTs) PBP2 and SgtB. We proposed that CAOs disaccharide moiety could function as a lipid II-disaccharide mimic and therefore represent a key feature for the binding of GTs. The only known natural products specifically inhibiting GTs are members of the moenomycin family (Goldman, Baizman, Branstrom, & Longley, 2000; Ostash & Walker, 2005, 2010; Welzel, 2005). Moenomycins bind to the catalytic site of GTs. In order to elucidate the mode of action of CAO, we assume that the catalytic site might be blocked in a similar fashion. Therefore the structure and potential key residues for an interaction were compared. Moenomycins mimic the  $\beta$ -1,4-linked MurNAc-GlcNAc-chain of lipid II and, thus, compete with the natural transglycosylase substrate. Moenomycin A (MOE) is the founding member of the moenomycin family and is comprised of a pentasaccharide (ring nomenclature B-F) with a C25 isoprene chain attached to the reducing sugar F via a phosphoglycerate unit on one end and a cyclopentenone (ring A) on the other. Crystal structure analysis of MOE bound to GTs (both PBP2 and SgtB) revealed the engagement of hydrogen bonds between catalytically essential amino acid residues of the active site and the oligosaccharide part of MOE (Gampe, Tsukamoto, Doud, Walker, & Kahne, 2013; Heaslet, Shaw, Mistry, & Miller, 2009; Lovering, de Castro, Lim, & Strynadka, 2007). MOE competes for the GT donor site with the elongating glycan chain (Derouaux, Sauvage, & Terrak, 2013).

PBP2 and SgtB both belong to the PGN glycosyltransferase protein family GT51, which are membrane bound murein polymerases and contain five signature motifs (I to V, or according to Punekar et al. (2018) additionally motif 0, motif IVa and motif IVb), which comprise residues for lipid II binding and catalysis (Figure 23A). PBP2 has two putative catalytic glutamic acid residues E114 and E171, which are conserved in SgtB (Lovering et al., 2007).

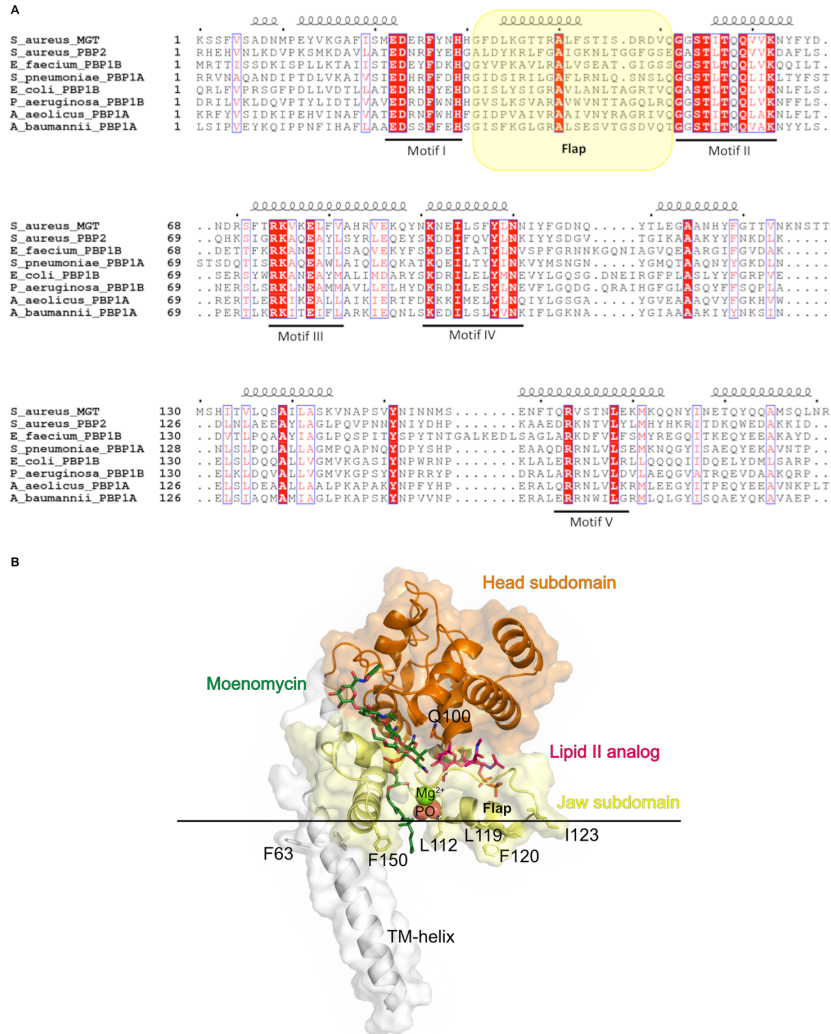


Figure 23: (A) Multiple sequence alignment of peptidoglycan GT domains in mono- and bifunctional (class A PBPs) glycosyltransferases. The pale yellow background indicates the protruding dynamic ‘flap’ region in the jaw subdomain. Conserved residues are shown in white on red background, and conservative substitutions are in red. Secondary structure of *S. aureus* monofunctional glycosyltransferase (SaMGT, also referred to as SgtB) is indicated above the alignment, and sequence motifs of the GT domain are indicated below the alignment. (B) Overall structure of ligand-bound SaMGT (SgtB). Model was made by superimposing and merging PDB ID codes 3HZS and 3VMT. The TM-helix is colored gray and the jaw subdomain and the head subdomain are colored pale yellow and orange respectively. MOE<sub>DON</sub> (green) in the donor site and lipid II analog (pink) in the acceptor site are shown as sticks. Magnesium and phosphate ions are shown as spheres. The residues located at the water-membrane interface are shown as sticks, labeled and colored by atom-type. Figure by Punekar et al. (2018).

Since PBP2 is a bifunctional PBP it possesses an additional TP domain, which is separated from the GT domain by a short linker. Crystal structure analysis shows that the GT51 domain has an  $\alpha$ -helical fold and is composed of two segments, a large globular “head region”, which is next to the linker and contains the first putative catalytic residue E114, and a small “jaw” region closer to the membrane, and containing the second active-site residue E171 (Lovering et al., 2007). The hydrophobic base of the jaw region is inferred to be involved in substrate recognition. Co-crystallization of PBP2 with MOE showed that binding occurred in the cleft between the head and jaw region, by mimicking the  $\beta$ 1,4 linkages of those of the growing glycan-chain donor. Despite being a monofunctional enzyme



the GT domain of SgtB adopts the similar fold (Figure 23B) as in PBP2 and binds MOE in the donor binding site (binding site of the growing sugar strand, Heaslet et al. (2009)). Furthermore, Punekar and coworkers (2018) could show an additional MOE bound to the jaw subdomain of SgtB and the positive cooperativity of the two MOE binding events. The additional MOE binding domain of SgtB might contribute to the fact that higher MOE concentrations were necessary to inhibit the SgtB reaction compared to inhibition of the PBP2 *in vitro* activity. It should be noted that the disaccharide unit of CAO contains a  $\beta$ 1,3 linked 6-deoxygulopyranosyl- $\alpha$ -rhamnopyranoside disaccharide, which differs structurally from the  $\beta$ 1,4-linked MurNAc-GlcNAc-chain of the lipid II substrate (Figure 24A and B). To evaluate if an interaction via a substrate mimic is at least plausible, relevant binding motifs of proposed GT inhibitors were compared to CAOs structure (Figure 24).

**Interestingly, positioning of the glycosidic bond or the exact identity of disaccharide hexoses seem to be no determinants for the potency of GT inhibitors.** Different semisynthetic GT inhibitors have been synthesized comprising  $\beta$ 1,2-,  $\beta$ 1,3- or  $\beta$ 1,4-linked disaccharides (or mono- and trisaccharide) moieties. It was reported that the  $\beta$ 1,2-linked E-F disaccharide portion of MOE (TS0514; Figure 24D) is sufficient to facilitate inhibition of PGN synthesis *in vitro* (Baizman et al., 2000). Based on the minimal moenomycin pharmacore, library derived analogues were generated including TS30663 (Figure 24E), a  $\beta$ 1,2-linked disaccharide analogue that further possessed *in vivo* activity (Goldman et al., 2000), and ACL19109 (Figure 24F), a  $\beta$ 1,3-linked EF-mimetic, where the carbon tail and the phosphoglyceric acid linker were replaced by a biphenyl moiety (Mesleh et al., 2015). There have also been many efforts to develop PGN synthesis inhibitors based on precursor analogues, which compete for the acceptor site of GTs with the natural lipid II substrate, with compound 62 being one of the most potent in this series regarding its *in vitro* GT inhibitory activity (Dumbre et al., 2012). Compound 62 is composed of a saturated C16 phosphoglycerate linked to  $\beta$ 1,4-MurNAc(-dipeptide)GlcNAc disaccharide, but showed only weak antibacterial activity. Even non-carbohydrate small molecule GT inhibitors, like HTS6-8 (Cheng et al., 2008, 2010) and compound 24 (Huang et al., 2012), have been identified, and show good antibacterial activity. Interestingly, a non-carbohydrate lipid II analogue (Compound 24, Figure 24G) showed superior inhibitory activity than a lipid II analogue comprising a  $\beta$ 1,4-MurNAc(-dipeptide)GlcNAc disaccharide (Compound 62, Figure 24C). The latter shows a higher structural similarity to the native GT substrate and would thus appear to be a more potent inhibitor, which did not hold true. The structural differences between the  $\beta$ 1,3 linked 6-deoxygulopyranosyl- $\alpha$ -rhamnopyranoside disaccharide unit of CAO and the natural GT substrate are therefore no criteria to rule out the possibility that CAO might mimic the lipid II disaccharide.

Apart from MOE and MOE-derivatives, there is evidence that semisynthetic glycopeptide analogues with hydrophobic substitutions, like chlorobiphenyl-vancomycin (Figure 24H), are also capable of directly inhibiting bacterial transglycosylases. The combination of the vancomycin aglycon and the hydrophobic chlorobiphenyl substitution enable binding of the peptidoglycan precursors lipid II and interaction with bacterial GTs respectively (Chen et al., 2003; Leimkuhler et al., 2005), which coincides with the dual mode of action proposed for CAO. The glycopeptide modifications enabled activity against vancomycin resistant microorganisms, and it was shown that the compounds retained their inhibitory activity when the D-Ala-D-Ala binding pockets were damaged (Chen et al., 2003; Leimkuhler et al., 2005).

In the case of MOE, structure-activity relationship studies demonstrated that the lipid moiety of MOE is crucial for antimicrobial activity and is likely to enable binding to the cytoplasmic membrane (Anikin et al., 1999). Indeed, various molecules are able to interfere with GT activity *in vitro* but hydrophobic substitutions seem to be essential for *in vivo* activity, presumably by guiding the inhibitors to the site of action. Even though MOE is a very potent microbial inhibitor, it has relatively poor bioavailability and has therefore not been used in the pharmaceutical area. If administered orally MOE has almost no curative, protective or toxic effects reflecting its extremely low absorption from the gastrointestinal tract (Ostash & Walker, 2010). The long C25-lipid moiety (moenocinol) is suggested to underlie these undesired effects (Adachi et al., 2006; Ostash & Walker,

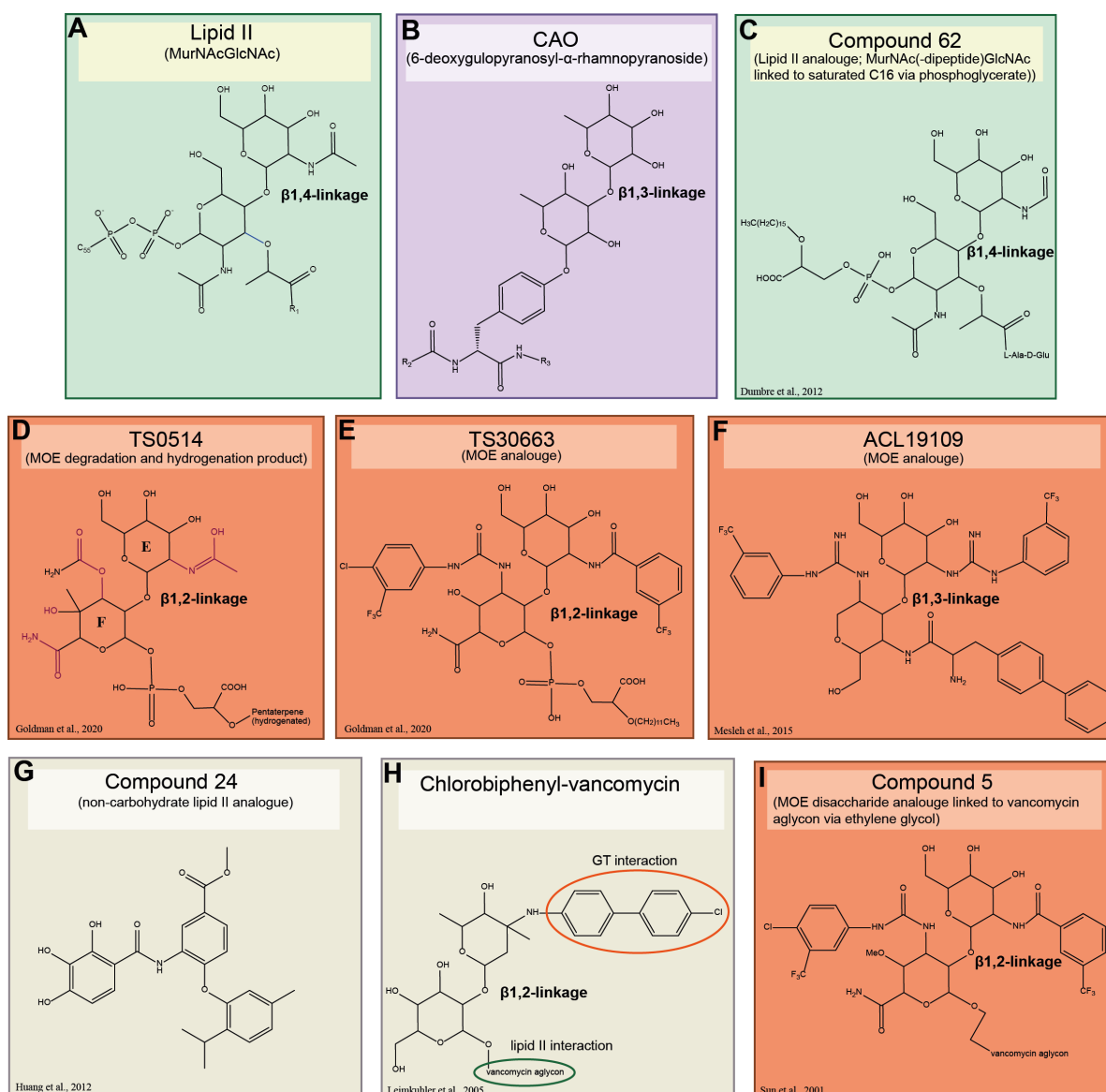


Figure 24: Structural comparison of the disaccharide and linkage unit of lipid II to the postulated glycosyltransferase (GT) binding motifs of CAO and known GT inhibitors. In the case of TS0514 the functional groups essential for activity are highlighted. Lipid II and analogues are displayed in green boxes, MOE derivatives or analogues in orange boxes, CAO in purple and others in grey. R1, L-Ala-D-Glu-L-Lys-D-Ala-D-Ala for a complete structure see Figure 16; R2, Ile-7-(D)Abu-6-Ala(S)5-NMe<sub>2</sub>Lan (Pro-4-Ala-3-Dha-2-NMe<sub>2</sub>Ala(S)-1); R3, Ala-9-(D)Ala-10-Val-11-(D)Ala-12-Ala-13-(D)Ala-14-Ile-15-(D)Ala-16-Ala-17-AviMeCys-18-Ala-19-Ser-20-Trp-21-Gly-22, for a complete CAO structure see Figure 1 of the publication in Chapter 4.2.

2010). Anyhow, MOE is still regarded as a promising lead for new antibiotics and its amphiphilic structure comprised of a hydrophilic pentasaccharide head and a hydrophobic lipid chain, provided helpful information for rational drug design. These findings indicate an effective GT inhibitor should comprise only a certain amount of hydrophobic substitutions to ensure target interaction *in vivo* and maintaining good pharmacokinetics. The high amount of hydrophobic residues combined with the disaccharide substitution of CAO confer the molecule an overall amphiphilic character.

**Hydrophobic substituents (in an overall amphiphilic molecule) enhance the inhibition of bacterial peptidoglycan glycosyltransferase activity.** The active site of GTs is hydrophilic and interacts with the disaccharide-peptide moiety of lipid II or with the pentasaccharide

unit in case of MOE. The adjacent surface of the active site is hydrophobic and thought to facilitate immersion into the membrane (Sung et al., 2009). An exposed hydrophobic region close to the active site most probably interacts with the lipid moiety of the substrate while it enters the active site (Sung et al., 2009)). Therefore, Wang et al. (2020) postulate that effective GT inhibitors should be amphiphilic in nature, comprising a hydrophilic moiety to interact with the active site of the enzyme and a hydrophobic group to interact with the transmembrane region of the enzyme as well as the membrane, which could assist the inhibitory molecule to approach the active-site pocket of GTs. With that in mind, Wang et al. (2020) used isatins, small molecules harboring antibacterial and moderate GT inhibitory activities (Wang et al., 2014), as a scaffold and tuned their hydrophobicity by addition of hydrophobic groups to create a series of isatin-based amphiphilic GT inhibitors. The results demonstrate it is feasible to generate GT inhibitors with broad-spectrum antibacterial activities against gram positives and gram negatives and that the activities can be tuned by adjusting the overall hydrophobicity of the amphiphilic inhibitors. Nevertheless, hydrophobicity has to be fine tuned to maintain bioavailability, because if it is too high the molecule could enter the bacterial cell and therefore prevent engagement with the target, which is anchored in the membrane with its active site facing into the periplasm.

In the end, crystal structures of the individual CAO-GT and CAO-lipid II complexes are required to pin down specific interaction sites. This could further guide SAR analysis and synthesis of hybrid antibiotics, i.e. incorporation of CAOs unprecedented disaccharide into synthetic drugs. With regard to the multiple target hypothesis, CAO poses an interesting candidate for this application, since it combines substrate binding and enzyme inhibition. Substrate binding antibiotics, as opposed to single-enzyme targeting antibiotics, have several advantages, such as that high-level resistance usually does not readily develop, except by horizontal transfer of genes originating from the producing organism. Anyhow, disadvantages of substrate binders are that they are often large, relatively polar and, consequentially, have a poor oral bioavailability and cannot penetrate outer membranes of gram negatives. The large size and inability to penetrate outer membranes are also features of CAO, while regarding its bioavailability no statements can be made, but the high amount of hydrophobic amino acids would suggest it is rather low. Considering the glycosyltransferase interaction, it was observed that CAOs antibiotic activity varied towards different gram positive bacteria, which might be partly explained by differential GT expression or structural and functional differences in the GT subsets among the tested strains. Actually, the latter was reported for MOE analogues (Baizman et al., 2000; Goldman et al., 2000; Sofia et al., 1999). The selective activity of  $\beta$ -lactams against different PBPs has also been observed (Miller et al., 2004). Even though enzyme inhibitors are more prone to induce resistance development and MOE was used as a growth promotor for decades, there have been no reports of resistance so far.

One major challenge for drug discovery is that the final evaluation of the safety and efficacy of a drug is only possible *in vivo* and it is not uncommon that drugs fail in the late clinical stage, after several years of work and resources have already been spent on the project. Improving our ability to identify promising targets early on and understand the physicochemical properties necessary for activity, specificity, and bioavailability might help in this regard.

Natural Products (NPs) represent the major source of oral drugs currently in use, are structurally optimized by evolution for target interaction, exhibit lower hydrophobicity, and occupy larger regions of chemical space compared to synthetic molecule libraries (Stratton, Newman, & Tan, 2015). Because of their genetically encoded precursor peptides, RiPPs are particularly well-suited for synthetic biology approaches to generate novel structures (Montalbán-López et al., 2021). The most challenging barrier in natural product discovery over the past decades represents the rediscovery of already known bioactives rather than novel compounds. To eliminate this error, effective dereplication

processes<sup>16</sup> need to be implemented. Other drawbacks of NPs for drug discovery are that screenings typically involve extract libraries from natural sources which might not be compatible with traditional target-based assays as well as assessing sufficient amounts of material to isolate and characterize.

Pharmaceutical companies shift away from focusing exclusively on classical, small molecule drug discovery marked by an increase of approvals of biologic therapeutics, e.g. monoclonal antibodies and vaccines. Further, alternative approaches to narrow the antibiotic spectrum towards a desired pathogenic bacterial population are of great interest, since broad-spectrum antibiotics also kill beneficial bacteria and thereby accelerate the spread of resistance across multiple bacterial species (Koyasseril-Yehiya et al., 2020). A targeted, organism-specific approach might also be beneficial when regarding the effects of broad spectrum antibiotics on the human microbiome, often resulting in dysbiosis and health consequences we are only starting to discover. The burden of antibiotic-resistant bacteria on public health just recently started to measure cases of attributable deaths **and** disability-adjusted life-years (DALYs).

It should be further pointed out that even new substances would need strict antibiotic stewardship.

---

<sup>16</sup>The dereplication process recognizes and excludes from further studies such hit mixtures that contain already known bioactive compounds.

## References

- Adachi, M., Zhang, Y., Leimkuhler, C., Sun, B., LaTour, J. V., & Kahne, D. E. (2006, nov). Degradation and Reconstruction of Moenomycin A and Derivatives: Dissecting the Function of the Isoprenoid Chain. *Journal of the American Chemical Society*, *128*(43), 14012–14013. doi: 10.1021/ja065905c
- Anikin, Buchynskyy, Kempin, Stembera, Welzel, & Lantzsch. (1999, December). Membrane Anchoring and Intervesicle Transfer of a Derivative of the Antibiotic Moenomycin A. *Angewandte Chemie (International ed. in English)*, *38*, 3703–3707. doi: 10.1002/(sici)1521-3773(19991216)38:24<3703::aid-anie3703>3.0.co;2-1
- Arnison, P. G., Bibb, M. J., Bierbaum, G., Bowers, A. A., Bugni, T. S., Bulaj, G., Camarero, J. A., Campopiano, D. J., Challis, G. L., Clardy, J., Cotter, P. D., Craik, D. J., Dawson, M., Dittmann, E., Donadio, S., Dorrestein, P. C., Entian, K.-D., Fischbach, M. A., Garavelli, J. S., Göransson, U., Gruber, C. W., Haft, D. H., Hemscheidt, T. K., Hertweck, C., Hill, C., Horswill, A. R., Jaspars, M., Kelly, W. L., Klinman, J. P., Kuipers, O. P., Link, A. J., Liu, W., Marahiel, M. A., Mitchell, D. A., Moll, G. N., Moore, B. S., Müller, R., Nair, S. K., Nes, I. F., Norris, G. E., Olivera, B. M., Onaka, H., Patchett, M. L., Piel, J., Reaney, M. J. T., Rebuffat, S., Ross, R. P., Sahl, H.-G., Schmidt, E. W., Selsted, M. E., Severinov, K., Shen, B., Sivonen, K., Smith, L., Stein, T., Süßmuth, R. D., Tagg, J. R., Tang, G.-L., Truman, A. W., Vederas, J. C., Walsh, C. T., Walton, J. D., Wenzel, S. C., Willey, J. M., & van der Donk, W. A. (2013). Ribosomally synthesized and post-translationally modified peptide natural products: overview and recommendations for a universal nomenclature. *Nat. Prod. Rep.*, *30*(1), 108–160. doi: 10.1039/c2np20085f
- Arthur, M., Reynolds, P., & Courvalin, P. (1996, oct). Glycopeptide resistance in enterococci. *Trends in Microbiology*, *4*(10), 401–407. doi: 10.1016/0966-842x(96)10063-9
- Asensio, J. L., Ardá, A., Cañada, F. J., & Jiménez-Barbero, J. (2012, jun). Carbohydrate–Aromatic Interactions. *Accounts of Chemical Research*, *46*(4), 946–954. doi: 10.1021/ar300024d
- Assoni, L., Milani, B., Carvalho, M. R., Nepomuceno, L. N., Waz, N. T., Guerra, M. E. S., Converso, T. R., & Darrieux, M. (2020, oct). Resistance Mechanisms to Antimicrobial Peptides in Gram-Positive Bacteria. *Frontiers in Microbiology*, *11*. doi: 10.3389/fmicb.2020.593215
- Atanasov, A. G., Zotchev, S. B., Dirsch, V. M., & Supuran, C. T. (2021, jan). Natural products in drug discovery: advances and opportunities. *Nature Reviews Drug Discovery*, *20*(3), 200–216. doi: 10.1038/s41573-020-00114-z
- Baizman, E. R., Branstrom, A. A., Longley, C. B., Allanson, N., Sofia, M. J., Gange, D., & Goldman, R. C. (2000, December). Antibacterial activity of synthetic analogues based on the disaccharide structure of moenomycin, an inhibitor of bacterial transglycosylase. *Microbiology (Reading, England)*, *146 Pt 12*, 3129–3140. doi: 10.1099/00221287-146-12-3129
- Baumgart, M., Schubert, K., Bramkamp, M., & Frunzke, J. (2016, aug). Impact of LytR-CpsA-psr proteins on cell wall biosynthesis in *Corynebacterium glutamicum*. *Journal of Bacteriology*, *198*(22), 3045–3059. doi: 10.1128/jb.00406-16
- Beltramini, A. M., Mukhopadhyay, C. D., & Pancholi, V. (2009, apr). Modulation of Cell Wall Structure and Antimicrobial Susceptibility by a *Staphylococcus aureus* Eukaryote-Like Serine/Threonine Kinase and Phosphatase. *Infection and Immunity*, *77*(4), 1406–1416. doi: 10.1128/iai.01499-08
- Bender, M. H., Cartee, R. T., & Yother, J. (2003, oct). Positive Correlation between Tyrosine Phosphorylation of CpsD and Capsular Polysaccharide Production in *Streptococcus pneumoniae*. *Journal of Bacteriology*, *185*(20), 6057–6066. doi: 10.1128/jb.185.20.6057-6066.2003
- Bera, A., Herbert, S., Jakob, A., Vollmer, W., & Götz, F. (2004, dec). Why are pathogenic staphylococci so lysozyme resistant? The peptidoglycan *O*-acetyltransferase OatA is the major determinant for lysozyme resistance of *Staphylococcus aureus*. *Molecular Microbiology*, *55*(3), 778–787. doi: 10.1111/j.1365-2958.2004.04446.x

- Bhasin, N., Albus, A., Michon, F., Livolsi, P. J., Park, J.-S., & Lee, J. C. (1998, jan). Identification of a gene essential for O-acetylation of the *Staphylococcus aureus* type 5 capsular polysaccharide. *Molecular Microbiology*, *27*(1), 9–21. doi: 10.1046/j.1365-2958.1998.00646.x
- Bierbaum, G., & Sahl, H.-G. (2009, jan). Lantibiotics: Mode of Action, Biosynthesis and Bioengineering. *Current Pharmaceutical Biotechnology*, *10*(1), 2–18. doi: 10.2174/138920109787048616
- Blin, K., Shaw, S., Steinke, K., Villebro, R., Ziemert, N., Lee, S. Y., Medema, M. H., & Weber, T. (2019, apr). antiSMASH 5.0: updates to the secondary metabolite genome mining pipeline. *Nucleic Acids Research*, *47*(W1), W81–W87. doi: 10.1093/nar/gkz310
- Böttiger, T., Schneider, T., Martínez, B., Sahl, H.-G., & Wiedemann, I. (2009, may). Influence of Ca<sup>2+</sup> Ions on the Activity of Lantibiotics Containing a Mersacidin-Like Lipid II Binding Motif. *Applied and Environmental Microbiology*, *75*(13), 4427–4434. doi: 10.1128/aem.00262-09
- Bouhss, A., Trunkfield, A. E., Bugg, T. D. H., & Mengin-Lecreulx, D. (2008, mar). The biosynthesis of peptidoglycan lipid-linked intermediates. *FEMS Microbiology Reviews*, *32*(2), 208–233. doi: 10.1111/j.1574-6976.2007.00089.x
- Brötz, H., Bierbaum, G., Leopold, K., Reynolds, P. E., & Sahl, H.-G. (1998, jan). The Lantibiotic Mersacidin Inhibits Peptidoglycan Synthesis by Targeting Lipid II. *Antimicrobial Agents and Chemotherapy*, *42*(1), 154–160. doi: 10.1128/aac.42.1.154
- Brötz-Oesterhelt, H., & Brunner, N. (2008, oct). How many modes of action should an antibiotic have? *Current Opinion in Pharmacology*, *8*(5), 564–573. doi: 10.1016/j.coph.2008.06.008
- Brown, D. G., May-Dracka, T. L., Gagnon, M. M., & Tommasi, R. (2014, dec). Trends and Exceptions of Physical Properties on Antibacterial Activity for Gram-Positive and Gram-Negative Pathogens. *Journal of Medicinal Chemistry*, *57*(23), 10144–10161. doi: 10.1021/jm501552x
- Brown, S., Maria, J. P. S., & Walker, S. (2013, sep). Wall Teichoic Acids of Gram-Positive Bacteria. *Annual Review of Microbiology*, *67*(1), 313–336. doi: 10.1146/annurev-micro-092412-155620
- Carvalho, S. M., Kloosterman, T. G., Manzoor, I., Caldas, J., Vinga, S., Martinussen, J., Saraiva, L. M., Kuipers, O. P., & Neves, A. R. (2018, mar). Interplay Between Capsule Expression and Uracil Metabolism in *Streptococcus pneumoniae* D39. *Frontiers in Microbiology*, *9*. doi: 10.3389/fmicb.2018.00321
- Cassini, A., Högberg, L. D., Plachouras, D., Quattrocchi, A., Hoxha, A., Simonsen, G. S., Colomb-Cotinat, M., Kretzschmar, M. E., Devleeschauwer, B., Cecchini, M., Ouakrim, D. A., Oliveira, T. C., Struelens, M. J., Suetens, C., Monnet, D. L., Strauss, R., Mertens, K., Struyf, T., Catry, B., Latour, K., Ivanov, I. N., Dobрева, E. G., Andrašević, A. T., Soprek, S., Budimir, A., Paphitou, N., Žemlicková, H., Olsen, S. S., Sönksen, U. W., Märtin, P., Ivanova, M., Lyytikäinen, O., Jalava, J., Coignard, B., Eckmanns, T., Sin, M. A., Haller, S., Daikos, G. L., Gikas, A., Tsiodras, S., Kontopidou, F., Tóth, Á., Hajdu, Á., Guólaugsson, Ó., Kristinsson, K. G., Murchan, S., Burns, K., Pezzotti, P., Gagliotti, C., Dumpis, U., Liuimienė, A., Perrin, M., Borg, M. A., de Greeff, S. C., Monen, J. C. M., Koek, M. B. G., Zabicka, P. E. D., Deptula, A., Hryniewicz, W., Caniça, M., Nogueira, P. J., Fernandes, P. A., Manageiro, V., Popescu, G. A., Serban, R. I., Schréterová, E., Litvová, S., Štefkovicová, M., Kolman, J., Klavs, I., Korošec, A., Aracil, B., Asensio, A., Pérez-Vázquez, M., Billström, H., Larsson, S., Reilly, J. S., Johnson, A., & Hopkins, S. (2019, jan). Attributable deaths and disability-adjusted life-years caused by infections with antibiotic-resistant bacteria in the EU and the European Economic Area in 2015: a population-level modelling analysis. *The Lancet Infectious Diseases*, *19*(1), 56–66. doi: 10.1016/s1473-3099(18)30605-4
- Cerca, N., Brooks, J. L., & Jefferson, K. K. (2008, jul). Regulation of the Intercellular Adhesin Locus Regulator (*icaR*) by SarA,  $\sigma^B$  and IcaR in *Staphylococcus aureus*. *Journal of Bacteriology*, *190*(19), 6530–6533. doi: 10.1128/jb.00482-08

- Chan, Y. G. Y., Frankel, M. B., Dengler, V., Schneewind, O., & Missiakas, D. (2013, aug). *Staphylococcus aureus* Mutants Lacking the LytR-CpsA-Psr Family of Enzymes Release Cell Wall Teichoic Acids into the Extracellular Medium. *Journal of Bacteriology*, *195*(20), 4650–4659. doi: 10.1128/jb.00544-13
- Chan, Y. G.-Y., Kim, H. K., Schneewind, O., & Missiakas, D. (2014, may). The Capsular Polysaccharide of *Staphylococcus aureus* Is Attached to Peptidoglycan by the LytR-CpsA-Psr (LCP) Family of Enzymes. *Journal of Biological Chemistry*, *289*(22), 15680–15690. doi: 10.1074/jbc.m114.567669
- Chen, L., Walker, D., Sun, B., Hu, Y., Walker, S., & Kahne, D. (2003, apr). Vancomycin analogues active against vanA-resistant strains inhibit bacterial transglycosylase without binding substrate. *Proceedings of the National Academy of Sciences*, *100*(10), 5658–5663. doi: 10.1073/pnas.0931492100
- Cheng, T.-J. R., Sung, M.-T., Liao, H.-Y., Chang, Y.-F., Chen, C.-W., Huang, C.-Y., Chou, L.-Y., Wu, Y.-D., Chen, Y.-H., Cheng, Y.-S. E., Wong, C.-H., Ma, C., & Cheng, W.-C. (2008, jan). Domain requirement of moenomycin binding to bifunctional transglycosylases and development of high-throughput discovery of antibiotics. *Proceedings of the National Academy of Sciences*, *105*(2), 431–436. doi: 10.1073/pnas.0710868105
- Cheng, T.-J. R., Wu, Y.-T., Yang, S.-T., Lo, K.-H., Chen, S.-K., Chen, Y.-H., Huang, W.-I., Yuan, C.-H., Guo, C.-W., Huang, L.-Y., Chen, K.-T., Shih, H.-W., Cheng, Y.-S. E., Cheng, W.-C., & Wong, C.-H. (2010, dec). High-throughput identification of antibacterials against methicillin-resistant *Staphylococcus aureus* (MRSA) and the transglycosylase. *Bioorganic & Medicinal Chemistry*, *18*(24), 8512–8529. doi: 10.1016/j.bmc.2010.10.036
- Chopra, I. (2012, nov). The 2012 Garrod Lecture: Discovery of antibacterial drugs in the 21st century. *Journal of Antimicrobial Chemotherapy*, *68*(3), 496–505. doi: 10.1093/jac/dks436
- Cieslewicz, M. J., Kasper, D. L., Wang, Y., & Wessels, M. R. (2000, oct). Functional Analysis in Type Ia Group B *Streptococcus* of a Cluster of Genes Involved in Extracellular Polysaccharide Production by Diverse Species of Streptococci. *Journal of Biological Chemistry*, *276*(1), 139–146. doi: 10.1074/jbc.m005702200
- Cocchiario, J. L., Gomez, M. I., Risley, A., Solinga, R., Sordelli, D. O., & Lee, J. C. (2006, feb). Molecular characterization of the capsule locus from non-typeable *Staphylococcus aureus*. *Molecular Microbiology*, *59*(3), 948–960. doi: 10.1111/j.1365-2958.2005.04978.x
- Cotter, P. D., Hill, C., & Ross, R. P. (2005, oct). Bacteriocins: developing innate immunity for food. *Nature Reviews Microbiology*, *3*(10), 777–788. doi: 10.1038/nrmicro1273
- de Jonge, B. L., Chang, Y. S., Gage, D., & Tomasz, A. (1992, jun). Peptidoglycan composition of a highly methicillin-resistant *Staphylococcus aureus* strain. *Journal of Biological Chemistry*, *267*(16), 11248–11254. doi: 10.1016/s0021-9258(19)49903-1
- D'Elia, M. A., Millar, K. E., Beveridge, T. J., & Brown, E. D. (2006, dec). Wall Teichoic Acid Polymers Are Dispensable for Cell Viability in *Bacillus subtilis*. *Journal of Bacteriology*, *188*(23), 8313–8316. doi: 10.1128/jb.01336-06
- D'Elia, M. A., Pereira, M. P., & Brown, E. D. (2009, oct). Are essential genes really essential? *Trends in Microbiology*, *17*(10), 433–438. doi: 10.1016/j.tim.2009.08.005
- Deng, L., Kasper, D. L., Krick, T. P., & Wessels, M. R. (2000, mar). Characterization of the Linkage between the Type III Capsular Polysaccharide and the Bacterial Cell Wall of Group B *Streptococcus*. *Journal of Biological Chemistry*, *275*(11), 7497–7504. doi: 10.1074/jbc.275.11.7497
- Derouaux, A., Sauvage, E., & Terrak, M. (2013). Peptidoglycan Glycosyltransferase Substrate Mimics as Templates for the Design of New Antibacterial Drugs. *Frontiers in Immunology*, *4*. doi: 10.3389/fimmu.2013.00078
- Doak, B. C., Over, B., Giordanetto, F., & Kihlberg, J. (2014, sep). Oral Druggable Space beyond the Rule of 5: Insights from Drugs and Clinical Candidates. *Chemistry & Biology*, *21*(9), 1115–1142. doi: 10.1016/j.chembiol.2014.08.013

- Donat, S., Streker, K., Schirmeister, T., Rakette, S., Stehle, T., Liebeke, M., Lalk, M., & Ohlsen, K. (2009, jul). Transcriptome and Functional Analysis of the Eukaryotic-Type Serine/Threonine Kinase PknB in *Staphylococcus aureus*. *Journal of Bacteriology*, *191*(13), 4056–4069. doi: 10.1128/jb.00117-09
- Dörr, T., Moynihan, P. J., & Mayer, C. (2019, sep). Editorial: Bacterial Cell Wall Structure and Dynamics. *Frontiers in Microbiology*, *10*. doi: 10.3389/fmicb.2019.02051
- Dumbre, S., Derouaux, A., Lescrinier, E., Piette, A., Joris, B., Terrak, M., & Herdewijn, P. (2012, may). Synthesis of Modified Peptidoglycan Precursor Analogues for the Inhibition of Glycosyltransferase. *Journal of the American Chemical Society*, *134*(22), 9343–9351. doi: 10.1021/ja302099u
- Duquesne, S., Destoumieux-Garzón, D., Peduzzi, J., & Rebuffat, S. (2007). Microcins, gene-encoded antibacterial peptides from enterobacteria. *Natural Product Reports*, *24*(4), 708. doi: 10.1039/b516237h
- Eberhardt, A., Hoyland, C. N., Vollmer, D., Bisle, S., Cleverley, R. M., Johnsborg, O., Håvarstein, L. S., Lewis, R. J., & Vollmer, W. (2012, jun). Attachment of Capsular Polysaccharide to the Cell Wall in *Streptococcus pneumoniae*. *Microbial Drug Resistance*, *18*(3), 240–255. doi: 10.1089/mdr.2011.0232
- Essig, A., Hofmann, D., Münch, D., Gayathri, S., Künzler, M., Kallio, P. T., Sahl, H.-G., Wider, G., Schneider, T., & Aebi, M. (2014, oct). Copsin, a Novel Peptide-based Fungal Antibiotic Interfering with the Peptidoglycan Synthesis. *Journal of Biological Chemistry*, *289*(50), 34953–34964. doi: 10.1074/jbc.m114.599878
- Férir, G., Petrova, M. I., Andrei, G., Huskens, D., Hoorelbeke, B., Snoeck, R., Vanderleyden, J., Balzarini, J., Bartoschek, S., Brönstrup, M., Süßmuth, R. D., & Schols, D. (2013, may). The Lantibiotic Peptide Labyrinthopeptin A1 Demonstrates Broad Anti-HIV and Anti-HSV Activity with Potential for Microbicidal Applications. *PLoS ONE*, *8*(5), e64010. doi: 10.1371/journal.pone.0064010
- Foucault, M.-L., Courvalin, P., & Grillot-Courvalin, C. (2009, jun). Fitness Cost of VanA-Type Vancomycin Resistance in Methicillin-Resistant *Staphylococcus aureus*. *Antimicrobial Agents and Chemotherapy*, *53*(6), 2354–2359. doi: 10.1128/aac.01702-08
- Fournier, J.-M., Vann, W. F., & Karakawa, W. W. (1984). Purification and characterization of *Staphylococcus aureus* type 8 capsular polysaccharide. *Infection and Immunity*, *45*(1), 87–93.
- Gale, R. T., Li, F. K. K., Sun, T., Strynadka, N. C. J., & Brown, E. D. (2017, dec). *B. subtilis* LytR-CpsA-Psr Enzymes Transfer Wall Teichoic Acids from Authentic Lipid-Linked Substrates to Mature Peptidoglycan In Vitro. *Cell Chemical Biology*, *24*(12), 1537–1546.e4. doi: 10.1016/j.chembiol.2017.09.006
- Gampe, C. M., Tsukamoto, H., Doud, E. H., Walker, S., & Kahne, D. (2013, mar). Tuning the Moenomycin Pharmacophore To Enable Discovery of Bacterial Cell Wall Synthesis Inhibitors. *Journal of the American Chemical Society*, *135*(10), 3776–3779. doi: 10.1021/ja4000933
- Geoghegan, J. A., & Foster, T. J. (2015). Cell Wall-Anchored Surface Proteins of *Staphylococcus aureus*: Many Proteins, Multiple Functions. In *Current topics in microbiology and immunology* (pp. 95–120). Springer International Publishing. doi: 10.1007/82\_2015\_5002
- George, S. E., Nguyen, T., Geiger, T., Weidenmaier, C., Lee, J. C., Liese, J., & Wolz, C. (2015, sep). Phenotypic heterogeneity and temporal expression of the capsular polysaccharide in *Staphylococcus aureus*. *Molecular Microbiology*, *98*(6), 1073–1088. doi: 10.1111/mmi.13174
- Goldman, R. C., Baizman, E. R., Branstrom, A. A., & Longley, C. B. (2000, oct). Differential antibacterial activity of moenomycin analogues on gram-positive bacteria. *Bioorganic & Medicinal Chemistry Letters*, *10*(20), 2251–2254. doi: 10.1016/s0960-894x(00)00443-1
- González-Lamothe, R., Mitchell, G., Gattuso, M., Diarra, M., Malouin, F., & Bouarab, K. (2009, jul). Plant Antimicrobial Agents and Their Effects on Plant and Human Pathogens. *International Journal of Molecular Sciences*, *10*(8), 3400–3419. doi: 10.3390/ijms10083400



- Grein, F., Schneider, T., & Sahl, H.-G. (2019, aug). Docking on Lipid II—A Widespread Mechanism for Potent Bactericidal Activities of Antibiotic Peptides. *Journal of Molecular Biology*, *431*(18), 3520–3530. doi: 10.1016/j.jmb.2019.05.014
- Gruszczyk, J., Fleurie, A., Olivares-Illana, V., Béchet, E., Zanella-Cleon, I., Moréra, S., Meyer, P., Pompidor, G., Kahn, R., Grangeasse, C., & Nessler, S. (2011). Structure Analysis of the *Staphylococcus aureus* UDP-*N*-acetyl-mannosamine Dehydrogenase Cap5O Involved in Capsular Polysaccharide Biosynthesis. *Journal of Biological Chemistry*, *286*(19), 17112–17121. doi: 10.1074/jbc.m110.216002
- Gruszczyk, J., Olivares-Illana, V., Nourikyan, J., Fleurie, A., Béchet, E., Gueguen-Chaignon, V., Freton, C., Aumont-Nicaise, M., Moréra, S., Grangeasse, C., & Nessler, S. (2013, oct). Comparative Analysis of the Tyr-Kinases CapB1 and CapB2 Fused to Their Cognate Modulators CapA1 and CapA2 from *Staphylococcus aureus*. *PLoS ONE*, *8*(10), e75958. doi: 10.1371/journal.pone.0075958
- Grzegorzewicz, A. E., de Sousa-d'Auria, C., McNeil, M. R., Huc-Claustre, E., Jones, V., Petit, C., kumar Angala, S., Zemanová, J., Wang, Q., Belardinelli, J. M., Gao, Q., Ishizaki, Y., Mikušová, K., Brennan, P. J., Ronning, D. R., Chami, M., Houssin, C., & Jackson, M. (2016, sep). Assembling of the *Mycobacterium tuberculosis* Cell Wall Core. *Journal of Biological Chemistry*, *291*(36), 18867–18879. doi: 10.1074/jbc.m116.739227
- Gwynn, M. N., Portnoy, A., Rittenhouse, S. F., & Payne, D. J. (2010, nov). Challenges of antibacterial discovery revisited. *Annals of the New York Academy of Sciences*, *1213*(1), 5–19. doi: 10.1111/j.1749-6632.2010.05828.x
- Hardt, P., Engels, I., Rausch, M., Gajdiss, M., Ulm, H., Sass, P., Ohlsen, K., Sahl, H.-G., Bierbaum, G., Schneider, T., & Grein, F. (2017, jan). The cell wall precursor lipid II acts as a molecular signal for the Ser/Thr kinase PknB of *Staphylococcus aureus*. *International Journal of Medical Microbiology*, *307*(1), 1–10. doi: 10.1016/j.ijmm.2016.12.001
- Hardy, G. G., Caimano, M. J., & Yother, J. (2000, apr). Capsule Biosynthesis and Basic Metabolism in *Streptococcus pneumoniae* Are Linked through the Cellular Phosphoglucomutase. *Journal of Bacteriology*, *182*(7), 1854–1863. doi: 10.1128/jb.182.7.1854-1863.2000
- Hübscher, J., Lüthy, L., Berger-Bächli, B., & Meier, P. S. (2008). Phylogenetic distribution and membrane topology of the LytR-CpsA-Psr protein family. *BMC Genomics*, *9*(1), 617. doi: 10.1186/1471-2164-9-617
- Hübscher, J., McCallum, N., Sifri, C. D., Majcherczyk, P. A., Entenza, J. M., Heusser, R., Berger-Bächli, B., & Meier, P. S. (2009, jun). MsrR contributes to cell surface characteristics and virulence in *Staphylococcus aureus*. *FEMS Microbiology Letters*, *295*(2), 251–260. doi: 10.1111/j.1574-6968.2009.01603.x
- Heaslet, H., Shaw, B., Mistry, A., & Miller, A. A. (2009, aug). Characterization of the active site of *S. aureus* monofunctional glycosyltransferase (Mtg) by site-directed mutation and structural analysis of the protein complexed with moenomycin. *Journal of Structural Biology*, *167*(2), 129–135. doi: 10.1016/j.jsb.2009.04.010
- Herbert, S., Newell, S. W., Lee, C., Wieland, K.-P., Dassy, B., Fournier, J.-M., Wolz, C., & Döring, G. (2001). Regulation of *Staphylococcus aureus* type 5 and type 8 capsular polysaccharides by CO<sub>2</sub>. *Journal of Bacteriology*, *183*(15), 4609–4613. doi: 10.1128/JB.183.15.4609-4613.2001
- Hiramatsu, K., Kayayama, Y., Matsuo, M., Aiba, Y., Saito, M., Hishinuma, T., & Iwamoto, A. (2014, dec). Vancomycin-intermediate resistance in *Staphylococcus aureus*. *Journal of Global Antimicrobial Resistance*, *2*(4), 213–224. doi: 10.1016/j.jgar.2014.04.006
- Homma, T., Nuxoll, A., Gandt, A. B., Ebner, P., Engels, I., Schneider, T., Götz, F., Lewis, K., & Conlon, B. P. (2016, nov). Dual Targeting of Cell Wall Precursors by Teixobactin Leads to Cell Lysis. *Antimicrobial Agents and Chemotherapy*, *60*(11), 6510–6517. doi: 10.1128/aac.01050-16

- Hsu, S.-T. D., Breukink, E., Bierbaum, G., Sahl, H.-G., de Kruijff, B., Kaptein, R., van Nuland, N. A. J., & Bonvin, A. M. J. J. (2003, apr). NMR Study of Mersacidin and Lipid II Interaction in Dodecylphosphocholine Micelles. *Journal of Biological Chemistry*, *278*(15), 13110–13117. doi: 10.1074/jbc.m211144200
- Hsu, S.-T. D., Breukink, E., Tischenko, E., Lutters, M. A. G., de Kruijff, B., Kaptein, R., Bonvin, A. M. J. J., & van Nuland, N. A. J. (2004, sep). The nisin–lipid II complex reveals a pyrophosphate cage that provides a blueprint for novel antibiotics. *Nature Structural & Molecular Biology*, *11*(10), 963–967. doi: 10.1038/nsmb830
- Hu, Q., Peng, H., & Rao, X. (2016, oct). Molecular Events for Promotion of Vancomycin Resistance in Vancomycin Intermediate *Staphylococcus aureus*. *Frontiers in Microbiology*, *7*. doi: 10.3389/fmicb.2016.01601
- Huang, C.-Y., Shih, H.-W., Lin, L.-Y., Tien, Y.-W., Cheng, T.-J. R., Cheng, W.-C., Wong, C.-H., & Ma, C. (2012, apr). Crystal structure of *Staphylococcus aureus* transglycosylase in complex with a lipid II analog and elucidation of peptidoglycan synthesis mechanism. *Proceedings of the National Academy of Sciences*, *109*(17), 6496–6501. doi: 10.1073/pnas.1203900109
- Hudson, K. L., Bartlett, G. J., Diehl, R. C., Agirre, J., Gallagher, T., Kiessling, L. L., & Woolfson, D. N. (2015, nov). Carbohydrate–Aromatic Interactions in Proteins. *Journal of the American Chemical Society*, *137*(48), 15152–15160. doi: 10.1021/jacs.5b08424
- Huo, L., & van der Donk, W. A. (2016, April). Discovery and Characterization of Bicareucin, an Unusual D-Amino Acid-Containing Mixed Two-Component Lantibiotic. *Journal of the American Chemical Society*, *138*, 5254–5257. doi: 10.1021/jacs.6b02513
- Hutchings, M. I., Truman, A. W., & Wilkinson, B. (2019, oct). Antibiotics: past, present and future. *Current Opinion in Microbiology*, *51*, 72–80. doi: 10.1016/j.mib.2019.10.008
- Imani, A. S., & Freeman, M. F. (2018, jun). RiPPing apart the rules for peptide natural products. *Synthetic and Systems Biotechnology*, *3*(2), 81–82. doi: 10.1016/j.synbio.2018.03.002
- Jarick, M., Bertsche, U., Stahl, M., Schultz, D., Methling, K., Lalk, M., Stigloher, C., Steger, M., Schlosser, A., & Ohlsen, K. (2018, sep). The serine/threonine kinase Stk and the phosphatase Stp regulate cell wall synthesis in *Staphylococcus aureus*. *Scientific Reports*, *8*(1). doi: 10.1038/s41598-018-32109-7
- Jevons, M. P. (1961). “Celbenin”-resistant staphylococci. *British medical journal*, *1*(5219), 124.
- Johnsborg, O., & Håvarstein, L. S. (2009, jul). Pneumococcal LytR, a Protein from the LytR-CpsA-Psr Family, Is Essential for Normal Septum Formation in *Streptococcus pneumoniae*. *Journal of Bacteriology*, *191*(18), 5859–5864. doi: 10.1128/jb.00724-09
- Jones, C. (2005, may). Revised structures for the capsular polysaccharides from *Staphylococcus aureus* Types 5 and 8, components of novel glycoconjugate vaccines. *Carbohydrate Research*, *340*(6), 1097–1106. doi: 10.1016/j.carres.2005.02.001
- Kalynych, S., Ruan, X., Valvano, M. A., & Cygler, M. (2011, August). Structure-Guided Investigation of Lipopolysaccharide O-Antigen Chain Length Regulators Reveals Regions Critical for Modal Length Control. *Journal of Bacteriology*, *193*(15), 3710–3721. doi: 10.1128/jb.00059-11
- Kalynych, S., Yao, D., Magee, J., & Cygler, M. (2012, may). Structural Characterization of Closely Related O-antigen Lipopolysaccharide (LPS) Chain Length Regulators. *Journal of Biological Chemistry*, *287*(19), 15696–15705. doi: 10.1074/jbc.m112.354837
- Katayama, Y., Murakami-Kuroda, H., Cui, L., & Hiramatsu, K. (2009, aug). Selection of Heterogeneous Vancomycin-Intermediate *Staphylococcus aureus* by Imipenem. *Antimicrobial Agents and Chemotherapy*, *53*(8), 3190–3196. doi: 10.1128/aac.00834-08
- Kawai, Y., Marles-Wright, J., Cleverley, R. M., Emmins, R., Ishikawa, S., Kuwano, M., Heinz, N., Bui, N. K., Hoyland, C. N., Ogasawara, N., Lewis, R. J., Vollmer, W., Daniel, R. A., & Errington, J. (2011, sep). A widespread family of bacterial cell wall assembly proteins. *The EMBO Journal*, *30*(24), 4931–4941. doi: 10.1038/emboj.2011.358

- Keinhörster, D., Salzer, A., Duque-Jaramillo, A., George, S. E., Marincola, G., Lee, J. C., Weidenmaier, C., & Wolz, C. (2019, jul). Revisiting the regulation of the capsular polysaccharide biosynthesis gene cluster in *Staphylococcus aureus*. *Molecular Microbiology*, *112*(4), 1083–1099. doi: 10.1111/mmi.14347
- Kiser, K. B., Bhasin, N., Deng, L., & Lee, J. C. (1999, aug). *Staphylococcus aureus cap5P* Encodes a UDP-N-Acetylglucosamine 2-Epimerase with Functional Redundancy. *Journal of Bacteriology*, *181*(16), 4818–4824. doi: 10.1128/jb.181.16.4818-4824.1999
- Klaenhammer, T. (1993, sep). Genetics of bacteriocins produced by lactic acid bacteria. *FEMS Microbiology Reviews*, *12*(1-3), 39–85. doi: 10.1016/0168-6445(93)90057-g
- Klevens, R. M., Morrison, M. A., Nadle, J., Petit, S., Gershman, K., Ray, S., Harrison, L. H., Lynfield, R., Dumyati, G., Townes, J. M., Craig, A. S., Zell, E. R., Fosheim, G. E., McDougal, L. K., Carey, R. B., & Fridkin, S. K. (2007, oct). Invasive Methicillin-Resistant *Staphylococcus aureus* Infections in the United States. *JAMA*, *298*(15), 1763. doi: 10.1001/jama.298.15.1763
- Kloosterman, A. M., Cimermancic, P., Elsayed, S. S., Du, C., Hadjithomas, M., Donia, M. S., Fischbach, M. A., van Wezel, G. P., & Medema, M. H. (2020, dec). Expansion of RiPP biosynthetic space through integration of pan-genomics and machine learning uncovers a novel class of lanthipeptides. *PLOS Biology*, *18*(12), e3001026. doi: 10.1371/journal.pbio.3001026
- Kneidinger, B., O'Riordan, K., Li, J., Brisson, J.-R., Lee, J. C., & Lam, J. S. (2002, dec). Three Highly Conserved Proteins Catalyze the Conversion of UDP-N-acetyl-D-glucosamine to Precursors for the Biosynthesis of O Antigen in *Pseudomonas aeruginosa* O11 and Capsule in *Staphylococcus aureus* Type 5. *Journal of Biological Chemistry*, *278*(6), 3615–3627. doi: 10.1074/jbc.m203867200
- Kojima, N., Araki, Y., & Ito, E. (1985). Structure of the Linkage Units Between Ribitol Teichoic Acids and Peptidoglycan. *Journal of Bacteriology*, *161*(1), 299–306. doi: 10.1128/jb.161.1.299-306.1985
- Koyasseril-Yehiya, T. M., García-Heredia, A., Anson, F., Rangadurai, P., Siegrist, M. S., & Thayumanavan, S. (2020). Supramolecular antibiotics: a strategy for conversion of broad-spectrum to narrow-spectrum antibiotics for *Staphylococcus aureus*. *Nanoscale*, *12*(40), 20693–20698. doi: 10.1039/d0nr04886k
- Kuipers, A., Stapels, D. A. C., Weerwind, L. T., Ko, Y.-P., Ruyken, M., Lee, J. C., van Kessel, K. P. M., & Rooijackers, S. H. M. (2016, jul). The *Staphylococcus aureus* polysaccharide capsule and Efb-dependent fibrinogen shield act in concert to protect against phagocytosis. *Microbiology*, *162*(7), 1185–1194. doi: 10.1099/mic.0.000293
- Lange, R., Locher, H., Wyss, P., & Then, R. (2007, oct). The Targets of Currently Used Antibacterial Agents: Lessons for Drug Discovery. *Current Pharmaceutical Design*, *13*(30), 3140–3154. doi: 10.2174/138161207782110408
- Larson, T. R., & Yother, J. (2017, may). *Streptococcus pneumoniae* capsular polysaccharide is linked to peptidoglycan via a direct glycosidic bond to  $\beta$ -D-N-acetylglucosamine. *Proceedings of the National Academy of Sciences*, *114*(22), 5695–5700. doi: 10.1073/pnas.1620431114
- Lassila, J. K., Zalatan, J. G., & Herschlag, D. (2011, jul). Biological Phosphoryl-Transfer Reactions: Understanding Mechanism and Catalysis. *Annual Review of Biochemistry*, *80*(1), 669–702. doi: 10.1146/annurev-biochem-060409-092741
- Lattar, S. M., Tuchscher, L. P. N., Cacuri, R. L., Centrón, D., Becker, K., Alonso, C. A., Barberis, C., Miranda, G., Buzzola, F. R., von Eiff, C., & Sordelli, D. O. (2009, mar). Capsule Expression and Genotypic Differences among *Staphylococcus aureus* Isolates from Patients with Chronic or Acute Osteomyelitis. *Infection and Immunity*, *77*(5), 1968–1975. doi: 10.1128/iai.01214-08
- Lazarevic, V., Margot, P., Soldo, B., & Karamata, D. (1992, sep). Sequencing and analysis of the *Bacillus subtilis* *lytRABC* divergon: A regulatory unit encompassing the structural genes of the N-acetylmuramoyl-L-alanine amidase and its modifier. *Journal of General Microbiology*, *138*(9), 1949–1961. doi: 10.1099/00221287-138-9-1949

- Lee, C. Y., & Lee, J. C. (2014, apr). Staphylococcal Capsule. In *Gram-positive pathogens* (pp. 456–463). ASM Press. doi: 10.1128/9781555816513.ch37
- Leimkuhler, C., Chen, L., Barrett, D., Panzone, G., Sun, B., Falcone, B., Oberthür, M., Donadio, S., Walker, S., & Kahne, D. (2005, mar). Differential Inhibition of *Staphylococcus aureus* PBP2 by Glycopeptide Antibiotics. *Journal of the American Chemical Society*, *127*(10), 3250–3251. doi: 10.1021/ja043849e
- Lewis, K. (2013, apr). Platforms for antibiotic discovery. *Nature Reviews Drug Discovery*, *12*(5), 371–387. doi: 10.1038/nrd3975
- Li, F., Zhai, D., Wu, Z., Zhao, Y., Qiao, D., & Zhao, X. (2020, apr). Impairment of the Cell Wall Ligase, LytR-CpsA-Psr Protein (LcpC), in Methicillin Resistant *Staphylococcus aureus* Reduces Its Resistance to Antibiotics and Infection in a Mouse Model of Sepsis. *Frontiers in Microbiology*, *11*. doi: 10.3389/fmicb.2020.00557
- Li, F. K. K., Rosell, F. I., Gale, R. T., Simorre, J.-P., Brown, E. D., & Strynadka, N. C. J. (2020, feb). Crystallographic analysis of *Staphylococcus aureus* LcpA, the primary wall teichoic acid ligase. *Journal of Biological Chemistry*, *295*(9), 2629–2639. doi: 10.1074/jbc.ra119.011469
- Li, W., Ulm, H., Rausch, M., Li, X., O’Riordan, K., Lee, J. C., Schneider, T., & Müller, C. E. (2014, nov). Analysis of the *Staphylococcus aureus* capsule biosynthesis pathway in vitro: Characterization of the UDP-GlcNAc C6 dehydratases CapD and CapE and identification of enzyme inhibitors. *International Journal of Medical Microbiology*, *304*(8), 958–969. doi: 10.1016/j.ijmm.2014.06.002
- Ligozzi, M., Pittaluga, F., & Fontana, R. (1993). Identification of a genetic element (*psr*) which negatively controls expression of *Enterococcus hirae* penicillin-binding protein 5. *Journal of Bacteriology*, *175*(7), 2046–2051. doi: 10.1128/jb.175.7.2046-2051.1993
- Ling, L. L., Schneider, T., Peoples, A. J., Spoering, A. L., Engels, I., Conlon, B. P., Mueller, A., Schäberle, T. F., Hughes, D. E., Epstein, S., Jones, M., Lazarides, L., Steadman, V. A., Cohen, D. R., Felix, C. R., Fetterman, K. A., Millett, W. P., Nitti, A. G., Zullo, A. M., Chen, C., & Lewis, K. (2015, jan). A new antibiotic kills pathogens without detectable resistance. *Nature*, *517*(7535), 455–459. doi: 10.1038/nature14098
- Lipinski, C. A., Lombardo, F., Dominy, B. W., & Feeney, P. J. (2001, mar). Experimental and computational approaches to estimate solubility and permeability in drug discovery and development settings. *Advanced Drug Delivery Reviews*, *46*(1-3), 3–26. (Article was originally published in *Advanced Drug Delivery Reviews* 23 (1997)) doi: 10.1016/s0169-409x(00)00129-0
- Liu, B., Park, S., Thompson, C. D., Li, X., & Lee, J. C. (2016, dec). Antibodies to *Staphylococcus aureus* capsular polysaccharides 5 and 8 perform similarly *in vitro* but are functionally distinct *in vivo*. *Virulence*, *8*(6), 859–874. doi: 10.1080/21505594.2016.1270494
- Lohans, C. T., Li, J. L., & Vederas, J. C. (2014, sep). Structure and Biosynthesis of Carnolysin, a Homologue of Enterococcal Cytolysin with D-Amino Acids. *Journal of the American Chemical Society*, *136*(38), 13150–13153. doi: 10.1021/ja5070813
- Lovering, A. L., de Castro, L. H., Lim, D., & Strynadka, N. C. J. (2007, mar). Structural Insight into the Transglycosylation Step of Bacterial Cell-Wall Biosynthesis. *Science*, *315*(5817), 1402–1405. doi: 10.1126/science.1136611
- Lovering, A. L., Safadi, S. S., & Strynadka, N. C. J. (2012, jul). Structural Perspective of Peptidoglycan Biosynthesis and Assembly. *Annual Review of Biochemistry*, *81*(1), 451–478. doi: 10.1146/annurev-biochem-061809-112742
- Ma, S., & Zhang, Q. (2020). Linaridin natural products. *Natural Product Reports*, *37*(9), 1152–1163. doi: 10.1039/c9np00074g
- Malanovic, N., & Lohner, K. (2016, may). Gram-positive bacterial cell envelopes: The impact on the activity of antimicrobial peptides. *Biochimica et Biophysica Acta (BBA) - Biomembranes*, *1858*(5), 936–946. doi: 10.1016/j.bbamem.2015.11.004

- Medeiros-Silva, J., Jekhmane, S., Paioni, A. L., Gawarecka, K., Baldus, M., Swiezewska, E., Breukink, E., & Weingarth, M. (2018, sep). High-resolution NMR studies of antibiotics in cellular membranes. *Nature Communications*, *9*(1). doi: 10.1038/s41467-018-06314-x
- Mendes, R. E., Deshpande, L. M., & Jones, R. N. (2014, apr). Linezolid update: Stable in vitro activity following more than a decade of clinical use and summary of associated resistance mechanisms. *Drug Resistance Updates*, *17*(1-2), 1–12. doi: 10.1016/j.drup.2014.04.002
- Mesleh, M. F., Rajaratnam, P., Conrad, M., Chandrasekaran, V., Liu, C. M., Pandya, B. A., Hwang, Y. S., Rye, P. T., Muldoon, C., Becker, B., Zuegg, J., Meutermans, W., & Moy, T. I. (2015, oct). Targeting Bacterial Cell Wall Peptidoglycan Synthesis by Inhibition of Glycosyltransferase Activity. *Chemical Biology & Drug Design*, *87*(2), 190–199. doi: 10.1111/cbdd.12662
- Miller, C., Thomsen, L. E., Gaggero, C., Mosseri, R., Ingmer, H., & Cohen, S. N. (2004, September). SOS response induction by beta-lactams and bacterial defense against antibiotic lethality. *Science (New York, N.Y.)*, *305*, 1629–1631. doi: 10.1126/science.1101630
- Miyafusa, T., Caaveiro, J. M. M., Tanaka, Y., & Tsumoto, K. (2013, oct). Dynamic elements govern the catalytic activity of CapE, a capsular polysaccharide-synthesizing enzyme from *Staphylococcus aureus*. *FEBS Letters*, *587*(23), 3824–3830. doi: 10.1016/j.febslet.2013.10.009
- Müller, A., Klöckner, A., & Schneider, T. (2017). Targeting a cell wall biosynthesis hot spot. *Natural Product Reports*, *34*(7), 909–932. doi: 10.1039/c7np00012j
- Münch, D., Roemer, T., Lee, S. H., Engeser, M., Sahl, H. G., & Schneider, T. (2012, jan). Identification and *in vitro* Analysis of the GatD/MurT Enzyme-Complex Catalyzing Lipid II Amidation in *Staphylococcus aureus*. *PLoS Pathogens*, *8*(1), e1002509. doi: 10.1371/journal.ppat.1002509
- Münch, D., & Sahl, H.-G. (2015, nov). Structural variations of the cell wall precursor lipid II in Gram-positive bacteria — Impact on binding and efficacy of antimicrobial peptides. *Biochimica et Biophysica Acta (BBA) - Biomembranes*, *1848*(11), 3062–3071. doi: 10.1016/j.bbamem.2015.04.014
- Mohamed, N., Timofeyeva, Y., Jamrozy, D., Rojas, E., Hao, L., de Monerri, N. C. S., Hawkins, J., Singh, G., Cai, B., Liberator, P., Sebastian, S., Donald, R. G. K., Scully, I. L., Jones, C. H., Creech, C. B., Thomsen, I., Parkhill, J., Peacock, S. J., Jansen, K. U., Holden, M. T. G., & Anderson, A. S. (2019, jan). Molecular epidemiology and expression of capsular polysaccharides in *Staphylococcus aureus* clinical isolates in the United States. *PLOS ONE*, *14*(1), e0208356. doi: 10.1371/journal.pone.0208356
- Montalbán-López, M., Scott, T. A., Ramesh, S., Rahman, I. R., van Heel, A. J., Viel, J. H., Bandarian, V., Dittmann, E., Genilloud, O., Goto, Y., Burgos, M. J. G., Hill, C., Kim, S., Koehnke, J., Latham, J. A., Link, A. J., Martínez, B., Nair, S. K., Nicolet, Y., Rebuffat, S., Sahl, H.-G., Sareen, D., Schmidt, E. W., Schmitt, L., Severinov, K., Süßmuth, R. D., Truman, A. W., Wang, H., Weng, J.-K., van Wezel, G. P., Zhang, Q., Zhong, J., Piel, J., Mitchell, D. A., Kuipers, O. P., & van der Donk, W. A. (2021). New developments in RiPP discovery, enzymology and engineering. *Natural Product Reports*, *38*(1), 130–239. doi: 10.1039/d0np00027b
- Moravvej, Z., Estaji, F., Askari, E., Solhjoui, K., Nasab, M. N., & Saadat, S. (2013, oct). Update on the global number of vancomycin-resistant *Staphylococcus aureus* (VRSA) strains. *International Journal of Antimicrobial Agents*, *42*(4), 370–371. doi: 10.1016/j.ijantimicag.2013.06.004
- Moreau, M., Richards, J. C., Fournier, J.-M., Byrd, R. A., Karakawa, W. W., & Vann, W. F. (1990, jul). Structure of the type 5 capsular polysaccharide of *Staphylococcus aureus*. *Carbohydrate Research*, *201*(2), 285–297. doi: 10.1016/0008-6215(90)84244-o
- Nichols, D., Cahoon, N., Trakhtenberg, E. M., Pham, L., Mehta, A., Belanger, A., Kanigan, T., Lewis, K., & Epstein, S. S. (2010, feb). Use of Ichip for High-Throughput *In Situ* Cultivation of “Uncultivable” Microbial Species. *Applied and Environmental Microbiology*, *76*(8), 2445–2450. doi: 10.1128/aem.01754-09

- Olivares-Illana, V., Meyer, P., Bechet, E., Gueguen-Chaignon, V., Soulat, D., Lazereg-Riquier, S., Mijakovic, I., Deutscher, J., Cozzone, A. J., Lapr evote, O., Morera, S., Grangeasse, C., & Nessler, S. (2008, jun). Structural Basis for the Regulation Mechanism of the Tyrosine Kinase CapB from *Staphylococcus aureus*. *PLoS Biology*, 6(6), e143. doi: 10.1371/journal.pbio.0060143
- Oman, T. J., Lupoli, T. J., Wang, T.-S. A., Kahne, D., Walker, S., & van der Donk, W. A. (2011, nov). Haloduracin  $\alpha$  Binds the Peptidoglycan Precursor Lipid II with 2:1 Stoichiometry. *Journal of the American Chemical Society*, 133(44), 17544–17547. doi: 10.1021/ja206281k
- O’neill, J. (2014). Antimicrobial Resistance: Tackling a crisis for the health and wealth of nations. *WHO GAP AMR Newsletter*(13). Retrieved from <https://amr-review.org/> (Accessed on 18th September 2021)
- O’Riordan, K., & Lee, J. C. (2004, jan). *Staphylococcus aureus* Capsular Polysaccharides. *Clinical Microbiology Reviews*, 17(1), 218–234. doi: 10.1128/cmr.17.1.218-234.2004
- Ortega, M. A., & van der Donk, W. A. (2016, jan). New Insights into the Biosynthetic Logic of Ribosomally Synthesized and Post-translationally Modified Peptide Natural Products. *Cell Chemical Biology*, 23(1), 31–44. doi: 10.1016/j.chembiol.2015.11.012
- Ostash, B., & Walker, S. (2005, oct). Bacterial transglycosylase inhibitors. *Current Opinion in Chemical Biology*, 9(5), 459–466. doi: 10.1016/j.cbpa.2005.08.014
- Ostash, B., & Walker, S. (2010). Moenomycin family antibiotics: chemical synthesis, biosynthesis, and biological activity. *Natural Product Reports*, 27(11), 1594. doi: 10.1039/c001461n
- Ouyang, S., Sau, S., & Lee, C. Y. (1999, apr). Promoter Analysis of the cap8 Operon, Involved in Type 8 Capsular Polysaccharide Production in *Staphylococcus aureus*. *Journal of Bacteriology*, 181(8), 2492–2500. doi: 10.1128/jb.181.8.2492-2500.1999
- Over, B., Heusser, R., McCallum, N., Schulthess, B., Kupferschmied, P., Gaiani, J. M., Sifri, C. D., Berger-B achi, B., & Meier, P. S. (2011, may). LytR-CpsA-Psr proteins in *Staphylococcus aureus* display partial functional redundancy and the deletion of all three severely impairs septum placement and cell separation. *FEMS Microbiology Letters*, 320(2), 142–151. doi: 10.1111/j.1574-6968.2011.02303.x
- Payne, D. J., Gwynn, M. N., Holmes, D. J., & Pompliano, D. L. (2006, dec). Drugs for bad bugs: confronting the challenges of antibacterial discovery. *Nature Reviews Drug Discovery*, 6(1), 29–40. doi: 10.1038/nrd2201
- Portol s, M., Kiser, K. B., Bhasin, N., Chan, K. H. N., & Lee, J. C. (2001, feb). *Staphylococcus aureus* Cap5O Has UDP-ManNAc Dehydrogenase Activity and Is Essential for Capsule Expression. *Infection and Immunity*, 69(2), 917–923. doi: 10.1128/iai.69.2.917-923.2001
- Punekar, A. S., Samsudin, F., Lloyd, A. J., Dowson, C. G., Scott, D. J., Khalid, S., & Roper, D. I. (2018, jun). The role of the jaw subdomain of peptidoglycan glycosyltransferases for lipid II polymerization. *The Cell Surface*, 2, 54–66. doi: 10.1016/j.tcs.2018.06.002
- Rasko, D. A., & Sperandio, V. (2010, jan). Anti-virulence strategies to combat bacteria-mediated disease. *Nature Reviews Drug Discovery*, 9(2), 117–128. doi: 10.1038/nrd3013
- Rausch, M. (2017). *Molecular Analysis of Regulatory Networks and Cell Envelope Biosynthesis Pathways of Gram-positive Bacteria* (Unpublished doctoral dissertation). Rheinische Friedrich-Wilhelms-Universit t Bonn.
- Rausch, M., Deisinger, J. P., Ulm, H., M ller, A., Li, W., Hardt, P., Wang, X., Li, X., Sylvester, M., Engeser, M., Vollmer, W., M ller, C. E., Sahl, H. G., Lee, J. C., & Schneider, T. (2019, March). Coordination of capsule assembly and cell wall biosynthesis in *Staphylococcus aureus*. *Nature Communications*, 10(1404). doi: 10.1038/s41467-019-09356-x
- Robbins, J. B., Schneerson, R., Egan, W. B., Vann, W., & Liu, D. T. (1980). Virulence properties of bacterial capsular polysaccharides-unanswered questions. *The molecular basis of microbial pathogenicity*, 115–132.
- Rodrigues, T., Reker, D., Schneider, P., & Schneider, G. (2016, apr). Counting on natural products for drug design. *Nature Chemistry*, 8(6), 531–541. doi: 10.1038/nchem.2479

- Rogers, L. A. (1928, nov). THE INHIBITING EFFECT OF STREPTOCOCCUS LACTIS ON LACTOBACILLUS BULGARICUS. *Journal of Bacteriology*, 16(5), 321–325. doi: 10.1128/jb.16.5.321-325.1928
- Roghmann, M., Taylor, K. L., Gupte, A., Zhan, M., Johnson, J. A., Cross, A., Edelman, R., & Fattom, A. I. (2005, jan). Epidemiology of capsular and surface polysaccharide in *Staphylococcus aureus* infections complicated by bacteraemia. *Journal of Hospital Infection*, 59(1), 27–32. doi: 10.1016/j.jhin.2004.07.014
- Román-Hurtado, F., Sánchez-Hidalgo, M., Martín, J., Ortiz-López, F., & Genilloud, O. (2021, apr). Biosynthesis and Heterologous Expression of Cacaoidin, the First Member of the Lanthidin Family of RiPPs. *Antibiotics*, 10(4), 403. doi: 10.3390/antibiotics10040403
- Rossolini, G. M., Arena, F., Pecile, P., & Pollini, S. (2014, oct). Update on the antibiotic resistance crisis. *Current Opinion in Pharmacology*, 18, 56–60. doi: 10.1016/j.coph.2014.09.006
- Ryan, M. P., Jack, R. W., Josten, M., Sahl, H. G., Jung, G., Ross, R. P., & Hill, C. (1999, December). Extensive post-translational modification, including serine to D-alanine conversion, in the two-component lantibiotic, lactacin 3147. *The Journal of biological chemistry*, 274, 37544–37550. doi: 10.1074/jbc.274.53.37544
- Sadykov, M. R., Mattes, T. A., Luong, T. T., Zhu, Y., Day, S. R., Sifri, C. D., Lee, C. Y., & Somerville, G. A. (2010, jan). Tricarboxylic Acid Cycle-Dependent Synthesis of *Staphylococcus aureus* Type 5 and 8 Capsular Polysaccharides. *Journal of Bacteriology*, 192(5), 1459–1462. doi: 10.1128/jb.01377-09
- Sau, S., Bhasin, N., Wann, E. R., Lee, J. C., Foster, T. J., & Lee, C. Y. (1997, jul). The *Staphylococcus aureus* allelic genetic loci for serotype 5 and 8 capsule expression contain the type-specific genes flanked by common genes. *Microbiology*, 143(7), 2395–2405. doi: 10.1099/00221287-143-7-2395
- Sau, S., Sun, J., & Lee, C. Y. (1997, March). Molecular characterization and transcriptional analysis of type 8 capsule genes in *Staphylococcus aureus*. *Journal of bacteriology*, 179, 1614–1621. doi: 10.1128/jb.179.5.1614-1621.1997
- Schaefer, K., Matano, L. M., Qiao, Y., Kahne, D., & Walker, S. (2017, feb). In vitro reconstitution demonstrates the cell wall ligase activity of LCP proteins. *Nature Chemical Biology*, 13(4), 396–401. doi: 10.1038/nchembio.2302
- Schaefer, K., Owens, T. W., Kahne, D., & Walker, S. (2018, feb). Substrate Preferences Establish the Order of Cell Wall Assembly in *Staphylococcus aureus*. *Journal of the American Chemical Society*, 140(7), 2442–2445. doi: 10.1021/jacs.7b13551
- Schatz, A., Bugle, E., & Waksman, S. A. (1944, jan). Streptomycin, a Substance Exhibiting Antibiotic Activity Against Gram-Positive and Gram-Negative Bacteria. *Experimental Biology and Medicine*, 55(1), 66–69. doi: 10.3181/00379727-55-14461
- Schulthess, B., Bloes, D. A., François, P., Girard, M., Schrenzel, J., Bischoff, M., & Berger-Bächi, B. (2011, sep). The  $\sigma^B$ -Dependent yabJ-spoVG Operon Is Involved in the Regulation of Extracellular Nuclease, Lipase, and Protease Expression in *Staphylococcus aureus*. *Journal of Bacteriology*, 193(18), 4954–4962. doi: 10.1128/jb.05362-11
- Schwartbeck, B., Birtel, J., Treffon, J., Langhanki, L., Mellmann, A., Kale, D., Kahl, J., Hirschhausen, N., Neumann, C., Lee, J. C., Götz, F., Rohde, H., Henke, H., Küster, P., Peters, G., & Kahl, B. C. (2016, nov). Dynamic *in vivo* mutations within the *ica* operon during persistence of *Staphylococcus aureus* in the airways of cystic fibrosis patients. *PLOS Pathogens*, 12(11), e1006024. doi: 10.1371/journal.ppat.1006024
- Sewell, E., & Brown, E. D. (2013, oct). Taking aim at wall teichoic acid synthesis: new biology and new leads for antibiotics. *The Journal of Antibiotics*, 67(1), 43–51. doi: 10.1038/ja.2013.100

- Shang, Z., Winter, J. M., Kauffman, C. A., Yang, I., & Fenical, W. (2019, feb). Salinipeptins: Integrated Genomic and Chemical Approaches Reveal Unusual D-Amino Acid-Containing Ribosomally Synthesized and Post-Translationally Modified Peptides (RiPPs) from a Great Salt Lake *Streptomyces* sp. *ACS Chemical Biology*, *14*(3), 415–425. doi: 10.1021/acscchembio.8b01058
- Shoji, M., Cui, L., Iizuka, R., Komoto, A., min Neoh, H., Watanabe, Y., Hishinuma, T., & Hiramatsu, K. (2011, may). *walk* and *clpP* Mutations Confer Reduced Vancomycin Susceptibility in *Staphylococcus aureus*. *Antimicrobial Agents and Chemotherapy*, *55*(8), 3870–3881. doi: 10.1128/aac.01563-10
- Siegel, S. D., Amer, B. R., Wu, C., Sawaya, M. R., Gosschalk, J. E., Clubb, R. T., & Ton-That, H. (2019, feb). Structure and Mechanism of LcpA, a Phosphotransferase That Mediates Glycosylation of a Gram-Positive Bacterial Cell Wall-Anchored Protein. *mBio*, *10*(1). doi: 10.1128/mbio.01580-18
- Silver, L. L. (2007, jan). Multi-targeting by monotherapeutic antibacterials. *Nature Reviews Drug Discovery*, *6*(1), 41–55. doi: 10.1038/nrd2202
- Silver, L. L. (2011, jan). Challenges of Antibacterial Discovery. *Clinical Microbiology Reviews*, *24*(1), 71–109. doi: 10.1128/cmr.00030-10
- Silver, L. L. (2016). Appropriate Targets for Antibacterial Drugs. *Cold Spring Harbor Perspectives in Medicine*, *6*(12), a030239. doi: 10.1101/cshperspect.a030239
- Silver, L. L., & Bostian, K. A. (1993). Discovery and Development of New Antibiotics: The Problem of Antibiotic Resistance. *Antimicrobial Agents and Chemotherapy*, *37*(3), 377.
- Skaugen, M., Nissen-Meyer, J., Jung, G., Stevanovic, S., Sletten, K., Inger, C., Abildgaard, M., & Nes, I. F. (1994, November). *In vivo* conversion of L-serine to D-alanine in a ribosomally synthesized polypeptide. *The Journal of biological chemistry*, *269*, 27183–27185.
- Sofia, M. J., Allanson, N., Hatzenbuehler, N. T., Jain, R., Kakarla, R., Kogan, N., Liang, R., Liu, D., Silva, D. J., Wang, H., Gange, D., Anderson, J., Chen, A., Chi, F., Dulina, R., Huang, B., Kamau, M., Wang, C., Baizman, E., Branstrom, A., Bristol, N., Goldman, R., Han, K., Longley, C., Midha, S., & Axelrod, H. R. (1999, aug). Discovery of Novel Disaccharide Antibacterial Agents Using a Combinatorial Library Approach. *Journal of Medicinal Chemistry*, *42*(17), 3193–3198. doi: 10.1021/jm990212a
- Sørensen, U. B. S., Henrichsen, J., Chen, H.-C., & Szu, S. C. (1990, may). Covalent linkage between the capsular polysaccharide and the cell wall peptidoglycan of *Streptococcus pneumoniae* revealed by immunochemical methods. *Microbial Pathogenesis*, *8*(5), 325–334. doi: 10.1016/0882-4010(90)90091-4
- Soulat, D., Grangeasse, C., Vaganay, E., Cozzone, A. J., & Duclos, B. (2007). UDP-Acetyl-Mannosamine Dehydrogenase Is an Endogenous Protein Substrate of *Staphylococcus aureus* Protein-Tyrosine Kinase Activity. *Journal of Molecular Microbiology and Biotechnology*, *13*(1-3), 45–54. doi: 10.1159/000103596
- Stähle, J., & Widmalm, G. (2019, nov). Lipopolysaccharides of Gram-Negative Bacteria: Biosynthesis and Structural Aspects. *Trends in Glycoscience and Glycotechnology*, *31*(184), J157–J168. doi: 10.4052/tigg.1749.7j
- Staubitz, P., Neumann, H., Schneider, T., Wiedemann, I., & Peschel, A. (2004, feb). MprF-mediated biosynthesis of lysylphosphatidylglycerol, an important determinant in staphylococcal defensin resistance. *FEMS Microbiology Letters*, *231*(1), 67–71. doi: 10.1016/s0378-1097(03)00921-2
- Stefanović, C., Hager, F. F., & Schäffer, C. (2021, jan). LytR-CpsA-Psr Glycopolymer Transferases: Essential Bricks in Gram-Positive Bacterial Cell Wall Assembly. *International Journal of Molecular Sciences*, *22*(2), 908. doi: 10.3390/ijms22020908
- Stratton, C. F., Newman, D. J., & Tan, D. S. (2015, nov). Cheminformatic comparison of approved drugs from natural product versus synthetic origins. *Bioorganic & Medicinal Chemistry Letters*, *25*(21), 4802–4807. doi: 10.1016/j.bmcl.2015.07.014



- Suligoy, C. M., Díaz, R. E., Gehrke, A.-K., Ring, N., Yebra, G., Alves, J., Gómez, M. I., Wendler, S., FITZGERALD, J. R., Tuchscher, L., Löffler, B., Sordelli, D. O., Llana, M. N., & Buzzola, F. R. (2020, aug). Acapsular *Staphylococcus aureus* with a non-functional agr regains capsule expression after passage through the bloodstream in a bacteremia mouse model. *Scientific Reports*, *10*(1), 14108. doi: 10.1038/s41598-020-70671-1
- Sung, M.-T., Lai, Y.-T., Huang, C.-Y., Chou, L.-Y., Shih, H.-W., Cheng, W.-C., Wong, C.-H., & Ma, C. (2009, may). Crystal structure of the membrane-bound bifunctional transglycosylase PBP1b from *Escherichia coli*. *Proceedings of the National Academy of Sciences*, *106*(22), 8824–8829. doi: 10.1073/pnas.0904030106
- Supa-amornkul, S., Mongkolsuk, P., Summpunn, P., Chaiyakunvat, P., Navaratdusit, W., Jiarpinitnun, C., & Chaturongakul, S. (2019, nov). Alternative Sigma Factor B in Bovine Mastitis-Causing *Staphylococcus aureus*: Characterization of Its Role in Biofilm Formation, Resistance to Hydrogen Peroxide Stress, Regulon Members. *Frontiers in Microbiology*, *10*. doi: 10.3389/fmicb.2019.02493
- Swoboda, J. G., Campbell, J., Meredith, T. C., & Walker, S. (2009, nov). Wall Teichoic Acid Function, Biosynthesis, and Inhibition. *ChemBioChem*, *11*(1), 35–45. doi: 10.1002/cbic.200900557
- Tamber, S., Schwartzman, J., & Cheung, A. L. (2010, aug). Role of PknB Kinase in Antibiotic Resistance and Virulence in Community-Acquired Methicillin-Resistant *Staphylococcus aureus* Strain USA300. *Infection and Immunity*, *78*(8), 3637–3646. doi: 10.1128/iai.00296-10
- Thakker, M., Park, J.-S., Carey, V., & Lee, J. C. (1998, nov). *Staphylococcus aureus* Serotype 5 Capsular Polysaccharide Is Antiphagocytic and Enhances Bacterial Virulence in a Murine Bacteremia Model. *Infection and Immunity*, *66*(11), 5183–5189. doi: 10.1128/iai.66.11.5183-5189.1998
- Tommasi, R., Brown, D. G., Walkup, G. K., Manchester, J. I., & Miller, A. A. (2015, jul). ESKAPEing the labyrinth of antibacterial discovery. *Nature Reviews Drug Discovery*, *14*(8), 529–542. doi: 10.1038/nrd4572
- Tuchscher, L., Löffler, B., Buzzola, F. R., & Sordelli, D. O. (2010, dec). *Staphylococcus aureus* adaptation to the host and persistence: role of loss of capsular polysaccharide expression. *Future Microbiology*, *5*(12), 1823–1832. doi: 10.2217/fmb.10.147
- Ulm, H. (2016). *Biosynthesis of soluble capsule precursors in Staphylococcus aureus* (Unpublished doctoral dissertation). Universitäts-und Landesbibliothek Bonn.
- Unsleber, S., Wohlleben, W., & Stegmann, E. (2019, sep). Diversity of peptidoglycan structure—Modifications and their physiological role in resistance in antibiotic producers. *International Journal of Medical Microbiology*, *309*(6), 151332. doi: 10.1016/j.ijmm.2019.151332
- Ventola, C. L. (2015a). The Antibiotic Resistance Crisis Part 1: Causes and Threats. *Pharmacy and therapeutics*, *40*(4), 277–283.
- Ventola, C. L. (2015b). The Antibiotic Resistance Crisis Part 2: Management Strategies and New Agents. *Pharmacy and Therapeutics*, *40*(5), 344–352.
- Verdier, I., Durand, G., Bes, M., Taylor, K. L., Lina, G., Vandenesch, F., Fattom, A. I., & Etienne, J. (2007, jan). Identification of the Capsular Polysaccharides in *Staphylococcus aureus* Clinical Isolates by PCR and Agglutination Tests. *Journal of Clinical Microbiology*, *45*(3), 725–729. doi: 10.1128/jcm.01572-06
- Wang, Y., Chan, F.-Y., Sun, N., Lui, H.-K., So, P.-K., Yan, S.-C., Chan, K.-F., Chiou, J., Chen, S., Abagyan, R., Leung, Y.-C., & Wong, K.-Y. (2014, aug). Structure-based Design, Synthesis, and Biological Evaluation of Isatin Derivatives as Potential Glycosyltransferase Inhibitors. *Chemical Biology & Drug Design*, *84*(6), 685–696. doi: 10.1111/cbdd.12361
- Wang, Y., Cheong, W.-L., Liang, Z., So, L.-Y., Chan, K.-F., So, P.-K., Chen, Y. W., Wong, W.-L., & Wong, K.-Y. (2020, apr). Hydrophobic substituents on isatin derivatives enhance their inhibition against bacterial peptidoglycan glycosyltransferase activity. *Bioorganic Chemistry*, *97*, 103710. doi: 10.1016/j.bioorg.2020.103710

- Wann, E. R., Dassy, B., Fournier, J.-M., & Foster, T. J. (1999, jan). Genetic analysis of the *cap5* locus of *Staphylococcus aureus*. *FEMS Microbiology Letters*, *170*(1), 97–103. doi: 10.1111/j.1574-6968.1999.tb13360.x
- Weidenmaier, C., & Lee, J. C. (2015). Structure and Function of Surface Polysaccharides of *Staphylococcus aureus*. In *Current topics in microbiology and immunology* (pp. 57–93). Springer International Publishing. doi: 10.1007/82\_2015\_5018
- Weidenmaier, C., & Peschel, A. (2008, mar). Teichoic acids and related cell-wall glycopolymers in Gram-positive physiology and host interactions. *Nature Reviews Microbiology*, *6*(4), 276–287. doi: 10.1038/nrmicro1861
- Welzel, P. (2005, dec). Syntheses around the Transglycosylation Step in Peptidoglycan Biosynthesis. *Chemical Reviews*, *105*(12), 4610–4660. doi: 10.1021/cr040634e
- Wiedemann, I., Bottiger, T., Bonelli, R. R., Wiese, A., Hagge, S. O., Gutschmann, T., Seydel, U., Deegan, L., Hill, C., Ross, P., & Sahl, H.-G. (2006, jul). The mode of action of the lantibiotic lactacin 3147 - a complex mechanism involving specific interaction of two peptides and the cell wall precursor lipid II. *Molecular Microbiology*, *61*(2), 285–296. doi: 10.1111/j.1365-2958.2006.05223.x
- Wiseman, B., Nitharwal, R. G., Widmalm, G., & Högbom, M. (2021, jan). Structure of a full-length bacterial polysaccharide co-polymerase. *Nature Communications*, *12*(1). doi: 10.1038/s41467-020-20579-1
- Wright, G. D. (2017). Opportunities for natural products in 21st century antibiotic discovery. *Natural Product Reports*, *34*(7), 694–701. doi: 10.1039/c7np00019g
- Wright, G. D. (2018, dec). Unlocking the potential of natural products in drug discovery. *Microbial Biotechnology*, *12*(1), 55–57. doi: 10.1111/1751-7915.13351
- Xu, D., & Lu, W. (2020, may). Defensins: A Double-Edged Sword in Host Immunity. *Frontiers in Immunology*, *11*. doi: 10.3389/fimmu.2020.00764
- Xu, M., Zhang, F., Cheng, Z., Bashiri, G., Wang, J., Hong, J., Wang, Y., Xu, L., Chen, X., Huang, S.-X., Lin, S., Deng, Z., & Tao, M. (2020, aug). Functional Genome Mining Reveals a Class V Lanthipeptide Containing ad-Amino Acid Introduced by an F420H2-Dependent Reductase. *Angewandte Chemie International Edition*, *59*(41), 18029–18035. doi: 10.1002/anie.202008035
- Yamakawa, J., Kurosawa, H., Kaneko, K., Yamakawa, J., Aminaka, M., Hori, S., Cui, L., Ito, T., Jin, J., Hiramatsu, K., Okuzumi, K., Kobayashi, H., Katayama, Y., Cui, L., Ito, T., Hiramatsu, K., Kondo, S., Nakamura, A., Oguri, T., Oguri, T., & Hiramatsu, K. (2012). Heterogeneously vancomycin-intermediate *Staphylococcus aureus* (hVISA) emerged before the clinical introduction of vancomycin in Japan: a retrospective study. *Journal of Infection and Chemotherapy*, *18*(3), 406–409. doi: 10.1007/s10156-011-0330-2
- Yokoyama, K., Miyashita, T., Araki, Y., & Ito, E. (1986, dec). Structure and functions of linkage unit intermediates in the biosynthesis of ribitol teichoic acids in *Staphylococcus aureus* H and *Bacillus subtilis* W23. *European Journal of Biochemistry*, *161*(2), 479–489. doi: 10.1111/j.1432-1033.1986.tb10469.x
- Yushchuk, O., Binda, E., & Marinelli, F. (2020, jun). Glycopeptide Antibiotic Resistance Genes: Distribution and Function in the Producer Actinomycetes. *Frontiers in Microbiology*, *11*. doi: 10.3389/fmicb.2020.01173
- Ziemert, N., Alanjary, M., & Weber, T. (2016). The evolution of genome mining in microbes – a review. *Natural Product Reports*, *33*(8), 988–1005. doi: 10.1039/c6np00025h

## List of Figures

1	Cell envelope of <i>S. aureus</i> . . . . .	5
2	Comparison of prevalent <i>S. aureus</i> capsular serotypes CP5 and CP8 . . . . .	7
3	Organization of the <i>cap5</i> and <i>cap8</i> operon . . . . .	8
4	Capsule biosynthesis of <i>S. aureus</i> serotype 5 . . . . .	9
5	Regulative reversible phosphorylation circuit of capsule biosynthesis . . . . .	11
6	PGN, WTA and capsule biosynthesis . . . . .	12
7	Shared precursor pool of PGN, WTA, and capsule biosynthesis and the role of <i>S. aureus</i> LCPs in glycopolymer attachment . . . . .	14
8	WTA-PGN linkage . . . . .	15
9	Various cell wall glycopolymers linked to PGN . . . . .	16
10	LCP domain organization . . . . .	18
11	LCP protein crystals of various organisms . . . . .	19
12	<i>S. aureus</i> LcpA-C and <i>B. subtilis</i> TagT-V sequence alignment and secondary LcpA structure . . . . .	21
13	Catalytic mechanism of WTA attachment catalyzed by LcpA . . . . .	22
14	A hydrophilic pocket within the LcpA structure as a putative drug target . . . . .	23
15	PGN synthesis and sites of antibiotic intervention . . . . .	24
16	Structure of lipid II and species-specific modifications . . . . .	26
17	Comparison of selected RiPP family representatives . . . . .	30
18	Mechanism of glycopolymer attachment catalyzed by LCPs . . . . .	163
19	Superimposed crystal structures of <i>S. aureus</i> LcpA, <i>B. subtilis</i> TagT and respective LcpC models . . . . .	166
20	(Putative) active site residues of <i>S. aureus</i> LcpA and modeled LcpC . . . . .	167
21	Structural comparison CapA1 and <i>E. coli</i> co-polymerase WzzB. . . . .	169
22	Comparison of predicted structure models of CapA1 and CapA2 . . . . .	170
23	Alignment of PGTs and structure of MOE bound to SgtB . . . . .	174
24	Structure comparison of glycosyltransferase inhibitors with the lipid II-disaccharide . . . . .	176

## 6 List of Publications

**Deisinger, J. P.**, Müller, A., Ortiz-López, F. J., Genilloud, O., & Schneider, T. (**under review**). Dual targeting of the lanthidin antibiotic Cacaoidin. *Cell iScience*

Drayton, M., **Deisinger, J. P.**, Ludwig, K. C., Raheem, N., Müller, A., Schneider, T., & Straus, S. K. (2021, sep). Host Defense Peptides: Dual Antimicrobial and Immunomodulatory Action. *International journal of molecular sciences*, 22(20), 11172. doi: 10.3390/ijms222011172

Ortiz-López, F. J., Carretero-Molina, D., Sánchez-Hidalgo, M., Martín, J., González, I., Román-Hurtado, F., Cruz, M., García-Fernández, S., Reyes, F., **Deisinger, J. P.**, Müller, A., Schneider, T., & Genilloud, O. (2020, jun). Cacaoidin, First Member of the New Lanthidin RiPP Family. *Angewandte Chemie International Edition*, 59 (31), 12654–12658. doi: 10.1002/anie.202005187  
Copyright Wiley-VCH GmbH. Reproduced with permission.

Rausch, M.\*, **Deisinger, J. P.\***, Ulm, H.\* (\*contributed equally), Müller, A., Li, W., Hardt, P., Wang, X., Li, X., Sylvester, M., Engeser, M., Vollmer, W., Müller, C. E., Sahl, H. G., Lee, J. C., & Schneider, T. (2019, mar). Coordination of capsule assembly and cell wall biosynthesis in *Staphylococcus aureus*. *Nature Communications*, 10 (1404). doi: 10.1038/s41467-019-09356-x

Shan, Y., Gandt, A. B., Rowe, S. E., **Deisinger, J. P.**, Conlon, B. P., & Lewis, K. (2017, mar). ATP-Dependent Persister Formation in *Escherichia coli*. *MBio*, 8 (1), e02267-16. doi: 10.1128/mbio.02267-16